TARGETED CELL-TYPE SPECIFIC GENE EXPRESSION PROFILING IN A TRANSGENIC MOUSE MODEL OF PARKINSON'S



KATHARINA WAGNER

DEPARTMENT OF PHYSIOLOGY, ANATOMY AND GENETICS

CHRIST CHURCH

UNIVERSITY OF OXFORD

TRINITY TERM 2017

A THESIS SUBMITTED TOWARDS THE DEGREE OF DOCTOR OF PHILOSOPHY

TARGETED CELL-TYPE SPECIFIC GENE EXPRESSION PROFILING IN A TRANSGENIC MOUSE MODEL OF PARKINSON'S

A THESIS SUBMITTED FOR THE DEGREE OF DOCTOR OF PHILOSOPHY, TRINITY TERM 2017

KATHARINA WAGNER, CHRIST CHURCH, UNIVERSITY OF OXFORD

Parkinson's disease is a neurodegenerative disorder that is pathologically characterised by the preferential cell death of vulnerable dopaminergic neurons (DAn) in the midbrain. Multiplications of the human alpha-Synuclein (aSyn) gene locus give rise to autosomal-dominant Parkinson's and elevated aSyn expression has been linked to an increased risk to develop sporadic Parkinson's. Thus, aSyn provides an important link between familial and sporadic forms of the disease. This thesis brings together cutting-edge transgenic mouse models to examine early translational changes in the specifically vulnerable DAn. Translating ribosome affinity purification (TRAP) methodology was combined with a mouse model of Parkinson's that over-expresses aSyn from the complete human *SNCA* locus. Immunoprecipitation of translated mRNA from midbrain DAn enabled the investigation of perturbations in gene expression early during disease progression. Next generation sequencing analysis of translated mRNAs determined the effect of aSyn over-expression on the translational profile of the "at-risk" population of DAn. This translatome analysis in THTR mice which express an eGFP-tagged ribosomal transgene (eGFP-L10a) under the endogenous mouse promoter of tyrosine hydroxylase (TH) identified a mitochondrial deficit in aged transgenic mice. In addition, a novel Cre-conditional TRAP line expresses eGFP-L10a inCre expressing cells upon crossing to a DAT-Cre driver. Pilot TRAP experiments successfully isolated translated mRNA from soma (midbrain) and axons (striatum) of DAn. Overall, data generated with the transgenic TRAP/Parkinson's mouse lines will allow to obtain a more complete understanding of the underlying pathological pathways and translational changes during Parkinson's.

DECLARATION

I confirm that the work presented in this thesis is my own unless otherwise indicated. Where information has been derived from other sources, I confirm that this has been indicated in the thesis. Any text, data, and representation that is not my own work are indicated as such, acknowledged and referenced appropriately.

The work for this thesis has been performed by the author at the University of Oxford. This work has not been submitted for any other degree in this or any other University.

PUBLICATIONS AND CONFERENCE PRESENTATIONS

Publications

Janezic S, Threlfell S, Dodson PD, Dowie MJ, Taylor TN, Potgieter D, Parkkinen L, Senior SL, Anwar S, Ryan B, Deltheil T, Kosillo P, Cioroch M, **Wagner K**, Ansorge O, Bannerman DM, Bolam JP, Magill PJ, Cragg SJ, Wade-Martins R. *Deficits in dopaminergic transmission precede neuron loss and dysfunction in a new Parkinson model*. Proc Natl Acad Sci U S A. 2013.

Conference presentations

Wagner K, Janezic S, Deltheil T, Cioroch M, Wade-Martins R (2014). *Characterisation of a transgenic mouse model of Parkinson's for dopamine neuron specific translational profiling.*
Poster presentation at the Parkinson's UK Research Conference 2014, York, UK.

Wagner K, Janezic S, Wessely F, Monzon Sandoval J, Webber C, Wade-Martins R (2016). *Dopamine neuron specific translational profiling in a TH-bacTRAP transgenic mouse model.*
Poster presentation at the 10th FENS Forum of Neuroscience Conference 2016, Copenhagen, Denmark.

Wagner K, Janezic S, Wessely F, Monzon Sandoval J, Webber C, Wade-Martins R (2016). *Dopamine neuron specific translational profiling in a transgenic mouse model of PD.*
Poster presentation at the Neuroscience 2016 - Society for Neuroscience Conference, San Diego, CA, USA.

Wagner K, Monzon Sandoval J, Wessely F, Janezic S, Webber C, Wade-Martins R (2017). *Analysis of the dopaminergic neuron translatome in a transgenic mouse model of Parkinson's.*
Poster presentation at the EMBO | EMBL Symposium: Mechanisms of Neurodegeneration 2017, Heidelberg, Germany.

ACKNOWLEDGEMENTS

First and foremost, I would like to thank my supervisor Professor Richard Wade-Martins for the opportunity to join his lab, for his mentoring and support which have always been very stimulating. Thank you for the encouragement and all the challenging questions that hopefully made me a better scientist. Furthermore, I would like to thank Parkinson's UK, especially their Oxford branch, for providing me with generous funding for my degree.

While the past four years changed my life for so many reasons, they also let me realise that you can achieve anything you set your mind to. When I look back on my time as a PhD student, remembering all ups and downs, the words of motivation and encouragement, I realise that this thesis would not have been possible without the help and support of many great people!

Thank you all for these amazing memories, I will miss you and Oxford.

TABLE OF CONTENTS

DECLARATION **1**

PUBLICATIONS AND CONFERENCE PRESENTATIONS **2**

ACKNOWLEDGEMENTS **3**

TABLE OF CONTENTS **4**

ABBREVIATIONS **7**

LIST OF FIGURES **9**

LIST OF TABLES **12**

- CHAPTER 1 - **13**

GENERAL INTRODUCTION 13

1.1 PARKINSON'S DISEASE 14

1.1.1 INTRODUCTION 14

1.1.2 CLINICAL FEATURES OF PARKINSON'S DISEASE 14

1.1.3 NEUROPATHOLOGICAL FEATURES 15

1.1.4 AETIOLOGY OF PARKINSON'S DISEASE 17

1.1.5 TREATMENT OPTIONS FOR PARKINSON'S DISEASE 23

1.2 ALPHA-SYNUCLEIN 25

1.2.1 INTRODUCTION 25

1.2.2 ALPHA-SYNUCLEIN STRUCTURE 25

1.2.3 ALPHA-SYNUCLEIN AND PARKINSON'S DISEASE 27

1.2.4 AGGREGATION AND PRION-LIKE PROPERTIES OF ALPHA-SYNUCLEIN 28

1.2.5 CELLULAR FUNCTIONS OF ALPHA-SYNUCLEIN 30

1.3 ALPHA-SYNUCLEIN TRANSGENIC MOUSE MODELS OF PARKINSON'S DISEASE 35

1.3.1 ALPHA-SYNUCLEIN KNOCK-OUT MODELS 37

1.4 TRANSLATING RIBOSOME AFFINITY PURIFICATION (TRAP) 38

1.4.1 TRAP METHODOLOGY 38

1.4.2 ADVANTAGES AND DISADVANTAGES OF TRAP COMPARED TO OTHER RNA ISOLATION METHODS 40

1.4.3 TRANSGENIC MOUSE MODELS FOR TRAP 42

1.5 AIMS 48

- CHAPTER 2 - **49**

MATERIALS AND METHODS 49

2.1 MATERIALS AND METHODS - ANIMAL HUSBANDRY. 50

2.2 MATERIALS AND METHODS - PROTEIN BIOCHEMISTRY. 57

2.3 MATERIALS AND METHODS - IMMUNOHISTOCHEMISTRY. 60

2.4 MATERIALS AND METHODS - MOLECULAR BIOLOGY. 63

2.5 MATERIALS AND METHODS - BIOINFORMATICS. 73

- CHAPTER 3 - 79

MOLECULAR CHARACTERISATION OF A BACTRAP TRANSGENIC ALPHA-SYNUCLEIN OVER-EXPRESSION MOUSE MODEL . 79

3.1 OVERVIEW 80

CHAPTER AIMS 80

3.2 INTRODUCTION 81

3.2.1 *HSNCA+* TRANSGENIC MOUSE LINE 81

3.2.2 *TH-BACTRAP* (*THTR*) TRANSGENIC MOUSE LINE 82

3.3 RESULTS 84

3.3.1 GENERATION, BREEDING AND MAINTENANCE OF BACTRAP TRANSGENIC MOUSE LINES 84

3.3.2 MOLECULAR CHARACTERISATION OF OUR NOVEL *THTR* TRANSGENIC MOUE LINE 85

3.3.3 REVISED BREEDING STRATEGY TO GENERATE A COHORT OF HOMOZYGOUS *THTR* TRANSGENIC MICE 98

3.3.4 ESTABLISHING AN ADDITIONAL GENETIC CONTROL FOR GENE EXPRESSION PROFILING USING BACTRAP MICE 99

3.3.5 ANALYSIS OF KEY PROTEIN EXPRESSION LEVELS IN THE STRIATUM DID NOT SHOW CHANGES IN BACTRAP TRANSGENIC MICE 101

3.3.6 *HSNCA* PROTEIN IS OVEREXPRESSED IN OUR PD MOUSE MODEL 104

3.3.7 INVESTIGATION OF NIGROSTRIATAL DOPAMINERGIC CELL LOSS 106

3.4 DISCUSSION AND CONCLUSION 108

- CHAPTER 4 - 115

ESTABLISHING TRANSLATING RIBOSOME AFFINITY PURIFICATION METHODOLOGY IN *THTR* MICE 115

4.1 OVERVIEW 116

CHAPTER AIMS 116

COLLABORATION STATEMENT 116

4.2 INTRODUCTION 117

4.2.1 GENOME-WIDE GENE EXPRESSION ANALYSIS 117

4.2.2 GENE EXPRESSION PROFILING TO STUDY NEURODEGENERATIVE DISEASES 118

4.3 RESULTS 119

4.3.1 ESTABLISHING TRAP METHODOLOGY IN OUR *THTR* TRANSGENIC MOUSE LINE 119

4.3.2 FEASIBILITY PILOT TRAP EXPERIMENTS USING THE *THTR* TRANSGENIC MOUSE LINE 120

4.3.3 MATRIX OPTIMISATION TRAP EXPERIMENTS IN YOUNG AND OLD THTR MICE 122

4.3.4 PILOT TRAP RNA-SEQ AND BIOINFORMATIC ANALYSIS 126

4.4 DISCUSSION AND CONCLUSION 136

- CHAPTER 5 - 140

ANALYSIS OF THE DAN TRANSLATOME IN A TRANSGENIC MOUSE MODEL OF PD 140

5.1 OVERVIEW 141

CHAPTER AIMS 141

COLLABORATION STATEMENT 141

5.2 INTRODUCTION 142

5.2.1 TRANSGENIC MOUSE MODELS TO STUDY NEURODEGENERATIVE DISEASES 142

5.2.2 GENE EXPRESSION PROFILING IN A MPTP MODEL OF PARKINSON'S DISEASE 143

5.3 RESULTS 144

5.3.1 CELL-TYPE SPECIFIC ANALYSIS OF DAN-SPECIFIC MRNAS FROM THTR MICE 144

5.3.2 GENE EXPRESSION PROFILING OF DAN-SPECIFIC MRNA USING A MOUSE MODEL OF PD 147

5.3.3 PRINCIPAL COMPONENT ANALYSIS IDENTIFIES OUTLIER SAMPLES 150

5.3.4 ANALYSIS OF GENE MARKER ENRICHMENTS CONFIRMS DOPAMINERGIC NATURE OF THE TRAP IP FRACTIONS 153
5.3.5 THE TRAP-SEQ DATA CLUSTERING FINDS OVERLAP WITH EXTERNAL DATASETS 160
5.3.6 DIFFERENTIAL EXPRESSION ANALYSIS FINDS UP-AND DOWN-REGULATED GENES FOR THE 'EXPERIMENT', 'DISEASE', AND 'AGE' COMPARISONS 162
5.3.7 FUNCTIONAL ANALYSIS OF DEGS IN THE 'AGE' DATASET 167
5.1.1 TRAP-SEQ VALIDATION EXPERIMENTS 172
5.2 DISCUSSION AND CONCLUSION 184

- CHAPTER 6 - 192

MOLECULAR CHARACTERISATION OF A NOVEL DOUBLE TRANSGENIC CONDITIONAL TRAP PARKINSON'S MODEL 192
6.1 OVERVIEW 193
CHAPTER AIMS 193
6.2 INTRODUCTION 194
6.2.1 6.2.1 THE *DAT-IRES-CRE* TRANSGENIC MOUSE MODEL 194
6.2.2 THE ROSA26-EGFP-L10A TRANSGENIC MOUSE MODEL 194
6.2.3 AXONAL TRANSLATION 195
6.3 RESULTS 197
6.3.1 GENERATION, BREEDING AND MAINTENANCE OF A NOVEL CONDITIONAL TRAP TRANSGENIC MOUSE LINE 197
6.3.2 MOLECULAR CHARACTERISATION OF THE NOVEL *RELFS/-::DATCRE/-(::HSNCA+)* LINE 200
6.3.3 ESTABLISHING TRAP METHODOLOGY IN CELL SOMA AND AXONS USING A CONDITIONAL TRAP TRANSGENIC MOUSE LINE 207
6.3.4 YOUNG REL MICE CAN BE SUCCESSFULLY USED FOR TRAP 208
6.3.5 TRAP CAN BE SUCCESSFULLY USED TO ISOLATE HIGH QUALITY RNA FROM CELL SOMA AND AXONS OF YOUNG AND AGED REL TRANSGENIC MICE 210
6.4 DISCUSSION AND CONCLUSION 215

- CHAPTER 7 - 222

GENERAL DISCUSSION 222
7.1 OVERVIEW 223
7.2 DISCUSSION - *TH-BACTRAP* (*THTR*) MICE 223
7.3 FUTURE DIRECTIONS - *TH-BACTRAP* (*THTR*) MICE 225
7.4 DISCUSSION - ROSA26-EGFP-L10A::DAT-CRE MICE 226
7.5 FUTURE DIRECTIONS - *ROSA26-EGFP-L10A::DAT-CRE* MICE 226
7.6 OUTLOOK 229

REFERENCES 230

- APPENDIX - I

APPENDIX - LIST OF FIGURES II
APPENDIX - LIST OF TABLES II
APPENDIX - CHAPTER 4 III
APPENDIX – CHAPTER 5 VII

ABBREVIATIONS

-/-	Knock-out (also KO)
+/-	Heterozygous
+	Hemizygous
++ or +/+	Homozygous
6-OHDA	6-hydroxydopamine
AADC	Aromatic L-amino acid decarboxylase
AAV	Adeno-associated virus
AB	Antibody
AD	Alzheimer's disease
ALS	Amyotrophic lateral sclerosis
ANOVA	Analysis of variance
APP	Amyloid precursor protein
aSyn	Alpha-Synuclein
ATP	Adenosine triphosphate
Aβ	Amyloid-beta
b-ME	Beta-mercaptoethanol
BAC	Bacterial artificial chromosome
BCA	Bicinchoninic acid
birA	Bacterial biotin ligase gene
bp	Base pair
BSA	Bovine serum albumin
bSyn	Beta-Synuclein
CAG	CMV early enhancer/chicken beta actin
CAV	Canine adenovirus
CB	Cerebellum
cDNA	Complementary DNA
CHX	Cycloheximide
CMV	Cytomegalovirus
CNS	Central nervous system
CNV	Copy number variant
CSPa	Cysteine string protein alpha
CTRL	Control
CTX	Cortex
DA	Dopamine
DAB	3,3'-diaminobenzidine
DAn	Dopaminergic neurons
DAPI	4',6-diamidino-2-phenylindole
DAT	Dopamine transporter
DBS	Deep brain stimulation
ddH_2O	Double distilled h2o
DEA	Differential expression analysis
DEGs	Differentially expressed genes
DEPC	Diethyl pyrocarbonate
DHPC	1,2-diheptanoyl-*sn*-glycero-3-phosphocholine
DLB	Dementia with Lewy body disease
DNA	Deoxyribonucleic acid
dNTP	Deoxynucleotide triphosphate
Dox	Doxycycline
DRP1	Dynamin-1-like
DTT	Dithiothreitol
EDTA	Ethylenediaminetetraacetic acid
Eef1a1	Eukaryotic translation elongation factor 1 alpha 1
eGFP	Enhanced green fluorescent protein
KO	Knock-out (also -/-)
L-DOPA	L-3,4-dihydroxyphenylalanine or levadopa
LB	Lewy body
LC	Locus coeruleus
LN	Lewy neurite
LRRK2	Leucine-rich repeat kinase 2
m	Mouse
MB	Midbrain
MeOH	Methanol
MFN2	Mitofusin 2
$MgCl_2$	Magnesium chloride
MPTP	1-methyl-4-phenyl-1,2,3-tetrahydropyridine
mRNA	Messenger RNA
MSA	Multiple system atrophy
mSnca	Mouse alpha-Synuclein
NAC	Non-amyloid-β component
NaCl	Sodium chloride
NACP	Non-amyloid-beta component precursor
$NaHCO_3$	Sodium bicarbonate
NaOH	Sodium hydroxide
ncRNA	Non-coding RNA
NDS	Normal donkey serum
neo	Neomycin
non-tg	Non-transgenic
NP-40	Nonylphenyl polyethylene glycol
O/N	Over-night
OVX	Over-expressed
OXPHOS	Oxidative phosphorylation
PARK2	Parkin
PBS	Phosphate buffered saline
PCA	Principal component analysis
PCR	Polymerase chain reaction
PD	Parkinson's disease
PDHa1	Pyruvate dehydrogenase alpha 1
PFA	Paraformaldehyde
PHB	Prohibitin
PINK1	PTEN-induced putative kinase 1
PLA	Proximity ligation assay
polyA	Polyadenylation sequence
PPI	Protein-protein interaction
PVDF	Polyvinylidene fluoride
QC	Quality control
qPCR	Quantitative real-time PCR
RanGAP1	RAN GTPase activating protein 1
RBD	Rem sleep behaviour disorder
rcf	Relative centrifugal force
REL	Rosa26-eGFP-L10a mouse line
REM	Rapid eye movement
RIN	RNA integrity number
RIPA	Radioimmunoprecipitation assay
RNA	Ribonucleic acid
RNA-Seq	RNA sequencing

eGFP-L10a	eGFP-tagged RPL10a fusion protein
ER	Endoplasmic reticulum
EtOH	Ethanol
FACS	Fluorescent-activated cell sorting
FDR	False discovery rate
FISH	Fluorescent *in situ* hybridisation
FLP	Flipase
FPKM	Fragments per kilobase million
FRT	FLP recombinase target
fs	Floxed
GAD2	Glutamate decarboxylase 2
GAPDH	Glyceraldehyde 3-phosphate dehydrogenase
GBA	Glucocerebrosidase
gDNA	Genomic DNA
GENSAT	Gene expression nervous system atlas
GFAP	Glial fibrillary acidic protein
GFP	Green fluorescent protein
GIRK2	G protein-activated inward rectifier potassium channel 2
GO	Gene ontology terms
gSyn	Gamma-Synuclein
GWAS	Genome-wide association study
h	Human
HBSS	Hank's balanced salt solution
HCl	Hydrogen chloride
hESC	Human embryonic stem cell
HI	Hippocampus
HRP	Horseradish
hSNCA	Human alpha-Synuclein
HSP60	Heat shock protein 60
IHC	Immunohostochemistry
INTACT	Isolation of nuclei tagged in specific cell-types
IP	Immunoprecipitation/ immunoprecipitated
iPSC	Induced pluripotent stem cell
IRES	Internal ribosome entry site
ISH	*In situ* hybridisation
kb	Kilobase
KCl	Potassium chloride
kDa	Kilo Dalton
KEGG	Kyoto Encyclopedia of Genes and Genomes
RNase	Ribonuclease
ROS	Reactive oxygen species
RPL10a	Ribosomal protein L 10a
rpm	Rotations per minute
rRNA	Ribosomal RNA
RT	Room temperature
SDHA	Succinate dehydrogenase complex, subunit A
SDS	Sodium dodecyl sulphate
SNAP23	Synaptosomal-associated protein 23
SNAP25	Synaptosomal-associated protein 25
SNARE	Soluble nsf attachment protein receptor
SNc	Substantia nigra pars compacta
Snca	Alpha-Synuclein (or asyn)
Sncaip	Asyn-interacting protein (or synphilin)
Sncb	Beta-Synuclein (or bsyn)
Sncg	Gamma-Synuclein (or gsyn)
SNP	Single nucleotide polymorphism
SOD1	Superoxide dismutase 1
STR	Striatum
TBE	Tris/borate/edta
TBS	Tris-buffered Saline
TBS-T	Tbs, tween-20
TBS-TX	Tbs, triton-x100
TBS+	Tbs, 10% nds, triton-x100
tetO	Tetracycline operator
TH	Tyrosine hydroxylase
THTR	TH-bacTRAP mouse line
TOMM20	Translocase of outer Mitochondrial membrane 20
TPM	Transcripts per million
TRAP	Translating ribosome affinity purification
tTA	Tetracycline-controlled trans-activator
TUJ1	Beta3-tubulin
UB	Unbound
UTR	Untranslated region
V	Volt
VDAC	Voltage-dependent anion channel
VTA	Ventricular tegmental area
WT	Wild-type
WTCHG	Wellcome Trust for Human Genetics

LIST OF FIGURES

CHAPTER 1

FIGURE 1. 1 PHASES OF PARKINSON'S DEVELOPMENT. 15

FIGURE 1. 2 SCHEMATIC REPRESENTATION OF ALPHA-SYNUCLEIN 26

FIGURE 1. 3 SUMMARY OF THE MYRIAD FUNCTIONS OF ALPHA-SYNUCLEIN IN NEURONS. 34

FIGURE 1. 4 TRANSLATING RIBOSOME AFFINITY PURIFICATION (TRAP). 40

CHAPTER 3

FIGURE 3. 1 PRELIMINARY IN VITRO RESULTS TESTING THE TH-BACTRAP VECTOR USED FOR THE GENERATION OF THE THTR TRANSGENIC MOUSE LINE. 83

FIGURE 3. 2 BREEDING SCHEME FOR THE DOUBLE TRANSGENIC THTR /HSNCA+ EXPERIMENTAL COHORT. 84

FIGURE 3. 3 NATIVE EGFP FLUORESCENCE IS RESTRICTED TO DAN IN THE MIDBRAINS OF HEMIZYGOUS AND HOMOZYGOUS THTR MICE COMPARING 3 MONTHS AND 18 MONTHS. 86

FIGURE 3. 4 TH AND EGFP ARE CO-EXPRESSED IN DAN IN THE MIDBRAIN (3 MONTHS). 87

FIGURE 3. 5 ANALYSIS OF EGFP-L10A TRANSGENE SHOWS NO SIGNS OF ECTOPIC EXPRESSION (3 MONTHS) 89

FIGURE 3. 6 ANALYSIS EGFP EXPRESSION IN MIDBRAIN DAN SHOWS CONSISTENT RESULTS IN AGED MICE (18 MONTHS). 90

FIGURE 3. 7 CONFIRMATION OF REGION-SPECIFIC EXPRESSION OF THE EGFP-L10A TRANSGENE IN AGED ANIMALS (18 MONTHS). 92

FIGURE 3. 8 TIMELINE ANALYSIS OF TH/GFP-DOUBLE POSITIVE CELLS IN DAN OF THTR MICE REVEALS A DECREASE IN GFP/TH DOUBLE POSITIVE CELLS. 93

FIGURE 3. 9 ANALYSIS OF EGFP-L10A TRANSGENE EXPRESSION IN CATECHOLAMINERGIC NEURONS OF THE LOCUS COERULEUS SHOWS SURPRISING RESULTS (3 MONTHS). 94

FIGURE 3. 10 ALPHA-SYNUCLEIN IS CO-EXPRESSED IN SOME EGFP-POSITIVE CELLS IN THE MIDBRAIN (3 MONTHS). 96

FIGURE 3. 11 ALPHA-SYNUCLEIN AND EGFP ARE ALSO CO-EXPRESSED IN AGED TRANSGENIC MICE (18 MONTHS) 97

FIGURE 3. 12 COMPARISON OF DIFFERENT GFP ANTIBODIES EXCLUDES THAT SITE-SPECIFIC DIFFERENCES IN ANTIBODY EPITOPE RECOGNITION INFLUENCE GFP LABELLING. 98

FIGURE 3. 13 OPTIMISED BREEDING SCHEME FOR THE DOUBLE TRANSGENIC THTR/HSNCA+ EXPERIMENTAL COHORT. 99

FIGURE 3. 14 BREEDING OVERVIEW FOR AN ADDITIONAL CONTROL FOR THE THTR LINE TO PERFORM TRAP EXPERIMENTS IN THTR+/+ MSNCA KO VERSUS THTR+/+ MSNCA WT ANIMALS. 100

FIGURE 3. 15 QUANTITATIVE WESTERN BLOT ANALYSIS IN THE STRIATUM OF THTR MICE AT 3 AND 12 MONTHS 102

FIGURE 3. 16 ANALYSIS OF STRIATAL DAT EXPRESSION LEVELS OF THTR MICE SHOWS NO DIFFERENCE (3 AND 12 MONTHS). 104

FIGURE 3. 17 HUMAN ALPHA-SYNUCLEIN EXPRESSION IN THE STRIATUM OF YOUNG AND AGED THTR/HSNCA+ MICE. .. 105

FIGURE 3. 18 STEREOLOGICAL CELL COUNT ANALYSIS OF DAN IN THE MIDBRAIN BY TH- AND EGFP- IMMUNOREACTIVITY. 107

CHAPTER 4

FIGURE 4. 1 PILOT TRAP EXPERIMENTS USING THE THTR TRANSGENIC MOUSE LINE SUCCESSFULLY ENRICH DAN-MARKERS IN THE IP FRACTION. 121

FIGURE 4. 2 TRAP AFFINITY MATRIX OPTIMISATION EXPERIMENTS ADAPT THE TRAP PROTOCOL TO THE THTR MOUSE LINE. 123

FIGURE 4. 3 SECOND ROUND OF TRAP AFFINITY MATRIX OPTIMISATION EXPERIMENTS CONFIRM OPTIMAL TRAP MATRIX AMOUNTS. 124

FIGURE 4. 4 OPTIMISED TRAP AFFINITY MATRIX CONDITIONS CAN BE SUCCESSFULLY USED FOR AGED THTR TRANSGENIC MICE. 125

FIGURE 4. 5 SAMPLE OVERVIEW FOR PILOT TRAP RNA-SEQ AND CORRESPONDING TRAP-QPCR ENRICHMENT GRAPHS. 127

FIGURE 4. 6 PRINCIPAL COMPONENT ANALYSIS (PCA) OF THE PILOT RNA-SEQ RESULTS. 129

FIGURE 4. 7 SCATTER PLOTS SHOWING A COMPARISON OF IP VS TOTAL TRAP RNA USING SELECTED MARKERS AND PUBLISHED GENES. 131

FIGURE 4. 8 SCATTER PLOTS SHOWING THE IP VS TOTAL TRAP RNA COMPARISON FOR AGED TRAP MICE. 132

FIGURE 4. 9 CHARACTERISTICS OF THE DIFFERENTIALLY EXPRESSED HOMOZYGOUS TRAP IP FRACTION REVEAL A DAN-SPECIFIC PROFILE. 133

FIGURE 4. 10 HIERARCHICAL CLUSTERING CLEARLY SEPARATES THE TRAP-HOMOZYGOUS IP SAMPLE FROM THE TRAP-NEGATIVE AND TRAP-HEMIZYGOUS IP SAMPLES 135

CHAPTER 5

FIGURE 5. 1 EXPERIMENTAL DESIGN OF THE THTR TRAP-SEQ STUDY. 145

FIGURE 5. 2 HIGH QUALITY RNA WAS ISOLATED FROM THTR MICE USING TRAP FOR DAN-SPECIFIC GENE EXPRESSION PROFILING. 147

FIGURE 5. 3 OVERVIEW OF THE READS PER LANE REVEALS 80% MAPPING SUCCESS TO PROTEIN CODING GENES. 150

FIGURE 5. 4 HIERARCHICAL CLUSTERING AND PCA ANALYSIS OF ALL 40 RNA-SEQ SAMPLES IDENTIFIES OUTLIER SAMPLES. 152

FIGURE 5. 5 PCA AFTER REMOVING THE OUTLIER SAMPLES SEPARATES TRAP IP SAMPLES BY AGE. 153

FIGURE 5. 6 DAN AND NON-DAN MARKER ENRICHMENTS PLOTS CONFIRM SUCCESSFUL ISOLATION OF DAN-SPECIFIC MRNA. 154

FIGURE 5. 7 SELECTED MARKER GENES ARE NOT ENRICHED IN THE TRAP IP FRACTIONS BY GLOBAL EXPRESSION LEVEL ANALYSIS. 155

FIGURE 5. 8 SELECTED MARKER GENES ARE ENRICHED IN THE TRAP IP FRACTIONS BY GLOBAL EXPRESSION LEVEL ANALYSIS. 156

FIGURE 5. 9 SYNUCLEIN FAMILY MEMBER GENES ARE EXPRESSED IN THE TRAP-SEQ SAMPLES 158

FIGURE 5. 10 COMPARISON OF THE TRAP-SEQ DATASET TO EXTERNAL DAN TRANSLATOME DATASETS CONFIRMS SUCCESSFUL ENRICHMENT OF DAN-SPECIFIC MRNA. 161

FIGURE 5. 11 KEY DEA SHOWS UP-AND DOWN-REGULATED GENES BY EXPERIMENT AND AGE, BUT NOT DISEASE 162

FIGURE 5. 12 GO TERMS AND PATHWAYS RELATING TO DOPAMINERGIC CELL POPULATION ARE DIFFERENTIALLY EXPRESSED IN THE TRAP IP FRACTIONS. 165

FIGURE 5. 13 HIGH CO-EXPRESSION IN THE BRAIN AMONG DIFFERENTIALLY EXPRESSED GENES WITH AGE. 169

FIGURE 5. 14 SIMILAR GO TERMS ARE FOUND UP- OR DOWN-REGULATED IN CTRL AND PD SAMPLES WITH AGE. 172

FIGURE 5. 15 GO TERMS AND KEGG PATHWAYS FOUND UP- OR DOWN-REGULATED IN PD SAMPLES WITH AGE. 173

FIGURE 5. 16 VALIDATION OF AGE AND PD-RELATED TRAP-SEQ DEGS. 175

FIGURE 5. 17 MITOCHONDRIAL RESPIRATORY CHAIN COMPLEXES 177

FIGURE 5. 18 EXPRESSION OF OXPHOS COMPLEXES IS DOWN-REGULATED WITH AGE. 178

FIGURE 5. 19 ANALYSIS OF PROTEINS INVOLVED IN MITOCHONDRIAL FUSION AND FISSION. 180

FIGURE 5. 20 ANALYSIS OF MITOCHONDRIA-RELATED PROTEINS SHOW A DECREASE IN EXPRESSION WITH AGE 181

FIGURE 5. 21 PROTEIN EXPRESSION ANALYSIS OF FURTHER MITOCHONDRIA-RELATED GENES. 183

CHAPTER 6

FIGURE 6. 1 CONDITIONAL TRAP TRANSGENIC MOUSE LINE. 195

FIGURE 6. 2 LOCALISATION OF ROSA26 AND ASYN ON MOUSE CHROSOMOSE 6. 197

FIGURE 6. 3 BREEDING SCHEME TO CROSS HSNCA+ MICE BACK ON A MSNCA BACKGROUND. 198

FIGURE 6. 4 BREEDING SCHEME TO GENERATE TRANSGENIC RELFS/-::DATCRE/-::(HSNCA+) EXPERIMENTAL COHORTS. 199

FIGURE 6. 5 NATIVE EGFP FLUORESCENCE IS DETECTABLE IN RELFS/-::DATCRE/- MICE AT 3, 6, AND 12 MONTHS. ... 201

FIGURE 6. 6 EGFP IS CO-EXPRESSED WITH DAN-SPECIFIC MARKERS IN THE MIDBRAIN (3 MONTHS). 202

FIGURE 6. 7 OVERVIEW OF EGFP-L10A-NEGATIVE BRAIN REGIONS (3 MONTHS). 204

FIGURE 6. 8 QUANTITATIVE WESTERN BLOT ANALYSIS OF TH AND RPL10A EXPRESSION IN THE STRIATUM OF YOUNG MICE DOES NOT SHOW A DIFFERENCE ACROSS DIFFERENT GENETIC BACKGROUNDS IN THE REL LINE (3 MONTHS). 205

FIGURE 6. 9 ASYN-POSITIVE NEURONS SHOW CO-EXPRESSION WITH EGFP IN TRANSGENIC MICE (3 MONTHS). 206

FIGURE 6. 10 ASYN IS OVER-EXPRESSED IN THE STRIATUM OF YOUNG RELFS/-::DATCRE/-::HSNCA+ MICE (3 MONTHS). 207

FIGURE 6. 11 NEURONAL TRANSLATING RIBOSOME AFFINITY PURIFICATION (TRAP) IN SOMA AND AXONS. 208

FIGURE 6. 12 TRAP PILOT EXPERIMENTS USING TRAP-TRANSGENIC MICE (3 MONTHS) SHOW SUCCESSFUL ISOLATION OF DAN-SPECIFIC MRNA FROM MIDBRAIN AND STRIATUM. 210

FIGURE 6. 13 MIDBRAIN AND STRIATUM FROM TRAP-TRANSGENIC MICE (6 MONTHS) CAN BE SUCCESSFULLY USED FOR THE ENRICHMENT OF MARKER GENES. 211

FIGURE 6. 14 TRAP RESULTS CAN BE SUCCESSFULLY RE-PRODUCED IN AGED TRANSGENIC MICE (12 MONTHS). 212

FIGURE 6. 15 TRAP ON MIDBRAIN AND STRIATUM INPUT TISSUE PRODUCES CONSISTENT RESULTS IN AGED MICE (18 MONTHS). 214

FIGURE 6. 16 EXPERIMENTAL DESIGN OF THE REL TRAP-SEQ STUDY. 221

LIST OF TABLES

CHAPTER 2

TABLE 2. 1 SUMMARY OF MOUSE LINES USED FOR THIS STUDY. 51

TABLE 2. 2 PRIMER SEQUENCES FOR GENOTYPING OF ALPHA-SYNUCLEIN TRANSGENIC MICE. 53

TABLE 2. 3 PRIMER SEQUENCES FOR GENOTYPING OF TRANSGENIC MICE. 54

TABLE 2. 4 PRIMER SEQUENCES FOR GENOTYPING OF ROSA26-EGFP-L10A AND DAT-CRE TRANSGENIC MICE. 55

TABLE 2. 5 QPCR PRIMER SEQUENCES FOR COPY/NUMBER GENOTYPING OF TH-BACTRAP AND ROSA26-EGFP-L10A TRANSGENIC MICE. 56

TABLE 2. 6 PRIMARY ANTIBODIES FOR WESTERN BLOT ANALYSIS 59

TABLE 2. 7 SECONDARY ANTIBODIES FOR WESTERN BLOT ANALYSIS 59

TABLE 2. 8 PRIMARY ANTIBODIES FOR IMMUNOFLUORESCENCE ANALYSIS. 61

TABLE 2. 9 SECONDARY ANTIBODIES FOR IMMUNOFLUORESCENCE ANALYSIS. 61

TABLE 2. 10 PRIMARY ANTIBODIES FOR IMMUNOHISTOCHEMISTRY ANALYSIS. 62

TABLE 2. 11 SECONDARY ANTIBODIES FOR IMMUNOHISTOCHEMISTRY ANALYSIS. 62

TABLE 2. 12 ANTIBODIES OF GFP ORDER # 1 FOR ALL THTR TRAP EXPERIMENTS. 65

TABLE 2. 13 ANTIBODIES OF GFP ORDER # 2 FOR ALL REL TRAP EXPERIMENTS. 65

TABLE 2. 14 QPCR HOUSEKEEPING PRIMERS. 72

TABLE 2. 15 QPCR PRIMERS USED FOR TRAP RNA ANALYSIS. 72

TABLE 2. 16 QPCR PRIMERS USED FOR RNA-SEQ VALIDATION 72

TABLE 2. 17 SUMMARY OF PILOT RNA-SEQ SAMPLES. 74

TABLE 2. 18 SUMMARY OF RNA-SEQ SAMPLES. 75

CHAPTER 4

TABLE 4. 1 PILOT TRAP-SEQ SAMPLES OVERVIEW 128

CHAPTER 5

TABLE 5. 1 TRAP-SEQ SAMPLES OVERVIEW. 148

TABLE 5. 2 GENE EXPRESSION OF THE SYNUCLEIN FAMILY. 158

TABLE 5. 3 TOP 25 GENES FOR THE DEA 'EXPERIMENT'. 163

TABLE 5. 4 TOP GENES FOR THE DEA 'DISEASE. 166

TABLE 5. 5 TOP 25 GENES FOR THE DEA 'AGE - CTRL'. 167

TABLE 5. 6 TOP 25 GENES FOR THE DEA 'AGE - PD'. 167

TABLE 5. 7 GENES SELECTED FOR QPCR ANALYSIS OUT OF THE 100 MOST SIGNIFICANTLY CHANGED GENES (DEA 'AGE - PD'). 174

TABLE 5. 8 GENES SELECTED FOR WESTERN BLOT ANALYSIS OUT OF THE 100 MOST SIGNIFICANTLY CHANGED GENES (DEA 'AGE' IP SAMPLES PD) – OXPHOS COMPLEXES. 176

TABLE 5. 9 GENES SELECTED FOR WESTERN BLOT ANALYSIS OUT OF THE 100 MOST SIGNIFICANTLY CHANGED GENES (DEA 'AGE' IP SAMPLES PD). 176

- CHAPTER 1 -

GENERAL INTRODUCTION

1.1 Parkinson's Disease

1.1.1 Introduction

Parkinson's disease (PD) is the second most common neurodegenerative disorder of the human brain after Alzheimer's disease (AD) (Lau and Breteler, 2006). PD pathology is not restricted to the central nervous system (CNS), it also presents peripheral and enteric nervous system involvement (Comi et al., 2014; Lebouvier et al., 2009). The first detailed description of PD was published in 1817 by James Parkinson in '*An essay on the shaking palsy*' (reprinted as (Parkinson et al., 2002)). Here, James Parkinson described the motor symptoms of PD that later became the cornerstone of clinical diagnosis (Parkinson et al., 2002). PD is a progressive disease. Less than 5% of all affected people are under the age of 50 years but the incidence rate rapidly increases in elderly people (Van Den Eeden, 2003) and sums up to more than 1% of the population older than 60 years and up to 4% of the population older than 80 years (Lau and Breteler, 2006).

1.1.2 Clinical Features of Parkinson's disease

Motor symptoms and non-motor symptoms

The cardinal clinical symptoms of PD motor dysfunction include resting tremor, bradykinesia (slowness of movement), rigidity (stiffness), and postural instability (Jankovic, 2008). These symptoms arise as a consequence of the loss of about 50-70% of the dopaminergic neurons (DAn) in the substantia nigra pars compacta (SNc). Subsequent loss of dopaminergic innervation in the striatum is causing an imbalance in the basal ganglia circuit (Fearnley and Lees, 1991).

The prodromal phase of PD is mainly characterised by non-motor symptoms that can precede clinical diagnosis of PD by several decades (Chaudhuri et al., 2006) (Figure 1. 1). Non-motor symptoms of PD include gastrointestinal dysfunction, hyposmia, anxiety, and depression, or they manifest as sleep disorders, rapid eye movement behaviour disorders (RBD), and others (Dickson et al., 2009). Pathological changes correlating with non-motor symptoms have been observed outside of the nigrostriatal system in brain regions, including in the olfactory bulb, the lower brainstem as well as in the autonomic nervous system (Dickson et al., 2009). Motor symptoms commonly respond well to treatment with dopamine (DA) replacement therapies, such as levodopa

(L- DOPA) but non-motor symptoms of PD are often poorly recognised and inadequately treated due to the limited availability of therapies (Chaudhuri et al., 2006). Thus, non-motor symptoms impose a significant burden on the quality of life for patients (Welsh, 2004).

Overall, clinical diagnosis is complicated by the lack of reliable biomarkers for the prodromal phase of PD. A clinical diagnosis can often only be made well after PD onset, when about 60% of the DAn are already lost, which can only be finally confirmed by post-mortem examinations of the brain (Dauer and Przedborski, 2003; Fearnley and Lees, 1991).

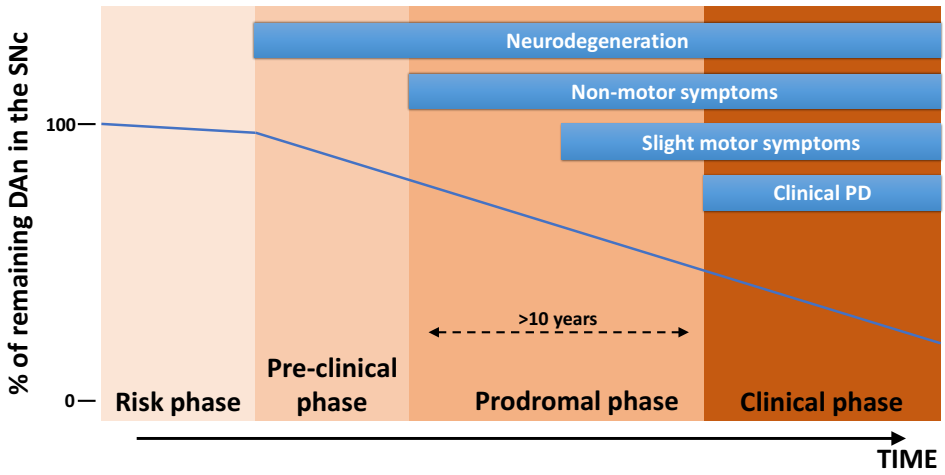


Figure 1. 1 ***Phases of Parkinson's development.***
PD neurodegeneration likely starts in the preclinical phase with no overt symptoms, before progressing to the prodromal phase, in which non-motor symptoms and slight motor signs can occur. The final clinical phase is characterised by a variety of (non-) motor symptoms. PD= Parkinson's disease. DAn= dopaminergic neuron. SNc= Substantia nigra.

1.1.3 Neuropathological features

Cell loss and regional vulnerability

The main pathophysiological feature at the cellular level of PD is the progressive degeneration of dopaminergic cell bodies in the SNc which leads to a loss of dopaminergic innervation from the corresponding nerve terminals in the dorsal striatum (Dauer and Przedborski, 2003). The dopaminergic cell populations in the midbrain are located in two major groups, the SNc neurons (A9) projecting to the dorsal striatum, and the ventral tegmental area (VTA) (A10) neurons projecting to the ventral striatum, limbic, and cortical areas (German and Manaye, 1993). Intriguingly, A9 neurons show the greatest vulnerability and degenerate predominantly in PD

(Hirsch et al., 1988; Sulzer, 2007). The pattern of cell loss observed during PD shows opposing patterns to the losses observed during healthy aging (Fearnley and Lees, 1991). It has not yet been discovered why DAn in the SNc are particularly susceptible to degeneration. The A9 and A10 neurons can be distinguished by certain characteristics; DAn in the VTA express the calcium binding protein Calbindin-D28k but only low levels of dopamine transporter (DAT), conversely, DAn in the SNc are Calbindin-D28k -negative and uniquely express the G protein-activated inward rectifier potassium channel 2 (GIRK2) (Björklund and Dunnett, 2007). Susceptible neurons tend to have an underlying high metabolic demand; A9 neurons are characterised by their highly branched, long, unmyelinated axons (Pissadaki and Bolam, 2013), and together with their typical autonomous pace-maker activity this could add to the burden of energy demand in these cells (Grace and Bunney, 1984; Guzman et al., 2009).

Lewy bodies and Lewy neurites

Another hallmark of PD is the presence of intracytoplasmic, eosinophilic inclusions in the surviving neurons, termed Lewy bodies (LBs) (Forno, 1987), first described in the brainstem of PD patients by Friedrich Lewy in 1912 (Lewy, 1912). These deposits of aggregated proteins are found in all PD-affected brain areas and are mostly composed of the protein alpha-Synuclein (aSyn) (Spillantini et al., 1997; Spillantini et al., 1998) but also other filamentous structures such as ubiquitin and neurofilament proteins (Galloway et al., 1992). Morphologically, two different forms of LBs can be distinguished, 'classical' brainstem and the 'cortical' LBs (Goedert et al., 2012). Classical LBs are characterised by a dense granular core with a surrounding pale halo at the periphery. Cortical LBs lack a halo and are poorly organised on the ultrastructural level (Jellinger, 2009). Abnormal inclusions containing aSyn in dystrophic neurons are termed Lewy neurites (LNs) (Braak et al., 1999) and could represent an early PD-pathological characteristic and a pre-stage to LBs (Braak et al., 2003). Since aSyn-positive inclusions are also characteristic of other neurodegenerative disorders such as Dementia with Lewy Bodies (DLB) and Multiple System Atrophy (MSA), all neurodegenerative diseases affected by aSyn pathology are collectively referred to as synucleinopathies (Spillantini and Goedert, 2000).

Braak and colleagues proposed a staging scheme for the progression of PD pathology that described six distinct pathological stages based on varying degrees of LB and LN pathology in post-mortem brains (Braak et al., 2003). The 'Braak hypothesis' suggests that the disease begins in structures of the lower brainstem and the olfactory bulbs (stage 1) from where it moves up the brainstem, traveling to the Locus Coeruleus (LC) (stage 2) until it reaches the SNc (stage 3). The olfactory bulb and the lower brainstem are thought to be implicated in the pre-clinical stages as key areas that mediate non-motor symptoms such as olfaction or sleep (Chaudhuri et al., 2006). At stage 3 and 4, typical motor symptoms of PD start to emerge with severe DAn loss in the SNc (stage 4). The final stages (stage 5 and 6) correlate with the presence of LBs in the neocortex. The disease is at its most severe in stage 6, affecting the motor and sensory areas in the brain which manifest as neuropsychiatric symptoms such as depression, cognitive impairment, and hallucinations (Braak et al., 2003; Chaudhuri et al., 2006). However, the Braak hypothesis does not provide an explanation for all preclinical symptoms seen in PD; furthermore, the staging is based on LBs distribution and not neuronal degeneration (Chaudhuri et al., 2006).

The role of LBs and LNs in the brain is not yet fully understood. Some PD patients with familial gene mutations, including *Parkin* (Cookson et al., 2008) or Leucine-rich repeat kinase 2 (*LRRK2*) (Gaig et al., 2007), exhibit neurodegeneration but no LB-pathology. Hence, the formation of LBs could pose a protective mechanism for sequestering toxic protein aggregates, helping the cells to maintain their normal cellular functions (Bengoa-Vergniory et al., 2017). This hypothesis is supported by the presence of LBs in a small number of neurologically normal brains by post-mortem analysis (Parkkinen et al., 2005).

1.1.4 Aetiology of Parkinson's disease

Significant progress has been made in the study of familial forms of PD caused by rare genetic alterations but the aetiology of sporadic disease-onset which accounts for most PD cases remains largely unknown (Dauer and Przedborski, 2003).

Genetic risk factors

The majority of PD cases are sporadic and about 10% of disease cases have known genetic implications (Thomas and Flint Beal, 2007). To date, eighteen chromosomal so called 'PARK' regions are known, named after their putative link to PD and numbered chronologically (Table 1. 1). Six of these specific chromosomal regions contain genes with known mutations sufficient to cause (monogenic) PD. Out of the six genes linked to heritable, monogenic PD, mutations in *SNCA* (PARK1/4) and *LRRK2* (PARK8) display autosomal-dominant inheritance, while mutations in *Parkin* (PARK2), *PINK1* (PARK6), ATP13A2 (PARK9), and *DJ-1* (PARK7) are inherited autosomal-recessive (Klein et al., 2012). The mutations explain 3-5% of sporadic PD cases (Klein et al., 2012).

The first genetic link that associated aSyn to PD was a A53T mutation in the *SNCA* gene that causes autosomal dominant PD (Polymeropoulos et al., 1997). Since then, several other mutations (A30P (Kruger et al., 1998), E46K (Zarranz et al., 2004), H50Q (Appel-Cresswell et al., 2013; Proukakis et al., 2013), G51D (Lesage et al., 2013), and A53E (Ghosh et al., 2014; Pasanen et al., 2014)) have been shown to cause familial forms of PD or DLB. Furthermore, copy number variants (CNVs) in the *SNCA* gene are now known to cause PD, including duplications (Chartier-Harlin et al., 2004; Ibáñez et al., 2004) and triplications (Olgiati et al., 2015; Singleton et al., 2003).

Mutations in another autosomal-dominant inherited gene *LRRK2* are estimated to account for up to 10% of familial PD (Lesage and Brice, 2009). Known mutations include I2020T, R1441C (Zimprich et al., 2004), and G2019S that is present in about 2% of sporadic PD cases (Gilks et al., 2005). Mutations in *VPS35* cause late-onset, autosomal-dominant PD that have been described in a Swiss family (Vilariño-Güell et al., 2011).

Gene	Locus	Protein	Pathology	Inheritance	Identification
SNCA	PARK1/4	alpha-Synuclein	early-onset PD	autosomal-dominant	Linkage analysis
Parkin	PARK2	Parkin	early-onset PD	autosomal-recessive	Linkage analysis
Unknown	PARK3		PD	autosomal-dominant	Linkage analysis
UCHL1	PARK5	Ubiquitin C-terminal hydroxylase	PD	autosomal-dominant	Candidate gene
PINK1	PARK6	PTEN-induced putative kinase 1	early-onset PD	autosomal-recessive	Linkage analysis
DJ-1	PARK7	DJ-1	early-onset PD	autosomal-recessive	Linkage analysis
LRRK2	PARK8	Leucine-rich repeat kinase 2	PD	autosomal-dominant	Linkage analysis
ATP13A2	PARK9	Lysosomal type 5 ATPase	atypical PD and others	autosomal-recessive	Linkage analysis
Unknown	PARK10		PD	Risk factor	Linkage analysis
Unknown	PARK11		Late-onset PD		Linkage analysis
Unknown	PARK12		PD	Risk factor	Linkage analysis
HTRA2	PARK13	HTRA serine peptidase 2	PD	autosomal-dominant or risk factor	Candidate gene
PLA2G6	PARK14	Phospholipase A2	Early-onset parkinsonism	autosomal-recessive	Linkage analysis
FBX07	PARK15	F-box only protein 7	Early-onset parkinsonism	autosomal-recessive	Linkage analysis
Unknown	PARK16		PD	Risk factor	GWAS
VPS35	PARK17	Vacuolar protein sorting 35	PD	autosomal-dominant	Exome sequencing
EIF4G1	PARK18	Eukaryotic translation initiating factor gamma 1	PD	autosomal-dominant	Linkage analysis

Table 1. 1 ***List of genes and proteins proposed to be associated with PD.***

PARK1 and PARK4 were initially assigned to separate loci but were later confirmed to both correspond to the same locus. Modified after Klein and Westenberger, 2012.

Genes associated with autosomal-recessive PD belong to the *Parkin* (PARK2), *PINK1* (PARK6), *DJ-1* (PARK7), *ATP13A2* (PARK9), *PLA2G6* (PARK14), and *FBXO7* (PARK15) loci.

Parkin was the first PD-related recessive locus discovered in a Japanese family and is responsible for a juvenile form of PD (Kitada et al., 1998). Overall, *Parkin* mutations account for about 50% of all known autosomal-recessive PD cases (Nuytemans et al., 2010).

- *PINK* and *DJ,* two other genes causing autosomal-recessive PD map to human chromosome 1. Mutations in *PINK1* are less frequent compared to *Parkin* mutations and mutations in *DJ-1* are generally quite rare (Nuytemans et al., 2010). The ubiquitous expressed and highly conserved protein DJ-1 has been suggested to play a role in the oxidative stress response (Bonifati, 2003), whereas the mitochondrial located PTEN-induced novel kinase 1 (PINK1) has suggested roles in cellular protection by phosphorylating mitochondrial proteins in response to cellular stress (Valente, 2004). Mutations in both genes are suggested to cause a loss-of-function (Nuytemans et al., 2010).
- *ATP13A2* mutations were first recorded in a Jordanian family in 2006. The transmembrane lysosomal type 5 P-type ATPase protein encoded by this gene is involved in Kufor-Rakeb syndrome that manifests as a neurodegenerative disorder characterised by early-onset PD symptoms with pyramidal tract degeneration and dementia (Ramirez et al., 2006).
- *PLA2G6* was identified by gene mapping and mutation analysis. Mutations in *PLA2G6* were first related to infantile neuro-axonal dystrophy (Khateeb et al., 2006) and have been subsequently identified in patients with early-onset, L-DOPA-responsive dystonia parkinsonism (Paisan-Ruiz et al., 2009).
- *FBX07* mutations were described in a Persian family (Shojaee et al., 2008) and later also in Italian and Dutch kindred (Di Fonzo et al., 2009). The early-onset disease pathology affects the extrapyramidal and pyramidal tracts.

Large genome-wide association studies (GWAS) or exome sequencing studies have been conducted in sporadic PD patients to identify new loci or single nucleotide polymorphisms (SNPs) which

increase PD risk. Two independent GWAS studies in a Japanese and European cohort, respectively, studied genetic risk factors for PD and both studies found a strong association of the *SNCA* (aSyn) and *MAPT* (tau) loci with PD (Satake et al., 2009; Simón-Sánchez et al., 2009). More recent large-scale meta-analyses have confirmed the associations of *SNCA* and *MAPT* as PD risk genes. In this context, another risk factors for the development of PD, beta-Glucocerebrosidase (*GBA*), was identified (Nalls et al., 2014; Pankratz et al., 2012). The latest GWAS study followed by a meta-analysis confirmed PD-related loci and further uncovered 17 novel and previously unreported risk loci which indicate a key role for autophagy and lysosomal pathways in PD (Chang et al., 2017). Another risk-related region was uncovered by Hamza et al. who found a genetic association in the human leukocyte antigen (HLA) region with PD (Hamza et al., 2010).

Non-genetic risk factors

Numerous epidemiological studies have tried to identify non-genetic risk factors but their identification is complicated by the underlying genetic predisposition of individuals. Variations in the prevalence of PD in different cultural backgrounds could result from differences in exposure to environmental factors (Van Den Eeden, 2003). By far greatest risk factor for the development of PD is age. Studies of non-human primates suggest that normal ageing underlies the same cellular mechanisms as the degeneration of DAn in PD. Cellular risk factors accumulate during normal ageing and accelerate or exaggerate in PD through a combination of genetic and environmental risk factors (Collier et al., 2011). The 'seven pillars' of the molecular and cellular changes that occur during ageing: proteostasis, adaptation to stress, inflammation, stem cells and regeneration, epigenetics, metabolism, and macromolecular damage, are also commonly involved in many neurodegenerative diseases (Kennedy et al., 2014). The 'multiple hit hypothesis' of PD proposes that a sequence of several events in the lifetime of an individual leads to the accumulation of toxic and genetic agents which accelerate the ageing-related loss of DAn that ultimately results in PD (Carvey et al., 2006; Sulzer, 2007). This hypothesis could explain the high clinical diversity observed in PD patients because the interplay of damaging insults might differ from individual to individual (Rodriguez et al., 2015). A similar 'multifactor hypothesis' has been proposed for healthy brain

ageing (Olson, 1987). In this context, Rodriguez et al. proposed that PD is the ultimate result of the slow neurodegenerative processes underlying normal ageing (Rodriguez et al., 2015).

The discovery of symptoms that closely resembled PD pathology in drug users after intravenous injection of drugs accidentally contaminated with 4-propyloxy-4-phenyl-N-methylpiperidine (MPTP) lead to the subsequent findings that MPTP can selectively damage DAn in the SNc (Davis et al., 1979; Langston et al., 1983). Since then, other epidemiological studies reported an association between exposure to pesticides or herbicides, heavy metal exposure, rural living/farming, and other environmental factors with the risk of PD. Since no general associations between these factors and PD could be found, it has been suggested that long-term exposure may be needed to contribute to the onset of PD (Lau and Breteler, 2006). The insecticide rotenone was found to cause degeneration of nigrostriatal DAn upon chronic exposure in rats and the accumulation of cytoplasmic, aSyn-positive inclusions (Betarbet et al., 2000). Similar, exposure to the herbicide paraquat was reported to cause the development of PD (Liou et al., 1997) and neurodegeneration of DAn with the accumulation of aSyn in mice (Manning-Bog et al., 2003). All three agents, MPTP, rotenone, and paraquat, act as selective inhibitors of Complex I of the mitochondrial electron transport chain and were shown to induce dopamine (DA) depletion in animal studies (Betarbet et al., 2000). In addition to pesticide exposure, it has also been hypothesised that chronic exposure to heavy metals such as aluminium, amalgam, copper, iron, lead, manganese, or zinc increases the risk of PD. These metals were thought to accumulate in the SNc and to act by increasing oxidative stress levels (Lai et al., 2002).

Smoking, caffeine consumption, and alcohol have all been studied in the context of PD (Checkoway et al., 2002). Cigarette smoking was inversely associated with PD in a meta-analysis for individual case-control studies (Hernán et al., 2002). A likely mechanism for the potential neuroprotective effect of cigarette smoke involves nicotine as a stimulant of DA release or as an antioxidant (Quik, 2004). Studies on caffeine consumptions suggest that caffeine intake may lower PD risk (Checkoway et al., 2002) and alleviate motor symptoms, as well as aid the management of non-motor symptoms

of PD (Prediger, 2010). For alcohol, there is limited epidemiologic evidence that it is correlated to PD (Checkoway et al., 2002).

1.1.5 Treatment options for Parkinson's disease

To date, treatment options for PD are focused on the amelioration of symptoms since no known agents can halt or reverse the neurodegenerative processes. Despite increasing awareness of the importance of non-motor symptoms, research on PD treatment options still mainly focuses on the nigrostriatal DAn pathway.

Introduced as a treatment for the motor symptoms of PD in the 1970s, the administration of L-DOPA, that replenishes DA levels in the striatum is still the most widely used treatment for PD (Fahn, 2015). However, long-term therapy of several years of L-DOPA treatment often results in the development of motor fluctuations, so called L-DOPA-induced dyskinesia (Ahlskog and Muenter, 2001). Other drugs are now often used in combination with L-DOPA to improve its effectiveness. Inhibitors of monoamine oxidase B, the enzyme that degrades DA, or inhibitors of catechol-O-methyltransferase, the enzyme that degrades L-DOPA, were successfully administered together with L-DOPA (Bonifácio et al., 2007; Riederer and Laux, 2011). Several DA agonists that selectively bind to DA receptors in the brain have similar effects to L-DOPA and are now used as a complementary therapy for individuals with L-DOPA-induced complications. Since DA agonists are less effective than L-DOPA at controlling PD symptoms and because dyskinesia is rare in younger PD patients, DA agonists are the preferred initial treatment for early-onset PD (Samii et al., 2004; Stocchi, 2009).

A promising alternative to the pharmacological treatment of PD is deep brain stimulation (DBS). DBS is carried out by inserting stimulating electrodes into brain areas such as the globus pallidus or sub-thalamic nucleus to transmit electrical pulses that disrupt the unbalanced neuronal activity that trigger PD motor symptoms (Kleiner-Fisman et al., 2006). Current therapies therefore pose a sympathetic relief. However, to develop targeted treatments and therapeutic intervention that can modify disease progression, a deeper understanding of the underlying molecular pathways is key.

Nowadays, it becomes more and more crucial to understand the molecular properties of a cell, its transcriptome and translatome. Classical drug discovery routes must be reconsidered. Research and Development efficiencies are declining despite increased investment and fewer drugs reach the market because many drug candidates fail in late-stage development due to safety issues or side-effects (Scannell et al., 2012). Today, thousands of genes associated with specific biological processes or involved in disease can be discovered while more than a decade ago, gene expression was understood as one gene at a time. Advanced understanding of gene expression underlying normal cellular processes and pathology are fundamental to aid the development of therapeutic strategies and for confirming their effectiveness. High-throughput, low-cost systems made it possible to apply gene expression profiling studies to basic research but also to the discovery of biomarkers, drug development, and clinical studies analysing human genome-scale variation (Heard et al., 2010). Changes in gene expression patterns reflect a sensitive measure of biological activity, processes, and changes. Knowledge gained with these studies can be used to identify mechanisms related to toxic insults or the action of novel compounds. Thus, gene expression data can even be used as a highly specific predictor of disease-related prognosis in addition to studying the molecular mechanisms underlying human disease (Dolginow, 2005). Such disease-related changes contributed to the ability to re-define diseases which in turn helped to influence clinical decisions and shape patient populations selected for clinical trials. Ultimately, this knowledge will help to target therapies to patients that are most likely to respond (Bates, 2011), to identify a wide range of novel drug-gable targets (Heard et al., 2010), and to re-purpose already approved drugs (Iorio et al., 2010; Pacini et al., 2013). The future of drug discovery will focus on reference collections of gene-expression profiles such as the "Connectivity Map" which pairs cultured human cells treated with bioactive small molecules with a software that uncovers functional connections among diseases, genetic perturbation, and drug action (Lamb et al., 2006) or programmes such as the web-based bioinformatics tool *DeSigN* which allows to search large public databases of differentially expressed gene signatures as starting points to associate these with drug response data (Lee et al., 2017).

1.2 Alpha-Synuclein

1.2.1 Introduction

A fragment of aSyn was first identified as a precursor to the non-amyloid-beta component (NAC) containing amyloid deposits in AD (Ueda et al., 1993), which was the human homologue of a protein originally found in the electric ray, *Torpedo californica* (Maroteaux et al., 1988). aSyn is further known as a protein implicated in the process of song learning found at pre-synaptic terminals in songbirds (George et al., 1995). Together with the two other closely related and highly evolutionary conserved beta- and gamma-Synuclein proteins (bSyn and gSyn, respectively), aSyn forms the Synuclein family (Lavedan, 1998). The aSyn sequence is highly-conserved across species but has only been described in vertebrates (George et al., 1995).

1.2.2 Alpha-Synuclein structure

The human aSyn protein is encoded by the *SNCA* gene on human chromosome 4 (4q21-q23) which spans a region of 111 kb (Campion et al., 1995; Chen et al., 1995) (Figure 1. 2 A). The *SNCA* gene comprises seven exons, five of which correspond to a coding region (George, 2002) containing the information for a 140-amino acid protein. The aSyn protein sequence can be divided into three regions with distinct structural characteristics (Figure 1. 2 B) (Beyer, 2006). The amphipathic N-terminal region is dominated by a series of 11 imperfect amino acid repeats including a consensus sequence, KTKEGV. These repeats form amphipathic alpha-helices under certain conditions and show similarities to the lipid-binding domains of apolipoproteins (Davidson et al., 1998). All known PD-related *SNCA* mutations (A30P, E46K, H50Q, G51D, and A53T/E) are located within the amphipathic domain. The central hydrophobic region includes the NAC region (Ueda et al., 1993) which associates with an increased propensity for aSyn aggregation (Giasson et al., 2001). The highly acidic C-terminal region contains mostly negatively charged amino acids and has no distinct structural tendency. While the N-terminal and NAC domain of aSyn are highly conserved, the length and amino acid composition of the C-terminus differs considerably between species (Recchia et al., 2004). Several post-transcriptional modifications have also been reported for aSyn. The most common phosphorylation site of aSyn lies at the Ser129 residue (Figure 1. 2 B) (Anderson et al.,

2006; Fujiwara et al., 2002). Other modifications include nitration (Giasson, 2000), ubiquitination (Hasegawa et al., 2002; Tofaris et al., 2001), and C-terminal truncations (Li et al., 2005; Oueslati et al., 2010).

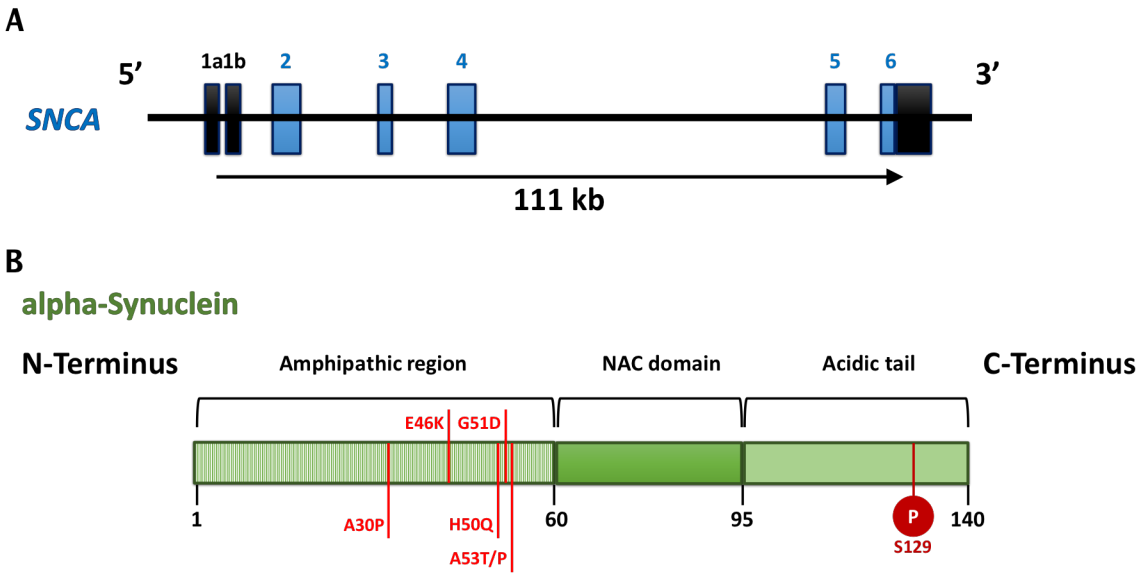


Figure 1. 2 ***Schematic representation of alpha-Synuclein***
(A) SNCA gene structure. (B) Protein domains. NAC= non-amyloid component. P= Phosphorylation site.

Based on its primary sequence, the predicted secondary structure of aSyn is considered natively unfolded (Weinreb et al., 1996). Upon binding to acidic phospholipid membranes, aSyn can adopt an alpha-helical structure (Davidson et al., 1998; Jo et al., 2000). Some studies show that aSyn proteins are present as disordered monomers within cells (Burré et al., 2013; Fauvet et al., 2012; Theillet et al., 2016). Recent data from Burré et al. suggested that aSyn exists in an equilibrium between monomeric free forms in the cytoplasm and multimeric membrane-bound proteins (Burré et al., 2013). The aSyn protein may underlie a great conformational flexibility to adopt different structures under specific conditions or interactions, which is influenced by several factors including oxidative stress (Hashimoto et al., 1999a), C-terminal truncations (Li et al., 2005), or fatty acid compositions (Sharon et al., 2003). On the other hand, a recent study by Bartels et al. showed that purified aSyn exists as a stable folded tetramer that is resistant to aggregation and fibril formation (Bartels et al., 2011). Nevertheless, these findings could not be replicated in other studies (Burré et al., 2013; Fauvet et al., 2012).

1.2.3 Alpha-Synuclein and Parkinson's disease

It is well established that aSyn has a prominent role in the underlying processes leading to PD. ASyn is considered a central link between familial and sporadic PD, since it plays a causative role in genetic PD and is pivotal in the identification of pathological hallmarks underlying both familial and idiopathic forms of the disease (Venda et al., 2010). The accumulation of misfolded aSyn in LBs found in DAn serves as a hallmark of PD pathology in both sporadic and familial cases (Baba et al., 1998; Spillantini et al., 1997). Elevated levels of aSyn have been shown to be prone to aggregation. The phosphorylation-site at the Ser129 residue increases the propensity of aSyn to aggregate *in vitro* (Anderson et al., 2006; Fujiwara et al., 2002) and phosphorylated aSyn proteins are often found in LBs (Fujiwara et al., 2002).

The *SNCA* gene was linked to autosomal dominant PD in 1996 in studies on a large Italian kindred with a familial history of early disease on-set (Polymeropoulos et al., 1996). Just one year later, a single base pair change in exon 4 of *SNCA* was found to cause the A53T mutation in a family of Greek origin and other unrelated individuals with familial PD (Polymeropoulos et al., 1997). Interestingly, human and mouse aSyn sequences share over 90% sequence identity apart from only very few amino acid differences such as the amino acid at position 53, which is alanine in humans and very few primates but threonine in mice and other vertebrates (Hamilton, 2004; Lavedan, 1998). In the following years, increasing evidence linked the aSyn locus to PD. In a family of German origin, the A30P mutation in aSyn exon 3 was causative of familial PD (Krüger et al., 1998). Another PD-relevant mutation (E46K) was described in a Spanish family (Zarranz et al., 2004). More recently, three novel mutations in *SNCA* have been reported. The H50Q substitution in exon 4 was reported in a female patient with L-DOPA responsive PD (Proukakis et al., 2013) and the G51D mutation was found in an exome sequencing approach of three PD patients who presented with early-onset pathology and death within a few years (Lesage et al., 2013). Their pathology involved not only the basal ganglia but extended to the pyramidal tract. Another single base exchange causes the A53E mutation with extensive aSyn-based pathology in both neurons and glia that was shown to cause PD but also MSA (Pasanen et al., 2014).

Multiplication of the aSyn locus with either duplication or triplication give rise to rare, familial forms of PD by causing an increase in aSyn expression levels (Chartier-Harlin et al., 2004; Ibáñez et al., 2004; Kara et al., 2014; Singleton et al., 2003). Since the degree of over-expression was found to correlate with the severity of the disease, a gene dosage-dependent effect of *SNCA* has been postulated. Individuals harbouring *SNCA* triplications have an earlier-onset with more severe and faster disease progression, such as rapid cognitive decline, severe non-motor symptoms, and widespread neurodegeneration compared to patients with *SNCA* locus duplication (Chartier-Harlin et al., 2004). So far, there are only few sporadic cases with aSyn multiplications (Ahn et al., 2008).

In the frontal cortex of PD patients, locus multiplications of the *SNCA* gene were directly correlated with an increase in aSyn mRNA levels and multiple copies lead to an increase in protein levels in whole blood samples (Miller et al., 2004). Elevated aSyn expression levels may also be caused by a genetic variability within the promoter and the 3' untranslated (UTR) region of *SNCA* (McCarthy et al., 2011; Miller et al., 2004). In a mouse study, a polymorphic microsatellite Rep1 in the promoter region located 10 kb upstream of the human *SNCA* transcription start site was shown to regulate *SNCA* expression by enhancing its transcription in the adult brain (Cronin et al., 2009). In this context, total aSyn mRNA levels were found to be increased in post-mortem midbrain tissue of sporadic patients compared to control (Chiba-Falek et al., 2006). The variability between patients was very high, which might explain contradictory results by others that showed a reduction of aSyn mRNA in surviving midbrain DAn (Dachsel et al., 2007; Kingsbury et al., 2004). Another confounding factor underlying the pathological processes in DAn is the massive cell loss accompanying PD progression.

1.2.4 Aggregation and prion-like properties of alpha-Synuclein

Under certain conditions, aSyn monomers can interact to form proto-fibrils/oligomers, which in turn can further aggregate to insoluble fibrils (Conway et al., 2000). It is not clear which molecular species of aSyn causes neurodegeneration. A widely-accepted hypothesis of aSyn toxicity proposes that oligomers are the cytotoxic species (Lashuel et al., 2012; Winner et al., 2011), whereas the

highly-aggregated fibrils of the protein could represent a protective mechanism in PD (Caughey and Lansbury, 2003). In support of this hypothesis, the aSyn oligomer-load is increased in the brains of patients with PD and DLB (Sharon et al., 2003; Tofaris et al., 2003). Additionally, aSyn-over-expressing cells (Outeiro et al., 2008) or mouse models have associated oligomers with increased neurotoxicity (Giasson et al., 2002; Kahle et al., 2001; Periquet et al., 2007). In flies, the aggregation of human aSyn resulted in PD-like pathology with age-dependent loss of DAn, locomotor deficits, and the formation of filamentous LBs-like inclusions (Feany and Bender, 2000). In *Caenorhabditis elegans,* the over-expression of aSyn similarly resulted in DAn cell loss and motor deficits (Lakso et al., 2004). It is possible that LBs could represent 'innocent bystanders' protecting the cells from toxic aSyn oligomers (Caughey and Lansbury, 2003). Recent work by Roberts et al. using a technique based on the Proximity Ligation Assay (PLA) gave insights into previously undetected PD pathology in only mildly affected brain regions such as the cingulate cortex or the medulla. Their PLA protocol allows to discriminate different molecular species of aSyn, including monomers, oligomers or fibrillary aggregates (Roberts et al., 2015).

Post-translational modification of aSyn or genetic mutations may modify its aggregation properties. C-terminal truncation of the aSyn protein caused accelerated aggregation *in vitro* (Crowther et al., 1998; Murray et al., 2003). Similarly, post-translational modifications such as oxidation, nitration and phosphorylation of the aSyn C-terminal region were shown to influence its propensity to aggregate *in vivo* (Giasson, 2000; Hashimoto et al., 1999a; Hashimoto et al., 1999b). The oligomerisation and aggregation of aSyn is also influenced by its mutations (Lázaro et al., 2014). Compared to the wild-type aSyn protein, E46K, A53T, and H50Q mutations were found to have an increased aggregation propensity (Ghosh et al., 2013; Ono et al., 2011; Rutherford et al., 2015), with A30P, A53E, and G51D being less prone to aggregate (Fares et al., 2014; Ono et al., 2011; Rutherford et al., 2015).

Increasing experimental evidence supports a prion-like propagation of aSyn by intercellular transfer from cell-to-cell seeding further aggregation. The Braak hypothesis already suggested a spread of aSyn pathology throughout the brain (Braak et al., 2003). Follow-up studies on PD patients after

more than 10 years with transplantations of foetal DAn grafts found LB-pathology in the grafted neurons (Kordower et al., 2008; Li et al., 2008), suggesting that aSyn pathology had spread from diseased neurons in the patients' brains to the grafted DAn. Others have shown that aSyn spreads across cells (Desplats et al., 2009) and seeds new aggregation of intracellular monomeric aSyn *in vitro* and *in vivo* (Luk et al., 2009; Luk et al., 2012a). Extracts of aggregated aSyn caused the development of lesions in the brain, motor dysfunction, and neurodegeneration after transmission from host cells to neurons grafted into the brain (Desplats et al., 2009; Hansen et al., 2011; Kordower et al., 2011). In a mouse model, it could be shown that the injection of brain lysates from human A53T transgenic mice in asymptomatic transgenic mice accelerated aggregation and disease pathology even at great distance from the injection sites (Luk et al., 2012b; Mougenot et al., 2012).

The pathology-spreading effects of diseased brain lysates could be replicated using recombinant aSyn fibrils (Volpicelli-Daley et al., 2011). These findings indicate that passive or active immunisation using aSyn could promote clearance of toxic aSyn species and reduce the intercellular transfer of aggregates. Immunisation with recombinant aSyn antibodies turned out to ameliorate aSyn-related synaptic pathology (Masliah et al., 2005), while treating the same transgenic mouse model with an antibody targeting the C-terminus of aSyn reduced behavioural deficits and axonal and synaptic pathology (Masliah et al., 2011). Thus, aSyn-induced immunisations might confer an effective mechanism-based therapy to reduce aSyn burden in synucleinopathies.

1.2.5 Cellular functions of alpha-Synuclein

To date, the precise cellular function of aSyn is still not fully understood. Several studies suggest a role at the synapse supported by its intracellular localisation and a variety of proposed protein-protein interactions; in particular, such interactions include cytoskeletal proteins such as tau (Giasson et al., 2003; Jensen et al., 1999) and beta-amyloid (Ono et al., 2012), as well as proteins involved in lipid metabolism such as the phospholipases D1 (Ahn et al., 2002).

Current knowledge of aSyn function has largely been gained through knock-out (KO) or over-expression studies using *in vitro* and *in vivo* systems (Surmeier, 2010). Research focusing on aSyn in

relation to DA synthesis, release, and re-uptake proposed a role in vesicle pool dynamics. Endogenous mouse aSyn KO suggested a cooperative but not necessarily essential function for aSyn in neurotransmitter release which was shown by alterations in synaptic DA handling (Abeliovich et al., 2000; Anwar et al., 2011). Other studies postulated a role for aSyn in the maintenance of these pools demonstrated *in vitro* and *in vivo* by changes to the vesicle pool dynamics in aSyn KO mice (Cabin et al., 2002; Murphy et al., 2000). In agreement, over-expression models of aSyn showed significantly inhibited synaptic DA release through impaired synaptic vesicle recycling caused by the reduction of readily releasable and recycling vesicle pools at the synapse (Nemani et al., 2010). This inhibitory role for aSyn in DA neurotransmission was supported by findings that demonstrated diminished vesicular release in response to over-expression of human aSyn mimicking protein changes seen in diseased human brains (Scott et al., 2010). The KO of chaperone cysteine string protein alpha (CSPa) in mice led to decreased levels of SNARE-complexes, degeneration of synaptic terminals, motor dysfunctions, and cell death (Chandra et al., 2005). In this context, increased expression of aSyn was shown to rescue this degenerative phenotype by restoring the levels of SNARE-complexes in the nerve terminals. Mice lacking both CSPa and aSyn exhibited severe synaptic dysfunctions and cell death suggesting that aSyn function can complement the molecular chaperone activity of CSPa that is needed for synaptic terminal integrity (Bonini and Giasson, 2005). Furthermore, Burré et al. could show that aSyn directly interacts with synaptobrevin-2/vesicle-associated membrane protein 2 at the synapse which is required for the maintenance of SNARE-complex assembly (Burre et al., 2010). More recently, the same group linked aSyn binding and multimerisation at cellular membranes to an aSyn-mediated chaperone function for SNARE proteins (Burré et al., 2014).

Another key aspect of aSyn functional properties is considered to be its involvement in DA homeostasis through the regulation of DA synthesis, storage, and re-uptake at the synapse. The enzyme tyrosine hydroxylase (TH) catalysis the rate-limiting step of the DA synthesis pathway which converts tyrosine into the DA precursor L-3,4-dihydroxyphenylalanine, L-DOPA. Aromatic L-amino acid decarboxylase (AADC) enzyme subsequently converts L-DOPA to DA. Cell culture studies

implicated aSyn over-expression in reduced activity of the TH promoter (Gao et al., 2007), decreased TH mRNA and protein levels (Baptista et al., 2003; Yu et al., 2004), and sequence homologies of aSyn to the TH-interacting chaperone molecule 14-3-3 suggested an aSyn-dependent interaction with TH. Indeed, binding to aSyn influences TH activity by stabilising its un-phosphorylated, inactive form (Perez et al., 2002). In contrast, suppression of aSyn in culture increased phosphorylation of TH resulting in increased activity (Liu et al., 2008). aSyn also binds to DAT in cell culture and the rat brain leading to a diminished uptake velocity of DA by DAT which is dependent on aSyn expression levels (Wersinger and Sidhu, 2003; Wersinger et al., 2003; Wersinger et al., 2004).

Pathologically, aSyn has been involved in several pathways related to neurodegenerative diseases, whereby aSyn dysfunction likely tips DAn over the edge. The potential issue of impaired protein degradation in the context of aberrant aSyn expression has attracted a lot of attention. Ubiquitin-dependent proteasomal degradation was shown to be decreased by aggregated forms of aSyn *in vitro* (Snyder et al., 2003) or mutant aSyn (Tanaka et al., 2001). Degradation via chaperone-mediated autophagy was also impaired in cells or transgenic mice over-expressing aSyn (Winslow et al., 2010) and was significantly reduced in post-mortem PD and AD brains (Alvarez-Erviti et al., 2010).

Other cellular compartments such as the endoplasmatic reticulum (ER) and the Golgi apparatus are also affected by aSyn. Mutant A53T cells exhibited cell death associated with decreased proteasome activity and increased intracellular levels of reactive oxygen species (ROS). In these cells, mitochondrial dysfunction was accompanied by ER stress mimicking aSyn cellular toxicity in PD patients (Smith et al., 2005).

Mitochondrial function and dysfunction have great pathological relevance in PD and the involvement of aSyn has been greatly explored. Electron microscopy in brains of PD patients showed the presence of αSyn in the mitochondrial matrix which is based on a cryptic mitochondrial targeting signal in the N-terminal region of aSyn (Devi et al., 2008). Other studies support the

localisation of aSyn in mitochondria/mitochondrial membrane often in association with increased oxidative stress (Nakamura et al., 2011; Parihar et al., 2008; Shavali et al., 2008). More recently, a study postulated that aSyn localises to the mitochondria-associated ER membrane, a structurally and functionally distinct subdomain of the ER, rather than to mitochondria themselves (Guardia-Laguarta et al., 2014). This association is reduced in mutant aSyn, thus, the intracellular localisation of aSyn could play a key role in pathological mechanisms underlying early PD pathogenesis (Guardia-Laguarta et al., 2015). In cultured cells, increased levels of aSyn but not bSyn or gSyn induced robust mitochondrial fragmentation in the absence of overt cell death or any visible morphologic changes on other organelles (Nakamura et al., 2011). Furthermore, aSyn was also shown to influence mitochondrial fusion/fission dynamics (Kamp et al., 2010). An A53T over-expressing transgenic mouse model of PD showed mitochondrial Complex I impairments in association with aSyn oligomers that associated with the mitochondrial membrane (Chinta et al., 2010). Complex I activity is significantly reduced in DAn in the SNc of PD patient brains (Janetzky et al., 1994; Schapira et al., 1990). Toxins that inhibit mitochondrial function were shown to increase oxidative stress by the generation of ROS and reduce the production of ATP in animals and cell models (Bates et al., 1994; Fountaine et al., 2008). Interestingly, aSyn knock-down was protective towards MPP+ toxicity, probably due to reduced DAT protein at the cell surface and the activation of protective cellular pathways (Fountaine et al., 2008). While aSyn KO mice were more resistant to MPTP-induced cellular toxicity (Dauer et al., 2002; Klivenyi et al., 2006), this vulnerability is completely restored upon over-expression of human wild-type or mutant A53T aSyn in mouse aSyn KO mice (Thomas et al., 2011). In addition to aSyn, the two familial recessive PD genes, Parkin and PINK1, were shown to be involved in mitochondrial homeostasis under both physiological and pathological conditions (Geisler et al., 2010; Poole et al., 2008). Figure 1. 3 summarises the functions of aSyn in neurons.

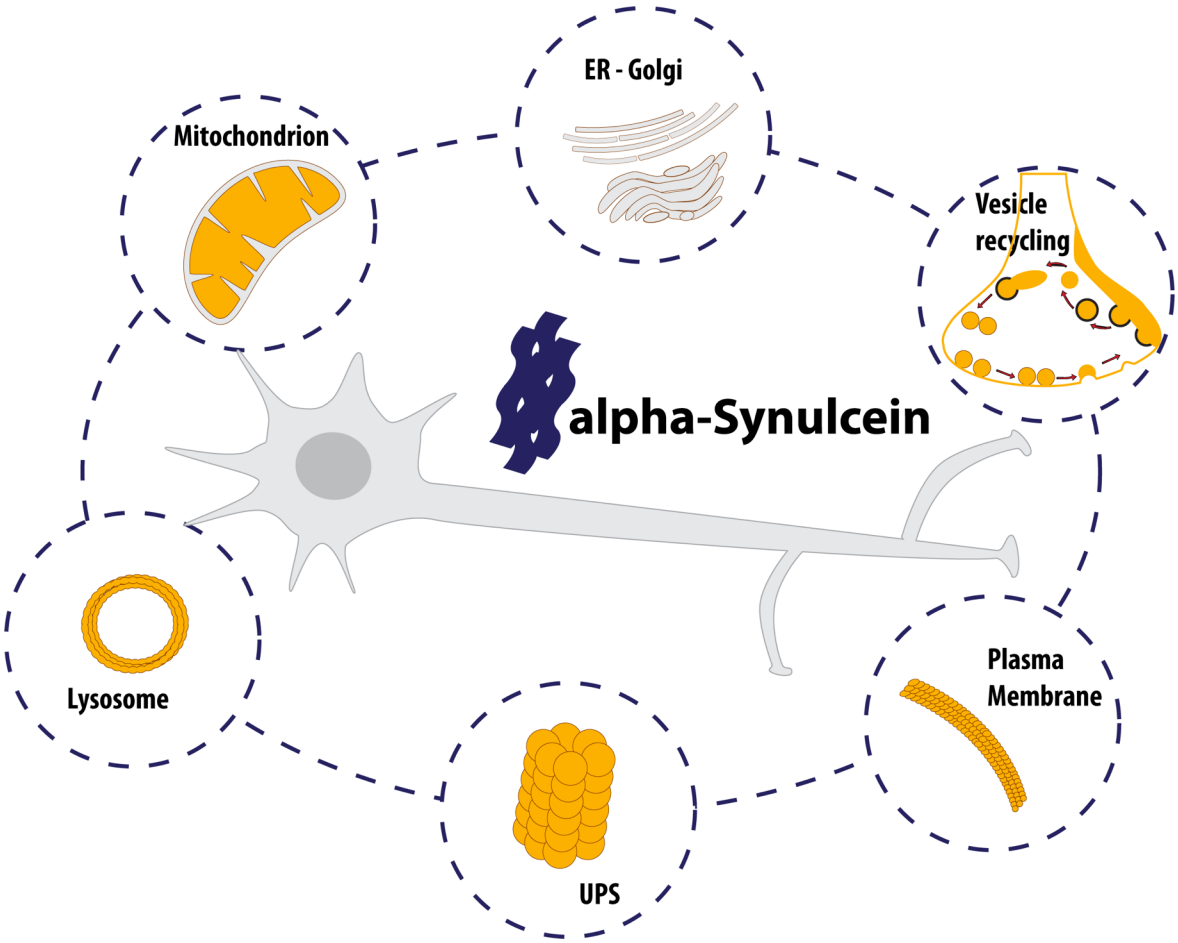


Figure 1. 3 ***Summary of the myriad functions of Alpha-Synuclein in neurons.***
Highlighted in this figure are six different intracellular pathways affected by Alpha-Synuclein (aSyn). Synaptic vesicles: aSyn protein is enriched at pre-synaptic neuron terminals and modulates synaptic function by participating in vesicle recycling. Membranes: aSyn strongly interacts with membranes, such as plasma membrane or the mitochondrial membranes. Ubiquitin-proteasome system (UPS) and lysosomes: aSyn can be degraded by the UPS and inside lysosomes. Misfolded aSyn protein is prone to aggregation forming toxic oligomeric structures that are believed to impair basic neuronal processes: impairment of ER-Golgi trafficking, inhibition of vesicle docking, membrane permeabilisation, impairment of lysosome and UPS function, alteration of mitochondrial physiology and morphology, dysregulation of calcium and cation homeostasis. Summary based on Dehay et al. Lancet Neurol. (2015).

1.3 Alpha-Synuclein transgenic mouse models of Parkinson's disease

Many genetic animal models make use of small cDNA constructs to drive transgene expression from strong heterologous promoters which often fail to recapitulate physiologically-relevant temporal changes in transgene levels and expression patterns (Fernagut and Chesselet, 2004). While these models have been useful to study isolated aspects of PD, they exhibit several limitations. Over the years, a range of different heterologous promoters have been used, including the prion (Giasson et al., 2002; Gispert et al., 2003; Lee et al., 2002), PDGF-β (Masliah et al., 2000), Thy-1 (Neumann et al., 2002), and rat TH (Richfield et al., 2002) promoters. Reduced specificity exhibited by of some of these promoters include the failure of aSyn expression in non-DAn circuits or strong ectopic transgene expression in cell-types not characteristically affected by PD (Fernagut and Chesselet, 2004).

Numerous transgenic mouse models which are over-expressing human WT, A53T, or A30P mutant aSyn were shown to have PD-like phenotypes (Visanji et al., 2016). The pathology correlates with increased expression levels which strongly supports a toxic gain-of-function mechanism for aSyn. Pathogenesis associated with aSyn aggregation is accelerated by PD-linked mutations or locus multiplications (Ibáñez et al., 2004; Miller et al., 2004; Singleton et al., 2003) and involves mitochondrial dysfunction, oxidative stress, and the activation of cell death pathways. Mice over-expressing aSyn by viral injections developed neurodegeneration-related symptoms such as cell loss, loss of striatal DA, and motor dysfunctions (Kirik et al., 2002) and aSyn bacterial artificial chromosomes (BACs) transgenic mouse models that over-express WT or mutant aSyn showed aSyn-related pathology with motor dysfunctions linked to loss of DAn at an advanced age (Hansen et al., 2013; Janezic et al., 2013; Kuo et al., 2010; Taylor et al., 2014). In addition, early non-motor symptoms of PD could be noted in some of the transgenic lines including gastrointestinal function (Hallett et al., 2012; Janezic et al., 2013; Noorian et al., 2012; Wang et al., 2008), olfaction (Fleming et al., 2008; Kim et al., 2011; Zhang et al., 2015), and disturbed sleep behaviour (McDowell et al., 2014; Rothman et al., 2013).

Larger DNA vectors such as BACs are capable of holding entire genomic loci (Shizuya and Kouros-Mehr, 2001; Shizuya et al., 1992), including native promoters flanked by endogenous regulatory elements. BACs have significant advantages for the generation of physiologically-relevant disease models (Heintz, 2001). BAC vectors faithfully reproduce endogenous transgene expression profiles in the correct spatio-temporal manner (Heintz, 2001). Indeed, the Gene Expression Nervous System Atlas (GENSAT) project has characterised a large number of BACs driving expression in specific CNS cell-types (Gong et al., 2003). To date, some aSyn BAC transgenic mouse models of PD have been generated (Janezic et al., 2013; Hansen et al., 2011; Kuo et al., 2010; Taylor et al., 2014; Yamakado et al., 2012) which recapitulate several disease-related phenotypes not limited to dopaminergic neuronal circuits. For example, Taylor et al. described a novel transgenic mouse line that expresses the A30P mutant form of human aSyn on a mouse aSyn KO background. They identified a deficit in evoked DA release only in the caudate putamen reflecting region-specific changes seen in PD (Taylor et al., 2014; Sawamoto et al., 2008). Nevertheless, A30P aSyn mice did not lose DAn, showed no LB-like aggregations, or any overt behavioural impairments (Taylor et al., 2014). Others found gastrointestinal impairments accompanied by aSyn immune-reactive aggregates in the enteric nervous system in A53T or A30P human mutant aSyn transgenic mice (Kuo et al., 2010). The Wade-Martins laboratory developed BAC transgenic mouse model over-expression aSyn from the human *SNCA* locus on a mouse aSyn KO background in the correct spatio-temporal manner (Janezic et al., 2013). The 2x aSyn expression in this model is mirroring the levels observed in PD patients with aSyn locus multiplications (Chartier-Harlin et al., 2004; Singleton et al., 2003). Consequently, the expression of developmentally regulated aSyn transgene in a BAC replicates the proteins expression patterns in a physiological manner which may represent an improved way of modelling the impact of genetic alterations in PD.

Another method that has been used to overcome pitfalls of cDNA based constructs or endogenous promoters were viral vector mediated expression of aSyn by injection of the virus directly into the area of interest. Both rodents and primates successfully reproduced the loss of DAn in the and even showed aSyn positive inclusions in some cases (Burre et al., 2015; Decressac et al., 2012; Kirik et al.,

2002; Kirik et al., 2003; Lo Bianco et al., 2002). The presence of endogenous aSyn protein might represent a confounding factor to investigate the molecular effects of human aSyn over-expression. Thus, choosing an endogenous aSyn KO background is essential in eliminating any confounding effects based on the presence of endogenous aSyn.

1.3.1 Alpha-Synuclein knock-out models

In a line of Harlan mice, a spontaneous genomic deletion included the entire *SNCA* locus (Specht and Schoepfer, 2001). These animals showed no overt phenotype which may suggest that the constitutive KO of *SNCA* allows for the initiation of a functional compensation mechanism during nervous system development, for example by b- or gSyn or an unrelated mechanism. The first targeted aSyn KO model was viable, with normal brain architecture but showed a decrease in striatal DA levels and altered activity-dependent regulation of DA neurotransmission (Abeliovich et al., 2000). Another aSyn KO model established by Cabin et al. showed an impaired ability to restore the synaptic vesicle pool in hippocampal neurons which was due to fewer vesicles in the reserve pool and an overall decrease in presynaptic vesicles (Cabin et al., 2002). ASyn KO mice treated with the neurotoxin MPTP showed a striking resistance to the toxin (Dauer et al., 2002) or rotenone (Zharikov et al., 2015) which was replicated by numerous other studies (Robertson et al., 2004; Schlüter et al., 2003). Surprisingly, mice lacking two members of the Synuclein family individually or in combinations display only a mild synaptic impact without neurodegeneration (Chandra et al., 2004; Senior et al., 2008). The lack of all three Synuclein in a/b/gSyn KO mice is characterised by synaptic alterations (Anwar et al., 2011; Greten-Harrison et al., 2010) which could be associated to SNARE-complex assembly deficits (Burre et al., 2010). Recently, the KO of every possible combination of members of the Synuclein family was systematically analysed by Connor-Robson et al. (Connor-Robson et al., 2016). Their study revealed specific functions for each of the Synucleins despite noticeable overall functional redundancy. Thus, knocking out a Synuclein gene might lead to some compensatory effects but the remaining Synucleins cannot fully compensate for the deficiency of a lost family member.

1.4 Translating Ribosome Affinity Purification (TRAP)

Recent advances in gene expression profiling using microarray or RNA sequencing (RNA-Seq) made it possible to simultaneously analyse RNA expression profiles of all genes in a genome (Wang et al., 2009). Profiling studies on the mammalian brain have been complicated by the high level of cellular heterogeneity and the close anatomical location of diverse cell-types within this complex tissue. Gene expression profiles derived from whole tissue may contain averaged information across different cell-types complicating the analysis of non-directional changes and changes specific to defined cell populations.

1.4.1 TRAP methodology

The Translating Ribosome Affinity Purification (TRAP) methodology relies on the distinct isolation of mRNAs attached to translating ribosomes (polysomes) of any genetically defined cell population by immunoaffinity purifications to achieve cell-type specific gene expression analysis (Heiman et al., 2008). The N-terminus of the large ribosomal subunit protein L10a (RPL10a) is tagged with an enhanced green fluorescent protein (eGFP) under the control of the regulatory sequences of a gene of interest. Thus, the eGFP-L10a fusion protein is expressed in genetically defined cell populations and eGFP-tagged ribosomes and their associated mRNAs can be isolated using anti-GFP antibodies (Heiman et al., 2008). TRAP methodology combines the purification of polysomes with downstream analysis of transgene expression, hence, the specific targeting of translated mRNAs using TRAP rather than total RNA serves as a better reflection of protein expression (Emery and Barres, 2008).

The idea for the TRAP methodology is based on a gene profiling strategy called ‘mRNA-tagging’ developed in *Caenorhabditis elegans* (Roy et al., 2002). First TRAP gene expression profiling experiments relied on the use of transgenic mice which had been established in the context of the GENSAT project (Gong et al., 2003). The GENSAT database comprises many BAC transgenic lines in which genes of interest were replaced by eGFP expression under the control of endogenous promoter sequences to allow the identification of spatial expression profiles in the brain (Gong et al., 2003). The expression of the eGFP-L10a fusion protein in a BAC vector under the control of cell-

type specific promoters led to the establishment of a variety of bacTRAP transgenic mouse lines (Doyle et al., 2008). While the originally published TRAP methodology required the generation of separate BAC transgenic lines for each cell-type of interest (Doyle et al., 2008; Heiman et al., 2008), recent conditional TRAP mouse lines circumvent these early limitations (Hupe et al., 2014; Zhou et al., 2013). To date, cell-type-specific gene expression profiling using TRAP has been achieved in plants (Mustroph et al., 2009), flies (Thomas et al., 2012), frogs (Watson et al., 2012), fish (Tryon et al., 2013), and worms (Gracida and Calarco, 2017).

Important steps for the successful purification of translating ribosomes using the TRAP protocol (Heiman et al., 2014) include the immediate homogenisation of target tissue in the presence of the eukaryotic protein synthesis inhibitor cycloheximide (CHX) which stops elongation and stabilises translating ribosomes on the mRNA (Obrig et al., 1971). The inhibition of translation by CHX is key as it provides a snap-shot of the translational status of the targeted cell populations and it further overcomes the need for chemical fixation, one of the obstacles of other cell isolation techniques. Subsequent centrifugation steps clear the homogenate of larger organelles and cell debris. Ribosomes are captured using an 'Affinity matrix' (magnetic beads coupled with a GFP antibody mix) in an overnight immunoprecipitation (IP) reaction (Heiman et al., 2014) (Figure 1. 4).

The affinity matrix components can be adjusted to the needs of the respective model used for TRAP to enhance isolation efficiency while simultaneously reducing background RNA binding. A variety of factors such as the number of cells expressing the TRAP transgene, its expression level, background RNA binding levels of the respective tissue but also more general factors, including cell-type, target cell-type abundance, translational state, and size all influence TRAP efficiency and RNA yields (Heiman et al., 2014). TRAP-isolated high-purity RNA can be directly used for various downstream applications, including quantitative real-time PCR (qPCR), microarray analysis or RNA sequencing (RNA-Seq). Ease and speed of mRNA purifications using TRAP enable paralleled analysis of different experimental and control genotypes or different experimental treatment groups (Emery and Barres, 2008).

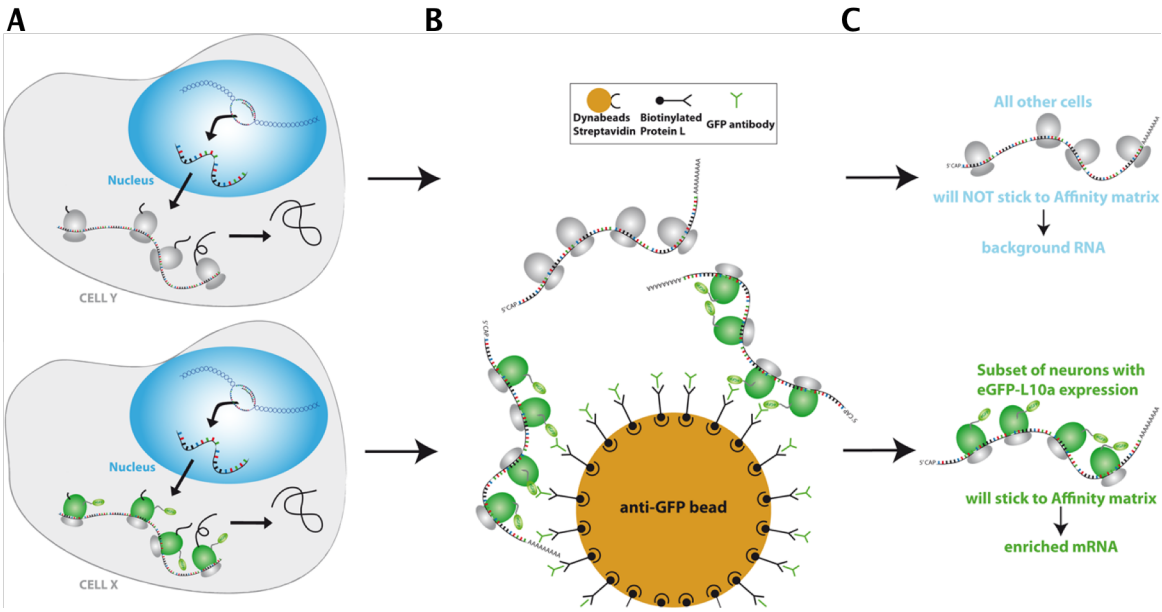


Figure 1. 4 ***Translating Ribosome Affinity Purification (TRAP).***

(A) Large ribosomal subunit protein RPL10a has been targeted with appropriate genetic elements to express the eGFP-L10a transgene in cell-type of interest. Only translating polyribosomes (polysomes) originating from targeted cells (Cell X) have an eGFP-tag on their ribosomes, whereas these originating from non-targeted cells (Cell Y) do not have an eGFP tag on their ribosomes. (B) anti-GFP beads ('Affinity matrix') were constructed using magnetic Strepavidin Dynabeads, a biotinylated Protein L-linker and anti-GFP antibodies. These anti-GFP beads capture eGFP-tagged ribosomes and actively translated mRNAs from cells of interest. Non-tagged ribosomes with attached mRNAs (and non-translated RNAs) do not bind to the beads. (C) During immunoprecipitation, mRNA from the subset of neurons with eGFP-L10a expression will stick to the Affinity matrix while background RNA and non-translated RNA does not bind the anti-GFP beads. blue= unbound (UB) RNA fraction. green = bound or immunoprecipitated (IP) RNA fraction.

1.4.2 Advantages and disadvantages of TRAP compared to other RNA isolation methods

High-resolution analysis at the cellular level can already be achieved with existing techniques, including *in situ* hybridisation (ISH) and immunohistochemistry (IHC), but these methods cannot be applied on a genome-wide scale (Emery and Barres, 2008). Other molecular profiling methods to study genome-wide expression profiles, such as manual sorting of (fluorescent) cells, laser-capture micro-dissection (LCM), or fluorescence-activated cell sorting (FACS), also face several challenges.

High levels of cellular heterogeneity and close anatomical proximity of diverse cell populations especially in the CNS complicate tissue dissections. While LCM is the most accurate method of tissue dissection by using morphological and locational clues to identify the cell-type of interest (Emmert-Buck et al., 1996), it is a laborious technique that provides only very low amount of tissue material. FACS is highly efficient but it requires complex equipment and relies on the fixation and dissociation of tissue before the sorting process (Meyer et al., 1980). RNA purification from fixed

tissue is technically challenging and isolation and fixation of cells may introduce stresses or lead to the loss of tissue-intrinsic signals which could ultimately introduce analytical artefacts (Emery and Barres, 2008; Heiman et al., 2014). Furthermore, FACS of neurons has long been limited to the use of cultured cells or embryonic brain tissue because mature neurons are highly fragile, with long and branched axons and dendrites, and shearing forces applied during the cell sorting process complicate successful applications (Guez-Barber et al., 2012; Saxena et al., 2012). Advances in sorting of adult neurons has been shown for GFP-expressing transgenic mice (Lobo et al., 2006) and only recently the requirement of transgenic animals could be overcome in a FACS study on adult rat brains (Guez-Barber et al., 2012). It is particularly advantageous that TRAP is compatible with the use of adult brain tissue allowing the study of neurodegenerative diseases. TRAP also enables the profiling of the mRNA distributed throughout the entire cell, including long axonal and dendritic protrusions, that might be lost by other cell isolation techniques (Heiman et al., 2008). Furthermore, rare as well as abundant cell-types can be isolated using TRAP (Emery and Barres, 2008). Overall, TRAP bypasses the need for tissue fixation or dissociation of cells, and thus, reduces experimental noise and the introduction of artefacts due to lengthy sorting procedures. Moreover, cell-types of interest can be directly visualised in IHC or electrophysiological studies due to the introduction of a GFP-tag with the TRAP transgene (Heiman et al., 2014).

With the TRAP methodology, translated mRNAs rather than total RNAs are targeted which is possibly a better reflection of protein expression. The identification of mRNAs that are under strong translational control is further enabled through the comparison of total with translated mRNA profiles (Emery and Barres, 2008). Nevertheless, possible pitfalls of the TRAP method include the co-isolation of some translationally inhibited mRNAs that remain bound to the ribosome or the loss of never translated, non-coding RNAs which could be detected by standard gene profiling methods (Emery and Barres, 2008). Another disadvantage of TRAP is the requirement of a genetic element to drive cell-type-specific expression of eGFP-L10a (Okaty et al., 2011). Despite their great popularity, bacTRAP mice may have underlying changes in TRAP efficiency due to fluctuations in endogenous promoter activity over time, hence, affecting eGFP-L10a expression simultaneously.

Furthermore, the BAC transgenic animals are generated by the non-specific integration of the transgene into the target genome. This integration can lead to the insertion of a variable number of copies, as well as the insertion of the transgene into an unknown locus in the target genome (Beil et al., 2012). The random integration or mislocalisation can lead to problems if important genes are destroyed, especially, if the BAC transgenic animal is bred to homozygosity. The use of conditional TRAP mouse lines (Hupe et al., 2014; Zhou et al., 2013) and recent viral-mediated TRAP approaches (Ekstrand et al., 2014; Nectow et al., 2015) have greatly improved its applicability. Whenever genetic modifications are not possible, including studies on human brain tissue, other methods such as LCM may be preferable despite being less sensitive (Okaty et al., 2011).

A key challenge in all gene expression profiling studies is background RNA contamination. The expression of eGFP-L10a from exogenous alleles must compete with endogenous RPL10a for ribosome occupancy, thus, extra-ribosomal presence of eGFP-L10a could reduce the efficiency of ribosome-tagging and subsequent TRAP isolations (Okaty et al., 2011). Furthermore, non-specific binding of mRNAs to the IP antibodies cannot be eliminated completely but the use of a TRAP-negative control animal can serve as a marker for non-specific binding (Shigeoka et al., 2016).

1.4.3 Transgenic mouse models for TRAP

Gene expression profiling serves as a useful strategy to study cells during development and disease but its success is greatly depended on the successful isolation of RNA from specific cell-types or distinct cellular compartments. Widespread application of TRAP has been limited by availability of bacTRAP transgenic mouse lines but recently developed inducible TRAP models make this approach more widely accessible.

Cre recombinase-mediated cell-type specificity for gene expression profiling

Many current mouse models make use of the Cre-Lox (or FLP-FRT) recombination systems to closely regulate location and timing of gene expression. The Cre-Lox system is based on site-specific DNA recombination initiated by the Cre-recombinase enzyme (Cre) that catalases the recombination of short target ‘LoxP’ sequences originally derived from bacteriophage P1 (Sauer and Henderson,

1988; Sternberg and Hamilton, 1981). Targeted DNA modifications, such as deletions, insertions, translocations, or inversion of specific genes in cell-types of interest are enabled by widely available transgenic Cre driver lines that express the Cre recombinase transgene under a tissue-specific promoter. The Cre driver can be crossed with any transgenic animal for which the genomic locus of interest is flanked by two *LoxP* sequences ('floxed') (Nagy et al., 2009; Orban et al., 1992). While Cre/LoxP recombination controls time and cell-type specific transgene expression, there is no way of silencing the transgene once it has been induced or rescuing a gene once it has been excised. Cre expression independent of endogenous gene regulatory elements, for example only during certain developmental stages, can be achieved with inducible gene expression systems such as doxycycline, tamoxifen, or RU-486 (Brocard et al., 1998; Kellendonk et al., 1999; Utomo et al., 1999). Similarly, FLP-FRT mediated site-specific recombination involves a DNA recombinase, flippase (FLP) derived from baker's yeast *Saccharomyces cerevisiae* (Sadowski, 1995) and a pair of FLP recombinase target (FRT) sequences that flank the genomic locus of interest. Both systems can be used combined in the germline of adult mice (Meyers et al., 1998).

In 2009, Sanz et al developed a 'RiboTagging' approach to analyse cell-type specific translatomes similar to TRAP (Sanz et al., 2009). Here, the floxed final exon of ribosomal protein L22 is replaced by three hemagglutinin (HA) epitopes upon Cre recombinase activation in the cell-type of interest. These epitope-tagged actively translating polyribosomes in genetically modified 'RiboTag' mice can be immunoaffinity-purified using HA antibodies (Sanz et al., 2009). In 2013, the first conditional TRAP mice developed at the Rockefeller University relied on the introduction of a 'floxed' eGFP-L10a cassette into the first intron of the eukaryotic translation elongation factor 1 alpha 1 (Eef1a1) (Stanley et al., 2013). The strong Eef1a1 promoter made this TRAP line particularly useful for the detection and profiling of lowly expressed genes such as glucose-sensing neurons using a neuronal/endocrine-specific glucokinase Cre driver (Stanley et al., 2013).

Targeting the ROSA26 locus to create a Cre conditional mouse model for TRAP

In the 1990s, the ROSAβgeo26 (or Gt(ROSA)26Sor; ROSA26) locus was discovered in gene-trap experiment using the retroviral ROSAβgeo vector to infect ES cells (Friedrich and Soriano, 1991).

ROSA26 is located on mouse chromosome 6, consists of three exons, and spans around 9 kb generating three polyadenylated RNAs with unknown function (Casola, 2010). Targeting the ROSA26 locus by homologous recombination to insert transgenes into mouse ES cells resulted in stable, frequent, and correctly targeted events achieving expression of single transgene copies (Soriano, 1999; Zambrowicz et al., 1997). Expression of transgenes in the ROSA26 locus can either be constitutively activated using the Cre/LoxP recombination system (Soriano, 1999), or temporally controlled and in a cell-type specific manner using the tetracycline (tet)-on/off system (Bäckman et al., 2009).

Conditional TRAP models enable polyribosome-tagging with subsequent affinity purification by activating floxed eGFP-L10a within the ROSA26 locus in all Cre expressing cells. Two recent TRAP studies reported a conditional TRAP model in which eGFP-L10a under the control of a strong synthetic cytomegalovirus (CMV) early enhancer element/chicken beta-actin/rabbit beta-globin (CAG) hybrid promoter was specifically and constitutively activated in Cre-expressing tissues (Hupe et al., 2014; Liu et al., 2014). This novel approach, different to previous TRAP studies, was based on the identification of transcripts on the fold-enrichment between cell-type specific translated mRNA and total RNA isolated from the input tissue or organ (Doyle et al., 2008; Heiman et al., 2008; Hupe et al., 2014). Zhou et al. developed a conditional TRAP mouse model (‘fs-TRAP’) that allowed combined Cre and FRT-mediated recombination (Zhou et al., 2013). The TRAP construct within the ROSA26 locus contained a CAG driven frt-flanked eGFP-L10a fusion protein controlled by a LoxP-flanked neo cassette but also a hemagglutinin-tagged bacterial biotin ligase (birA). A single recombination event using Cre activates eGFP-L10a expression. On the other hand, a double recombination event using FLP removes the frt-flanked eGFP-L10a and subsequent Cre-mediated recombination constitutively activates birA by removing the floxed-neo cassette (Zhou et al., 2013). Cell-type specific gene expression profiling in endothelial cells, cardiomyocytes, or melanin-concentrating hormone neurons assured the wide-range versatility of the fs-TRAP’ line (Zhou et al., 2013).

Control of both spatial and temporal eGFP-L10a expression is the major advantage of the tet-on/off method which is mediated through cell-type specific expression of the tetracycline-controlled trans-activator protein (tTA) or inhibition of expression through the administration of tetracycline/doxycycline, respectively. In a 'tetO-TRAP' mouse line, eGFP-L10a is controlled by a tetracycline-responsive regulatory element (tetracycline operator= tetO) and expression can be regulated with tetracycline or its analogue doxycycline (dox) when this line is crossed to a strain expressing tTA (Ainsley et al., 2014; Drane et al., 2014)

Simultaneous profiling of the translatome and epigenome from defined cell-types

The integrated analysis of data gained by combined profiling of the translatome and epigenome can help to gain valuable insight into cellular identity, physiology, and pathophysiology. Cell-type specific gene expression and chromatin profiling analysis was enabled by a technology termed INTACT (isolation of nuclei tagged in specific cell-types), a transgenic nuclei-tagging strategy which circumvents the need to dissociate or mechanically separate cells (Deal and Henikoff, 2010). A nuclear targeting fusion protein consisting of a RAN GTPase activating protein 1 (RanGAP1) for nuclear envelope association, GFP for visualisation, and a biotin ligase recognition peptide, enables the affinity purification of the biotinylated nuclei. Initially established in plants, INTACT has been utilised to characterise the epigenomes in worms, flies, and mice (Amin et al., 2014; Deal and Henikoff, 2010; Henry et al., 2012; Steiner et al., 2012).

While the 'fs-TRAP' model described by Zhou et al. is suitable to isolate tagged-nuclei in addition to mRNAs as described above, it requires a Cre driver and an additional Flp driver line (Zhou et al., 2013). In contrast, 'H2B-TRAP' mice developed by Long et al. enable isolation of nuclear material in combination with translating mRNA in polysome complexes by expressing a mCherry-tagged human histone 1 H2bj and eGFP-L10a fusion protein separated by a self-cleaving viral 2A peptide under control the CAG promoter (Long et al., 2014). Adipocyte-specific Cre-mediated recombination labelled the nucleus and ribosomes in the cytoplasm with mCherry-H2B and eGFP-L10a, respectively (Long et al., 2014), but since the mice failed to model the desired adipocyte-related phenotype an improved model was developed (Roh et al., 2017). Optimised 'NuTRAP'

(nuclear-tagging and translating ribosome affinity purification) mice combine TRAP-based ribosome-tagging with the INTACT-based nuclear-tagging strategy by substituting mCherry-H2B for BirA-RanGAP1. They provide a powerful *in vivo* tool for studies on simultaneous isolation of mRNA (translatome) and nuclei (epigenome) from specific cell-types (Roh et al., 2017).

Viral-mediated translating ribosome affinity purifications

Traditionally, classification of neuronal cell populations was based on criteria such as morphology and location, electrophysiological properties, and the expression of marker genes. Neural circuits could be mapped in high-resolution using classical microscopy-based neuroanatomical methods but connectivity-mediated molecular profiling of neurons was not possible until very recently. While TRAP can provide detailed information about neuronal cell identity, it fails to provide information about interconnected neurons in complex connectivity circuits.

To solve problems posed by complexity and cellular heterogeneity of neural circuits, the Friedman laboratory developed a 'Retro-TRAP' methodology which combined transgenic and viral approaches with TRAP (Ekstrand et al., 2014; Nectow et al., 2015). High-throughput molecular profiling of projection neurons was achieved by a two-component system (GFP plus anti-GFP camelid nanobody-tagged RPL10A) that enabled ribosomes to bind GFP for projection-specific affinity purifications (Ekstrand et al., 2014). In a proof-of-principle experiment, molecular profiling was achieved in a transgenic mouse line that expressed the nanobody fusion protein in all neuronal cells. Next, cell-types giving input to the target region, the nucleus accumbens (NAc), were identified using canine adenovirus (CAV)-mediated injections of GFP into the targeted brain region to retrogradely label all neurons that were projecting to this area. Subsequently, selective molecular profiling of the heterologous DAn in the VTA projecting to the NAc was enabled by the stereotaxic injections of adeno-associated virus (AAV) that conditionally express the nanobody fusion protein in the presence of Cre-recombinase (Ekstrand et al., 2014; Nectow et al., 2015).

Another viral tool for gene expression profiling of projection neurons with anatomically-defined location of soma and axon terminals utilised a retrograde AAV that expressed eGFP-L10a-tagged ribosomes under control of the alpha-calcium/calmodulin-dependent protein kinase II (Camk2a)

promoter (Cook-Snyder et al., 2015). While utility and cell-type specific expression could be shown for retrograde transduced basal amygdala projection neurons, it should be noted that complete cell-type specificity around the site of injection could not be conferred (Cook-Snyder et al., 2015).

Two very recent additional publications use viral expression of eGFP-tagged ribosomes to identify cell populations based on their projection patterns. Neural components of the complex polysynaptic circuits of the mesolimbic DA pathway was analysed using a Cre-dependent pseudorabies virus (PRV) (Pomeranz et al., 2017). The virus labelled presynaptic neurons in Cre-expressing neurons and depicted the molecular profiles of mesolimbic DAn and their presynaptic inputs (Pomeranz et al., 2017). Recently, Nectow et al. developed 'viral TRAP' using an engineered Cre-dependent AAV that expressed eGFP-L10a to access translating mRNAs in a spatio-temporal restricted manner from any neuronal population that expresses Cre (Nectow et al., 2015).

Viral-TRAP approaches improve TRAP by providing a tool to study molecular connectivity within the brain of previously anatomically restricted cell-types. Furthermore, viral-TRAP circumvents the need for difficult genetic modifications, thus, it could be applied to other mammalian species whose genetic modifications have been proven difficult if suitable Cre driver lines exist.

1.5 Aims

Here, we will make use of the TRAP technology to study gene expression changes during Parkinson's disease. Thereby, the overall aim focuses on the investigation of changes in the DAn-specific translatome in a *hSNCA+* transgenic mouse model of Parkinson's disease (Janezic et al., 2013). We make use of several advantages of the TRAP methodology such as the specific analysis of translated mRNA rather than total RNA, the cell-type specific isolation of mRNA from dopaminergic neurons - the main cell-type affected by Parkinson's - and the isolation of translated mRNAs *in vivo* without the need for lengthy dissociations, fixations, staining or cell-sorting strategies. While previous studies mainly focused on gene expression profiling analysis of whole midbrain neurons, these results represent the profiles of a variety of cell-types and cannot be generalised for DAn. Thus, our aim for cell-type specific profiling of degenerating DAn and the bioinformatic analysis of their specific regulatory network will aid the identification of underlying molecular factors driving neuronal loss and the pathology of Parkinson's.

This will be detailed in four results Chapters:

- Molecular characterisation of a bacTRAP transgenic Alpha-Synuclein over-expression mouse model (**Chapter 3**).
- Establishing Translating Ribosome Affinity Purifications (TRAP) in bacTRAP mice (**Chapter 4**).
- Analysis of the dopamine neuron translatome in a transgenic mouse model of Parkinson's (**Chapter 5**)
- Molecular characterisation and pilot TRAP experiments of a novel double transgenic conditional TRAP-Parkinson's model (**Chapter 6**)

- CHAPTER 2 -

MATERIALS AND METHODS

2.1 Materials and Methods - Animal husbandry.

2.1.1 Animals.

mSnca-/-, hemizygous *hSNCA+,* and hemizygous *TH-bacTRAP* (*THTR*) transgenic mouse colonies which were backcrossed on a pure C57BL/6 background over several generations have been established previously (DPhil Thesis: S. Senior, 2007; S. Anwar, 2011; S. Janezic, 2013; Chapter 3). *hSNCA+* and *THTR* mice were kept on a *mSnca-/-* background unless otherwise indicated. The *hSNCA* transgene was maintained in a hemizygous state, the *THTR* colony was bred to homozygosity.

ROSA26-eGFP-L10a (REL) fs/fs mice were purchased from Jackson Laboratories (B6.129S4-Gt(ROSA)26Sor$^{tm1(CAG-EGFP/RPL10a,-birA)Wtp}$/J; Stock No: 022367; (Zhou et al., 2013)). Homozygous *RELfs/fs* mice are viable and fertile and have been backcrossed on a pure C57BL/6 background over several generations. The targeting vector was inserted into the ROSA26 locus; the strong synthetic CAG promoter (C: cytomegalovirus (CMV) enhancer element; A: promoter, first exon and intron of chicken beta-Actin; G: splice acceptor of rabbit beta-Globin (Miyazaki et al., 1989)) drives frt-flanked enhanced green fluorescence-ribosomal fusion protein (eGFP-L10a) controlled by a loxP-flanked (floxed)-neomycin (neo) resistance cassette including a polyadenylation (polyA) sequence. Cre-mediated recombination leads to the removal of the neo sequence, ribosomes of selected tissues are labelled by constitutively activated eGFP-L10a only where Cre is expressed.

DAT^{IRES}cre (DAT-Cre) transgenic mice for breeding were kindly provided by the Cragg laboratory (DPAG, University of Oxford). Homozygous DAT-Cre mice are viable and fertile and have been backcrossed on a pure C57BL/6 background over several generation (Jackson Laboratories B6.SJL-*Slc6a3$^{tm1.1(cre)Bkmn}$*/J; Stock No: 006660; (Bäckman et al., 2006)). Internal ribosome entry site-linked Cre recombinase gene (IRES-Cre) was inserted into the 3' untranslated region (3'UTR) of the endogenous dopamine transporter (DAT) gene to enable co-expression of both genes from the endogenous promoter with correct spatio-temporal expression patterns and minimal interference with endogenous DAT gene function.

Animals were group-housed in a 12-12 hours' light-dark cycle and all experiments were conducted during the light cycle. Food and water was available to mice *ad libitum*. All experimental animals were matched for age and both, male and female mice were used as indicated. All experiments were carried out in accordance with the United Kingdom Animals (Scientific Procedures) Act of 1986 and approved by the local ethical review panel at the Department of Physiology, Anatomy and Genetics (DPAG), University of Oxford.

Name	Zygosity	Colony name in mouse database	Abbreviations in mouse database
mSnca-/-	Homozygous KO for mSnca	Littermates of THTR	KO
hSNCA+ mSnca-/-	Hemizygous for hSNCA; homozygous KO for mSnca	Littermates of THTR	OVX
THTR+ (hSNCA+) mSnca-/-	Hemizygous for THTR (hemizygous for hSNCA); homozygous KO for mSnca	THTR	+ (OVX)
THTR+/+ (hSNCA+) mSnca-/-	Homozygous for THTR (hemizygous for hSNCA); homozygous KO for mSnca	THTR	++ (OVX)
THTR+/+ mSnca-/-	Homozygous for THTR; homozygous KO for mSnca	THTRctrl	++, KO
THTR+/+ mSnca WT	Homozygous for THTR WT for mSnca	THTRctrl	++, WT
RELfs/fs (hSNCA+) mSnca WT	Homozygous for floxed REL; (hemizygous for hSNCA); WT for mSnca	TRAP	Fs/fs (OVX)
RELfs/-::DAT cre/- (hSNCA+) mSnca WT	Heterozygous for floxed REL; heterozygous for DAT-Cre; (hemizygous for hSNCA); WT for mSnca	REL	Fs/-::cre/- (OVX)
DATcre/cre mSnca WT	Homozygous for DAT-cre transgene; WT for mSnca	DATC, used for breeding only	/

Table 2. 1 Summary of mouse lines used for this study.
THTR= TH-bacTRAP. REL= ROSA26-eGFP-L10a. KO= knock-out. WT= wild-type. mSnca= mouse alpha-Synuclein. hSNCA= human alpha-Synuclein. DAT= dopamine transporter. TH= tyrosine hydroxylase. fs= floxed. OVX= over-expressed.

2.1.2 Crude lysate DNA extraction from ear tissue clips.

Transgenes of genetic modified mice were identified by genotyping PCR. DNA was extracted from ear tissue by digestion of the sample in 450 µl of lysis buffer (50 mM KCl, 1.5 mM $MgCl_2$, 10 mM Tris pH 8.5, 0.45% CA-630 (Igepal), 0.45% Tween-20, ddH_20) and 20 µg/ml of proteinase K (Sigma) for 2-3 hours at 55°C until the tissue has been lysed completely and no tissue clumps were visible. Proteinase K activity was inactivated by incubating samples at 95°C for 20 minutes. Extracted DNA samples were stored at 4°C.

2.1.3 Purified genomic DNA extraction from ear clips.

Genomic DNA (gDNA) was extracted from ear clips by digestion using the MasterPure kit (Epicentre). gDNA was extracted from ear tissue by digestion of the sample in 150 µl Tissue Cell and Lysis Solution (Epicentre) and 4.33 µl Proteinase K (20 µg/ml, Sigma) for 2 hours at 55°C until the tissue has been lysed completely and no tissue clumps were visible. Samples were cooled to 37°C for 30 minutes with added 0.7 µl RNase A (5 mg/ml, Sigma), followed by incubation on ice (3-5 minutes). 90 µl MPC Protein Precipitation Reagent (Epicentre) was added, followed by centrifugation at 10,000*xg* (4°C, 10 minutes). To precipitate the gDNA, the supernatant was mixed with 250 µl Isopropanol by inverting the tube 30-40 times. gDNA was pelleted by centrifugation at 10,000*xg* (4°C, 10 minutes), washed twice with 250 µl 75% ethanol (EtOH) and air-dried upside down with open lid (about 15 minutes, until all drops of EtOH have disappeared). gDNA was re-suspended in 50 µl Nuclease-free water and purified gDNA was stored at -20°C.

2.1.4 DNA quantification.

gDNA was quantified using the NanoDrop 1000 Spectrophotometer at a wavelength of 260 nm. Protein contamination was assessed by measuring 260/280 nm ratio. The 230/260 nm ratio was used to access the purity of the nucleic acid preparation from other contaminants; this ratio is expected to be >2 for pure DNA. Following quantification, gDNA was diluted to 4 ng/µl with Nuclease-free water for downstream applications and stored at -20°C.

2.1.5 Genotyping PCR.

Polymerase chain reaction (PCR) was performed for the purposes of genotyping. Specific primers were designed to amplify the separate transgenes. PCR master mixes were prepared for each primer pair using a HotStar Taq DNA Polymerase kit (QIAGEN) according to the following protocol (20 µl PCR reaction):

Reaction Mix	Volume/ reaction
ddH_2O	13.5 µl
10x Buffer	2 µl
8 mM dNTP mix	0.4 µl
10 mM primer pair mix	2 µl
HotStar Taq DNA Polymerase	0.1 µl

For each sample, 18 µl of PCR master mix was added to the well of a 96-well plate with 2 µl of template DNA. Samples were run on a DNA Engine Tetrad 2 Peltier Thermal Cycler (Bio-Rad) using the specific PCR programmes as described below. Following DNA amplification, 10 µl PCR product was separated by gel electrophoresis using a 1-2% agarose gel (w/v) in 1x Tris/Borate/EDTA (TBE) buffer (Sigma-Aldrich) and 0.25 µg/mL of ethidium bromide alongside the Gene Ruler 1 kb Plus DNA ladder (Thermo Scientific). Electrophoresis was performed using standard electrophoresis tanks (Bio-Rad) at 100-120V in TBE buffer until the desired separation. Gels were imaged using the GelDoc XR system (Bio-Rad).

mSnca-/-, hSNCA+ mSnca-/- or hSNCA+ mSnca WT mice.

Junctions between the BAC vector and the *hSNCA* genomic DNA insert were amplified by PCR. In addition, primers were used to detect presence or absence of endogenous *mSnca*. The primers were previously designed in the laboratory (DPhil Thesis: S. Senior, 2007) and are listed below.

Primer name	Forward primer	Reverse primer	Product size
3' BAC-hSNCA junction	GGCCTCTGTCGTTTCCTTTCTCTG	ACGTGCATAGGCAGAGCTAAAACT	450 bp
5' BAC-hSNCA junction	CACTGAGTATTGTTCTGGTAAC	TCAAACATGAGAATTGGTCG	450 bp
mSnca WT	CAGCTCAAGTTCAGCCACGA (common upstream primer)	AAGGAAAGCCGAGTGATGTAC (WT downstream primer)	485 bp
mSnca KO	CAGCTCAAGTTCAGCCACGA (common upstream primer)	ATGGAAGGATTGGAGCTACG (KO downstream primer)	550 bp

Table 2. 2 Primer sequences for genotyping of alpha-Synuclein transgenic mice.

The PCR was run using the following programme:

95°C	15 min	
95°C	30 sec	Repeat for 34 cycles
55°C	30 sec	
72°C	60 sec	
72°C	3 min	
15°C	forever	

TH-bacTRAP (THTR) transgenic mice.

Junctions between the endogenous tyrosine hydroxylase (TH) promoter and the eGFP transgene, the transgene and the BAC vector and the BAC vector and the endogenous TH promoter were amplified by PCR. In addition, presence or absence of endogenous *mSnca* or the *hSNCA* transgene was detected as described above. The primers were previously designed in the laboratory (DPhil Thesis: S. Janezic, 2013) and are listed below.

Primer name	Forward primer	Reverse primer	Product size
TH_EGFP junction	TGGTGCAGATGAACTTCAGG	GGGCTGTGGAGACAGAACTC	190 bp
Amp_BAC junction	ACATTTCCCCGAAAAGTGC	TTTGAGGCTTAGGCACAAGG	183 bp
BAC_TH junction	GGGGCACATTTCATTACCTC	GATGACACCAATGGACATGC	386 bp

Table 2. 3 Primer sequences for genotyping of transgenic mice.

The PCR was run using the following programme:

95°C	15 min	
95°C	30 sec	Repeat for 34 cycles
55°C	30 sec	
72°C	60 sec	
72°C	3 min	
15°C	forever	

ROSA26-eGFP-L10a (REL) and DAT-Cre transgenic mice.

Primer sequences amplifying either the wild-type (WT) *ROSA26* or the modified ROSA26-eGFP-L10a locus were purchased from Jackson Laboratories for strain 22367. Additional primer pairs to specifically amplify the eGFP-L10a transgene have been designed. All sequences are listed below. To detect successful Cre-mediated recombination, primer to either detect WT DAT or DAT-cre have been used. These primer sequences were obtained from the Cragg laboratory (DPAG, University of Oxford) and are listed below.

Primer name	Forward primer	Reverse primer	Product size
WT ROSA26 locus (WT)	AAGGGAGCTGCAGTGGAGTA (common upstream primer)	CCGAAAATCTGTGGGAAGTC (WT downstream primer)	297 bp
ROSA26-eGFP-L10a locus (MUT)	AAGGGAGCTGCAGTGGAGTA (common upstream primer)	CGGGCCATTTACCGTAAGTTAT (MUT downstream primer)	284 bp
eGFP-L10a_1	TATCATGGCCGACAAGCAGA	CACCGTCTCCAGAAACTTGC	395 bp
eGFP-L10a_2a	CAAAGACCCCAACGAGAAGC	CTCCACCGTCTCCAGAAACT	227 bp
eGFP-L10a_2b	CAAAGACCCCAACGAGAAGC	TTGGCTTCATCACAGTGCTG	361 bp
DAT WT	TGGCTGTTGGTGTAAAGTGG	GGACAGGGACATGGTTGACT	264 bp
DAT-cre	CCGGGCTGCCACGACCAA	GGCGCGGCAACACCATTTTT	445 bp

Table 2. 4 Primer sequences for genotyping of ROSA26-eGFP-L10a and DAT-cre transgenic mice.

Transgenic Mouse	Expected Bands	Product size
REL WT mice	Only REL WT band	297 bp
REL MUT homozygous mice	Only REL MUT band	284 bp
REL MUT heterozygous mice	REL WT and REL MUT bands	297 bp; 284 bp
DAT WT mice	Only DAT WT band	264 bp
DAT-Cre homozygous mice	Only DAT Cre band	445 bp
DAT-Cre heterozygous mice	DAT WT and DAT Cre bands	264 bp

The PCR was run using the following programme:

95°C	15 min	
95°C	30 sec	Repeat for 34 cycles
62°C	30 sec	
72°C	60 sec	
72°C	3 min	
15°C	forever	

2.1.6 Copy-number genotyping by quantitative real-time PCR (qPCR).

Zygosity of *TH-bacTRAP (THTR)* or *ROSA26-eGFP-L10a (REL)* transgenic mice (hemizygous/ heterozygous= one copy of the transgene; homozygous= two copies of the transgene) were identified by copy-number genotyping via qPCR (Wishart et al., 2007) on a StepOnePlus Real-Time PCR System (Applied Biosystems). Copy-thresholds for the transgene of interest compared to the geometric mean of reference gene amplifications (GAPDH and beta-Tubulin) were established using the comparative C_t method, whereby two known hemizygous *THTR* or homozygous *REL* mice served as calibrators. Copy-number genotyping qPCR master mixes were prepared using FastSYBR Green Master Mix (Invitrogen) according to the following protocol (25 µl qPCR reaction).

Reaction Mix	Volume/ reaction
FastSYBR Green Master mix	12.5 µl
Forward Primer (10 µM)	0.2 µl
Reverse Primer (10 µM)	0.2 µl
Nuclease-free Water	7.1 µl
gDNA Template (4 ng/µl)	5 µl

The qPCR was run using the following programme.

95°C	20s	
95°C	3 sec	Repeat for 40 cycles
60°C	30 sec	

Primer name	Forward primer	Reverse primer	Mouse line
Beta-Tubulin	GCCAGAGTGGTGCAGGAAAT	TCACCACGTCCAGGACAGAGT	THTR; REL
GAPDH	ATCCTGTAGGCCAGGTGATG	GGGCTTTTAAGGCTAATAAGGTG	THTR; REL
TH-bacTRAP	TGGTGCAGATGAACTTCAGG	GGGCTGTGGAGACAGAACTC	THTR
ROSA26 WT	AAGGGAGCTGCAGTGGAGTA (common upstream primer)	CCGAAAATCTGTGGGAAGTC (WT downstream primer)	REL
ROSA26-eGFP-L10a (MUT)	AAGGGAGCTGCAGTGGAGTA (common upstream primer)	CGGGCCATTTACCGTAAGTTAT (MUT downstream primer)	REL
eGFP-L10a	CAAAGACCCCAACGAGAAGC	CTCCACCGTCTCCAGAAACT	REL

Table 2. 5 qPCR primer sequences for copy/number genotyping of TH-bacTRAP (THTR) and ROSA26-eGFP-L10a (REL) transgenic mice.

2.2 Materials and Methods - Protein biochemistry.

2.2.1 Standard protein extraction.

Proteins were extracted from snap-frozen brain tissue (usually one hemisphere striatum or midbrain) which was stored at -80°C. Brains were thawed on ice and re-suspended in 3 ml/g Radio immunoprecipitation assay buffer (RIPA buffer) (1% NP-40, 0.1% sodium dodecyl sulphate (SDS), 0.5% sodium deoxy cholate, 150 mM NaCl, 50 mM Tris pH 8) containing protease inhibitors (cOmplete EDTA-free, Roche). Samples were homogenised with the tissue tearor (Biospec Products, Inc) for approximately 15 seconds and left on ice for 1 hour. The lysate was centrifuged at 500 rpm for 10 minutes at 4°C. The protein lysate was stored at -80°C. Protein content was quantified using a bicinchoninic acid (BCA) assay Kit (Sigma).

2.2.2 Protein quantification.

Protein concentration in tissue homogenates was quantified by BCA assay. Bovine serum albumin (BSA) solutions of increasing concentrations ranging from 0-1000 µg/ml were used as protein standards. Protein lysates were diluted to concentrations within the range of the standard curve. BCA solution was added to the samples according to standard protocol. Following incubation for 30 minutes at 37°C, the absorbance was measured at 562 nm using a microplate reader (Synergy HT, Biotek).

2.2.3 Western blotting.

Proteins in tissue lysates were reduced and denatured by boiling samples for 5-10 minutes in Laemmli buffer (60 mM Tris pH 6.8, 2% SDS, 10% glycerol, 5% β-mercaptoethanol, 0.01% bromophenol blue). Samples (5-10 µg depending on protein of interest) were loaded onto 4-15% Criterion Tris-HCl polyacrylamide gels (Bio-Rad), electrophoresis was performed at 200 V for 45 min. Spectra Multicolour Broad Range Protein Ladder (Thermo Scientific) was used to determine target protein weight. Proteins were then transferred to a polyvinylidene fluoride (PVDF) (Bio-Rad) membrane using a Trans- Blot Turbo Transfer System (Bio-Rad) using Trans-Blot Turbo Midi PVDF transfer packs (Bio-Rad) as per the manufacturer's instructions. Membranes were blocked in TBS

supplemented with 0.1% Tween-20 (TBS-T) and 5% skim milk powder for 1 h at room temperature (RT) and incubated in primary antibody solution overnight (O/N) at 4°C. Membranes were washed in TBS-T (3x 10 minutes) followed by incubation in horseradish peroxidase (HRP)-conjugated secondary antibodies (Bio-Rad) in antibody solution for 1 h. All antibodies were diluted in 5% skim milk/ TBS-T. After washing in TBS-T (3x 10 minutes), membranes were developed using ECL+ solution (Milipore). Western blots were imaged using the GelDoc XR system (Bio-Rad). The blots were quantified using Imagelab software (QuantityOne, Bio-Rad) and normalised for the loading control beta-Actin and the average of the control samples. For statistical analysis, Prism software version 5.0 (GraphPad) was used. Data from Western blot analysis were analysed using a one-way or two-way ANOVA followed by Tukey's or Dennett's post hoc analysis unless otherwise indicated. Data are shown ±SEM.

Antibody	Host species	Company	Catalogue number	Dilution	Approx. size
Alpha-Synuclein	Mouse	BD biosciences	610786	1/1,000	19 kDa
Alpha-Synuclein Purified (4B12)	Mouse	Covance	SIG-39730-200	1/1,000	16 kDa
Beta-actin (HRP conjugated)	Mouse	Abcam	ab49900	1/30,000	42 kDa
CI subunit NDUFB8	Mouse	Abcam, OXPHOS Kit	110409	1/1,000	20 kDa
CII-30 kDa/ SDHB	Mouse	Abcam, OXPHOS Kit	110410	1/1,000	28 kDa
CIII-Core protein 2/ UQCRC2	Mouse	Abcam, OXPHOS Kit	110411	1/1,000	48 kDa
CIV subunit I/ mt-CO1	Mouse	Abcam, OXPHOS Kit	110412	1/1,000	40 kDa
CV alpha subunit/ ATP5A	Mouse	Abcam, OXPHOS Kit	110413	1/1,000	55 kDa
Cytochrome c, somatic/ CYTO c	Rabbit	Cell signalling, Mitochondrial Marker Kit	8674	1/1,000	14 kDa
DAT (C-20)	Goat	Santa Cruz	sc-1433	1/750	50+80 kDa
DAT (N-20)	Rat	Millipore	MAB369	1/500	70-85 kDa
DRP1/ DNML1	Rabbit	Cell Signalling	8570	1/1,000	78-82 kDa
GFP	Chicken	Abcam	ab13970	1/1,000	26 kDa
GFP	Goat	Abcam	ab6673	1/1,000	26 kDa
GFP	Rabbit	Invitrogen	A11122	1/1,000	26 kDa
GFP	Mouse	Invitrogen	A11120	1/1,000	26 kDa
HSP60	Rabbit	Cell signalling, Mitochondrial Marker Kit	8674	1/1,000	60 kDa
L10a (RPL10a)	Mouse	Sigma	WH0004736M1	1/2,000	25 kDa
Mitofusin 2/ MFN2	Rabbit	Sigma	M6319	1/1,000	86 kDa
OPA1	Mouse	BD biosciences	612606	1/1,000	80+100 kDa
Parkin/ PARK2	Rabbit	Abcam	ab15954	1/2,000	52 kDa
PGC1a	Rabbit	Abcam	ab54481	1/1,000	105 kDa
Porin/ VDAC	Rabbit	Cell signalling, Mitochondrial Marker Kit	8674	1/1,000	32 kDa
Prohibitin/ PHB	Rabbit	Cell signalling, Mitochondrial Marker Kit	8674	1/1,000	32 kDa
Pyruvate Dehydrogenase/ PDHA1	Rabbit	Cell signalling, Mitochondrial Marker Kit	8674	1/1,000	43 kDa
SDHA	Rabbit	Cell signalling, Mitochondrial Marker Kit	8674	1/1,000	70 kDa
Superoxide Dismutase 1/ SOD1	Rabbit	Abcam	ab16831	1/2,000	17 kDa
TH	Rabbit	Millipore	AB152	1/2,000	62 kDa
TOMM20	Rabbit	Santa Cruz	sc-11415	1/1,000	18-20 kDa
TOMM40	Rabbit	Santa Cruz	sc-11414	1/1,000	40 kDa

Table 2. 6 Primary antibodies for Western blot analysis

Target species	Host species	Target	Conjugate	Dilution	Company	Cat number
Chicken	Rabbit	IgG	HRP	1/5,000	Millipore	12-341
Goat	Donkey	IgG (H+L)	HRP	1/5,000	Santa Cruz	sc-2020
Goat	Rabbit	IgG (H+L)	HRP	1/5,000	Bio-Rad	172-1034
Mouse	Goat	IgG (H+L)	HRP	1/5,000	Bio-Rad	170-6516
Rabbit	Goat	IgG (H+L)	HRP	1/5,000	Bio-Rad	170-6515
Rat	Rabbit	IgG (H+L)	HRP	1/5,000	Invitrogen	61-9520

Table 2. 7 Secondary antibodies for Western blot analysis

2.3 Materials and Methods - Immunohistochemistry.

2.3.1 Transcardial perfusion.

Mice were deeply anaesthetised by intraperitoneal injection of an overdose of pentobarbital injected intraperitoneally (0.15-0.2 ml per animal) and perfused transcardially with phosphate buffered saline (PBS) followed by 4% paraformaldehyde (PFA) in PBS. Following removal from the skull, the brains were post-fixed in 4% PFA O/N at 4°C and cryo-protected in 30% sucrose for 24-48 hours at 4°C. Brains were sectioned in coronal orientation using a sliding microtome (SM 2000R, Leica) at 35 or 50 μm and stored in 96-well plates in anti-freeze solution (500 ml PBS, 250 ml ethylene glycol, 250 ml glycerol) at -20°C in the dark.

2.3.2 Immunofluorescence.

All steps in the labelling process were carried out at 70-100 rpm on an orbital shaker (SI50, Stuart Equipment) at RT unless otherwise indicated. Free-floating sections (35 μm) were washed in PBS (3x 10 minutes) and treated with 50 mM glycine in PBS for 15 minutes followed by another wash in PBS (3x 10 minutes). The sections were blocked in TBS+ (1x TBS, 10 % normal donkey serum (NDS), 0.1% Triton X-100) for 1 hour and incubated with primary antibody in TSB+ at 4°C O/N on a rocker. Next, sections were washed in PBS (3x 10 minutes) and incubated in Alexa Fluor fluorescent secondary antibodies (Life Technologies) for 1 hour in TBS+. Sections were washed in PBS (3x 10 minutes), incubated in 4',6-diamidino-2-phenylindole (DAPI) (40 mg/ml DAPI stock solution in PBS) for 10 minutes followed by a further wash in PBS (3x 10 minutes). Sections were mounted on Polysine slides (VWR International), cover-slipped using FluoroMount (Sigma-Aldrich) and imaged using an EVOS FL Auto Cell Imaging System (Thermo Fisher).

Antibody	Host species	Company	Catalogue number	Dilution
Alpha-Synuclein	Mouse	BD biosciences	610786	1/500
Alpha-Synuclein Purified (4B12)	Mouse	Covance	SIG-39730-200	1/500
Beta-III tubulin (TUJ1)	Mouse	Covance	MMS-435P	1/500
DAT (C-20)	Goat	Santa Cruz	sc-1433	1/250
GFAP	Rabbit	Dako	Z0334	1/1,000
GFP	Chicken	Abcam	ab13970	1/500
GFP	Chicken	aveslab	GFP-1020	1/500
GFP	Goat	Abcam	ab6673	1/500
GFP	Mouse	Invitrogen	A11120	1/500
GFP	Rabbit	Invitrogen	A11122	1/500
TH	Rabbit	Millipore	AB152	1/1000
TH	Sheep	Millipore	AB1542	1/500

Table 2. 8 Primary antibodies for Immunofluorescence analysis.

Excitation	Target species	Host species	Conjugate	Dilution	Company	Cat number
488	Chicken	Donkey	1/1,000	1/5,000	Jackson	703-454-155
	Goat	Donkey	1/1,000	1/5,000	Jackson	705 -485-003
	Mouse	Donkey	1/1,000	1/5,000	Invitrogen	A21202
	Rabbit	Donkey	1/1,000	1/5,000	Invitrogen	A21206
	Sheep	Donkey	1/1,000	1/5,000	Invitrogen	A11015
594	Goat	Donkey	1/1,000	1/5,000	Invitrogen	A11058
	Mouse	Donkey	1/1,000	1/5,000	Invitrogen	A21203
	Rabbit	Donkey	1/1,000	1/5,000	Invitrogen	A21207
	Sheep	Donkey	1/1,000	1/5,000	Invitrogen	A11016

Table 2. 9 Secondary antibodies for Immunofluorescence analysis.

2.3.3 Immunohistochemistry (IHC).

Free-floating coronal brain sections (50 μm) were stained by IHC. All steps were carried out at RT on an orbital shaker (~100 rpm) unless otherwise indicated. Sections were washed in TBS (3x 10 minutes) and endogenous peroxidase activity was quenched by incubation in 3% H_2O_2 in TBS for 10 mins. Sections were rinsed in TBS (3x 10 minutes) and blocked in TBS+ (1x TBS, 10 % NDS, 0.1% Triton X-100) for 1 hour. After incubation with primary antibody in TSB+ at 4°C O/N on a rocker, sections were rinsed in TBS (3x 10 minutes) to remove excess antibody. Subsequently, sections were incubated in biotin-SP-conjugated secondary antibody in TBS+ (Vectorlabs) for 1 hour and washed in TBS (3x 10 minutes). After incubation in ABC reagent (Vectastain Elite ABC Kit, Vectorlabs) in TBS for 1 hour and further washes in TBS (3x 10 minutes), sections were incubated in 3,3'-diaminobenzidine (DAB) solution (Thermo Scientific Pierce), washed in TBS-T (3x 10 minutes) and left to dry on SuperFrost Plus slides (VWR) O/N.

Antibody	Host species	Dilution	Company	Catalogue number
TH	Rabbit	1/2,000	Millipore	AB152
eGFP	Rabbit	1/1,000	Invitrogen	A11122

Table 2. 10 Primary antibodies for Immunohistochemistry analysis.

Antibody	Target species	Host species	Dilution	Company	Catalogue number
Biotin-SP	Rabbit	Goat	1/2,000	Jackson	11-065-144

Table 2. 11 Secondary antibodies for Immunohistochemistry analysis.

2.3.4 Haematoxylin counterstain and dehydration.

Immunohistochemistry sections were counterstained with haematoxylin (Gill's Formula, Vectorlabs) for 30 sec. Slides were washed 2x 1 minutes in water. Tissue was then dehydrated by subsequently submerging slides for 1 minute in 50% EtOH, 75% EtOH, 95% EtOH, 2x 1 minute in 100% EtOH, 50% xylenes/50% EtOH and 2x 2 minutes in 100% xylenes before being cover slipped using DPX mountant (Fluka Biochemika).

2.3.5 Stereological cell count analysis.

The total numbers of either TH or eGFP-immunoreactive, haematoxylin-counterstained nigra dopaminergic neurons (DAn) were estimated with the optical fractionator method of unbiased stereology using the Stereo Investigator software (MicroBrightField). Free-floating sections (50 µm) were processed for eGFP or TH immunoreactivity as described above; every fourth section was counted for a total of 6-7 sections per mouse. Mice of each genotype were processed together in each age group to prevent technical differences. The substantia nigra pars compacta (SNc) and ventral tegmental area (VTA) were delineated according to the mouse brain atlas (Paxinos and Franklin, 2012) using a 10x objective. Cells were counted under a 100x objective of a Zeiss Imager M2 microscope using a randomly placed counting frame of 60x60 µm on a sample grid of 120x120 µm. A 10 µm optical dissector with 2 µm upper and lower guard zones was used. The sampling parameters were established using pilot experiments.

2.4 Materials and Methods - Molecular biology.

All reagents and equipment used in this section were specified RNase-free, diethyl pyro carbonate (DEPC)-treated or rinsed with RNA-Zap and RNase-free water or 100% EtOH to remove possible contamination and all RNases.

2.4.1 Pre-Treatments of Dynabeads for RNA manipulation.

Streptavidin MyOne T1 Dynabeads (Invitrogen) were pre-treated to make them suitable for RNA manipulations. All steps were carried out at RT using 1 ml of solution in a 1.5 ml reaction tube unless otherwise indicated. During all wash-steps, supernatant was removed by aspiration with a pipette while the tube was on the magnet. The beads were re-suspended in the original vial by rotation or vortexing. The beads were washed on a magnetic rack to remove preservatives in RNase-free PBS for 1-2 minutes by adding the solution along the inside of the tube where the beads were collected and re-suspended by pipetting for a total of three washes. Next, the beads were washed twice in Solution A (DEPC-treated 0.1 M NaOH, DEPC-treated 0.05 M NaCl) for 2 minutes, followed by one wash in Solution B (DEPC-treated 0.1 M NaCl). After the last wash, beads were re-suspended in RNase-free PBS and taken forward for the TRAP “affinity matrix” preparation.

2.4.2 TRAP reagents preparation.

TRAP reagent aliquots were prepared according to the following protocols and stored as per the manufacturer’s instructions:

1,2-diheptanoyl-*sn*-glycero-3-phosphocholine (DHPC) powder (Generon) was stored at −20°C and thawed to RT for about 30 minutes before opening to reconstitute. Powder reconstituted with RNase-free water to 300 mM was left at RT with occasional vortexing for another 30 minutes. Once reconstituted in water DHPC was stored at 4°C in its glass packaging for up to 7 days.

Cycloheximide powder (CHX; Sigma) was aliquoted directly in pre-weighed empty 1.5 ml reaction tubes and stored at 4°C. On the day of use, CHX aliquots were weighed out and re-suspended in methanol (MeOH) at 100 mg/ml. The made-up aliquot was stored at 4°C for up to one day.

Biotinylated Protein L (recombinant, purified; Fisher Scientific) was reconstituted as recommended by the manufacturer to 1 µg/µl in RNase-free water. Excess Protein L was aliquoted in single-use aliquots and stored at −80°C.

Translating ribosome affinity purification buffers were prepared according to the following protocols and stored at 4°C for up to several months:

TRAP Dissection buffer (D):

Hank's balanced salt solution (HBSS, 10x, calcium, magnesium, no phenol red; Invitrogen), 2.5 mM HEPES-KOH (1 M, pH 7.4; Affimetrix), 35 mM glucose (Sigma), and 4 mM sodium bicarbonate ($NaHCO_3$; Sigma) in RNase-free water. Immediately before use, 100 µg/ml CHX (100 mg/ml in MeOH; Sigma) was added to a buffer aliquot.

TRAP Tissue-lysis buffer (L):

20 mM HEPES KOH, 150 mM KCl (potassium chloride, 2 M, RNase-free; Applied Biosystems), and 10 mM $MgCl_2$ (magnesium chloride, 1 M, RNase-free; Applied Biosystems), in RNase-free water. Immediately before use, protease inhibitors (one mini tablet per 10 ml; Mini-complete EDTA-free, Roche), 0.5 mM DTT (100 mM; Superscript III kit, Invitrogen), 100 µg/ml CHX (100 mg/ml in MeOH; Sigma), and 10 µl/ml rRNasin (recombinant Ribonuclease Inhibitor, 20-40 U/µl; Promega) and Superasin (SUPERase In RNase Inhibitor, 20 U/µl; Applied Biosystems) were added to a L buffer aliquot.

TRAP Low-salt buffer (LS):

20 mM HEPES KOH (pH 7.4), 150 mM KCl, 10 mM $MgCl_2$, and 1% nonylphenyl polyethylene glycol (NP-40, 10%; AG scientific) in RNase-free water. Immediately before use, 0.5 mM DTT, and 100 µg/ml CHX were added to a LS buffer aliquot. 10 µl/ml rRNasin and Superasin were only added to the LS buffer on TRAP day 1.

TRAP High-salt buffer (HS):

20 mM HEPES KOH (pH 7.4), 350 mM KCl, 10 mM $MgCl_2$, and 1% NP-40 in RNase-free water. Immediately before use, 0.5 mM DTT, 100 µg/ml CHX, and 10 µl/ml RNasin and Superasin were added to a HS buffer aliquot.

2.4.3 TRAP GFP antibody preparation.

Monoclonal GFP antibodies (clone Htz-GFP-19F7 and Htz-GFP-19C8, bioreactor supernatant purity) were ordered from the Memorial Sloan-Kettering Monoclonal Antibody Facility. Antibodies that arrived unfrozen were mixed gently before dividing each antibody into single-experiment aliquots. Tubes were snap-frozen on dry-ice and stored at −80°C. Antibodies that arrived frozen were stored immediately at −80°C or thawed on ice and treated as outlined above. On the day of use, aliquots were thawed on ice and centrifuged at maximum speed (>13,000x*g*) in a micro-centrifuge for 10 minutes at 4°C. The supernatants were transferred to new tubes and either stored on ice until use or kept at 4°C for a few days with the addition of sodium azide (SIGMA).

GFP order #1 has been used for all THTR TRAP experiments. The concentrations and volumes used for the different affinity matrix concentration are outlined in the following table.

	Total Volume	Concentration	Amount for matrix	Volume for matrix
Htz-GFP-19F7 (GFP F7)	1.67 ml	3.0 mg/ml	50 µg	17 µl
			25 µg	8.5 µl
			12.5 µg	4.25 µl
			6.25 µg	2.13 µl
Htz-GFP-19C8 (GFP C8)	5.56 ml	0.9 mg/ml	50 µg	56 µl
			25 µg	28 µl
			12.5 µg	14 µl
			6.25 µg	7 µl

Table 2. 12 Antibodies of GFP order # 1 for all THTR TRAP experiments.

GFP order #2 has been used for all REL TRAP experiments. The concentrations and volumes used for the different affinity matrix concentration are outlined in the following table.

	Total Volume	Concentration	Amount for matrix	Volume for matrix
Htz-GFP-19F7 (GFP F7)	1.8 ml	2.77 mg/ml	50 µg	18 µl
			25 µg	9 µl
			12.5 µg	4.5 µl
			6.25 µg	2.25 µl
Htz-GFP-19C8 (GFP C8)	5.0 ml	1.0 mg/ml	50 µg	50 µl
			25 µg	25 µl
			12.5 µg	12.5 µl
			6.25 µg	6.25 µl

Table 2. 13 Antibodies of GFP order # 2 for all REL TRAP experiments.

2.4.4 TRAP affinity matrix preparation.

The affinity matrix used for the same experiment has been aliquoted to samples from a common source; either all matrices were prepared in one larger tube or prepared in batches in smaller tubes and combined into a larger tube for mixing before making aliquots. As recommended by the manufacturer, the volume of beads was kept close to the original volume from the source bottle throughout all manipulations. The ratio of beads/protein L/antibody must remain the same when reducing the total affinity matrix concentration. The ratio of affinity matrix used for each specific experiment is indicated where appropriate.

After washing and cleaning the beads, they were collected on the magnet and re-suspended in RNase-free PBS (original bead volume minus the volume of biotinylated protein L to be added) with biotinylated protein L (ideally a 1 ml total volume when using a 1.5 ml tube) for 35 minutes at RT by using gentle end-over-end mixing in a tube rotator. To remove excess biotinylated protein, the coated beads were washed 5x with PBS 3% IgG and protease-free BSA (w/v) (Affimetrix). Antibody binding was carried out using equal amounts of each GFP antibody, C8 and F7, in 1 ml total volume of LS buffer for 1 h by gentle end-over-end rotation in a tube rotator. It is important not to vortex the affinity matrix after antibody binding. After antibody binding, the beads were washed 3x with LS buffer and re-suspended in a total volume of LS buffer that each IP received an aliquot (200 µl final aliquot volume) of the affinity matrix components listed above. The affinity matrices were either used immediately, or stored for up to 2 weeks at 4°C with the addition of 0.02% sodium azide. In case of sodium azide addition to the pre-prepared affinity matrix, it was washed 3x quickly in LS buffer before use.

2.4.5 Translating Ribosome Affinity Purification.

On day 1, mice were schedule 1 culled and brains were rapidly manually dissected on ice. The following brain regions were used for TRAP unless otherwise indicated. For THTR TRAP experiments, the midbrain (MB) hemispheres of two males or females; for REL TRAP experiments, the MB or striatum (STR) hemispheres of one male or female, respectively were placed in ice-cold D buffer with added CHX (500 µl per hemisphere) and kept on ice until lysis. The other brain regions

(cerebellum (CB), hippocampus (Hi), cortex (CTX) (THTR + REL), STR (THTR mice only)) were snap-frozen on dry-ice and stored at -80°C, ear tissue was stored at -20°C.

Samples were transferred to pre-chilled 1.5 ml reaction tubes containing 500 µl L buffer with added extras and homogenised using cooled down polypropylene Pellet Pestles (Kimble Kontes) on ice. Lysates of left and right hemisphere (and of the two THTR mice per n= 1) were pooled in pre-chilled 2 ml reaction tubes and a 100 µl input aliquot per sample was snap-frozen on dry-ice and stored at -80°C for later analysis (Total RNA). The TRAP post-nuclear supernatant 'S2' fraction was prepared by centrifugation for 10 minutes at 2,000x*g* (4°C). The supernatant was transferred to a new, pre-chilled 2 ml reaction tube on ice. To the S2 fraction, 1/9 of the sample volume of 10% NP-40 (final concentration = 1%), was added and mixed by gently inverting the tube, followed by pulse-centrifugation of the sample in a micro-centrifuge to collect the liquid at the bottom of the tube. A further 1/9 of the sample volume of 300 mM DHPC (final concentration= 30 mM) was added and mixed by gently inverting the tube before incubating the mixture on ice for 5 min. The TRAP post-mitochondrial supernatant 'S20' fraction was prepared by centrifugation for 10 minutes at 20,000x*g* (4°C). The supernatant was transferred to a new, pre-chilled 2 ml reaction tube on ice and proceeded immediately to the immunoprecipitation (IP) in 2 ml reaction tube. To each sample, an aliquot of 200 µl of freshly re-suspended affinity matrix was added and the samples were incubated at in the cold room for 16-18 h with gentle end-over-end mixing in a tube rotator O/N.

On day 2, the beads were collected with a magnet (well-chilled in an ice bucket) and a 100 µl unbound fraction aliquot per sample was snap-frozen on dry-ice and stored at -80°C for later analysis (Unbound (UB) RNA). The beads were re-suspended in 1 ml ice-cold HS buffer with added extras and collected with the magnet as described above for a total of four washes. A micro-centrifuge was used to spin down beads from the caps between washes. After the beads were visibly re-suspended, the mix was pipetted gently at least 4x. Since high background can result from insufficient bead resuspension during washes, the tubes have been changed between all wash steps. After the fourth wash, all remaining wash buffer was removed and the tubes were allowed to warm to RT before re-suspension of the beads in 100 µl RLT PLUS lysis buffer (QIAGEN) with 1%

beta-mercaptoethanol (β-ME). The mixture was vortexed, spun down quickly and incubated for 10 minutes at RT. The RNA (now in lysis buffer) was removed from the beads with the magnet and proceeded immediately to the RNA clean-up using the RNeasy Micro PLUS Kit (QIAGEN) as per the manufacturer's instructions. All steps of the procedure were performed at RT, all centrifugation steps were performed at 20-25°C in a standard micro-centrifuge.

Briefly, for the IP RNA clean-up, the lysate was transferred to a gDNA Eliminator spin column and centrifuged for 30 s at 10,000 rpm and the flow-through was saved. The lysate mixed with one volume of 70% EtOH (about 100 µl) was added to an RNeasy MinElute spin column for centrifugation (10,000 rpm, 15 seconds for the following steps). Columns were washed with 700 µl Buffer RW1, followed by 500 µl Buffer RPE and a longer wash with 500 µl of 80% EtOH (10,000 rpm, 2 minutes) with a fresh collection tube. A spin with open lid at full speed for 5 minutes dried the spin column membrane, before RNA elution with 14 µl RNase-free water twice into the same tube (1 minutes at full speed). Eluted RNA was placed on ice immediately, snap-frozen on dry ice and stored at -80°C including two 2.2 µl aliquots for RiboGreen and Bioanalyzer assays.

2.4.6 RNA extraction from TRAP samples.

RNeasy Mini Kit (QIAGEN) was used to extract RNA from UB and TOTAL TRAP samples. The kit was used as per the manufacturer's instructions including DNase I treatment and modifications where indicated. Briefly, 100 µl aliquots were thawed on ice and 350 µl Buffer RLT, 1% β-ME was added. After mixing with 250 µl 100% EtOH the lysate was applied to an RNeasy spin column for centrifugation (10,000 rpm, 15 seconds for the following steps), and washed with 350 µl Buffer RW1. The column was incubated with 10 µl DNase I in 70 µl Buffer RDD for 20 minutes at RT before washing with 350 µl Buffer RW1, 500 µl Buffer RPE, and a longer wash with 500 µl Buffer RPE (10,000 rpm, 2 minutes) using a fresh collection tube. Columns were dried for 1-2 minutes at 10,000 rpm. UB and Total RNA were eluted with 30 µl water into a new tube by centrifugation (10,000 rpm, 1 minutes). This step was repeated for Total RNA into the same tube. Eluted RNA was placed on ice

immediately, snap-frozen on dry ice and stored at -80°C including two 2.2 µl aliquots for RiboGreen and Bioanalyzer assays.

2.4.7 RNA extraction from mouse brain tissue.

RNA was extracted from MB or STR tissue using TRIzol (Life Technologies), followed by purification using the RNeasy Mini Kit (QIAGEN). Tissue was lysed in 500 µl TRIzol per hemisphere using a Tissue-Tearor (Biospec) and left to homogenise at RT for at least 15 minutes, followed by centrifugation to get rid of debris (10,000 rpm, 10 minutes, 4°C). Supernatant was transferred to a fresh tube and 150 µl of chloroform was added for phase separation. The solution was mixed by shaking vigorously for 15 seconds and incubated at RT for 2 minutes. After centrifugation (10,000 rpm, 10 minutes, 4°C), the upper aqueous phase was transferred to a new tube, an equal volume of 70% EtOH was added slowly and loaded onto a RNeasy mini column and centrifuged at 10,000 rpm for 30 seconds. The rest of the protocol was carried out as described for the RNA extraction from TRAP samples. Eluted RNA was placed on ice immediately and RNA concentration was determined by Nanodrop (Thermo Scientific). The RNA was snap-frozen on dry ice and stored at -80°C.

2.4.8 Agilent Bioanalyzer Pico Assay.

RNA integrity (RIN) was assed using the Agilent RNA 6000 Pico Kit (Agilent) as per the manufacturer's instructions. All reagents were allowed to equilibrate to RT for 30 minutes before use while protecting them from light. Briefly, for gel preparation, 550 µl of RNA 6000 Pico gel matrices were placed into a spin filter and centrifuged for 10 minutes at 1,500*xg*. To run the chip, RNA 6000 Pico dye concentrate was mixed by vortexing for 10 seconds and spun down before adding 1 µl to a 65 µl aliquot of gel matrix. The gel-dye mix was vortexed thoroughly and centrifuged for 10 minutes at RT (13,000*xg*). Excess prepared gel-dye mix was stored at 4°C for up to one day (equilibrated to RT before use). The chip was carefully loaded with 9 µl of the gel-dye mix in the chip priming station (well "G"). The plunger of the syringe was pressed down for exactly 30 seconds, released and slowly pulled back up to the 1 ml position after 5 seconds. Next, 9 µl of the gel-dye mix ("G"-wells) and 9 µl of the RNA 6000 Pico conditioning solution (well "CS") were added. All 11

sample wells and the ladder well were filled with 5 µl of the RNA 6000 Pico marker and 1 µl of heat denatured RNA aliquots (70°C, 2 minutes) or 1 µl of the diluted RNA 6000 Pico ladder, respectively. TRAP UB and Total RNA aliquots were diluted 1:10 after heat denaturation to fit within the analysis range of the Agilent Pico chip (50-5,000 pg/µl in water). Unused sample wells were filled with 1 µl of ddH_2O. The chip was vortexed (IKA vortex mixer (Agilent)) for 60 seconds at 2,400 rpm and the run was started within 5 minutes (Pico RNA protocol, Agilent 2100 Bioanalyzer Instrument).

2.4.9 Quant-iT RiboGreen Assay.

RNA quantity was assed using the low-range assay (1-50 pg/µl) of Quant-iT RiboGreen RNA Assay Kit (Invitrogen) as per the manufacturer's instructions. Briefly, RiboGreen RNA Reagent was equilibrated at RT for 30 minutes protected from light. RNA was quantified (Excitation 485 nm; Emission 530 nm) using a fluorescence microplate reader (Synergy HT, Biotek). Fluorescence emission of unknown RNA concentration was plotted versus a standard curve (increasing concentrations of ribosomal (r)RNA standard 16S/23S *E. coli*). Concentrated RNA reagent was diluted 2,000-fold in TE buffer (10 mM Tris-HCl, 1 mM EDTA, pH 7.5) to a RNA reagent working solution and kept aside protected from light for up to a few hours. For the standard curve, a 100 µg/ml RNA solution was diluted 50-fold into TE (2 µg/ml). This 2 µg/ml RNA solution was further diluted 20-fold into TE (100 ng/ml) to prepare the dilution series. For the serial dilution of the standard curve 100 µl of standard #1-10 was pipetted in a 96-well plate in duplicates. Also in duplicates, 1 µl of TRAP RNA (UB/Total RNA 1:10 diluted) was added. After adding 100 µl of the RNA Reagent working solution to all wells, the plate was incubated for 2-5 minutes at RT, protected from light before measuring the sample fluorescence.

2.4.10 cDNA synthesis.

RNA was transcribed into complementary DNA (cDNA) with a SuperScript III or IV VILO Reverse Transcriptase Master Mix (Life Technologies) according to manufacturer's instructions. For each 20 µl reaction, the following components were added:

Reaction Mix	Volume/ reaction
RNA	Different amounts (3-100 ng), depending on experiment
SuperScript III/ IV VILO Master Mix	4 µl
ddH_2O	Up to 20 µl

The reaction was run on DNA Engine Tetrad 2 Peltier Thermal Cycler (Bio-Rad). For each reaction, a "no RNA" sample was added as a control. The cDNA was stored at -20°C until PCR amplification.

2.4.11 Quantitative real-time PCR analysis.

All qPCR reactions were run on a StepOnePlus Real-Time PCR System (Applied Biosystems). The cDNA was 1:10 diluted with nuclease-free water before running the reaction. The reaction mix was pipetted in a 96-well plate in duplicates including a negative and a "no RNA" control. Copy-thresholds for the gene of interest compared to the geometric mean of reference gene amplifications (GAPDH, beta-Actin, and UBI c) were established using the comparative C_t method. qPCR master mixes were prepared using FastSYBR Green Master Mix (Invitrogen) according to the following protocol (25 µl qPCR reaction):

Reaction Mix	Volume/ reaction
FastSYBR Green Master mix	12.5 µl
Forward Primer (10 uM)	0.2 µl
Reverse Primer (10 uM)	0.2 µl
Nuclease-free Water	7.1 µl
cDNA (1:10 dilution)	5 µl

The qPCR was run using the following programme:

95°C	20s	
95°C	3 sec	Repeat for 40 cycles
60°C	30 sec	

Gene	# in -20°C	Forward Sequence (5'->3')	TM [°C]	Reverse Sequence (5'->3')	TM [°C]	Product length [bp]
Beta-Actin	F	GGCTGTATTCCCCTCCATCG	61.4	CCAGTTGGTAACAATGCCATGT	58.4	154
GAPDH	M	AACTTTGGCATTGTGGAAGG	55.3	GGATGCAGGGATGATGTTCT	57.3	125
Ubiquitin C	G	CGTACCTTCCTCACCACAGT`	59.4	AAACTAAGACACCTCCCCCA	57.3	80

Table 2. 14 ***qPCR housekeeping primers.***
Primer stock: 100 µmol. Primer working: 1:10 dilution.

Gene	# in -20°C	Forward Sequence (5'->3')	TM [°C]	Reverse Sequence (5'->3')	TM [°C]	Product length [bp]
DAT	J	ACACCCGCTGCTGAGTATTT	57.3	AGGTCATCAATGCCACGACT	57.3	68
GAD2	K	TGGGTTTGAGGCACACATTG	57.3	GTGTGTTGAGGCTTCCCATC	59.4	111
GFAP	L	ACCGCATCACCATTCCTGTA	57.3	GCCTTCTGACACGGATTTGG	59.4	83
TH	I	TGTTGGCTGACCGCACAT	56	GCCCCCAGAGATGCAAGTC	61	61

Table 2. 15 ***qPCR primers used for TRAP RNA analysis.***
Primer stock: 100 µmol. Primer working: 1:10 dilution.

Gene	# in -20°C	Forward Sequence (5'->3')	TM [°C]	Reverse Sequence (5'->3')	TM [°C]	Product length [bp]
Atp5e	5	GACAGGCTGGACTCAGCTAC	60	CCCGAAGTCTTCTCAGCGTT	60	103
BMP7	9	CGAGACCTTCCAGATCACAGT	59.2	CAGCAAGAAGAGGTCCGACT	59.4	73
COX20	13	CGGGGCGATGGAGAGGA	60.5	TCTCGAGCACATGGAGTGTT	59	118
CTsB	17	GGCTCTTGTTGGGCATTTGG	60	ACTCGGCCATTGGTGTGAAT	60	71
CtsS	21	TTTGGAGTGAGCACCACACTT	60	CACACCAGGGGCATCCAAAA	60.8	90
Snap23	27	AGTGAGCTTCACTTCTGAACCC	60.2	AATGGGACCATGCCATGACT	59.4	141
SNAP25	29	TTTCTCAGTGGCGTTTGCTG	59.3	GTGGCAGTAGCTCTGTGGAAT	60	117
Timm8b	33	AGCGGACGAAGCGGAGTTA	61.3	TTTTCAGTGCGGGAGTCTAGC	60.3	144

Table 2. 16 ***qPCR primers used for RNA-Seq validation.***
Primer stock: 100 µmol. Primer working: 1:10 dilution.

2.4.12 TRAP qPCR data analysis

First the TRAP IP RNA for each gene was divided by the TRAP Total RNA (whole MB/STR input), to determine the fold-enrichment (IP/Input) to measure the degree to which the transcript is enriched in the IP relative to the whole input tissue. Because the IP is divided by the input, changes in the absolute expression level of a transcript within the tissue have no effect on the fold-enrichment. For statistical analysis, Prism software version 5.0 (GraphPad) was used. Data from qPCR analysis were analysed using a one-way or two-way ANOVA followed by Tukey's or Dennett's post hoc analysis unless otherwise indicated. Data are shown ±SEM.

2.5 Materials and Methods - Bioinformatics.

Bioinformatics analysis have been performed by Dr Frank Wessely and Dr Jimena Monzon-Sandoval (Webber group, DPAG, University of Oxford). The materials and methods section of this thesis has been written with support by Dr Jimena Monzon-Sandoval.

2.5.1 Pilot RNA-Sequencing.

For the Pilot RNA-Sequencing (RNA-Seq), RNA of two *THTR* TRAP pilot experiments was analysed at the High-Throughput Genomics Group at the Wellcome Trust Centre for Human Genetics (WTCHG, Oxford). The TRAP Total and IP RNA from either young (3 months; *mSnca-/-*, *THTR+ mSnca-/-*, *THTR+/+ mSnca-/-*) or old (18 months; *THTR+ mSnca-/-*) were used. For both experiments, 5.6 ng of RNA was converted to cDNA using the SMARTer Ultra Low RNA Kit for Illumina Sequencing (Clontech) followed by end-repair, A-tailoring, and adapter-ligation of the cDNA. The resulting libraries were size selected and multiplexed and sequenced together on two lanes of an Illumina HiSeq2500 Rapid Mode 51 System. Resulting reads were aligned to the mouse37 reference genome. Quality control (QC) was performed with FastQC and Rqc packages which found an adapter contamination for read 1 and 2 that presented as an over-represented sequence of 31 bp:

AAGCAGTGGTATCAACGCAGAGTACATGGGG

This feature stems from the SMARTer oligo and is a common problem of the 2nd read due to the amplification chemistry of the SMARTer protocol (Email communication with Dr Sarah Lamble, WTCHG, Oxford).

Sample Name	RNA-Seq ID	TRAP fraction	Genotype	Age (months)	Gender	Pooled
THTR++ IP RNA	IP++	IP	THTR+/+	3	mixed	false
THTR++ Total RNA	Total++	Total	THTR+/+	3	mixed	false
THTR+ IP RNA	IP+	IP	THTR+	3	mixed	false
THTR+ Total RNA	Total+	Total	THTR+	3	mixed	false
non-tg IP RNA	IP-	IP	Non-tg	3	mixed	false
non-tg Total RNA	Total-	Total	Non-tg	3	mixed	false
THTR+ IP RNA	IP+ old	IP	THTR+	18	mixed	false
THTR+ Total RNA	Total+ old	Total	THTR+	18	mixed	false
THTR++ IP RNA	IP++	IP	THTR+/+	3	mixed	false
THTR++ Total RNA	Total++	Total	THTR+/+	3	mixed	false
THTR+ IP RNA	IP+	IP	THTR+	3	mixed	false
THTR+ Total RNA	Total+	Total	THTR+	3	mixed	false
non-tg IP RNA	IP-	IP	Non-tg	3	mixed	false
non-tg Total RNA	Total-	Total	Non-tg	3	mixed	false
THTR+ IP RNA	IP+ old	IP	THTR+	18	mixed	false
THTR+ Total RNA	Total+ old	Total	THTR+	18	mixed	false

Table 2. 17 Summary of pilot RNA-Seq samples.

2.5.2 RNA-Sequencing and data processing.

For the RNA-Seq, RNA of *THTR* TRAP experiments in young and old *THTR+/+ mSnca-/-* versus *THTR+/+ hSNCA+ mSnca-/-* mice was analysed at the WTCHG, Oxford. Here, 2.4 ng of four IP RNA samples per genotype, age and gender, as well as pooled IP and pooled Total TRAP RNA for each genotype plus age group were converted to cDNA using the SMARTer Ultra Low RNA Kit for Illumina Sequencing (Clontech) followed by end-repair, A-tailoring, and adapter-ligation of the cDNA. The resulting libraries were size selected and multiplexed and sequenced together over five lanes of a flow cell of an Illumina HiSeq4000 75 bp System. Around 8 million (± 1.5 M) reads per sample per lane were obtained. The total number of reads per sample ranged from 26 million to 63 million. The resulting reads have been aligned to the reference mouse transcriptome (*Mus musculus GRCm38*) using *Kallisto v0.43.0* (Bray et al., 2016). cDNA and non-coding (nc) RNA sequences available in ENSEMBLE (ftp release 87) were used to create an index against which reads were aligned and from which transcript abundances were estimated. Default parameters were used, except for the number of bootstraps which has been increased to 100. The number of counts and transcripts per million (TPM) has been summarised for each protein coding gene using *tximport* function in R (Soneson et al., 2016).

Sample Name	RNA-Seq ID	TRAP Fraction	Disease	Age (months)	Gender	Pooled
THTR++ A* IP RNA	IP1F12m	IP	CTRL	12	F	false
THTR++ B* IP RNA	IP2F12m	IP	CTRL	12	F	false
THTR++ C* IP RNA	IP3F12m	IP	CTRL	12	F	false
THTR++ D* IP RNA	IP4F12m	IP	CTRL	12	F	false
THTR++PD A* IP RNA	IP1F12mPD	IP	PD	12	F	false
THTR++PD B* IP RNA	IP2F12mPD	IP	PD	12	F	false
THTR++PD C* IP RNA	IP3F12mPD	IP	PD	12	F	false
THTR++PD D* IP RNA	IP4F12mPD	IP	PD	12	F	false
THTR++ A IP RNA	IP1M12m	IP	CTRL	12	M	false
THTR++ B IP RNA	IP2M12m	IP	CTRL	12	M	false
THTR++ C IP RNA	IP3M12m	IP	CTRL	12	M	false
THTR++ D IP RNA	IP4M12m	IP	CTRL	12	M	false
THTR++PD A* IP RNA	IP1M12mPD	IP	PD	12	M	false
THTR++PD B IP RNA	IP2M12mPD	IP	PD	12	M	false
THTR++PD C IP RNA	IP3M12mPD	IP	PD	12	M	false
THTR++PD D IP RNA	IP4M12mPD	IP	PD	12	M	false
THTR++ a* IP RNA	IP1F3m	IP	CTRL	3	F	false
THTR++ b* IP RNA	IP2F3m	IP	CTRL	3	F	false
THTR++ c* IP RNA	IP3F3m	IP	CTRL	3	F	false
THTR++ d* IP RNA	IP4F3m	IP	CTRL	3	F	false
THTR++PD a* IP RNA	IP1F3mPD	IP	PD	3	F	false
THTR++PD b* IP RNA	IP2F3mPD	IP	PD	3	F	false
THTR++PD c* IP RNA	IP3F3mPD	IP	PD	3	F	false
THTR++PD d* IP RNA	IP4F3mPD	IP	PD	3	F	false
THTR++ a IP RNA	IP1M3m	IP	CTRL	3	M	false
THTR++ b IP RNA	IP2M3m	IP	CTRL	3	M	false
THTR++ c IP RNA	IP3M3m	IP	CTRL	3	M	false
THTR++ d IP RNA	IP4M3m	IP	CTRL	3	M	false
THTR++PD a IP RNA	IP1M3mPD	IP	PD	3	M	false
THTR++PD b IP RNA	IP2M3mPD	IP	PD	3	M	false
THTR++PD c IP RNA	IP3M3mPD	IP	PD	3	M	false
THTR++PD d IP RNA	IP4M3mPD	IP	PD	3	M	false
	IPpool12m	IP	CTRL	12	B	true
	Totalpool12m	Total	CTRL	12	B	true
	IPpool12mPD	IP	PD	12	B	true
	Totalpool12mPD	Total	PD	12	B	true
	IPpool3m	IP	CTRL	3	B	true
	Totalpool3m	Total	CTRL	3	B	true
	IPpool3mPD	IP	PD	3	B	true
	Totalpool3mPD	Total	PD	3	B	true

Table 2. 18 Summary of RNA-Seq samples.

2.5.3 Principal component analysis (PCA).

For Principal component analysis (PCA), log transformed expression data given in TPM (*log2 (TPM + 1)*) and the *prcomp* functions from the stats R package (R Development Core Team, 2016) R Foundation for Statistical Computing, Vienna, Austria. https://www.R-project.org/) were used.

2.5.4 Hierarchical clustering.

For clustering analysis, TPM expression data have been used. Similarity between expression profiles was measured by the Spearman correlation (*p*) between each pair of samples, the Euclidean

distance based on (*1 - p*) was then used as an input for *hclust* using the Ward's clustering criterion. If the range of *p* included negative values, then the distance was based on (*2 – (p + 1)*). Only for comparisons with external datasets, we have first ranked gene expression (based on TPM data). In such cases, the removal of the principal component associated with the differences between datasets was done using *kill.pc* function from *swamp* R package ((Lauss et al., 2013) swamp: R package version 1.2.3. https://CRAN.R-project.org/package=swamp).

2.5.5 Differential expression analysis (DEA).

For differential expression analysis (DEA), data were pre-filtered, outlier samples, as well as lowly expressed genes were removed, defined as these with less than one TPM across the remaining 35 selected samples. *DESeq2* R package (Love et al., 2014) has been used for differential expression analysis (DEA). *DESeq* function has been used with default parameters, except for the minimum number of replicates for replace which has been set to infinite. Finally, the alpha threshold has been set to 0.05 in the results function of the same package.

2.5.6 Gene Ontology Enrichment analysis.

Gene Ontology (GO) annotations were accessed using *biomaRt* R package to *Ensembl mart version 87* (Durinck et al., 2005; Durinck et al., 2009). For each subset of differentially expressed genes (DEGs) the corresponding background gene population (i.e. including only genes that were tested for differential expression in a comparison) has been considered. Given the large number of GO terms, only biological process terms containing at least 50 genes in each background population have been tested. A p value has been estimated for each GO term tested, which comes from a Z-score derived from 1000 randomisations, from which an expected mean and standard error has been obtained. Finally, all p values have been adjusted for multiple testing. Only these GO terms with at least 2 genes and false discovery rate (FDR) <0.05 have been considered overrepresented.

2.5.7 Co-expression.

RNA-Seq expression data comprising several human brain structures across developmental ages from “BrainSpan” has been used to measure coordinated patterns of expression (Miller et al.,

2014). Only genes with a one to one orthologue relationship between mouse and human were considered for further co-expression analysis. Co-expression was measured as the Pearson correlation between gene expression levels across all samples between each gene pair.

Co-expression among differentially expressed genes.

For selected subsets of DEGs the average co-expression between all possible gene pairs has been measured. Further, the average co-expression of each set to that of 10,000 equally sized random samples of genes drawn from the gene background population has been compared. Here, the background population consisted of all one to one orthologues between human and mouse with gene expression data in both *BrainSpan* and our own dataset (not these pre-filtered for differential expression analysis). Next, a p value from the random samples counting the number of cases in which the average co-expression was equal or higher than the observed for each subset of DEGs was estimated.

Co-expression between differentially expressed genes and PD associated genes.

The co-expression between two subsets of genes (i.e. DEGs and genes associated to PD) has been measured. If no overlapping genes were found, the average co-expression between them was measured and compared with the 10,000 randomisations. In each randomisation, two non-overlapping random samples of genes were selected, each of them with an equivalent size to the original subsets, followed by measuring the average correlation between them (excluding correlations between gene pairs of the same subset). In the alternative case where a subgroup of genes is simultaneously contained in the two subsets, average co-expression between 1) genes only contained in subset A and these only contained in the subset B, 2) genes only contained in subset A and overlapping genes, 3) genes only contained in subset B and overlapping genes were measured. Accordingly, for 10,000 randomisations 3 subsets were created, representing A and B subsets and their corresponding overlap, each of them of an equivalent size and with measured average co-expression as described for the original subsets. Finally, a p-value has been estimated from 10,000 randomisations as previously described.

2.5.8 Protein-protein interactions.

A protein-protein interaction (PPI) network has been obtained by combining different resources: Protein-protein interactions from (*Biogrid*, *HitPredict* and *IntAct*), protein links (*STRING*, only these with an experimental score different to zero), protein complexes (*CORUM*) and interactions from shared reactions (*Reactome*). For each subset of DEGs the number of edges between them in the merged protein-protein interaction network has been counted. Then, by comparing the observed number of edges to that expected by chance was obtained by drawing 10,000 equally sized random samples of genes with a similar degree distribution. To take the degree distribution into account, the degree distribution for all the genes contained in the merged protein-protein interaction network was obtained, log transformed such distribution and then divided all genes in 20 bins according to their degree. In each randomisation from a bin the same number of random genes as these that fell in that bin from the original subset of genes has been observed. Finally, a p-value from 10,000 randomisations counting the number of cases in which the number of edges was equal or higher than the observed for the set of DEGs was estimated. In a similar way, the average clustering between each subset of DEGs using transitivity function in *igraph* R package was measured (Csárdi and Nepusz, 2006). When looking at the number of edges between two subsets of genes (i.e. links between DEGs and genes associated to PD) only edges between genes that do not belong simultaneously to both subsets were considered; thus, if there were overlapping genes the number of edges between subsets was not overestimated. Again, for comparison 10,000 equally sized random samples with similar degree distribution were obtained and a corresponding p-value was estimated.

2.5.9 Overlapping genes.

For an observed overlap between subsets of genes a p-value using equally sized random samples of genes has been estimated by considering only genes contained in the intersection of the background populations from which each gene list has been drawn from.

- CHAPTER 3 -

MOLECULAR CHARACTERISATION OF A BACTRAP TRANSGENIC ALPHA-SYNUCLEIN OVER-EXPRESSION MOUSE MODEL

3.1 Overview

This chapter covers the generation and in-depth molecular characterisation of our novel *TH-bacTRAP* (THTR) transgenic mouse line. The data presented in this chapter include the analysis of fluorescent ribosomal transgene (eGFP-L10a) expression in dopaminergic neurons (DAn), as well as in a range of other brain regions. Characterisation experiments were performed to prove that transgene expression follows the correct temporal and spatial expression profile of endogenous mouse tyrosine hydroxylase (TH). To confirm that the insertion of the bacTRAP vector did not have any effects on protein expression, protein and integrity analysis of human wild-type (WT) alpha-Synuclein (aSyn), ribosomal protein L10a (RPL10a), and nigrostriatal dopaminergic markers (TH and dopamine transporter (DAT)) was performed. Finally, the chapter investigates the susceptibility of nigrostriatal dopaminergic cell populations to progressive neurodegeneration in aged double transgenic *THTR*/*hSNCA+* mice and discusses the expression analysis of TH and eGFP by stereological cell counts.

Chapter aims

1) To generate experimental cohorts of *THTR* and double transgenic *THTR/hSNCA+* mice on a mouse aSyn knock-out (KO) and mouse aSyn WT background for future genome-wide gene expression profiling studies.
2) To investigate fluorescent eGFP-L10a transgene expression in the *THTR* mouse line.
3) To characterise the eGFP-L10a-positive dopaminergic cell population.

3.2 Introduction

3.2.1 *hSNCA+* transgenic mouse line

Previously, the Wade-Martins laboratory generated a BAC transgenic mouse line in which human aSyn (*hSNCA*) is over-expressed (OVX) on a mouse aSyn KO (*mSnca-/-*) background. The BAC contains the complete human aSyn gene locus of 111 kb plus approximately 20 kb of upstream regulatory elements. The new aSyn transgenic mouse line, here abbreviated *hSNCA+*, was produced by pronuclear injection using C57Bl/6/CBA F1 hybrid embryos and the transgene integration site was found close to the centromere on one copy of chromosome 4 using fluorescent *in-situ* hybridisation (FISH). The resulting *hSNCA+* line was backcrossed for over nine generations on a pure C57Bl/6 background before further crossing onto a *mSnca-/-* background to preclude confounding interactions with endogenous mouse aSyn (DPhil Thesis: S. Senior, 2007; S. Anwar thesis, 2011; S. Janezic, 2013).

Over-expression of aSyn in a transgenic mouse model enables the study of the deleterious effects of aSyn dysfunction as seen in sporadic and familial PD (Gründemann et al., 2008; Miller et al., 2004). The transgene expression profile in *hSNCA+* mice accurately recapitulates endogenous mouse aSyn expression but at a 2x increased level compared to endogenous mouse aSyn in age matched C57Bl/6 animals (Janezic et al., 2013). The model is mirroring the levels observed in PD patients with aSyn locus multiplications (Chartier-Harlin et al., 2004; Singleton et al., 2003). Aged *hSNCA+* mice display progressive motor deficits accompanying a loss of DAn specifically in the SNc, whereas neurons in the VTA are largely spared recapitulating events as seen in patients with PD. At young age the dorsal striatum of these mice shows a DA release deficit with no change in overall striatal DA content which persists the entire lifespan of the animal (Janezic et al., 2013). This change demonstrated by fast-scan cyclic voltammetry could represent one of the earliest stages of PD neurodegeneration (Sawamoto et al., 2008) which is in line with previous work on Synuclein double- or triple-KO mice which showed that Synuclein proteins negatively regulate DA release only in the dorsal but not the ventral striatum (Anwar et al., 2011; Senior et al., 2008). Until now, early disease-related changes in DAn are largely unclear making *hSNCA+* mice an important tool in

providing insight into the potential early neural processes that take place at the onset of neurodegeneration in PD.

3.2.2 *TH-bacTRAP* (*THTR*) transgenic mouse line

To enable the study of cell-type specific gene expression profiling of mRNA isolated from DAn, the Wade-Martins laboratory has designed a second BAC vector for the generation of an additional transgenic mouse line. This second BAC transgenic line enables a technique, developed by the Heintz laboratory, called TRAP (Heiman et al., 2008; Heiman et al., 2014) that allows the isolation of actively translated mRNAs from a cell population of interest. Here, we put the eGFP-L10a transgene expression under the control of the mouse TH promoter, a defining marker for DAn (Haavik and Toska, 1998). Since TH catalyses the rate limiting step in the biosynthesis of catecholamines including DA and noradrenaline, eGFP-L10a expression should be present in all catecholamine-containing cells (Nagatsu et al., 1964).

The bacTRAP vector was constructed by a former PhD student (DPhil Thesis: S. Janezic, 2013) based on the original TRAP vector 'S296' (Dr Nathaniel Heintz; Rockefeller University, New York) and a fully sequenced plasmid (pBACe3.6; BACPAC Resources Centre at the Children's Hospital Oakland Research Institute) that contained the mouse *TH* genomic locus and promoter (DPhil Thesis: S. Janezic, 2013). In the *TH-bacTRAP* construct, the eGFP-L10a transgene was placed directly after the ATG start site of the mouse *TH* promoter, replacing the first exon of the mouse *TH* gene. The BAC contains 43 kb of the upstream *TH* promoter region including an alternative first *TH* exon located 30 kb upstream of the transcription start site. However, further exonic, intronic, as well as the downstream 3' UTR of the native mouse *TH* locus has been removed from the BAC (Figure 3. 1 B).

Functionality of the bacTRAP vector has been tested by preliminary experiments *in vitro*. Transient transfection of HEK-293 cells with the bacTRAP vector enabled analysis of native fluorescence from the eGFP-L10a fusion protein under the native *TH* promoter. Fluorescence microscopy at 48 hours' post-transfection shows that eGFP-L10a localises to the cytoplasm and nucleolus of transfected cells (Figure 3. 1 A) as previously demonstrated (Heiman et al., 2008; Thomas et al., 2012). Further,

western blot analysis from HEK-293 cell lysates using an anti-GFP or anti-RPL10A antibodies showed the expected 52 kDa band for the fusion protein (eGFP: 27 kDa; L10a: 25 kDa; eGFP-L10a: 52 kDa) and anti-RPL10a also detects endogenous L10a at 25 kDa (Figure 3. 1 C, C'). The caesium chloride purified bacTRAP construct was pronuclear-injected into C57Bl/6 oocytes to ensure that *THTR* mice were generated on the same genetic background as *hSNCA+* mice, to aid in subsequent crosses generating a double transgenic *THTR/hSNCA+* mouse line. The *THTR/hSNCA+* mice will serve as a useful tool for the analysis of gene expression profiles of dopaminergic cell populations in our *hSNCA+* PD mouse model.

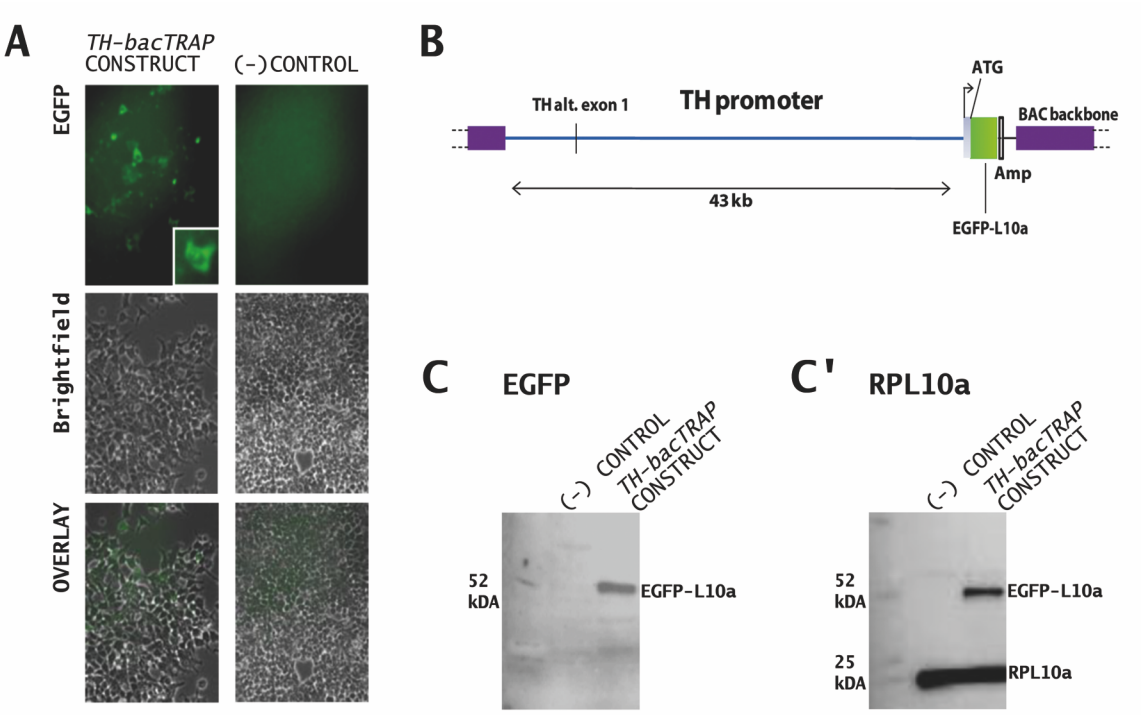


Figure 3. 1 ***Preliminary in vitro results testing the TH-bacTRAP vector used for the generation of the THTR transgenic mouse line.***

(A) Analysis of transient transfection of HEK-293 cells with the TH-bacTRAP vector using native fluorescence from the eGFP-L10a fusion protein at 48 hours' post-transfection. GFP fluorescence localised to the cytoplasm and nucleolus of transfected cells. (B) Schematic depicting the design of the TH-bacTRAP construct which contains 43 kb of TH promoter region including an alternative first exon in the upstream promoter region. The eGFP-L10a transgene was placed directly below the TH mouse promoter ATG start site while further exonic, intronic, as well as downstream regions have been removed from the BAC. (C, C') western blotting using an anti-GFP or anti-RPL10A antibodies show the expected 52 kDa band for the fusion protein. Anti-RPL10a also detects endogenous L10a at 25 kDa. Experiments performed by S. Janezic.

3.3 Results

3.3.1 Generation, breeding and maintenance of bacTRAP transgenic mouse lines

To generate a genetic tool for the genome-wide gene expression analysis of DAn in our transgenic *hSNCA+* PD mouse model, *THTR* transgenic mice were interbred with *hSNCA+* mice. Initially, breeding pairs were set up to cross *hSNCA*+ transgenic mice with hemizygous *THTR* (*THTR+)* mice. All mice were maintained on a homozygous m*Snca*-/- background unless otherwise indicated; the human aSyn transgene was maintained in a hemizygous state. The breeding scheme (Figure 3. 2 A) allowed the generation of TRAP-positive (*THTR+ hSNCA+* m*Snca*-/-*; THTR+* m*Snca*-/-) and TRAP-negative (*hSNCA+* m*Snca*-/-*;* m*Snca*-/-) littermate control animals in each generation (DPhil Thesis: S. Janezic, 2013); TRAP-positive mice were utilised for experiments, TRAP-negative mice served as controls. Control mice, *hSNCA*+ and *mSnca*-/-, were utilised as negative controls for the TRAP-mediated pull-down of mRNA allowing the estimation of non-specific background RNA binding. (Figure 3. 2 C).

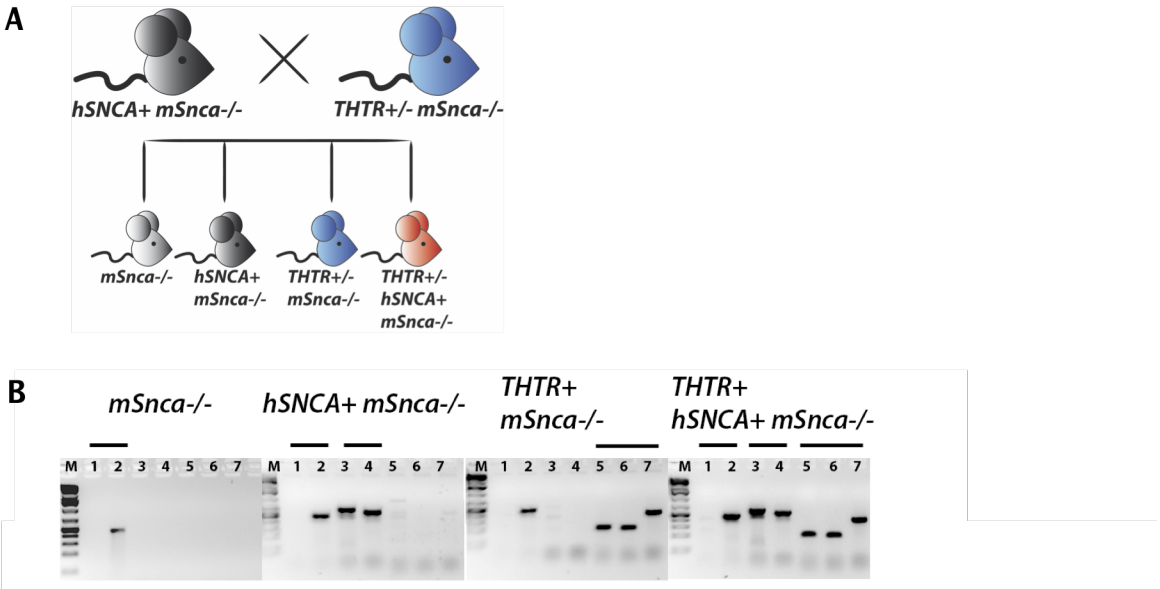


Figure 3. 2 ***Breeding Scheme for the double transgenic* THTR */hSNCA+ experimental cohort.***

(A) Overview of the initial breeding strategy (S. Janezic Thesis, 2013). (B) Representative genotyping results. Two primer pairs detect presence/absence of wild-type (1) and knock-out (2) mouse alpha-Synuclein to verify the mSnca-/- background. Other primers detect the hSNCA+ construct at the 3' (3) and 5' junctions (4) of the BAC backbone. (5-7) Three primer pairs detect the TH-bacTRAP construct via junctions of the eGFP-L10a transgene, the TH genomic locus and the TH-bacTRAP construct, respectively (5= TH-eGFP; 6= Amp-BAC; 7= BAC-TH). THTR= TH-bacTRAP. -/-= Knock-out. += Heterozygous. +/+= Homozygous. += Hemizygous. OVX= over-expressed. mSnca= mouse alpha-Synuclein. hSNCA= human alpha-Synuclein.

3.3.2 Molecular characterisation of our novel *THTR* transgenic moue line

We used the TH promoter to drive eGFP-L10a expression aiming to express eGFP-L10a specifically in catecholaminergic neurons, with focus on the midbrain (SNc and VTA). Since eGFP-L10a was placed under control of the endogenous mouse TH promoter within the BAC, the eGFP-L10a fusion protein should be expressed in DAn, thus, all TH-positive cells. TH catalyses the rate-limiting step in the biosynthesis of catecholamines which includes DAn (Nagatsu et al., 1964), therefore no eGFP-L10a transgene expression was expected in non-catecholaminergic brain regions. In the following paragraphs, we confirm that eGFP-L10a expression is restricted to DAn of the midbrain (SNc and VTA), without ectopic expression in non-dopaminergic brain regions, such as hippocampus or cortex. Furthermore, expression in the striatum and locus coeruleus (LC) was analysed.

eGFP-L10a is expressed in DAn of young and aged THTR mice

Initial molecular characterisation of *THTR* mice by native eGFP fluorescence from the eGFP-L10a fusion protein was investigated in unstained coronal midbrain sections of hemizygous and homozygous *THTR* mice. The sections were mounted directly after cutting on a vibrating microtome without further processing. Fluorescence was compared at 3 months and 18 months of age using stitched images covering the complete slide (Figure 3. 3). As expected, eGFP fluorescence was restricted to the SNc/VTA area where TH is expressed. Comparing hemizygous and homozygous *THTR* mice, a more pronounced eGFP expression was visible in homozygous *THTR* mice compared to hemizygous littermates. eGFP expression seemed to decrease with age for both hemizygous and homozygous mice; aged *THTR* mice exhibited less eGFP fluorescence when compared to the younger age time-point (Figure 3. 3). The intracellular localisation of transgene expression was detected in the cytoplasm and nucleolus of cells in the SNc which matches the intracellular localisation seen in HEK-293 cells transiently transfected with the bacTRAP construct (Figure 3. 3 E, E'). This intracellular localisation is consistent with previously reported expression patterns of the eGFP-L10a protein (Heiman et al., 2008; Thomas et al., 2012).

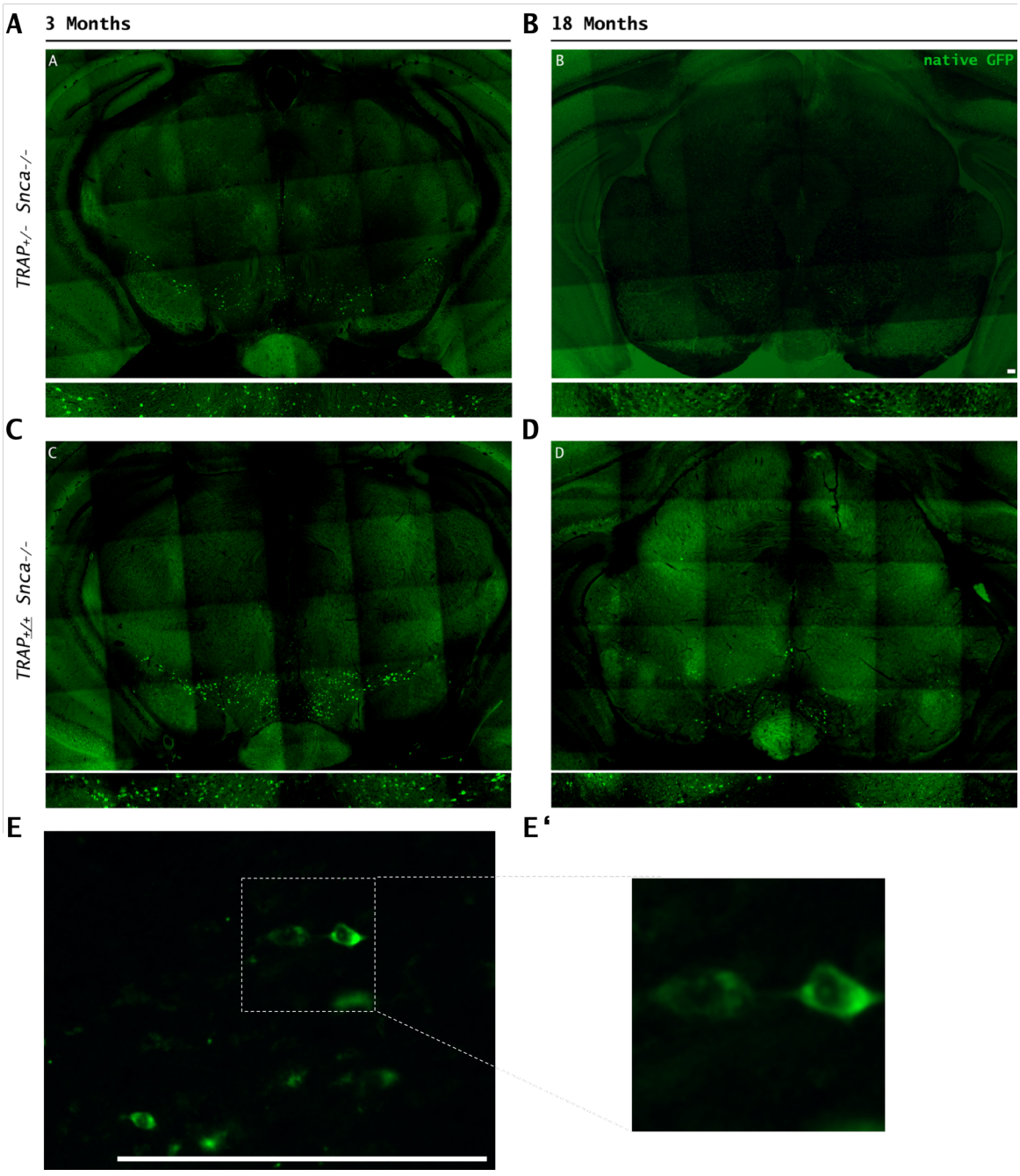


Figure 3. 3 ***Native eGFP fluorescence is restricted to DAn in the midbrains of hemizygous and homozygous THTR mice comparing 3 months and 18 months.***

(A-D) eGFP-L10a is expressed in the Substantia nigra pars compacta (SNc) and ventral tegmental area (VTA) of TRAP-positive mice (stitching of 36 images). A horizontal close-up through the SNc and VTA region is shown below the image. Hemizygous mice (upper panel) show less eGFP at 3 (A, C) and 18 months (B, D) compared to homozygous mice (lower panel). Reduced eGFP expression at 18 months compared to young animals. Scale bar= 200 µm. (E, E') The intracellular profile of eGFP-L10a expression in young TRAP-positive mice (3 months) is detectable in the cytoplasm and nucleolus of nigrostriatal cells in TRAP-positive mice only. Scale bar= 200 µm. TRAP+(+)= THTR mouse line. -/-= Knock-out. += Hemizygous. +/+= Homozygous. mSnca= mouse alpha-Synuclein. eGFP= enhanced green fluorescent protein.

Analysis of DAn-specific translatome using eGFP-L10a requires the accurate reproduction of endogenous TH expression profiles. Thus, cellular identity of DAn in young (3 months) and aged (18 months) *THTR* mice was assessed by double immunofluorescence labelling using anti-GFP and anti-TH fluorescent antibodies on sequential coronal brain sections. In greater detail, Figure 3. 4 shows restricted eGFP expression in TH-positive cells of the SNc and VTA in young TRAP-positive animals with TRAP-negative animals not showing any GFP-positive cells. Surprisingly, only a sub-set of DAn co-expressed GFP and TH. Since transgene expression is controlled by the endogenous mouse *TH* promoter the presence of eGFP-L10a in only a small sub-set of TH-positive neurons was unexpected. Homozygous *THTR* mice show more GFP-positive cells compared to hemizygous mice, as seen before by native fluorescence.

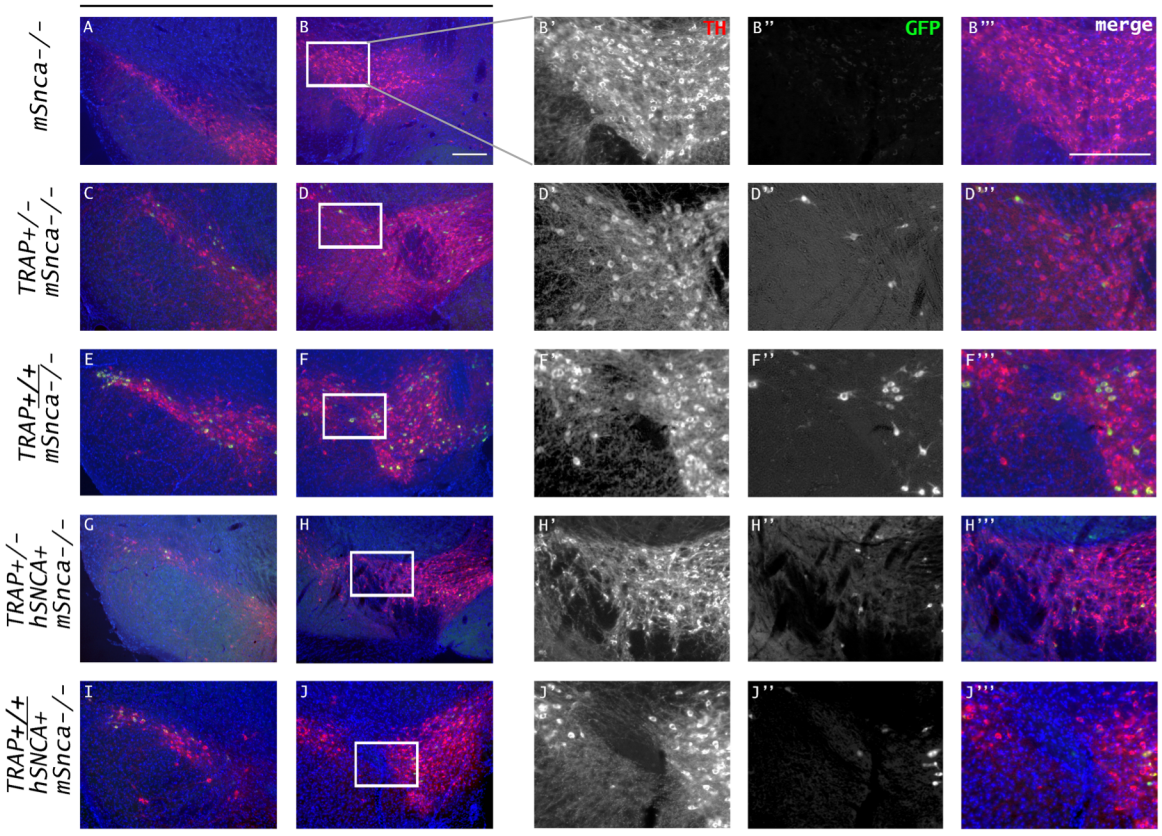
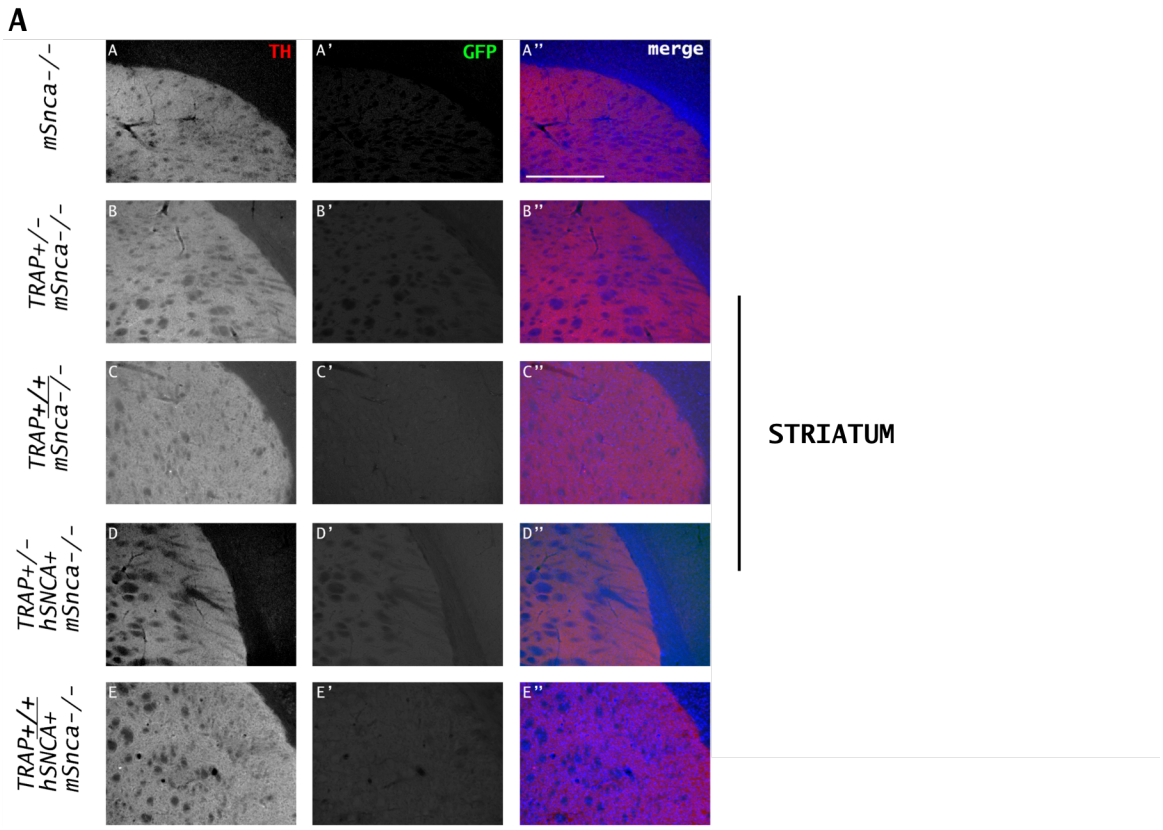


Figure 3. 4 ***TH and eGFP are co-expressed in DAn in the midbrain (3 months).***

Coronal midbrain sections were stained for tyrosine hydroxylase (TH) (red) and GFP (green). ***LEFT PANELs*** *(A-J)****:*** *Labelling confirm TH/eGFP co-expression in DAn of the Substantia nigra (SNc) and Ventral tegmental area (VTA). Not all TH-positive cells express eGFP despite being controlled by the same promoter. Homozygous mice express more eGFP-positive cells compared to hemizygous littermates. No GFP reactivity is found in TRAP-negative mice. Representative images are shown.* ***RIGHT PANELs*** *(B', D', F' H' J')****:*** *Close-up of the inserts (panel 1). Scale bars= 200 µm. TRAP+(+)= THTR mouse line. -/-= Knock-out. +/+= Homozygous. += Hemizygous. mSnca= mouse alpha-Synuclein. hSNCA= human alpha-Synuclein. GFP= green fluorescent protein. DAn= dopaminergic neurons.*

The correct regionally restricted expression of eGFP was investigated in further brain regions. As expected, Figure 3. 5 shows that no transgene expression was found in the hippocampus or the cortex. Interestingly, no expression of eGFP was found in the striatum either, where DAn axonal terminals are found (Figure 3. 5). This lack of expression may be caused by the fact that eGFP-L10a is a ribosomal protein with expression restricted to cell bodies rather than the terminals of DAn where TH expression is found. Furthermore, it could be possible that immunofluorescence is not sensitive enough to reveal eGFP-tagged ribosomes located at the synapse or in axons.



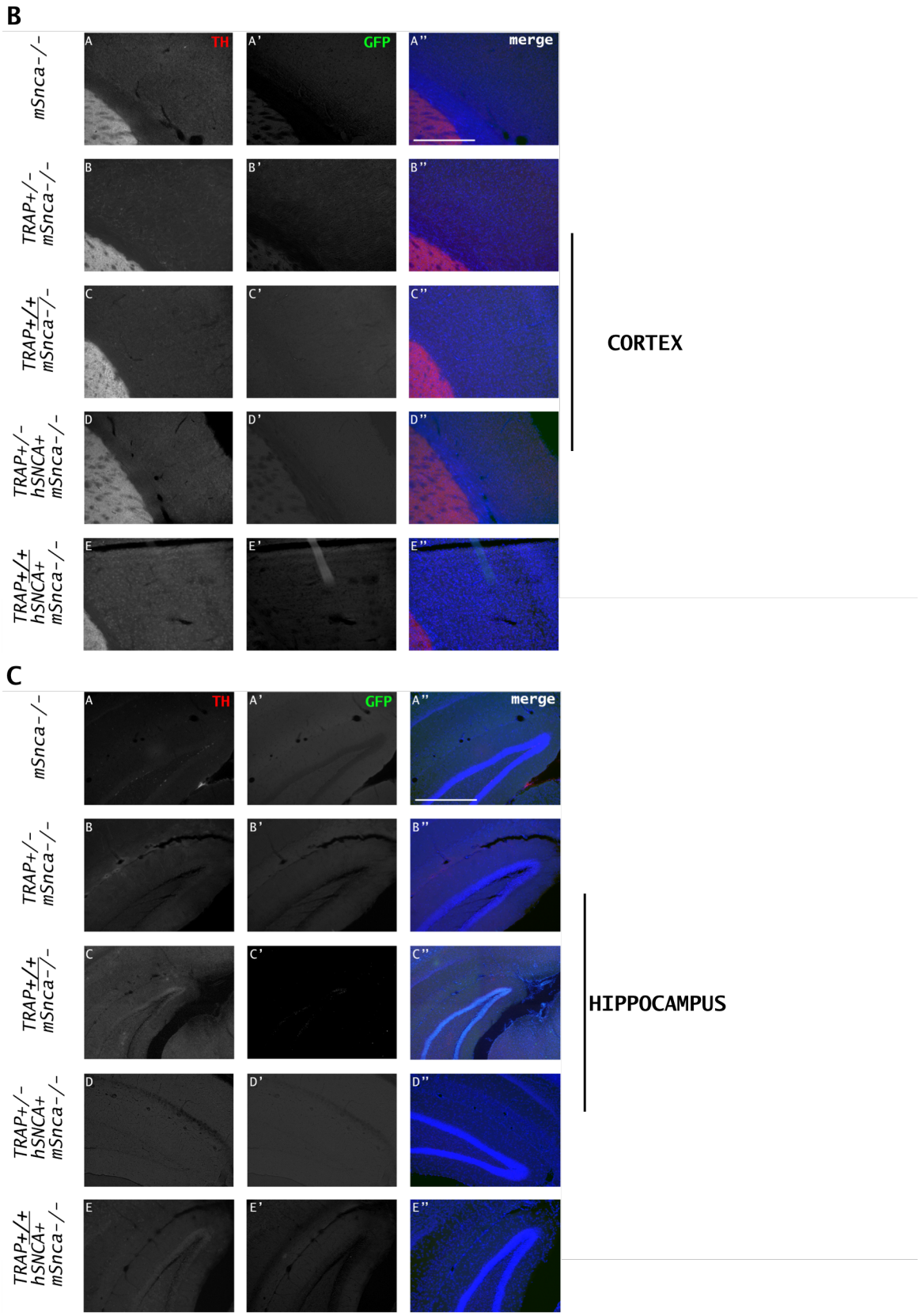


Figure 3. 5 ***Analysis of eGFP-L10a transgene shows no signs of ectopic expression (3 months).***

Coronal midbrain sections were stained for TH (red) and GFP (green). (A $^{(A-E)}$) No GFP-immunoreactivity could be detected in TH-positive neurons of the striatum. GFP is not expressed in brain regions were TH is not expressed ((B $^{(A-E)}$) cortex or (C $^{(A-E)}$) hippocampus). Representative images are shown. Scale bars= 200 µm. TRAP+(+)= THTR mouse line. -/-= Knock-out. +/+= Homozygous. += Hemizygous. mSnca= mouse alpha-Synuclein. hSNCA= human alpha-Synuclein. TH= tyrosine hydroxylase. GFP= green fluorescent protein.

Double TH/GFP immunofluorescence was repeated on sequential coronal brain sections in aged *THTR* animals and littermate controls (18 months). Figure 3. 6 shows eGFP-L10a transgene expression in the SNc and VTA, mirroring the findings in young mice. Despite the low eGFP signal by native fluorescence in aged mice, antibodies could pick up stronger GFP expression in DAn. Again, only a small fraction of TH-positive cells also co-expressed GFP.

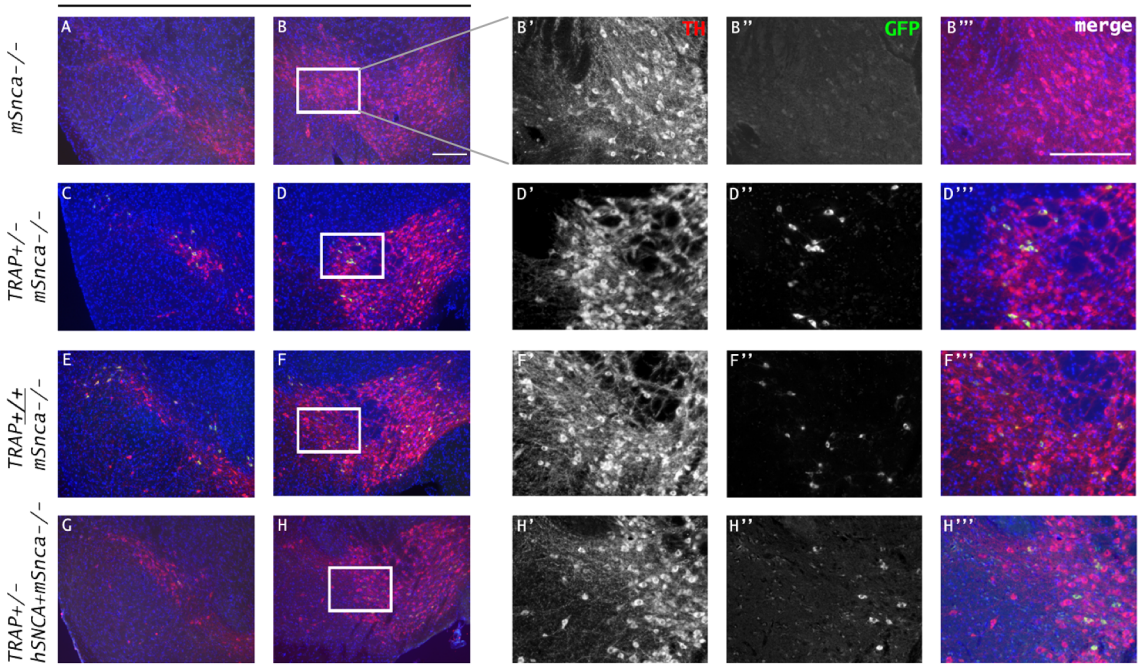
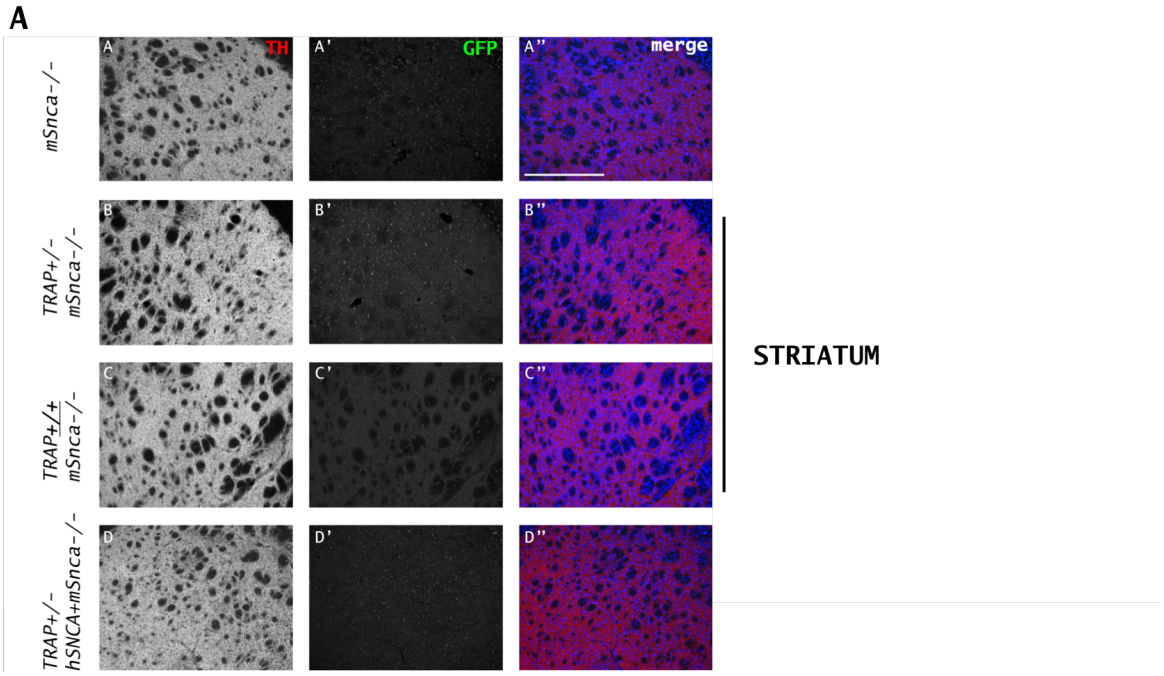
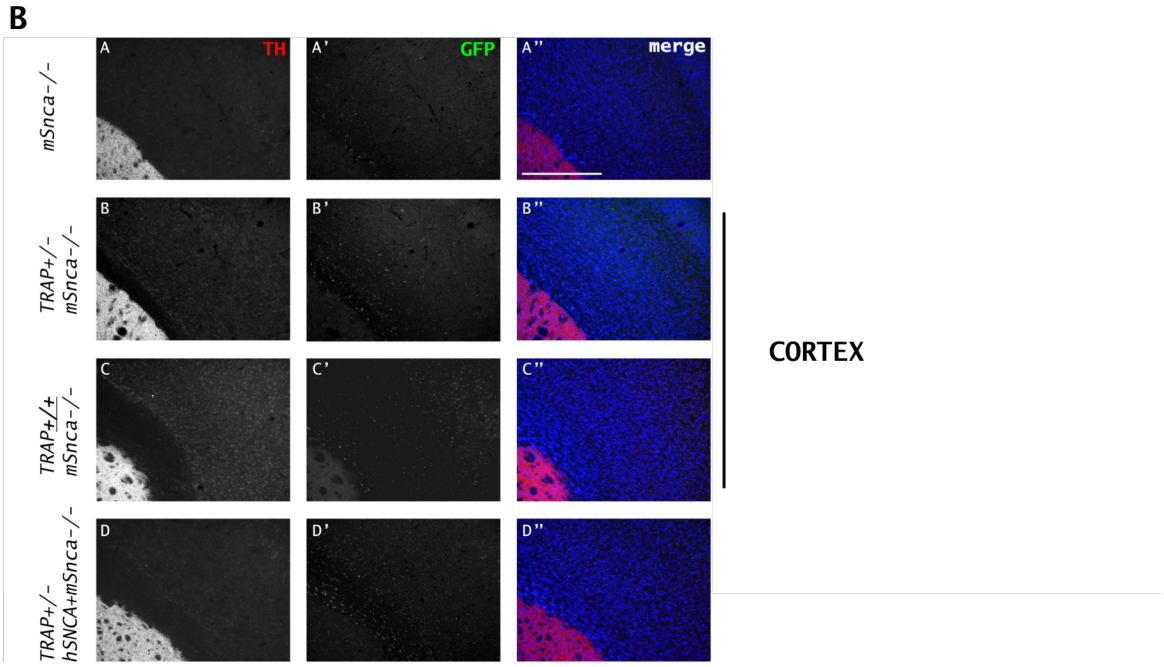


Figure 3. 6 ***Analysis eGFP expression in midbrain DAn shows consistent results in aged mice (18 months).***
Coronal midbrain sections stained for either tyrosine hydroxylase (TH) (red, A) and GFP (green). ***LEFT PANELs*** $^{(A\text{-}J)}$***:*** *TH and eGFP are co-expressed in some but not all dopaminergic neurons of the Substantia nigra (SNc) and Ventral tegmental area (VTA). Not all TH-positive cells express eGFP despite being controlled by the same promoter. No GFP reactivity is found in TRAP-negative mice.* ***RIGHT PANELs*** $^{(B', D', F' H' J')}$***:*** *Close-up of the inserts (panel 1). Scale bars= 200 µm. TRAP+(+)= THTR mouse line. -/-= Knock-out. +/+= Homozygous. += Hemizygous. mSnca= mouse alpha-Synuclein. hSNCA= human alpha-Synuclein. GFP= green fluorescent protein. DAn= dopaminergic neurons.*

Immunofluorescence analysis of striatum, cortex, and hippocampus in aged transgenic *THTR* mice recapitulated the results seen at 3 months, eGFP-L10a expression was absent from these brain regions (Figure 3. 7).


A
mSnca-/-
TRAP+/- mSnca-/-
TRAP+/+ mSnca-/-
TRAP+/- hSNCA+mSnca-/-
A TH
A' GFP
A'' merge
B
B'
B''
C
C'
C''
D
D'
D''
STRIATUM


B
mSnca-/-
TRAP+/- mSnca-/-
TRAP+/+ mSnca-/-
TRAP+/- hSNCA+mSnca-/-
A TH
A' GFP
A'' merge
B
B'
B''
C
C'
C''
D
D'
D''
CORTEX

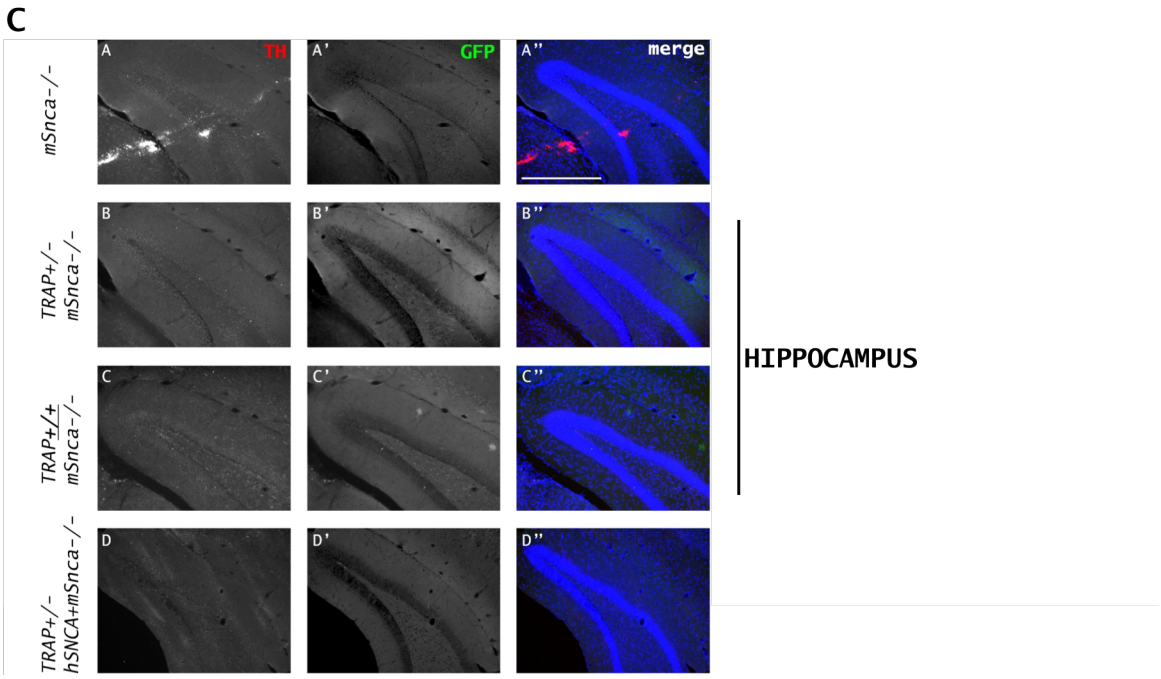


Figure 3. 7 ***Confirmation of region-specific expression of the eGFP-L10a transgene in aged animals (18 months).***
Coronal midbrain sections stained for tyrosine hydroxylase (TH) (red) and GFP (green). No GFP-positive cells were found in TH-positive neurons of the striatum (A), cortex (B) or hippocampus (C). Representative images are shown. Scale bars= 200 µm. TRAP+(+)= THTR mouse line. -/-= Knock-out. +/+= Homozygous. += Hemizygous. mSnca= mouse alpha-Synuclein. hSNCA= human alpha-Synuclein. TH= tyrosine hydroxylase. GFP= green fluorescent protein.

Analysis of eGFP and TH co-expression in THTR transgenic mice shows a decrease over time

TH and GFP expression in the midbrain was analysed in a time-line fashion, to investigate if the reduction in GFP signal as shown for the native GFP fluorescence in Figure 3. 3 is consistent in immunofluorescent labelled brain sections. For this analysis, we used sequential coronal brain sections of young (3-6 months) and aged (12-18 months) homozygous *THTR* transgenic mice. TH-positive and TH/GFP-double positive cells were outlined using a pipeline created with the Cell Profiler software (http://cellprofiler.org/) (Figure 3. 8, experiments performed by Laura Klinger). Overall, the analysis showed that only a small proportion of all TH-positive cells co-expressed GFP (young mice: ~10%; aged mice: ~7%). Analysis of TH/GFP co-expression as a percentage of all TH-positive over time reveals a significant decrease in aged mice (Figure 3. 8; unpaired t-test; mean ± SEM; * $p \leq 0.05$).

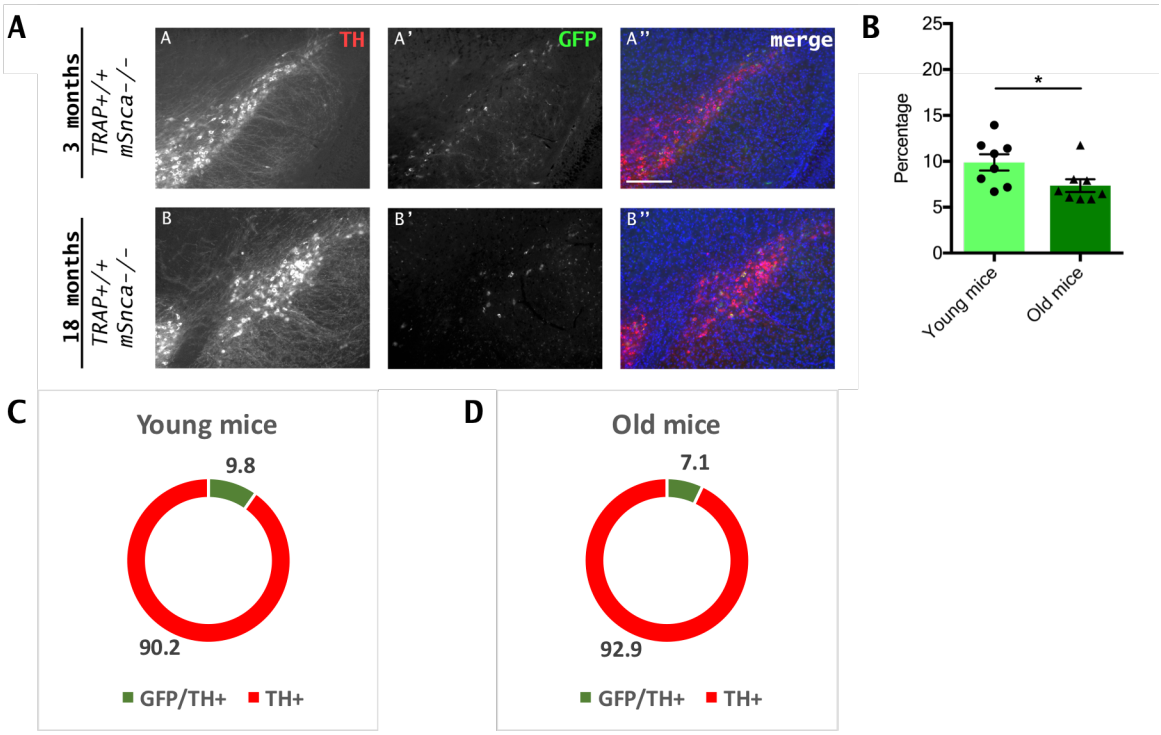


Figure 3. 8 ***Timeline analysis of TH/GFP-double positive cells in DAn of THTR mice reveals a decrease in GFP/TH double positive cells.***

*(A) Immunofluorescence labelling of TH- and GFP-positive DAn in the midbrain of homozygous young (3-6 months) and aged (12-18 months) THTR mice. Exemplary images shown (n= 8 mice per age group). (B, C, D) Percentage of TH/GFP-double-positive cells relative to all TH-positive cells as analysed by Cell Profiler software (unpaired t-test; mean ± SEM; * p ≤ 0.05). Experiments performed by Laura Klinger. DAn= dopaminergic neurons. GFP= green fluorescent protein. TH= tyrosine hydroxylase. TRAP+(+)= THTR mouse line. mSnca= mouse alpha-Synuclein. +/+= Homozygous. -/-= knock-out.*

eGFP-L10a is not co-expressed in TH-positive neurons in the Locus coeruleus

TH is involved in the biosynthesis pathway of catecholamines and its expression is also found in the LC, the principal site for the synthesis of norepinephrine (Nagatsu et al., 1964). In all TRAP-positive animals, TH and eGFP could be detected at a young (3 months, Figure 3. 9 A) and old age (18 months, results not shown). Unexpectedly, TH and eGFP presented as two almost exclusively distinct cellular subpopulations at both ages. The eGFP-L10a transgene was expressed in a TH-negative cell population in the LC. The eGFP-L10a expressing population was found in close proximity to the TH expressing cells but almost no TH/eGFP double positive cells could be found. Very few double positive cells could only be found in homozygous *THTR* mice. Based on comparisons of the GFP-positive region with the Allen Brain Atlas (http://www.brain-map.org), this region could likely correspond to the medial parabrachial nucleus which has been shown to be affected in PD (Goto and Hirano, 1991). To rule out the possibility that non-neural cell types in the LC express eGFP-L10a, a co-labelling of eGFP with neuron-specific Class III β-tubulin (TUJ1) in all

TRAP-positive animals confirmed neuronal specificity with no overlap between eGFP and the astrocyte marker, glial fibrillary acidic protein (GFAP) (Figure 3. 9 B, C).

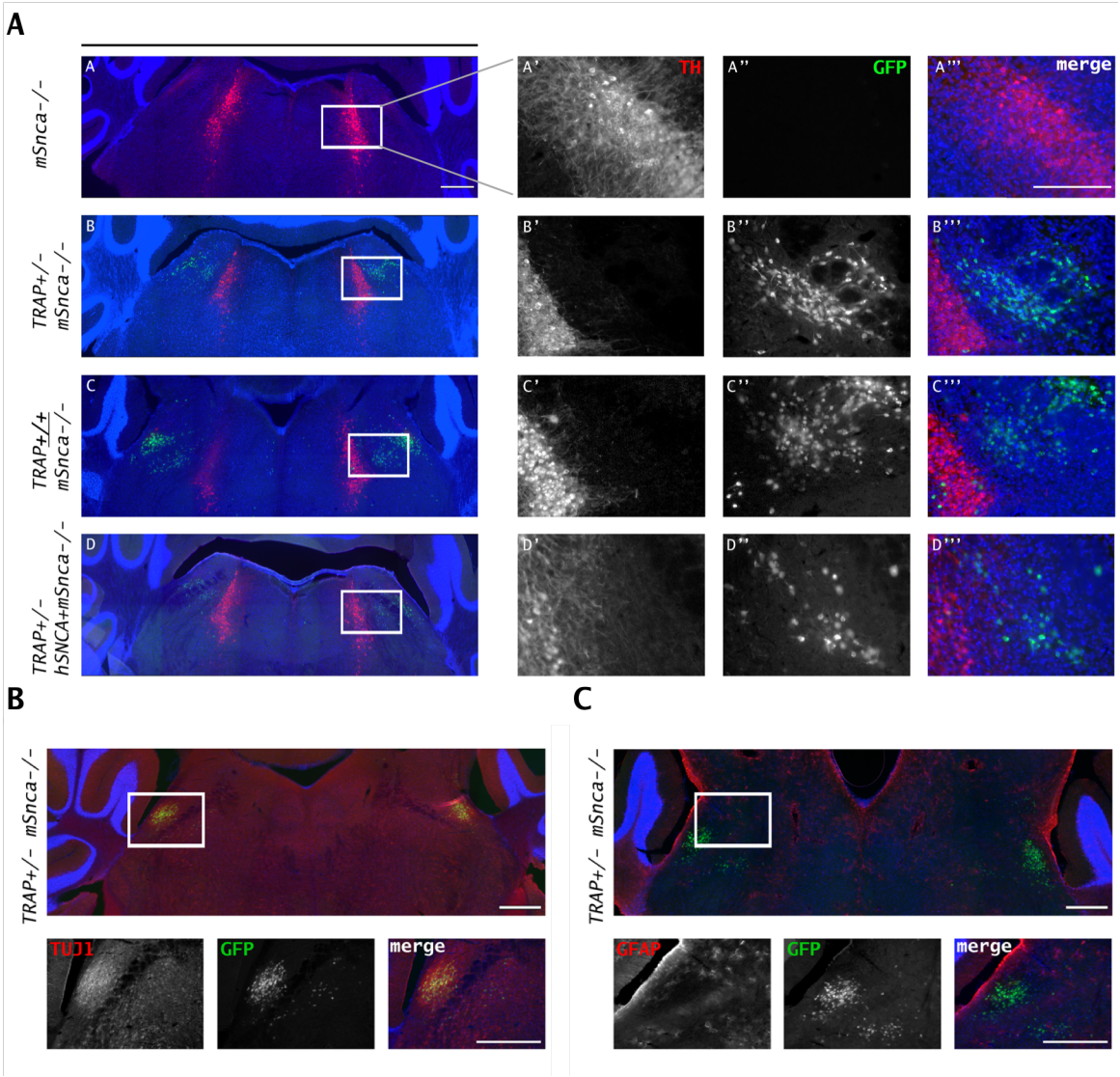
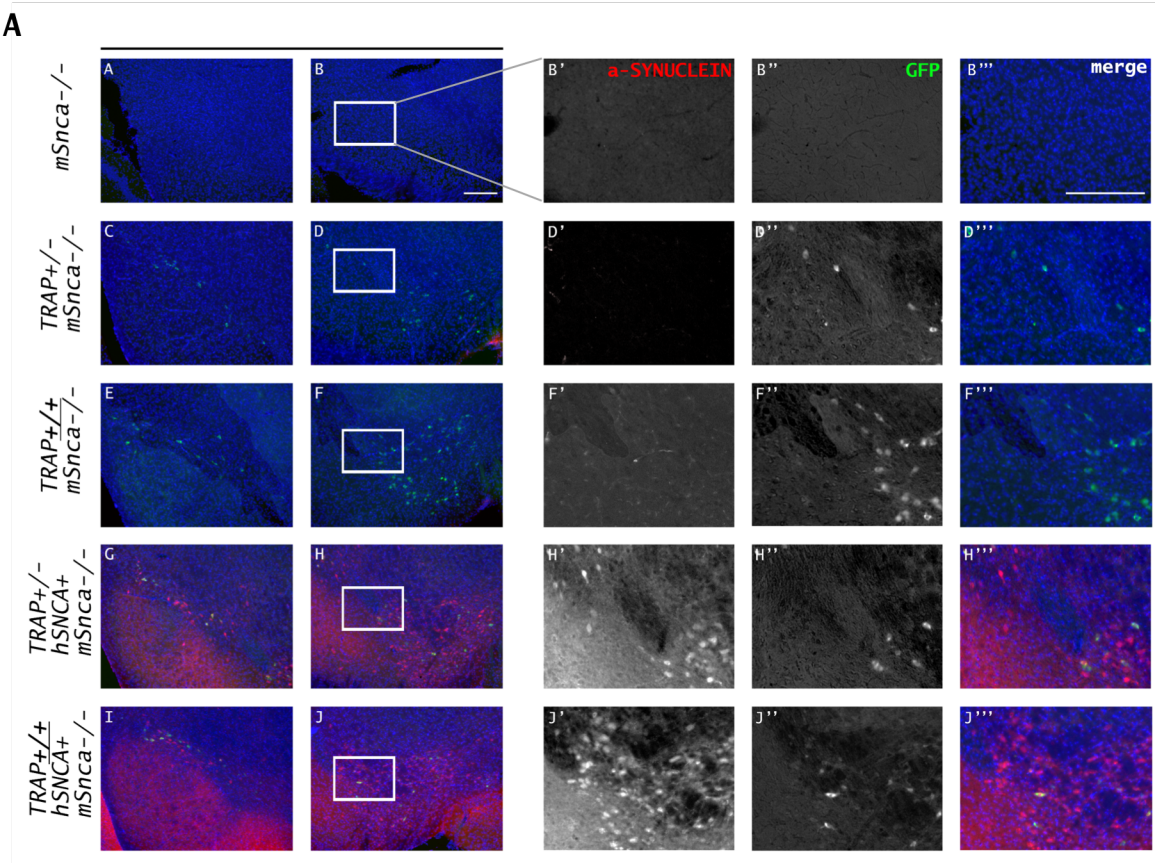


Figure 3. 9 ***Analysis of eGFP-L10a transgene expression in catecholaminergic neurons of the locus coeruleus shows surprising results (3 months).***

(A) Coronal locus coeruleus (LC) sections were stained for TH (red) and GFP (green). ***LEFT PANELS*** $^{(A\text{-}J)}$***:*** *Labelling confirms the expression of TH and eGFP in catecholaminergic neurons of the LC. Surprisingly, TH- and eGFP-positive cell populations do not overlap but lay close to each other. Homozygous mice express more eGFP-positive cells compared to their hemizygous littermates. No GFP reactivity is found in TRAP-negative mice. Representative images are shown.* ***RIGHT PANELS*** $^{(B', D', F' H' J')}$***:*** *Close-up of the inserts (panel 1). (B, C) Labelling using TUJ1 and GFAP confirm that eGFP-positive cells shown above are indeed neurons. Scale bars= 200 µm. Representative images are shown. TRAP+(+)= THTR mouse line. -/-= Knock-out. +/+= Homozygous. += Hemizygous. mSnca= mouse alpha-Synuclein. hSNCA= human alpha-Synuclein. TH= tyrosine hydroxylase. GFP= green fluorescent protein. TUJ1= Neuron-specific Class III β-tubulin. GFAP= Glial fibrillary acidic protein.*

THTR/hSNCA+ mice show aSyn expression in DAn

The accurate recapitulation of the endogenous spatio-temporal expression pattern of aSyn in *hSNCA+* mice under its native promoter and its native control elements has been validated previously (DPhil Thesis: S. Janezic, 2013). Here, coronal sections from 3 months old transgenic mice were probed with either a human-specific or a pan-species aSyn antibody to analyse aSyn/GFP co-expression (Figure 3. 10). The later recognises both mouse and human aSyn. As previously observed, the *hSNCA* transgene expression profile closely mirrored the expression profile of endogenous mouse aSyn in WT C57Bl/6 mice in the DAn of the SNc and VTA (DPhil Thesis: S. Janezic, 2013). As expected, no human aSyn expression was detected in the *mSnca-/-* control line and mice on a *THTR mSnca-/-* background (Figure 3. 10). Only few aSyn-positive cells in the SNc and VTA co-expressed GFP which might be due to the general low expression of GFP. On the other hand, almost all GFP-positive cells co-expressed aSyn (Figure 3. 10). The intracellular localisation of aSyn was observed in the axons, cell bodies, and nuclei of our *hSNCA+* transgenic mice.



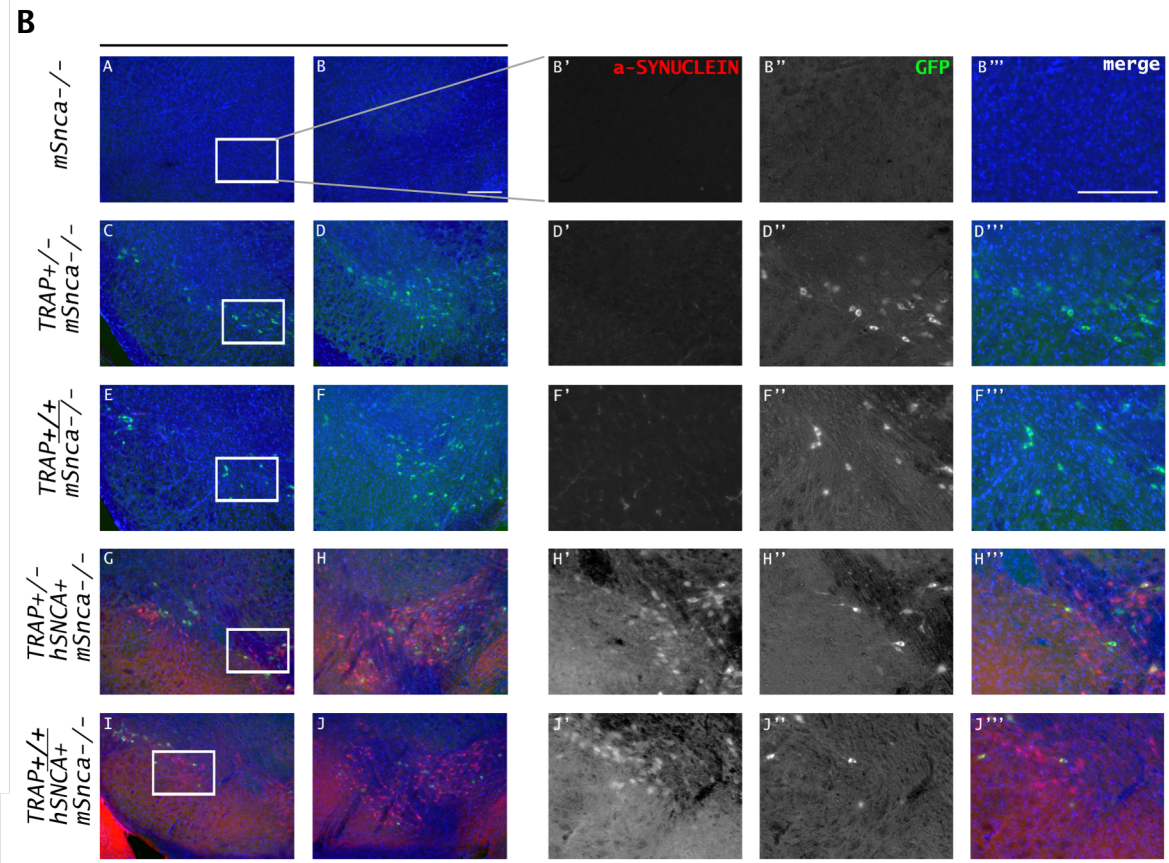


Figure 3. 10 Alpha-Synuclein is co-expressed in some eGFP-positive cells in the midbrain (3 months).

Coronal midbrain sections stained for aSyn using either a human-specific (A) or a pan-aSyn antibody (B) (red) in combination with an anti-GFP antibody (green). ***LEFT PANELs*** *(A-J)****:*** *Immunohistochemistry, confirms expression of the alpha-Synuclein transgene in some eGFP-positive dopaminergic cells of the Substantia nigra (SNc) and Ventral tegmental area (VTA). No alpha-Synuclein reactivity is found in mSnca-/- mice. Representative images are shown.* ***RIGHT PANELs*** *(B', D', F' H' J')****:*** *Close-up of the inserts (panel 1). Scale bars= 200 µm. TRAP+(+)= THTR mouse line. -/-= Knock-out. +/+= Homozygous. += Hemizygous. mSnca= mouse alpha-Synuclein. hSNCA= human alpha-Synuclein. GFP= green fluorescent protein.*

Furthermore, aSyn/GFP co-expression using the human-specific aSyn antibody was analysed in aged transgenic animals (Figure 3. 11). Similar to the results in young animals, aged *hSNCA+* animals contained aSyn localised to axons, cell bodies, and nuclei with only few aSyn-positive cells co-expressing eGFP (Figure 3. 11).

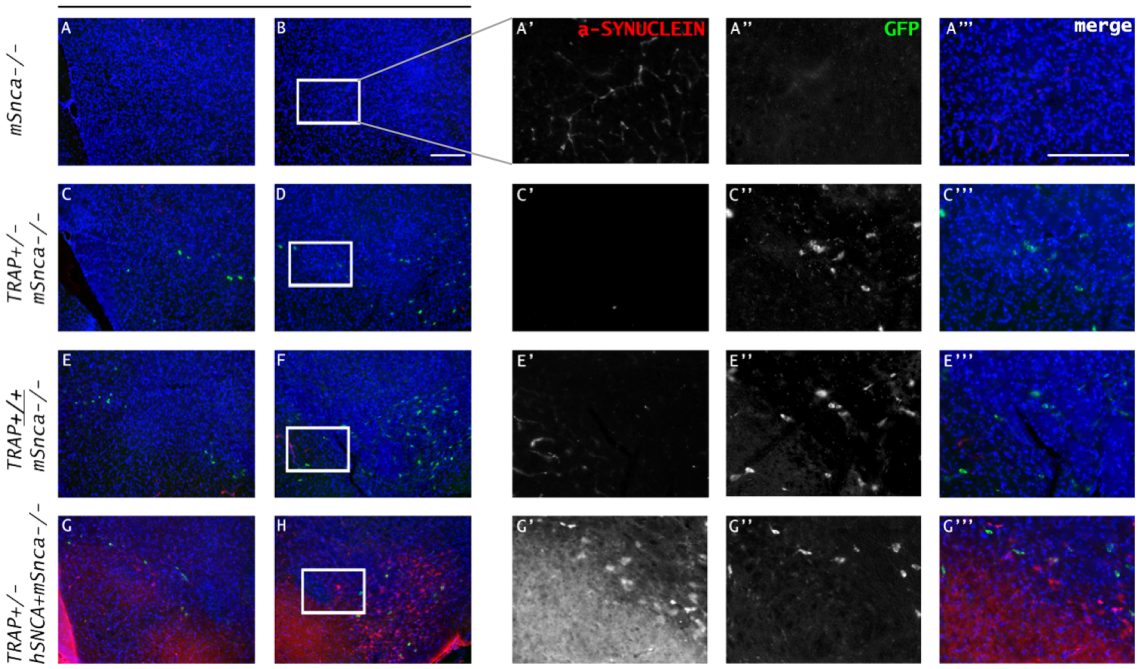


Figure 3. 11 ***Alpha-Synuclein and eGFP are also co-expressed in aged transgenic mice (18 months).***
LEFT PANELs $^{(A\text{-}J)}$***:*** *hSNCA+ mice express the alpha-Synuclein transgene in the Substantia nigra (SNc) and Ventral tegmental area (VTA). A few alpha-Synuclein-positive cells co-express eGFP. No alpha-Synuclein reactivity is found in mSnca-/- mice. Representative images are shown.* ***RIGHT PANELs*** $^{(B', D', F' H' J')}$***:*** *Close-up of the inserts (panel 1). Scale bars= 200 µm. TRAP+(+)= THTR mouse line. -/-= Knock-out. +/+= Homozygous. += Hemizygous. mSnca= mouse alpha-Synuclein. hSNCA= human alpha-Synuclein. GFP= green fluorescent protein.*

Low numbers of eGFP-L10a positive neurons are not attributable to the GFP-antibody used for detection

To exclude that the anti-GFP antibody used for immunofluorescence labelling does not detect all truly GFP-positive cells within the SNc and VTA, four different anti-GFP antibodies were used in comparison (Figure 3. 12). Brain sections from young, hemizygous *THTR* transgenic mice co-stained for TH and GFP with various anti-GFP antibodies did not show any differences in number or location of GFP/TH double positive cells.

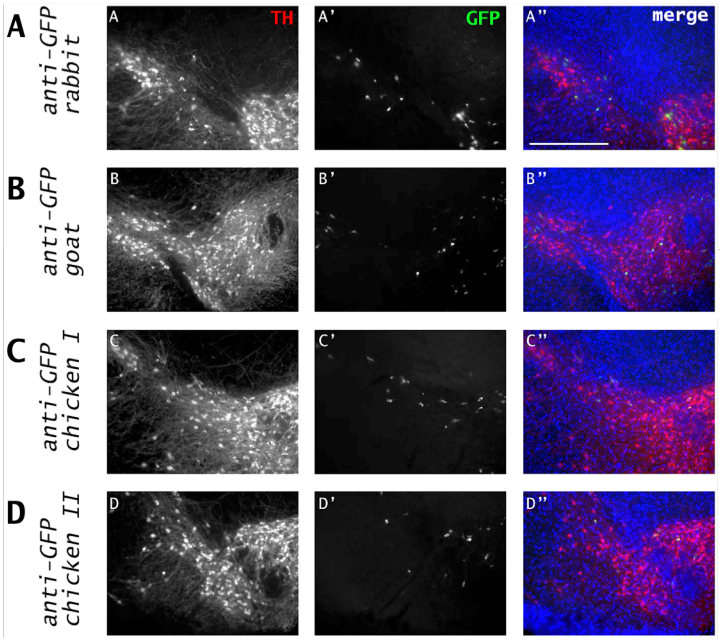
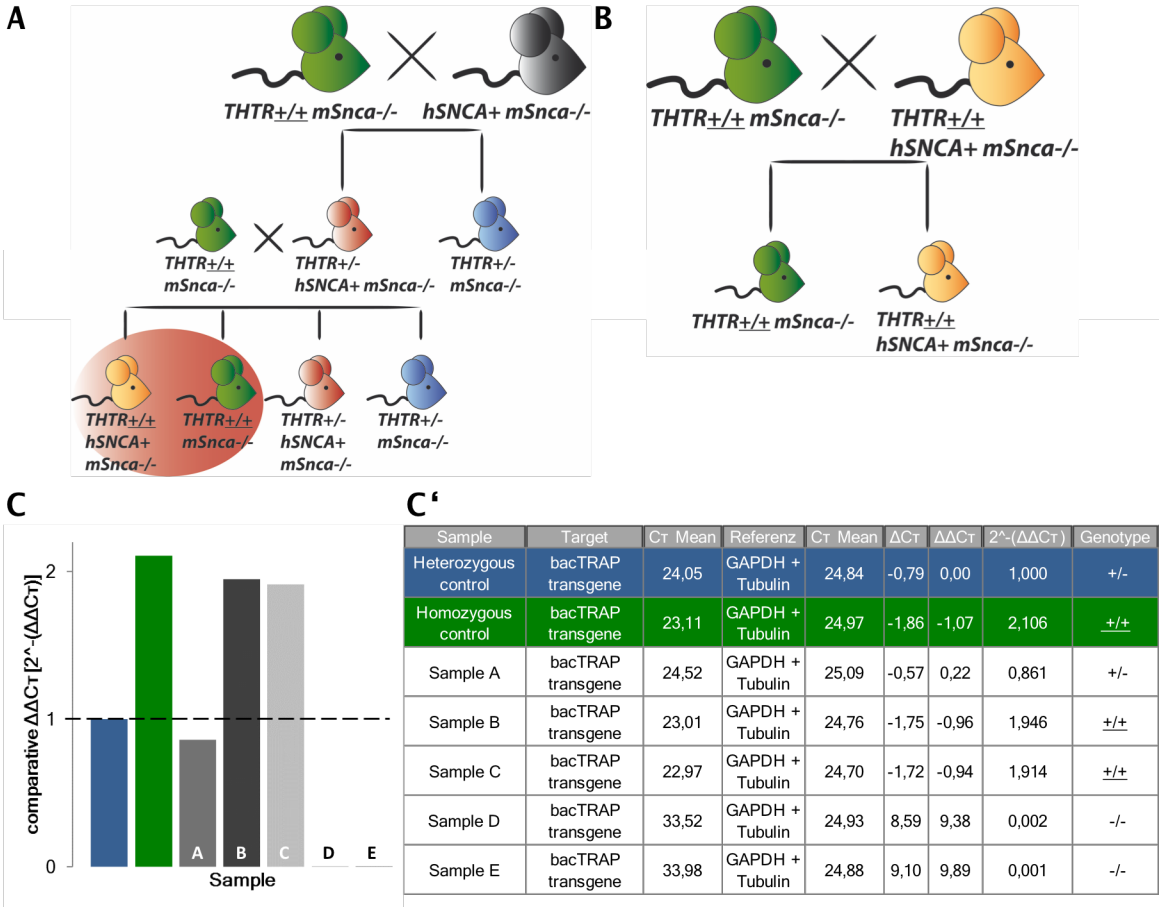


Figure 3. 12 Comparison of different GFP antibodies excludes that site-specific differences in antibody epitope recognition influence GFP labelling.

The SNc and VTA of TRAP-positive mice stained with different antibodies recognising GFP reveals no differences in labelling pattern. (A $^{(A\text{-}A''')}$) anti-GFP rabbit (Invitrogen, A11122). (B $^{(B\text{-}B''')}$) anti-GFP goat (Abcam, ab6673). (C $^{(C\text{-}C''')}$) anti-GFP chicken I (Abcam, ab13970). (D $^{(D\text{-}D''')}$) anti-GFP chicken II (Aveslab, GFP-1020). For all labelling young hemizygous THTR mice have been used (3 months). Representative images shown. TH= tyrosine hydroxylase. GFP= green fluorescent protein. SNc= Substantia nigra. VTA= ventral tegmental area.

3.3.3 Revised breeding strategy to generate a cohort of homozygous *THTR* transgenic mice

Because of the first molecular characterisation experiments, the breeding scheme was revised to breed the *THTR* transgenic mice to homozygosity for the *TH-bacTRAP* transgene in order to enhance eGFP-L10a expression in DAn (Figure 3. 13). Stronger eGFP-L10a expression allows for an improved immunoaffinity-precipitation of eGFP-tagged ribosomes using TRAP from homozygous mice as discussed in the following chapter (Chapter 4). To distinguish hemizygous from homozygous littermates, a copy-number genotyping protocol via real-time PCR based on a previously published method has been established for this mouse line (Wishart et al., 2007). Copy-thresholds for the bacTRAP transgene were compared to the geometric mean of reference gene amplifications (GAPDH and beta-Tubulin) using the comparative Ct method, whereby one known hemizygous and homozygous *THTR* mouse served as calibrators to identify the correct zygosity. Copy-number genotyping of TRAP-negative mice did not give any detectable Ct values for the bacTRAP transgene (Figure 3. 13 C).



Sample	Target	CT Mean	Referenz	CT Mean	ΔCT	ΔΔCT	2^-(ΔΔCT)	Genotype
Heterozygous control	bacTRAP transgene	24,05	GAPDH + Tubulin	24,84	-0,79	0,00	1,000	+/-
Homozygous control	bacTRAP transgene	23,11	GAPDH + Tubulin	24,97	-1,86	-1,07	2,106	+/+
Sample A	bacTRAP transgene	24,52	GAPDH + Tubulin	25,09	-0,57	0,22	0,861	+/-
Sample B	bacTRAP transgene	23,01	GAPDH + Tubulin	24,76	-1,75	-0,96	1,946	+/+
Sample C	bacTRAP transgene	22,97	GAPDH + Tubulin	24,70	-1,72	-0,94	1,914	+/+
Sample D	bacTRAP transgene	33,52	GAPDH + Tubulin	24,93	8,59	9,38	0,002	-/-
Sample E	bacTRAP transgene	33,98	GAPDH + Tubulin	24,88	9,10	9,89	0,001	-/-

Figure 3. 13 Optimised breeding Scheme for the double transgenic THTR/hSNCA+ experimental cohort.

A) Revised breeding scheme to breed the TH-bacTRAP transgene to homozygosity on the hSNCA+ background. Desired genotypes are indicated by red circle. (B) Final optimised breeding scheme to generate the homozygous THTR experimental cohort. (C) Representative copy-number genotyping results. qPCR primers detect the bacTRAP construct. The genotype is defined by comparative Ct method using a hemizygous and homozygous THTR mouse as a calibrator and the geometric mean of two housekeeping genes as reference samples. This resolves the unknown samples as follows: Blue= hemizygous control. Green= homozygous control. A= hemizygous; B/C= homozygous; D/E= non-transgenic. THTR= TH-bacTRAP. -/-= Knock-out. +/+= Homozygous. += Hemizygous. OVX= over-expressed. mSnca= mouse alpha-Synuclein. hSNCA= human alpha-Synuclein.

3.3.4 Establishing an additional genetic control for gene expression profiling using bacTRAP mice

As detailed in previous chapters (Chapter 1), the KO of mouse aSyn was shown to cause some slight molecular alterations (Al-Wandi et al., 2010; Robertson et al., 2004). When analysing the effects of human aSyn overexpression using our *THTR* mice, some of the gene expression changes could be caused by the KO of mouse aSyn itself. An additional mouse aSyn WT control cohort for immunoaffinity purifications of DAn-specific mRNAs and subsequent gene expression profiling by next generation sequencing in our analysis controlled for this. Since our transgenic mice did not express mouse aSyn, the *TH-bacTRAP* transgene had to be bred back onto a mouse aSyn WT

background (Figure 3. 14). In the first generation, homozygous *THTR* mice were crossed with WT C57Bl/6 mice resulting in mice hemizygous for *THTR* and *mSnca* (Figure 3. 14 A). Further inter-crossing of their offspring generated a range of genotypes. Mice homozygous for *THTR* and hemizygous for *mSnca* were kept for further breeding (Figure 3. 14 B), mice homozygous for *THTR* with either aSyn WT or KO backgrounds were kept as experimental groups. The final breeding scheme allowed the generation of the two desired experimental groups, as well as littermates for additional breeding.

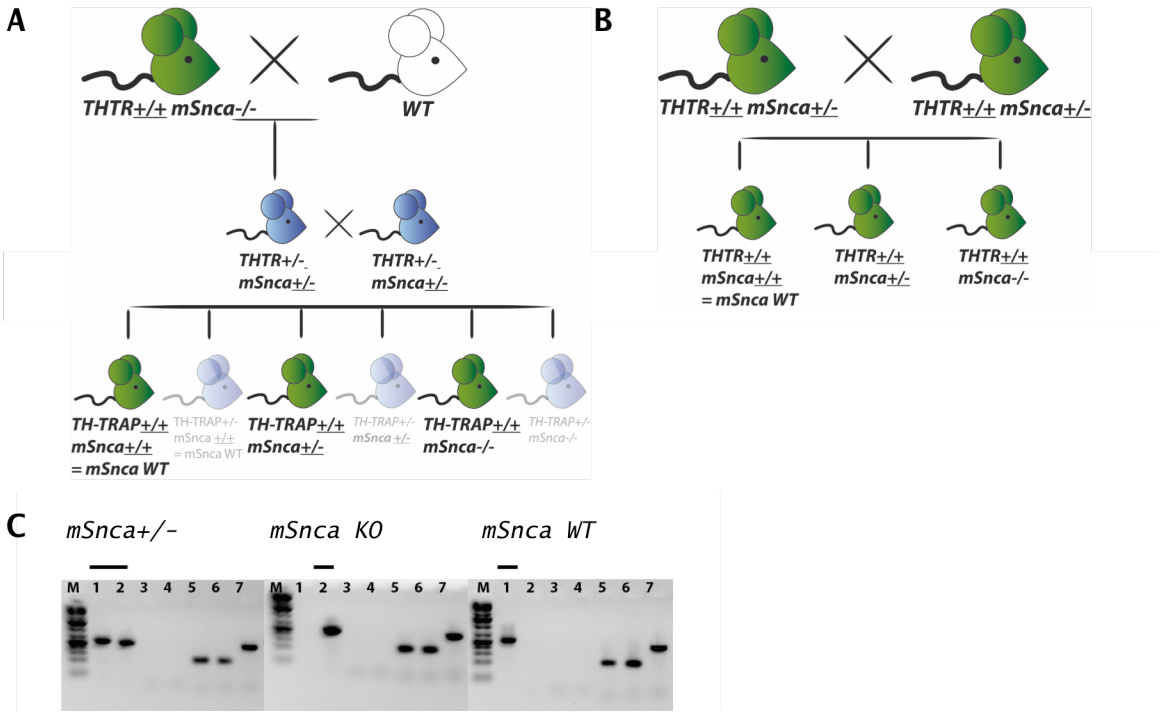


Figure 3. 14 Breeding overview for an additional control for the THTR line to perform TRAP experiments in THTR+/+ mSnca KO versus THTR+/+ mSnca WT animals.

(A) Breeding strategy to cross the homozygous TH-bacTRAP transgene on the mSnca WT background. (B) Breeding strategy for additional TRAP control experiments. Littermates from this cross were used for further breeding or as experimental animals to compare the effect of mSnca KO with mSnca WT on the dopaminergic neuronal translatome using translated mRNA isolated by TRAP followed by gene expression profiling. (C) Exemplary Genotyping results. Two primer pairs detect presence/absence of wild-type (1) and knock-out (2) mSnca to verify the Snca-/- background. THTR= TH-bacTRAP. -/-= Knock-out. +/-= Heterozygous. +/+= Homozygous. += Hemizygous. mSnca= mouse alpha-Synuclein. WT= wild-type.

3.3.5 Analysis of key protein expression levels in the striatum did not show changes in bacTRAP transgenic mice

Expression of the eGFP-L10a fusion protein was analysed in whole midbrain tissue lysates of 3-month-old homozygous THTR animals compared to non-transgenic controls using four different anti-GFP antibodies and an antibody against RPL10a. Protein band sizes were expected to run at approximately 52 kDa for the eGFP-L10a fusion protein and at 25 kDa for endogenous RPL10a. Unfortunately, the eGFP-L10a fusion protein could not be detected with any of the antibodies used (results not shown). This was not unexpected since whole midbrain lysates have been used for western blotting. Overall, the eGFP-L10a transgene might be too lowly expressed in the *THTR* line as suggested by Immunofluorescence labelling as shown above. In general, immunoblotting might be not sensitive enough to detect eGFP-L10a in whole tissue lysates. Concentrated lysates from the TRAP fractions or sucrose gradient fractions that enrich for eGFP-L10a tagged ribosomes could be used for western blotting instead which has been successfully applied in some TRAP-studies (Nectow et al., 2015; Zhou et al., 2013).

A similar TRAP study using DAT-bacTRAP mice performed molecular characterization experiments to confirm that their mice presented normal brain morphology and biochemical characteristics. In their study, they did not observe any significant differences in striatal levels of TH and DAT between adult transgenic DAT-bacTRAP mice and WT littermates (Brichta et al., 2015). For our THTR mice we similarly investigated protein expression in the striatal tissues because all markers are expressed in this tissue and to save the midbrain for further experiments. Immunoblotting using anti-TH and the previously used anti-RPL10a antibody revealed no differences in the overall striatal protein expression levels at either 3 (Figure 3. 15 A) or 12 months (Figure 3. 15 B) of age between any of the analysed genotypes (one-way ANOVA, non-significant (n.s.)). The eGFP-L10a fusion protein could also not be detected using the anti-RPL10a antibody on striatal tissue at approximately 52 kDa.

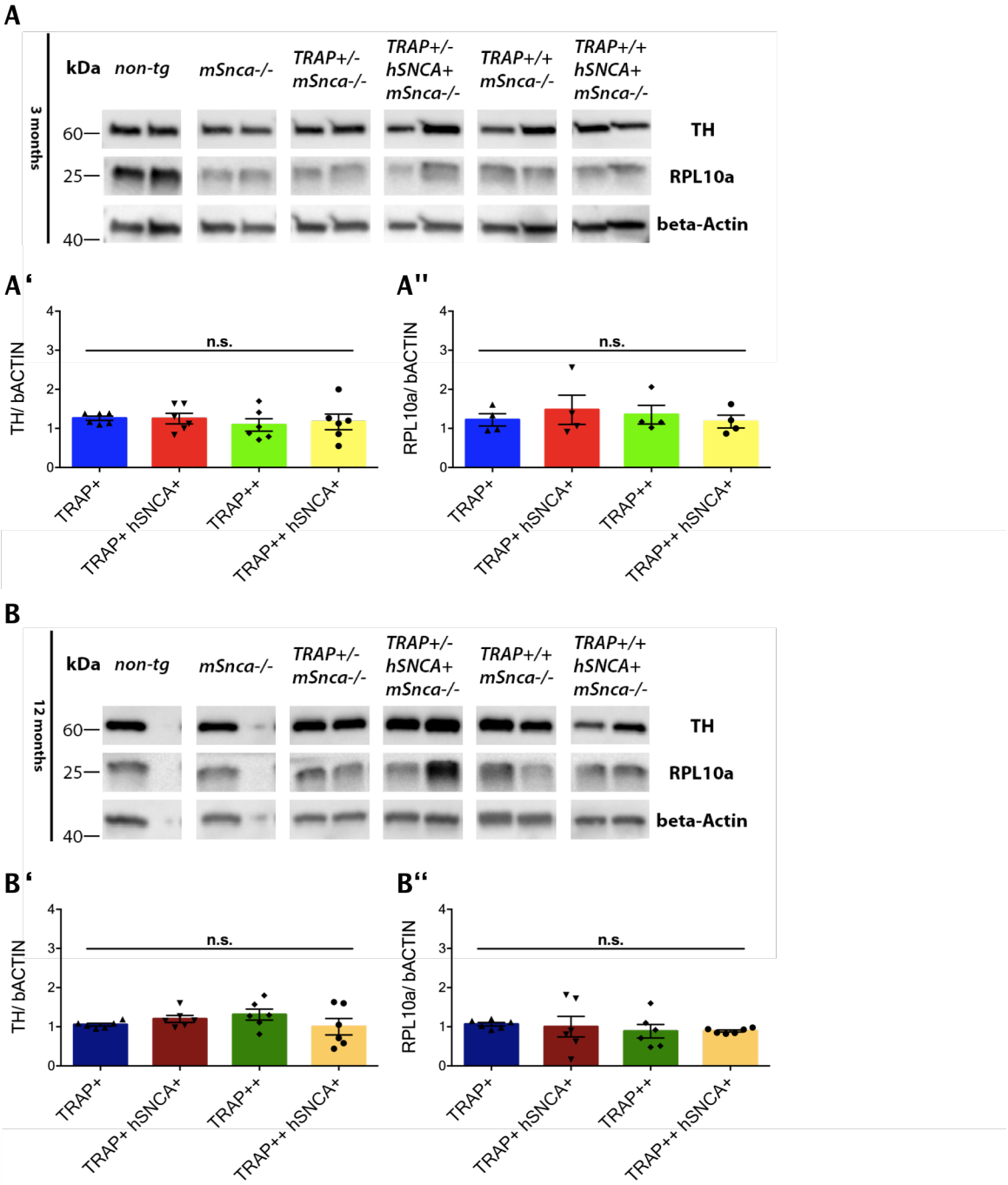
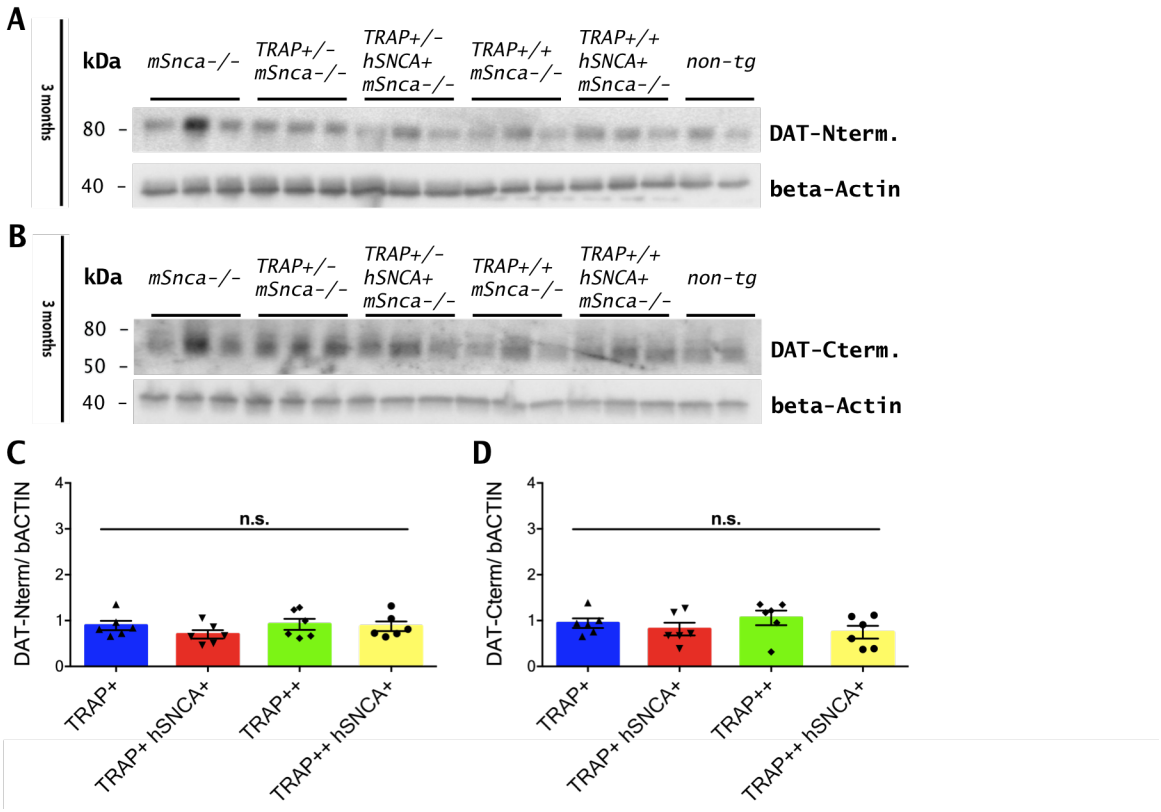


Figure 3. 15 Quantitative Western blot analysis in the striatum of THTR mice at 3 and 12 months.

Immunoblot analysis of TH, RPL10a and beta-Actin protein levels in striatal tissue from THTR mice or non-transgenic controls at 3 months (A) and 12 months (B) (three independent replicates of n= 1-2 mice per genotype). The molecular weight standard is shown on the left, blot images are cropped, representative blots are shown. Three independent experiments were carried out. Quantitative Western blot analysis of TH (A' + B') protein levels normalised to beta-Actin shows no change in the overall striatal expression levels. Normalised RPL10a protein levels (A'' + B'') showed a higher variation across the various genotypes and experiments which however was also non-significant. (Two-way ANOVA with Tukey post-hoc analysis; mean ± SEM). Normalised bar graphs are displayed relative to non-tg. TRAP+(+)= THTR mouse line. Non-tg= non-transgenic, here C57BL/6 wild type mice. -/- or KO= Knock-out. += Hemizygous. ++= Homozygous. mSnca= mouse alpha-Synuclein. hSNCA= human alpha-Synuclein. TH= tyrosine hydroxylase. RPL10a= ribosomal protein L10a. n.s.= non-significant.

Another key DAn marker, DAT, is a membrane transporter whose function of clearing DA from the synaptic cleft of DAn synapses is regulated through glycosylation of its N-terminus. Therefore, two different anti-DAT antibodies were used, which recognise structural epitopes at the N- and C-terminus of DAT, respectively. The N-terminal-specific antibody (#MAB369, Millipore) recognises the glycosylated mature form of DAT at approximately 80 kDa. The C-terminal raised antibody (#sc-1433, Santa Cruz) further recognises a non-glycosylated immature form of DAT which runs at approximately 55 kDa in addition to the glycosylated mature form (Figure 3. 16). Analysis of DAT showed no difference for the young animals between the analysed genotypes. Results from the aged animals were very variable. More replicates will be necessary to confirm DAT protein expression levels (Figure 3. 16; experiments performed by Laura Klinger).

All in all, our mice present normal biochemical characteristics for the markers analysed as seen by others using similarly genetically modified mice (Brichta et al., 2015). In these mice, EGFP-L10a seems to be very lowly expressed as it cannot be picked up with immunoblotting technology.



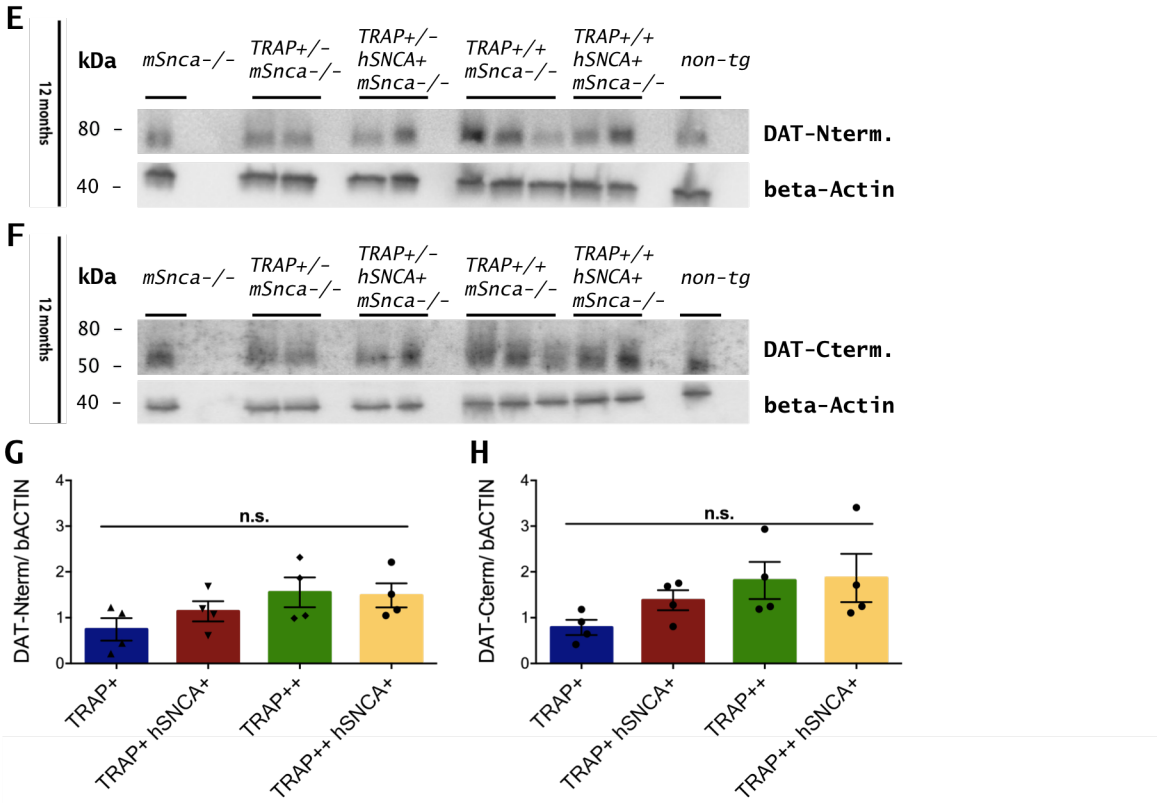


Figure 3. 16 Analysis of striatal DAT expression levels of THTR mice shows no difference (3 and 12 months).

Immunoblot analysis of DAT and beta-Actin protein levels in striatal tissue from THTR mice or non-transgenic controls at 3 (A, B) or at 12 months (E, F). Antibodies against DAT N- (Nterm) or C-terminus (Cterm) were used, blot images are cropped, representative blots are shown. Three independent experiments were carried out. Quantitative Western blot analysis of DAT-Nterm (A') or DAT-Cterm (B') protein levels normalised to beta-Actin show no change in the striatal protein expression levels for 3 or 12 months old animals (Two-way ANOVA with Tukey post-hoc analysis; mean ± SEM). Normalised bar graphs are displayed relative to non-tg. TRAP+(+)= THTR mouse line. Non-tg= non-transgenic, here C57BL/6 wild-type mice. -/- or KO= Knock-out. += Hemizygous. ++= Homozygous. mSnca= mouse alpha-Synuclein. hSNCA= human alpha-Synuclein. DAT= dopamine transporter. n.s.= non-significant. Experiments performed by Laura Klinger.

3.3.6 *hSNCA* protein is overexpressed in our PD mouse model

Previous work has shown that human aSyn expression levels in *hSNCA+* mice increased by approximately 2x compared to endogenous mouse aSyn levels in WT C57Bl/6 animals are (DPhil Thesis: S. Janezic, 2013). Here, the over-expression of the human aSyn transgene in double transgenic mice *THTR/hSNCA+* compared to age-matched, non-transgenic C57Bl/6 animals was confirmed by western blot analysis using either a human-specific or a pan-species anti-aSyn antibody (Figure 3. 17). Average aSyn expression levels detected by the pan-species anti-aSyn antibody were significantly increased by at least 2x in young (3 months, Figure 3. 17 B) and aged (12 months, Figure 3. 17 C) (unpaired t-test, * $p \leq 0.05$, ** $p \leq 0.01$, *** $p \leq 0.001$) double transgenic hemizygous and homozygous *THTR/hSNCA+* animals compared to levels of endogenous mouse

aSyn in age-matched C57Bl/6 mice. *hSNCA+* transgenic mice at 3 and 12 months of age showed comparable expression levels of human aSyn, while animals on the C57Bl/6 background did not show human aSyn protein expression (Figure 3. 17).

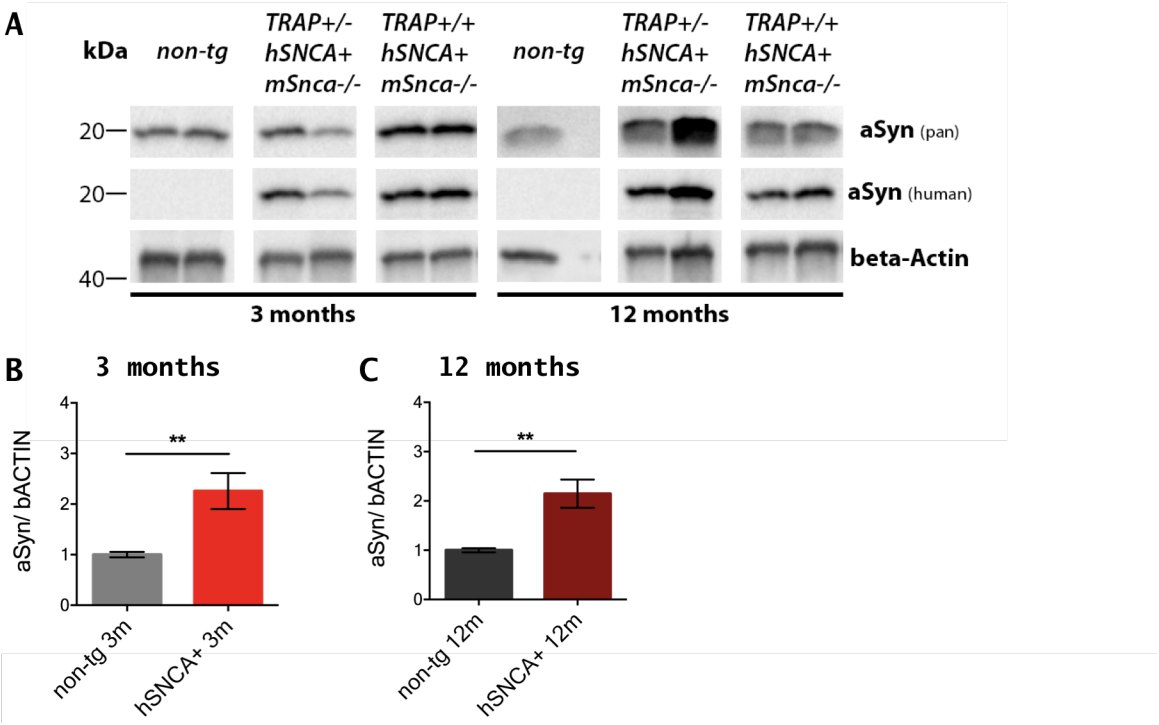


Figure 3. 17 Human alpha-Synuclein expression in the striatum of young and aged THTR/hSNCA+ mice.

*(A) Immunoblot analysis of aSyn expression in the striatum of hemizygous and homozygous THTR/hSNCA+ using a pan-species anti-aSyn or a human-specific anti-aSyn antibody. Protein expression in transgenic mice at 3 months and 12 months (three independent replicates of n= 2 mice per genotype) was compared to non-transgenic controls. The molecular weight standard is shown on the left, blot images are cropped, representative blots are shown. Three independent experiments were carried out. Quantitative Western blot analysis of pan-species anti-aSyn antibody in 3 (B) and 12 months (C) old animals normalised to beta-Actin shows an increase of 2-4-fold in the striatum of young and aged THTR/hSNCA+ transgenic mice compared to endogenous aSyn expression in C57Bl/6 mice (non-tg). (unpaired t-test; mean ± SEM; * $p \leq 0.05$, ** $p \leq 0.01$, *** $p \leq 0.001$). As expected no human aSyn expression was detected in non-tg mice. TRAP+(+)= THTR mouse line. Non-tg= non-transgenic, here C57Bl/6 wild type mice. -/- or KO= Knock-out. += Hemizygous. ++= Homozygous. mSnca= mouse alpha-Synuclein. hSNCA= human alpha-Synuclein. aSyn= alpha-Synuclein. n.s.= non-significant.*

3.3.7 Investigation of nigrostriatal dopaminergic cell loss

Progressive degeneration of DAn is a cardinal clinical feature of PD and the loss of more than 50% of nigrostriatal DAn results in the on-set of characteristic motor symptoms of PD (Fearnley and Lees, 1991). Unbiased stereological cell counts of either TH- or GFP-immuno-reactive DAn were performed in the SNc and VTA of 3 and 12 months old homozygous *THTR* or homozygous *THTR*/*hSNCA*+ mice to assess whether progressive degeneration of nigrostriatal DAn occurs based on the over-expression of the human aSyn transgene.

Neuropathological post-mortem studies of PD patients revealed a preferential loss of neuromelanin-positive DAn in the ventrolateral areas of the SNc (Fearnley and Lees, 1991), resulting in a decreased innervation of the caudate putamen (dorsal striatum). DAn of the VTA that projects to the ventral striatum have been shown to be more resistant to neuronal death in PD (Maingay et al., 2006). The regional selectivity in our aged PD model on the bacTRAP background was investigated by separately counting TH- or GFP-positive neurons. DAn in the SNc and VTA were counted combined in this approach. No significant difference could be found for either TH-positive (Figure 3. 18 A, C) or GFP-positive neurons (Figure 3. 18 B, D) for any of the analysed age groups or genotypes (non-significant). Nevertheless, 12 months old *THTR*/*hSNCA*+ mice showed the lowest number of TH-positive cells.

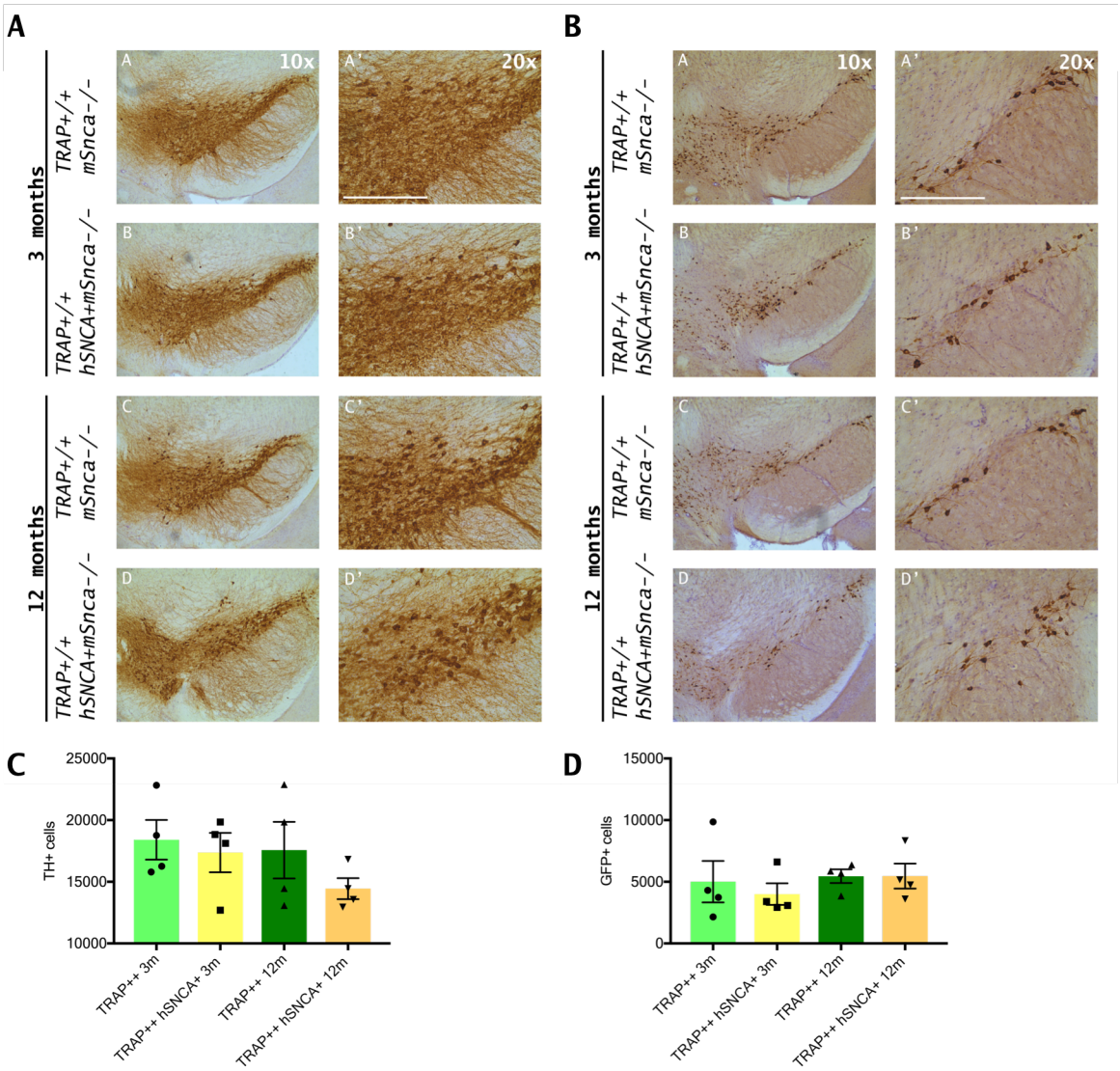


Figure 3. 18 Stereological cell count analysis of DAn in the midbrain by TH- and eGFP- immunoreactivity.

(A, B) Immunohistochemically stained DAn in the midbrain using either a TH (A) or a GFP (B) antibody. (C, D) No significance difference was detected in the number of immunoreactive TH or GFP-positive neurons in the SNc and VTA of 3 or 12 months old double transgenic homozygous THTR/hSNCA+ mice as compared to THTR mice (Two-way ANOVA, non-significant, n=4 mice per genotype). Data are expressed as mean ± SEM. Representative images are shown. TRAP+(+)= THTR mouse line. -/-= Knock-out. +/+= Homozygous. += Hemizygous. mSnca= mouse alpha-Synuclein. hSNCA= human alpha-Synuclein. DAn= dopaminergic neurons. TH= tyrosine hydroxylase. GFP= green fluorescent protein. GFP labelling and stereological counting was performed by Laura Klinger.

3.4 Discussion and Conclusion

The objective of this chapter was to describe the generation and in-depth molecular characterisation of a *THTR/hSNCA+* double transgenic mouse line. These mice enable the investigation of the impact of aSyn over-expression on translational profiles of dopaminergic cell populations in a PD model that replicates aSyn expression levels seen in familial PD patients.

I will highlight four major areas for discussion:

1) Establishment of a double transgenic THTR/hSNCA+ mouse line

Double transgenic *THTR(/hSNCA+)* mice carrying the eGFP-L10a transgene (DPhil Thesis: S. Janezic, 2013) were successfully established on a *mSnca*-/- null background (Figure 3. 2). Molecular characterisation experiments outlined in this chapter suggested that the homozygous background for the bacTRAP transgene could be advantageous to increase the total number of eGFP-positive cells. Since surprisingly low number of TH-positive cells co-expressed eGFP-L10a (Figure 3. 4) even though eGFP expression is controlled by the endogenous mouse TH promoter in the bacTRAP construct (Figure 3. 1). The breeding scheme was adjusted to generate the homozygous *THTR* mice (Figure 3. 13). Mice aged to 18 months did not show any obvious phenotypic or behavioural differences to their TRAP-negative littermates. All mice, hetero- or homozygous for the bacTRAP transgene were fertile and produced normal litter sizes, with no observed increase in embryonic lethality or early death of pups.

The deletion of endogenous mouse aSyn has been beneficial to avoid confounding interactions when over-expressing human aSyn protein but the effect of aSyn KO on gene expression in DAn has not been addressed so far. Studies on mouse aSyn null mice found a subtle reduction of DA in the striatum with synaptic dysfunction under repetitive stimuli and a resistance to neurodegeneration caused by MPTP (Abeliovich et al., 2000; Dauer et al., 2002). Since the knock-out of mouse aSyn itself could influence gene expression profiling, we wanted to include an additional control in our analysis. After intensive backcrossing, the *TH-bacTRAP* transgene was bred on a mouse aSyn WT

background, to serve as essential additional controls in subsequent TRAP experiments and gene expression profiling (Figure 3. 14).

2) Transgene vs endogenous TH expression in DAn

eGFP-L10a is expressed in DAn of the midbrain

The eGFP-L10a bacTRAP transgene is targeted to DAn as it is expressed under the control of the defining marker for DAn, TH, using the endogenous mouse promoter. Analysis of native eGFP expression in the midbrain of hemizygous and homozygous THTR mice showed decreased expression with age (Figure 3. 3). This finding could indicate that DA neurons are lost simply due to ageing, which correlates with what has been seen in the human SNc where up to 5–10% of the DA neurons are lost per decade during healthy normal ageing (Fearnley and Lees, 1991; Naoi and Maruyama, 1999).

Otherwise TH protein expression intensity could be down-regulated in the aged SNc as shown previously (Emborg et al., 1998; Ma et al., 1999). In a study using non-human primates the intensity of TH immunoreactivity labelling decreased with age in all three midbrain dopamine regions analysed (Collier et al., 2011). Thus, TH-positive neurons might be harder to detect in aged mice since the overall expression intensity per cell is decreased. Since eGFP-L10a is expressed under the TH promoter, transgene expression might be lost or the intensity might be decreased with age which would explain why we see less eGFP-positive DAn in aged bacTRAP mice (Figure 3. 6).

Furthermore, the expression of the eGFP-L10a transgene was confirmed to be present in key dopaminergic cell populations, such as the SNc/VTA (Figure 3. 4, young animals; Figure 3. 6, aged animals), with the absence of ectopic transgene expression. Neither cortex, nor hippocampus expressed GFP-positive cells (Figure 3. 5, young animals; Figure 3. 7, aged animals). This was expected since none of these regions express endogenous TH. Overall, no obvious morphological differences of DA cell populations between TRAP-transgenic and TRAP-negative mice could be observed and additional analyses revealed no significant differences in the striatal protein expression levels of TH, RPL10a (Figure 3. 15), and DAT (Figure 3. 16). Of note, aged THTR mice showed a high variability of DAT expression.

eGFP-L10a fusion protein expression levels could not be detected by immunoblotting using either an antibody against RPL10a or different anti-GFP antibodies. This could be due to the fact that total midbrain lysates contain too little GFP-tagged ribosomes. Immunoblotting analysis of the TRAP immunoprecipitated (IP) fraction might be concentrated enough to show eGFP-L10a fusion protein expression levels as it has been shown by Heiman at al. who detected tagged RPL10a in their IP fraction (Heiman et al., 2008).

Surprisingly, not all TH-positive neurons co-expressed eGFP. The low overlap of detectable TH/GFP co-expressing cells (Figure 3. 8) could either represent the true biological situation in these transgenic mice or it could have underlying by technical reasons. For example, one possibility could have been that the specific epitope of the anti-GFP antibody could be masked in some of the eGFP-positive cells, thereby hindering the antibody to bind and to recognise the transgene. Nevertheless, none of the immunolabellings using different GFP antibodies detected no differences in numbers of GFP-positive cells (Figure 3. 12). Thus, it can be excluded that the lack of eGFP expression is due to a recognition problem of the antibody.

Overall, GFP is expressed at a much lower rate than expected already from a young age (Figure 3. 3). Only a sub-set of DAn TH-positive co-expresses GFP in the midbrain (Figure 3. 4). This problem could have arisen based on the construction of the TH-bacTRAP vector. Only the promoter region with the 5'UTR was retained in the BAC, while exon, intron, and downstream regions of TH were removed. Literature provides evidence that important regulatory cues are embedded in exons, introns, and the flanking UTRs of genes (Barrett et al., 2012). Both, the 3'UTR and polyA signals are interconnected with the regulation of transcription and mRNA processing of genes. Furthermore, they are also able to directly affect the stability of transcripts (Proudfoot, 2011). All these important regulatory regions are missing from the bacTRAP construct.

Several other studies used TH promoter constructs to drive gene expression. A study that generated transgenic mice using the human TH locus showed that expression generally matched that of mouse TH. Nevertheless, they found some ectopic expression in non-catecholaminergic regions, although

the construct contained all exons and introns including 2.5 kb 5' promoter and 0.5 kb of the downstream region (Kaneda et al., 1991). Similarly, studies that drive reporter gene expression in transgenic mice have shown ectopic expression when using limited portions of the human TH 5' promoter (Kessler et al., 2003; Nagatsu et al., 1994). Notably, the 11 kb TH promoter construct was successfully used to generate a rat model showing minimal ectopic expression of the GFP transgene (Iacovitti et al., 2014). The construct used in this study included regulatory elements at a greater distance to the TH 5' promoter region in the BAC which may be necessary for accurate expression of the TH driven transgene. Our bacTRAP construct contains 43 kb of TH promoter region including an alternative first exon 30 kb upstream of the promoter region but the transgene cassette replaced the first coding exon and all further downstream regions of the TH locus (Figure 3. 1). Importantly, another study mirrored our transgene expression results. A knock-in approach using a yellow fluorescent protein (YFP) that replaced the first exon and intron of the TH gene only produced about 6% of TH-positive cells which additionally expressed YFP in midbrain regions (Kelly et al., 2006). Thus, the deleted intron or exon sequences of the TH locus may be necessary to provide important temporal and spatial expression clues and the lack of these in the bacTRAP construct may be hindering the eGFP-L10a reporter construct to accurately mimic TH expression. Accordingly, the TH locus might contain important sequences for its own transcriptional regulation. For the human TH promoter, it has been shown that a polymorphic microsatellite located in the first intron of the TH gene can act as a transcription regulatory element *in vitro* (Meloni et al., 1998) and might participate in the transcriptional regulation of the TH gene by exhibiting a silencing effect (Albanèse et al., 2001). However, human, mouse, and rat TH promoters only share very small evolutionary conserved regions that do not have the same positions alongside the promoter sequences (Gandelman et al., 1990; Kessler et al., 2003; Kim et al., 2003). Thus, TH gene regulation might be achieved through different mechanisms among species.

eGFP-L10a fusion protein cannot be detected in DAn axons

Unexpectedly, the striatum did not show GFP immunofluorescence even though TH expression was found there (Figure 3. 5, young animals; Figure 3. 7, aged animals). This finding indicates that eGFP-

tagged ribosomes might not extend to the projections of DAn to the striatum and that the fusion protein eGFP-L10a expression is likely limited to cell bodies. Similar results have been observed by others studying DAn using TRAP (Brichta et al., 2015). Alternatively, eGFP-tagged ribosomal number could be undetectably low in axons and at the synapse, especially when considering the generally low expression in the midbrain itself, thereby accounting for the lack of expression. Furthermore, it could be possible that immunofluorescence is not sensitive enough to pick up axonally located eGFP-tagged ribosomes. To account for this, electron microscopy images might be needed to investigate the presence or absence of eGFP-tagged ribosomes in DAn projections but the presence of actively translated ribosomes in the axon is still under debate (Holt and Schuman, 2013). On the other hand, performing TRAP after inducing eGFP-L10a transgene expression by viral injections indeed showed the presence of eGFP-L10a in neuronal projections, e.g. in Camk2a-positive projection neurons that were retrograde transduced by AAV9-Camk2a-TRAP (Cook-Snyder et al., 2015). In another recent publication, a Cre-conditional GFP virus was injected into the nucleus accumbens of GFP-nanobody-L10A transgenic mice and translating ribosomes were successfully immunoprecipitated from infected neurons after retrograde tracing (Pomeranz et al., 2017). Since strong viral promoters enable a local over-expression of the transgene, the presence of eGFP-L10a in neuronal projections might not be surprising.

eGFP-L10a and endogenous TH expression do not overlap in catecholaminergic cell populations of the LC

In the LC, TH- and GFP-immunoreactive cell populations were found as two separate populations next to each other with little or no overlap (Figure 3. 9). This was an unexpected finding which could be further investigated by *in situ* hybridisation (ISH) experiments. It would be interesting to investigate if only TH and GFP protein expression is regionally separated or if also TH and GFP RNAs are located at different regions within the LC region. Generally, the final construction of the bacTRAP vector might lack essential spatial cues for correct expression in the LC.

3) Analysis of hSNCA protein expression and aSyn/eGFP co-labelling

Co-labelling of eGFP with aSyn revealed the expression of only a few aSyn/GFP-double positive cells (Figure 3. 9, young animals; Figure 3. 11, old animals). This might be due to the general low expression of GFP. Nevertheless, almost all GFP-positive cells co-expressed aSyn, a promising finding since these eGFP-positive cells will be analysed by gene expression profiling in our PD model after TRAP. The findings are consistent in young and aged THTR mice. Additionally, as observed previously, the presence of the *hSNCA+* transgene lead to increased aSyn levels compared to endogenous mouse aSyn in non-transgenic mice (Figure 3. 17 and DPhil Thesis: S. Janezic, 2013). Thus, we could show that our PD model is mirroring the levels observed in PD patients with aSyn locus multiplications (Chartier-Harlin et al., 2004; Singleton et al., 2003), which makes *hSNCA+* mice a promising tool for translatome profiling analysis in DAn.

4) Analysis of potential cell loss of DAn in our mouse model of PD

To eliminate confounding effects or protective functions due to the presence of endogenous mouse aSyn, our model was generated on a mouse aSyn KO background. The presence of endogenous mouse aSyn resulted in higher cell numbers of DAn in the SNc of WT C57Bl/6 mice compared to aSyn KO mice (Garcia-Reitboeck et al., 2013). Al Wandi et al. and others demonstrated a general decrease in DAn number in the SNc of aSyn KO mice compared to their WT littermates at a young age (Al-Wandi et al., 2010; Robertson et al., 2004), while others failed to replicate this loss (Abeliovich et al., 2000; Cabin et al., 2002). However, it might not be of importance for the study of *THTR* mice if cells are lost since all mice are kept on the same mouse aSyn KO background. Any effect on DAn number would display the effect of human aSyn presence or absence. However, discrepancies in total DAn number should be kept in mind when conducting comparisons with other studies based on counts on a different genetic background.

Unbiased stereological cell counts in young and aged THTR mice could not find a difference for either TH- or GFP-positive DAn in the midbrain (Figure 3. 18). Although we could confirm the significant up-regulation of aSyn in our *THTR/hSNCA+* double transgenic mouse model, a longer duration of aSyn exposure might be needed to initiate cell loss as seen in PD. Previously, cell loss

pathology has been successfully assessed in aged *hSNCA+* mice (+18 months, Janezic et al., 2013). Unfortunately, the here selected time-point at 12 months was the best compromise between age and feasibility of TRAP methodology (as discussed in the following chapters). Due to the overall low expression of eGFP-L10a in DAn in the midbrain with only about 10% TH/GFP-overlap, gross cell losses would have negatively impacted the success of TRAP-mediated RNA isolation from these cells. Thus, we are likely profiling an 'at-risk' population of DAn which might get us important insight in underlying cellular processes leading to the establishment of PD pathology.

The newly established *THTR/hSNCA+* double transgenic mouse line provides a promising tool to investigate the impact of aSyn over-expression on translational profiles of DAn. In the following chapters, we will address:

1) Can TRAP be used to successfully isolate DAn-specific translated mRNA from the midbrain of THTR mice?
2) Do the translatome profiles of DAn differ between control and PD TH-positive neurons?
3) Can translational profiling of dopaminergic cell populations identify potential progressive changes between young and aged *THTR/hSNCA+* double transgenic mice?
4) Do we see any early disease-related changes in the translatome of young mice bearing the *hSNCA+* transgene?

- CHAPTER 4 -

ESTABLISHING TRANSLATING RIBOSOME AFFINITY PURIFICATION METHODOLOGY IN *THTR* MICE

4.1 Overview

This chapter describes the technical optimisation of the translating ribosome affinity purification (TRAP) protocol published by Heiman et al. (Heiman et al., 2008; Heiman et al., 2014) and application to our novel *TH-bacTRAP* (THTR) transgenic mouse line. qPCR based enrichment analysis of marker genes after pilot TRAP experiments in young hemizygous and homozygous THTR mice, as well as TRAP-negative littermate controls demonstrated the successful establishment of the TRAP protocol and application in aged mice. In addition, this chapter describes a pilot RNA-Seq study on the RNA isolated by TRAP. The pilot RNA-Seq study was undertaken to confirm the successful establishment of the TRAP protocol in our hands on a genome wide scale, proving that THTR mice can indeed be used to isolate DAn-specific mRNA. Moreover, the pilot RNA-Seq results allowed us to establish the TRAP genotype and age for further analysis.

Chapter aims

1) To set up TRAP using a *TH-bacTRAP* (THTR) transgenic mouse line.
2) To optimise the TRAP protocol.
3) To perform a pilot RNA-Seq study using TRAP-isolated RNA.

Collaboration statement

The work in this chapter was conducted in collaboration with the laboratory of Professor Caleb Webber (DPAG, University of Oxford). I performed all wet lab experiments and was involved in the bioinformatic analysis of the RNA-Seq dataset (e.g. defining the project underlying hypothesis and questions, providing literature examples of similar work, choosing genes for enrichment analysis). Library preparation and RNA-Seq runs were undertaken at the Oxford Genomics Centre, Wellcome Trust for Human Genetics (WTCHG), Oxford. The bioinformatic analysis of the RNA-Seq data in this chapter was performed in collaboration with Dr Frank Wessely.

4.2 Introduction

4.2.1 Genome-wide gene expression analysis

Genome-wide gene expression profiling provides a unique and valuable tool to gain insights into cellular function and molecular characteristics of distinct cell populations. It can be used to create a picture of cellular and molecular pathways which are specifically related to disease. This unique capture of the mRNA profile not only provides novel insights into pathological disease pathways but also holds potential to facilitate the discovery of new therapeutic targets. Recent successes in high-throughput gene expression analysis, including microarray and RNA-Seq, has provided a breakthrough in the field allowing more sensitive and specific detection of mRNA (Lashkari et al., 1997; Nagalakshmi et al., 2008; Wang et al., 2009). Nevertheless, when analysing regional gene expression of whole tissues, changes in rare cell-types can be missed because they represent only a small proportion of the mRNAs of the total pool of transcripts. Furthermore, information is lost when different cell-types are averaged within the analysed tissue. Gene expression can be rapidly altered in response to exogenous stimuli, whereby changes on the mRNA level do not necessarily reflect changes on the level of encoded proteins since the correlation between mRNA and protein levels is often insufficient (Gygi et al., 1999). Thus, detailed analysis of changes in polysome-associated mRNAs (translatome) rather than total mRNA (transcriptome) might be a better readout of gene expression changes (Halbeisen and Gerber, 2009) and better reflect the actual protein content of a cell.

Gene expression profiling in the CNS is difficult as the brain is composed of multiple distinct regions which are still ill-defined and contain a variety of heterogeneous, intermixed neuronal subtypes (Emery and Barres, 2008). To study neurodegenerative diseases, there is a great need for methodologies that allow the investigation of neurodegenerative diseases by giving insights into the temporal events leading to neuronal dysfunction and pathologies observed in patients.

4.2.2 Gene expression profiling to study neurodegenerative diseases

The accessibility of CNS tissue is another important drawback for the study of neurodegenerative diseases. Since CNS tissue is largely inaccessible before death, gene expression profiling to study human neurodegenerative diseases relies on the use of post-mortem brain tissue which solely represents the end-stage of disease. Cell culture models *in vitro* such as human embryonic stem cells (hESCs) or induced pluripotent stem cells (iPSCs) hold a great potential for the identification and verification of specific molecular dysfunctions in a dish.

IPSCs provide a promising alternative, especially because the problem of possible oncogene reactivation during IPSC generation due to the introduction of reprogramming factors by lentivirus (Takahashi and Yamanaka, 2006; Takahashi et al., 2007) could be significantly reduced by recent non-integrating approaches (Okita et al., 2008). Nevertheless, reprogramming might still affect the genetic and epigenetic status of clones which makes cautious selection of stable iPSC lines for differentiation studies inevitable. Although reprogrammed fibroblasts from patients contain mutations in known disease-related genes, most neurodegenerative disorders are age-dependent which is difficult to model in long-term culture. Thus, some iPSCs may not reflect the entire disease relevant pathogenesis (Xie and Zhang, 2014). More generally, *in vitro* models have their own disadvantages. Cell culture models lack the ability to replicate complex interactions between neuronal circuits and sub-populations, features which may underlie neurodegenerative disease pathology.

Consequently, the use of transgenic animal models still serve as a valuable tool to obtain insights into the molecular mechanisms underlying neuronal dysfunction seen in human neurodegenerative disease. Animal models enable the long-term combined analysis of pathological alterations at the genomic, as well as proteomic level, and allow multidisciplinary analysis at the electrophysiological, pharmacological and behavioural level (Dawson et al., 2010).

4.3 Results

4.3.1 Establishing TRAP methodology in our *THTR* transgenic mouse line

As described in Chapter 3, hemizygous (*THTR+)* and homozygous (*THTR+/+) THTR* mice that express an eGFP-tagged ribosomal transgene (eGFP-L10a) under the mouse TH promoter, and TRAP-negative littermate controls (*mSnca*-/-) were successfully established. Initially, affinity purifications of DAn-specific mRNA from the THTR line was based on the protocol published in 2008 as part of the original TRAP study by Heiman et al. (Heiman et al., 2008). This version of the protocol required the use of a high amount of input tissue; therefore, pooling of several mouse midbrains was required (results not shown). Since an updated version of the protocol including many technical optimisations, as well as the use of new, more specific reagents was available shortly after the first few pilot experiments, all subsequent pilot TRAP experiments were based on the updated TRAP protocol version (Heiman et al., 2014).

The possibility to freeze and thaw tissue before its use for TRAP would prove technically beneficial simplifying the use of the TRAP protocol on pooled mouse brains, especially for aged mice. To test the effect of freezing and thawing on TRAP efficiency, manually dissected and snap-frozen tissue of THTR mice was taken forward for analysis. Unfortunately, this approach did not enable successful mRNA isolation (results not shown). This was not unexpected, since others also found a disadvantageous effect of freezing tissue on polyribosome integrity and mRNA yields; polysomes and about 50% of the monosomes were lost after flash-freezing of tissue and storage at −80°C (Heiman et al., 2014).

First TRAP experiments shown here were performed according to the protocol published by Heiman et al. in 2014 unless otherwise indicated (Heiman et al., 2014). The same batch of monoclonal GFP antibodies Htz-GFP-19C8 and Htz-GFP-19F7 was used for all TRAP (pilot) experiments performed on the THTR mouse line.

4.3.2 Feasibility pilot TRAP experiments using the *THTR* transgenic mouse line

Preliminary results from the molecular characterisation of the THTR mouse line revealed that the overall eGFP-L10a expression in the midbrain was surprisingly low (Chapter 3). Thus, four brains from young hemizygous and homozygous TRAP-positive or TRAP-negative mice were pooled for initial feasibility pilot TRAP experiments. To limit the total brain tissue mass for the lysis and reduce potential non-specific background binding, midbrains were manually dissected and lysed and processed according to the TRAP protocol. Figure 4. 1 shows that high-quality RNA can be isolated from TRAP-positive midbrains. qPCR experiments using the immunoprecipitated RNA (bound to the beads; immunoprecipitated= IP) or the RNA isolated from the supernatant (not bound to the beads; unbound= UB), detected higher levels of the DAn markers DAT (1.4x) and TH (1.2x) but not for the two non-neural markers GAD2 (Glutamate decarboxylase 2) and GFAP (Glial fibrillary acidic protein) in the IP RNA fraction of TRAP-positive mice when normalised to the IP RNA isolated from TRAP-negative mice. The expression of these DAn markers was about 2x higher in homozygous THTR mice (Figure 4. 1 C) compared to TRAP-negative mice. The markers tested for the UB RNA fraction from TRAP-positive mice were undistinguishable when normalised to the UB RNA fraction of TRAP-negative mice (Figure 4. 1 F). Later, a Total (input) RNA fraction has been saved before each TRAP immunoprecipitation to calculate the individual enrichment scores for each IP fraction.

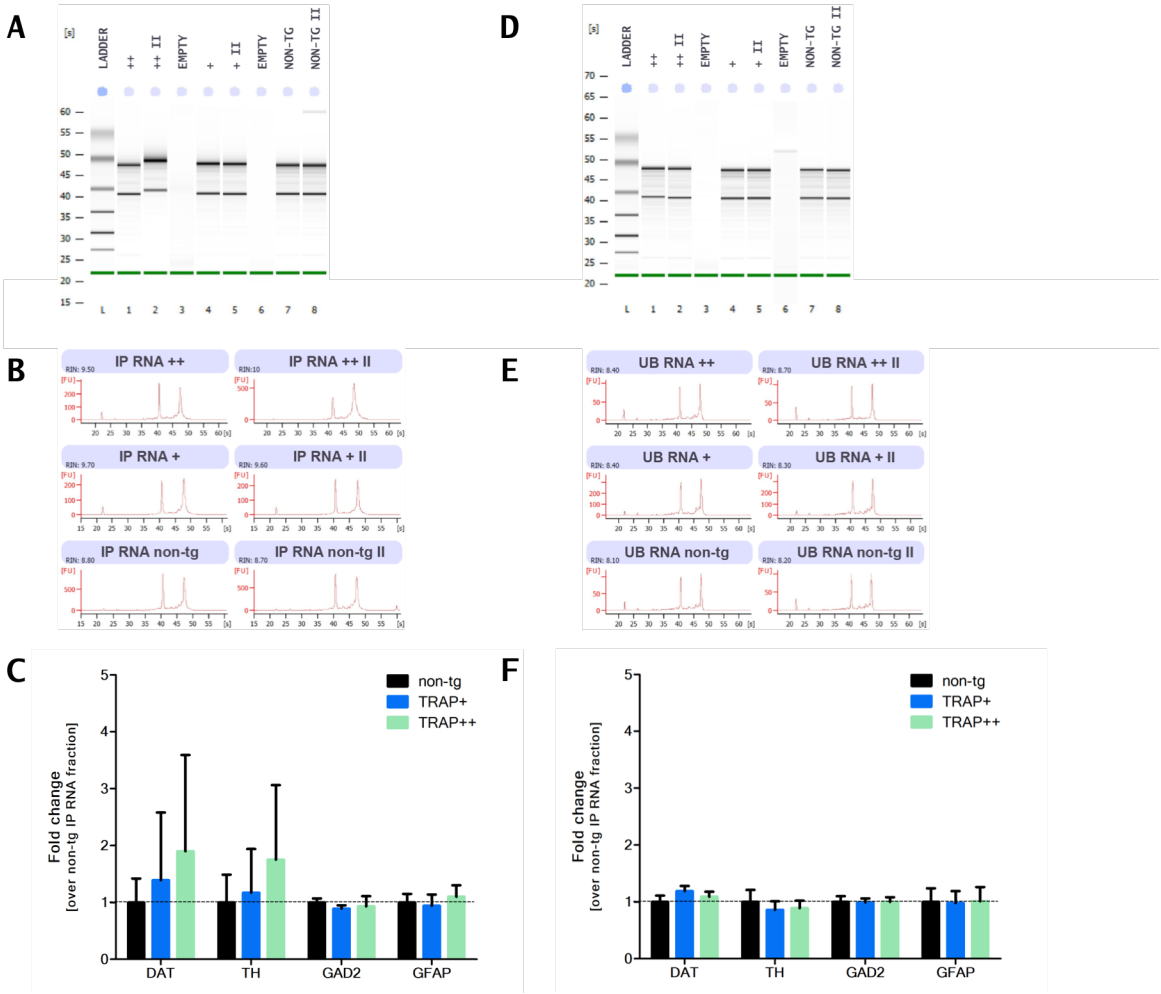


Figure 4. 1 ***Pilot TRAP experiments using the THTR transgenic mouse line successfully enrich DAn-markers in the IP fraction.***

The TRAP protocol (Heiman et al., 2014) was used to isolate DAn-specific mRNAs from midbrains of young THTR mice and TRAP-negative littermate controls. Representative Agilent bioanalyzer densitometry plots (A, D) and electropherogram results (B, E) for the IP RNA (A, B) and the UB RNA fraction (D, E) confirm good quality of the isolated RNA. (C) Summary of qPCR results of the TRAP IP RNA fraction shows enrichment for DAn markers TH and DAT only in TRAP-positive mice. No enrichment is seen for non- DAn markers (GAD2, GFAP). (F) qPCR analysis of the UB fraction did not enrich any of the marker tested. The qPCR results were normalised to the mean of two reference genes and fold-enrichment values were calculated over non-tg gene expression using the comparative Ct method (n= 3 independent TRAP experiments; one-way ANOVA with Tukey post-hoc analysis; mean ± SEM). IP= bound or immunoprecipitated RNA fraction. UB= unbound RNA fraction. Non-tg= non-transgenic (TRAP-negative). ++ or TRAP++= Homozygous THTR mice. + or TRAP+= Hemizygous THTR mice. DAT= Dopamine transporter. TH= Tyrosine hydroxylase. GAD2= Glutamate decarboxylase 2. GFAP= Glial fibrillary acidic protein.

The total RNA amount in the IP fraction isolated from these mice was surprisingly high because molecular characterisation experiments (Chapter 3) revealed low GFP-positive cell numbers in the midbrain. TRAP-negative mice also yielded high amounts of RNA after TRAP which suggested that most of the isolated RNA was non-specific background (THTR++: 32.02 ng ± 8.65; THTR+: 44.89 ng ± 3.90; TRAP-negative: 49.45 ng ± 13.83). Brain tissue is known to be a fatty tissue with high lipid content, the tissue tends to have the highest background RNA levels when processed using the TRAP protocol (Heiman et al., 2014). Thus, it was expected that a certain amount of non-specific

RNA would also be isolated from TRAP-negative samples due to the 'stickiness' of the magnetic beads used to construct the affinity matrix for TRAP.

In contrast to the high yield of RNA, we detected only a relatively low enrichment for DAn markers. This might be caused by the low number of GFP-positive cells in the midbrain (Chapter 3). In any case, the absence of a specific enrichment for any certain cell-type in the background RNA suggests that the presence of non-specific RNA is negligible and should not pose a problem in subsequent analysis. This RNA could result even in a positive effect serving as carrier RNA. Because the variability of the fold-enrichment after qPCR was too variable and the isolated RNA amounts in the TRAP-negative fractions were very high, further optimisation experiments were carried out to optimise the published protocol to the needs of this transgenic line.

4.3.3 Matrix optimisation TRAP experiments in young and old THTR mice

Next, the matrix component amounts were altered as recommended in the updated protocol version (Heiman et al., 2014) in order to find an optimal amount of matrix that captures all tagged mRNAs. Because the amount of affinity matrix needed is influenced by abundance, size, and translational state of the cell-type of interest, the overall amount of affinity matrix components was doubled (2x), left unchanged (1x), halved (0.5x), and quartered (0.25x) in a set of pilot experiments. The first round of optimisation experiments used **one** single mouse midbrain per experimental 'n' (Figure 4. 2). As before, high quality RNA could be successfully isolated but the amount of RNA isolated from any of the fractions was very low. Since the qPCR analysis for the 2x and 1x matrix conditions (Figure 4. 2 A, B) showed a variable enrichment pattern for the markers tested, only 0.5x or 0.25x matrix conditions (Figure 4. 2 C, D) were taken forward for further optimisations. For a more comparable read-out of marker gene enrichment before and after IP, the fold-change for these experiments was calculated individually for each IP sample over its input (Total) RNA fraction.

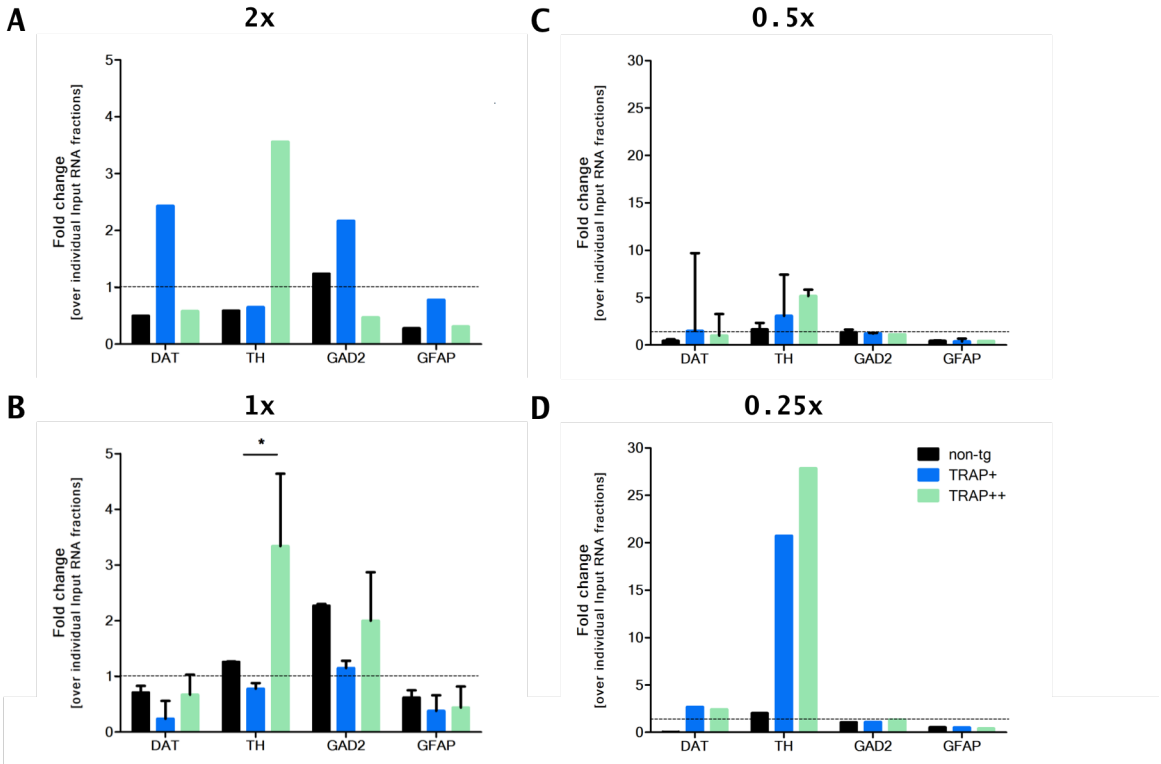


Figure 4. 2 ***TRAP Affinity matrix optimisation experiments adapt the TRAP protocol to the THTR mouse line.***

*Per experimental 'n', **one** midbrain of young hemizygous or homozygous THTR mice and TRAP-negative littermate controls was used to analyse the effect of modifying the 'Affinity matrix' components on the successful isolation of DAn-specific mRNAs. 'Affinity matrix' components (Heiman et al., 2014) were doubled (A), kept unchanged (B), halved (C), and quartered (D). Enrichment for the DAn markers TH and DAT was a success, while no enrichment for non-DAn markers (GAD2, GFAP) was desired. The qPCR results were normalised to the mean of two reference genes and fold-enrichment values were calculated separately for each sample based on expression of sampled input RNA before TRAP using the comparative Ct method (n= 1 (A, D) or 2 (B, C) independent TRAP experiments; one-way ANOVA with Tukey post-hoc analysis; mean ± SEM; *p≤ 0.05). IP= bound or immunoprecipitated RNA fraction. UB= unbound RNA fraction. Non-tg= non-transgenic (TRAP-negative). ++ or TRAP++= Homozygous THTR mice. + or TRAP+= Hemizygous THTR mice. DAT= Dopamine transporter. TH= Tyrosine hydroxylase. GAD2= Glutamate decarboxylase 2. GFAP= Glial fibrillary acidic protein.*

In order to find the optimal compromise between enough RNA for downstream applications and best possible enrichment of DAn markers, the amount of input tissue was doubled (using **two** midbrains per experimental 'n') and tested again with the 0.5x and 0.25x matrix conditions. The second round of matrix optimisation experiments confirmed that halving the initially described affinity matrix component amounts led to successful enrichment of DAn markers in homozygous samples as visualised by qPCR also when using more input tissue (Figure 4. 3 A). Even better results could be achieved with 0.25x matrix component amounts; under these conditions IP RNA isolated TRAP-positive mice enriched significantly for DAT (hemizygous THTR mice: 1.1x; homozygous THTR mice: 5.4x) and TH mRNA (hemizygous THTR mice: 2.2x; homozygous THTR mice: 3.9x). Non-DAn markers were not enriched in any of the IP fractions over Total RNA input. For both conditions, the

RNA integrity numbers (RIN) were suitable for a gene expression profiling study by RNA-Seq (Figure 4. 3 A', B'; RIN of ≥7). RIN values are a direct read-out for the integrity of RNA molecules based on a technique that relies on an algorithm that assigns integrity values to RNA measurements gained during electrophoretic RNA separation in an automated high-throughput approach (Schroeder et al., 2006). Determining RNA integrity prior to sequencing studies is of paramount importance as low quality or even degraded RNA samples can significantly impact on gene expression profiling results (Gallego Romero et al., 2014).

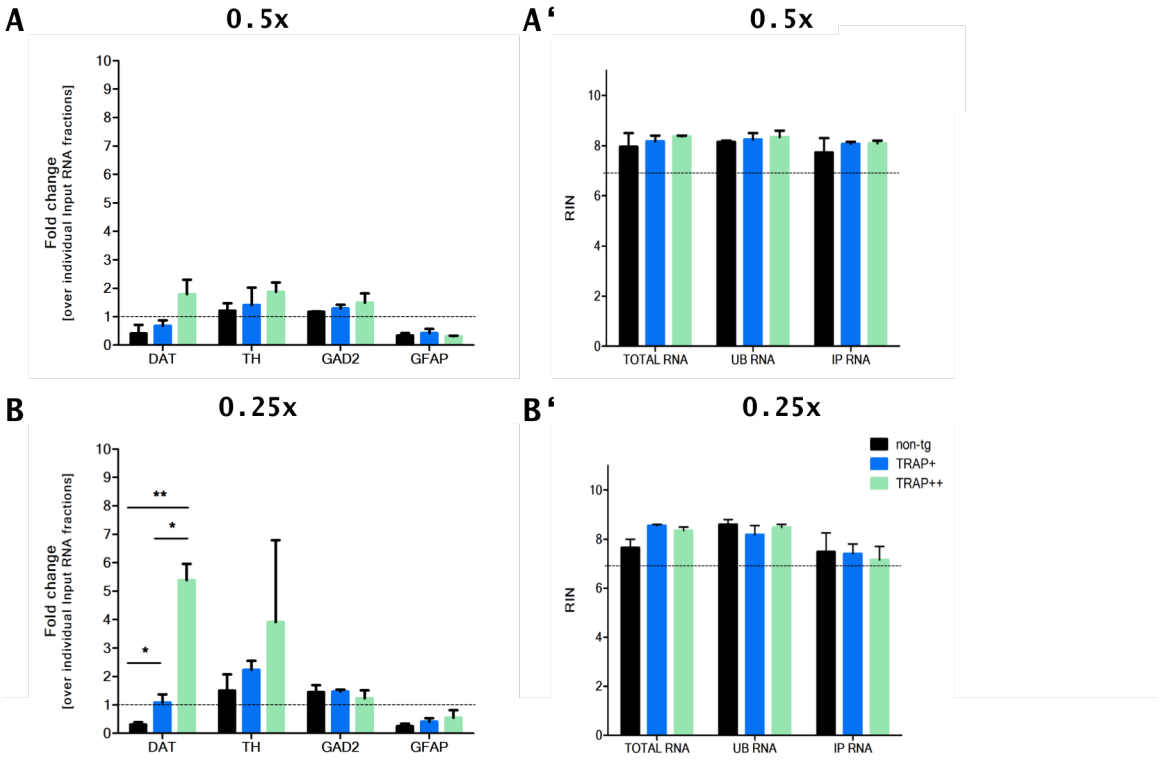


Figure 4. 3 ***Second round of TRAP Affinity matrix optimisation experiments confirm optimal TRAP matrix amounts.*** *Per experimental 'n', **two** midbrains of young hemizygous or homozygous THTR mice and TRAP-negative littermate controls were used. (A, A') 'Affinity matrix' using 0.5x matrix component amounts (Heiman et al., 2014). DAT and TH were slightly enriched after qPCR only for homozygous THTR mice. (B, B') qPCR using 0.25x matrix component amounts on TRAP isolated RNA show a clear enrichment for DAn marker DAT and TH mRNA in TRAP-positive mice, whereas non-DAn markers are not enriched in the IP fractions. RIN values showed good RNA quality for all conditions and genotypes (A', B'). qPCR results are normalised to the mean of two reference genes and fold-enrichment values were calculated separately for each sample based on input RNA expression before TRAP using the comparative Ct method (n= 2 independent TRAP experiments; one-way ANOVA with Tukey post-hoc analysis; mean ± SEM; *p≤ 0.05, **p≤ 0.01). IP= bound or immunoprecipitated RNA fraction. UB= unbound RNA fraction. RIN= RNA integrity number. Non-tg= non-transgenic (TRAP-negative). ++ or TRAP++= Homozygous THTR mice. + or TRAP+= Hemizygous THTR mice. DAT= Dopamine transporter. TH= Tyrosine hydroxylase. GAD2= Glutamate decarboxylase 2. GFAP= Glial fibrillary acidic protein.*

As a next step, 0.25x matrix component amounts were tested using midbrain tissue isolated from aged THTR mice (n= 1 equals **two** midbrains). Here, due to the limited availability of aged mice for a pilot study, no non-transgenic mice were used. Results in 18 months old mice confirmed that high quality mRNA can still be isolated from aged *THTR* transgenic mice using TRAP. Hemizygous *THTR* showed a slight enrichment for DAn marker mRNA after qPCR on the IP RNA fraction compared to Total RNA input, mirroring the results seen in 3 months old mice (Figure 4. 4 A, A'). Again, this enrichment was significantly more pronounced for the IP RNA isolated from homozygous aged THTR mice (DAT: 2.2x; TH: 5.3x). A general slight decrease in fold-change for DAn markers was expected since ageing in general can trigger the loss of dopamine containing neurons in the brain (Naoi and Maruyama, 1999) and molecular characterisation indicated a reduction in GFP-positive cells in 18 months old mice (Chapter 3).

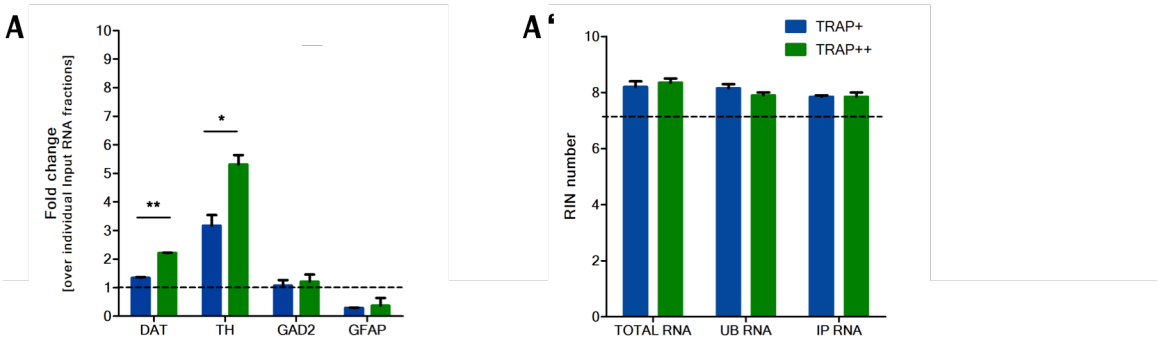


Figure 4. 4 ***Optimised TRAP Affinity matrix conditions can be successfully used for aged THTR transgenic mice.***

*Per experimental 'n', **two** midbrains of 18 months old hemizygous or homozygous THTR mice were used. (A) qPCR results after TRAP using 0.25x 'Affinity matrix' component amounts (Heiman et al., 2014). Old homozygous THTR animals show the best enrichment for DAT and TH mRNA. While TH is enriched in hemizygous THTR, there is no enrichment for DAT enrichment. (A') RIN values prove success of good quality RNA isolation from aged mice after TRAP for all fraction and all genotypes. The qPCR results were normalised to the mean of two reference genes and fold-enrichment values were calculated separately for each sample based on input RNA expression before TRAP using the comparative Ct method (n= 2 independent TRAP experiments; one-way ANOVA with Tukey post-hoc analysis; mean ± SEM; *p≤ 0.05, **p≤ 0.01). IP= bound or immunoprecipitated RNA fraction. UB= unbound RNA fraction. RIN= RNA integrity number. Non-tg= non-transgenic (TRAP-negative). ++ or TRAP++= Homozygous THTR mice. + or TRAP+= Hemizygous THTR mice. DAT= Dopamine transporter. TH= Tyrosine hydroxylase. GAD2= Glutamate decarboxylase 2. GFAP= Glial fibrillary acidic protein.*

In addition to optimising the matrix component amounts, other modifications of the originally published TRAP protocol were undertaken to optimise its use further. These modifications are outlined in the Materials and Methods section of this thesis (Chapter 2).

After confirming that high-quality RNA can be isolated from the midbrains of our bacTRAP mice at a young (3 months) and old age (18 months) using the TRAP methodology, we went on to perform a pilot RNA-Seq study. This study was undertaken to confirm the successful isolation of DAn-specific mRNA from our bacTRAP model on a genome-wide scale. Moreover, we intended to confirm the genetic background (hemizygous or homozygous THTR mice) for the further analysis of DAn-specific mRNA based on the pilot RNA-Seq results.

4.3.4 Pilot TRAP RNA-Seq and bioinformatic analysis

qPCR analysis of selected markers confirmed the successful establishment of the TRAP protocol in our laboratory and its adaption for the use with our *THTR* transgenic mouse line, especially in homozygous THTR mice. The pilot RNA-Seq study on TRAP-isolated IP and Total RNA from young (3 months) and aged (18 months) THTR mice aimed to answer whether the TRAP protocol could be successfully used to isolate midbrain-specific mRNA ((midbrain) dopaminergic profile). Since RNA-Seq enables high-throughput analysis of genome-wide gene expression, a greater variety of dopaminergic and non-DAn markers could be tested for fold-changes in IP vs Total fractions. Lastly, the pilot RNA-Seq study aimed to confirm that TRAP-isolated RNA samples from the aged THTR mice can still be used to enrich DAn-specific markers.

Integrity was checked on the Agilent Bioanalyzer pico chip and quantity was measured using the RiboGreen assay before submitting the RNA to sequencing at the WTCHG, Oxford. In this pilot study, a total of 8 samples was analysed (Figure 4. 5 A and C). The colour scheme for each sample depicted in Figure 4. 5 is consistent throughout the following analysis. At the 3-month time-point, TRAP-negative, TRAP-positive hemizygous, and homozygous IP and Total RNA samples were prepared for sequencing. At the time of the pilot RNA-Seq analysis, only hemizygous aged THTR (18 months) sample were sequenced alongside the THTR samples at 3 months since no aged

homozygous THTR were available at the time of the pilot RNA-Seq study. The fold-enrichment graphs as gained by qPCR analysis for the respective samples are shown below (Figure 4. 5 B, D). The SMARTer synthesis kit for low level RNA was used for cDNA synthesis, the cDNA was end-repaired, A-tailed, and adapter-ligated. The prepared libraries were size selected and multiplexed before sequencing on two lanes as 50 bp paired-end reads (PE) on an Illumina HiSeq Rapid sequencer (Table 4. 1). The quality control (QC) performed with FastQC and Rqc package detected an adapter contamination for both reads, lane 1 and 2, with more adapter contamination for read 2. The over-represented sequence has a length of 31 bp: AAGCAGTGGTATCAACGCAGAGTACATGGGG. This is a commonly found issue in the performed library preparation method (Clontech manual) and can be addressed by simply trimming the reads.

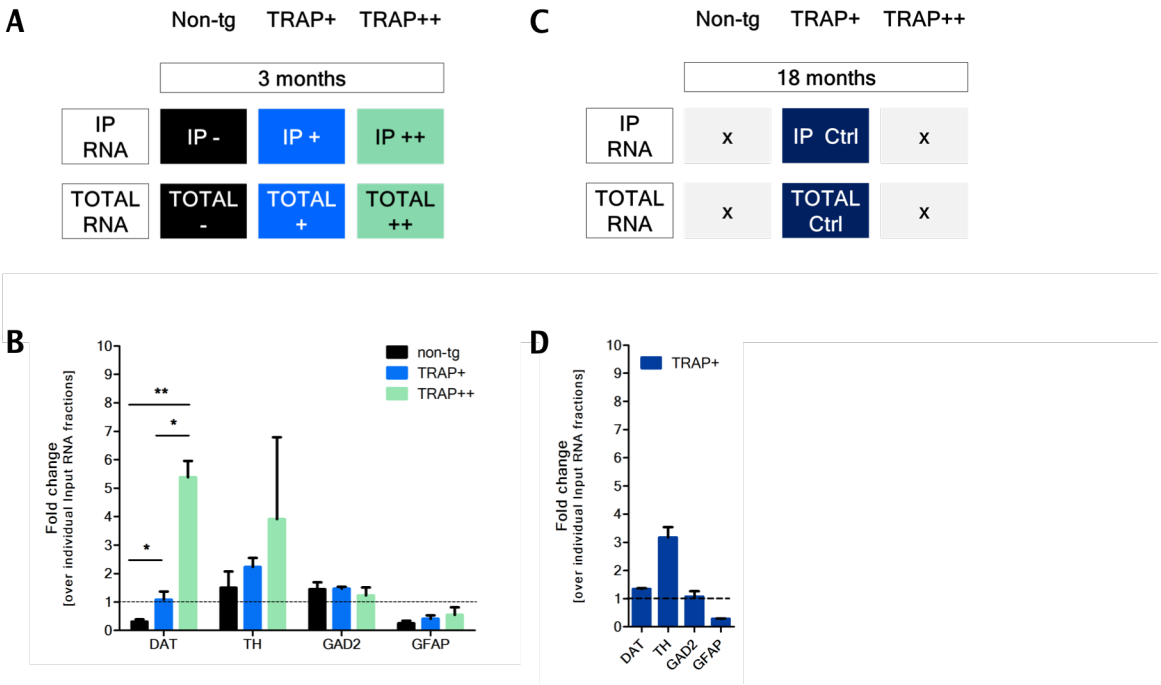


Figure 4. 5 Sample overview for Pilot TRAP RNA-Seq and corresponding TRAP-qPCR enrichment graphs.

*IP and Total TRAP RNA sample for each of the here shown genetic backgrounds from either young THTR mice (A; 3 months) or aged THTR mice (C; 18 months) was analysed in a pilot RNA-Seq study. (B, D) Corresponding qPCR results after TRAP of the samples analysed in the pilot RNA-Seq study. Young and aged TRAP-positive mice show enrichment for DAT and TH, but not non-DAn marker genes tested. The qPCR results were normalised to the mean of two reference genes and fold-enrichment values were calculated separately for each sample the comparative Ct method (n= 2 independent TRAP experiments; one-way ANOVA with Tukey post-hoc analysis; mean ± SEM; *p≤ 0.05, **p≤ 0.01). IP= bead-bound or immunoprecipitated RNA fraction. Total= input RNA fraction. Non-tg= non-transgenic (TRAP-negative). ++ or TRAP++= Homozygous THTR mice. + or TRAP+= Hemizygous THTR mice. DAT= Dopamine transporter. TH= Tyrosine hydroxylase. GAD2= Glutamate decarboxylase 2. GFAP= Glial fibrillary acidic protein.*

Sample Name	Age (months)	TRAP fraction	RNA-Seq ID	Sequencing Index	Wellcome Trust File Name	Lane	Read count
THTR++ IP RNA	3	IP	IP++	S241	WTCHG_217911_241	1	15,940,257
THTR++ Total RNA	3	Total	Total++	S242	WTCHG_217911_242	1	16,917,611
THTR+ IP RNA	3	IP	IP+	S243	WTCHG_217911_243	1	17,370,601
THTR+ Total RNA	3	Total	Total+	S244	WTCHG_217911_244	1	20,543,593
non-tg IP RNA	3	IP	IP-	S245	WTCHG_217911_245	1	15,751,104
non-tg Total RNA	3	Total	Total-	S246	WTCHG_217911_246	1	19,421,331
THTR+ IP RNA	18	IP	IP+ old	S249	WTCHG_217911_249	1	16,300,727
THTR+ Total RNA	18	Total	Total+ old	S250	WTCHG_217911_250	1	16,590,227
THTR++ IP RNA	3	IP	IP++	S241	WTCHG_217912_241	2	15,925,039
THTR++ Total RNA	3	Total	Total++	S242	WTCHG_217912_242	2	16,915,652
THTR+ IP RNA	3	IP	IP+	S243	WTCHG_217912_243	2	17,395,075
THTR+ Total RNA	3	Total	Total+	S244	WTCHG_217912_244	2	20,546,711
non-tg IP RNA	3	IP	IP-	S245	WTCHG_217912_245	2	15,769,417
non-tg Total RNA	3	Total	Total-	S246	WTCHG_217912_246	2	19,428,299
THTR+ IP RNA	18	IP	IP+ old	S249	WTCHG_217912_249	2	16,293,880
THTR+ Total RNA	18	Total	Total+ old	S250	WTCHG_217912_250	2	16,588,655

Table 4. 1 Pilot TRAP-Seq samples overview.

Summary of the 8 samples processed in the pilot TRAP RNA-Seq study. The samples were multiplexed and sequenced together over two lanes (lane 1+2). WTCHG= Wellcome Trust centre for Human Genetics. IP= TRAP immunoprecipitated RNA fraction. Total= TRAP input RNA fraction. Young= 3 months old mice. Old= 18 months old mice. Non-tg= non-transgenic. –= TRAP-negative or non-tg mice; mSnca-/-. += hemizygous THTR mice. ++= homozygous THTR mice. Analysis performed in collaboration with F. Wessely.

PCA confirmed successful separation of the homozygous TRAP IP samples from the input fraction

Next, a principal component analysis (PCA) using the fragments per kilo base million (FPKM) values could show that the homozygous TRAP IP sample (3 months) successfully separated from the Total/Input TRAP RNA samples, as well as the hemizygous and TRAP-negative (non-tg) IP samples. Figure 4. 6 A shows an overview of the samples used for this analysis. In more detail, focusing on the samples of the 3 months old mice, the PCA plot (PC1 vs PC2) revealed a clear separation of all IP TRAP RNA (circles) on the left from the Total/Input TRAP RNA samples (hexagon) on the right (Figure 4. 6 B). Surprisingly, the Total fraction from THTR++ mice separates from the Total of THTR+ and TRAP-negative samples. Due to the random integration of the bacTRAP construct in to the genome, breeding BAC mice to homozygosity always harbours the risk of interfering with important genomic regions, which is a likely cause of the detected variance in THTR++ mice. Combining 3 and 18 month samples for PCA maintains the above-mentioned separation between IP (circles) and

Total (hexagons) samples in the PC1 vs PC2 plot which account for the greatest proportion of the detected variation (Figure 4. 6 C; PC1: 78.5%; PC2: 9.9%). Concentrating on the IP samples, the PC1 vs PC2 plot showed a strong separation between the TRAP-negative (IP-) and the homozygous THTR IP samples (IP++) with the hemizygous THTR samples (IP+) in-between both. Of note, animals of the hemizygous THTR genetic background clustered closer together irrespectively of their age (3 vs 18 month) (Figure 4. 6 C; PC1 vs PC2).

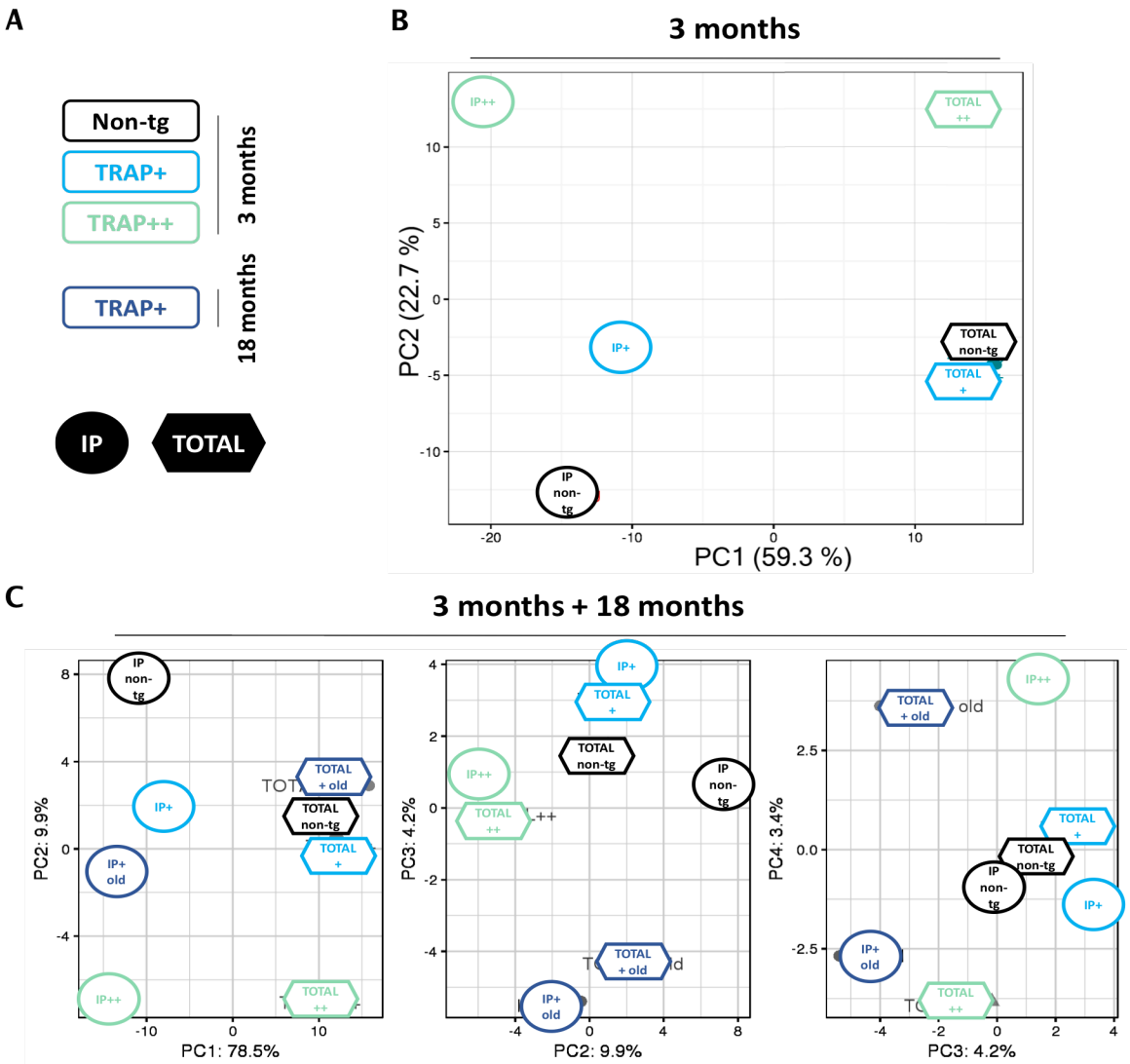


Figure 4. 6 ***Principal Component Analysis (PCA) of the Pilot RNA-Seq results.***

(A) Sample overview. (B) PC plot representing the variation between the IP and Total samples (3 months). Plotted are the FPKM values of 2000 most variable genes. PC1 and 2 explain up to 82% of the total variance. IP samples (circle) cluster away from Total samples (hexagon). (C) Combined PCA (3 and 18 month). IP and Total samples do not overlap. IP= bead-bound or immunoprecipitated RNA fraction. Total= input RNA fraction. Non-tg= non-transgenic (TRAP-negative). ++ or TRAP++= Homozygous THTR mice. + or TRAP+= Hemizygous THTR mice. Modified after F. Wessely. Analysis performed in collaboration with F. Wessely.

Scatter plots show enrichment of DAn markers in the IP fractions of homozygous TRAP IP samples

To verify the dopaminergic character of the IP fraction, the fold-changes in FPKM values comparing IP vs Total TRAP fraction were plotted for selected markers (Figure 4. 7 A-C) or compared to a set of published genes found as enriched or depleted in DAn in another study also employing TRAP methodology (Brichta et al., 2015) (Figure 4. 7 A'-C'). The DAn markers used for Figure 4. 7, the FPKM values, and fold-changes (FC) for DAn and non-DAn genes shown in the scatter plots are listed in the Appendix (Appendix Table 4. 1, Appendix Table 4. 2, Appendix Table 4. 3). Using scatter plot analysis, we could show that only homozygous TRAP IP samples achieved successful enrichment of DAn marker mRNA in the IP vs Total TRAP fraction using a few selected markers (Figure 4. 7 C), or a global comparison of genes found enriched or depleted in DAn (Figure 4. 7 C').

In greater detail, the comparison of selected markers in the TRAP-negative IP- vs Total- RNA (black box) showed no clear separation. In contrast, a few of the DAn markers start to separate away from the midline for the hemizygous IP+ vs Total+ RNA (light blue box) comparison, but we could only detect a clear enrichment for most of the DAn marker genes (turquoise) in the homozygous IP++ vs Total++ RNA (light green box) comparison. For example, mRNA for DAn markers TH, DAT, and PITX3 was enriched more than 5x in the IP fraction (12.8x, 5.9x, and 7.4x, respectively). Non-DAn specific genes (red) were more highly present in the Total midbrain input fraction (Figure 4. 7 A-C).

For the global gene comparison, TRAP-negative and TRAP hemizygous RNA fractions showed no clear separation of the genes previously associated with DAn (turquoise) and the genes associated with total midbrain (red) (Figure 4. 7 A' - C'). Figure 4. 7 C' represents the homozygous TRAP RNA samples for which a good separation of the two gene fractions was shown. Many 'turquoise genes' were enriched by at least 1.5 x in the IP RNA fraction, whereas the 'red genes' mainly clustered on the Total RNA side of the plot.

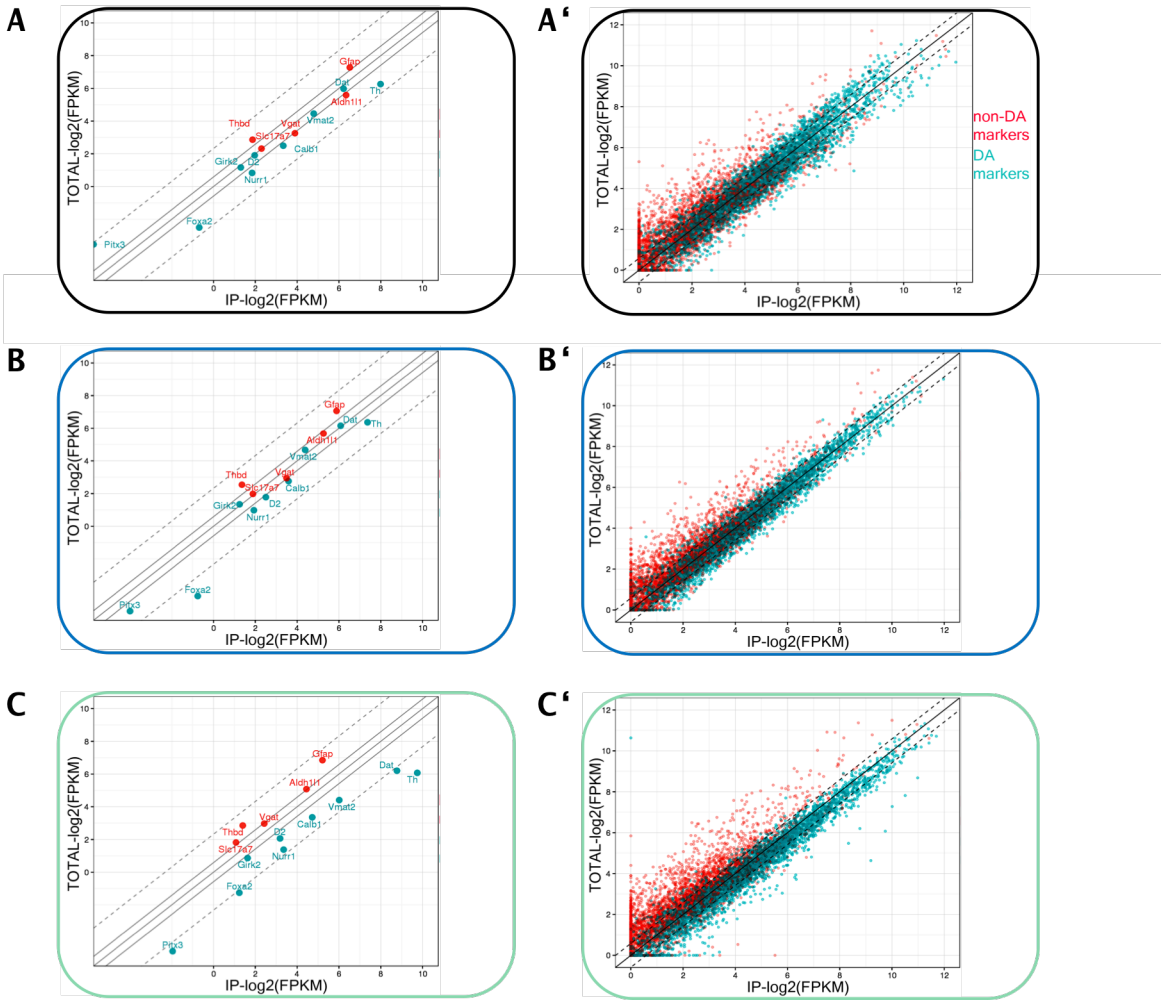


Figure 4. 7 ***Scatter plots showing a comparison of IP vs Total TRAP RNA using selected markers and published genes.*** *Fold changes of TRAP IP vs Total RNA were tested for: (A, A’) non-transgenic (black). (B, B’) THTR+ (light blue). (C, C’) THTR++ (light green). (A-C) Here, a selection of dopaminergic (turquoise) and non-DAn marker (red) genes are shown. Negative values after log2 transformation (i.e. FPKM < 1) were set to zero, and the diagonal lines indicate the thresholds for a fold-change in FPKM values of 1 (i.e. no change, middle line), 1.5 (grey lines) or 5 (dashed grey lines). (A’- C’) Plotted are the untrimmed IP versus Total reads using all genes found enriched or depleted in DAn in the study by Brichta et al. Mapped are all genes listed in Supplement table 1 (Brichta et al., 2015; 4381 genes enriched in DAn; turquoise) and 2 (Brichta et al., 2015; 5616 genes enriched in total midbrain; red) to the ENSEMBL gene IDs using biomaRt R-package. A few genes were not mapped, but 4325 DAn and 5431 total midbrain ENSEMBL genes are shown in the plots. Negative values after log2 transformation (i.e. FPKM < 1) were set to zero, and the dashed lines represent a fold change of FPKM values of 1.5 in either direction. IP= bead-bound or immunoprecipitated RNA fraction. Total= input RNA fraction. Non-tg= non-transgenic (TRAP-negative). ++ or TRAP++= Homozygous THTR mice. + or TRAP+= Hemizygous THTR mice. REFERENCE: Brichta et al. 2015. Analysis performed in collaboration with F. Wessely.*

The same analysis was performed on the aged TRAP RNA samples. Fold-changes in FPKM values (IP vs Total TRAP RNA) are summarised in the Appendix. Similar to the young hemizygous TRAP-positive animals, no clear separation of the DAn and non-DAn marker genes could be achieved for either selected markers (Figure 4. 8 A) or the global gene comparison (Figure 4. 8 A’).

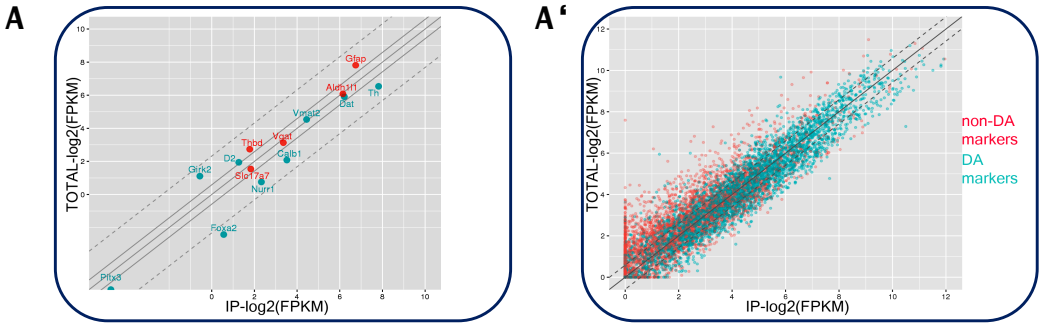


Figure 4. 8 Scatter plots showing the IP vs Total TRAP RNA comparison for aged TRAP mice.

(A) Fold-changes of TRAP IP vs Total RNA for a selection of DAn (turquoise) and non-DAn marker (red) genes. Negative values after log2 transformation (i.e. FPKM < 1) were set to zero, and the diagonal lines indicate the thresholds for a fold-change in FPKM values of 1 (i.e. no change, middle line), 1.5 (grey lines) or 5 (dashed grey lines). (A') Plotted are the untrimmed IP versus Total reads using all genes found enriched or depleted in DAn in the study by Brichta et al. Mapped are all genes listed in Supplement table 1 (Brichta et al., 2015; 4381 genes enriched in DAn; turquoise) and 2 (Brichta et al., 2015; 5616 genes enriched in total midbrain; red) to the ENSEMBL gene IDs using biomaRt R-package. A few genes were not mapped, but 4325 DAn and 5431 total midbrain ENSEMBL genes are shown in the plots. Negative values after log2 transformation (i.e. FPKM < 1) were set to zero, and the dashed lines represent a fold change of FPKM values of 1.5 in either direction. IP= bead-bound or immunoprecipitated RNA fraction. Total= input RNA fraction. + or THTR+= Hemizygous THTR mice. REFERENCE: Brichta et al., 2015. Analysis performed in collaboration with F. Wessely.

TRAP successfully isolates DAn-specific mRNA from homozygous THTR mice

The comparison of fold-changes for the top 50 differentially expressed genes (DEGs) in the THTR++ IP sample showed that the IP++ fraction is very different from the hemizygous genetic background (Figure 4. 9). Many genes, including some known DAn markers, are up-regulated in the THTR++ IP fraction, e.g. TH 13.3x, LMX1A 7.5x, DAT (Slc6a3) 6.3x, or FOXA2 5.8x. The same pattern could be reproduced in the other TRAP IP RNA fractions. To further highlight the DAn profile of the THTR++ IP RNA fractions, the top 500 DEGs of the IP vs Total comparison were analysed using DAVID (https://david.ncifcrf.gov (Huang et al., 2008)) to determine whether they enrich for specific functional categories and pathways. The chosen genes were all up-regulated by more than 2x in the IP fraction compared to total midbrain RNA. KEGG (Kyoto Encyclopaedia of Genes and Genomes) pathways overrepresented in these fractions represented 'calcium signalling pathway' (11 genes, p-value= 3.10 x 10-4), 'synaptic vesicle cycle' (5 genes, p-value= 1.30 x 10-2), and 'dopaminergic synapse' (7 genes, p-value= 1.40 x 10-2) (Figure 4. 9 B). The THTR++ IP RNA-enriched genes were primarily associated with biological processes, such as 'dopamine biosynthetic process' (5 genes, p-value= 9.20 x 10-5), 'negative regulation of neuron apoptotic process' (12 genes, p-value= 7.20 x 10-4), 'aminergic neurotransmitter loading into synaptic vesicle' (3 genes, p-value=

2.70 x 10-3), and 'calcium ion-regulated exocytosis of neurotransmitter' (5 genes, p-value= 2.90 x 10-3) (Figure 4. 9 C). TRAP could be successfully used to isolate DAn-specific mRNA from homozygous THTR mice.

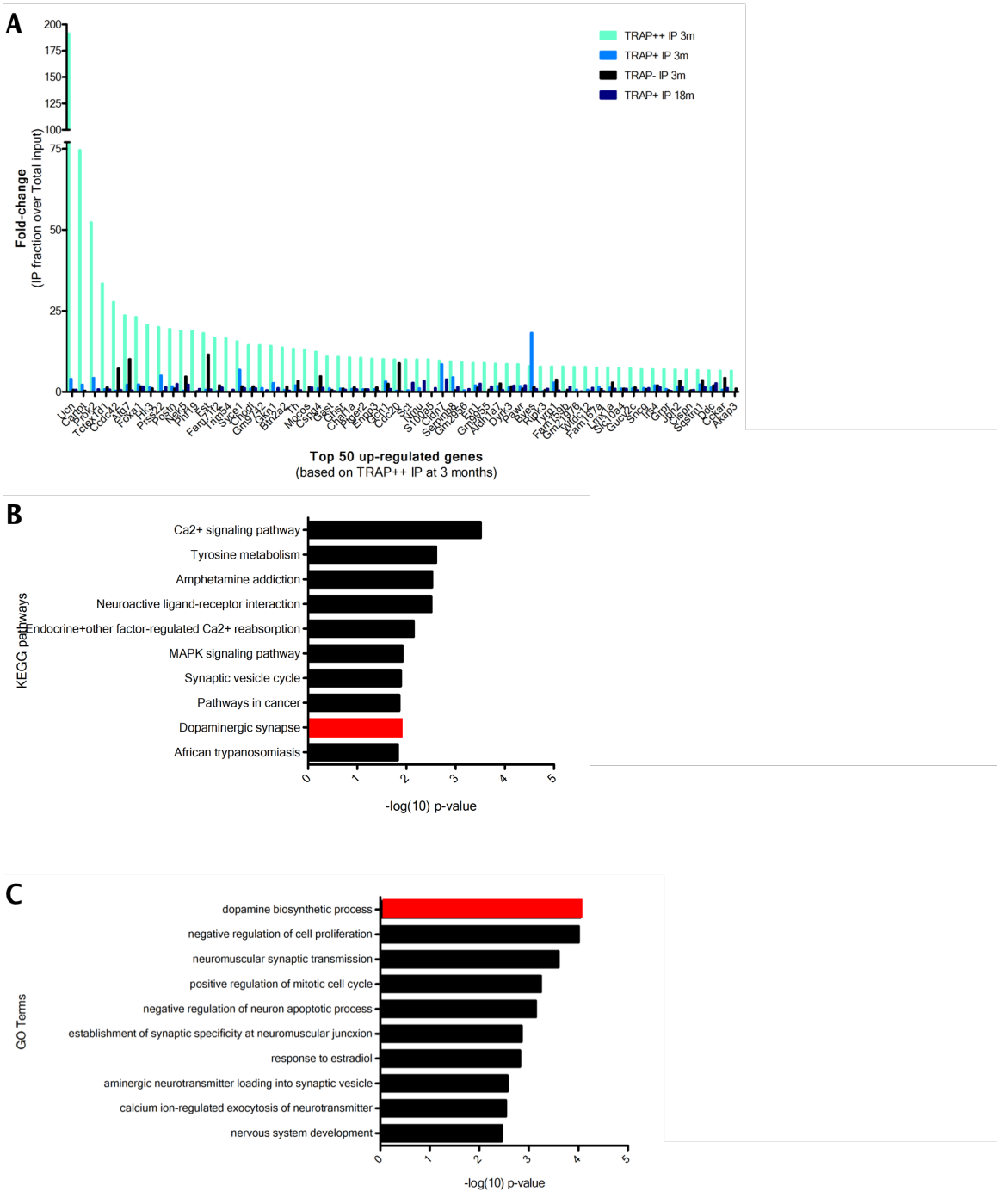


Figure 4. 9 ***Characteristics of the differentially expressed homozygous TRAP IP fraction reveal a DAn-specific profile.*** *(A) Top 50 gene fold-changes based on the TRAP IP vs Total RNA comparison showing the same genes across all samples in the pilot RNA-Seq study. (B, C) Top 10 KEGG pathways and gene ontology biological process (GO-BP) categories using the 500 most changed genes in the THTR++ IP RNA fraction. Analysis was performed using Database for Annotation, Visualisation and Integrated Discovery (DAVID) v6.8. Plotted here is the –log (10) p-value. IP= bead-bound or immunoprecipitated RNA fraction. Total= input RNA fraction. Non-tg= non-transgenic (TRAP-negative). ++ or TRAP++= Homozygous THTR mice. + or TRAP+= Hemizygous THTR mice.*

Hierarchical clustering analysis of DEGs reveals a separate cluster for homozygous TRAP IP samples

In a last analysis, we compared the gene expression of our RNA fractions to a set of midbrain (DAn) markers previously used for the analysis of 96 genes in a microfluidic chip array with the aim to study different midbrain DAn-subtypes (Poulin et al., 2014). The specific set of 96 candidate genes was selected based on their reported differential expression between SNc and VTA (Chung et al., 2005; Greene et al., 2005; Grimm et al., 2004), their previous validation as DAn markers (DDC, TH, DAT, and VMAT2), their link to PD (Atp13a2, LRRK2, PARK2, PARK7, PINK1, and aSyn), as well as their known-role as housekeeping genes (ACTB, GAPDH, and HPRT) (Poulin et al., 2014), summarised in the Appendix. The unbiased hierarchical clustering in a heat map is based on the FPKM values of the all 8 TRAP IP and Total samples and resulted in the presence of three clusters (Figure 4. 10). A separate cluster can be found for the homozygous TRAP IP RNA which is specifically highlighting a DAn profile. Within this cluster, many of the DAn population markers are highly upregulated compared to the two other clusters, for example PITX3, DAT, DRD2, CALB1, FOXA2, DDC, and TH. These genes are expressed at a much lower level in the second cluster comprising all midbrain input RNA samples, representing a mixed midbrain profile for the 96 chosen genes. Since all input midbrain fractions do cluster together nicely, this confirms the consistency in tissue dissection as input for the translating ribosome affinity precipitation. Interestingly, both TRAP hemizygous and TRAP-negative IP RNA samples together formed a third cluster; it is not distinguishable from the non-specific background RNA population, represented here by the TRAP-negative IP sample (Figure 4. 10). This cluster does not show a specific enrichment for a dopaminergic cell population. Overall, the heat map highlights that hemizygous THTR TRAP mice are not suitable for on-going analysis. Bionformatic analysis of this early pilot study was performed by Dr Frank Wessely and was based on FPKM values. Later analysis by Dr Jimena Monzon-Sandoval was based on transcript per million (TPM) values which are more and more used by the bioinformatic field. TPM values are normalised for gene length first, before normalising for sequencing depth. Consequently, the sum of all TPMs in each sample are the same making it easier to compare the proportion of reads that mapped to a gene (Dillies et al., 2013).

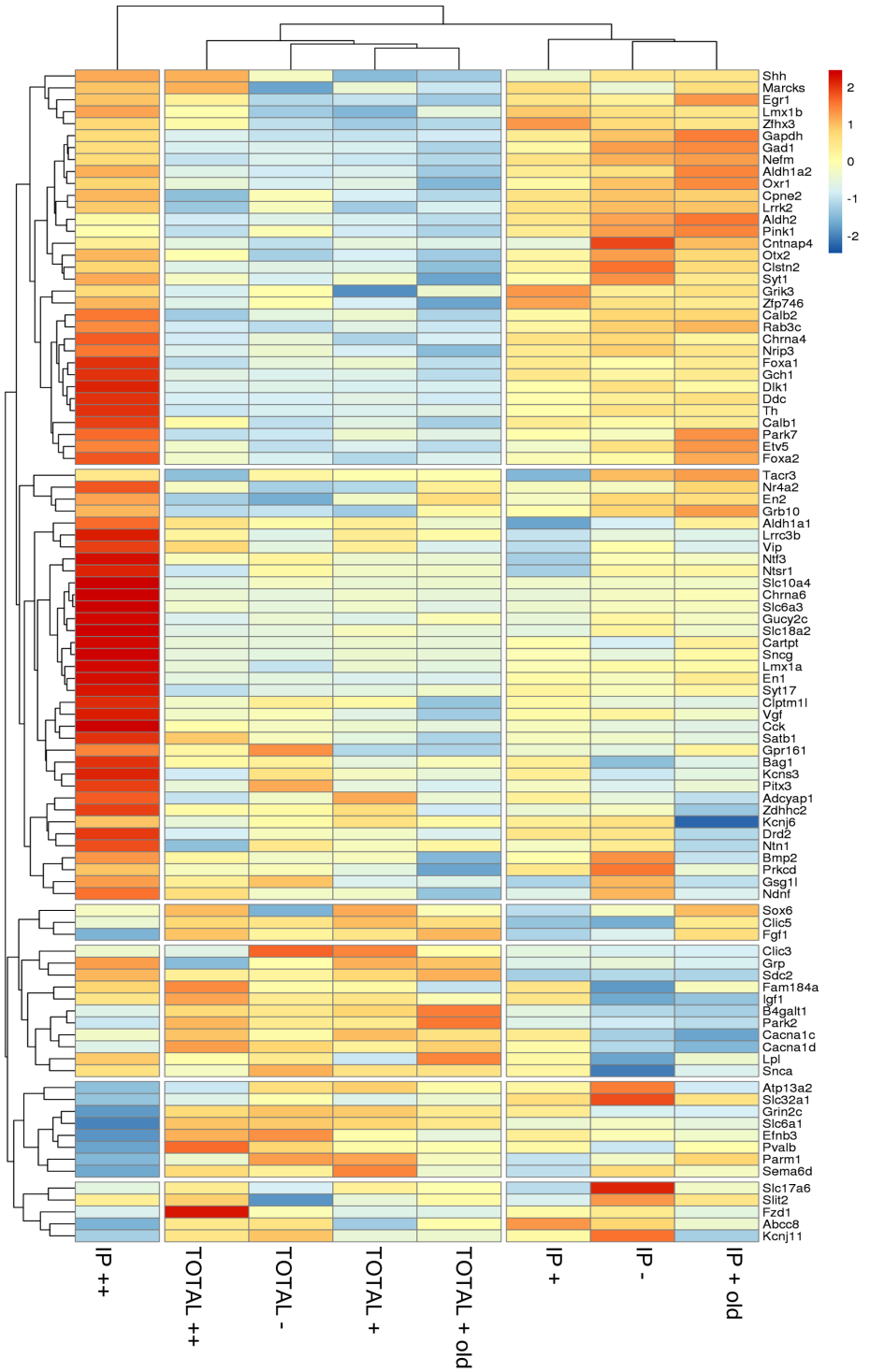


Figure 4. 10 Hierarchical clustering clearly separates the TRAP-homozygous IP sample from the TRAP-negative and TRAP-hemizygous IP samples.

Transformed FPKM values [log2 (FPKM +1)] were used as input for the heat map and clustering of the THTR TRAP RNA samples and 96 selected genes. The expression level of each gene is depicted on a logarithmic scale showing the z-score with red indicating high expression and blue representing a low expression. Unbiased clustering analysis of all 8 samples revealed the presence of a separate cluster for the homozygous TRAP IP RNA, whereas all other TRAP IP RNA fractions form a separate cluster together (TRAP hemizygous young/old, TRAP-negative IP RNA samples). Another cluster is made up of all Total RNA fractions, representing the complete midbrain profile. IP= bead-bound or immunoprecipitated RNA fraction. Total= input RNA fraction. Non-tg= non-transgenic (TRAP-negative). ++ or TRAP++= Homozygous THTR mice. + or TRAP+= Hemizygous THTR mice. REFERENCE: Poulin et al., 2014. Analysis performed in collaboration with F. Wessely.

4.4 Discussion and Conclusion

The aim of this chapter was to describe the optimisation and adaption of the TRAP protocol to be used with our *THTR* transgenic mouse line. The changes to the protocol allowed successful isolation of DAn-specific mRNA from midbrains of THTR mice. The pilot RNA-Seq study helped to define the optimal genetic background and determined the age frame that enabled best results using TRAP in combination with translatome profiling in THTR mice.

The experiments outlined above focused on answering the following questions:

- Can the TRAP protocol be used to successfully isolate DAn-specific translated mRNA from the midbrain of THTR mice?
- Is dopaminergic mRNA enriched and are the translatome profiles of DAn different between TRAP-positive and TRAP-negative (background) samples?
- Is homozygous breeding of THTR mice required for successful TRAP experiments?
- Can aged THTR mice still be used to successfully isolate actively translated mRNAs using TRAP?

1) Matrix optimisation experiments optimised TRAP results in THTR mice

The first pilot experiments in this chapter confirm successful affinity purifications of translated DAn-specific mRNA from the midbrains of our *THTR* transgenic mouse line. Nevertheless, the enrichment of DAn markers was low and variable between experiments and a large amount of input tissue was needed. Unfortunately, we were not able to effectively use flash-frozen tissue for TRAP, a result that was not unexpected since others have already shown a loss of about 50% of the monosomes upon flash-freezing of tissue and storage at −80 °C (Heiman et al., 2014). In order to reduce the number of mice per experimental 'n' and to reduce experimental variation, further essential optimisation experiments have been carried out. These optimisation experiments adjusted the protocol to the here used THTR mouse line.

Considerable cellular heterogeneity within the midbrain cell populations of the SNc and VTA (Grimm et al., 2004) with close anatomical proximity of intermingled cell-types such as glutamate neurons especially within the VTA (Nair-Roberts et al., 2008; Yamaguchi et al., 2007) enlarge the potential of cross-contamination with unwanted cell-types. The determination of cross-

contamination is particularly important for the analysis of genes that are expressed at low levels in the cell population of interest compared to surrounding cells. To control the degree of contamination with unwanted cell-types, the DAn-associated gene expression in TRAP samples (IP fraction) was analysed relative to the whole midbrain (Total fraction) by qPCR. The expression levels of the DAn-specific genes, DAT and TH, were analysed and to determine the contamination of our DAn-specific mRNA samples with glial cells or GABA neurons we used GFAP and GAD2 markers, respectively. Similarly, a study which enriched midbrain DAn by LCM to a high degree of purity used the fold-enrichments to reflect the relative number of target and non-target cells (Brown et al., 2013). In addition to determining non-specific background signal, the fold-enrichment further serves as a read-out of the efficiency of the TRAP process. In a series of TRAP 'affinity matrix' optimisation experiments, we found optimal amounts for the matrix components which allowed a successful enrichment of DAn markers as shown by qPCR, as well as gained sufficient amounts of RNA for downstream applications (Figure 4. 3). The optimised protocol was successfully used in aged *THTR* mice (18 months). Overall, enrichment of marker genes was more robust and pronounced in homozygous compared to hemizygous THTR mice with a slight but expected decrease in enrichment for DAn markers in aged mice compared to the young age (Figure 4. 3 and (Figure 4. 4).

2) Pilot RNA-Seq comparing TRAP-isolated mRNA and total midbrain RNA successfully enriched for DAn markers in the TRAP-IP fraction

We defined the parameters for our actual TRAP experiments with subsequent gene expression profiling with the help of a pilot RNA-Seq study using TRAP IP and Total RNA fractions at different age time-points and genetic backgrounds. First, only the homozygous bacTRAP genetic background was sufficient to truly resemble a DAn-specific translatome (Figure 4. 6; Figure 4. 7; Figure 4. 9). Despite the fact that the TRAP IP fraction from non-transgenic mice presented some RNA, no specific neuronal profile could be detected in this background RNA population by RNA-Seq (Figure 4. 7). Ideally, the use of TRAP-negative mice should not lead to any RNA isolation since the beads are specifically designed to capture eGFP-polysomes only.

Very likely, non-specific RNA binds to the sticky beads which cannot be completely removed during the washing steps. Beads get lost with every wash step but too harsh pipetting techniques could disintegrate the mRNA-ribosome connection or introduce too many bubbles in the tube. Thus, it is a fine line between how much background can be removed without losing any truly bound mRNAs. Probably, RNA can bind to the beads non-specifically because the number of eGFP-positive cells is generally quite low in the THTR line (Chapter 3). There might not be enough eGFP-positive ribosomes in the lysate to saturate all beads, leaving room for non-specific binding. Reducing the number of beads used to set up the affinity matrix even further was tested as well (results not shown) but this did not lead to any significant improvements. Thus, for future TRAP experiments, it must be assumed that a proportion of the isolated RNA will always be non-specific background despite optimising the TRAP protocol for this mouse line.

3) Homozygous THTR mice are necessary for successful TRAP experiments

Underlining former molecular characterisation results, qPCR analysis of TRAP IP RNA in young or aged THTR mice showed that the homozygous genetic background for the bacTRAP transgene is more suitable for the use in TRAP experiments. In addition, DAn markers exhibited an almost 2x higher fold-change compared to the hemizygous genetic background by qPCR analysis (Figure 4. 3 B). The pilot RNA-Seq study revealed that homozygous breeding of the THTR line is necessary to successfully carry out TRAP and enrich dopaminergic mRNA. In the pilot study, we were able to confirm that we isolated a DAn-specific translatome profile on a translatome-wide level. The gene expression profiles did not differ between hemizygous TRAP-positive and TRAP-negative (background) samples, the enrichment of a DAn-specific profile was only possible for homozygous THTR mice.

4) Aged THTR mice might not be suitable for the enrichment of DAn-markers by TRAP

PD is a progressive disease in which the majority of symptoms become apparent at an advanced age. Ideally, it would have been beneficial to carry out translatome profiling experiments in age-matched double transgenic *THTR/hSNCA+* mice (resembling the diseased stage) and *THTR* mice (serving as a healthy control) at two time-points to cover young adult (3-4 months) and aged adult

(18 months) mice for the investigation of early changes in gene expression as well as translational changes during PD manifestation. However, taking together the results from this chapter and the molecular characterisation results (Chapter 3), we decided that performing TRAP experiments and subsequent gene expression profiling on aged 18 months old mice was suboptimal. Despite breeding the mice to homozygosity, double transgenic *THTR/hSNCA+* mice might have too few eGFP-positive neurons remaining to successfully perform TRAP experiments. We decided that with the loss of TH-positive DAn in our PD model (Janezic et al., 2013), too many eGFP-positive neurons might be lost simultaneously, a fact that could significantly reduce the success of the immunoaffinity purifications since the eGFP cell population was already much smaller than the TH-positive population to begin with. A low specific mRNA signal isolated from these lines could be masked by the background RNA population covering any disease-relevant changes in our aged PD mice. TRAP experiments in middle-aged (12 months) mice were considered as an alternative. At this stage, DAn might not yet be lost but we argued that profiling of cells under stress (cell that are dying but are not lost yet) will let us gain insight into molecular mechanisms underlying the specific vulnerability of DAn. This can serve as a read-out of early translatomic changes underlying PD. Thus, the final experimental comparison as outlined in the following chapter entails 3 vs 12 months old mice on either the *THTR/hSNCA+* or the *THTR* genetic background.

Overall, the newly established *THTR* transgenic mouse line provides a powerful tool to investigate the impact of aSyn overexpression in our PD transgenic mouse model on translational profiles of DA neurons.

- CHAPTER 5 -

ANALYSIS OF THE DAN TRANSLATOME IN A TRANSGENIC MOUSE MODEL OF PD

5.1 Overview

This chapter details the TRAP-based isolation of translated mRNA from dopaminergic cell populations in the midbrain to study gene expression changes during the progression of PD. The work entails RNA preparation by TRAP (RNA quality, quantity, and assessment of enrichment of selected marker genes by qPCR); RNA-Seq and quality control (QC), the bioinformatic analysis of differentially expressed genes (DEGs). The analysis has been clustered to answer questions related the effect of: 'experiment', 'disease', or 'age'. Independent follow-up experiments confirmed potential gene hits and pathways.

Chapter aims

1) To obtain DAn-specific mRNA using TRAP from young and aged *THTR* mice and to compare healthy controls (homozygous *THTR*) with our PD model (homozygous *THTR/hSNCA+*).
2) To perform gene expression profiling by RNA-Seq on the TRAP-isolated RNA.
3) To investigate and follow up potential differentially expressed genes and affected pathways due to disease progression or ageing by qPCR and immunoblotting.

Collaboration statement

The work in this chapter was conducted in collaboration with the laboratory of Professor Caleb Webber (DPAG, University of Oxford). I performed all wet lab experiments and was involved in the bioinformatic analysis of the RNA-Seq dataset (e.g. defining the project underlying hypothesis and questions, providing literature examples of similar work, choosing genes for enrichment analysis). Library preparation and RNA-Seq runs were undertaken at the Oxford Genomics Centre, Wellcome Trust for Human Genetics (WTCHG), Oxford (Project details: Quotation #: Q160900; Project #: P160668; Project Manager: Dr Simon Engledow). The bioinformatic analysis of the RNA-Seq data in this chapter was performed in collaboration with Dr Frank Wessely and Dr Jimena Monzon-Sandoval.

5.2 Introduction

5.2.1 Transgenic mouse models to study neurodegenerative diseases

Successful new therapies in the clinic are highly dependent on our understanding of the molecular pathways underlying the disease and are influenced by the model used for preclinical testing. Thus, it is of great importance to develop well-characterised disease models, e.g. for drug testing, which recapitulate all or at least most features of the studied disease (Dauer and Przedborski, 2003). Only the pathological disease end-state of most neurodegenerative disease, such as PD, is generally well described from post-mortem tissue. Early changes in the physiology of the selectively vulnerable DAn are unclear. The in-depth analysis of molecular changes in these cells before the manifestations of clinical symptoms (the prodromal phase) or during disease progression, requires better model systems. For this reason, animal models provide a pivotal tool in the discovery of molecular processes that are underlying disease pathology when studying age-related neurodegenerative diseases. They can significantly aid our understanding of disease progression or help with the development of novel therapies (Dauer and Przedborski, 2003).

Current transgenic models of PD can be broadly divided into neurotoxin-induced and genetic models. The injection or administration 6-OHDA (Ungerstedt, 1968), MPTP (Chiueh et al., 1984; Meredith and Rademacher, 2011), or paraquat and rotenone (Ossowska et al., 2006; Pan-Montojo et al., 2010) can cause selective lesions of the nigrostriatal dopaminergic system in neurotoxin-induced models. While these toxins have been extremely useful in examining the consequences of DAn loss, their usefulness on studying the progressive character of PD is limited due to their rapid or immediate onset of symptoms (Dawson et al., 2010). Genetic models on the other hand, have been primarily created based on known PD-related genes such as aSyn, LRRK2, PINK1 or Parkin to identified molecular pathways underlying PD in humans even though the pathological and behavioural phenotypes they reproduce are often quite different from the human condition (Blesa and Przedborski, 2014; Dawson et al., 2010).

5.2.2 Gene expression profiling in a MPTP model of Parkinson's disease

Recently, the Greengard laboratory successfully established a DAT-bacTRAP model that expresses eGFP-tagged ribosomes under the control of the mouse DAT promoter from a BAC containing the entire DAT locus (Brichta et al., 2015). Their study aimed to profile midbrain DAn to characterise their baseline translational molecular signatures compared to conditions of degenerative stress. In DAT-bacTRAP mice, PD was modelled using MPTP injections. A combinatorial approach of translational profiling and the construction of brain regulatory network analysis revealed intrinsic regulators upstream of the dopaminergic stress response although the intrinsic regulators did not show expression changes themselves (Brichta et al., 2015). The study by Brichta et al. aimed to identify key determinants of the molecular mechanisms underlying neuronal survival or death, but it did not display the progressive character of PD. The inability to mirror gradual disease development or progression is one of the disadvantages of chemically-induced neurodegenerative disease models (Dawson et al., 2010). On the other hand, disease progression could be modelled with a genetic disease model but so far, no genetic PD model has been paired with TRAP methodology.

Our genetic human aSyn over-expressing model of PD will be paired with TRAP methodology and translatome analysis in this chapter to analyse the progressive changes underlying PD pathology.

5.3 Results

5.3.1 Cell-type specific analysis of DAn-specific mRNAs from THTR mice

Experimental design and strategy

After optimising the TRAP protocol (Chapter 4), it was used to isolate DAn-specific translated mRNAs from the midbrain of homozygous *THTR* mice (control= CTRL) and *THTR/hSNCA+* mice (disease model= PD). An overview of the experimental design for the RNA-Seq ('TRAP-Seq') study can be found in Figure 5. 1 A. We analysed CTRL mice compared to our PD model at two different time-points - young (3 months) and aged (12 months). According to research by others, 12 months in mice approximately correspond to 45-50 years of age in humans (Dutta and Sengupta, 2016; Flurkey et al., 2007). With an average age of onset for PD of about 60 years (Samii et al., 2004), we are looking at the prodromal phase of the disease in our RNA-Seq study. Furthermore, sexes have been kept separate to allow for the analysis of male vs female samples if necessary since PD has been previously shown to have different incident rates relating to gender (Van Den Eeden, 2003).

Overall, the samples for the TRAP-Seq study were divided by gender (male vs females), age (3 vs 12 months), and control vs disease (CTRL vs PD) (Figure 5. 1 A). Four replicates per experimental condition were taken forward to RNA sequencing at the WTCHG, Oxford. Each experimental 'n' consists of a pool of two mice of the same sex and genotype. In addition, all IP and Total samples at either 3 or 12 months and CTRL or PD (male and female samples combined) have been pooled and sequenced alongside the non-pooled samples (Figure 5. 1 A). The colour scheme for each sample depicted in the following Figure 5. 1 is consistent throughout the rest of the analysis (light green: *THTR* 3 months; light yellow: *THTR/hSNCA+* 3 months; green: *THTR* 12 months; yellow: *THTR/hSNCA+* 12 months). The aim of our RNA-Seq experiment was to answer a range of questions:

- **EXPERIMENT**: Do we enrich DAn-specific mRNA in our TRAP-IP fractions?
- **DISEASE**: Do we see a difference in gene expression by comparing the translational profiles of our *THTR/hSNCA+* PD model with unaffected control genotypes at a young or an advanced age?
- **AGE**: Do we see a difference in gene expression by comparing the translational profiles of young and aged *hSNCA+* mice (disease-affected ageing) or of young and aged healthy control mice (normal ageing)?

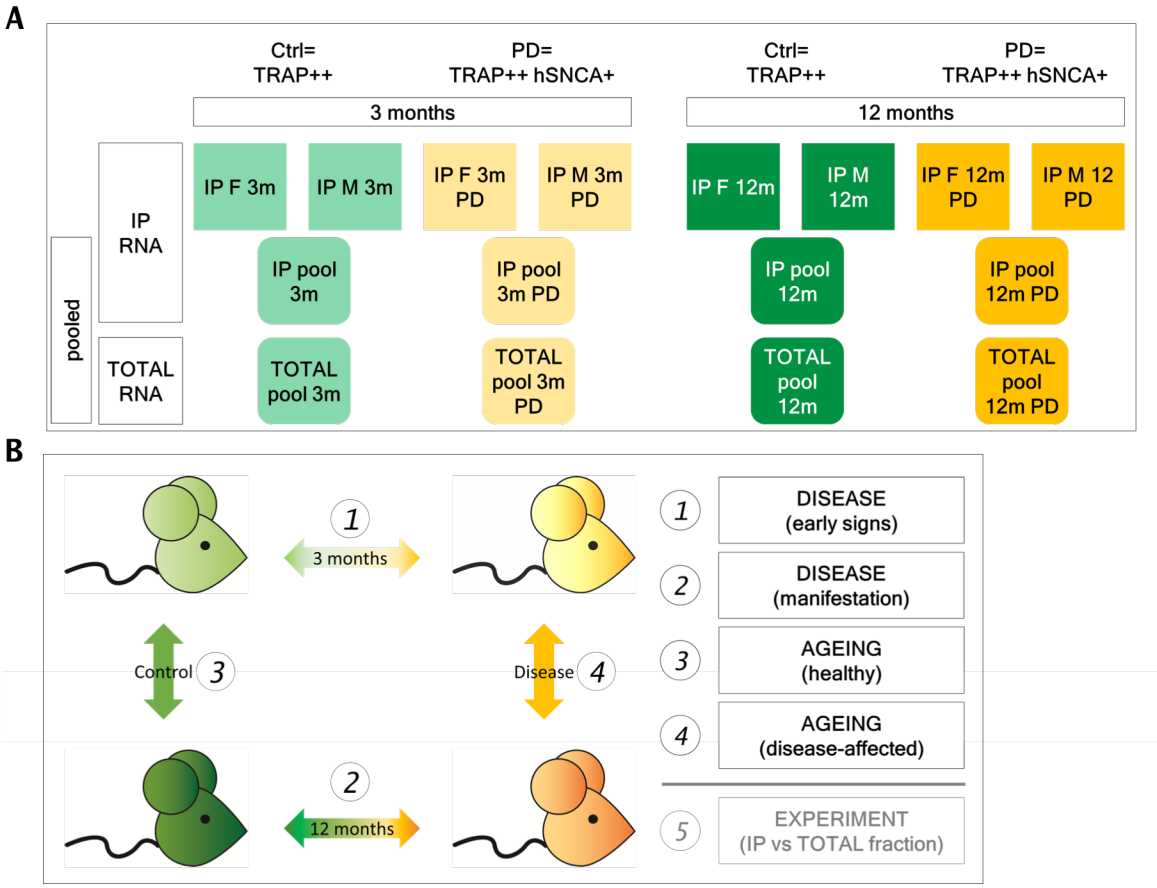


Figure 5. 1 ***Experimental design of the THTR TRAP-Seq study.***

(A) Four female (IP F #1-4) and four male TRAP IP (IP M #1-4) samples per genotype (CTRL or PD) and age (3 or 12 months) will be obtained for RNA-Seq (Total of 32 samples). Further, all TRAP IP and TRAP Total RNA samples will be pooled per genotype (IP/ Total pool 3 months CTRL or PD; IP/ Total pool 12 months CTRL or PD; Total of 8 samples). (B) The experimental design allows to answer a set of questions asking for 1) effect of PD at a young age or 2) advanced age (and disease progression), 3) gene expression changes due to healthy or 4) disease-affected ageing, and 5) changes specific to DAn by comparing the pooled IP and Total RNA fractions. light green: THTR++ 3m; light yellow: THTR++hSNCA+ 3m; green: THTR++ 12m; yellow: THTR++hSNCA+ 12m. IP= bound or immunoprecipitated fraction. Total= input fraction. F= female. M= male. CTRL= Control (THTR mice). PD= Parkinson's disease model (THTR/hSNCA+ mice). ++ or THTR++= Homozygous THTR mice. hSNCA+= human alpha-Synuclein. DAn= dopaminergic neuron.

Generation of RNA-Seq samples

For all conditions, RINs ≥ 7 were considered suitable quality for RNA-Seq. Three IP samples with lower RIN (about 6) were included in the study (Figure 5. 2 A, A'). The average RNA amount after TRAP in the young IP samples was very similar (*THTR++* 3m: 19.84 ng ± 1.22; *THTR++hSNCA+* 3m: 18.64 ng ± 0.96) (Figure 5. 2 B). Surprisingly, the amount of isolated RNA was consistently higher for the aged TRAP IP samples with a greater spread between the individual values by experiment (*THTR++* 12m: 45.35 ng ± 1.78; *THTR++hSNCA+* 12m: 55.08 ng ± 2.23) (Figure 5. 2 B'). Potentially, there was a higher amount of non-specific background RNA isolated from these samples. All TRAP IP RNA fractions were successfully enriched for the two DAn markers tested (DAT and TH). The enrichment was slightly higher in the young samples (**DAT**: *THTR++* 3m: **3.8 x ± 0.59**; *THTR++hSNCA+*

3m: **4.6 x ± 0.54**; **TH**: *THTR++* 3m: **11 x ± 0.93**; *THTR++hSNCA+* 3m: **9.9 x ± 0.66**) (Figure 5. 2 C) compared to their fold-enrichment over TRAP Total RNA in older animals (**DAT**: *THTR++* 12m: **3.4 x ± 0.38**; *THTR++hSNCA+* 12m: **3.6 x ± 0.38**; **TH**: *THTR++* 12m: **6.3 x ± 0.5**; *THTR++hSNCA+* 12m: **7.3 x ± 0.6**) (Figure 5. 2 C'). The lower enrichment in aged mice could be caused by a higher amount of background RNA as suggested above. None of the non-DAn markers (GFAP and GAD) were enriched in any of the IP fractions over the TRAP Total fractions. Figure 5. 2 and Appendix Table 5. 1. shows a summary of the RNA-Seq samples from *THTR* (CTRL) and *THTR/hSNCA+* mice (PD) (left panel: 3 months; right panel: 12 months). A Total volume of 8 µl RNA (0.3 ng/µl) was submitted for sequencing including the pooled IP and Total samples after combining equal amounts of RNA from the separate fractions.

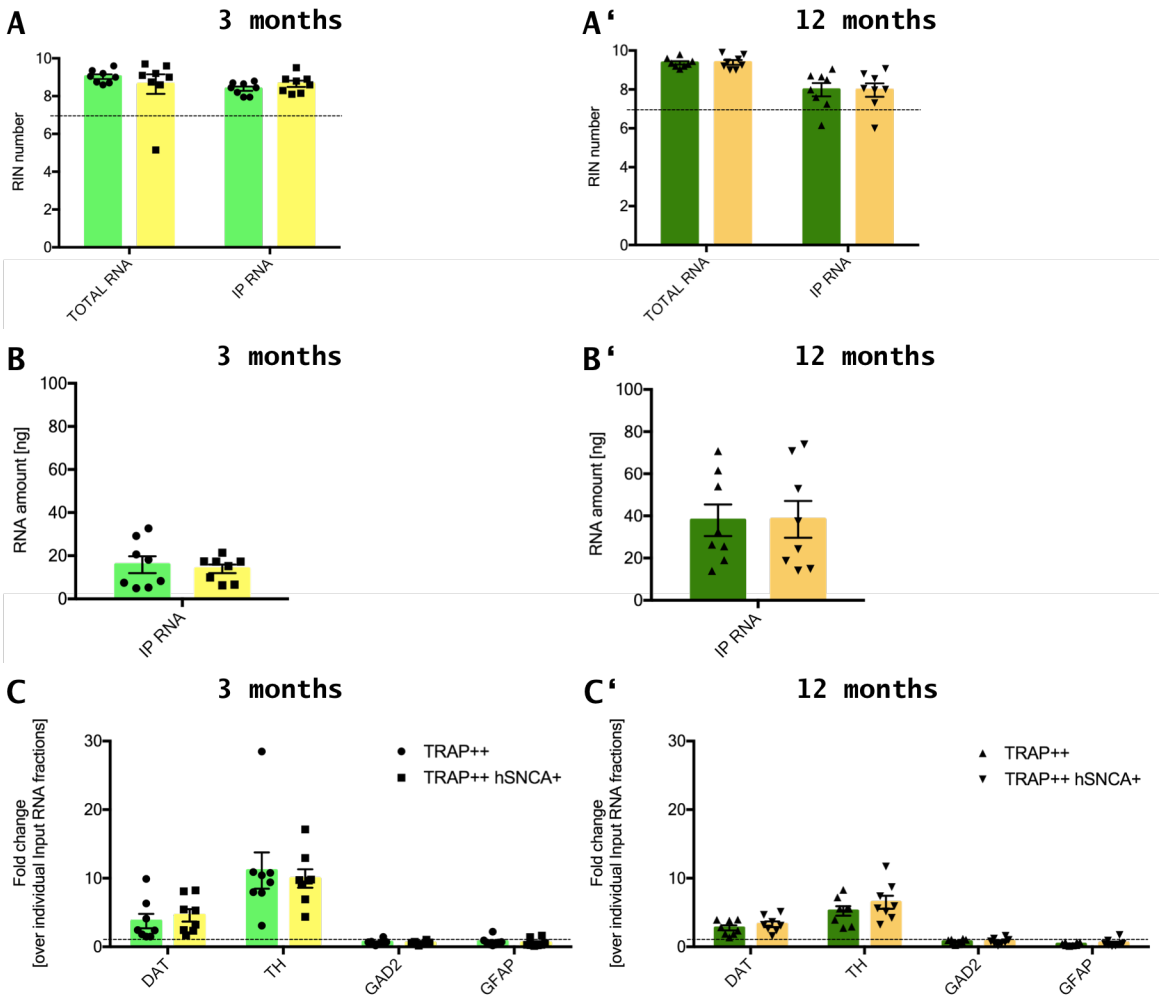


Figure 5. 2 High quality RNA was isolated from THTR mice using TRAP for DAn-specific gene expression profiling.
(A, A') RIN values of the Total/IP RNA fractions for young (A) and aged (A') mice. All RNA fractions show a RIN value >7 (three exceptions with RIN about 6). (B, B') Total IP RNA amount after TRAP are more variable in aged mice (B') compared to young mice (B). (C, C') Fold-changes for a set of DAn and non-DAn marker genes for young (C) and aged (C') mice. TRAP mice show a consistent enrichment of DAn markers only but no enrichment for non-DAn markers. Fold-changes for DAT and TH are slightly lower in aged animals compared to young mice. The qPCR results were normalised to the geometric mean of two reference genes and fold-enrichment values were calculated over individual input TRAP RNA fractions using the comparative Ct method (n= 4 per genotype; One-way ANOVA with Dunnett post-hoc analysis; mean ± SEM). light green: THTR++; light yellow: THTR++hSNCA+; green: THTR++; yellow: THTR++hSNCA+. RIN= RNA integrity number. IP= bound or immunoprecipitated RNA fraction. Total= input midbrain RNA fraction. ++ or THTR++= Homozygous THTR mice. hSNCA+= human alpha-Synuclein. DAT= dopamine transporter. TH= tyrosine hydroxylase. GAD2= glutamate decarboxylase 2. GFAP= glial fibrillary acidic protein. DAn= dopaminergic neuron. Pool= pooled IP/Total samples across either control or disease model at 3/12 months.

5.3.2 Gene expression profiling of DAn-specific mRNA using a mouse model of PD

General RNA-Sequencing details and quality control of reads

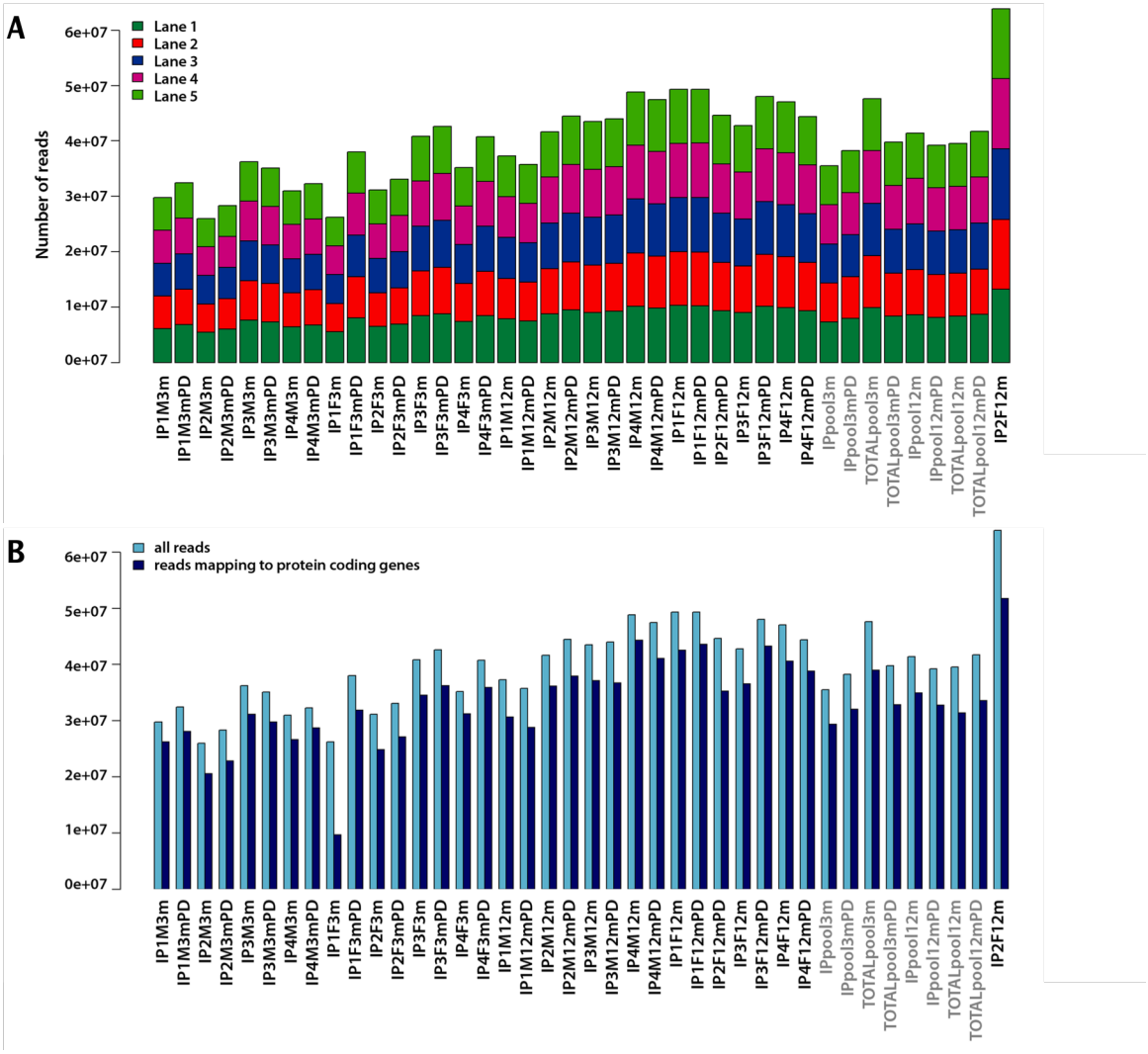
SMARTer library preparation for low input RNA samples and sequencing was undertaken by the WTCHG, Oxford (32 TRAP IP samples plus 8 pooled samples; Table 5. 1). All 40 samples have been multiplexed to minimise sequencing-related lane bias and were sequenced on the Illumina HiSeq4000 as paired-end 75 bp reads over five lanes. After sequencing, all samples-specific reads across the five lanes were combined and aligned to the mouse genome (*mouse37* reference genome).

Sample Name	RNA-Seq ID	TRAP Fraction	Disease	Age (months)	Gender	Pooled	Sequencing Index	Lane	Total read count
THTR++ A*	IP1F12m	IP	CTRL	12	F	false	225104	1-5	42,544,603.53
THTR++ B*	IP2F12m	IP	CTRL	12	F	false	301301	1-5	51,761,354.22
THTR++ C*	IP3F12m	IP	CTRL	12	F	false	229152	1-5	36,537,577.20
THTR++ D*	IP4F12m	IP	CTRL	12	F	false	231176	1-5	40,588,999.55
THTR++PD A*	IP1F12mPD	IP	PD	12	F	false	226116	1-5	43,548,807.24
THTR++PD B*	IP2F12mPD	IP	PD	12	F	false	228140	1-5	35,287,013.62
THTR++PD C*	IP3F12mPD	IP	PD	12	F	false	230164	1-5	43,233,167.13
THTR++PD D*	IP4F12mPD	IP	PD	12	F	false	232188	1-5	38,828,174.85
THTR++ A	IP1M12m	IP	CTRL	12	M	false	217103	1-5	30,671,763.99
THTR++ B	IP2M12m	IP	CTRL	12	M	false	219127	1-5	36,117,809.09
THTR++ C	IP3M12m	IP	CTRL	12	M	false	221151	1-5	37,123,791.65
THTR++ D	IP4M12m	IP	CTRL	12	M	false	223175	1-5	44,286,426.40
THTR++PD A*	IP1M12mPD	IP	PD	12	M	false	218115	1-5	28,842,271.12
THTR++PD B	IP2M12mPD	IP	PD	12	M	false	220139	1-5	37,931,370.04
THTR++PD C	IP3M12mPD	IP	PD	12	M	false	222163	1-5	36,746,849.72
THTR++PD D	IP4M12mPD	IP	PD	12	M	false	224187	1-5	41,070,659.66
THTR++ a*	IP1F3m	IP	CTRL	3	F	false	209102	1-5	9,663,360.24
THTR++ b*	IP2F3m	IP	CTRL	3	F	false	211126	1-5	24,843,708.52
THTR++ c*	IP3F3m	IP	CTRL	3	F	false	213150	1-5	34,508,213.20
THTR++ d*	IP4F3m	IP	CTRL	3	F	false	215174	1-5	31,204,274.75
THTR++PD a*	IP1F3mPD	IP	PD	3	F	false	210114	1-5	31,905,968.62
THTR++PD b*	IP2F3mPD	IP	PD	3	F	false	212138	1-5	27,108,208.20
THTR++PD c*	IP3F3mPD	IP	PD	3	F	false	214162	1-5	36,229,310.00
THTR++PD d*	IP4F3mPD	IP	PD	3	F	false	216186	1-5	35,903,515.21
THTR++ a	IP1M3m	IP	CTRL	3	M	false	201101	1-5	26,245,753.27
THTR++ b	IP2M3m	IP	CTRL	3	M	false	203125	1-5	20,546,255.07
THTR++ c	IP3M3m	IP	CTRL	3	M	false	205149	1-5	31,163,967.10
THTR++ d	IP4M3m	IP	CTRL	3	M	false	207173	1-5	26,636,465.77
THTR++PD a	IP1M3mPD	IP	PD	3	M	false	202113	1-5	28,109,309.94
THTR++PD b	IP2M3mPD	IP	PD	3	M	false	204137	1-5	22,827,750.65
THTR++PD c	IP3M3mPD	IP	PD	3	M	false	206161	1-5	29,747,190.99
THTR++PD d	IP4M3mPD	IP	PD	3	M	false	208185	1-5	28,693,715.30
	IPpool12m	IP	CTRL	12	B	true	237153	1-5	34,940,036.38
	Totalpool12m	Total	CTRL	12	B	true	239177	1-5	31,384,307.94
	IPpool12mPD	IP	PD	12	B	true	238165	1-5	32,791,348.55
	Totalpool12mPD	Total	PD	12	B	true	240189	1-5	33,603,651.22
	IPpool3m	IP	CTRL	3	B	true	233105	1-5	29,344,332.24
	Totalpool3m	Total	CTRL	3	B	true	235129	1-5	38,958,719.42
	IPpool3mPD	IP	PD	3	B	true	234117	1-5	32,019,863.78
	Totalpool3mPD	Total	PD	3	B	true	236141	1-5	32,848,595.17

Table 5. 1 TRAP-Seq samples overview.

The 40 samples processed in the TRAP RNA-Seq study were multiplexed and sequenced together over five lanes (lane 1-5). WTCHG= Wellcome Trust centre for Human Genetics. RIN= RNA integrity number. IP= bound or immunoprecipitated RNA fraction. Total= input midbrain RNA fraction. F= female. M= male. B= both; males and female samples pooled. PD= Parkinson's disease model; THTR/hSNCA+ mice. CTRL= Control; THTR mice. ++= homozygous THTR mice.

The quality control (QC) of the RNA-Seq reads revealed equal sequencing depth across the five separately sequenced lanes for each sample (Figure 5. 3 A). All samples had at least 20,000,000 reads, only sample IP1F3m was underrepresented with less than 10,000,000 reads. Most reads (about 80%) mapped to protein-coding genes (Figure 5. 3 B, C) confirming the success of the sequencing (Figure 5. 3 A). Sample IP2F12m showed the highest number of reads across all five lanes; sample IP1F3m showed fewer than 40% reads mapping to protein-coding genes. Furthermore, we found that some samples showed high % of reads mapping to rRNA (Appendix Figure 5.1).



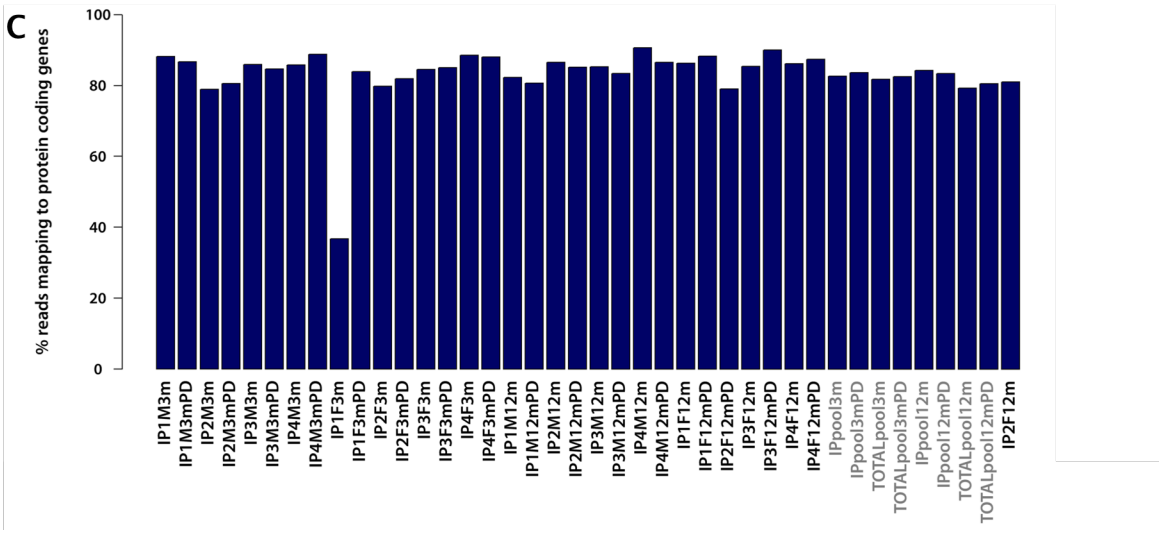


Figure 5. 3 Overview of the reads per lane reveals 80% mapping success to protein coding genes.

(A) Number of reads per sequencing lane (1-5). The five lanes show an equal distribution of reads/lane. For all five lanes sample IP2F12mPD shows the highest number of reads. (B) Comparison of all reads (light blue) and reads that map to protein coding genes (dark blue). While many genes map to protein coding genes for IP2F12mPD, this number is very low for sample IP1F3m. (C) Percentage of reads that map to protein coding genes. On average about 80% of all reads map to protein coding genes. The only exception is sample IP1F3m. IP= bound or immunoprecipitated RNA fraction. Total= midbrain input RNA fraction. F= female. M= male. 3m= 3 months old mice. 12m= 12 months old mice. PD= Parkinson's disease model. Pool= pooled IP/Total samples across either control or disease model at 3/12 months (grey text). Analysis performed in collaboration with J. Monzon-Sandoval. Adapted from J. Monzon-Sandoval.

5.3.3 Principal Component Analysis identifies outlier samples

Hierarchical clustering and principal component analysis (PCA) identified five outlier samples. The first outlier (IP1F3m) had the lowest mapping rates (< 40%) and a decreased library complexity due to the highest read duplication rates among all samples. Overall, the reads from this sample were characterised by many non-expressed genes (Appendix Figure 5.1) with only few highly-expressed genes that account for a large proportion of the total library.

In the hierarchical clustering (Figure 5. 4 A), the most obvious difference was found between the TRAP IP samples (translatome) and whole midbrain TRAP Total samples (transcriptome). Apart from five outlier samples, most IP samples (yellow) clustered together separately from the Total samples (blue) (Figure 5. 4). While the main branching point separated outlier IP1F3m in its own cluster, a set of additional four outliers (IP1M12m, IP1M12mPD, IP2F12m, and IP2F12mPD) was found in a cluster together with the pooled Total samples. Focusing on the remaining IP samples, no specific clusters were found. No cluster was specific to one sub-set of samples, e.g. based on gender, age, or disease status. Similarly, the PCA (Figure 5. 4 B, C) identified the major sources of variation,

whereby the first component (PC1) approximately separated the IP from the Total samples. Again, the same four outlier IP samples as mentioned above clustered closely to the Total samples as outliers. PC2 separated all samples from outlier IP1F3m.

Comparison of the RNA QC data for the outlier samples (Figure 5. 4 and Appendix Table 5.1) pointed out that they were among the samples with the lowest RINs (e.g. IP2F12mPD: RIN 6.0; IP1M12m: RIN 6.2), by far the highest average RNA amounts (e.g. IP2F12m: 93.4 ng; IP2F12mPD: 104.91 ng; IP1M12mPD: 131.5 ng) and the lowest DAT and TH mRNA fold-enrichments in the IP fractions (**DAT**: IP2F12m 1.4x; IP2F12mPD 2.4x; IP1M12m 1.5x; IP1M12mPD 2.5x and **TH**: IP2F12m 2.8x; IP2F12mPD 4.2x; IP1M12m 3.6x; IP1M12mPD 3.8x). All identified outliers have been excluded from most down-stream analysis as indicated.

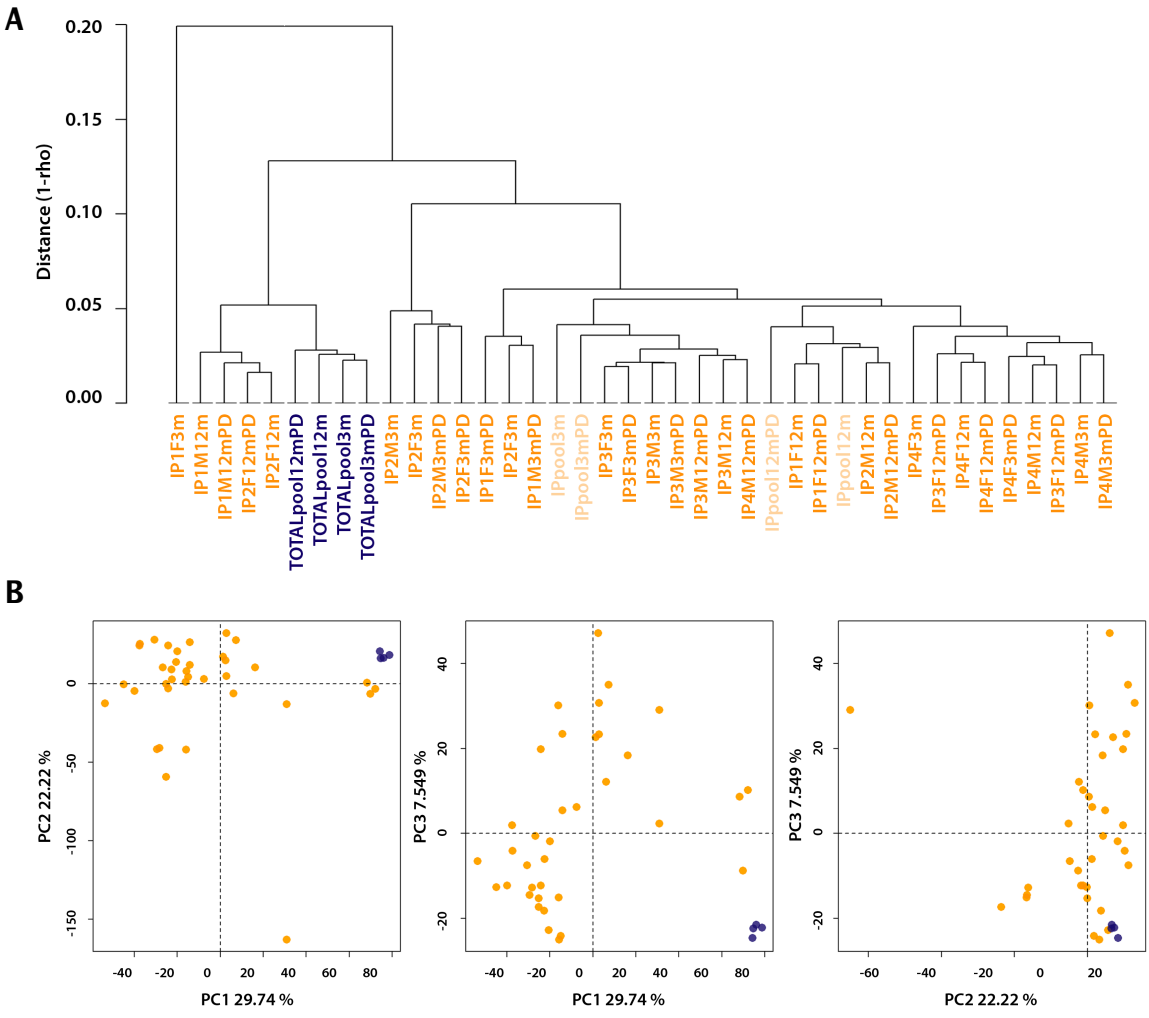
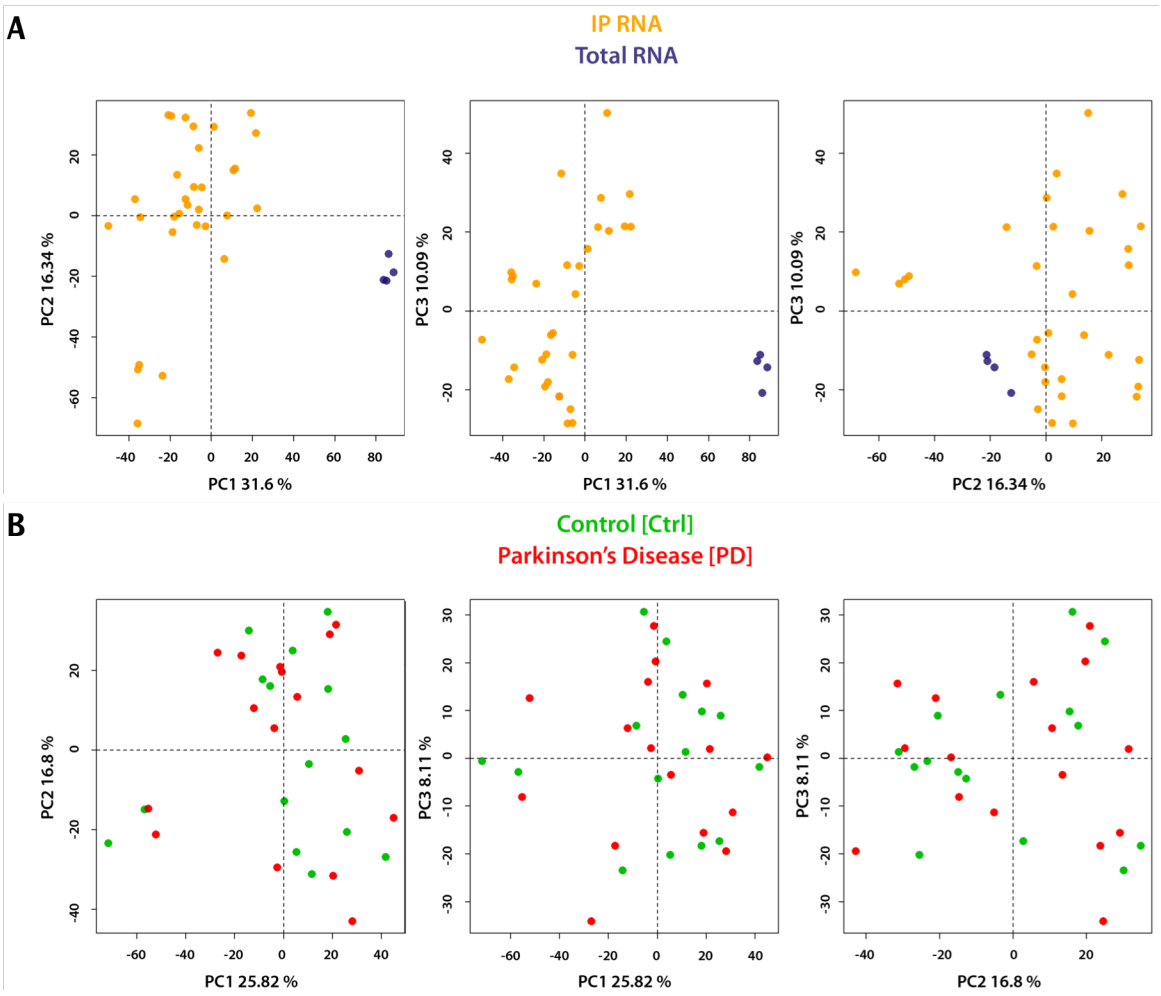


Figure 5. 4 Hierarchical clustering and PCA analysis of all 40 RNA-Seq samples identifies outlier samples.

(A) Clustering analysis shows a clear separation of the TRAP Total RNA samples (purple). A set of TRAP IP RNA samples is more closely related to the Total samples than the other IP RNA samples (IP1F3m, IP1M12m, IP1M12mPD, IP2F12mPD, IP2F12m). (B) PCA (log2(TPM +1)). Total RNA samples cluster away from the main IP cluster except for 5 IP samples. TPM= transcript per million. PCA= Principal component analysis. IP= bound or immunoprecipitated RNA fraction. Total= midbrain input RNA fraction. F= female. M= male. 3m= 3 months. 12m= 12 months. PD= Parkinson's disease model. Pool= pooled IP/Total samples across either control or disease model at 3/12 months. Analysis performed in collaboration with J. Monzon-Sandoval. Adapted from J. Monzon-Sandoval.

After removing the outlier samples (IP1F3m, IP2F12m, IP2F12mPD, IP1M12m, IP1M12mPD), the PCA plot clearly showed the experimental separation of IP (orange) from Total samples (purple) (Figure 5. 5 A). Figure 5. 5 B, C shows the PCA using **only** IP samples (outliers excluded) aiming to see a separation by gender (results not shown), disease (B), or age sub-sets (C). No separation could be seen for gender and disease between CTRL (green) and PD (red) groups in any of the analysed PCA (Figure 5. 5 B) but the samples tend to separate by age, (3m: dark blue; 12m: yellow) (Figure 5. 5 C).



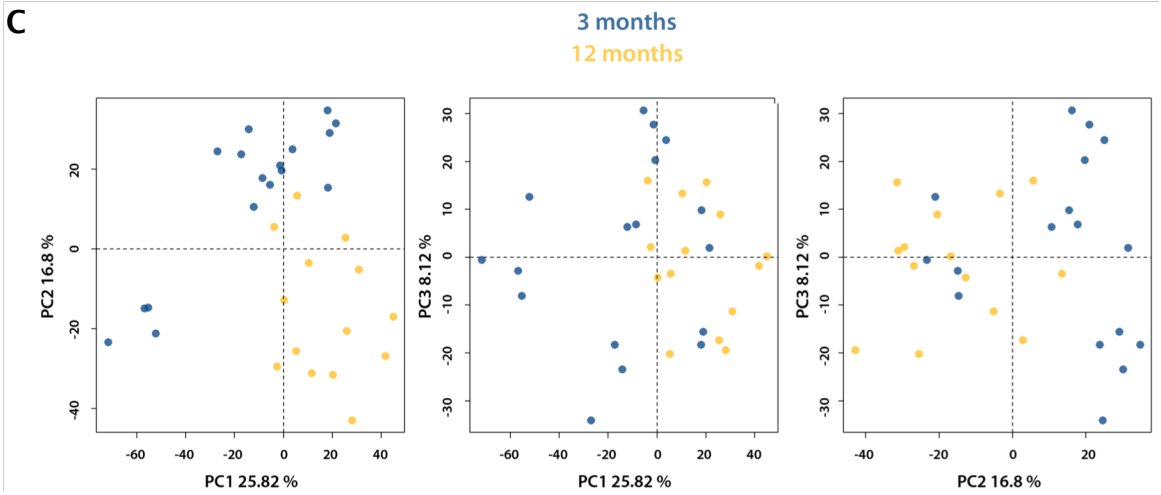


Figure 5. 5 ***PCA after removing the outlier samples separates TRAP IP samples by age.***
(A) PCA showing the experimental separation of IP (orange) vs Total (purple) TRAP RNA samples. The following PCA only show the IP samples. (B) Control (green) and Disease (red) samples show no separation in any of the analysed comparisons. (C) Samples, 3 (dark blue) or 12 months (yellow), do separate across different PCA despite a few exceptions. Five outlier samples were removed from the plots (IP1F3m, IP2F12m, IP2F12mPD, IP1M12m, IP1M12mPD). PCA= Principal component analysis. IP= bound or immunoprecipitated RNA fraction. Total= midbrain input RNA fraction. PD= Parkinson's disease model. Analysis performed in collaboration with J. Monzon-Sandoval. Adapted from J. Monzon-Sandoval.

5.3.4 Analysis of gene marker enrichments confirms dopaminergic nature of the TRAP IP fractions

Next, we tested if we had successfully enriched dopaminergic mRNAs in the IP samples, whilst depleting marker genes specific to other cellular sub-types. First, the pooled IP vs. Total TRAP RNA fractions were compared using a set of genes found as enriched or depleted in DAn in a study from the Greengard laboratory (Brichta et al., 2015), as performed for the pilot TRAP RNA-Seq study (Chapter 4). Marker genes that were shown to be specific for DAn or other cell-types are highlighted in the scatter plots (Figure 5. 6, Appendix Table 5.2 and 5.3). The plots summarise the fold-changes in FPKM values for 3 months CTRL/PD (Figure 5. 6 A, B) and 12 months CTRL/PD samples (Figure 5. 6 C, D). All RNA fractions showed an enrichment of the genes previously known to associate with DAn (red) in the IP fractions; TH was most enriched for all fractions with an average fold-change of about 14x. The non-DAn marker genes (blue) mainly clustered on the Total RNA side of the plots.

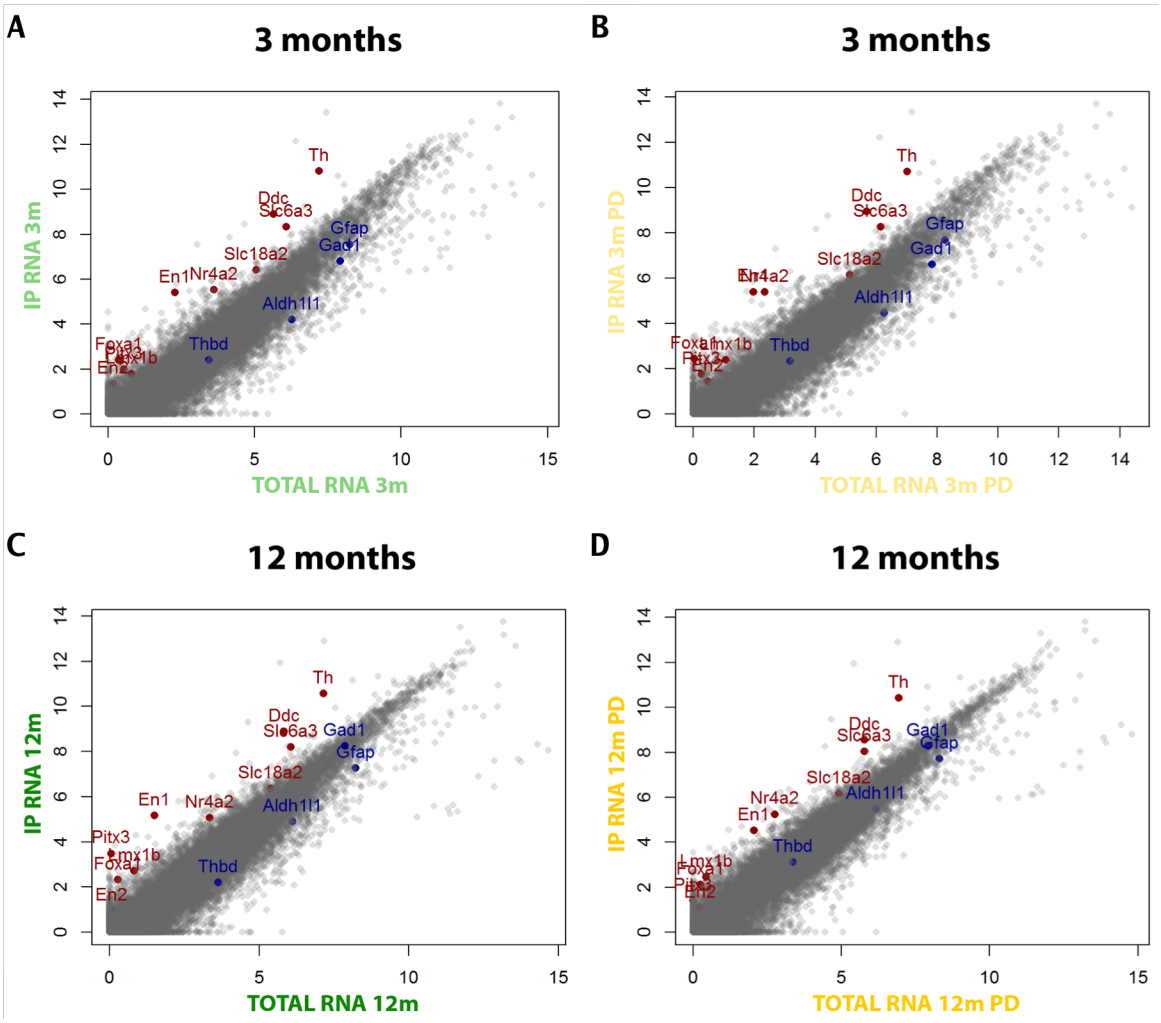


Figure 5. 6 ***DAn and non-DAn marker enrichments plots confirm successful isolation of DAN-specific mRNA.***

The enrichment of DAn (red) and non-DAn (blue) marker genes are shown for the pooled Total vs. pooled IP TRAP RNA expression plots. (log2(TPM + 1)). Plotted are all genes found enriched or depleted in DAn in a study of Brichta et al. 2015 (Nature Neuroscience). (A) 3m pooled CTRL (light green), (B) 3m pooled PD (light yellow), (C) 12m pooled CTRL (green), and (D) 12m pooled PD samples (yellow). For all four blots, there is a clear separation between the DAn enriched in the TRAP IP samples and the non-DAn, which are higher in the TRAP Total samples. TPM= transcript per million. IP= bound or immunoprecipitated RNA fraction. Total= midbrain input RNA fraction. F= female. M= male. 3m= 3 months old mice. 12m= 12 months old mice. PD= Parkinson's disease model. Pool= pooled IP/Total samples across either control or disease model at 3/12 months. Analysis performed in collaboration with J. Monzon-Sandoval. Adapted from J. Monzon-Sandoval.

Furthermore, we analysed the fold-changes of marker genes in greater detail. This analysis aimed to visualise the spread between the individual samples and helped to identify and confirm outlier samples. Only sample IP1F3m was excluded from the beginning. None of the analysed **non-DAn** markers showed a higher expression in the pooled IP samples compared to the pooled Total samples; such as GFAP, Aldh1l1, Slc17a7, and THBD (Figure 5. 7).

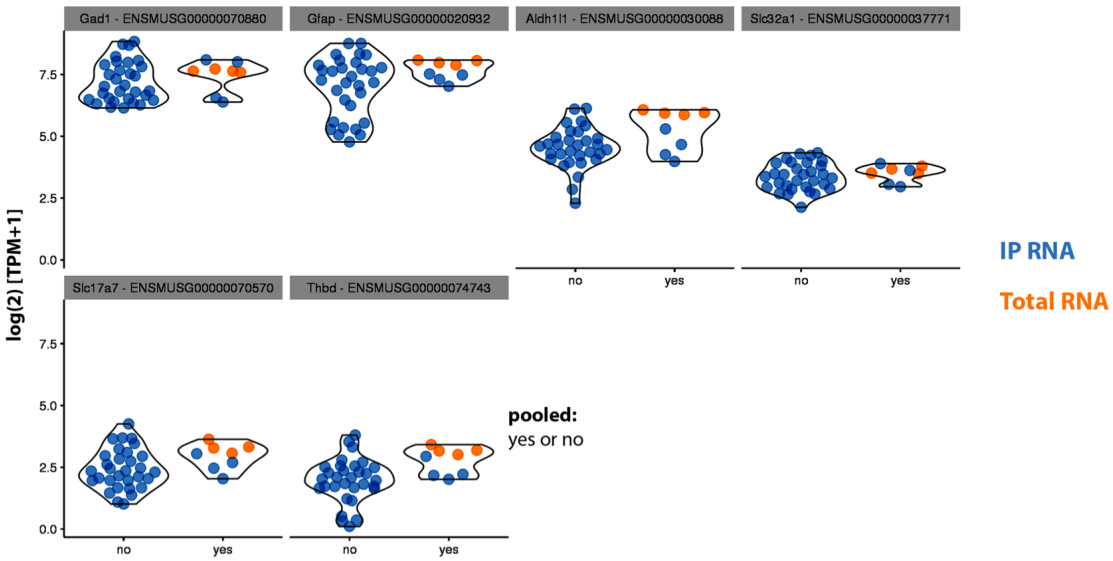


Figure 5. 7 ***Selected marker genes are not enriched in the TRAP IP fractions by global expression level analysis.***
Global expression levels of selected marker genes across the TRAP-Seq samples (Log2(TPM +1)). Selected non-DA marker genes. (Pooled) IP samples (blue) compared to pooled Total (orange) samples do not show any enrichment for the markers tested. TPM= transcript per million. IP= bound or immunoprecipitated RNA fraction. Total= midbrain input RNA fraction. Analysis performed in collaboration with F. Wessely. Adapted from F. Wessely.

Focusing on **DAn markers** (Figure 5. 8 A), these tended to have a higher expression in the pooled IP samples compared to the pooled Total fractions, e.g. TH, DDC, DAT, and VMAT2. Generally, lowly expressed genes show a less clear separation, e.g. GIRK2 (Kcnj6), PITX3, and LMX1B. A higher resolution of the separate TH expression across all 40 samples is shown in Figure 5. 8 B. A sub-set of 8 samples had a lower TH expression (IP2F3m, IP2F3mPD, IP2M3m, IP2M3mPD, IP2F12m, IP2F12mPD, IP1M12m, IP1M12mPD). Four of them were previously identified as outliers on the PCA blot (IP2F12m, IP2F12mPD, IP1M12m, IP1M12mPD).

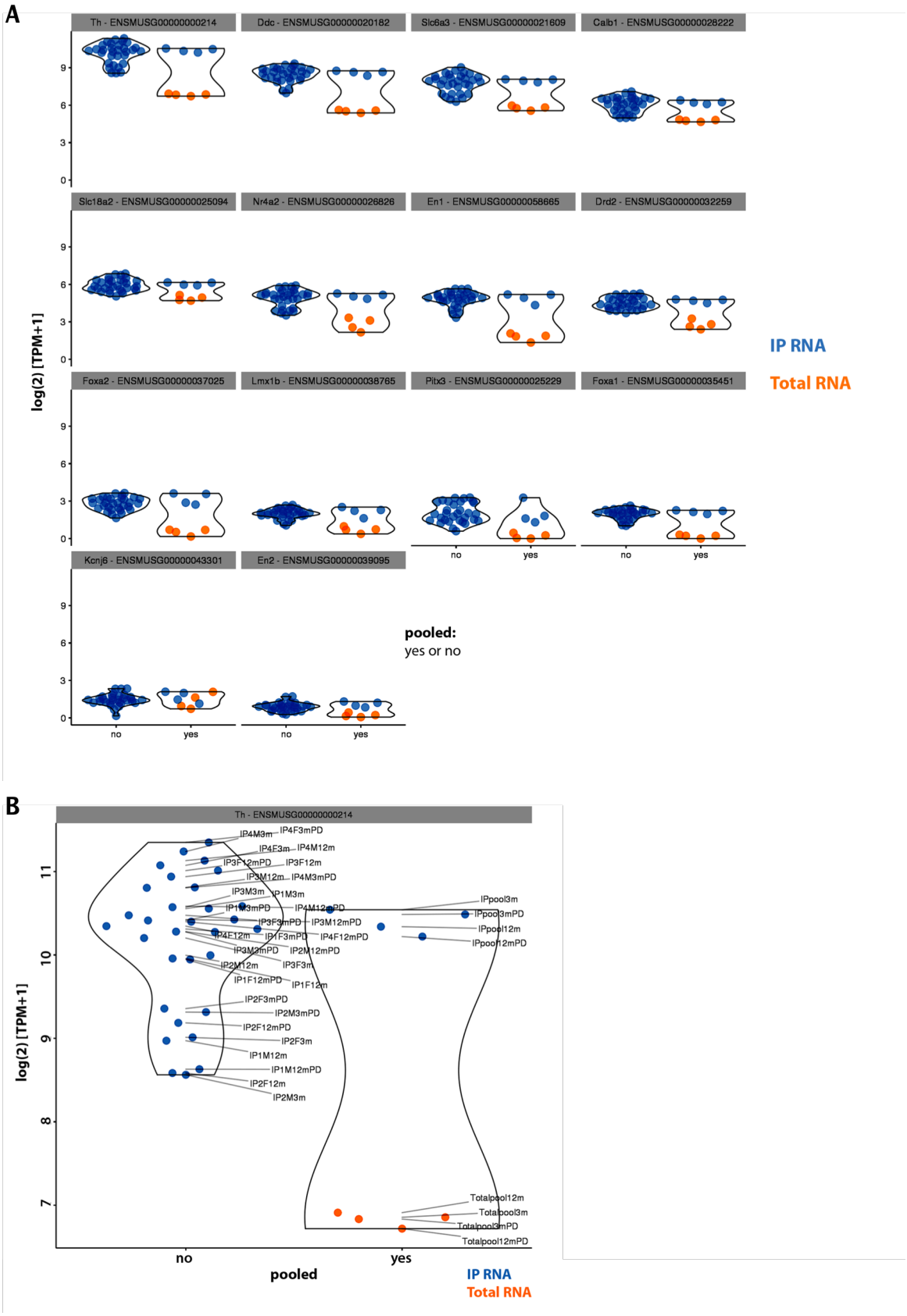
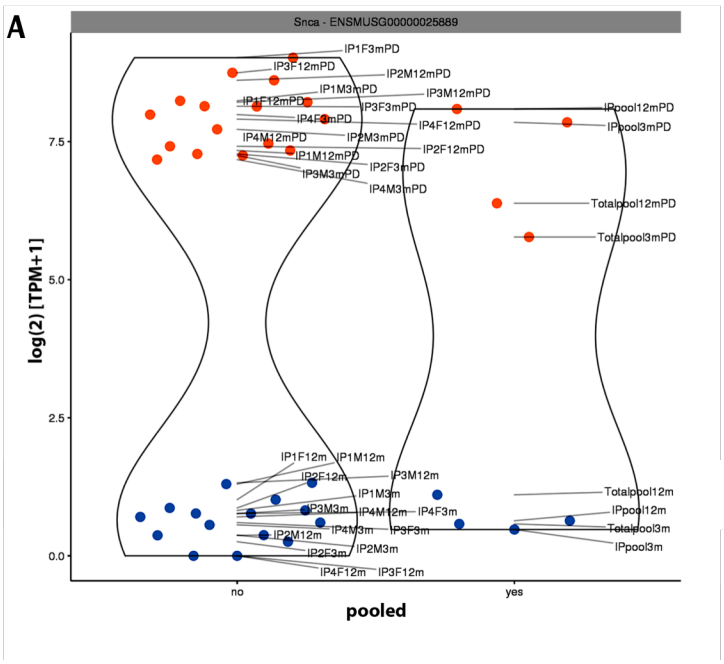


Figure 5. 8 ***Selected marker genes are enriched in the TRAP IP fractions by global expression level analysis.***

Global expression levels of selected marker genes across the TRAP-Seq samples (Log2()). (A) Selected DAn marker genes. (Pooled) IP samples (blue) show higher expression across several DAn markers compared to pooled Total samples (orange). (B) TH gene expression across all samples. There is a sub-set of 8 samples with lower TH expression (IP2F3m, IP2F3mPD, IP2M3m, IP2M3mPD, IP2F12m, IP2F12mPD, IP1M12m, IP1M12mPD). TPM= transcript per million. IP= bound or immunoprecipitated RNA fraction. Total= midbrain input RNA fraction. Analysis performed in collaboration with F. Wessely. Adapted from F. Wessely.

Our *hSNCA+* PD model over-expresses human aSyn on an endogenous mouse aSyn KO (*mSnca-/-)* background (Janezic et al., 2013). Therefore, we also checked the gene expression of the three Synuclein family members (alpha-Synuclein (*SNCA*), beta-Synuclein (*SNCB*), gamma-Synuclein (*SNCG*) and the aSyn-interacting protein (synphilin) (*SNCAIP*) (Figure 5. 9). As expected, only the samples corresponding to the PD group showed elevated *SNCA* expression (Figure 5. 9). Although the gene for mouse aSyn has been knocked-out, *DESeq* analysis assigned some reads to *SNCA* (Table 5. 2). An inherent analysis of the *DESeq* method is designed to detect and to correct too low dispersion estimates through pooling information across genes which are expressed at similar levels under the assumption that genes of similar average expression have similar sample-to sample variation (Anders and Huber, 2010; Love et al., 2014). Furthermore, the Synuclein family members share a high degree of sequence similarities (George, 2002), which could have let to false-positive assignment of reads to *SNCA*. For *SNCAIP* and *SNCB*, no difference was detectable between PD and CTRL samples for either all IP or pooled IP/Total samples. However, *SNCG* was enriched in all IP samples compared to the Total samples but not differentially expressed across PD and CTRL samples (Figure 5. 9).



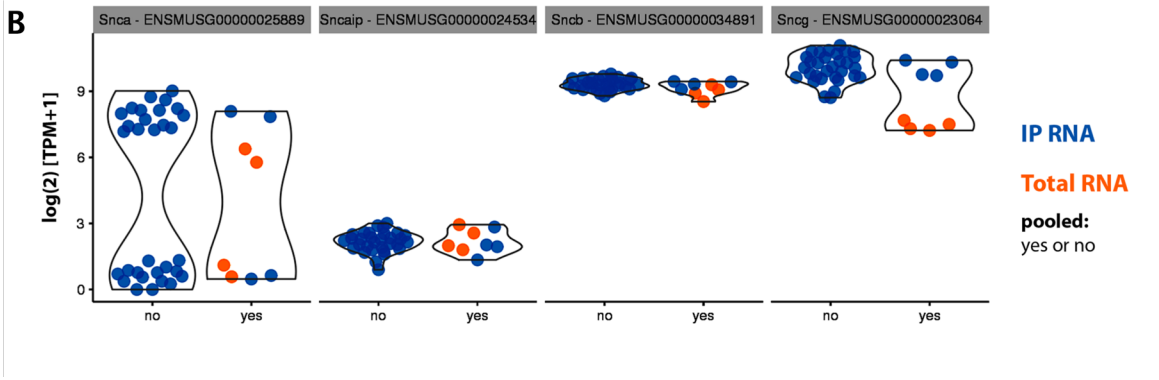


Figure 5. 9 ***Synuclein family member genes are expressed in the TRAP-Seq samples.***

Gene expression of the three Synuclein family members (SNCA, SNCB, SNCG) and SNCAIP (Log2(TPM + 1)). Non-pooled IP samples (blue) corresponding to the PD samples and all pooled IP (blue) or pooled Total (orange) show SNCA expression, but none of the CTRL samples. No difference between PD and CTRL for SNCAIP and SNCB. SNCG is enriched in all IP samples compared to the Total samples. TPM= transcript per million. IP= bound or immunoprecipitated RNA fraction. Total= midbrain input RNA fraction. PD= Parkinson's disease model. Pool= pooled IP/Total samples across either control or disease model at 3/12 months. Snca= aSyn or alpha-Synuclein. Sncaip= alpha-Synuclein interacting protein (synphilin). Sncb= beta-Synuclein. Sncg= gamma-Synuclein. Analysis performed in collaboration with F. Wessely. Adapted from F. Wessely.

Symbol	ENSEMBL	IP CTRL 3-months	IP PD 3-months	IP CTRL 12-months	IP PD 12-months
Snca	ENSMUSG00000025889	13.3	7732.0	15.6	7295.3
Sncaip	ENSMUSG00000024534	296.3	155.8	256.9	246.6
Sncb	ENSMUSG00000034891	20961.5	26069.2	22382.6	19369.6
Sncg	ENSMUSG00000023064	28589.1	29711.8	15625.3	15154.3

Symbol	ENSEMBL	Total CTRL 3-months	Total PD 3-months	Total CTRL 12-months	Total PD 12-months
Snca	ENSMUSG00000025889	12.6	1358.2	26.3	2219.3
Sncaip	ENSMUSG00000024534	150.5	209.8	292.4	194.9
Sncb	ENSMUSG00000034891	15627.1	17898.9	14029.9	11244.3
Sncg	ENSMUSG00000023064	3033.9	2446.9	2662.3	3587.0

Table 5. 2 ***Gene expression of the Synuclein family.***

DESeq assignment of RNA-seq reads to the three Synuclein family members (alpha-Synuclein (SNCA), beta-Synuclein (SNCB), gamma-Synuclein (SNCG) and the aSyn-interacting protein (synphilin) (SNCAIP). Pooled IP/Total samples shown. CTRL= control. PD= Parkinson's disease. Red= SNCA reads in mSnca KO samples.

Meaningful interpretation of gene expression profiles requires detailed knowledge of the targeted cell population. Potential contamination with unwanted cells must be identified; if the specific cell population (here: DAn) expresses the genes of interest at a low level compared to surrounding cells that might be inadvertently included in the analysis. Thus, we determined the amount and composition of non-specific background RNA contamination in our IP fractions. A range of marker genes for different cellular sub-types (selected neuronal, astrocyte, oligodendrocyte, microglia/macrophage, endothelial, fibroblast, and mitochondrial marker genes) was tested for differential expression between IP and Total samples across all 40 RNA-Seq samples. The list of neuronal- and non-neuronal sub-types used here was compiled based on a literature search (mainly based on (Tasic et al., 2016), Appendix Table 5.2).

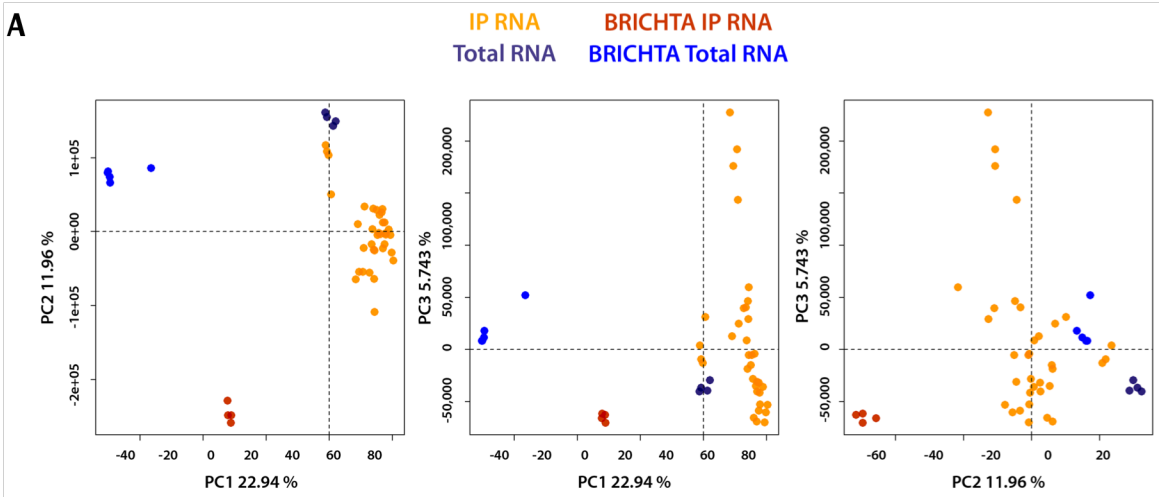
While some **neuronal** markers are expressed more highly in the IP fractions compared to the Total RNA fractions, they show no clear enrichment (Appendix Figure 5.2). Most of the **astrocyte-related** marker genes (Appendix Figure 5.3) are more lowly expressed in the IP fractions compared to the Total fractions. For all tested **oligodendrocyte** marker genes, we found a lower expression in the IP fractions, except for unchanged SOX10 levels (Appendix Figure 5.3). None of the overall very low expression **microglia** or **macrophage** marker genes showed a clear profile. Global expression level analysis of **endothelial** and **fibroblast** marker genes showed a wide-spread distribution of expression (Appendix Figure 5.4) but none of the tested marker genes showed a clear difference between IP and Total TRAP RNA samples. The expression of a **Y chromosome-specific gene** was only present in all male samples, as expected (Appendix Figure 5.4). Lastly, most of the **mitochondrial** gene markers showed a lower expression in the IP fractions compared to the pooled Total fractions (Appendix Figure 5.5). However, upon closer inspection, a sub-set of four IP samples showed higher expression for some mitochondrial markers (e.g. mt-Co1, mt-Co2, and mt-Co3) than the bulk of IP samples. When separating out the sample-specific expression for two of these mitochondrial genes, the set of four samples with higher expression for most mitochondrial genes was identified as IP2F3m, IP2F3mPD, IP2M3m, IP2M3mPD (Appendix Figure 5.5). We noticed that these four samples formed a separate cluster on hierarchical clustering shown above (Figure 5. 4) but overall clustering analysis did not justify classifying these four samples as outliers. Their RNA QC data revealed that all of them have been processed using TRAP with the same matrix stock solutions and they all showed a low expression for the two DAn marker genes compared to the other IP samples (except for previously identified outliers) (Appendix Table 5.1).

All in all, the global expression analysis showed that the TRAP IP samples were indeed enriched for DA genes. However, the RNA composition was not purely dopaminergic but contained some non-specific background RNA from other cell-types. This ‘contamination’ was most likely caused by non-specific binding of background RNA to the sticky magnetic beads.

5.3.5 The TRAP-Seq data clustering finds overlap with external datasets

We identified a study that was performing a TRAP-Seq study similar to ours. The Greengard laboratory analysed DAn-specific mRNA isolated from a *DAT-bacTRAP* mouse line using TRAP (Brichta et al., 2015). In this paper, TRAP was used to obtain gene expression profiles for DAn compared to whole midbrain. Thus, we wished to see whether published data from a similar experiment aligned with our dataset. To better compare both gene expression datasets, the 'Brichta' data were re-aligned and re-analysed using the same analysis pipeline that the TRAP-Seq data have undergone.

Upon ranking the expression profiles by PCA and hierarchical clustering, the main source of variation, as well as the main branching points were found based on the dataset origin (Figure 5. 10 A, B). After removing the component associated with the variance between datasets (PC1), an agreement between the dopaminergic profiles (IP samples) and both whole midbrain expression profiles (Total samples) was uncovered and the data clustered together as shown by hierarchical clustering (Figure 5. 10 C). Again, the previously identified TRAP-Seq outlier samples clustered together with all whole midbrain RNA samples. This comparison showed that we and others could successfully enrich DAn-specific mRNA using TRAP



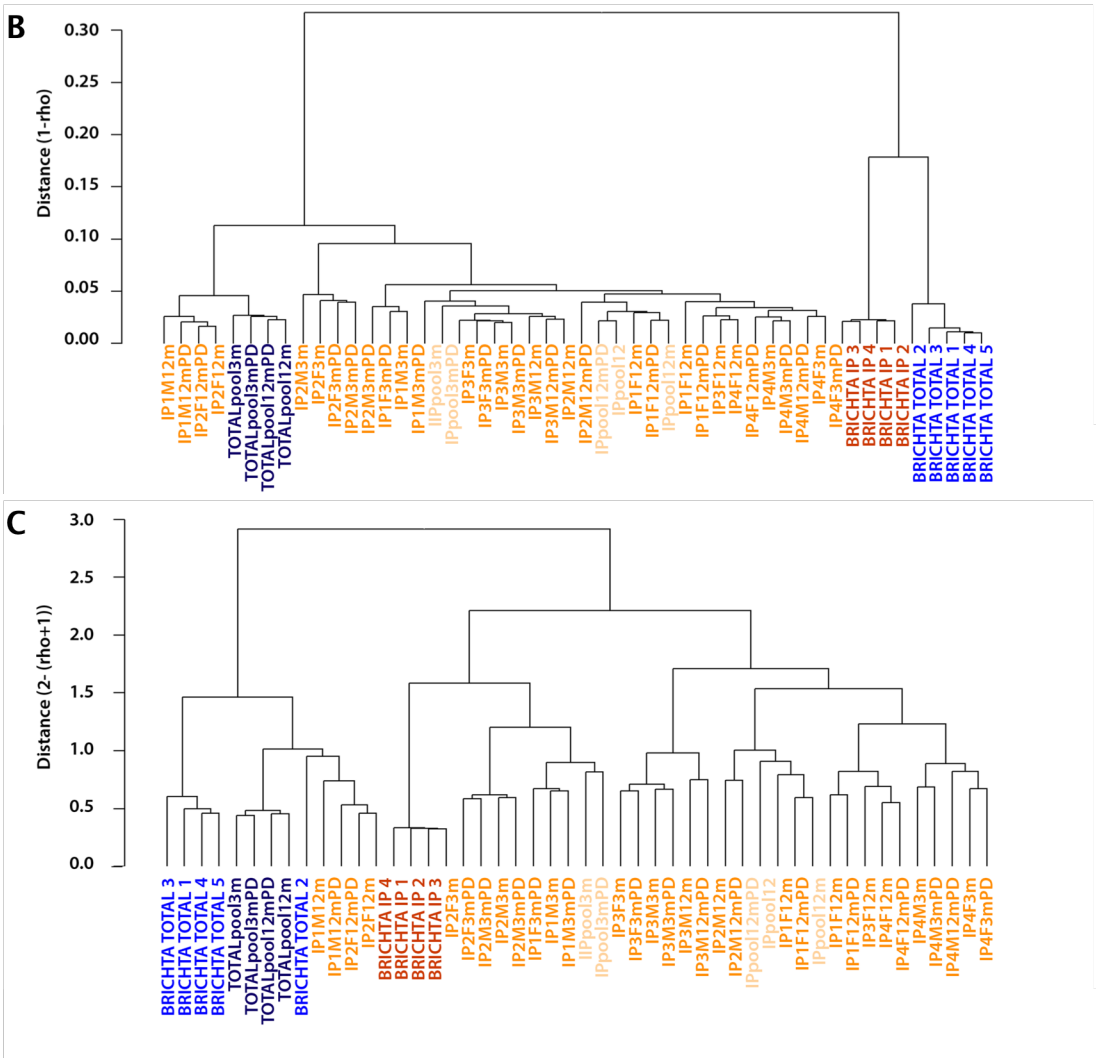


Figure 5. 10 Comparison of the TRAP-Seq dataset to external DAn translatome datasets confirms successful enrichment of DAn-specific mRNA.

The 'Brichta' (Brichta et al. 2015) RNA-Seq data ('Brichta Total', 'Brichta IP') was used for comparison. Ranked TPM for both datasets found 22237 features in common. Outlier sample IP1F3m was removed (TRAP-Seq dataset). (A) PCA [log2(TPM + 1)] and (B) hierarchical clustering show a clear separation of the two datasets. Some TRAP-Seq IP samples clusters with the Total samples (IP1M12m, IP1M12mPD, IP2F12mPD, IP2F12m). (C) Clustering after removing PC1 from ranked TPM leads to combined Total and IP RNA clusters despite dataset origin. TPM= transcript per million. IP= bound or immunoprecipitated RNA fraction. Total= midbrain input RNA fraction. F= female. M= male. 3m= 3 months. 12m= 12 months. PD= Parkinson's disease. Pool= pooled IP/Total samples across either control or disease model at 3/12 months. DAn= dopaminergic neuron. Analysis performed in collaboration with J. Monzon-Sandoval. Adapted from J. Monzon-Sandoval.

5.3.6 Differential expression analysis finds up-and down-regulated genes for the 'Experiment', 'Disease', and 'Age' comparisons

For the analysis of differential expressed genes (DEGs), we conducted three comparisons: by **experiment** (Total vs IP), by **disease** (CTRL vs PD), and by **age** (3 vs 12 months) (Figure 5. 11). Low expression genes were removed from the differential expression analysis (DEA), keeping 15,451 protein coding genes. A further sub-division of our three comparison groups according to other parameters, e.g. age, sex, or disease status, was performed to find out if changes are accountable for a specific sub-set. Most of these sub-set comparisons did not show any relevant differences (data not shown).

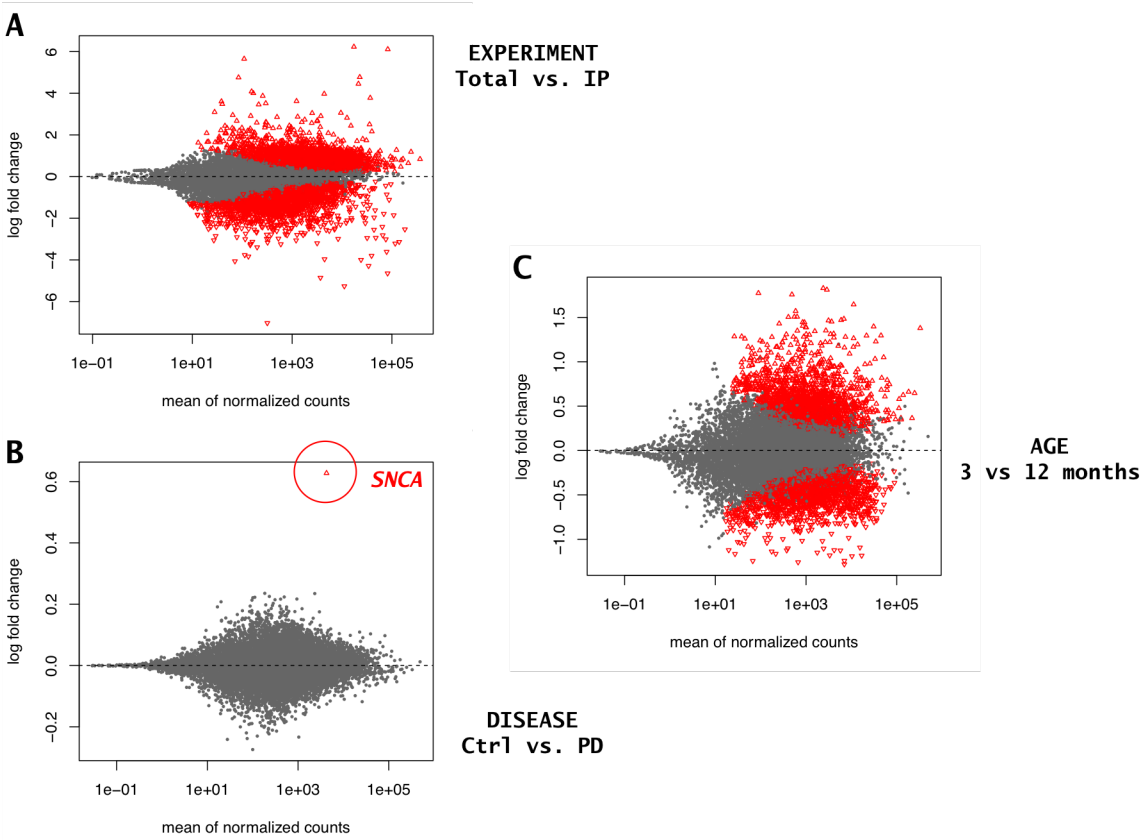


Figure 5. 11 Key DEA shows up-and down-regulated genes by Experiment and Age, but not Disease.

MA-plot of the log2 fold-changes (y-axis) versus the mean of normalised counts (x-axis) (red symbols: DEGs with adjusted p-value<0.05).
(A) DEA for 'experiment' using 8 pooled samples#. UP: 3255 (21%), DOWN: 2920 (19%) out of 15407 DEGs.
(B) DEA for 'disease' using 27 non-pooled IP samples. UP: 1 (0.0065 %), DOWN: 0 (0%) out of 15441 DEGs.*
(C) DEA for 'age' using 27 non-pooled IP samples (see B). UP: 1878 (12%), DOWN: 1932 (13%) out of 15441 DEGs. DEA= differential expression analysis. DEG= differentially expressed gene. LFC > 0= up. LFC < 0= down. IP= bound or immunoprecipitated RNA fraction. Total= midbrain input RNA fraction. F= female. M= male. 3m= 3 months old mice. 12m= 12 months old mice. PD= Parkinson's disease model. Pool= pooled IP/Total samples across either control or disease model at 3/12 months. Analysis performed in collaboration with J. Monzon-Sandoval. Adapted from J. Monzon-Sandoval.
 # IPpool3m (PD), Totalpool3m (PD), IPpool12m (PD), Totalpool12m (PD).
**IP1M3m, IP1M3mPD, IP2M3m, IP2M3mPD, IP3M3m, IP3M3mPD, IP4M3m, IP4M3mPD, IP1F3mPD, IP2F3m, IP2F3mPD, IP3F3m, IP3F3mPD, IP4F3m, IP4F3mPD, IP2M12m, IP2M12mPD, IP3M12m, IP3M12mPD, IP4M12m, IP4M12mPD, IP1F12m, IP1F12mPD, IP3F12m, IP3F12mPD, IP4F12m, IP4F12mPD.*

1) DEA 'Experiment'

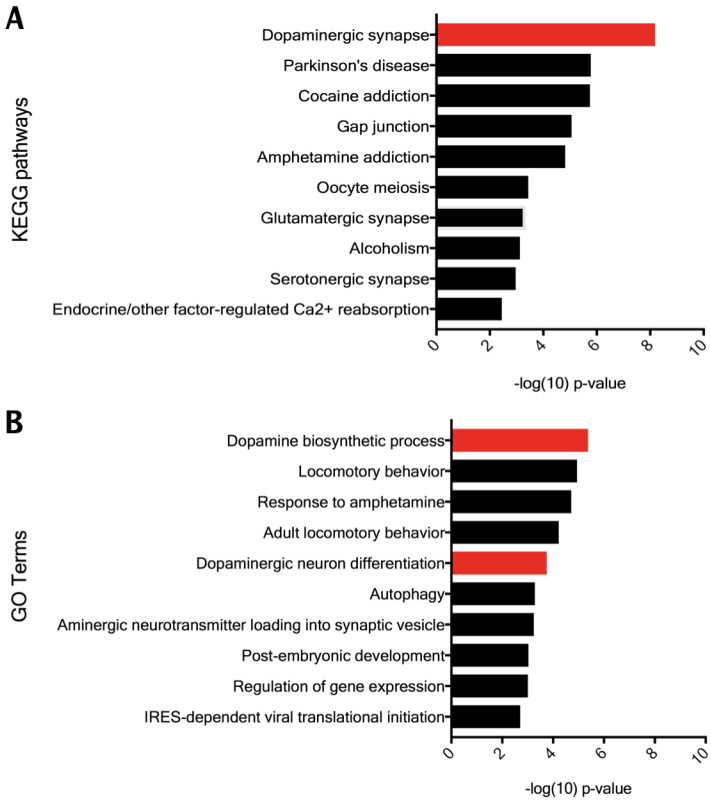
Many DEGs were found for the '**experiment**' comparison between the pooled IP and pooled Total samples. In total, 3255 and 2920 genes were up- and down-regulated in the IP sample, respectively. We selected the genes with the smallest false-discovery rate (FDR) for further analysis (Table 5. 1). Among the up-regulated genes, Cocaine- and amphetamine-regulated transcript (CARTPT), Urocortin (UCN), Ubiquitin protein Ligase E3 component N-recognin 3 (UBR3), Autophagy related 7 (ATG7), and TH had the smallest FDR closely followed by known DAn markers (DDC, DAT (Slc6a3), CALB1, and Nr4a2) (Table 5. 1). Among down-regulated genes with the smallest FDR were a few mitochondrial encoded genes (mt-Atp8, mt-Nd3, mt-Nd4l), Myelin basic protein (MBP), and Cystatin C.

Symbol	ENSEMBL	Log2 FC	FC	FDR
CARTPT	ENSMUSG00000021647	6.27	77.02	3.7692E-274
UCN	ENSMUSG00000038676	6.41	84.89	6.0641E-255
UBR3	ENSMUSG00000044308	4.52	22.88	2.4154E-252
ATG7	ENSMUSG00000030314	4.86	29.02	2.3336E-233
TH	ENSMUSG00000000214	3.85	14.37	3.0983E-148
mt-ATP8	ENSMUSG00000064356	-5.48	0.02	8.7601E-128
YEATS2	ENSMUSG00000041215	4.07	16.82	5.2131E-116
MBP	ENSMUSG00000041607	-2.56	0.17	2.4933E-107
mt-ND5	ENSMUSG00000064367	-4.43	0.05	8.3219E-104
mt-ND4L	ENSMUSG00000065947	-5.08	0.03	6.60135E-97
DDC	ENSMUSG00000020182	3.11	8.66	1.55752E-93
CST3	ENSMUSG00000027447	-1.98	0.25	7.41633E-91
SELENOP	ENSMUSG00000064373	-2.32	0.20	7.22489E-87
SDC4	ENSMUSG00000017009	-2.57	0.17	1.04926E-85
PLEKHB1	ENSMUSG00000030701	-2.01	0.25	1.14635E-79
APOE	ENSMUSG00000002985	-2.87	0.14	9.06091E-76
GM2A	ENSMUSG00000000594	-2.34	0.20	7.42763E-74
mt-ND6	ENSMUSG00000064368	-4.13	0.06	5.17041E-73
ATP1B2	ENSMUSG00000041329	-2.26	0.21	4.19977E-71
CMTM5	ENSMUSG00000040759	-2.25	0.21	2.00206E-70
DLK1	ENSMUSG00000040856	2.74	6.67	3.9696E-70
AC165954.1	ENSMUSG00000098411	2.74	6.67	3.9696E-70
MLC1	ENSMUSG00000035805	-2.43	0.19	2.29881E-68
PMP22	ENSMUSG00000018217	-2.23	0.21	2.55403E-64
SLC1A3	ENSMUSG00000005360	-2.66	0.16	2.60344E-63
SLC6A3	ENSMUSG00000021609	2.48	5.59	6.74232E-63

Table 5. 3 Top 25 genes for the DEA 'experiment'.

Shown are the log2 FC MLE and the FC MLE (MLE= maximum-likelihood estimate). FDR= false discovery rate. DEA= differential expression analysis. Log2 FC= log2 fold-change. FC= Fold-change. Blue= down-regulated. Red= up-regulated.

Next, we used the Database for Annotation, Visualization and Integrated Discovery (DAVID) software (Huang et al., 2008) to determine Kyoto Encyclopaedia of Genes and Genomes (KEGG) pathways and Gene Ontology (GO) terms of the top 200 genes with the lowest FDR that were enriched in the IP fraction for the '**experiment**' comparison (CTRL and PD samples analysed together) (Figure 5. 12). Several specific functional categories and pathways were found overrepresented, e.g. 'dopaminergic synapse' (14 genes, p-value= 6.58 x 10-9) and 'Parkinson's disease' (12 genes, p-value= 1.67 x 10-6). The genes associated with the 'dopaminergic synapse' pathway included DDC, DRD2, GNAI1, SLC6A3, TH, GNB2, PPP2CA, PPP2CB, SLC18A2, PPP3CB, GNAS, PRKACA, PPP3CA, and GNG4 (Figure 5. 12 A, C). Furthermore, the IP RNA-enriched genes were primarily associated with biological processes, such as 'dopamine biosynthetic process' (5 genes, p-value= 4.23 x 10-6) and 'dopaminergic neuron differentiation' (5 genes, p-value= 1.78 x 10-4) (Figure 5. 12 B). These results confirmed that the TRAP IP RNA fractions contained DAn-specific mRNA.



C

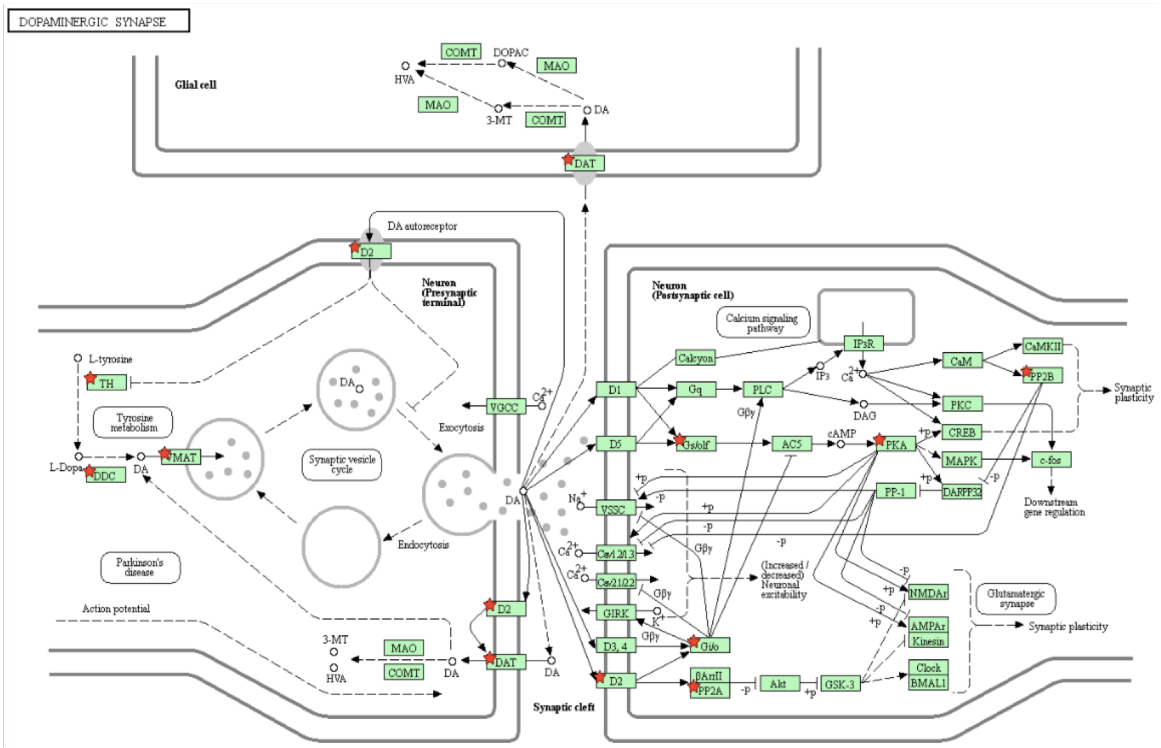


Figure 5. 12 GO terms and pathways relating to dopaminergic cell population are differentially expressed in the TRAP IP fractions.

The top 200 genes enriched for the TRAP pooled IP vs pooled Total RNA comparison (CTRL and PD samples analysed together) were analysed using Database for Annotation, Visualisation and Integrated Discovery (DAVID) v6.8. (A) Top 10 KEGG pathways with the lowest –log (10) p-value. 'Dopaminergic synapse' is the most significant pathway detected (red bar graph). (B) Top 10 GO-BP terms with the lowest –log (10) p-value. Significant gene ontology biological processes (GO-BP) represent 'dopaminergic biosynthetic process' or 'dopaminergic neuron differentiation' (red bar graphs). (C) Pathway map for 'dopaminergic synapse' generated using KEGG pathway analysis. Mapped objects are marked in red such as DAT, TH, and VMAT2.

2) DEA 'Disease'

For the '**disease**' comparison, CTRL and PD samples were analysed at 3 or 12 months (up- or downregulated DEGs relative to the PD sub-sets), focussing only on the IP samples (outliers and pooled samples removed). The only gene detected as differentially expressed (FDR < 0.05) in the PD samples was aSyn for both, 3 and 12 months Table 5. 4. We summarised the top 10 up-and down-regulated DEGs for the '**3 months - disease**' and '**12 months - disease**' comparison in Appendix Table 5.3 and 5.4. For 3 months, the highest up-regulated gene after aSyn was mucin 1 cell surface associated (MUC1), the most down-regulated gene was cysteine rich c-terminal 1 (CRCT1). For 12 months, the highest up-regulated gene after aSyn was mitochondrial amidoxime reducing component 1 (MARC1), the most down-regulated gene was adhesion g protein-coupled receptor g5 (ADGRG5).

	Symbol	ENSEMBL	Log2 FC	FC	FDR
3 months	ENSMUSG00000025889	Snca	8.99	508.81	1.72E-56
12 months	ENSMUSG00000025889	Snca	9.01	514.18	7.29E-07
both	ENSMUSG00000025889	Snca	8.99	509.81	7.99E-17

Table 5. 4 ***Top genes for the DEA 'disease.***

Shown are the log2 FC MLE and the FC MLE (MLE= maximum-likelihood estimate). FDR= false discovery rate. DEA= differential expression analysis. Log2 FC= log2 fold-change. FC= Fold-change. Red= up-regulated.

3) DEA 'Age'

For gene expression changes with '**age**', up- and down-regulated genes were analysed relative to 12 months. Here, several analyses were performed. First, all samples (CTRL and PD combined) were analysed together. In addition, the analysis was split into different sub-sets (CTRL or PD separately). Lastly, a separate analysis for each of the sub-sets for either males or females was conducted (results not shown). Most genes were found differentially expressed when CTRL and PD samples were analysed together. Even upon separation of the two conditions, many genes were commonly found to be differentially expressed in both conditions (marked in orange). We selected the top 25 most significantly changed genes for the DEA '**age CTRL**' or '**age PD**' sorted by their FDR (Table 5. 5; Table 5. 6). In both cases, all top 25 genes were up-regulated genes. Only within the top 50 most changed genes for the '**age – PD**' list (data not shown), mitochondrial respiratory complex I gene NADH:ubiquinone oxidoreductase subunit C1 (NDUFC1) was significantly down-regulated.

Symbol	ENSEMBL	Log2 FC	FC	FDR
CLPX	ENSMUSG00000015357	1.96	3.89	3.06E-16
ARC	ENSMUSG00000022602	1.51	2.85	1.16E-15
EFR3A	ENSMUSG00000015002	1.76	3.40	4.96E-14
ATRN	ENSMUSG00000027312	1.73	3.31	6.96E-13
MAP6	ENSMUSG00000055407	1.46	2.75	7.22E-13
CX3CL1	ENSMUSG00000031778	1.66	3.15	1.08E-12
TRIM9	ENSMUSG00000021071	1.10	2.14	1.21E-12
APP	ENSMUSG00000022892	1.51	2.84	4.99E-11
TIMM44	ENSMUSG00000002949	1.46	2.76	5.56E-11
CIT	ENSMUSG00000029516	1.12	2.17	7.84E-11
D8ERTD82E	ENSMUSG00000050271	1.49	2.80	6.06E-10
PTCD3	ENSMUSG00000063884	1.59	3.00	1.75E-09
TRIM66	ENSMUSG00000031026	1.30	2.47	6.92E-09
STXBP4	ENSMUSG00000020546	1.32	2.50	7.84E-09
CLCN6	ENSMUSG00000029016	1.51	2.84	7.84E-09
GPC5	ENSMUSG00000022112	1.94	3.83	7.84E-09
SERINC5	ENSMUSG00000021703	1.72	3.30	1.06E-08
SNAP25	ENSMUSG00000027273	1.50	2.84	1.61E-08
ACSBG1	ENSMUSG00000032281	1.77	3.40	1.95E-08
FSTL4	ENSMUSG00000036264	1.93	3.81	2.37E-08
LRRN1	ENSMUSG00000034648	1.42	2.68	2.74E-08
KDM3A	ENSMUSG00000053470	1.47	2.76	1.30E-07
PCDHB3	ENSMUSG00000045498	1.53	2.90	1.49E-07
CTSB	ENSMUSG00000021939	1.09	2.13	1.69E-07
SNAP23	ENSMUSG00000027287	1.77	3.41	1.69E-07

Table 5. 5 ***Top 25 genes for the DEA 'age - CTRL'.***

log2 FC MLE and the FC MLE (MLE= maximum-likelihood estimate). FDR= false discovery rate. DEA= differential expression analysis. Log2 FC= log2 fold-change. FC= Fold-change. Red= up-regulated. Orange= common to both lists of 25 genes (CTRL + PD). Analysis performed in collaboration with J. Monzon-Sandoval.

Symbol	ENSEMBL	Log2 FC	FC	FDR
EFR3A	ENSMUSG00000015002	1.75	3.36	1.38E-12
CLPX	ENSMUSG00000015357	2.02	4.04	6.19E-10
MAP6	ENSMUSG00000055407	1.27	2.42	1.85E-09
LRIG2	ENSMUSG00000032913	1.33	2.52	3.76E-09
SNAP25	ENSMUSG00000027273	1.45	2.74	4.11E-09
SMOC1	ENSMUSG00000021136	1.68	3.21	4.11E-09
SPTLC2	ENSMUSG00000021036	1.33	2.51	4.39E-09
ATRN	ENSMUSG00000027312	1.40	2.64	6.75E-09
APP	ENSMUSG00000022892	1.47	2.77	1.23E-08
MEGF10	ENSMUSG00000024593	2.27	4.82	4.33E-08
DTWD1	ENSMUSG00000023330	1.74	3.33	5.98E-08
CPEB2	ENSMUSG00000039782	0.88	1.84	7.15E-08
CX3CL1	ENSMUSG00000031778	1.51	2.85	7.15E-08
PTCD3	ENSMUSG00000063884	1.58	2.99	2.39E-07
TIMM44	ENSMUSG00000002949	1.34	2.53	5.87E-07
UNC5C	ENSMUSG00000059921	1.54	2.90	1.00E-06
TRIM9	ENSMUSG00000021071	1.01	2.01	1.08E-06
RGS17	ENSMUSG00000019775	1.33	2.51	1.96E-06
DPYD	ENSMUSG00000033308	1.82	3.52	2.23E-06
ZC3HAV1	ENSMUSG00000029826	0.85	1.81	2.68E-06
APLP2	ENSMUSG00000031996	1.38	2.60	2.88E-06
TRIM66	ENSMUSG00000031026	1.05	2.08	4.09E-06
CLCN6	ENSMUSG00000029016	1.26	2.40	4.09E-06
GAP43	ENSMUSG00000047261	0.74	1.67	6.99E-06
STXBP4	ENSMUSG00000020546	1.21	2.32	7.56E-06

Table 5. 6 ***Top 25 genes for the DEA 'age - PD'.***

log2 FC MLE and the FC MLE (MLE= maximum-likelihood estimate). FDR= false discovery rate. DEA= differential expression analysis. Log2 FC= log2 fold-change. FC= Fold-change. Red= up-regulated. Orange= common to both lists of 25 genes (CTRL + PD). Analysis performed in collaboration with J. Monzon-Sandoval.

5.3.7 Functional analysis of DEGs in the 'age' dataset

The following functional analysis focused on the resulting sub-sets of DEGs with '**age**' since the '**disease**' comparison did not show any significantly changed hits apart from aSyn. For the functional analysis of DEGs in the '**age**' datasets (all IP, CTRL IP, PD IP), we first focused on co-expression network analysis. Co-expression was measured as the correlation between the TRAP-Seq DEGs with gene expression levels in a *BrainSpan* atlas. The online resource *BrainSpan* contains information on transcriptional mechanisms involved in human brain development (http://www.brainspan.org/). Only human orthologues from the TRAP-Seq DEGs with 'age' were used. The average co-expression of each dataset was compared to that of 10,000 random samples of genes drawn from a background population (all protein coding genes () with measured expression level in *BrainSpan*) to test whether the co-expression between them is equal or higher than the real/observed co-

expression for each of the TRAP-Seq DEGs with age. Overall, the co-expression between the genes was higher than expected by chance (Figure 5. 13). Thereby, the co-expression was stronger among down-regulated genes than among up-regulated genes at 12 months. Nevertheless, we could not detect a difference between the '**CTRL**' or '**PD**' sub-sets.

Next, a combined protein-protein interaction (PPI) network was constructed from diverse resources using published PPIs (*Biogrid*, *HitPredict* and *IntAct*), protein links (STRING), protein complexes (*CORUM*), and interactions from shared reactions (*Reactome*). In this way, the number of edges/links among the proteins encoded by the TRAP-Seq DEGs with age and their clustering (Figure 5. 13 B, C) within the PPI network was measured by comparing the observed and expected number of edges or clustering by chance. Both the number of interactions and the clustering between down-regulated genes with age were higher than expected by chance. For the up-regulated genes with age in PD and CTRL samples combined, the number of PPIs were higher than expected by chance. However, the average clustering was not higher compared to random samples of genes. Appendix Table 5.6 - 5.8 detail the analysed values. Overall, we found higher co-expression values, number of edges, and clustering in the PPI network than compared by chance but the data-sets for DEGs of all IP, CTRL IP, and PD IP with age were indistinguishable.

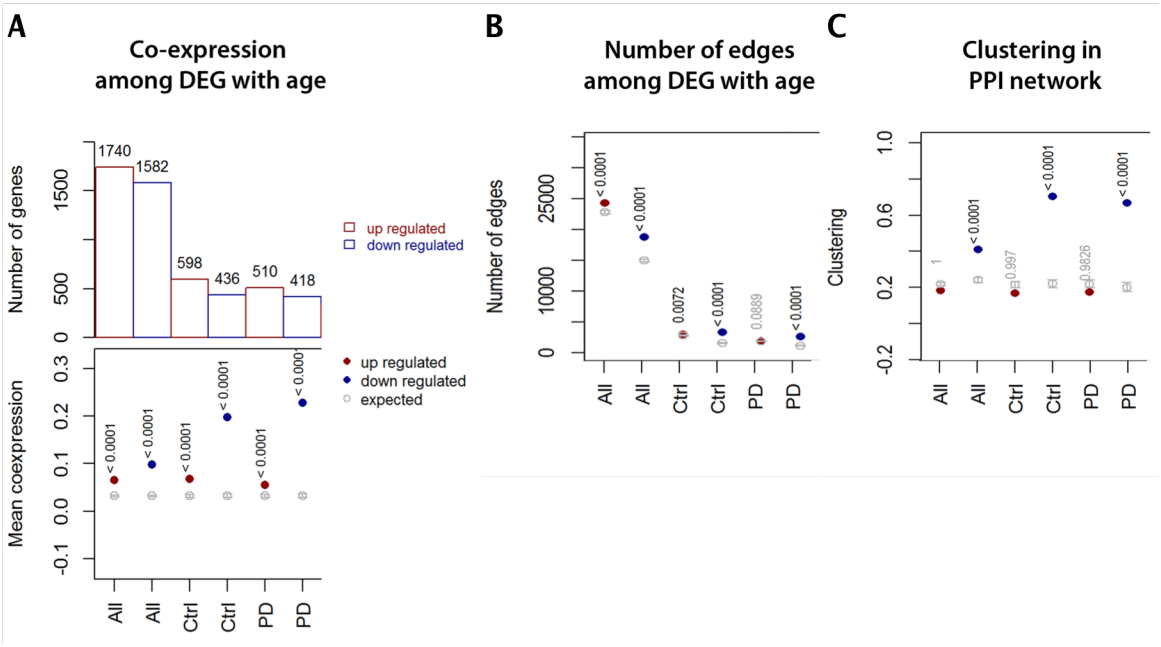


Figure 5. 13 High co-expression in the brain among differentially expressed genes with age.

(A) Co-expression among DEGs measured as the Pearson correlation between sets of DEGs from the TRAP-Seq dataset with expression levels in a 'BrainSpan' dataset. Average co-expression to 10,000 random samples of genes drawn from a background population was assed. ***Upper panel****: Total number of DEGs considered for the analysis.* ***Lower panel****: Observed and expected co-expression levels for each sub-set of DEGs with age and the estimated p-value plotted next to the corresponding co-expression levels. The average co-expression among up- and down regulated genes with age is higher than expected by chance. There is an overall higher co-expression among down-regulated genes with age, than among up-regulated genes. (B) PPI network considering the number of edges or the clustering (C) among the proteins encoded by the TRAP-Seq DEGs with age. Observed and expected numbers of edges are generated comparing 10,000 random samples of genes to that of the TRAP-Seq DEGs with age. Grey dots= expected values. Red dots= observed up-resulted values. Blue dots= observed down-regulated values. PPI= protein-protein interaction network. Analysis performed in collaboration with J. Monzon-Sandoval. Modified after J. Monzon-Sandoval.*

Overlap of the age-related DEGs with known PD relevant genes

We found no clear distinction between 'normal' age-related gene expression changes and these specific to our *hSNCA+* model. In order to find a link between age-driven DEGs and the PD phenotype, we tested associations of known PD-associated genes with our DEGs focusing on the '**age – PD**' sub-set. The PD gene lists have been curated based on literature researches (communication with J. Monzon-Sandoval, Appendix Tables 5.9 -5.11). Among the DEGs in the '**age'** dataset, there was some overlap to previously known PD-related genes: MAPT, ASH1L, MCCC1, SIPA1L2, NMD3, ZNF668, DNAJC6, SYNJ1, ATP6AP2, SYNJ1, and VPS13C were up-regulated; NUCKS1, PARK2, PARK7, and GCH1 were down-regulated. However, the number of overlapping genes was not higher than between a random sample-set of genes and there was no preferential overlap for DEGs with age detectable from the PD samples ('**age – PD**').

Comparison of the TRAP-Seq age-related DEGs to known age-associated genes

We were unable to distinguish 'normal' from 'disease-relevant' DEGs with age, thus, we concentrated our analysis on general ageing. Therefore, the TRAP-Seq dataset was compared to up- and down-regulated gene expression profiles of the mouse SNc at 2 and 18 months of age generated by microarray analysis (Gao et al., 2013). Upon comparison of the TRAP-Seq 'age' dataset to this study, a high overlap between the up-regulated genes with age could be detected (p-value < 0.05) (Appendix 5.9). Among the genes that were up-regulated in the SNc in the Gao et al. study and the TRAP-Seq 'age' data-set, EFEMP1, IL33, SERPINA3N, ZC3HAV1, DPYD, PCDHB3, PCDHB9, ITGB2, ABCA8A, and HEXB were found.

Furthermore, Goa et al. obtained a more general set of age-dependent DEGs in the brain by re-analysing four formerly published mouse-specific transcriptomic datasets for young (2 - 5 months) and old (24 - 30 months) groups (Gao et al., 2013). Also for this more general transcriptional signature of the aged mouse brain, some up-regulated genes with age could be found in common with the TRAP-Seq dataset (Appendix 5.9). Genes in common with this meta-analysis were: CTSS, SPP1, IL33, CTSZ, SERPINA3N, ZC3HAV1, PCDHB3, PCDHB9, C1QB, C1QA, LAMP2, FCGR2B, B3GALT5, ITGB2, H2-D1, ABCA8A, TRIM9, and XDH. No overlap was detected with down-regulated genes. This comparison confirmed that we were detecting age-related changes in the mouse SNc in our TRAP-Seq dataset. Therefore, we focused the further analysis and the validation of the TRAP-Seq hits on general ageing.

Various Gene Ontology terms associate with TRAP-Seq dataset for 'age'

The TRAP-Seq datasets were tested for overrepresented biological processes among the corresponding sets of DEGs using GO term analysis. Generally, we found more GO terms for up-regulated than down-regulated genes for all sub-sets, and the largest number of terms was found when all IP samples were considered focusing on pooled sexes to increase our statistical power for the analysis (Appendix Figure 5.10). GO terms for **all** up-regulated IP samples included 'cell adhesion', 'axon guidance', 'positive regulation of axon guidance', 'negative regulation of neuron apoptotic process', and 'oxidative reduction process'. 'Translation' was the most prominent feature for down-regulated DEGs. Further, down-regulated terms for 'mRNA or rRNA processing', and 'response to oxidative stress' were found (Appendix Figure 5.10).

Separated CTRL- and PD-related GO term analysis found no striking differences in the overrepresented biological processes among the age-related DEGs detected from either **CTRL** (Figure 5. 14 A, A') or **PD** samples separately (Figure 5. 14 B, B'). Overrepresented GO terms for up-regulated genes included 'axon guidance' (CTRL + PD), 'locomotor behaviour' and 'negative regulation of neuron apoptotic process' (CTRL only) (Figure 5. 14 A), or 'oxidation reduction process' and 'phosphorylation' (PD only) (Figure 5. 14 B). On the other hand, down-regulated GO terms found in both sets were 'translation', 'rRNA processing', 'oxidation reduction process', and

'response to oxidative stress' (Figure 5. 14 A', B'). Thereby, it was striking that although there were overall less down-regulated terms, they reached a –log (10)(FDR) of up to 80, whereas top up-regulated overrepresented GO terms only represented a –log (10)(FDR) of less than 10. Again, 'Translation' was by far the most significantly down-regulated GO term, especially for the 'age-PD' sub-set.

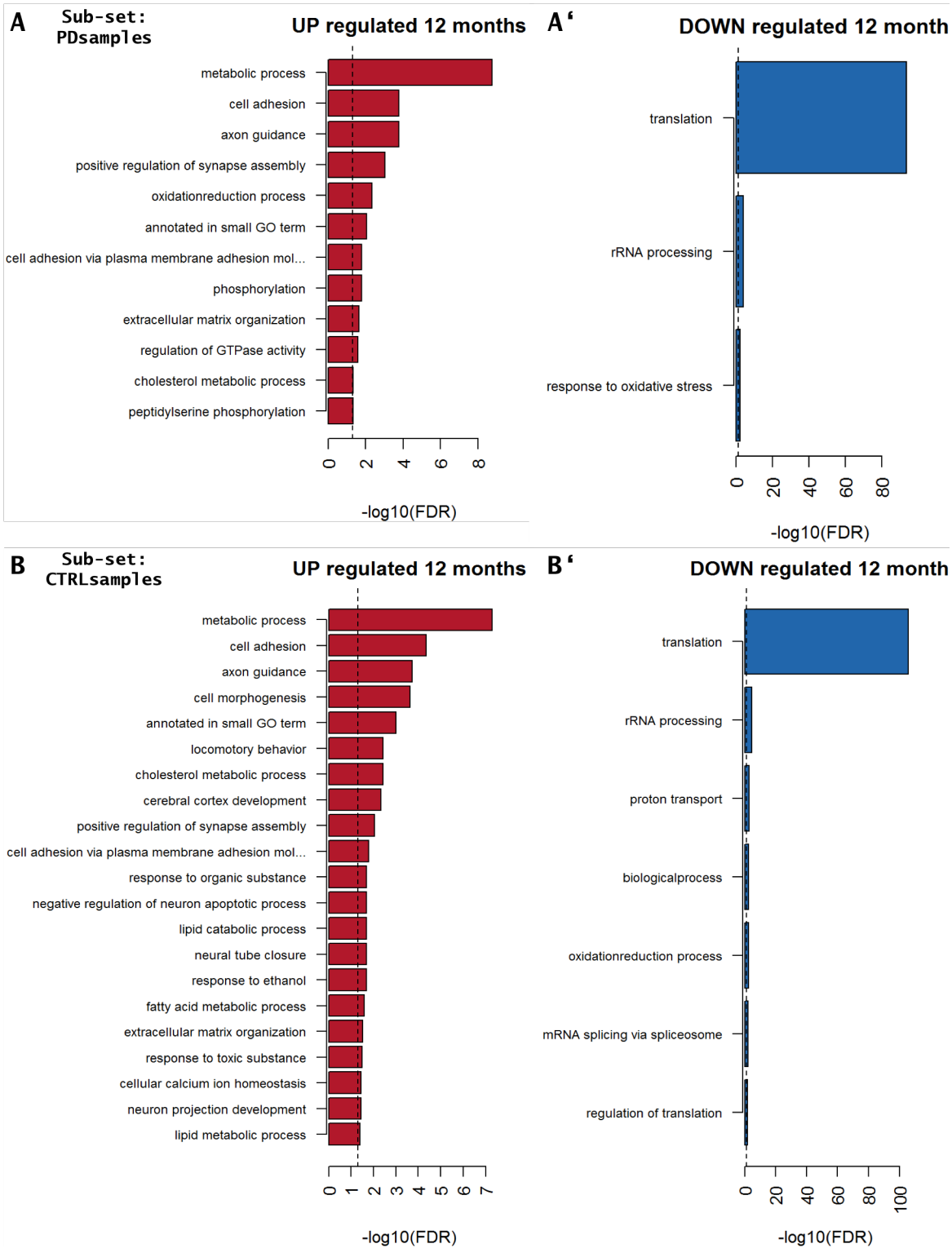


Figure 5. 14 Similar GO terms are found up- or down-regulated in CTRL and PD samples with age.

Age-related changes comparing 3 and 12 months old mice for DEGs(FDR < 0.05, n >= 2). UP (A, B) and DOWN (A', B') regulation is shown relative to 12 months. Bar plots represent -log 10 (FDR), dotted line is drawn at -log 10 (0.05). GO terms relevant for the sub-set of PD samples (A, A') and CTRL samples (B, B') (all IP samples, except (IP1F3m, IP1M12m, IP1M12mPD, IP2F12mPD, IP2F12m) and pooled samples). Overall, GO terms represent a greater variety of bps for UP-regulated than DOWN-regulated genes for both, CTRL and PD. Many bps are overlapping for CTRL and PD. FDR= false-discovery rate. GO= gene ontology. bp= biological process. DEG= differentially expressed gene. IP= bound or immunoprecipitated RNA fraction. 3m= 3 months old mice. 12m= 12 months old mice. PD= Parkinson's disease model. Analysis performed in collaboration with J. Monzon-Sandoval. Adapted from J. Monzon-Sandoval.

5.1.1 TRAP-Seq validation experiments

Selection of genes for RNA-Seq validation based on their associations to PD-relevant or mitochondria-related GO-term

To validate TRAP-Seq hits, selected targets were analysed on the gene and protein level. qPCR and western blotting analysis were performed on RNA isolated from the midbrain (1 hemisphere for each qPCR or western blotting) of *THTR++* and *THTR++hSNCA+* mice at 3 and 12 months (n= 3 mice per genotype and age, males and females used).

The top 100 up-regulated and down-regulated hits for the '**age - PD**' dataset (IP samples only, FDR < 0.05) were analysed for overrepresented KEGG pathways and biological processes (Figure 5. 15). Up-regulated DEGs associated with GO terms such as 'extracellular matrix organisation' or 'synaptic vesicle priming', including OTOF, **SNAP23**, and **SNAP25** (Figure 5. 15 A). Down-regulated DEGs associated with GO terms such as 'translation', 'small ribosome subunit assembly', or were found in the KEGG pathway analysis for 'oxidative phosphorylation', including mitochondrial respiratory complex genes **ATP5E**, NDUFA3, **UQCR11**, **NDUFC1**, **UQCRQ**, NDUFA1, and ATP5K (Figure 5. 15 B').

Out of this analysis (Figure 5. 15), we selected up- and down-regulated genes from the '**age – PD**' dataset for validation by qPCR analysis (Table 5. 7). Some of the selected genes (UQCR11, UQCRQ, ATP5E, and NDUFC1) came up in several mitochondrial respiration-related GO terms and pathways (down-regulated with '**age – PD**') and were chosen to assess mitochondrial complex integrity. Taking the full DEGs list into account, many more genes related to the mitochondrial respiratory complexes were found changed, mainly down-regulated.

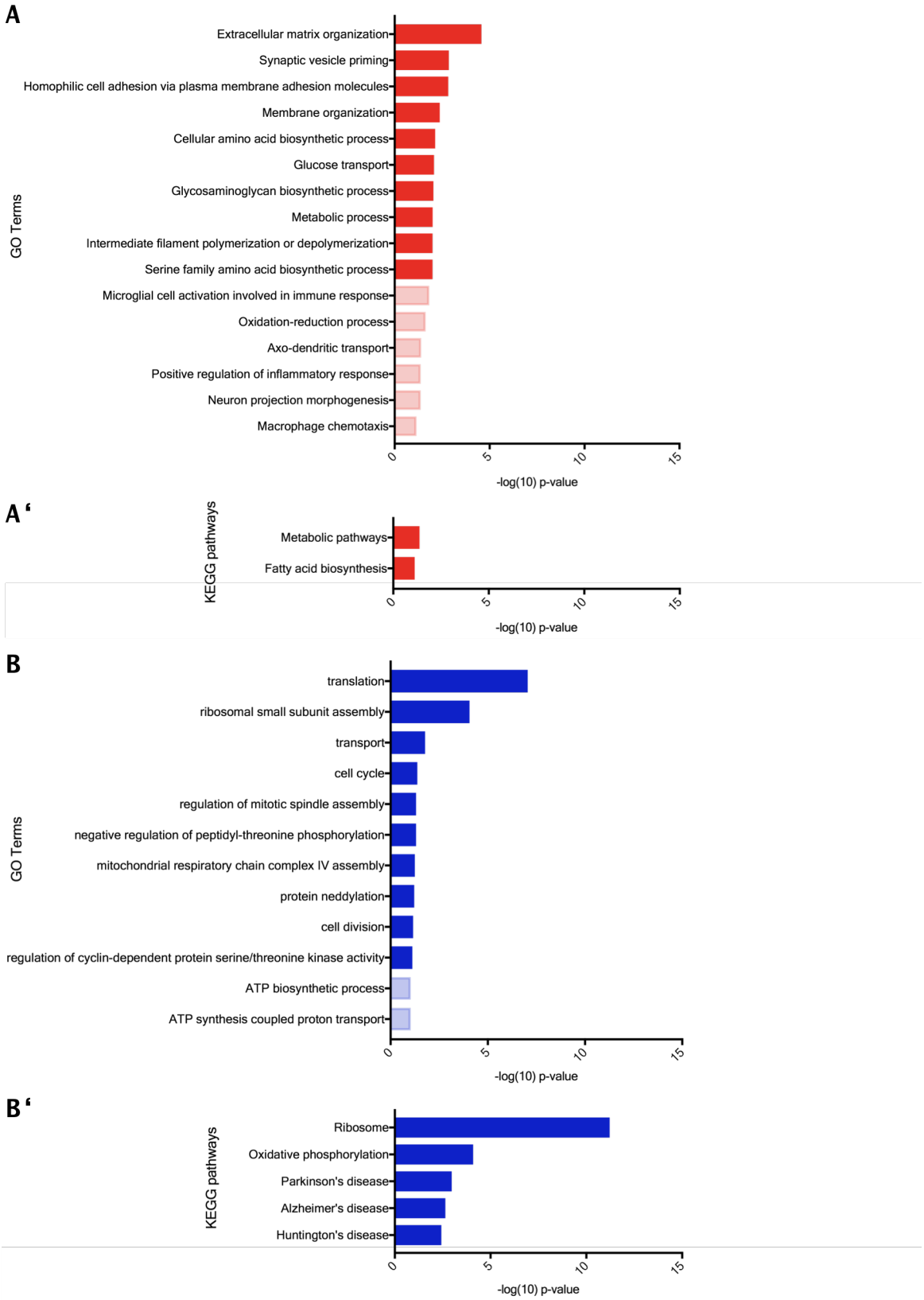


Figure 5. 15 GO terms and KEGG pathways found up- or down-regulated in PD samples with age.

Age-related changes comparing PD sub-set for DEGs (top 100 genes, FDR < 0.05) for up- (red) and down-regulated (blue) genes relative to 12 months. GO terms and KEGG pathways are presented as bar plots of the most significant hits (-log 10 (FDR)). (A, A') GO-bp or KEGG pathways relevant for up-regulated genes, such as 'synaptic vesicle priming' or 'oxidative reduction process'. (B, B') Terms relevant for down-regulated genes, such as 'translation' or 'oxidative phosphorylation', as well as neurodegenerative diseases (PD, AD, HD). FDR= false-discovery rate. GO= gene ontology. bp= biological process. DEG= differentially expressed gene. PD= Parkinson's disease model.

TRAP-Seq validation by qPCR using whole midbrain samples finds little overlap with DEGs

For each gene in Table 5. 7, qPCR primers were designed, tested for efficiency and a single product, and all primers that did not meet these criteria were excluded. Some of the analysed genes had to be excluded (UQCR11, UQCRQ, TIMM44, NDUFC1) as their detection by qPCR was unreliable. Figure 5. 16 summarises the validation results. No significant differences could be detected between the analysed samples. Bone morphogenetic protein 7 (BMP7) which is up-regulated in the TRAP-Seq dataset (Table 5. 7) shows the same trend in 12 months *hSNCA+* mice despite large sample-to-sample variation (Figure 5. 16 C, n.s.). More animals might be needed to clarify the chosen genes. Otherwise, total midbrain samples might not be specific enough to reproduce the results seen in DAn-specific TRAP IP RNA by RNA-Seq.

Symbol	Gene name	ENSEMBL	Log2 FC	FC	FDR
APP	Amyloid Beta Precursor Protein	ENSMUSG00000022892	1.47	2.77	1,23E-08
ATP5E	ATP Synthase, H+ Transporting, Mitochondrial F1 Complex, Epsilon Subunit	ENSMUSG00000016252	-0.86	0.55	1,23E-04
BMP7	Bone morphogenetic protein 7	ENSMUSG00000008999	1.26	2.39	2,94E-03
COX20	COX20, Cytochrome C Oxidase Assembly Factor	ENSMUSG00000026500	-0.95	0.52	4,30E-04
CTSB	Cathepsin B or APP Secretase	ENSMUSG00000021939	1.07	2.10	1,79E-05
CTSS	Cathepsin S	ENSMUSG00000038642	1.74	3.35	1,83E-04
NDUFC1	NADH:Ubiquinone Oxidoreductase Subunit C1	ENSMUSG00000037152	-0.87	0.55	2,19E-05
SNAP23	Synaptosome Associated Protein 23	ENSMUSG00000027287	1.67	3.18	2,55E-05
SNAP25	Synaptosome Associated Protein 25	ENSMUSG00000027273	1.45	2.74	4,11E-09
TIMM44	Translocase of Inner Mitochondrial Membrane 44	ENSMUSG00000002949	1.34	2.53	5,87E-07
TIMM8B	Translocase of Inner Mitochondrial Membrane 8 Homolog B	ENSMUSG00000039016	-0.79	0.58	2,44E-04
UQCR11	Ubiquinol-Cytochrome C Reductase, Complex III Subunit XI	ENSMUSG00000020163	-0.87	0.55	1,51E-04
UQCRQ	Ubiquinol-Cytochrome C Reductase Complex III Subunit VII	ENSMUSG00000044894	-0.78	0.58	4,81E-04

Table 5. 7 ***Genes selected for qPCR analysis out of the 100 most significantly changed genes (DEA 'age - PD').***
Log2 FC= log2 fold-change. FC= Fold-change. MLE= maximum-likelihood estimate. FDR= false discovery rate. DEA= differential expression analysis. Blue= down-regulated. Red= up-regulated.

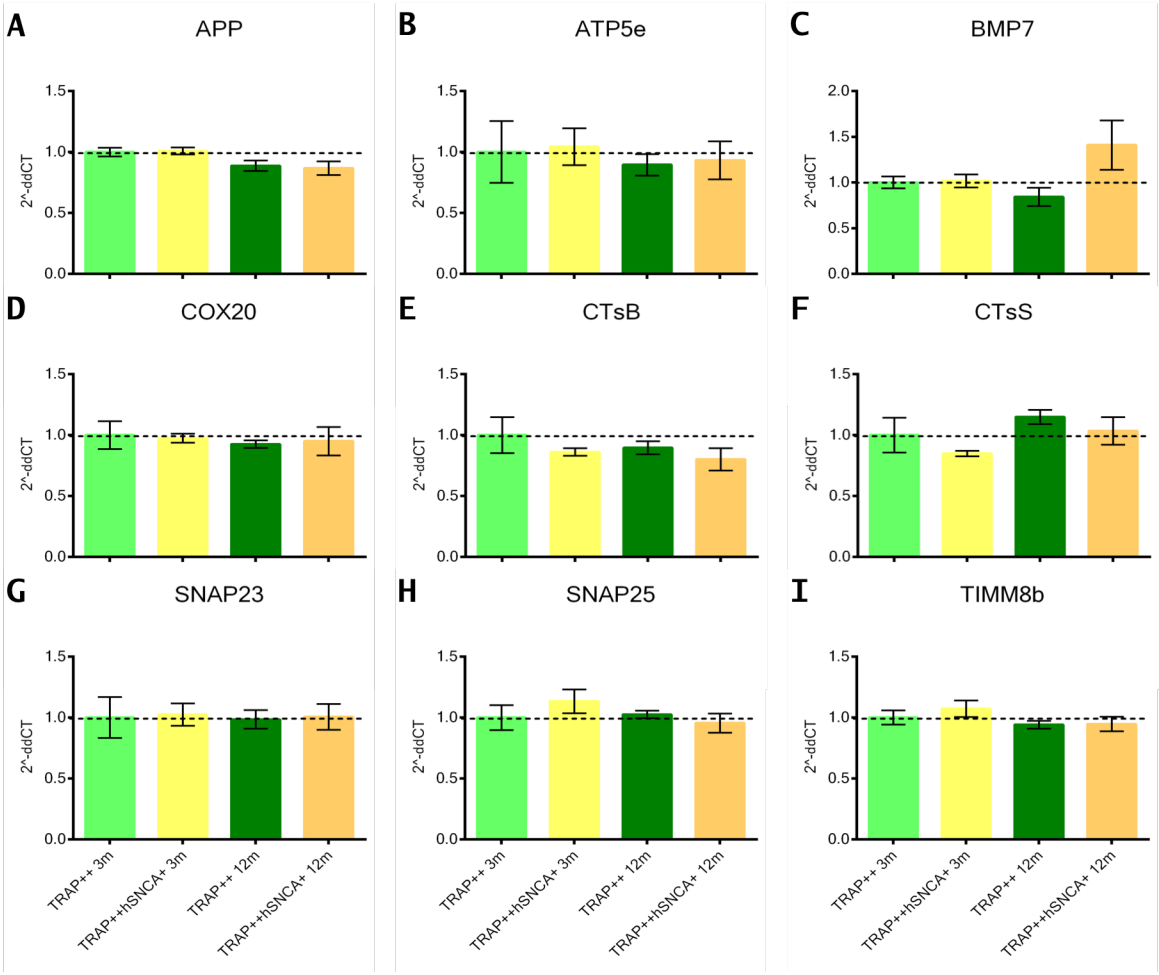


Figure 5. 16 Validation of age and PD-related TRAP-Seq DEGs.

qPCR analysis of various TRAP-Seq hits the midbrain of young (light green: THTR++; light yellow: THTR++hSNCA+) and aged (green: THTR++; yellow: THTR++hSNCA+) THTR mice. The qPCR results were normalised to the geometric mean of three reference genes and fold-changes were calculated relative to 3 months ++ TRAP results (n= 3 mouse midbrains per genotype; two-way ANOVA with Tukey post-hoc analysis; mean ± SEM). ++ or THTR++= Homozygous THTR mice. hSNCA+= human alpha-Synuclein.

Protein-based validation of TRAP-Seq hits reveals a mitochondrial phenotype

GO terms associated with oxidative stress, mitochondrial respiration, or oxidative phosphorylation (OXPHOS) were re-occurring features for the '**age – PD**' DEGs and they can be linked to studies that have reported mitochondrial dysfunction in animal or cell model of PD based on either mutant or over-expressed aSyn (Ryan et al., 2014; Smith et al., 2005). Pathway-analysis linked the '**age – PD**' dataset to OXPHOS deficits, thus, genes related to OXPHOS have been followed up by western blotting. OXPHOS is known to be involved in neurodegenerative disease such as PD or AD, as well as ageing (Finkel and Holbrook, 2000; Lin and Beal, 2006). The Wade-Martins laboratory found mitochondria-related deficits in cell culture studies using patient-derived IPSCs that carry mutations in aSyn (F. Zambon et al. Neuroscience 2016, USA). In order to validate the mitochondria-related

GO terms found in the TRAP-Seq analysis, proteins outlined in Table 5. 8 and Table 5. 9 were chosen for western blot analysis.

	Symbol	Gene name	ENSEMBL	Log2 FC	FC	FDR
I	NDUFB8	NADH:Ubiquinone Oxidoreductase Subunit B8	ENSMUSG00000025204	-0.45	0.73	0.1300
II	SDHB	Succinate Dehydrogenase Complex Flavoprotein Subunit B	ENSMUSG00000009863	0.03	1.02	0.9486
III	UQCRC2	Ubiquinol-Cytochrome C Reductase Core Protein II	ENSMUSG00000030884	0.41	1.33	0.2543
IV	mt-CO1	Mitochondrially Encoded Cytochrome C Oxidase I	ENSMUSG00000064351	-2.03	0.25	0.1438
V	ATP5A1	ATP Synthase, H+ Transporting, Mitochondrial F1	ENSMUSG00000025428	0.48	1.39	0.1531

Table 5. 8 ***Genes selected for western blot analysis out of the 100 most significantly changed genes (DEA 'age' IP samples PD) – OXPHOS complexes.***

Log2 FC= log2 fold-change. FC= Fold-change. MLE= maximum-likelihood estimate. FDR= false discovery rate. DEA= differential expression analysis. Blue= down-regulated. Red= up-regulated.

Symbol	Gene name	ENSEMBL	Log2 FC	FC	FDR
DRP1/DNM1L	Dynamin 1 Like	ENSMUSG00000022789	0,16	1,12	0,5512
HSPD1	Heat Shock Protein Family D (Hsp60) Member 1	ENSMUSG00000025980	0,18	1,13	0,5794
MFN2	Mitofusin 2	ENSMUSG00000029020	0,20	1,15	0,4046
OPA1	OPA1, Mitochondrial Dynamin Like GTPase	ENSMUSG00000038084	0,59	1,51	0,0228
PARK2	Parkin	ENSMUSG00000023826	-0,37	0,77	0,2342
PDHA1	Pyruvate Dehydrogenase (Lipoamide) Alpha 1	ENSMUSG00000031299	0,80	1,74	0,0204
PHB	Prohibitin	ENSMUSG00000038845	-0,06	0,96	0,7840
SDHA	Succinate Dehydrogenase Complex Flavoprotein Subunit A	ENSMUSG00000021577	0,55	1,47	0,2031
SOD1	Superoxide Dismutase 1	ENSMUSG00000022982	-0,42	0,75	0,0262
TOMM20	Translocase of Outer Mitochondrial Membrane	ENSMUSG00000093904	-0,33	0,80	0,1624
VDAC1	Voltage Dependent Anion Channel 1	ENSMUSG00000020402	0,29	1,22	0,3599

Table 5. 9 ***Genes selected for western blot analysis out of the 100 most significantly changed genes (DEA 'age' IP samples PD).***

Log2 FC= log2 fold-change. FC= Fold-change. MLE= maximum-likelihood estimate. FDR= false discovery rate. DEA= differential expression analysis. Blue= down-regulated. Red= up-regulated. Underlined= significant changes (FDR < 0.05).

First, we analysed the integrity of the mitochondrial respiratory complexes (**complex I**: nicotinamide adenine dinucleotide ((NADH)-ubiquinone oxidoreductase; **complex II**: succinate-ubiquinone oxidoreductase; **complex III**: ubiquinol-cytochrome c oxidoreductase; **complex IV**: cytochrome c oxidase; **complex V**: ATP synthase) summarised in Figure 5. 17.

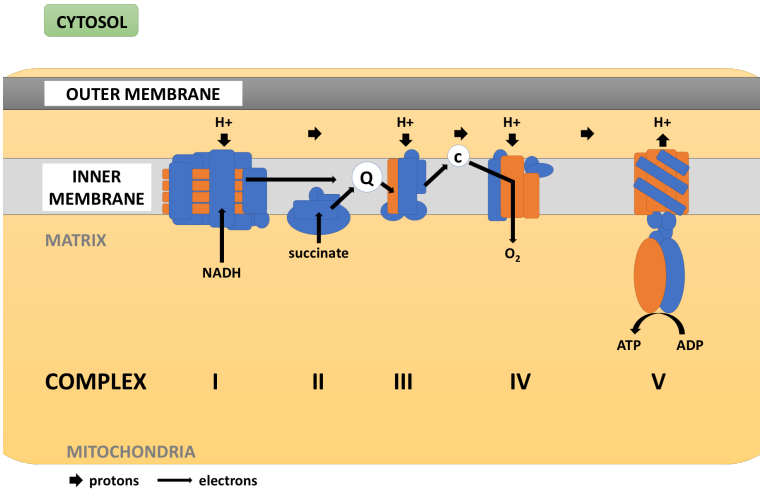


Figure 5. 17 Mitochondrial respiratory chain complexes

Diagram illustrating a mitochondrion and the mitochondrial respiratory enzyme complexes located on the inner mitochondrial membrane: ***Complex I*** *[NADH: ubiquinone oxidoreductase].* ***Complex II*** *[succinate: ubiquinone oxidoreductase].* ***Complex III*** *[ubiquinol: cytochrome c oxidoreductase].* ***Complex IV*** *[cytochrome c oxidase].* ***Complex V*** *[H+-translocating ATP synthase]. Q= Quinone. C= cytochrome c. ARROWS: direction of electron flux and the proton-pumping capability of complexes I, III and IV.*

In the TRAP-Seq 'age – PD' DEA, complex I and IV (NDUFB8, mt-CO1) were down-regulated, whereas complex III and V (UQCRC2, ATP5A1) were slightly up-regulated (Table 5. 8). The proteins corresponding to all five complexes were lower expressed with age relative to 3 months old *THTR++* control mice (light green) (n.s. for complex II). Complex I (Figure 5. 18 B, p-value= 0.13) and complex III (Figure 5. 18 D, p-value= 0.09) show decreased expression in aged *THTR++/hSNCA+* (dark yellow) animals compared to aged *THTR++* control mice (dark green).

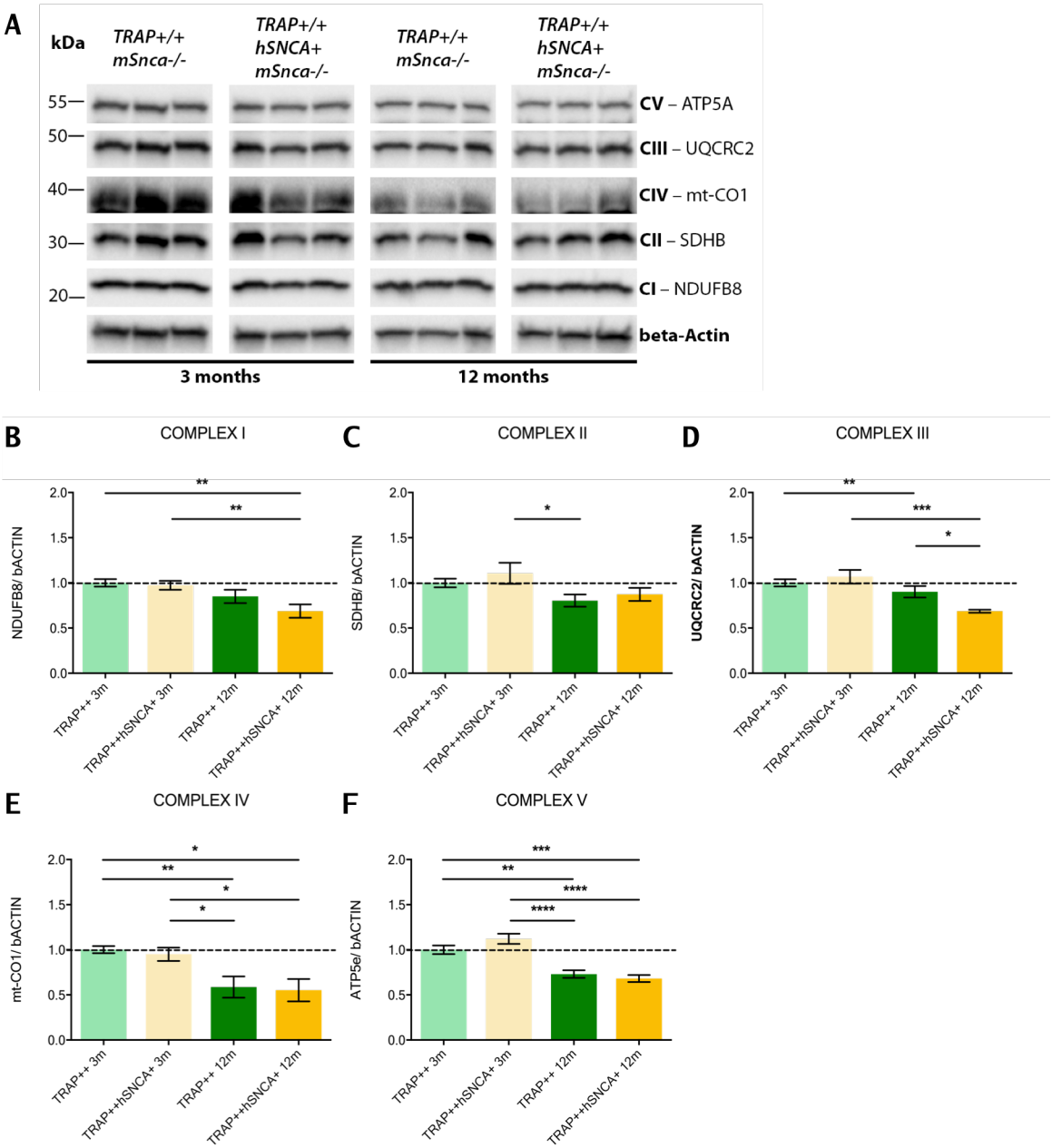


Figure 5. 18 Expression of OXPHOS complexes is down-regulated with age.

*(A) Western blot analysis using midbrain tissue of young (light green: THTR++; light yellow: THTR++hSNCA+) and aged (green: THTR++; yellow: THTR++hSNCA+) THTR mice to analyse C I – IV. The molecular weight is shown on the left, blot images are cropped, representative blots are shown. Four independent experiments were carried out. (B-D) The protein expression for each complex was normalised to beta-Actin and values shown here are calculated relative to 3 months ++ TRAP results (three independent replicates of n= 3 mice per genotype; two-way ANOVA with Tukey post-hoc analysis; mean ± SEM; * p ≤ 0.05, ** p ≤ 0.01, *** p ≤ 0.001). OXPHOS= oxidative phosphorylation. CI-IV= mitochondrial respiratory complexes 1-5. ++ or THTR++= Homozygous THTR mice. hSNCA+= human alpha-Synuclein.*

Next, we assessed proteins involved in mitochondrial fusion and fission which tightly regulate mitochondria function. Mitochondrial fusion is known to be regulated by both the long and short isoform of the protein Dynamin-like 120 kDa protein, L-OPA1 and S-OPA1 respectively (Song et al., 2007). L-OPA1 and S-OPA1 could be detected but neither was changed between any of the genotypes at 3 or 12 months (Figure 5. 19 A, n.s.). Contrary, OPA1 was significantly up-regulated on the gene level for the '**age – PD**' DEGs (Table 5. 9). Levels for another protein involved in mitochondrial fusion, Mitofusin 2 (MFN2) (Westermann, 2010) were also unchanged (Figure 5. 19 B, n.s.). In addition, levels of the mitochondrial fission protein Dynamin-1-like (DRP1) (Westermann, 2010) were unchanged between genotypes (Figure 5. 19 C, n.s.). While we detected changes in mitochondrial respiratory complexes (Figure 5. 18), other mechanisms regulating mitochondrial functions seemed mostly unaffected (Figure 5. 19).

We analysed a range of further proteins involved in mitochondria protein import (Heat shock protein 60 (HSP60) (Cheng et al., 1989), mitophagy (Parkin (PARK2) (Narendra et al., 2008), mitochondria complexes (Pyruvate dehydrogenase alpha 1 (PDHa1) (Patel et al., 2014); succinate dehydrogenase complex, subunit A (SDHA) (Bourgeron et al., 1995), or a mitochondria membrane protein (voltage-dependent anion channel (VDAC) (Hoogenboom et al., 2007). HSP60 was not significantly changed on the protein and gene level (Figure 5. 20 A, Table 5. 9, n.s.). PD-related gene Parkin was down-regulated with age on the protein (Figure 5. 20 B) and the gene level (Table 5. 9, n.s.). The mitochondrial matrix multi-enzyme complex protein PDHa1 was non-significantly changed (Figure 5. 20 C, n.s.) but the gene was up-regulated for the aged PD sample (Table 5. 9). The proteins SDHA (Figure 5. 20 D) and VDAC (Figure 5. 20 E) were significantly down-regulated with age.

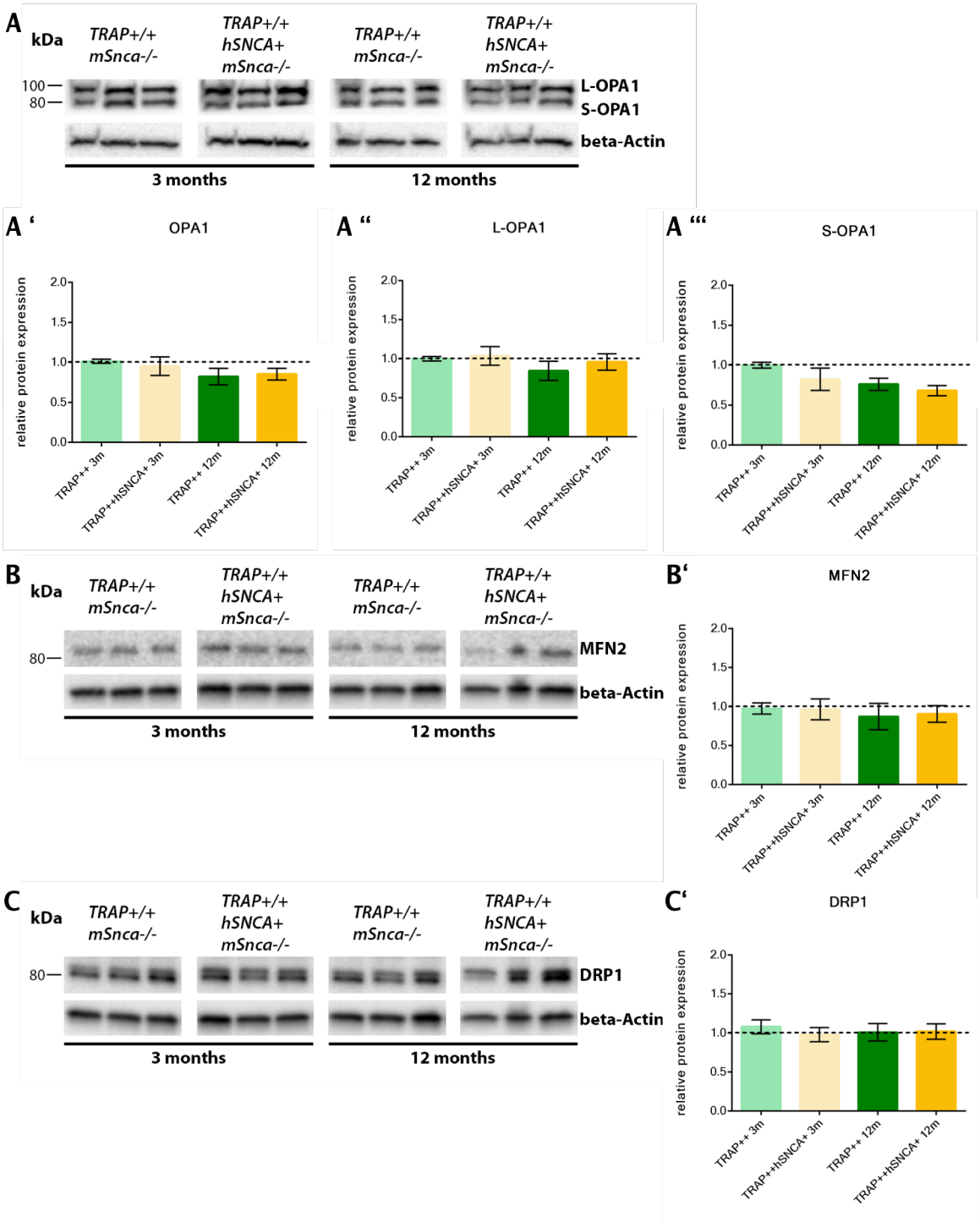


Figure 5. 19 Analysis of proteins involved in mitochondrial fusion and fission.

Western blot analysis using midbrain tissue (light green: THTR++; light yellow: THTR++hSNCA+) and aged (green: THTR++; yellow: THTR++hSNCA+). The molecular weight is shown on the left, blot images are cropped, representative blots are shown. Three independent experiments were carried out. (A, A', A'') L-OPA1 and S-OPA1 were detected but neither was changed between genotypes. Neither mitochondrial fusion as measured by (B, B') MFN2 levels, nor mitochondrial fission (C, C') measured by DRP1 levels were changed. The protein expression for each protein was normalised to beta-Actin and values shown here are calculated relative to 3 months ++ TRAP results (three independent replicates of n= 3 mice per genotype; two-way ANOVA with Tukey post-hoc analysis; mean ± SEM, not significant). ++ or THTR++= Homozygous THTR mice. hSNCA+= human alpha-Synuclein. OPA1= Dynamin-like 120 kDa protein. S= short isoform. L= long isoform. MFN2= Mitofusin 2. DRP1= Dynamin-1-like protein.

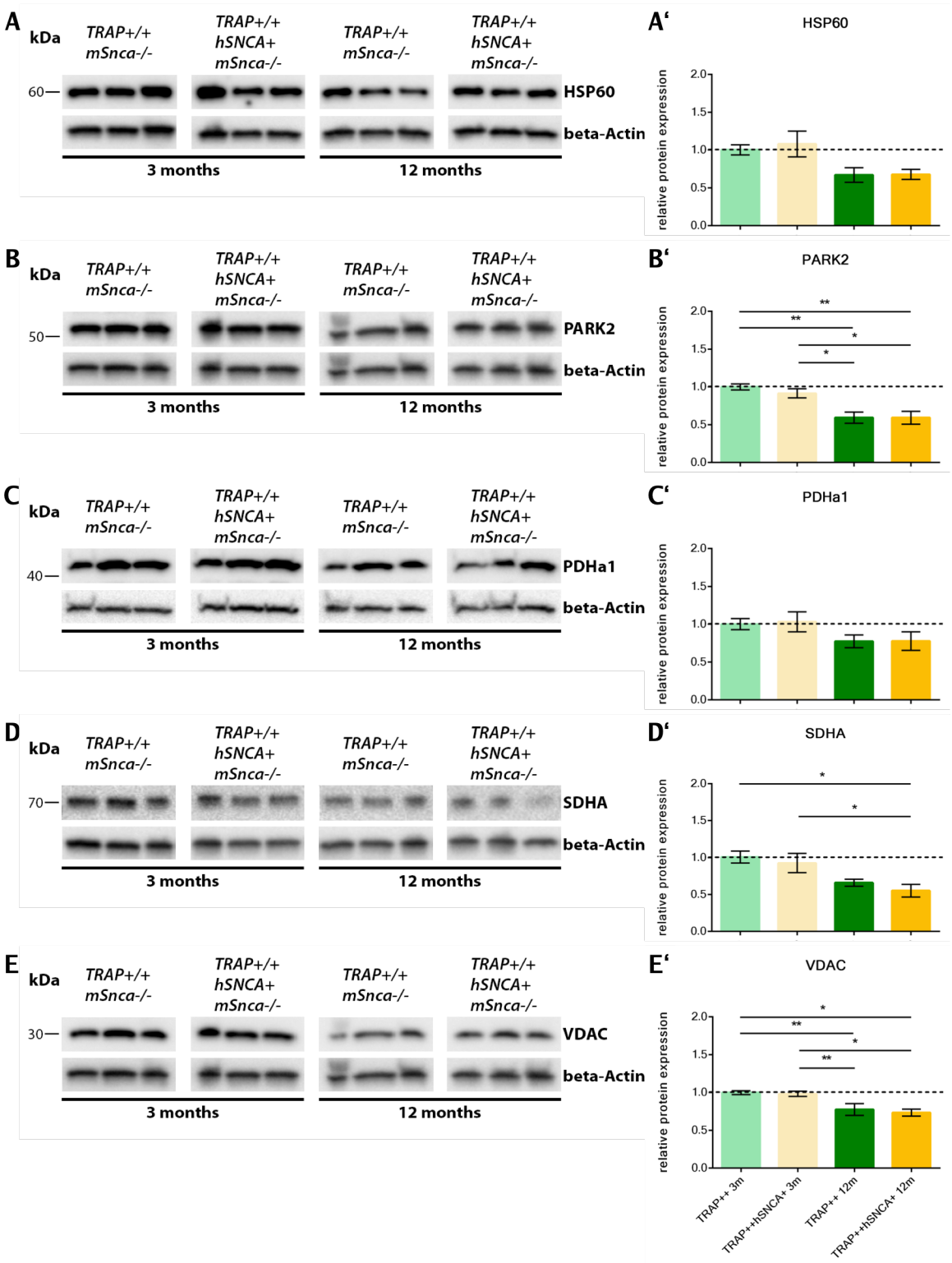


Figure 5. 20 Analysis of mitochondria-related proteins show a decrease in expression with age.

Western blot analysis using midbrain tissue of young (light green: THTR++; light yellow: THTR++hSNCA+) and aged (green: THTR++; yellow: THTR++hSNCA+) THTR mice for proteins involved in mitochondria protein import (HSP60, A), mitophagy (PARK2, B), mitochondria complexes (PDHa1, C; SDHA, D), or a mitochondria membrane protein (VDAC, E). The molecular weight is shown on the left, blot images are cropped, representative blots are shown. Three independent experiments were carried out. The protein expression for each protein was normalised to beta-Actin and values shown here are calculated relative to 3 months ++ TRAP results (three independent replicates of n= 3 mice per genotype; two-way ANOVA with Tukey post-hoc analysis; mean ± SEM). ++ or THTR++= Homozygous THTR mice. hSNCA+= human alpha-Synuclein. HSP60= Heat shock protein 60. PARK2= Parkin. PDHa1= Pyruvate dehydrogenase alpha 1. SDHA= Succinate dehydrogenase complex, subunit A, flavoprotein variant. VDAC= Voltage-dependent anion channel.

The inner mitochondrial membrane protein prohibitin (PHB) has multiple described roles in maintenance of cristae morphology, mitochondria functional integrity, or control of ROS production by complex I (Merkwirth and Langer, 2009; Zhou et al., 2012). We could not detect a change on protein level (Figure 5. 21 A, n.s.) in our *THTR* mice although it was shown to be increased in patient-derived aSyn A53T IPSCs (personal communication with Dr F. Zambon). The mitochondrial membrane translocase of outer membrane 20 (TOMM20) protein (Becker et al., 2008) (Figure 5. 21 B, n.s.) was not changed although the gene was down-regulated (Table 5. 9). Interestingly, the superoxide dismutase 1 (SOD1) protein was significantly down-regulated in the young *THTR/hSNCA+* mice, as well as in the aged mice (Figure 5. 21 C). The two intracellular SOD enzymes, the primarily cytosolic SOD1 and the mitochondrial matrix located SOD2, play a major role in the antioxidant response during the oxygen metabolism (Fukai and Ushio-Fukai, 2011).

Overall, we found reduced expression of some mitochondrial proteins, especially of the proteins within the mitochondrial respiratory complexes. In order to further investigate mitochondrial involvement in ageing and PD, immunoblotting for other proteins, e.g. TOMM40 or SOD2, as well as microscopic analysis of mitochondrial morphology and network integrity could be performed.

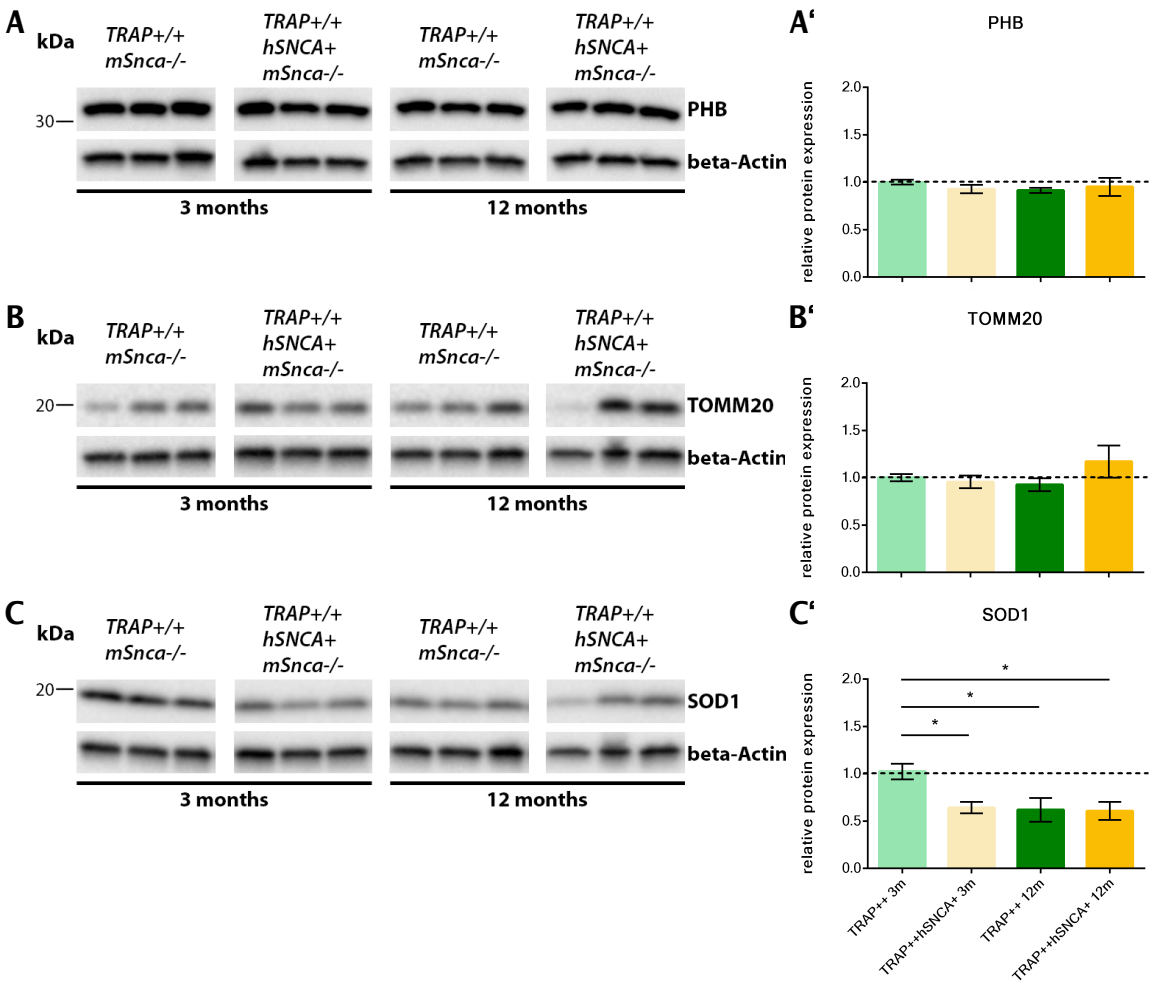


Figure 5. 21 Protein expression analysis of further mitochondria-related genes.

Western blot analysis using midbrain tissue of young (light green: THTR++; light yellow: THTR++hSNCA+) and aged (green: THTR++; yellow: THTR++hSNCA+) THTR mice for proteins with a function related to mitochondria, such as the inner mitochondria membrane protein PHB (A), mitochondrial import receptor subunit TOMM20 (B), or the superoxide dismutase enzyme (SOD1, C). The molecular weight is shown on the left, blot images are cropped, representative blots are shown. Three independent experiments were carried out. The protein expression for each protein was normalised to beta-Actin and values shown here are calculated relative to 3 months ++ TRAP results (three independent replicates of n= 3 mice per genotype; two-way ANOVA with Tukey post-hoc analysis; mean ± SEM). ++ or THTR++= Homozygous THTR mice. hSNCA+= human alpha-Synuclein. PHB= Prohibitin. TOMM20= Translocase of Outer Mitochondrial Membrane 20. SOD1= Superoxide dismutase 1.

5.2 Discussion and Conclusion

The work of this chapter is based on the analysis of DAn-specific mRNA by gene expression profiling comparing healthy and PD conditions at a young (3 months) and a middle age (12 months). High quality mRNA was successfully isolated using the TRAP protocol and gene expression profiling successfully showed enriched DAn-specific mRNA in our TRAP-IP fractions (**Experiment**). Unfortunately, the only significant difference in the translational profiles comparing our *THTR/hSNCA+* PD model with unaffected control genotypes was aSyn (3 or 12 months) (**Disease**). Nevertheless, gene expression changes in DAn linked many age-related changes to OXPHOS and mitochondria proteins (**Age**). Some genes were changed in the aged PD sub-set of DEGs but randomisation experiments failed to verify the uniqueness of these DEGs in relation to the presence of the *hSNCA* transgene.

1) DAn profile in our IP fractions confirms the success of the immuno-affinity purifications (Experiment)

Our results show that high-quality mRNA can be successfully isolated from our *THTR/hSNCA+* mouse line using TRAP (Figure 5. 2). Out of the 40 samples that were analysed by RNA-Seq, a set of five outlier samples (IP1F3m, IP2F12m, IP2F12mPD, IP1M12m and IP1M12mPD) was identified based on their read-complexity or clustering behaviour on the PCA and hierarchical clustering (Figure 5. 4).

TRAP methodology could be used for the identification of large numbers of DEGs between IP samples (dopaminergic translatome) and Total samples (whole midbrain transcriptome) (Figure 5. 11). The expression of DAn markers was higher in IP samples when compared to Total samples (Figure 5. 6), whereas non-neuronal cell markers (astrocytes, oligodendrocytes, microglia, endothelial cells) tended to have a lower expression in IP samples (Appendix). Although a clear dopaminergic profile was detected, relatively high background levels of non-specific RNA complicated down-stream analysis. Doyle et al. commented on the contamination problem in TRAP samples and found a few consistently enriched genes in every dataset, even in TRAP-negative mice (Doyle et al., 2008). In their study, they suggest that some mRNAs might interact with the beads or

the monoclonal GFP antibodies. Thereby, background contamination was more prominent in some transgenic mouse lines than others, likely depending on the cell-types and the levels of transgene expression (Dougherty et al., 2010). Furthermore, non-specific RNA might be isolated alongside unlabelled polysomes that are non-specifically pulled down during the IP or very abundant transcripts may stick to the beads by themselves.

In addition to the expected up-regulation of DAn-markers in the IP samples, cocaine and amphetamine-regulated transcript (CARTPT) and urocortin (UCN) were found as top hits (Table 5. 3). The widely-distributed protein CARTPT is involved in the regulation of many processes, such as food intake, body weight control, or reward (Rogge et al., 2008) and is found in the VTA where it was shown to produce similar behaviour in animals to cocaine and amphetamine. It is further released in response to repeated DA release in the nucleus accumbens (Hubert et al., 2008). The neuropeptide UCN is involved in stress responses mainly in DAn in the SNc. It was shown to exhibit a neuroprotective function on DAn (Abuirmeileh et al., 2007; Huang et al., 2011). Interestingly, CARTPT was found to be up-regulated by RNA-Seq and qPCR in other TRAP approaches characterising the molecular properties of a neuronal sub-population in the hypothalamus (Nectow et al., 2015; Zhou et al., 2013) and both CARTPT and UCN were identified in a TRAP study by Allison et al. (Allison et al., 2015). CARTPT or UCN have not been further investigated as they did not come up in any of the other DEA. Their enrichment in the IP samples might be specific to DAn but could also be an artefact due to their abundant expression in the midbrain.

Upon comparison to a similar TRAP-study, the expression profiles for IP (DAn translatome) and Total (midbrain transcriptome) samples aligned with analogous expression profiles for DAn and total midbrains previously reported by Brichta et al. (Brichta et al., 2015) (Figure 5. 10). The main source of variation and the main branching points was given by the datasets, as expected. This analysis ensured that the here presented TRAP-Seq study investigated gene expression changes on dopaminergic cell populations.

2) SNCA is differentially expressed between PD and CTRL groups (Disease)

As expected, *SNCA* was detected as differentially expressed between PD (*THTR/hSNCA+* model) and CTRL samples (*THTR*) at 3 and 12 months (Figure 5. 11) and highly enriched in PD samples. Comparably very few but some reads have been assigned to *SNCA* in CTRL samples which should represent *mSnca* KO. This assignment is probably due to great similarities in the gene sequences of the Synuclein family members leading to false-positive assignment of reads to *SNCA* in CTRL samples (George, 2002). Furthermore, the bioinformatical analysis method *DESeq* is based on a correction factor for each sample to normalise gene counts which is calculated by pooling information across genes. Hereby, to be conservative, the algorithm focuses primarily on 'housekeeping genes' with lesser variation across samples while excluding genes with a too high variation or genes that are not expressed in one condition. The correction factor is then applied to all genes of a sample to correct gene expression throughout the whole dataset (Anders and Huber, 2010; Love et al., 2014). Thus, *SNCA* expression seen in CTRL samples might not reflect 'true' gene expression. This 'background noise' is an analytical artefact of the data analysis software and does not necessarily represent intrinsic variability introduced by the experimental method.

However, no other DEGs were detected, even for a FDR < 0.1 or upon splitting the samples into sub-groups relating to age, gender, or age and gender. This finding was surprising since our study was carefully designed and a PD-related phenotype including an age-related decrease in DAn and a PD motor phenotype, as well as a DA release deficit in the dorsal striatum already from a young age has been reported for our PD mouse model (Janezic et al., 2013). A longer duration of aSyn pathology in aged *hSNCA+* mice (+18 months) might have led to a clearer picture of molecular dysfunctions. Unfortunately, the here selected time-point at 12 months was the best compromise between feasibility of TRAP methodology and age of the mice (Chapter 3 and 4). The overall low expression of eGFP-L10a in the midbrain, only about 10% of TH/GFP-double positive cells (Chapter 3), might have complicated the analysis. Nevertheless, the significant up-regulation of aSyn confirms the validity of our model.

The analysis split by gender did not find gender-depend differences in our PD model. In patients, male subjects have been shown to have an earlier disease onset (Haaxma et al., 2007), and twice as many men than women suffer from PD (Gillies et al., 2014; Van Den Eeden, 2003). So far, gender differences have been given little attention in genetic animal models of PD, whereas some toxin-induced models of PD could be used to reproduce gender-based differences in PD as seen in humans (Gillies et al., 2014).

3) Age-related gene expression changes are linked to deficits in mitochondrial respiration (Age)

In general, analysis of age-related changes between 3 and 12 months old mice resulted in many DEGs. Thereby, the number of DEGs fluctuated depending on the sub-set of samples that were considered for the analysis (e.g. all IP samples, only CTRL, only PD) (Figure 5. 11). Since some of the DEGs up-regulated with age (at 12 months) were common to genes previously reported to change their expression patterns with age, either in the SNc (at 18 months) or the whole brain (at least 24 months) (Appendix) confirmed that here detected changes in the midbrain using TRAP-Seq were age-related.

Unfortunately, we could not link our DEGs with age to PD; we failed to detect unique differences between the DEGs with age in CTRL and these found in PD samples that were not also detected by randomisation analysis of CTRL and PD DEGs (Appendix). This made it difficult to distinguish normal age-related changes and these specific to the *hSNCA+* PD model; thus, DEGs related to general ageing were further investigated.

The validation of TRAP-Seq DEGs

The genes for RNA-Seq validation by qPCR (Table 5. 7) and western blotting (Table 5. 8 and Table 5. 9) have been selected because either the genes themselves or the pathways they are associated with have been linked to PD or aSyn previously. Unfortunately, qPCR analysis on whole midbrain found no significant difference for any of the chosen genes (Figure 5. 16). TRAP enables analysis of gene expression changes specifically in DAn, small changes that are specific to this cell population might not be uniform in the whole midbrain. Any changes that are not unidirectional in all cells may

not be detected because of averaging of information across different cell-types in the target tissue. TRAP-isolated DAn-specific RNA as input material for the qPCR-based RNA-Seq validation would be needed to address this question more specifically. Unfortunately, further TRAP experiments are underway but will not be completed in the time-course of this thesis. Nevertheless, the gene expression changes found in the TRAP-Seq study are linked to PD by a range of other studies.

Mitochondrial accumulation of proteins such as amyloid precursor protein (APP) or amyloid-beta (Aβ) peptides derived from APP, and aSyn have been linked to the pathogenesis of mitochondrial dysfunction in AD and PD, respectively (Devi and Anandatheerthavarada, 2010; Devi et al., 2006; Devi et al., 2008). Interactions between Aβ and aSyn are well documented, a putative interactive mechanisms might involve inflammation and impaired protein degradation (Marsh and Blurton-Jones, 2012; Masliah et al., 2001). Hence, the up-regulation of APP in DAn of the *hSNCA+* models found by TRAP-Seq (Table 5. 7) might represent a combined pathological mechanism of both proteins which could be further investigated.

Therapies for PD ease motor symptoms by targeting the restoration of DA in the striatum but ultimately, these transient approaches fail to halt or reverse the loss of DAn. Neurotrophic factors, such as BMP7 promote the formation of neural dendrites *in vivo* and could positively support DAn (Chiocco et al., 2007). Human recombinant BMP7 has already been approved by the Food and Drug Administration (FDA) for the use in clinical trials in a variety of diseases (Chiocco et al., 2007). Its upregulation in DAn in the TRAP-Seq study could represent a defence mechanism of cells under cellular stress (Table 5. 7). Furthermore, it was postulated by a study by Grimm et al. that the sparing and neuroprotection of VTA neurons might be mediated by selective expression of neurotrophic factors (Grimm et al., 2004).

The protease cathepsin D (CtsD) is suggested to be the main protease for aSyn clearance within lysosomes (McGlinchey and Lee, 2015). Here, differentially expressed cathepsins B (CTsB) and S (CTsS) (Table 5. 7) belong to the family of lysosomal cysteine proteinase that may participate in the cleavage of aSyn as it has already been shown for CtsB and CtsL (Tsujimura et al., 2015).

Synaptic SNARE (**SNAP** (Soluble NSF Attachment Protein) **RE**ceptor) proteins were found redistributed in an age-dependent manner simultaneously with the synaptic accumulation and gain of toxic function of aSyn in the mouse striatum, which could represent an early event in the pathogenesis of PD (Garcia-Reitboeck et al., 2013). Here, t-SNARE protein synaptosomal-associated protein 25 (SNAP25) and synaptosomal-associated protein 23 (SNAP23) were found up-regulated in PD samples with age (Table 5. 7) which could be an early result of aSyn-induced toxicity in aged DAn. In our *hSNCA*+ model of PD, DA vesicle distribution is altered at the synapse but SNARE complex formation and striatal protein levels of SNAP25 and others were found unchanged (Janezic et al., 2013), whereas the TRAP-Seq found up-regulated levels for SNAP23 and SNAP25 genes in DAn (Table 5. 7).

Mitochondria use OXPHOS to generate cellular energy in form of ATP. Free radicals in form of ROS escape from the mitochondrial respiratory chain and cause oxidative damage within the cell (Lin and Beal, 2006). The 'Free Radical Theory of Aging' postulated by Denham Harman in the 1950s stated that a disrupted balance between ROS production and antioxidant defence causes damage to mitochondria and its components, thereby initiating degenerative processes (Harman, 1956). It is nowadays known as the 'Mitochondrial theory of aging' and was expanded to include not only aging but also age-related (neurodegenerative) diseases (Harman, 2009).

The first link between mitochondrial dysfunction and idiopathic PD was made after the discovery of mitochondrial complex I deficiency in the SNc (Schapira et al., 1990). Post-mortem analysis of patients with PD found decreased Complex I proteins in the SNc (Mizuno et al., 1989). In this regard, we could show that Complex I down-regulation on the gene level (Table 5. 8) and protein level with age; complex I and III show a trend towards down-regulation in the aged PD sample (Figure 5. 18). The age-dependent drop in protein expression was found for all other complexes.

Parkin is involved in multiple aspects of mitochondrial dysfunction in the context of PD (Ryan et al., 2015) and aSyn and Parkin are linked to genetic PD. The interaction of Parkin which was shown to ubiquitinate the glycosylated form of aSyn (Shimura et al., 2001) or synphilin (Chung et al., 2001)

suggests a common mechanism underlying PD pathology. Increased expression levels of Parkin were shown to protect aSyn-induced PD symptoms in a variety of studies (Haywood and Staveley, 2004; Petrucelli et al., 2002; Shimura et al., 2001). Here, Parkin protein levels are down-regulated in aged mice (Figure 5. 20), suggesting the lack of Parkin-mediated protection in *hSNCA*+ mice.

A study in yeast suggested a functional interaction between aSyn and VDAC (Rostovtseva et al., 2015) and others showed that VDAC and over-expressed aSyn co-immunoprecipitate from the SNc of rats (De Pinto et al., 2010). Furthermore, reduced VDAC expression is associated with aSyn accumulation in patients with PD, which was reproduced in a rat model over-expressing mutant aSyn A30P (Chu et al., 2014). In the TRAP-Seq dataset, VDAC gene levels were unchanged (Table 5. 9), while protein levels were down-regulated with age and PD (Figure 5. 20) which could be an effect of aSyn overexpression.

Mutations in the SOD1 protein are involved in amyotrophic lateral sclerosis (ALS) (Rosen et al., 1993) and have been linked to defects in mitochondrial complexes, abnormalities in mitochondrial structure, number, and localisation (Lin and Beal, 2006). Here, we found down-regulated SOD1 gene levels in DAn related to PD and age (Table 5. 9) and down-regulated SOD1 protein levels in the young PD sample and with age (Figure 5. 21). SOD1 and aSyn were shown to interact by influencing their aggregation tendency in a recent cell culture and mouse brain study (Helferich et al., 2015). A down-regulation for SOD1 could also be shown by a study investigating gene expression changes in laser micro-dissected DAn from the SNc of idiopathic PD patients compared to control (Simunovic et al., 2009).

A study on gene expression changes in the aged human frontal cortex of individuals ranging from their mid-twenties to 100+ years of age could show that the group of ≤40 years and ≥70 years olds showed a relative homogeneous patterns of gene expression that were negatively correlated with each other. In contrast, the middle-aged group (40-70 years) exhibited overall much greater heterogeneity, whereas some cases resembled the young group (≤40), while others resembled the aged group (≥70) (Lu et al., 2004). Thus, age-related changes in gene expression are potentially not

yet detectable at a middle age because large underlying heterogeneity masks a common trend which may become apparent at a later stage.

Impaired mitochondrial function may trigger damage of vulnerable genes or proteins by increased ROS or reduced energy supply, which is required for repair mechanisms in the ageing brain. These defects accumulate over time; hence, the starting points and rates of ageing might be divergent in middle-aged individuals until they approach a state of 'old age'. This effect of ageing may be worsened in combination with the burden of disease.

Although we found an age-related burden on mitochondrial function, the analysis of the TRAP-Seq data-sets is still on-going. Future directions could include the analysis of underlying causes of mitochondria respiratory complex dysfunctions by confocal or electron microscopy to investigate mitochondrial morphology and size and to describe the mitochondrial network. In addition, we established an improved, conditional TRAP model that will be crossed with our PD moue model for gene expression profiling in DAn (Chapter 6).

- CHAPTER 6 -

MOLECULAR CHARACTERISATION OF A NOVEL DOUBLE TRANSGENIC CONDITIONAL TRAP PARKINSON'S MODEL

6.1 Overview

As shown in previous chapters, we could successfully isolate high quality translated mRNAs from midbrains of our *THTR* transgenic mice, which was successful applied to gene expression profiling of DAn-specific mRNAs. Based on these results, this chapter will describe for the first time the establishment and in-depth molecular characterisation of an improved TRAP model (*ROSA26-eGFP-L10a::DATcre(::hSNCA+)*) for the analysis of the translatome during PD progression. Here, we optimised the TRAP protocol for the use with our novel *ROSA26-eGFP-L10a::DATcre* transgenic line and show that TRAP can successfully be used to isolate DAn-specific mRNA from soma (midbrain), as well as axons (striatum) of DAn.

Chapter aims

1) To establish and characterise a novel Cre-conditional *ROSA26-eGFP-L10a::DATcre(::hSNCA+)* transgenic mouse line for TRAP.
2) To optimise the TRAP protocol for the use with *ROSA26-eGFP-L10a::DATcre* transgenic mice.
3) To perform pilot TRAP experiments on soma and axons of *ROSA26-eGFP-L10a::DATcre* transgenic mice at different ages.

Aim 4) outlined below will not be addressed as part of this thesis but experiments are already underway:

4) To use TRAP for the isolation of DAn-specific mRNA from our young (3 months) and old (18 months) Cre-conditional TRAP transgenic mouse model, comparing healthy controls (*ROSA26-eGFP-L10a::DAT-Cre*) with our PD model (*ROSA26-eGFP-L10a::DAT-Cre*::*hSNCA+)* by gene expression profiling (experiments underway; not part of this thesis).

6.2 Introduction

6.2.1 The *DAT-IRES-Cre* transgenic mouse model

The work in this chapter is based on a Cre-conditional DAT-driven TRAP model for gene expression profiling of DAn. DAT labels DAn of the midbrain and regulates neurotransmission by transporting DA back into the presynaptic terminals. The Cre-driver line of choice (*DAT-IRES-Cre*) is based on a knock-in of Cre recombinase into the 3' untranslated region (UTR) of the DAT gene driven by an internal ribosomal entry sequence (IRES) under the transcriptional control of the endogenous DAT promoter (Bäckman et al., 2006). The IRES helps to preserve both DAT alleles to minimise interference with endogenous DAT function. Molecular characterisation of the DAT-Cre model revealed co-localised DAT/Cre expression in DAn. The pattern and intensity of DAT expression did not differ in the midbrain or striatum compared to wild-type by IHC, whereas striatal DAT protein levels have been shown to be decreased by western blotting (Bäckman et al., 2006). Cre-mediated recombination after breeding with a LoxP-strain will result in the deletion of the floxed gene region of interest in DAn, making the DAT-Cre line a useful tool to facilitate the analysis of gene function in DAn in the context of neurodegenerative diseases, such as PD.

6.2.2 The ROSA26-eGFP-L10a transgenic mouse model

In addition to the DAT-Cre mice, we make use of a conditional TRAP model ('fs-TRAP') developed by Zhou et al. (Zhou et al., 2013). The targeting vector containing eGFP-L10a under the control of the strong synthetic CAG hybrid promoter inserted into the ROSA26 locus enables two different conditional modifications (Zhou et al., 2013). In the absence of Cre, transcription of the frt-flanked eGFP-L10a fusion protein is prevented by a loxP-flanked neoresistance cassette (Figure 6. 1). Only after Cre-mediated recombination leading to the removal of the floxed STOP sequence, are ribosomes of selected tissues labelled by the now constitutively-activated eGFP-L10a only where Cre recombinase (here: DAT-Cre) is expressed (Figure 6. 1). The second manipulation enabled by the 'fs-TRAP' model uses a two-step modification, FLP-mediated recombination removes the frt-flanked eGFP-L10a while subsequent Cre-mediated recombination removes the floxed-neo cassette to constitutively activate hemagglutinin-tagged bacterial biotin ligase (birA) expression.

This enables the highly specific biotinylation and purification of biotin-tagged proteins. The biotinylation approach was not investigated further in the study by Zhou et al. (Zhou et al., 2013).

Here, we will make use of the *ROSA26-eGFP-L10a* TRAP model (Zhou et al., 2013) paired with a DAT-Cre driver line (Bäckman et al., 2006) in combination with our transgenic mouse model of Parkinson's (Janezic et al., 2013) to study DAn-related gene expression changes in a mouse model of PD.

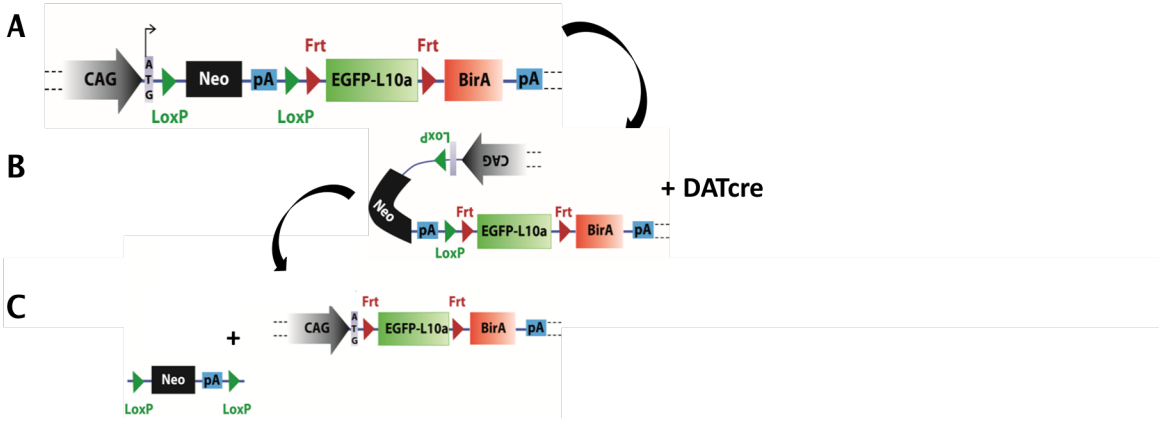


Figure 6. 1 ***Conditional TRAP transgenic mouse line.***

The fs-TRAP mice drive eGFP-L10a fusion protein (frt-flanked) expression from a CAG promoter in the ROSA26 locus. In the absence of Cre, gene expression is prevented by a loxP-flanked neo-polyA cassette (A). After removal of the neo cassette via Cre-mediated recombination (B, here DAT-Cre), eGFP-L10a will be constitutively activated and label ribosomes in tissues where Cre is expressed (C). REFERENCE: Zhou et al. (2013). eGFP= enhanced green fluorescence protein. RPL10a= ribosomal protein L10a, an integral component of the 60S ribosomal subunit. CAG= synthetic hybrid promotoer. Neo= neomycin resistance. Cre= Cre-recombinase. 2xHA= hemagglutinin. birA= bacterial bifunctional protein (biotin ligase).

6.2.3 Axonal Translation

The presence of actively translating ribosomes in axons is controversially discussed in the literature but there is increasing evidence that mRNAs are actively translated not only in the soma but in distal axons and dendrites (Jung et al., 2012). Neurons are highly compartmentalised structures and gene expression profiling studies on developing or mature axons (Gumy et al., 2011; Zivraj et al., 2010) have provided insight in to the distinct axonal translatomes. Overall, studies of local mRNA translation in axons date back to the 1960s (Giuditta et al., 1968) which found local protein synthesis in axons and dendrites as a common response to extracellular stimuli. Indeed, cell culture studies of stimulus-induced responses to chemokines (Campbell and Holt, 2001) or axonal

regeneration after injury (Verma, 2005) provide comprehensive information on the complex and dynamic nature of mRNAs and clearly lay out the need for local protein synthesis.

Translating ribosome affinity purification of axonal ribosomes

Cell-type specific translational profiling of axonally located mRNA provides an intriguing approach to aid the debate of local translation in neurons. In 2012, a transgenic mouse expressing eGFP-tagged ribosomes in cortical neurons depicted ribosomes in myelinated axons of the adult CNS, selectively enriched at the nodes of Ranvier (Walker et al., 2012b). Furthermore, axon-specific transcripts were analysed in *Xenopus leavis* using a tissue transplantation technique. Following eGFP-labelling of ribosomes in developing retinal ganglion cell (RGC) axons, transgenic tissue was transplanted into wild-type animals allowing new-born RGC axons to inherit axonally transported eGFP-L10a (Yoon et al., 2012). In a recent study, Shigeoka et al. developed an 'axon-TRAP-RiboTag' method that allowed specific isolation of ribosome-bound mRNAs in the distal compartment of RGC axons *in vivo*. By analysing axon-specific translatomes at multiple ages Shigeoka et al. could show that mRNAs were actively translated in axons which continued in adulthood (Shigeoka et al., 2016). In addition, eGFP-L10a labelled ribosomes were found surrounding synapses via electron microscopy in an astrocyte study (Sakers et al., 2017). In this way, distal astrocyte processes were found to carry out localised translation of specific transcripts allowing them to respond to or fine-tune synaptic activity.

In this study, we will apply 'axon-TRAP' to our *ROSA26-eGFP-L10a::DATcre* transgenic mouse line of PD to analyses the translatome of soma and axons specific to DAn.

6.3 Results

6.3.1 Generation, breeding and maintenance of a novel conditional TRAP transgenic mouse line

Initial breeding strategy to avoid interference of mouse aSyn and ROSA26

In order to optimise the isolation of DAn-specific mRNA for gene expression profiling from our transgenic mouse model of PD (*hSNCA+)*, we established a new conditional TRAP line. For this purpose, *ROSA26-eGFP-L10a (REL)* mice purchased from Jackson Laboratories (# 022367) were crossed to a DAT-Cre driver line to specifically express eGFP-L10a in DAn. We aimed to cross this *ROSA26-eGFP-L10a::DAT-Cre* line with our *hSNCA+* mouse model of PD that overexpresses human aSyn on a mouse aSyn knock-out background (*mSnca-/-*) (Janezic et al., 2013). Unfortunately, the ROSA26 locus and mouse aSyn are located on the same chromosome, mouse chromosome 6 (Figure 6. 2).

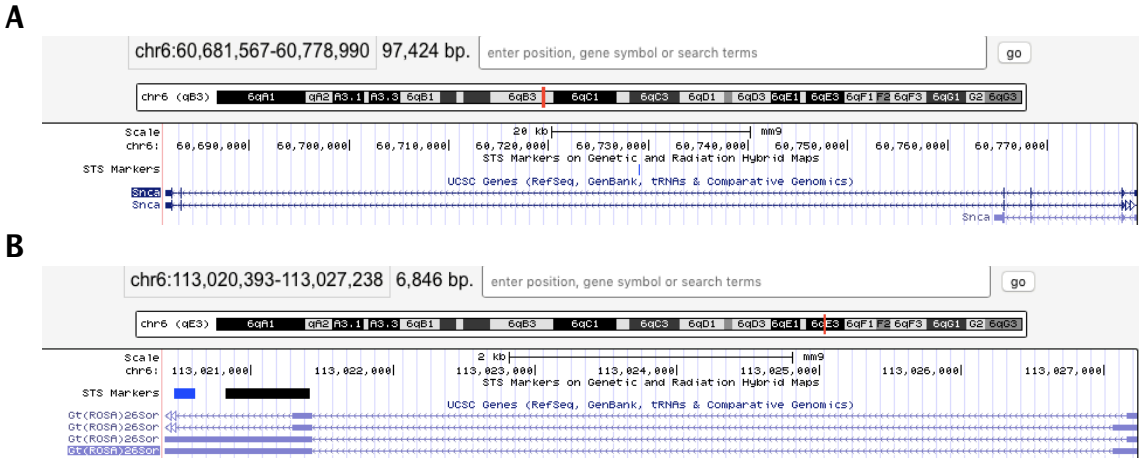


Figure 6. 2 Localisation of ROSA26 and aSyn on mouse Chrosomose 6.

UCSC Genome Browser showing the localisation of (A) aSyn and (B) the ROSA26 gene locus on the mouse chromosome 6.

To avoid any potential problems or interference with our planned experiments, we crossed the *hSNCA+* transgene back onto an aSyn WT mouse background. In the first generation, a homozygous *hSNCA+* mouse was crossed with a WT C57Bl/6 mouse, resulting in mice hemizygous for human (*hSNCA+)* and heterozygous mouse (*mSnca)* aSyn (Figure 6. 3 A). Further inter-crossing of the offspring generated a variety of genotypes of which only mice homozygous for WT *mSnca* and hemizygous for *hSNCA+* were kept for further breeding (Figure 6. 3).

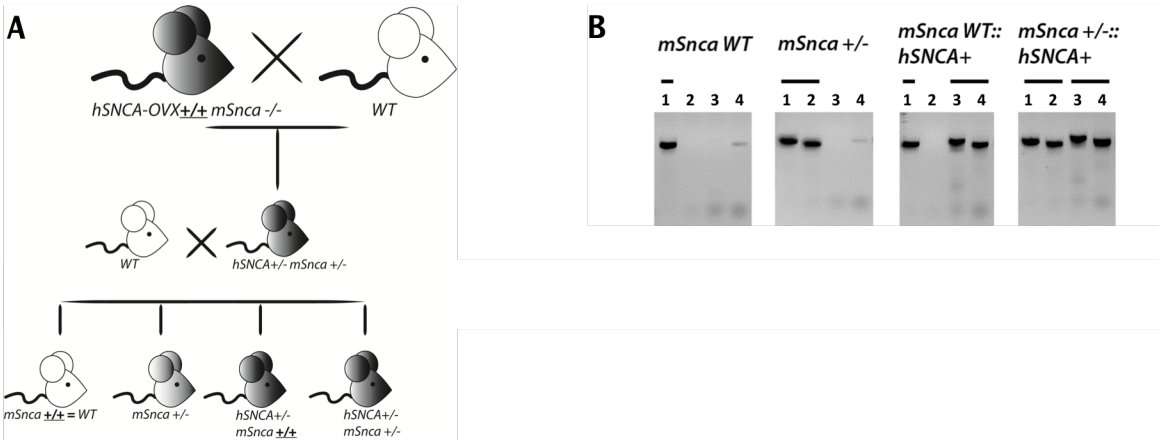
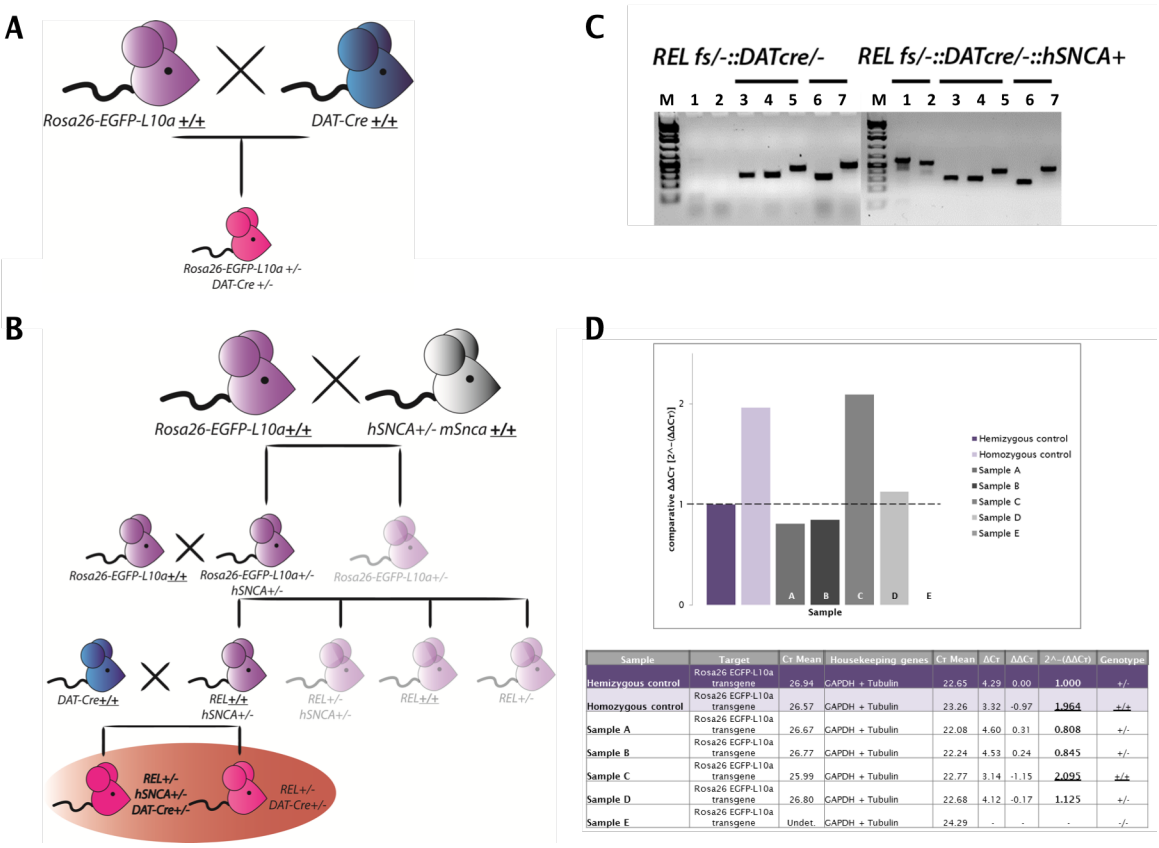


Figure 6. 3 Breeding scheme to cross hSNCA+ mice back on a mSnca background.

(A) Overview of the breeding strategy to cross hSNCA+ transgene is crossed back onto a mouse aSyn WT background. (B) Representative genotyping results. Two primer pairs detect presence/absence of WT (1) and KO (2) mouse aSyn to verify the mSnca-/- background. Other primers detect the hSNCA+ construct at the 3' (3) and 5' junctions (4) of the BAC backbone. -/-= Knock-out. +/-= Heterozygous. +/+= Homozygous. += Hemizygous. OVX= over-expressed. mSnca= mouse aSyn. hSNCA= human aSyn. WT= wild-type.

Establishing double transgenic ROSA26-eGFP-L10a::DATcre mice

For initial TRAP pilot experiments, the homozygous *ROSA26-eGFP-L10a::DATcre* mice (*RELfs/fs*) were interbred with homozygous DAT-Cre mice (*DATcre/cre*) (Figure 6. 4 A). The breeding resulted in Cre-mediated recombination specifically in DAn, triggering the deletion of the *loxP*-flanked neo cassette and subsequent eGFP-L10a expression. Figure 6. 4 B shows the breeding schematic to generate the *RELfs/-::DATcre/-::(hSNCA+)* experimental cohorts. This three-step breeding scheme generated double transgenic *RELfs/fs::hSNCA+* mice in a first generation; subsequent breeding allowed the generation of our desired transgenic experiments cohorts for TRAP and subsequent gene expression profiling, *RELfs/-::DATcre/-* (CTRL) and *RELfs/-::DATcre/-::hSNCA+* (PD model) (Figure 6. 4). qPCR-based copy-number genotyping (Figure 6. 4 D) was modified to distinguish heterozygous from homozygous REL littermates (Figure 6. 4 D) (Wishart et al., 2007). Mice without eGFP-L10a insertions in the ROSA26 locus did not give any detectable Ct values (Figure 6. 4 D).



Sample	Target	Ct Mean	Housekeeping genes	Ct Mean	ΔCt	ΔΔCt	2^-(ΔΔCt)	Genotype
Hemizygous control	Rosa26 EGFP-L10a transgene	26.94	GAPDH + Tubulin	22.65	4.29	0.00	1.000	+/-
Homozygous control	Rosa26 EGFP-L10a transgene	26.57	GAPDH + Tubulin	23.26	3.32	-0.97	1.964	+/+
Sample A	Rosa26 EGFP-L10a transgene	26.67	GAPDH + Tubulin	22.08	4.60	0.31	0.808	+/-
Sample B	Rosa26 EGFP-L10a transgene	26.77	GAPDH + Tubulin	22.24	4.53	0.24	0.845	+/-
Sample C	Rosa26 EGFP-L10a transgene	25.99	GAPDH + Tubulin	22.77	3.14	-1.15	2.095	+/+
Sample D	Rosa26 EGFP-L10a transgene	26.80	GAPDH + Tubulin	22.68	4.12	-0.17	1.125	+/-
Sample E	Rosa26 EGFP-L10a transgene	Undet.	GAPDH + Tubulin	24.29	-	-	-	-/-

Figure 6. 4 ***Breeding scheme to generate transgenic RELfs/-::DATcre/-::(hSNCA+) experimental cohorts.***

(A) Breeding scheme to generate animals for TRAP pilot experiments. (B) Final breeding scheme to generate the RELfs/-::DATcre/-::(hSNCA+) experimental cohort. Desired genotypes are indicated by red circle. (C) Representative genotyping results. Two primer pairs detect the hSNCA+ construct at the 3' (1) and 5' junctions (2) of the BAC backbone. Further primers detect the WT (3) and modified ROSA26 locus (4) or eGFP-L10a specifically (5) and the WT DAT (6) and DAT-Cre (7). (D) Representative copy-number genotyping results. qPCR primers detect the eGFP-L10a TRAP construct. The genotype is defined by comparative Ct method using a homozygous RELfs/fs mouse as a calibrator and the geometric expression mean of two housekeeping genes as reference samples. This resolves the unknown samples as follows: Purple= heterozygous control. Light Purple= homozygous control. A, B, D= heterozygous; C= homozygous; E= non-transgenic. REL= ROSA26-eGFP-L10a. Fs= floxed. Cre= Cre recombinase. -/- or KO= Knock-out. +/-= Heterozygous. +/+= Homozygous. OVX= over-expressed. mSnca= mouse alpha-Synuclein. hSNCA= human alpha-Synuclein. WT= wild-type.

6.3.2 Molecular characterisation of the novel *RELfs/-::DATcre/-(::hSNCA+)* line

We aimed to express eGFP-L10a specifically in DAn; since Cre recombinase is expressed under control of the endogenous mouse DAT promoter, the eGFP-L10a fusion protein should only be constitutively activated in Cre expressing, thus, DAT-positive cells. In the following paragraphs, we confirmed that eGFP-L10a expression is restricted to the midbrain (SNc and VTA), without ectopic expression in non-DAn brain regions, such as hippocampus or cortex.

DAn of young and aged RELfs/-::DATcre/- transgenic mice strongly express the eGFP-L10a fusion protein in the midbrain

Analysis of native eGFP fluorescence from the eGFP-L10a fusion protein showed a strong GFP signal in the SNc and VTA of *RELfs/-::DATcre/-* transgenic mice at 3, 6, and 12 months of age by fluorescence microscopy in unstained brain sections (Figure 6. 5). No ectopic fluorescence of native eGFP was detectable in the hippocampus or cortex areas, and REL-negative mice did not show any eGFP-positive cells (results not shown). In contrast to the bacTRAP mouse line (Chapter 3), REL mice express more eGFP-positive cells in the midbrain. In addition, 12 months old REL mice still strongly expressed eGFP-L10a (Figure 6. 5) in contrast to aged *THTR* mice (Chapter 3).

DAn-specific expression of the eGFP-L10a fusion protein was analysed in greater depth by co-expression of GFP with DAn-markers TH and DAT using double immunofluorescence labeling on sequential coronal brain sections. Overall, GFP transgene expression was detected in the midbrain (Figure 6. 6) but no other regions, such as the cortex and hippocampus (Figure 6. 7). Figure 6. 6 shows that eGFP-L10a expression is restricted to TH- or DAT positive DAn in the SNc and VTA. Cre-negative animals (*RELfs/fs*) do not express any GFP-positive cells (Figure 6. 6). Here, GFP is highly co-expressed in TH/DAT-positive neurons in contrast to the bacTRAP transgenic line for which only a subset of DAn co-expressed GFP and TH (Chapter 3). Here, we found that some cells did not co-expressed TH/GFP especially within the VTA (Figure 6. 6 C), something that has already been reported by others (Li et al., 2013).

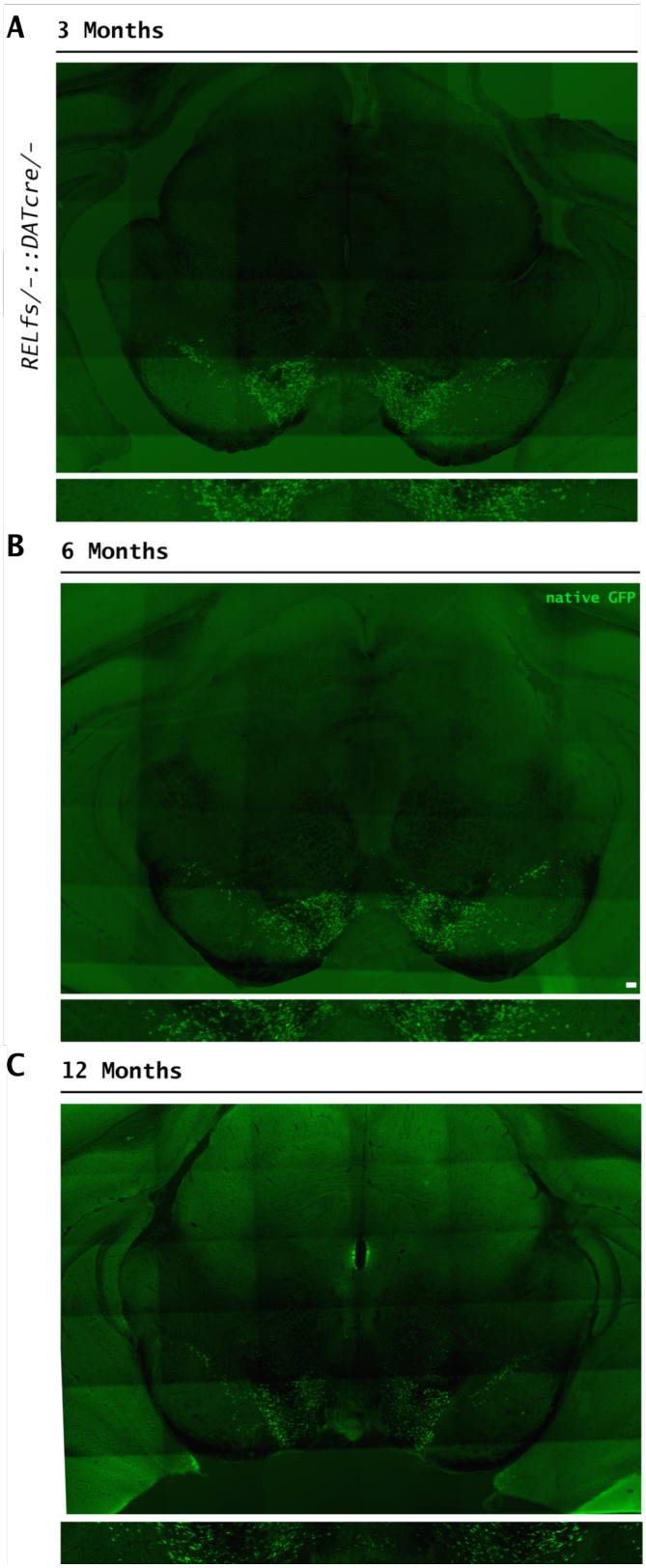


Figure 6. 5 Native eGFP fluorescence is detectable in RELfs/-::DATcre/- mice at 3, 6, and 12 months.

(A-C) eGFP-L10a is expressed in the SNc and VTA of RELfs/-::DATcre/- mice at different ages (stitching of 36 images). A horizontal close-up through the SNc and VTA region is shown below the image. Scale bar= 200 µm. REL= ROSA26-eGFP-L10a. Fs= floxed. Cre= Cre recombinase. SNc= substantia nigra pars compacta. VTA= ventral tegmental area. eGFP= enhanced green fluorescent protein.

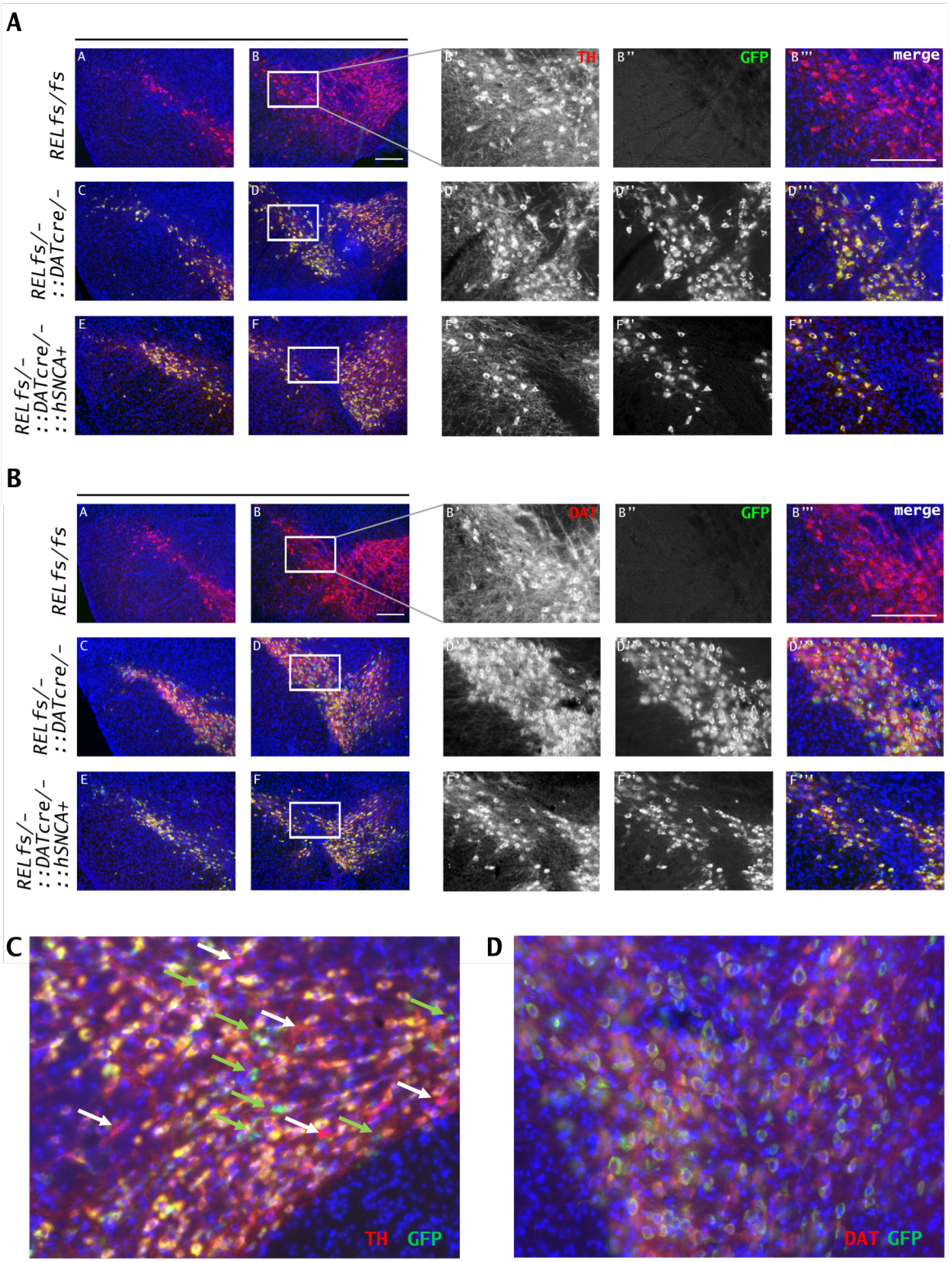
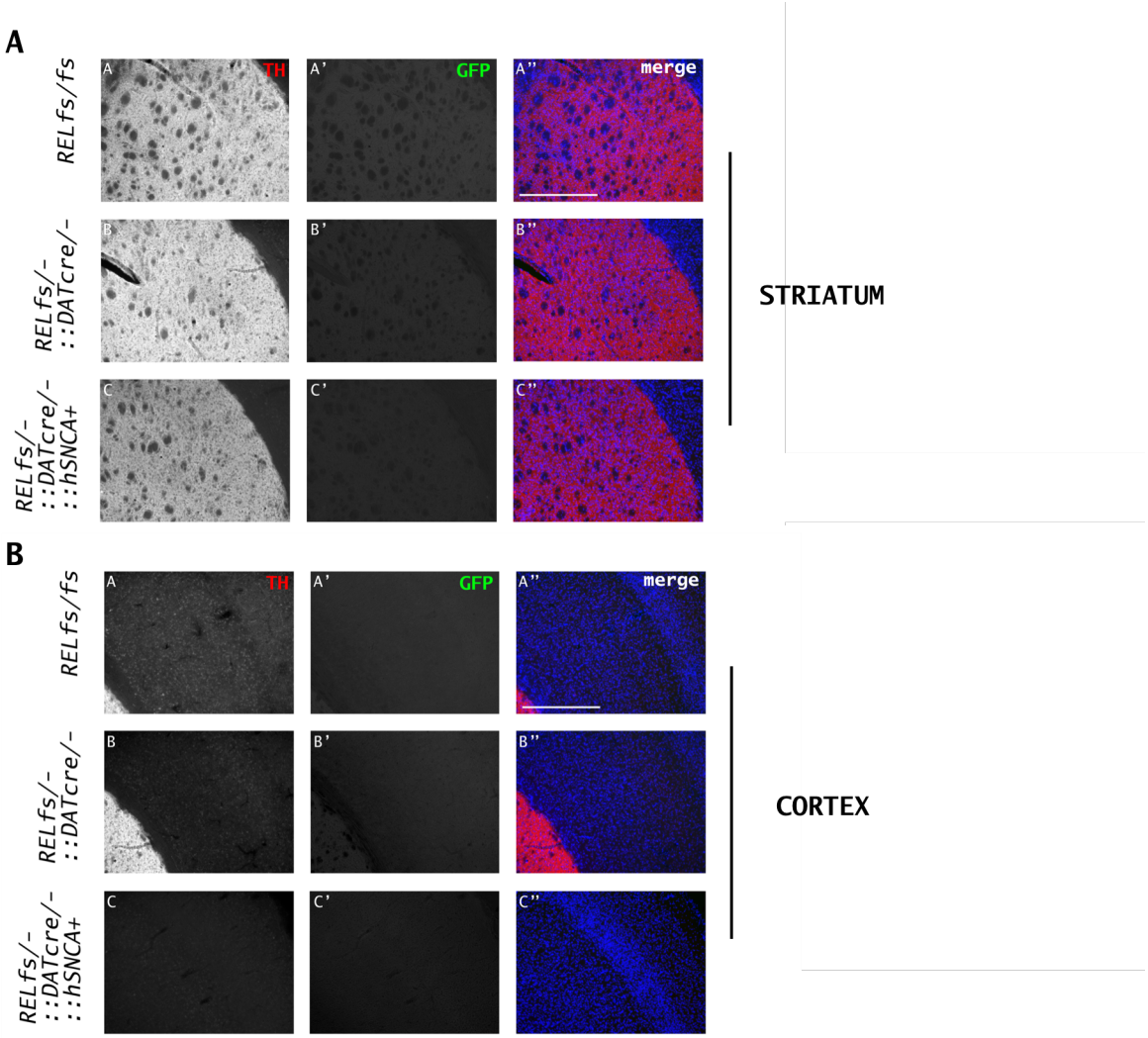


Figure 6. 6 ***eGFP is co-expressed with DAn-specific markers in the midbrain (3 months).***

Coronal midbrain sections were stained for tyrosine hydroxylase (TH) (red) and GFP (green) (A) or dopamine transporter (DAT) (red) and GFP (green) (B). ***LEFT PANELs*** *(A-J)****:*** *Labelings confirm the co-expression of TH and eGFP or DAT and eGFP in DAn of the SNc and VTA of RELfs/-::DATcre/- and RELfs/-::DATcre/-::hSNCA+ mice.* ***RIGHT PANELs*** *(B', D', F' H' J')****:*** *Close-up of the inserts (panel 1). Scale bars= 200 µm. Representative images are shown. (C) Not all TH-positive cells in the VTA express eGFP and vice versa (White arrows: TH-positive only. Green arrows: GFP-positive only). (D) DAT and GFP are co-expressed throughout the VTA. REL= ROSA26-eGFP-L10a. Fs= floxed. Cre= Cre recombinase. SNc= substantia nigra pars compacta. VTA= ventral tegmental area. eGFP= enhanced green fluorescent protein. hSNCA= human aSyn. DAn= DAn.*

Since the eGFP-L10a transgene should only be expressed in Cre-expressing DAT-positive cells, no eGFP fluorescence was expected in non-DAn brain regions. Absence of a GFP-signal in further brain regions - hippocampus, cortex, and striatum - confirmed the regional expression of eGFP-L10a (Figure 6. 7). As shown previously, GFP expression was not found in the hippocampus or the cortex of *THTR* mice (Chapter 3). Unexpectedly, but similar to the results using the *THTR* mouse line (Chapter 3), no eGFP expression was seen in the striatum despite the overall much stronger GFP signal in the midbrain and higher GFP-positive DAn cell numbers compared to the *THTR* line (Chapter 3).



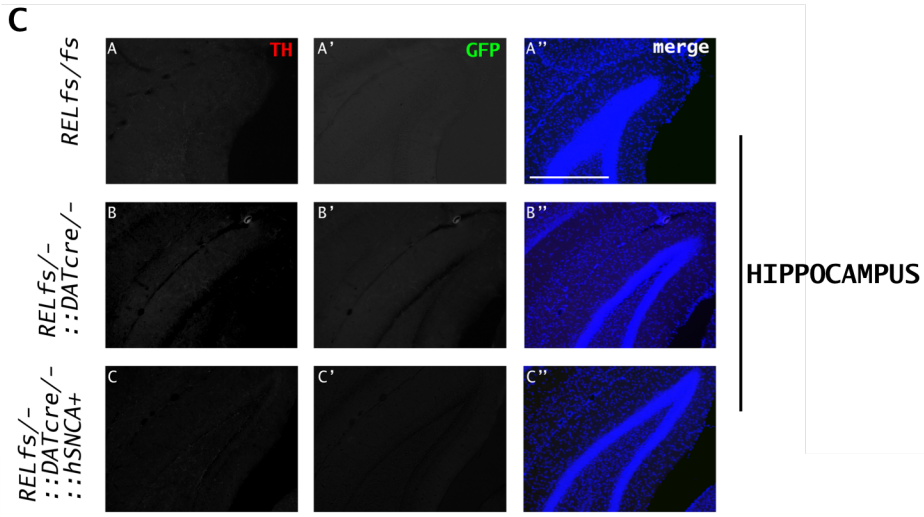
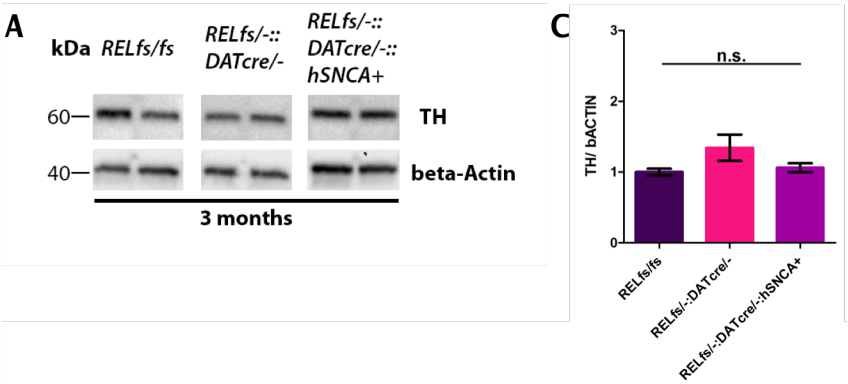


Figure 6. 7 Overview of eGFP-L10a-negative brain regions (3 months).

Coronal midbrain sections were stained for tyrosine hydroxylase (TH) (red) and GFP (green). Neither the striatum (A [(A-E)]), cortex (B [(A-E)]) nor hippocampus (C [(A-E)]) show GFP-immunoreactivity. Representative images are shown. Scale bars= 200 µm. REL= ROSA26-eGFP-L10a. Fs= floxed. Cre= Cre recombinase. SNc= substantia nigra pars compacta. VTA= ventral tegmental area. eGFP= enhanced green fluorescent protein. hSNCA= human aSyn.

Quantitative immunoblotting analysis of TH and endogenous RPL10a showed strong expression and no significant differences in the overall striatal expression levels at 3 months between any of the analysed genotypes (Figure 6. 8; one-way ANOVA, n.s.). As already shown for the *THTR* mouse line (Chapter 3), only endogenous RPL10a (25 kDa) but not the transgenic eGFP-L10a fusion protein (52 kDa) were detected in the striatum using an anti-RPL10a antibody. Analyses of eGFP-L10a fusion protein expression on whole midbrain tissue lysates of 3 months old REL animals using four different GFP antibodies and the previously used anti-RPL10a antibody were not sensitive enough to detect the eGFP-L10a fusion protein at 52 kDa (results not shown). These results mirror what was already shown for the *THTR* mouse line (Chapter 3).



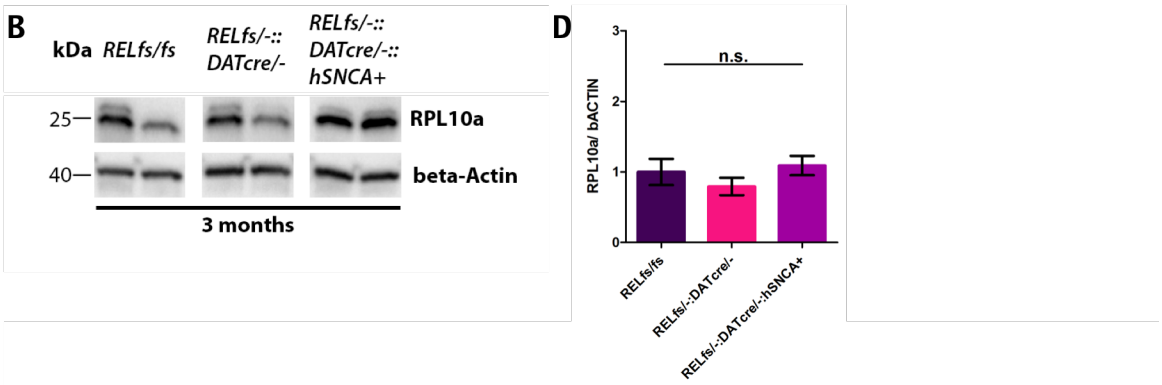


Figure 6. 8 ***Quantitative Western blot analysis of TH and RPL10a expression in the striatum of young mice does not show a difference across different genetic backgrounds in the REL line (3 months).***

(A, B) Immunoblot analysis of TH, RPL10a and beta-Actin protein levels in striatal tissue from REL mice at 3 months (three independent replicates of n=2 mice per genotype). The molecular weight is shown on the left, blot images are cropped, representative blots are shown. Three independent experiments were carried out. Quantitative Western blot analysis of TH (C) or RPL10a (D) protein levels normalised to beta-Actin showed no change in the overall striatal expression levels (One-way ANOVA with Dunnett post-hoc analysis; mean ± SEM; n.s.). Normalised bar graphs are displayed relative to RELfs/fs. REL= ROSA26-eGFP-L10a. Fs= floxed. Cre= cre recombinase. hSNCA= human aSyn. TH= tyrosine hydroxylase. RPL10a= ribosomal protein 10a. n.s.= not significant.

aSyn and GFP are co-expressed in DAn

The expression pattern of aSyn was analysed by immunofluorescence labeling using a human-specific (Figure 6. 9 A), or a pan-species aSyn antibody (Figure 6. 9 B), in combination with anti-GFP to analyse aSyn/GFP co-expression in the midbrain on coronal sections (3 months). As previously observed, human aSyn is only detected in *hSNCA+* transgenic animals (Figure 6. 9 A). The human aSyn over-expression profile closely mirrors endogenous mouse aSyn in the DAn of the SNc and VTA (Figure 6. 9 B). The intracellular localisation of aSyn was observed in the axons, cell bodies, and nuclei. In contrast to our THTR mouse line (Chapter 3), GFP is highly co-expressed with aSyn in the midbrain in *RELfs/-::DATcre/-* and *RELfs/-::DATcre/-::hSNCA+* animals (Figure 6. 9).

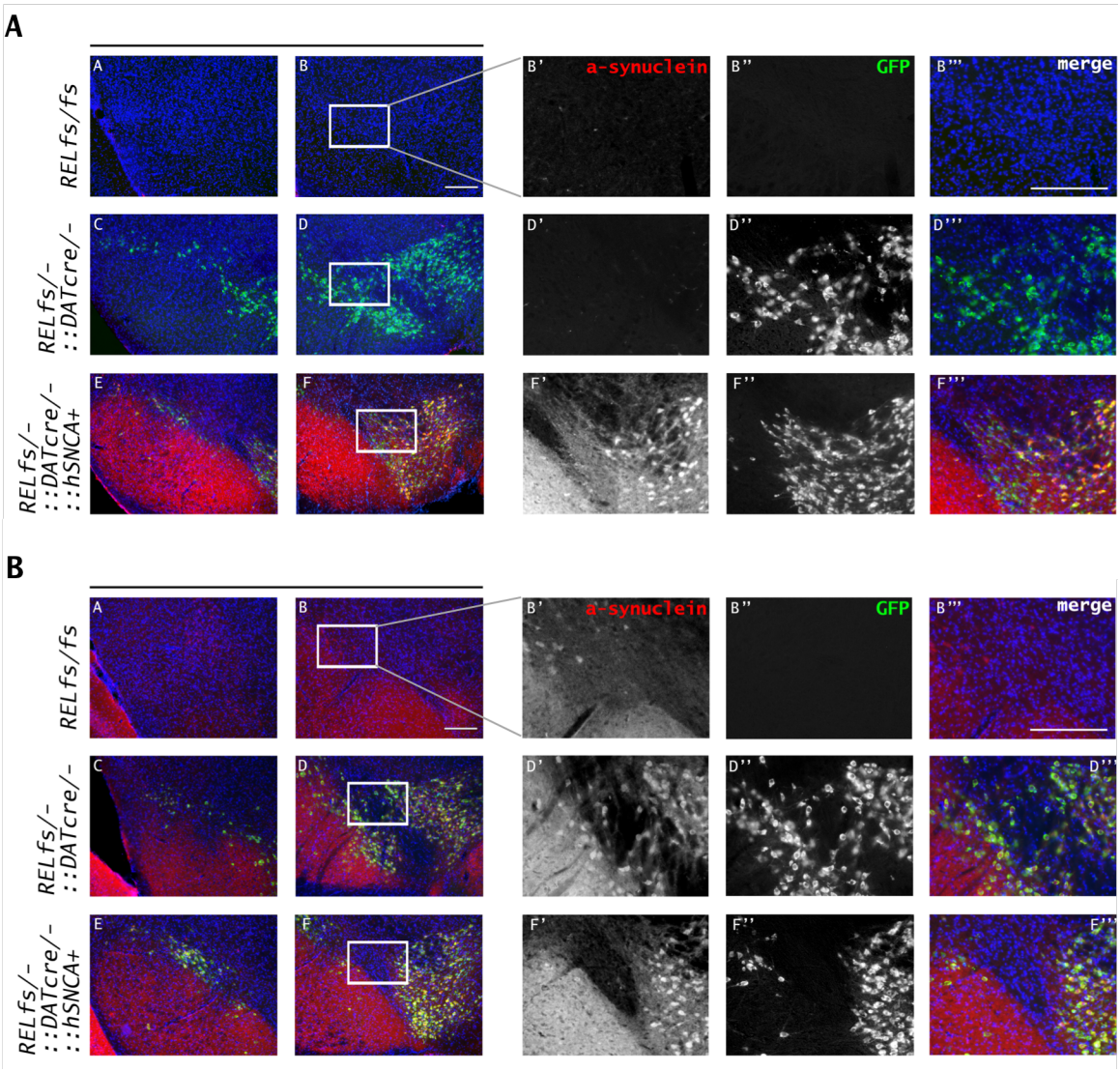


Figure 6. 9 ***aSyn-positive neurons show co-expression with eGFP in transgenic mice (3 months).***
Coronal midbrain sections were stained for aSyn using either a human-specific aSyn antibody (A) or a pan-aSyn antibody (B) (red) in combination with an anti-GFP antibody (green). ***LEFT PANELs*** *[A-J]****:*** *Labelings confirm co-expression of human (A) and mouse and human (B) aSyn with eGFP in DAn of the SNc and VTA.* ***RIGHT PANELs*** *[B', D', F' H' J']****:*** *Close-up of the inserts (panel 1). Scale bars= 200 µm. Representative images are shown. REL= ROSA26-eGFP-L10a. Fs= floxed. Cre= Cre recombinase. SNc= substantia nigra pars compacta. VTA= ventral tegmental area. eGFP= enhanced green fluorescent protein. hSNCA= human aSyn. DAn= DAn. aSyn= alpha-Synuclein.*

As expected, immunoblotting analysis of aSyn protein expression in the striatum clearly showed an up-regulation in REL animals carrying the *hSNCA+* transgene compared to mice carrying only mouse aSyn (Figure 6. 10 A). The successful expression of the human aSyn transgene in *RELfs/-::DATcre/-::hSNCA+* mice could be confirmed using a human-specific anti-aSyn antibody (Figure 6. 10 B).

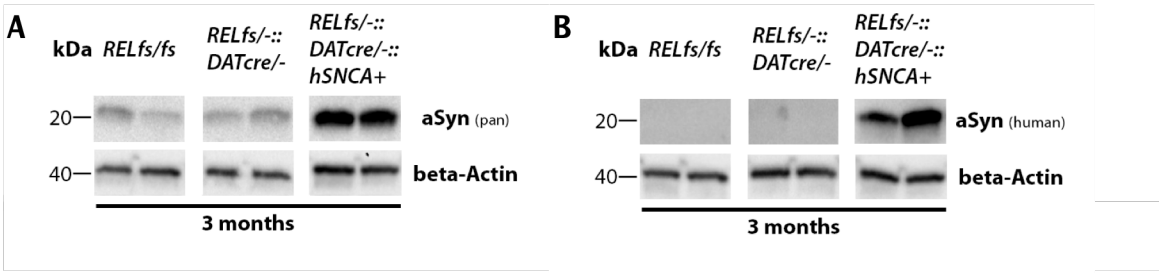


Figure 6. 10 ASyn is over-expressed in the striatum of young RELfs/-::DATcre/-::hSNCA+ mice (3 months).

(A) Immunoblot analysis of aSyn expression in the striatum of REL transgenic mice using a pan-species anti-aSyn antibody (#610786, BD Biosciences) or a human-specific anti-aSyn antibody (4B12, #MA1-90346, Invitrogen). Protein expression was compared to RELfs/fs mice (mice without DAT-Cre expression). The molecular weight is shown on the left, blot images are cropped, representative blots are shown. Two independent experiments were carried out. (B). Quantitative Western blot analysis of the pan-species anti-aSyn antibody in 3 months old animals (three independent replicates of n=2 mice per genotype; not quantified). hSNCA= human aSyn. REL= Rosa26-eGFP-L10a. Fs= floxed. Cre= cre recombinase. hSNCA= human aSyn. TH= tyrosine hydroxylase. RPL10a= ribosomal protein 10a. aSyn= alpha-Synuclein.

6.3.3 Establishing TRAP methodology in cell soma and axons using a conditional TRAP transgenic mouse line

Chapter 4 described the establishment of the TRAP protocol tailored to our new *THTR* mouse model (Heiman et al., 2014). Here, our adapted TRAP protocol was used to isolate DAn-specific mRNA from our conditional *ROSA26-eGFP-L10a::DAT-Cre* transgenic mouse line. Initial molecular characterisation experiments confirmed that only double transgenic *RELfs/-::DATcre/-* but not *RELfs/fs* mice express the eGFP-tagged ribosomal transgene in DAT-positive DAn (see above). Cre-mediated expression of eGFP-L10a in DAT-positive neurons led to strong eGFP signal in the midbrain and a complete overlap of GFP and DAT-positive cells (Figure 6. 6). We could circumventing initial difficulties caused by low cell numbers of GFP-positive cells in the midbrain of the *THTR* line (Chapter 3 and 4). Although we still could not visualise GFP-positive DAn in the striatum (Figure 6. 7), we used striatal tissue for TRAP in addition to midbrain tissue (Figure 6. 11).

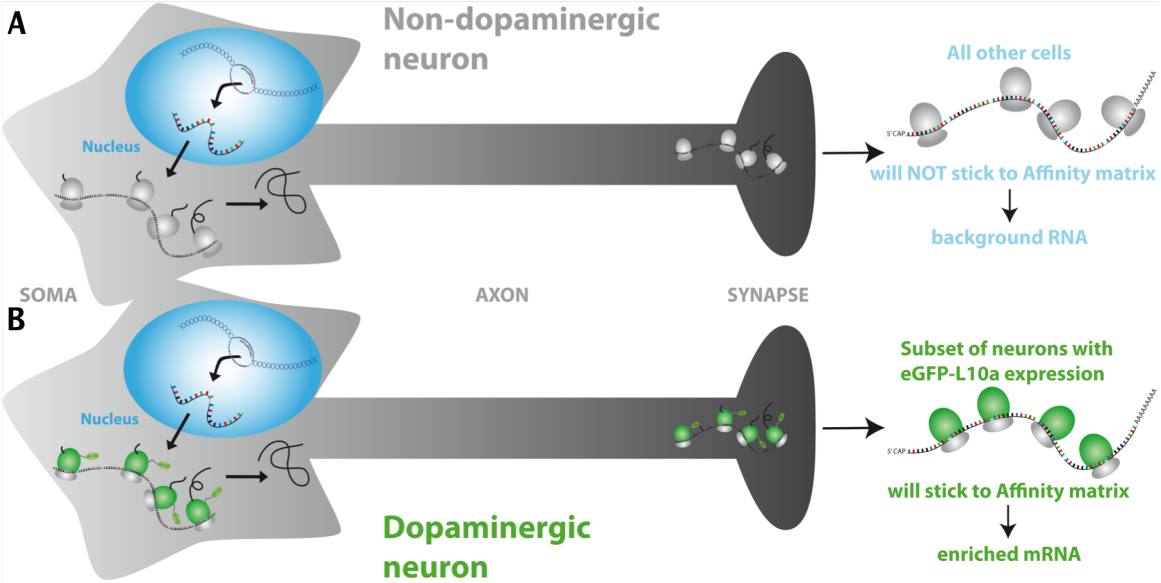


Figure 6. 11 Neuronal Translating Ribosome Affinity Purification (TRAP) in soma and axons.

Large ribosomal subunit protein RPL10a has been targeted with appropriate genetic elements to express the eGFP-L10a transgene in cell type of interest. Only translating polyribosomes (polysomes) originating from DAn (B, green) but not non-DAn (A, grey) express eGFP-tagged ribosomes. anti-GFP beads ('Affinity matrix') constructed using magnetic beads, a biotinylated linker and anti-GFP antibodies capture eGFP-tagged ribosomes and actively translated mRNAs from DAn. Non-tagged ribosomes (and non-translated RNAs) do not bind to the beads. During immunoprecipitation, mRNA from the soma or axons of DAn stick to the Affinity matrix. light blue= unbound (UB) RNA fraction. green= bound or immunoprecipitated (IP) RNA fraction.

6.3.4 Young REL mice can be successfully used for TRAP

The first TRAP experiments shown here were performed on one mouse midbrain or one striatum using halved (0.5x) matrix conditions. The same batch of monoclonal GFP antibodies Htz-GFP-19F7 and Htz-GFP-19C8 was used for all TRAP pilot experiments performed on the REL mouse line.

TRAP pilot experiments – 3 months

Pilot TRAP experiments in young (3 months) TRAP-positive mice (*RELfs/-::DATcre/-*) or TRAP-negative (*RELfs/fs* or non-tg) confirmed that DAn-specific mRNA can be successfully isolated from TRAP-positive tissue (Figure 6. 12). In the midbrain (Figure 6. 12 A), isolation of mRNA from *RELfs/-::DATcre/-* mice showed a significant enrichment of DAT (***RELfs/-::DATcre/-*:** 16.3x; ***RELfs/fs***: 0.29x; **non-tg**: 0.26x) and TH mRNA (***RELfs/-::DATcre/-*:** 30.7x; ***RELfs/fs***: 1.17x; non-tg: 1.21x), while non-DAn marker mRNA was not enriched in any of the IP fractions over Total RNA input. In the striatum, even higher enrichment results could be seen (Figure 6. 12 B). Here, isolation of mRNA from *RELfs/-::DATcre/-* mice led to a significant enrichment of DAT (***RELfs/-::DATcre/-*:** 267.6x; ***RELfs/fs***: 0.16x; **non-tg**: 0.25x) and TH mRNA (***RELfs/-::DATcre/-*:** 52.1x; ***RELfs/fs***: 0.99x; **non-tg**: 1.21x) in the IP

fractions normalised to Total RNA input while none of the non-DAn markers tested showed an enrichment. For both conditions, the RINs were suitable for a gene expression profiling study by RNA-Seq (RIN of ≥7; Figure 6. 12 A', B'). Tissue isolated from the midbrain had high total RNA amounts in the IP fractions only for the *RELfs/-::DATcre/-* genetic background as desired (Figure 6. 12 A'') (***RELfs/-::DATcre/-*:** 133.31 ng ± 25.61; ***RELfs/fs***: 4.59 ng ± 0.23; **non-tg**: 5.12 ng ± 0.37). Here, the amount of non-specific RNA isolated from TRAP-negative mice was negligible. In addition, tissue isolated from the striatum yielded relatively low amounts of RNA after TRAP (Figure 6. 12 B'') (***RELfs/-::DATcre/-*:** 18.29 ng ± 9.19; ***RELfs/fs***: 14.29 ng ± 8.26; **non-tg**: 4.96 ng ± 0.48). However, the amount of input tissue might have been too low to for the analysis of striatal DAn-specific mRNA. Additional pilot experiments to optimise the TRAP matrix conditions using striatal input tissue are underway. In general, as discussed in previous chapters, it was expected that a certain amount of non-specific RNA would be isolated alongside DAn-specific mRNA due to the 'stickiness' of the magnetic beads used to construct the affinity matrix for TRAP.

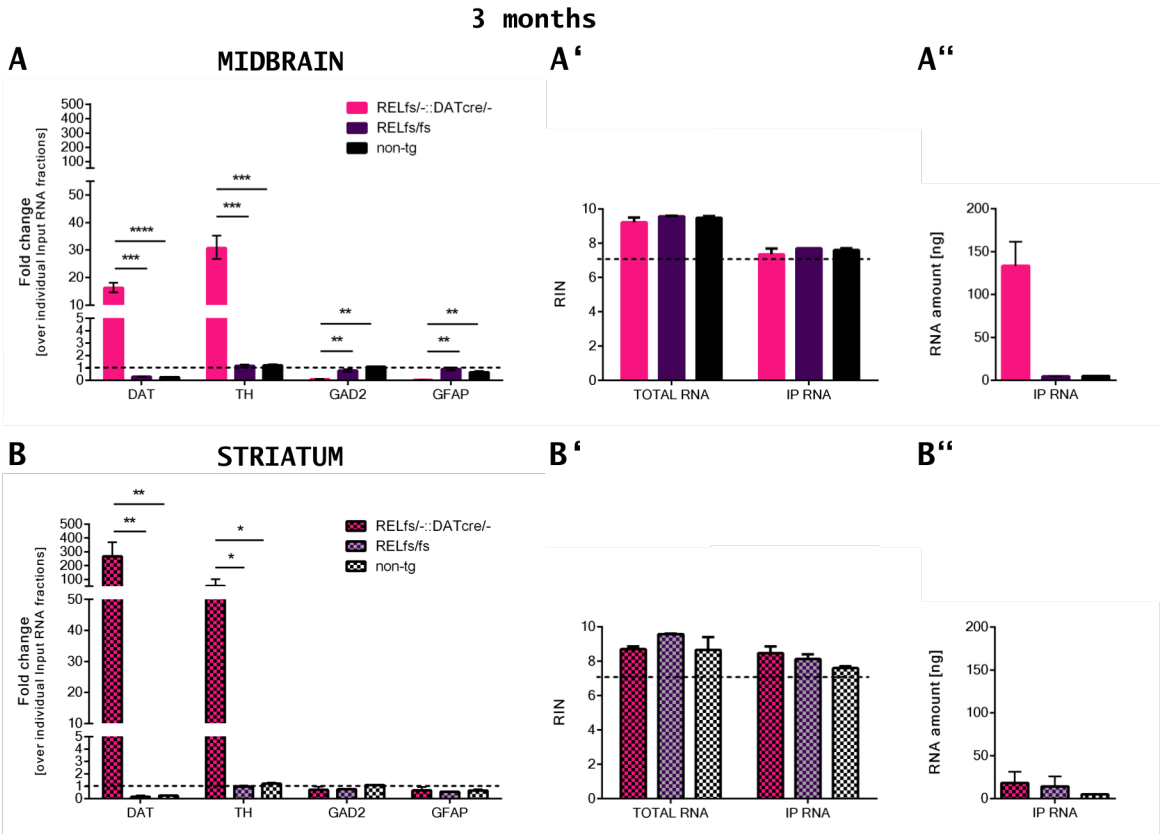


Figure 6. 12 TRAP pilot experiments using TRAP-transgenic mice (3 months) show successful isolation of DAn-specific mRNA from midbrain and striatum.

*Pilot TRAP experiments using the midbrain (A) or striatum (B) of 3 months old REL mice and non-tg controls (modified Heiman et al., 2014). Per experimental 'n', one midbrain or striatum per genotype were used. (A, B) DAT and TH are significantly enriched in DAn of the midbrain or striatum of RELfs/-::DATcre/- mice (pink), whereas non-DAn marker are not enriched in the IP fractions. eGFP-L10a-negative mice (purple) or non-tg control (black) do not show an enrichment for DAn markers. The qPCR results were normalised to the geometric expression mean of two reference genes and fold-enrichment values were calculated separately for each sample based on input RNA expression before TRAP using the comparative Ct method (n= 4 independent TRAP experiments; one-way ANOVA with Tukey post-hoc analysis; mean ± SEM; *p≤ 0.05, **p≤ 0.01, ***p≤ 0.001). (A', B') RIN values show good RNA quality for all Total and IP RNA fractions. (A'', B'') Overview of the total IP RNA amount [ng] isolated using with TRAP. Using midbrain tissue, RELfs/-::DATcre/- (pink) yield the highest amount of RNA. RNA amounts from the striatum are very low for all fractions. REL= ROSA26-eGFP-L10a. Fs= floxed. Cre= Cre recombinase. Non-tg= non-transgenic. IP= bound or immunoprecipitated fraction. Total= input midbrain fraction. DAn= DAn. RIN= RNA integrity number. Non-tg= non-transgenic (TRAP-negative). DAT= Dopamine transporter. TH= Tyrosine hydroxylase. GAD2= Glutamate decarboxylase 2. GFAP= Glial fibrillary acidic protein.*

6.3.5 TRAP can be successfully used to isolate high quality RNA from cell soma and axons of young and aged REL transgenic mice

Further pilot TRAP experiments using striatal or midbrain tissue isolated from TRAP-positive *RELfs/-::DATcre/-* and TRAP-negative *RELfs/fs* mice were undertaken along a time-line comparing 6, 12, and 18 months old mice. We aimed for high enrichment of DAn markers (DAT, TH) in TRAP-positive *RELfs/-::DATcre/-* mice only, as well as sufficient RNA quantity and quality for subsequent gene expression profiling analysis by RNA-Seq.

TRAP pilot experiments – 6 months

Subsequent pilot TRAP experiments in 6 months old mice confirmed the success of DAn-specific mRNA isolation from TRAP-positive tissue (Figure 6. 13). Midbrain tissue (Figure 6. 13 A) from *RELfs/-::DATcre/-* mice showed significant enrichment of DAT (***RELfs/-::DATcre/-*:** 11.4x; ***RELfs/fs***: 0.2x) and TH mRNA (***RELfs/-::DATcre/-*:** 34.7x; ***RELfs/fs***: 1.0x), while non-DAn marker mRNA was not enriched in any of the IP fractions normalised to Total RNA input. Similarly, striatal tissue (Figure 6. 13 B) isolated from *RELfs/-::DATcre/-* mice showed a significant enrichment of DAT (***RELfs/-::DATcre/-*:** 138.8x; ***RELfs/fs***: 1.2x) and TH mRNA (***RELfs/-::DATcre/-*:** 10.7x; ***RELfs/fs***: 1.1x) in the IP fractions normalised to Total RNA input, which was not the case for any non-DAn markers tested. High quality RNA could be isolated from both input tissues (RIN of ≥7; Figure 6. 13 A', B'). Total RNA amounts in the midbrain-IP fractions were high only for the *RELfs/-::DATcre/-* genetic background (Figure 6. 13 A'') (***RELfs/-::DATcre/-*:** 124.35ng ±16.46; ***RELfs/fs***: 9.01ng ±1.76), whereas the total

RNA amounts in the striatum-IP fractions were generally lower (Figure 6. 13 B'') (***RELfs/-::DATcre/-*** **:** 13.02ng ±5.88; ***RELfs/fs***: 8.05ng ±4.63).

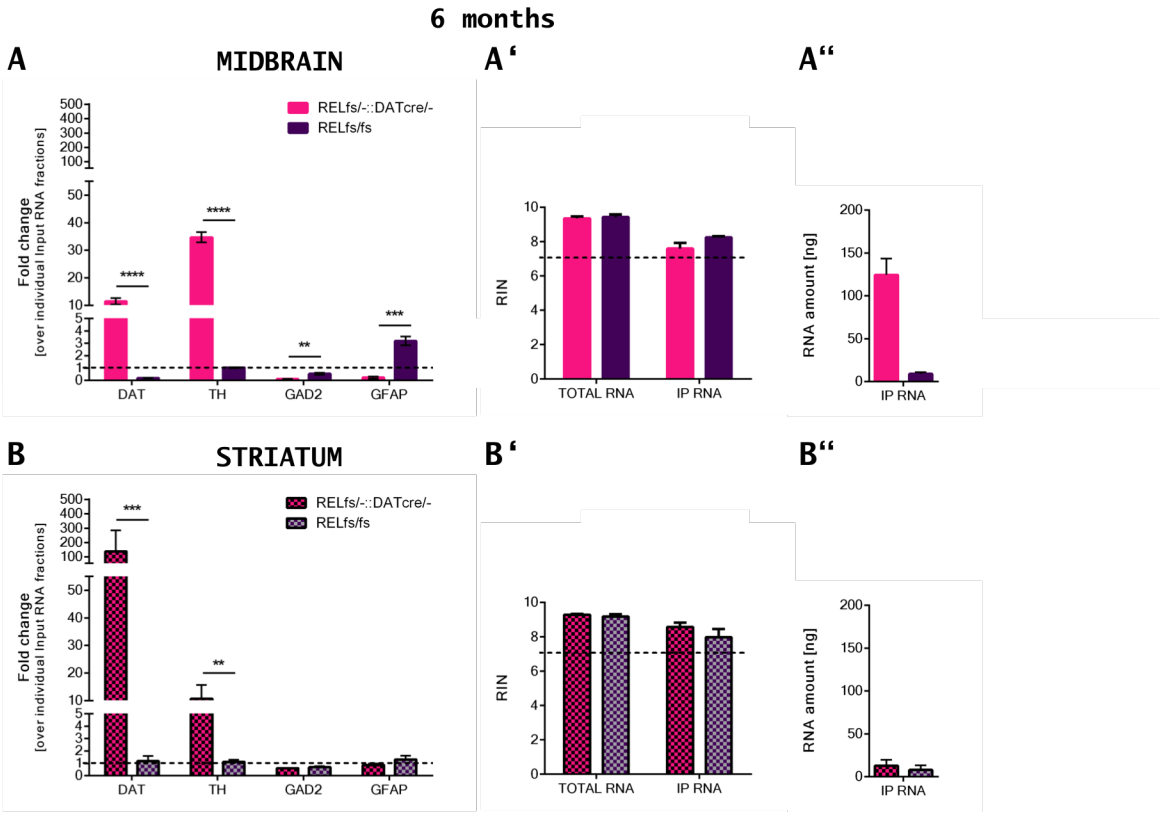


Figure 6. 13 Midbrain and striatum from TRAP-transgenic mice (6 months) can be successfully used for the enrichment of marker genes.

*Pilot TRAP experiments using the midbrain (A) or striatum (B) of 6 months old REL mice and TRAP-negative controls (modified Heiman et al., 2014). Per experimental 'n', one midbrain or striatum per genotype were used. (A, B) Similarly to the results from 3 months old mice, only markers DAT and TH are significantly enriched in the midbrain or striatum of RELfs/-::DATcre/- mice (pink). The qPCR results were normalised to the geometric expression mean of two reference genes and fold-enrichment values were calculated separately for each sample based on input RNA expression before TRAP using the comparative Ct method (n= 4 independent TRAP experiments; one-way ANOVA with Tukey post-hoc analysis; mean ± SEM; *p≤ 0.05, **p≤ 0.01, ***p≤ 0.001). (A', B') RNA of high quality for all Total and IP RNA fractions can be isolated at 6 months. (A'', B'') RELfs/-::DATcre/- (pink) can be successfully used to isolate RNA from midbrains after TRAP. The RNA amount is much lower when using the striatum as input for TRAP. REL= ROSA26-eGFP-L10a. Fs= floxed. Cre= Cre recombinase. Non-tg= non-transgenic. IP= bound or immunoprecipitated fraction. Total= input midbrain fraction. DAn= DAn. RIN= RNA integrity number. Non-tg= non-transgenic (TRAP-negative). DAT= Dopamine transporter. TH= Tyrosine hydroxylase. GAD2= Glutamate decarboxylase 2. GFAP= Glial fibrillary acidic protein.*

TRAP pilot experiments – 12 months

Furthermore, we could successfully show that DAn-specific mRNA can be isolated from aged mice (12 months) using TRAP. Using either midbrain (Figure 6. 14 A) or striatum (Figure 6. 14 B) as input tissue for TRAP, DAn marker RNA was significantly enriched in TRAP-positive mice only (MIDBRAIN: ***RELfs/-::DATcre/-*****:** DAT= 9.1x and TH= 33.4x; ***RELfs/fs***: DAT= 0.3x and TH= 1.5x. STRIATUM: ***RELfs/-::DATcre/-*****:** DAT= 70.6x and TH= 6.9x; ***RELfs/fs***: DAT= 0.3x and TH= 0.7x). RNA isolated from either

midbrain or striatum was of high quality (Figure 6. 14 A', B'; RIN of ≥7 except for the TRAP-negative IP fraction) and quantity (Figure 6. 14 A'', B''; MIDBRAIN: ***RELfs/-::DATcre/-*:** 63.4 ng ± 7.33; ***RELfs/fs*:** 0.48 ng ± 0.03. STRIATUM: ***RELfs/-::DATcre/-*:** 16.68 ng ± 1.33; ***RELfs/fs*:** 1.59 ng ± 0.54). As before the total RNA amounts the striatum-IP fractions were generally lower (Figure 6. 14 B'') compared to the midbrain.

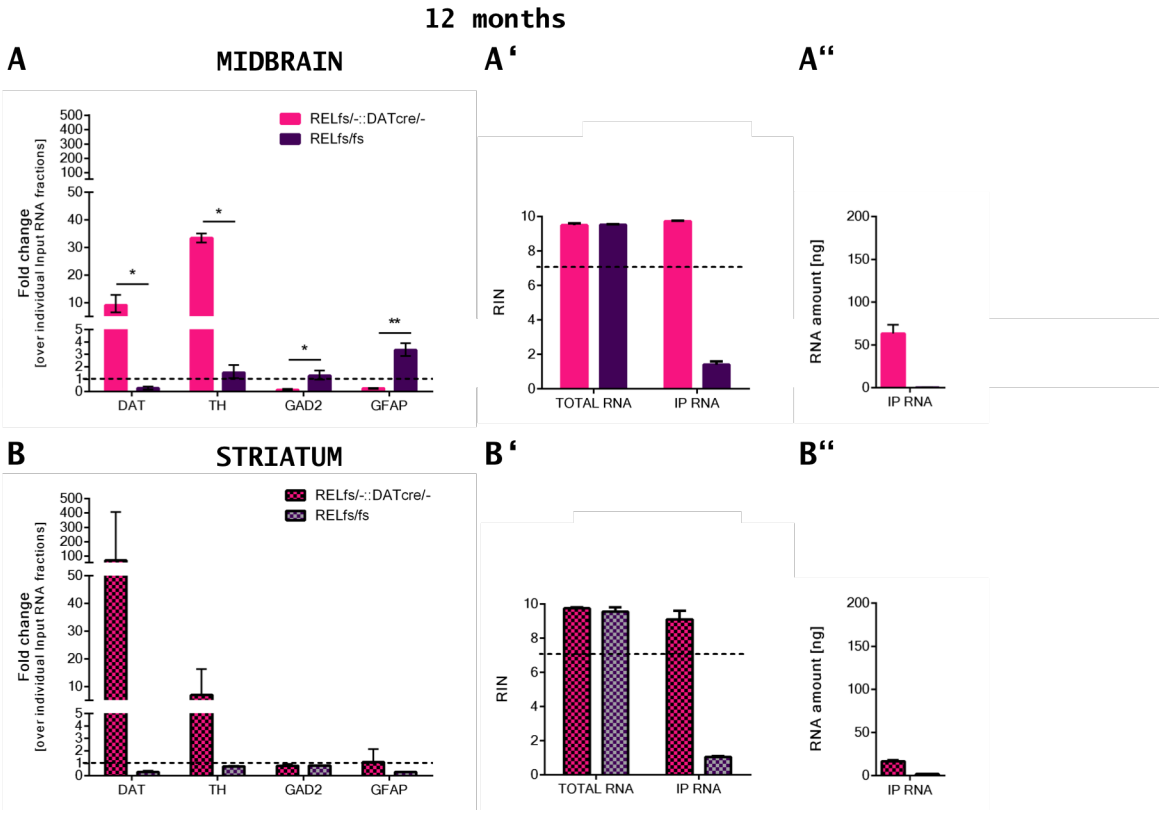


Figure 6. 14 TRAP results can be successfully re-produced in aged transgenic mice (12 months).

*Pilot TRAP experiments using the midbrain (A) or striatum (B) of 12 months old REL mice and TRAP-negative controls (modified Heiman et al., 2014). Per experimental 'n', one midbrain or striatum per genotype were used. (A, B) Midbrain and striatum of aged (12 months) RELfs/-::DATcre/- mice (pink) can be successfully used to enrich for markers (DAT, TH) in the IP fractions after TRAP. The qPCR results were normalised to the geometric expression mean of two reference genes and fold-enrichment values were calculated separately for each sample based on input RNA expression before TRAP using the comparative Ct method (n= 2 independent TRAP experiments; one-way ANOVA with Tukey post-hoc analysis; mean ± SEM; *p≤ 0.05). (A', B') RNA quality for all Total fractions is high. Only IP RNA fractions of RELfs/-::DATcre/- mice (pink) gained a sufficient RIN quality. (A'', B'') The RNA amount of the IP fractions of RELfs/-::DATcre/- (pink) is much higher compared to eGFP-L10a-negatove mice (purple). TRAP is less successful to gain much RNA using the striatum as input tissue. REL= ROSA26-eGFP-L10a. Fs= floxed. Cre= Cre recombinase. Non-tg= non-transgenic. IP= bound or immunoprecipitated fraction. Total= input midbrain fraction. DAn= DAn. RIN= RNA integrity number. Non-tg= non-transgenic (TRAP-negative). DAT= Dopamine transporter. TH= Tyrosine hydroxylase. GAD2= Glutamate decarboxylase 2. GFAP= Glial fibrillary acidic protein.*

TRAP pilot experiments – 18 months

Results in 18 months old mice show that high quality mRNA can still be isolated using TRAP in aged transgenic mice. Unlike for the THTR mouse line (Chapter 4), we could show in our TRAP-conditional REL transgenic mouse line that DAn marker genes show an enrichment in the mRNA isolated from midbrains or striata of old trangenic mice (18 months) using TRAP (MIDBRAIN: ***RELfs/-::DATcre/-*:** DAT= 14.5x and TH= 40.9x; ***RELfs/fs***: DAT= 0.4x and TH= 1.2x. STRIATUM: ***RELfs/-::DATcre/-*:** DAT= 210.9x and TH= 20.1x; ***RELfs/fs***: DAT= 0.1x and TH= 0.9x). The RNA isolated from both midbrain and striatum was of high quality (Figure 6. 15 A', B'; RIN of ≥7 except for the TRAP-negative IP fraction). Sufficient RNA amounts were isolated from the midbrains of old *RELfs/-::DATcre/-* mice (Figure 6. 15 A''; ***RELfs/-::DATcre/-*:** 161.25 ng ± 14.81; ***RELfs/fs***: 0.84 ng ± 0.15). RNA isolated from the striatum was lower (Figure 6. 15 B''; ***RELfs/-::DATcre/-*:** 7.58 ng ± 2.89; ***RELfs/fs***: 0.64 ng ± 0.08) as seen before for the younger ages.

However, the amount of input tissue might have been too low to for the analysis of striatal DAn-specific mRNA. Additional pilot experiments to optimise the TRAP matrix conditions using striatal input tissue are underway. In general, as discussed in previous chapters, it was expected that a certain amount of non-specific RNA would be isolated alongside DAn-specific mRNA due to the 'stickiness' of the magnetic beads used to construct the affinity matrix for TRAP.

All in all, we could show that TRAP can be successfully used to isolate high quality and quantity DAn-specific mRNA from the midbrain and striatum of *RELfs/-::DATcre/-* mice regardless of age (3, 6, 12, and 18 months).

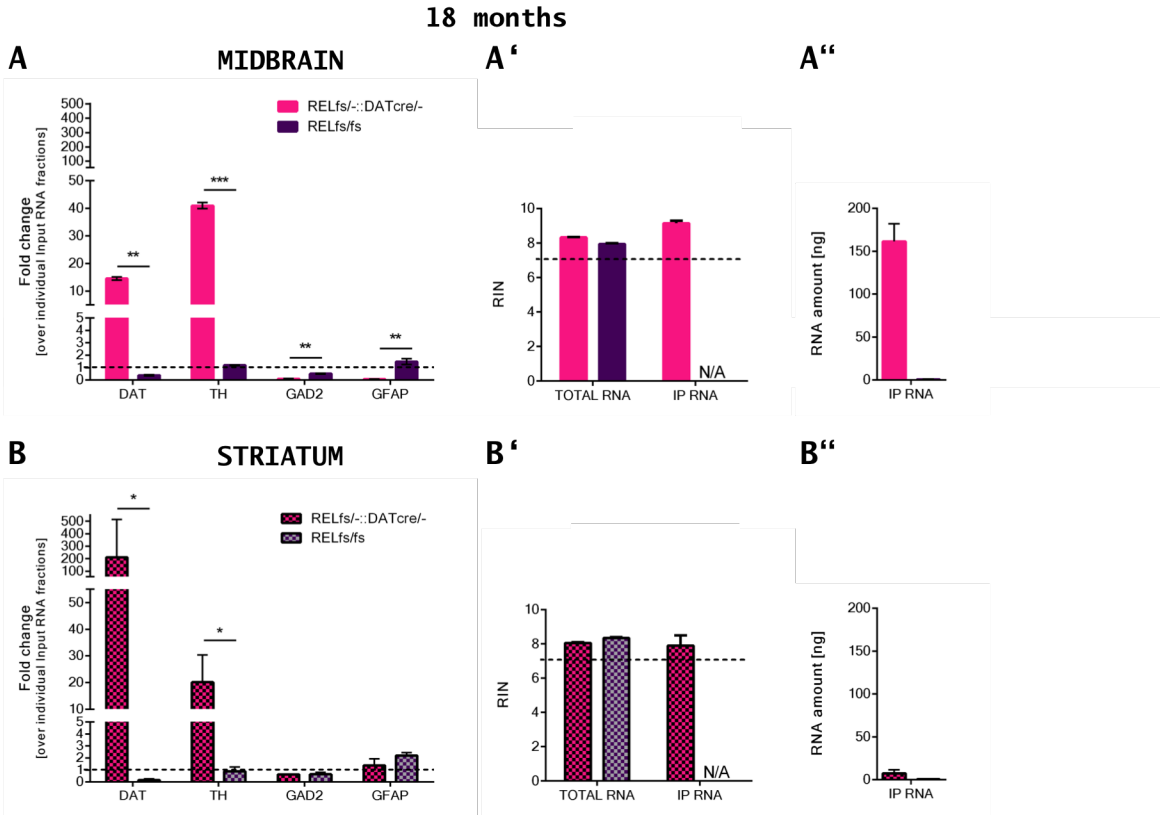


Figure 6. 15 TRAP on midbrain and striatum input tissue produces consistent results in aged mice (18 months).

*Pilot TRAP experiments using the midbrain (A) or striatum (B) of 18 months old REL mice and TRAP-negative controls (modified Heiman et al., 2014). Per experimental 'n', one midbrain or striatum per genotype were used. (A, B) Enrichment of markers (DAT, TH) in the IP fractions after TRAP using midbrain and striatum of old (18 months) shows consistent results in RELfs/-::DATcre/- mice (pink). Non-DAn markers are not enriched. The qPCR results were normalised to the geometric expression mean of two reference genes and fold-enrichment values were calculated separately for each sample based on input RNA expression before TRAP using the comparative Ct method (n= 2 independent TRAP experiments; one-way ANOVA with Tukey post-hoc analysis; mean ± SEM; *p≤ 0.05, **p≤ 0.01, ***p≤ 0.001). (A'/'', B'/''') RNA quality for all Total fractions and IP RNA fractions and RNA amount for the IP RNA fractions of RELfs/-::DATcre/- mice (pink) shows consistent high quality of RNA. REL= ROSA26-eGFP-L10a. Fs= floxed. Cre= Cre recombinase. Non-tg= non-transgenic. IP= bound or immunoprecipitated fraction. Total= input midbrain fraction. DAn= DAn. RIN= RNA integrity number. Non-tg= non-transgenic (TRAP-negative). DAT= Dopamine transporter. TH= Tyrosine hydroxylase. GAD2= Glutamate decarboxylase 2. GFAP= Glial fibrillary acidic protein.*

6.4 Discussion and Conclusion

The aim of this chapter was to describe the establishment, molecular characterisation, and optimisation of the TRAP protocol for our novel TRAP REL transgenic mouse line (*RELfs/-::DATcre/-(::hSNCA+)*). Molecular characterisation experiments confirmed that eGFP-L10a is highly and specifically expressed in DAn. Adaption of the TRAP protocol to use with our REL transgenic mouse line enabled the successful isolation of DAn-specific mRNA from soma (midbrain) and axons (striatum). Pilot TRAP experiments at different ages confirmed that we will be able to combine DAn-specific mRNA isolation using TRAP with translatome profiling in young (3 months) and old (18 months) REL mice.

I have highlighted four major areas for discussion:

1) Establishment of the ROSA26-eGFP-L10a::DATcre(::hSNCA+) transgenic mouse line

Our previously developed *THTR* model was successfully used for the DAn-specific isolation of mRNAs using TRAP (Chapter 3 and 4). Unfortunately, the background RNA amount was high and experimental noise complicated the analysis of our RNA-Seq datasets (Chapter 3-5). To circumvent the problem of low eGFP-L10a expression, we decided to establish here in Chapter 6 a second TRAP mouse line for which eGFP-L10a is driven by the strong synthetic CAG hybrid promoter (Zhou et al., 2013). The CAG vector was constructed to allow high levels foreign gene expression in mammalian expression vectors (Hitoshi et al., 1991; Miyazaki et al., 1989) and has been successfully used to drive Cre recombinase expression (Sakai and Miyazaki, 1997). The Cre conditional TRAP model that we have chosen (*ROSA26-eGFP-L10a (REL)*) was shown to display robust GFP-L10a expression without any detectable GFP fluorescence in the absence of Cre (Zhou et al., 2013). Other available TRAP-Cre mouse models were considered unreliable because they showed weak eGFP transgene expression in the absence of Cre-dependent recombination caused by bypass of the transcriptional stop cassette (Liu et al., 2014) or the mouse models expressed the eGFP-L10a fusion protein downstream of a lox-stop-lox cassette knocked into the ROSA26 locus without any further elements to prevent potential leakage of the floxed construct (Long et al., 2014).

We successfully combined the REL line with a DAT-Cre driver line (Figure 6. 4). We aimed to breed the *RELfs/-::DATcre/-* mice with our PD model *(hSNCA+),* which has been generated on a mouse aSyn KO background. Since the mouse aSyn gene and the ROSA26 locus are located on the same chromosome (Figure 6. 2) we wanted to prevent any potential interference between these two loci. Thus, the *hSNCA+* transgene had to be bred back onto a mouse WT background (Figure 6. 3). Preferably, we would have wanted to over-express human aSyn in the absence of the endogenous mouse aSyn such as in our *THTR/hSNCA+* mouse line (Chapter 3). Ideally, human aSyn is over-expressed on a mouse aSyn KO background to avoid potential confounding effects due to the presence of endogenous mouse protein. A confounding interaction was shown in a publication from Cabin et al. where the presence of mouse aSyn was protective against the deleterious effects of human mutant A53T aSyn protein in a transgenic mouse line (Cabin et al., 2005). The A53T substitution in the aSyn protein was observed in some familial cases of PD (Polymeropoulos, 1997). However, human and mouse aSyn sequences share over 90% sequence identity apart from only very few amino acid differences. Interestingly, one of them is the amino acid at position 53, which is alanine in humans but threonine in mice (Lavedan, 1998). This discrepancy in mouse and human aSyn sequences might be responsible for the protective effects that mouse aSyn exhibits in the study by Cabin et al. A study by Chandra et al. generally suggested that aSyn protein might play an important protective role at the synapse (Chandra et al., 2005). Hence, the presence of endogenous aSyn in neurons throughout development might increase their internal tolerance to this protein which prepare them to combat increased aSyn expression during ageing (Buchman and Ninkina, 2008). Contrary, neurons that never expressed any aSyn are more vulnerable to this protein as they never got prompted to develop any defense mechanisms, e.g. (in)activate certain intracellular pathways (Buchman and Ninkina, 2008).

Our BAC human aSyn over-expressing model of PD (*hSNCA+*) on a mouse aSyn KO background faithfully replicates the spatio-temporal expression profile of aSyn (Janezic et al., 2013). The human aSyn transgene and its complete genomic locus are expressed under the control of its native promoter, circumventing limitations that arise when using exogenous promoters. So far, we have

not analysed if the additional presence of mouse endogenous aSyn might interfere with human aSyn function. All in all, studies on aSyn over-expressing mouse models strongly suggest that the induction of neuronal dysfunction requires reaching a certain threshold of aSyn protein expression and that the general pathogenesis is closely linked to the duration of transgene expression. Others who aimed to model human aSyn over-expression in mice could report disease-related phenotypes despite the presence of endogenous mouse aSyn protein (e.g. (Giasson et al., 2002; Masliah et al., 2000)). The first model that over-expressed human WT aSyn generated by Masliah et al., displayed aSyn- and ubiquitin-reactive intraneuronal inclusion bodies in the midbrain and other PD-affected brain regions, as well as motor deficits from the age of 12 months (Masliah et al., 2000). Another mouse line that developed dramatic motor impairments at the age of 8 month expressed either WT or A53T aSyn under an exogenous promoter (Giasson et al., 2002).

In our case, it cannot be excluded that the presence of endogenous mouse aSyn could mediate potential protective effects or delay otherwise deleterious effects of human aSyn over-expression in our *RELfs/-::DATcre/-::hSNCA+* PD model. However, even if we might not be able to see extensive DA neuronal death, alterations of the nigrostriatal pathway, as well as behavioural deficits in aged mice due to the accumulation of aSyn as seen by others might be sufficient to change the DAn translatome (Giasson et al., 2002; Masliah et al., 2000). Potentially, we will be able to analyse dopaminergic dysfunction in the early phase of disease progression with subsequent cell death caused by accumulation aSyn protein over time.

2) DAn-specific expression of the eGFP-L10a fusion protein

We could show that eGFP-L10a is strongly expressed from the CAG promoter after Cre-mediated recombination in DAT-expressing DAn in the midbrain (Figure 6. 6). Strong native eGFP fluorescence can be detected as expected in the midbrain of young REL animals and this persists throughout ageing of our transgenic mice (Figure 6. 5). Hence, we could reproduce the widespread constitutively activated expression of eGFP from the ROSA26 locus as originally reported by Zhou et al. (Zhou et al., 2013). Cre expression is constitutively activated in all cells that have ever activated its promoter (here: DAT promoter) even if the promoter is only transiently activated. For the DAT

gene, transient promoter activity during development is not a problem since others also found no DAT-Cre driven transgene expression patterns in non-DAn (Turiault et al., 2007).

To make both of our TRAP lines (*THTR* line (Chapter 3) and *ROSA26-eGFP-L10a::DATcre* line (Chpater 6)) as comparable as possible, it would have been ideal to use same promoter in both cases. However, the DAT promoter serves as a better driver for Cre transgene expression compared to the TH promoter. For the TH promoter, ectopic expression of TH driven Cre recombinase has been seen by others (e.g. (Iacovitti et al., 2014; Kelly et al., 2006); see discussion in Chapter 3). Ectopic expression could possibly be a result of transient TH promoter activity during development in cell populations that stop to produce TH protein in adulthood (Lindeberg et al., 2004). It would be particularly disadvantageous if transient TH promoter activity constitutively activated Cre-mediated transgene expression that persists even if endogenous TH activity has long been turned down. Since the TH-Cre driver lines has been shown to ectopically express Cre (Lammel et al., 2015), we opted for a DAT-Cre driver instead as the best option for our second TRAP line.

DAT or TH co-expression with eGFP-L10a

The eGFP-L10a fusion protein is co-expressed in DAT- and TH-positive cells in the SNc and VTA (Figure 6. 6) confirming the correct spatio-temporal expression of Cre recombinase under control of the endogenous DAT promoter. Nevertheless, upon closer examination of GFP and TH co-labelings in our REL mouse line, it became apparent that not all TH-positive cells co-expressed GFP (Figure 6. 6 C). However, it has previously been shown that high levels of DAT expression (and Cre in our mice) were restricted to cells that were also highly enriched for TH in the SNc, whereas TH-positive cells in the VTA did not overlap completely with DAT-positive neurons (Li et al., 2013).

Furthermore, the absence of ectopic transgene expression of the eGFP-L10a transgene was confirmed by analysing cortex and hippocampus (Figure 6. 7). This was expected since none of these regions express endogenous DAT. Overall, no obvious morphological differences of DA cell populations (Figure 6. 6) or the striatal protein expression levels of TH and RPL10a (Figure 6. 8) between TRAP-transgenic and TRAP-negative mice could be observed. DAT/GFP and TH/GFP immunofluorescence co-labelings and western blot analysis of TH and RPL10a, and DAT protein

expression levels will also be measured for aged REL transgenic animals. It will be expected that DAT protein levels in the striatum are reduced in DAT-Cre expressing animals, which has already been shown by others (Bäckman et al., 2006). No eGFP-L10a fusion protein expression levels were detected by immunoblotting using either an antibody against RPL10a or different GFP antibodies (results not shown). Despite the increased numbers of eGFP-positive DAn, total midbrain lysates might still contain too little GFP-tagged ribosomes as discussed previously (Chapter 3).

eGFP-L10a fusion protein is undetectable in DAn axons

Similar to our *THTR* mouse line (Chapter 3) and TRAP lines by others (Brichta et al., 2015), eGFP-L10a could not be detected in the striatum although DAT and TH expression are found there. To clarify whether immunofluorescence is not sensitive enough to pick up axonally located eGFP-tagged ribosomes, electron microscopic analysis of immuno-gold labelled GFP-tagged ribosomes is underway. Although ribosomes were identified by electron microscopy in embryonic neurons in mammals (Bunge, 1973; Yamada et al., 1971), and the squid giant axons (Giuditta et al., 1986; Giuditta et al., 1991), the detection of polysomes in the axons shaft could not be reproduced by electron microscopy in a study using adult rats (Steward and Ribak, 1986). It was speculated that axonal translation only occurs during development (Zivraj et al., 2010) or in response to an external stimulus, such as regeneration following injury (Verma, 2005). It might also be possible that the ultrastructural identification of polysomes in the axons is generally complicated by a specialised morphology since several electron microscopy studies have failed to identify axonal ribosomes or axonal ER (Bunge, 1973; Steward and Ribak, 1986; Yamada et al., 1971). Polysomes located in mature axons might not follow conventional ultrastructural criteria, as suggested by an electron microscopy study that showed eGFP-tagged RPL10a at the nodes of Ranvier in corticospinal tract axons (Walker et al., 2012a). To further investigate the question of axonally located polysomes, we performed TRAP experiments using the striatum as input tissue (Figure 6. 12-Figure 6. 15). We could successfully isolate DAn-specific mRNA from our TRAP-positive animals as discussed further below.

3) aSyn/eGFP are co-expression in DAn

Analysis of human aSyn expression in our REL mouse line revealed the co-labelling of eGFP with aSyn in the midbrain (Figure 6. 9). A high number of aSyn-positive cells also expressed GFP, an improvement compared to GFP/human aSyn co-stains in our THTR mouse line (Chapter 3). Furthermore, only *hSNCA+* mice showed immunoreactivity for the human-specific anti-aSyn antibody, whereas the pan-species anti-aSyn antibody picked up aSyn-positive cells in all genotypes (Figure 6. 10). As observed previously, the *hSNCA+* transgene increased aSyn levels compared to endogenous mouse aSyn (Chapter 3 and DPhil Thesis: S. Janezic, 2013), mirroring aSyn levels observed in PD patients (Chartier-Harlin et al., 2004; Singleton et al., 2003).

4) Successful establishment of TRAP methodology in cell soma and axons

Previously optimised TRAP protocol and 'affinity matrix' conditions (THTR moue line, Chapter 4) were successfully adjusted for the use with the REL line. We could show that high quality RNA (RIN ≥7) DAn-specific mRNA can be successfully isolated from midbrains and striata of TRAP-positive animals regardless of age (3, 6, 12, 18 months). Pilot TRAP experiments using midbrain input tissue lead to the successful enrichment of DAn markers in TRAP-positive *RELfs/-::DATcre/-* mice only (Figure 6. 12: 3 months; Figure 6. 13: 6 months; Figure 6. 14: 12 months; Figure 6. 15: 18 months). The enrichment of DAn marker mRNA using our new REL mouse line with approximately 10x for DAT and 40x for TH was much higher than previously seen for our THTR line (Chapter 4 or 5), for which DAT and TH were enriched by 5x and 10x, respectively. The enrichment values obtained with our new *RELfs/-::DATcre/-* mouse line were very similar to the fold-changes achieved by a recent TRAP-based RNA-Seq study using a *DAT-bacTRAP* mouse line (Brichta et al., 2015).

The study by Brichta et al. claimed that the number of eGFP-L10a ribosomes in the DAn axons might be either undetectably low or that eGFP-tagged ribosomes are completely absent from the midbrain DA neuronal projections to the striatum (Brichta et al., 2015). Nevertheless, we could show that TRAP can indeed be used to isolate DAn-specific mRNA from the striata of *RELfs/-::DATcre/-* mice, which is consistent from young to aged animals. While the 'axonal TRAP' experiments serve as a proof of concept, further optimisation experiments are needed to improve

RNA yield in TRAP-positive animals and reduce non-specific background RNA binding in TRAP-negative mice. Affinity matrix optimisation experiments as performed for the THTR line (Chapter 4) are already underway to find the optimal compromise between DAn marker enrichment and RNA quantity and quality.

All in all, we could show that young and aged *ROSA26-eGFP-L10a::DATcre* mice express high levels of eGFP-L10a in DAn neurons and that these mice can be successfully used to isolate DAn-specific mRNA from the midbrain and striatum using TRAP. Ultimately, *ROSA26-eGFP-L10a::DATcre* mice will be paired with our *hSNCA+* transgenic mouse model of PD for a detailed analysis of the DAn-specific translatomic changes during PD progression. Experiments are already underway to collect TRAP-gained mRNA at 3 and 18 months comparing translatome profiles of healthy *ROSA26-eGFP-L10a::DATcre* mice with our PD model *ROSA26-eGFP-L10a::DATcre::hSNCA+* (Figure 6. 16).

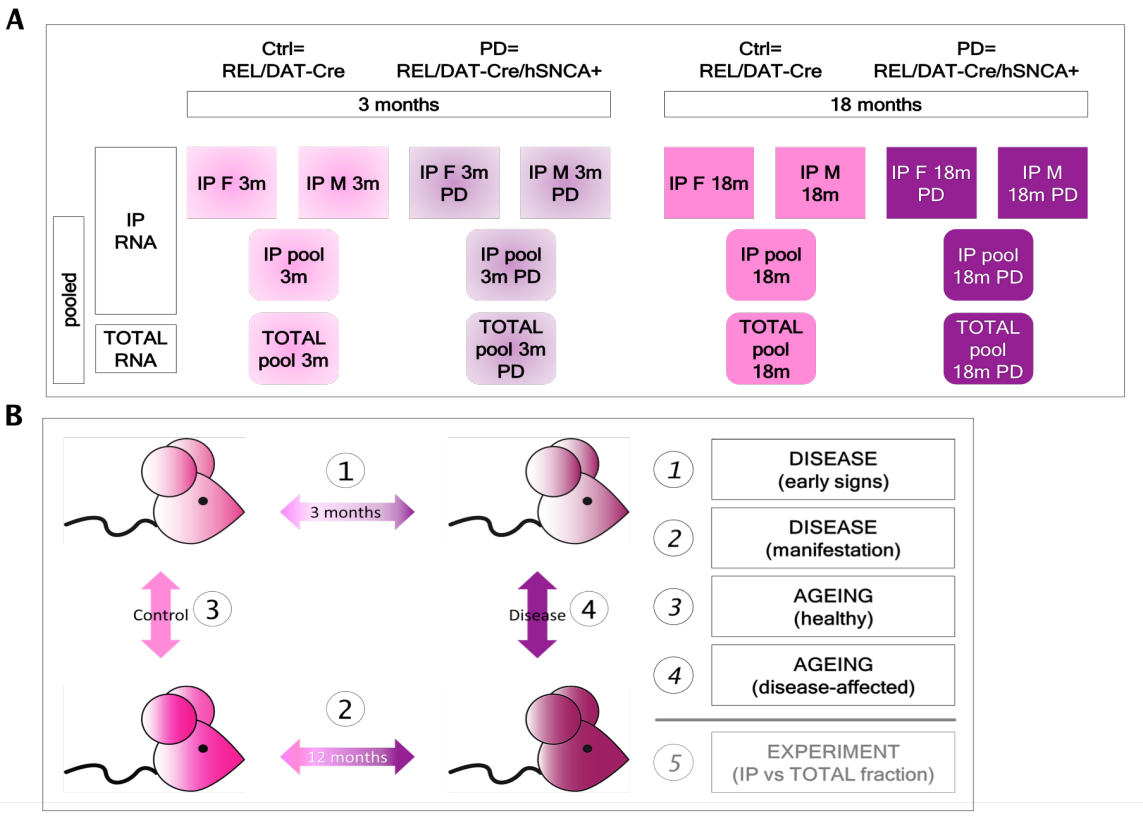


Figure 6. 16 Experimental design of the REL TRAP-Seq study.

(A) Four female (IP F #1-4) and four male TRAP IP (IP M #1-4) samples per genotype (CTRL or PD) and age (3 or 18 months) will be collected for RNA-Seq (total of 32 samples). All TRAP IP and Total samples will be pooled per genotype (IP/ Total 3/18 months CTRL or PD; total of 8 samples). (B) Possible questions asking for 1) effect of PD at a young or 2) advanced age (disease progression), 3) gene expression changes due to healthy or 4) disease-affected ageing, and 5) changes specific to DAn by comparing the pooled IP and Total RNA fractions. light pink: REL/DAT-Cre 3m; light purple: REL/DAT-Cre/hSNCA+ 3m; pink: REL/DAT-Cre 12m; purple: REL/DAT-Cre/hSNCA+ 12m. IP= bound or immunoprecipitated fraction. Total= input fraction. F= female. M= male. CTRL= Control (REL/DAT-Cre mice). PD= Parkinson's disease model (REL/DAT-Cre/hSNCA+ mice). hSNCA+= human alpha-Synuclein. DAn= dopaminergic neuron.

- CHAPTER 7 -

GENERAL DISCUSSION

7.1 Overview

The work in this thesis aimed to understand the pathological mechanisms underlying aSyn over-expression on the level of gene expression in PD. Firstly, the molecular characterisation of a *THTR* transgenic mouse line and optimisation of the translating ribosome affinity methodology in this line were necessary for subsequent gene expression profiling studies. Secondly, a pilot RNA-Seq study on TRAP isolated mRNA defined the age-frame and genotypes for the actual TRAP-Seq study using the *THTR* line. Next, analysis of the dopaminergic neuronal translatome found age-related changes in mitochondrial respiratory complexes and proteins involved in mitochondrial import and integrity. Lastly, a novel and improved conditional TRAP mouse line was successfully established and pilot TRAP experiments could already show that mRNA from dopaminergic cell populations in the soma (midbrain) and axons (striatum) can be successfully isolated using *ROSA26-eGFP-L10a::DAT-Cre* transgenic mice. Combining this new successful TRAP mouse line with our *hSNCA+* model of PD will in the future enable the analysis of gene expression profiles linked to the molecular pathway, which underlie the development of disease.

7.2 Discussion - *TH-bacTRAP* (*THTR*) mice

7.2.1 TRAP captures DAn-specific mRNAs from *THTR* mice

Molecular characterisations of the *TH-bacTRAP* (THTR) line in Chapter 3 revealed that the eGFP-L10a transgene is expressed in the correct spatio-temporal manner in the midbrain under the control of the mouse TH promoter. Work described in Chapter 4 could successfully show that the purification of cell type-specific mRNAs using TRAP methodology can be achieved on a genetic basis, by isolating eGFP-tagged ribosomal protein L10a from DAn. Therewith, we could circumvent physical enrichment strategies including FACS or LCM which suffer from several limitations, such as the introduction of experimental noise due to tissue fixation or very low cell and RNA yields (Emery and Barres, 2008; Heiman et al., 2014). Nevertheless, our study using the transgenic *THTR* line has limitations. First, our transgenic mice do not express eGFP in all TH-positive cells, something we expected. Only a small proportion of DAn in the midbrain is TH/eGFP-double positive which made

the affinity purification of DAn-specific mRNA challenging. Likely, the construction of the BAC vector affected transgene expression from the TH promotor since intronic and extronic sequences of the TH locus may be necessary to provide important temporal and spatial expression clues. The lack of these sequences in the bacTRAP construct may be hindering the eGFP-L10a reporter construct to accurately mimic TH expression (Kelly et al., 2006; Kessler et al., 2003; Nagatsu et al., 1994). Furthermore, we detected a decrease of eGFP native fluorescence in aged 18 months old transgenic mice in line with a lower enrichment of DAn markers after qPCR in the TRAP-isolated RNA from aged bacTRAP mice compared to a young age. These findings supported the decision to analyse younger, middle-aged 12 months old mice in the actual TRAP-Seq study in order to rule out any gross cell losses at a later time-point. The pilot RNA-Seq study successfully confirmed a dopaminergic profile for the homozygous bacTRAP background but failed to differentiate RNA isolated from the hemizygous *THTR* genetic background from non-specific RNA isolated in non-transgenic control mice. Thus, homozygous *THTR*(*/hSNCA+)* were taken forward for TRAP-Seq.

7.2.2 Gene expression profiling *THTR/hSNCA+* double transgenic mice

Genome-wide gene expression profiling provides a powerful tool to gain insights into early molecular alterations responsible for pathological changes and the progressive nature of human neurodegenerative diseases. The work described in Chapter 5 was based on the purification of translated mRNAs using TRAP methodology in combination with DAn-specific translatome profiling. We aimed to compare the translational profiles of young and aged *THTR/hSNCA+* double transgenic mice with unaffected control genotypes for the identification of genes and pathways that may be altered at an early stage in the disease process and during disease progression.

Analysis of genes differentially expressed with age rather than disease state found an expression decrease of genes encoding mitochondria respiratory complexes, a down-regulation which could be successfully confirmed on the protein level for the *THTR/hSNCA+* mice. Mitochondrial complex I deficiency in the SNc idiopathic PD patients was the first link between the disease and mitochondrial dysfunction (Mizuno et al., 1989; Schapira et al., 1990).

Up-regulation of Parkin expression levels was shown to protect from aSyn-induced PD symptoms in a variety of studies (Haywood and Staveley, 2004; Petrucelli et al., 2002; Shimura et al., 2001). Parkin was down-regulated on the gene and protein level in our TRAP-Seq study, which may potentially promote the deleterious effects of aSyn over-expression. In this context, we found an up-regulation of BMP7 on the gene level. The up-regulation of neurotrophic factors, such as BMP7 could aid DAn survival and serve as a neuroprotection mechanism as it has already been shown by others (Chiocco et al., 2007; Grimm et al., 2004). Administration of human recombinant BMP7 may serve as a potent treatment in a variety of diseases as already tested in clinical trials (Chiocco et al., 2007).

7.3 Future directions - *TH-bacTRAP* (*THTR*) mice

Future direction for the expression data gained with the *TH-bacTRAP* (THTR) line centre on the identification of PD-relevant changes on the midbrain DAn-specific translatome. A study by Brichta et al. focused on the discovery of key upstream regulators that mediate the observed gene expression changes in their MPTP-treated *DAT-bacTRAP* model (Brichta et al., 2015). So far, gene expression studies in neurodegenerative diseases have mainly relied on the identification of molecular players underlying the progressive cell loss by comparing gene expression levels in healthy and diseased tissue. DEGs are ranked simply based on the fold-change of their transcript levels. Computational modelling using the ARACNe algorithm can map the relationship between downstream target genes and their upstream transcriptional regulators in a tissue-specific network (Lachmann et al., 2016; Margolin et al., 2006). The Brichta study used computational modelling with ARACNe and MAster Regulator INference Algorithm (MARINa) which interrogate engineered networks with genome-wide expression signatures. Within this network, master regulators and key intrinsic upstream transcriptional regulators that mediate the response of DAn to degenerative stress can be identified, an approach that has previously been used in other studies (Carro et al., 2010; Chen et al., 2016).

A similar approach could be applied to the TRAP-Seq dataset generated in this thesis. Thereby, network or pathway analysis of differentially expressed genes can reveal clusters of altered biological functions that may underlie the development or manifestation of PD. Even though there are no overall changes in expression in the control or disease DEG-lists, it is possible to detect gene expression changes when analysing the coordinated patterns of expression (Tesson et al., 2010). The already obtained DAn translatome data will be analysed for organisation in differential co-expression gene modules in combination with the ARACNe algorithm to search for key regulators within these modules.

7.4 Discussion - ROSA26-eGFP-L10a::DAT-Cre mice

7.4.1 Conditional *ROSA26-eGFP-L10a::DAT-Cre* mice hold great potential for the analysis of changes in the disease-affected translatome in soma and axons

Work in Chapter 6 details the establishment of a Cre-conditional *ROSA26-eGFP-L10a::DAT-Cre* transgenic mouse line for translatome analysis in DAn. A DAT-Cre driver successfully mediated Cre recombination and expression of constitutively activated eGFP-L10a in DAn. In addition to the greater specificity of the DAT-Cre line as discussed previously (Lammel et al., 2015), the DAT promoter is also arguably more specific to DAn since TH is also present in other catecholaminergic neurons which requires careful microdissection to exclude the locus coeruleus from TRAP analysis. Pilot TRAP experiments successfully isolated high quality mRNA from the from dopaminergic cell populations of *ROSA26-eGFP-L10a::DAT-Cre* transgenic mice in the soma (midbrain) and axons (striatum) regardless of age.

7.5 Future directions - *ROSA26-eGFP-L10a::DAT-Cre* mice

Gene expression profiling ROSA26-eGFP-L10a::DAT-Cre::hSNCA+ transgenic mice

For future analysis, it will be important to carry out the next translatome profiling study ideally at a range of age-points covering young adult (3-6 months), middle-aged adult (12 months), and aged adult (18 months) mice using age-matched *ROSA26-eGFP-L10a::DAT-Cre::hSNCA+* and *ROSA26-eGFP-L10a::DAT-Cre* mice. PD is a progressive disease in which the majority of symptoms become

apparent at an advanced age. Furthermore, our gene expression profiling study in middle-aged bacTRAP mice was complicated by high variability between our biological replicates. Changes in underlying gene expression may provide insights into the molecular mechanisms underlying the phenotypes observed in young *hSNCA*+ mice, such as the decreased DA release in the dorsal striatum, changes in vesicle clustering, as well as the DAn degeneration and motor impairments in aged *hSNCA*+ mice as observed by the Wade-Martins laboratory (Janezic et al., 2013). Based on previous findings in our *THTR/hSNCA+* mouse line, we are particularly interested in changes associated to known DAn markers or genes involved in PD progression, as well as genes linked to inflammatory response and oxidative stress (Nakamura et al., 2011; Parihar et al., 2008; Shavali et al., 2008). Furthermore, translatome-related changes in genes involved in the ubiquitin-proteasome or autophagy system are also of great interest because they have been extensively studied in PD (Alvarez-Erviti et al., 2010; Chang et al., 2017; Snyder et al., 2003; Tanaka et al., 2001; Winslow et al., 2010)

Differential vulnerability of DAn in PD

The midbrain clusters in a variety of molecularly distinct DAn subtypes with specialised molecular, anatomical, and functional properties (Poulin et al., 2014) and their detailed analysis would aid the development of targeted therapeutics, or generally enlarge our understanding of the differential vulnerability of DAn. 'Soma TRAP' comparing SNc- and VTA-specific translatomes in our *ROSA26-eGFP-L10a::DATcre* mice could be analysed similarly to a study by Brichta et al. on their *DAT-bacTRAP* line (Brichta et al., 2015). The comparative analysis of translated mRNAs from DAn residing in the SNc and VTA could provide information on transcripts that are enriched in either of the two regions, thus, TRAP-Seq may facilitate the discovery of genes underlying differential DAn vulnerability. The analysis of SNc vs VTA transcripts during PD progression using our *hSNCA*+ model could aid the understanding of molecular complexity in midbrain DAn sub-types to finally refine and develop new therapeutic approaches for PD. A microfluidic dynamic array study by Poulin et al. identified multiple midbrain DAn sub-types by single-cell gene profiling (Poulin et al., 2014). It

would be highly interesting to broaden our analysis to include translatome-related differences in these distinct DAn clusters using TRAP in combination with our *ROSA26-eGFP-L10a::DATcre* mice.

DAn-specific changes on the axonal translatome

Translatome profiling of mRNAs located at the terminals of DAn projecting to the striatum may reveal pathological changes which affect the function of these nerve terminals and the regulation of DA release. In this context, 'axonal TRAP' could help to gain further insight into the molecular origins underlying the altered DA release profiles in the dorsal striatum and DA vesicle clustering that we see in young *hSNCA+* mice (Janezic et al., 2013). Midbrain DA neurons located in the SNc are mainly responsible for the control of movement, whereby the majority of their projections innervate the dorsal striatum. DA neurons originating in the VTA are involved in the regulation of reward, emotional behaviour and addiction and mainly project to the ventral striatum as well as cortical areas (Smith and Kieval, 2000). Thus, the dorsal striatum might be more vulnerable in PD while the ventral striatum might be more resistant (German and Manaye, 1993). In this context, our *ROSA26-eGFP-L10a::DAT-Cre* enables the analysis of midbrain-specific (DAn soma) vs striatum-specific (DAn axons and synapses) translatomes using TRAP. After optimising the TRAP methodology for the isolation of DAn-specific mRNA from axons (striatum), we aim to define the DA axonal translatome of the dorsal vs ventral striatum by 'axonal TRAP' to analyse regional vulnerability of DAn. Thereby, genes and pathways relating to synaptic function, neurotransmitter release or calcium signalling are of particular interest (Janezic et al., 2013; Nemani et al., 2010).

In a broader context, 'axonal TRAP' and subsequent gene expression profiling could be exploited to gain a better understanding of neuroplasticity, or axonal regeneration. Neurodegeneration could even be analysed in a greater variety of cell-types by making use of spatially and temporally controllable virus injections paired with TRAP. So-called 'viral-TRAP' has already been used for the analysis of a wide selection of cell-types, in which viral-injections mediated the retrograde labelling of projecting neurons to enable the isolation of specific mRNAs using TRAP (Ekstrand et al., 2014; Nectow et al., 2015; Pomeranz et al., 2017).

7.6 Outlook

Altogether, the work reported in this thesis demonstrates the relevance of gene expression profiling analysis to find disease-underlying changes of PD pathology. The innate heterogeneity of CNS cell populations has complicated gene expression profiling from distinct neuronal populations in the past and the distinct isolation of specific cell populations was time-consuming or inaccurate. We provide two TRAP mouse models that enable the specific isolation of DAn and subsequent gene expression profiling. Both serve as valuable tools to study gene expression changes in DAn. In addition, our Cre-conditional TRAP line can be crossed to any existing Cre driver making it a versatile tool to study the effects of human aSyn over-expression in a range of different cell types. The TRAP lines could even be crossed to any other available disease model or paired with the injection of aSyn fibrils to further drive PD pathology (Luk et al., 2012b; Masuda-Suzukake et al., 2013; Peelaerts et al., 2015).

Ultimately, 'soma and axonal TRAP' during PD progression will help to gain a better understanding of the translational changes underlying human aSyn-induced pathology in DAn. Studying these changes holds great potential for the identification of novel biomarkers and drug targets that can aid an earlier clinical diagnosis and treatment of PD. In this way, we can gain fundamental insight into anatomic and functional properties of the DAn that are crucial to PD pathology.

REFERENCES

Abeliovich, A., Schmitz, Y., Farinas, I., Choi-Lundberg, D., Ho, W. H., Castillo, P. E., Shinsky, N., Verdugo, J. M., Armanini, M., Ryan, A., et al. (2000). Mice lacking alpha-synuclein display functional deficits in the nigrostriatal dopamine system. *Neuron* **25**, 239–252.

Abuirmeileh, A., Harkavyi, A., Lever, R., Biggs, C. S. and Whitton, P. S. (2007). Urocortin, a CRF-like peptide, restores key indicators of damage in the substantia nigra in a neuroinflammatory model of Parkinson's disease. *J. Neuroinflammation* **4**, 19.

Ahlskog, J. E. and Muenter, M. D. (2001). Frequency of levodopa-related dyskinesias and motor fluctuations as estimated from the cumulative literature. *Mov. Disord.* **16**, 448–458.

Ahn, B. H., Rhim, H., Shi Yeon Kim, Y. M. S., Lee, M. Y., Choi, J. Y., Wolozin, B., Chang, J. S., Lee, Y. H., Kwon, T. K., Chung, K. C., et al. (2002). α-synuclein interacts with phospholipase D isozymes and inhibits pervanadate-induced phospholipase d activation in human embryonic kidney-293 cells. *J. Biol. Chem.* **277**, 12334–12342.

Ahn, T. B., Kim, S. Y., Kim, J. Y., Park, S. S., Lee, D. S., Min, H. J., Kim, Y. K., Kim, S. E., Kim, J. M., Kim, H. J., et al. (2008). α-Synuclein gene duplication is present in sporadic Parkinson disease. *Neurology* **70**, 43–49.

Ainsley, J. A., Drane, L., Jacobs, J., Kittelberger, K. A. and Reijmers, L. G. (2014). Functionally diverse dendritic mRNAs rapidly associate with ribosomes following a novel experience. *Nat. Commun.* **5**,.

Al-Wandi, A., Ninkina, N., Millership, S., Williamson, S. J. M., Jones, P. A. and Buchman, V. L. (2010). Absence of α-synuclein affects dopamine metabolism and synaptic markers in the striatum of aging mice. *Neurobiol. Aging* **31**, 796–804.

Albanèse, V., Biguet, N. F., Kiefer, H., Bayard, E., Mallet, J. and Meloni, R. (2001). Quantitative effects on gene silencing by allelic variation at a tetranucleotide microsatellite. *Hum. Mol. Genet.* **10**, 1785–1792.

Allison, M. B., Patterson, C. M., Krashes, M. J., Lowell, B. B., Myers, M. G. and Olson, D. P. (2015). TRAP-seq defines markers for novel populations of hypothalamic and brainstem LepRb neurons. *Mol. Metab.* **4**, 299–309.

Alvarez-Erviti, L., Rodriguez-Oroz, M. C., Cooper, J. M., Caballero, C., Ferrer, I., Obeso, J. A. and Schapira, A. H. V. (2010). Chaperone-Mediated Autophagy Markers in Parkinson Disease Brains. *Arch. Neurol.* **67**,.

Amin, N. M., Greco, T. M., Kuchenbrod, L. M., Rigney, M. M., Chung, M.-I., Wallingford, J. B., Cristea, I. M. and Conlon, F. L. (2014). Proteomic profiling of cardiac tissue by isolation of nuclei tagged in specific cell types (INTACT). *Development* **141**, 962–973.

Anders, S. and Huber, W. (2010). Differential expression analysis for sequence count data. *Genome Biol.* **11**,.

Anderson, J. P., Walker, D. E., Goldstein, J. M., De Laat, R., Banducci, K., Caccavello, R. J., Barbour, R., Huang, J., Kling, K., Lee, M., et al. (2006). Phosphorylation of Ser-129 is the dominant pathological modification of α-synuclein in familial and sporadic lewy body disease. *J. Biol. Chem.* **281**, 29739–29752.

Anwar, S., Peters, O., Millership, S., Ninkina, N., Doig, N., Connor-Robson, N., Threlfell, S., Kooner, G., Deacon, R. M., Bannerman, D. M., et al. (2011). Functional alterations to the nigrostriatal system in mice lacking all three members of the synuclein family. *J. Neurosci.* **31**, 7264–7274.

Appel-Cresswell, S., Vilarino-Guell, C., Encarnacion, M., Sherman, H., Yu, I., Shah, B., Weir, D., Thompson, C., Szu-Tu, C., Trinh, J., et al. (2013). Alpha-synuclein p.H50Q, a novel pathogenic mutation for Parkinson's disease. *Mov. Disord.* **28**, 811–813.

Baba, M., Nakajo, S., Tu, P. H., Tomita, T., Nakaya, K., Lee, V. M., Trojanowski, J. Q. and Iwatsubo, T. (1998). Aggregation of alpha-synuclein in Lewy bodies of sporadic Parkinson's disease and dementia with Lewy bodies. *Am. J. Pathol.* **152**, 879–84.

Bäckman, C. M., Malik, N., Zhang, Y., Shan, L., Grinberg, A., Hoffer, B. J., Westphal, H. and Tomac, A. C. (2006). Characterization of a mouse strain expressing Cre recombinase from the 3' untranslated region of the dopamine transporter locus. *Genesis* **44**, 383–90.

Bäckman, C. M., Zhang, Y. J., Malik, N., Shan, L., Hoffer, B. J., Westphal, H. and Tomac, A. C. (2009). Generalized tetracycline induced Cre recombinase expression through the ROSA26 locus of recombinant mice. *J. Neurosci. Methods* **176**, 16–23.

Baptista, M. J., O'Farrell, C., Daya, S., Ahmad, R., Miller, D. W., Hardy, J., Farrer, M. J. and Cookson, M. R. (2003). Co-ordinate transcriptional regulation of dopamine synthesis genes by alpha-synuclein in human neuroblastoma cell lines. *J Neurochem* **85**, 957–968.

Barrett, L. W., Fletcher, S. and Wilton, S. D. (2012). Regulation of eukaryotic gene expression by the untranslated gene regions and other non-coding elements. *Cell. Mol. Life Sci.* **69**, 3613–3634.

Bartels, T., Choi, J. G. and Selkoe, D. J. (2011). α-Synuclein occurs physiologically as a helically folded tetramer that resists aggregation. *Nature* **477**, 107–110.

Bates, S. (2011). The role of gene expression profiling in drug discovery. *Curr. Opin. Pharmacol.* **11**, 549–556.

Bates, T. E., Heales, S. J., Davies, S. E., Boakye, P. and Clark, J. B. (1994). Effects of 1-methyl-4-phenylpyridinium on isolated rat brain mitochondria: evidence for a primary involvement of energy depletion. *J. Neurochem.* **63**, 640–648.

Becker, T., Vögtle, F.-N., Stojanovski, D. and Meisinger, C. (2008). Sorting and assembly of mitochondrial outer membrane proteins. *Biochim. Biophys. Acta* **1777**, 557–63.

Beil, J., Fairbairn, L., Pelczar, P. and Buch, T. (2012). Is BAC transgenesis obsolete? State of the art in the era of designer nucleases. *J. Biomed. Biotechnol.* **2012**,.

Bengoa-Vergniory, N., Roberts, R. F., Wade-Martins, R. and Alegre-Abarrategui, J. (2017). Alpha-synuclein oligomers: a new hope. *Acta Neuropathol.* 1–20.

Betarbet, R., Sherer, T. B., Mackenzie, G., Garcia-osuna, M., Panov, A. V and Greenamyre, J. T. (2000). Chronic systemic pesticide exposure reproduces features of Parkinson's disease. *Nat. Neurosci.* **3**, 1301–1306.

Beyer, K. (2006). α-Synuclein structure, posttranslational modification and alternative splicing as aggregation enhancers. *Acta Neuropathol.* **112**, 237–251.

Björklund, A. and Dunnett, S. B. (2007). Dopamine neuron systems in the brain: an update. *Trends Neurosci.* **30**, 194–202.

Blesa, J. and Przedborski, S. (2014). Parkinson's disease: animal models and dopaminergic cell vulnerability. *Front Neuroanat* **8**, 155.

Bonifácio, M. J., Palma, P. N., Almeida, L. and Soares-Da-Silva, P. (2007). Catechol-O-methyltransferase and its inhibitors in Parkinson's disease. *CNS Drug Rev.* **13**, 352–379.

Bonifati, V. (2003). Mutations in the DJ-1 Gene Associated with Autosomal Recessive Early-Onset Parkinsonism. *Science (80-.).* **299**, 256–259.

Bonini, N. M. and Giasson, B. I. (2005). Snaring the function of α-synuclein. *Cell* **123**, 359–361.

Bourgeron, T., Rustin, P., Chretien, D., Birch-Machin, M., Bourgeois, M., Viegas-Péquignot, E., Munnich, a and Rötig, a (1995). Mutation of a nuclear succinate dehydrogenase gene results in mitochondrial respiratory chain deficiency. *Nat. Genet.* **11**, 144–149.

Braak, H., Sandmann-Keil, D., Gai, W. and Braak, E. (1999). Extensive axonal Lewy neurites in Parkinson's disease: A novel pathological feature revealed by Alpha-synuclein immunocytochemistry. *Neurosci. Lett.* **265**, 67–69.

Braak, H., Del Tredici, K., Rüb, U., De Vos, R. A. I., Jansen Steur, E. N. H. and Braak, E. (2003). Staging of brain pathology related to sporadic Parkinson's disease. *Neurobiol. Aging* **24**, 197–211.

Bray, N. L., Pimentel, H., Melsted, P. and Pachter, L. (2016). Near-optimal probabilistic RNA-seq quantification. *Nat. Biotechnol.* **34**, 525–527.

Brichta, L., Shin, W., Jackson-Lewis, V., Blesa, J., Yap, E.-L., Walker, Z., Zhang, J., Roussarie, J.-P., Alvarez, M. J., Califano, A., et al. (2015). Identification of neurodegenerative factors using translatome–regulatory network analysis. *Nat. Neurosci.* **18**, 1325–1333.

Brocard, J., Feil, R., Chambon, P. and Metzger, D. (1998). A chimeric Cre recombinase inducible by synthetic,but not by natural ligands of the glucocorticoid receptor. *Nucleic Acids Res.* **26**, 4086–90.

Brown, A. L., Day, T. A., Dayas, C. V. and Smith, D. W. (2013). Purity and enrichment of laser-microdissected midbrain dopamine neurons. *Biomed Res. Int.* **2013**,.

Buchman, V. L. and Ninkina, N. (2008). Modulation of alpha-synuclein expression in transgenic animals for modelling synucleinopathies--is the juice worth the squeeze? *Neurotox Res* **14**, 329–341.

Bunge, M. B. (1973). Fine structure of nerve fibers and growth cones of isolated sympathetic neurons in culture. *J. Cell Biol.* **56**, 713–35.

Burre, J., Sharma, M., Tsetsenis, T., Buchman, V., Etherton, M. R. and Sudhof, T. C. (2010). Alpha-Synuclein Promotes SNARE-Complex Assembly in Vivo and in Vitro. *Science (80-.).* **329**, 1663–1667.

Burre, J., Sharma, M. and Sudhof, T. C. (2015). Definition of a Molecular Pathway Mediating -Synuclein Neurotoxicity. *J. Neurosci.* **35**, 5221–5232.

Burré, J., Vivona, S., Diao, J., Sharma, M., Brunger, A. T. and Südhof, T. C. (2013). Properties of native brain α-synuclein. *Nature* **498**, E4–E6.

Burré, J., Sharma, M. and Südhof, T. C. (2014). α-Synuclein assembles into higher-order multimers upon membrane binding to promote SNARE complex formation. *Proc. Natl. Acad. Sci.* **111**, E4274–E4283.

Cabin, D. E., Shimazu, K., Murphy, D., Cole, N. B., Gottschalk, W., McIlwain, K. L., Orrison, B., Chen, A., Ellis, C. E., Paylor, R., et al. (2002). Synaptic vesicle depletion correlates with attenuated synaptic responses to prolonged repetitive stimulation in mice lacking alpha-synuclein. *J. Neurosci.* **22**, 8797–807.

Cabin, D. E., Gispert-Sanchez, S., Murphy, D., Auburger, G., Myers, R. R. and Nussbaum, R. L. (2005). Exacerbated synucleinopathy in mice expressing A53T SNCA on a Snca null background. *Neurobiol. Aging* **26**, 25–35.

Campbell, D. S. and Holt, C. E. (2001). Chemotropic responses of retinal growth cones mediated by rapid local protein synthesis and degradation. *Neuron* **32**, 1013–1026.

Campion, D., Martin, C., Heilig, R., Charbonnier, F., Moreau, V., Flaman, J. M., Petit, J. L., Hannequin, D., Brice, A. and Frebourg, T. (1995). The NACP/synuclein gene: chromosomal assignment and screening for

alterations in Alzheimer disease. *Genomics* **26**, 254–257.

Carro, M. S., Lim, W. K., Alvarez, M. J., Bollo, R. J., Zhao, X., Snyder, E. Y., Sulman, E. P., Anne, S. L., Doetsch, F., Colman, H., et al. (2010). The transcriptional network for mesenchymal transformation of brain tumours. *Nature* **463**, 318–325.

Carvey, P. M., Punati, A. and Newman, M. B. (2006). Progressive dopamine neuron loss in Parkinson's disease: The multiple hit hypothesis. *Cell Transplant.* **15**, 239–250.

Casola, S. (2010). Mouse models for miRNA expression: the ROSA26 locus. *Methods Mol. Biol.* **667**, 145–163.

Caughey, B. and Lansbury, P. T. (2003). PROTOFIBRILS, PORES, FIBRILS, AND NEURODEGENERATION: Separating the Responsible Protein Aggregates from The Innocent Bystanders. *Annu. Rev. Neurosci.* **26**, 267–298.

Chandra, S., Fornai, F., Kwon, H.-B., Yazdani, U., Atasoy, D., Liu, X., Hammer, R. E., Battaglia, G., German, D. C., Castillo, P. E., et al. (2004). Double-knockout mice for alpha- and beta-synucleins: effect on synaptic functions. *Proc. Natl. Acad. Sci. U. S. A.* **101**, 14966–71.

Chandra, S., Gallardo, G., Fernández-Chacón, R., Schlüter, O. M. and Südhof, T. C. (2005). Alpha-synuclein cooperates with CSPalpha in preventing neurodegeneration. *Cell* **123**, 383–396.

Chang, D., Nalls, M. A., Hallgrímsdóttir, I. B., Hunkapiller, J., van der Brug, M., Cai, F., Kerchner, G. A., Ayalon, G., Bingol, B., Sheng, M., et al. (2017). A meta-analysis of genome-wide association studies identifies 17 new Parkinson's disease risk loci. *Nat. Genet.*

Chartier-Harlin, M. C., Kachergus, J., Roumier, C., Mouroux, V., Douay, X., Lincoln, S., Levecque, C., Larvor, L., Andrieux, J., Hulihan, M., et al. (2004). alpha-Synuclein locus duplication as a cause of familial Parkinson's disease. *Lancet* **364**, 1167–1169.

Chaudhuri, K. R., Healy, D. G. and Schapira, A. H. (2006). Non-motor symptoms of Parkinson's disease: diagnosis and management. *Lancet Neurol.* **5**, 235–245.

Checkoway, H., Powers, K., Smith-Weller, T., Franklin, G. M., Longstreth, W. T. and Swanson, P. D. (2002). Parkinson's Disease Risks Associated with Cigarette Smoking, Alcohol Consumption, and Caffeine Intake. *Am. J. Epidemiol.* **155**, 732–738.

Chen, X., de Silva, H. A. R., Pettenati, M. J., Rao, P. N., George-Hyslop, P. St., Roses, A. D., Xia, Y., Horsburgh, K., Uéda, K., Saitoh, T., et al. (1995). The human NACP/α-synuclein gene: chromosome assignment to 4q21.3–q22 and TaqI RFLP analysis. *Genomics* **26**, 425–427.

Chen, J. C., Alvarez, M. J., Talos, F., Dhruv, H., Rieckhof, G. E., Iyer, A., Diefes, K. L., Aldape, K., Berens, M., Shen, M. M., et al. (2016). Identification of Causal Genetic Drivers of Human Disease through Systems-Level Analysis of Regulatory Networks (Cell (2014) 159(2) (402–414)). *Cell* **166**, 1055.

Cheng, M. Y., Hartl, F.-U., Martin, J., Pollock, R. A., Kalousek, F., Neuper, W., Hallberg, E. M., Hallberg, R. L. and Horwich, A. L. (1989). Mitochondrial heat-shock protein hsp60 is essential for assembly of proteins imported into yeast mitochondria. *Nature* **337**, 620–625.

Chiba-Falek, O., Lopez, G. J. and Nussbaum, R. L. (2006). Levels of alpha-synuclein mRNA in sporadic Parkinson disease patients. *Mov. Disord.* **21**, 1703–1708.

Chinta, S. J., Mallajosyula, J. K., Rane, A. and Andersen, J. K. (2010). Mitochondrial alpha-synuclein accumulation impairs complex I function in dopaminergic neurons and results in increased mitophagy in vivo. *Neurosci. Lett.* **486**, 235–239.

Chiocco, M. J., Harvey, B. K., Wang, Y. and Hoffer, B. J. (2007). Neurotrophic factors for the treatment of Parkinson's disease. *Parkinsonism Relat. Disord.* **13 Suppl 3**, S321-8.

Chiueh, C. C., Markey, S. P., Burns, R. S., Johannessen, J. N., Pert, A. and Kopin, I. J. (1984). Neurochemical and behavioral effects of systematic and intranigral administration of N-methyl-4-phenyl-1,2,3,6-tetrahydropyridine in the rat. *Eur. J. Pharmacol.* **100**, 189–194.

Chu, Y., Goldman, J. G., Kelly, L., He, Y., Waliczek, T. and Kordower, J. H. (2014). Abnormal alpha-synuclein reduces nigral voltage-dependent anion channel 1 in sporadic and experimental Parkinson's disease. *Neurobiol. Dis.* **69**, 1–14.

Chung, K. K., Zhang, Y., Lim, K. L., Tanaka, Y., Huang, H., Gao, J., Ross, C. a, Dawson, V. L. and Dawson, T. M. (2001). Parkin ubiquitinates the alpha-synuclein-interacting protein, synphilin-1: implications for Lewy-body formation in Parkinson disease. *Nat.Med.* **7**, 1144–1150.

Chung, C. Y., Seo, H., Sonntag, K. C., Brooks, A., Lin, L. and Isacson, O. (2005). Cell type-specific gene expression of midbrain dopaminergic neurons reveals molecules involved in their vulnerability and protection. *Hum. Mol. Genet.* **14**, 1709–1725.

Collier, T. J., Kanaan, N. M. and Kordower, J. H. (2011). Ageing as a primary risk factor for Parkinson's disease: evidence from studies of non-human primates. *Nat. Rev. Neurosci.* **12**, 359–366.

Comi, C., Magistrelli, L., Oggioni, G. D., Carecchio, M., Fleetwood, T., Cantello, R., Mancini, F. and Antonini, A. (2014). Peripheral nervous system involvement in Parkinson's disease: Evidence and controversies. *Park. Relat. Disord.* **20**, 1329–1334.

Connor-Robson, N., Peters, O. M., Millership, S., Ninkina, N. and Buchman, V. L. (2016). Combinational losses of synucleins reveal their differential requirements for compensating age-dependent alterations in motor behavior and dopamine metabolism. *Neurobiol. Aging* **46**, 107–112.

Conway, K. A., Lee, S.-J., Rochet, J.-C., Ding, T. T., Williamson, R. E. and Lansbury, P. T. (2000). Acceleration of oligomerization, not fibrillization, is a shared property of both alpha -synuclein mutations linked to early-onset Parkinson's disease: Implications for pathogenesis and therapy. *Proc. Natl. Acad. Sci.* **97**, 571–576.

Cook-Snyder, D. R., Jones, A. and Reijmers, L. G. (2015). A retrograde adeno-associated virus for collecting ribosome-bound mRNA from anatomically defined projection neurons. *Front. Mol. Neurosci.* **8**,.

Cookson, M. R., Hardy, J. and Lewis, P. A. (2008). Genetic neuropathology of Parkinson's disease. *Int. J. Clin. Exp. Pathol.* **1**, 217–231.

Cronin, K. D., Ge, D., Manninger, P., Linnertz, C., Rossoshek, A., Orrison, B. M., Bernard, D. J., El-Agnaf, O. M. A., Schlossmacher, M. G., Nussbaum, R. L., et al. (2009). Expansion of the Parkinson disease-associated SNCA-Rep1 allele upregulates human α-synuclein in transgenic mouse brain. *Hum. Mol. Genet.* **18**, 3274–3285.

Crowther, R. A., Jakes, R., Spillantini, M. G. and Goedert, M. (1998). Synthetic filaments assembled from C-terminally truncated α-synuclein. *FEBS Lett.* **436**, 309–312.

Csárdi, G. and Nepusz, T. (2006). The igraph software package for complex network research. *InterJournal Complex Syst.* **1695**, 1–9.

Dauer, W. and Przedborski, S. (2003). Parkinson's disease: Mechanisms and models. *Neuron* **39**, 889–909.

Dauer, W., Kholodilov, N., Vila, M., Trillat, A. C., Goodchild, R., Larsen, K. E., Staal, R., Tieu, K., Schmitz, Y., Yuan, C. A., et al. (2002). Resistance of alpha-synuclein null mice to the parkinsonian neurotoxin MPTP. *Proc. Natl. Acad. Sci.* **99**, 14524–14529.

Davidson, W. S., Jonas, a, Clayton, D. F. and George, J. M. (1998). Stabilization of alpha-synuclein secondary structure upon binding to synthetic membranes. *J. Biol. Chem.* **273**, 9443–9.

Davis, G. C., Williams, A. C., Markey, S. P., Ebert, M. H., Caine, E. D., Reichert, C. M. and Kopin, I. J. (1979). Chronic parkinsonism secondary to intravenous injection of meperidine analogues. *Psychiatry Res.* **1**, 249–254.

Dawson, T. M., Ko, H. S. and Dawson, V. L. (2010). Genetic Animal Models of Parkinson's Disease. *Neuron* **66**, 646–661.

Deal, R. B. and Henikoff, S. (2010). A simple method for gene expression and chromatin profiling of individual cell types within a tissue. *Dev. Cell* **18**, 1030–40.

De Pinto, V., Messina, A., Lane, D. J. R. and Lawen, A. (2010). Voltage-dependent anion-selective channel (VDAC) in the plasma membrane. *FEBS Lett.* **584**, 1793–1799.

Decressac, M., Mattsson, B., Lundblad, M., Weikop, P. and Björklund, A. (2012). Progressive neurodegenerative and behavioural changes induced by AAV-mediated overexpression of α-synuclein in midbrain dopamine neurons. *Neurobiol. Dis.* **45**, 939–953.

Desplats, P., Lee, H.-J., Bae, E.-J., Patrick, C., Rockenstein, E., Crews, L., Spencer, B., Masliah, E. and Lee, S.-J. (2009). Inclusion formation and neuronal cell death through neuron-to-neuron transmission of Alpha-synuclein. *Proc. Natl. Acad. Sci.* **106**, 13010–13015.

Devi, L. and Anandatheerthavarada, H. K. (2010). Mitochondrial trafficking of APP and alpha synuclein: Relevance to mitochondrial dysfunction in Alzheimer's and Parkinson's diseases. *Biochim. Biophys. Acta - Mol. Basis Dis.* **1802**, 11–19.

Devi, L., Prabhu, B. M., Galati, D. F., Avadhani, N. G. and Anandatheerthavarada, H. K. (2006). Accumulation of amyloid precursor protein in the mitochondrial import channels of human Alzheimer's disease brain is associated with mitochondrial dysfunction. *J. Neurosci.* **26**, 9057–9068.

Devi, L., Raghavendran, V., Prabhu, B. M., Avadhani, N. G. and Anandatheerthavarada, H. K. (2008). Mitochondrial import and accumulation of alpha-synuclein impair complex I in human dopaminergic neuronal cultures and Parkinson disease brain. *J. Biol. Chem.* **283**, 9089–9100.

Di Fonzo, A., Dekker, M. C. J., Montagna, P., Baruzzi, A., Yonova, E. H., Correia Guedes, L., Szczerbinska, A., Zhao, T., Dubbel-Hulsman, L. O. M., Wouters, C. H., et al. (2009). FBXO7 mutations cause autosomal recessive, early-onset parkinsonian-pyramidal syndrome. *Neurology* **72**, 240–5.

Dickson, D. W., Fujishiro, H., Orr, C., DelleDonne, A., Josephs, K. A., Frigerio, R., Burnett, M., Parisi, J. E., Klos, K. J. and Ahlskog, J. E. (2009). Neuropathology of non-motor features of Parkinson disease. *Park. Relat. Disord.* **15**,.

Dillies, M. A., Rau, A., Aubert, J., Hennequet-Antier, C., Jeanmougin, M., Servant, N., Keime, C., Marot, N. S., Castel, D., Estelle, J., et al. (2013). A comprehensive evaluation of normalization methods for Illumina high-throughput RNA sequencing data analysis. *Brief. Bioinform.* **14**, 671–683.

Dolginow, Y. D. (2005). The next decade of gene expression profiling. *Drug Discov. World* **6**, 55–62.

Dougherty, J. D., Schmidt, E. F., Nakajima, M. and Heintz, N. (2010). Analytical approaches to RNA profiling data for the identification of genes enriched in specific cells. *Nucleic Acids Res.* **38**, 4218–4230.

Doyle, J. P., Dougherty, J. D., Heiman, M., Schmidt, E. F., Stevens, T. R., Ma, G., Bupp, S., Shrestha, P., Shah, R. D., Doughty, M. L., et al. (2008). Application of a translational profiling approach for the comparative analysis of CNS cell types. *Cell* **135**, 749–762.

Drane, L., Ainsley, J. A., Mayford, M. R. and Reijmers, L. G. (2014). A transgenic mouse line for collecting ribosome-bound mRNA using the tetracycline transactivator system. *Front. Mol. Neurosci.* **7**,.

Durinck, S., Moreau, Y., Kasprzyk, A., Davis, S., De Moor, B., Brazma, A. and Huber, W. (2005). BioMart and

Bioconductor: A powerful link between biological databases and microarray data analysis. *Bioinformatics* **21**, 3439–3440.

Durinck, S., Spellman, P. T., Birney, E. and Huber, W. (2009). Mapping identifiers for the integration of genomic datasets with the R/Bioconductor package biomaRt. *Nat. Protoc.* **4**, 1184–1191.

Dutta, S. and Sengupta, P. (2016). Men and mice: Relating their ages. *Life Sci.* **152**, 244–248.

Ekstrand, M. I., Nectow, A. R., Knight, Z. A., Latcha, K. N., Pomeranz, L. E. and Friedman, J. M. (2014). Molecular profiling of neurons based on connectivity. *Cell* **157**, 1230–1242.

Emborg, M. E., Ma, S. Y., Mufson, E. J., Levey, A. I., Taylor, M. D., Brown, W. D., Holden, J. E. and Kordower, J. H. (1998). Age-related declines in nigral neuronal function correlate with motor impairments in rhesus monkeys. *J. Comp. Neurol.* **401**, 253–265.

Emery, B. and Barres, B. A. (2008). Unlocking CNS cell type heterogeneity. *Cell* **135**, 596–8.

Emmert-Buck, M. R., Bonner, R. F., Smith, P. D., Chuaqui, R. F., Zhuang, Z., Goldstein, S. R., Weiss, R. A. and Liotta, L. A. (1996). Laser Capture Microdissection. *Science (80-.).* **274**, 998–1001.

Fahn, S. (2015). The medical treatment of Parkinson disease from James Parkinson to George Cotzias. *Mov. Disord.* **30**, 4–18.

Fares, M. B., Ait-Bouziad, N., Dikiy, I., Mbefo, M. K., Jovičić, A., Kiely, A., Holton, J. L., Lee, S. J., Gitler, A. D., Eliezer, D., et al. (2014). The novel Parkinson's disease linked mutation G51D attenuates in vitro aggregation and membrane binding of α-synuclein, and enhances its secretion and nuclear localization in cells. *Hum. Mol. Genet.* **23**, 4491–4509.

Fauvet, B., Mbefo, M. K., Fares, M. B., Desobry, C., Michael, S., Ardah, M. T., Tsika, E., Coune, P., Prudent, M., Lion, N., et al. (2012). α-Synuclein in central nervous system and from erythrocytes, mammalian cells, and Escherichia coli exists predominantly as disordered monomer. *J. Biol. Chem.* **287**, 15345–15364.

Feany, M. B. and Bender, W. W. (2000). A Drosophila model of Parkinson's disease. *Nature* **404**, 394–398.

Fearnley, J. M. and Lees, A. J. (1991). Ageing and Parkinson's disease: substantia nigra regional selectivity. *Brain* **114 (Pt 5**, 2283–2301.

Fernagut, P. O. and Chesselet, M. F. (2004). Alpha-synuclein and transgenic mouse models. *Neurobiol Dis* **17**, 123–130.

Finkel, T. and Holbrook, N. J. (2000). Oxidants, oxidative stress and the biology of ageing. *Nature* **408**, 239–247.

Fleming, S. M., Tetreault, N. A., Mulligan, C. K., Hutson, C. B. C. B., Masliah, E. and Chesselet, M.-F. F. (2008). Olfactory deficits in mice overexpressing human wildtype alpha-synuclein. *Eur. J. Neurosci.* **28**, 247–256.

Flurkey, K., M. Currer, J. and Harrison, D. E. (2007). *The Mouse in Biomedical Research*.

Forno, L. S. (1987). The Lewy body in Parkinson's disease. *Adv Neurol* **45**, 35–43.

Fountaine, T. M., Venda, L. L., Warrick, N., Christian, H. C., Brundin, P., Channon, K. M. and Wade-Martins, R. (2008). The effect of alpha-synuclein knockdown on MPP plus toxicity in models of human neurons. *Eur. J. Neurosci.* **28**, 2459–2473.

Friedrich, G. and Soriano, P. (1991). Promoter traps in embryonic stem cells: A genetic screen to identify and mutate developmental genes in mice. *Genes Dev.* **5**, 1513–1523.

Fujiwara, H., Hasegawa, M., Dohmae, N., Kawashima, A., Masliah, E., Goldberg, M. S., Shen, J., Takio, K. and Iwatsubo, T. (2002). α-Synuclein is phosphorylated in synucleinopathy lesions. *Nat. Cell Biol.* **4**, 160–164.

Fukai, T. and Ushio-Fukai, M. (2011). Superoxide Dismutases: Role in Redox Signaling, Vascular Function, and Diseases. *Antioxid. Redox Signal.* **15**, 1583–1606.

Gaig, C., Martí, M. J., Ezquerra, M., Rey, M. J., Cardozo, A. and Tolosa, E. (2007). G2019S LRRK2 mutation causing Parkinson's disease without Lewy bodies. *J. Neurol. Neurosurg. Psychiatry* **78**, 626–8.

Gallego Romero, I., Pai, A. A., Tung, J. and Gilad, Y. (2014). RNA-seq: impact of RNA degradation on transcript quantification. *BMC Biol.* **12**, 42.

Galloway, P. G., Mulvihill, P. and Perry, G. (1992). Filaments of Lewy bodies contain insoluble cytoskeletal elements. *Am. J. Pathol.* **140**, 809–822.

Gandelman, K. Y., Coker, G. T., Moffat, M. and O'Malley, K. L. (1990). Species and regional differences in the expression of cell-type specific elements at the human and rat tyrosine hydroxylase gene loci. *J. Neurochem.* **55**, 2149–52.

Gao, N., Li, Y.-H., Li, X., Yu, S., Fu, G.-L. and Chen, B. (2007). Effect of alpha-synuclein on the promoter activity of tyrosine hydroxylase gene. *Neurosci. Bull.* **23**, 53–7.

Gao, L., Hidalgo-Figueroa, M., Escudero, L. M., Díaz-Martín, J., López-Barneo, J. and Pascual, A. (2013). Age-Mediated Transcriptomic Changes in Adult Mouse Substantia Nigra. *PLoS One* **8**,.

Garcia-Reitboeck, P., Anichtchik, O., Dalley, J. W., Ninkina, N., Tofaris, G. K., Buchman, V. L. and Spillantini, M. G. (2013). Endogenous alpha-synuclein influences the number of dopaminergic neurons in mouse substantia nigra. *Exp. Neurol.* **248**, 541–545.

Geisler, S., Holmström, K. M., Skujat, D., Fiesel, F. C., Rothfuss, O. C., Kahle, P. J. and Springer, W. (2010). PINK1/Parkin-mediated mitophagy is dependent on VDAC1 and p62/SQSTM1. *Nat. Cell Biol.* **12**, 119–131.

George, J. M. (2002). The synucleins. *Genome Biol.* **3**, REVIEWS3002.

George, J. M., Jin, H., Woods, W. S. and Clayton, D. F. (1995). Characterization of a novel protein regulated during the critical period for song learning in the zebra finch. *Neuron* **15**, 361–372.

German, D. C. and Manaye, K. F. (1993). Midbrain dopaminergic neurons (nuclei A8, A9, and A10): Three-dimensional reconstruction in the rat. *J. Comp. Neurol.* **331**, 297–309.

Ghosh, D., Mondal, M., Mohite, G. M., Singh, P. K., Ranjan, P., Anoop, A., Ghosh, S., Jha, N. N., Kumar, A. and Maji, S. K. (2013). The Parkinson's disease-associated H50Q mutation accelerates alpha-Synuclein aggregation in vitro. *Biochemistry* **52**, 6925–6927.

Ghosh, D., Sahay, S., Ranjan, P., Salot, S., Mohite, G. M., Singh, P. K., Dwivedi, S., Carvalho, E., Banerjee, R., Kumar, A., et al. (2014). The newly discovered Parkinsons disease associated finnish mutation (A53E) attenuates Alpha-synuclein aggregation and membrane binding. *Biochemistry* **53**, 6419–6421.

Giasson, B. I. (2000). Oxidative Damage Linked to Neurodegeneration by Selective alpha-Synuclein Nitration in Synucleinopathy Lesions. *Science (80-.).* **290**, 985–989.

Giasson, B. I., Murray, I. V. J., Trojanowski, J. Q. and Lee, V. M. Y. (2001). A Hydrophobic Stretch of 12 Amino Acid Residues in the Middle of alpha-Synuclein Is Essential for Filament Assembly. *J. Biol. Chem.* **276**, 2380–2386.

Giasson, B. I., Duda, J. E., Quinn, S. M., Zhang, B., Trojanowski, J. Q. and Lee, V. M.-Y. (2002). Neuronal alpha-synucleinopathy with severe movement disorder in mice expressing A53T human alpha-synuclein. *Neuron* **34**, 521–533.

Giasson, B. I., Lee, V. M.-Y. and Trojanowski, J. Q. (2003). Interactions of amyloidogenic proteins. *Neuromolecular Med.* **4**, 49–58.

Gilks, W. P., Abou-Sleiman, P. M., Gandhi, S., Jain, S., Singleton, A., Lees, A. J., Shaw, K., Bhatia, K. P., Bonifati, V., Quinn, N. P., et al. (2005). A common LRRK2 mutation in idiopathic Parkinson's disease. *Lancet* **365**, 415–416.

Gillies, G. E., Pienaar, I. S., Vohra, S. and Qamhawi, Z. (2014). Sex differences in Parkinson's disease. *Front. Neuroendocrinol.* **35**, 370–384.

Gispert, S., Del Turco, D., Garrett, L., Chen, A., Bernard, D. J., Hamm-Clement, J., Korf, H. W., Deller, T., Braak, H., Auburger, G., et al. (2003). Transgenic mice expressing mutant A53T human alpha-synuclein show neuronal dysfunction in the absence of aggregate formation. *Mol. Cell. Neurosci.* **24**, 419–429.

Giuditta, A., Dettbarn, W. D. and Brzin, M. (1968). Protein synthesis in the isolated giant axon of the squid. *Proc. Natl. Acad. Sci. U. S. A.* **59**, 1284–7.

Giuditta, A., Hunt, T. and Santella, L. (1986). Messenger RNA in squid axoplasm. *Neurochem. Int.* **8**, 435–42.

Giuditta, A., Menichini, E., Capano, C. P., Langella, M., Martin, R., Castigli, E. and Kaplan, B. B. (1991). Active polysomes in the axoplasm of the squid giant axon. *J. Neurosci. Res.* **28**, 18–28.

Goedert, M., Spillantini, M. G., Del Tredici, K. and Braak, H. (2012). 100 years of Lewy pathology. *Nat. Rev. Neurol.* **9**, 13–24.

Gong, S., Zheng, C., Doughty, M. L., Losos, K., Didkovsky, N., Schambra, U. B., Nowak, N. J., Joyner, A., Leblanc, G., Hatten, M. E., et al. (2003). A gene expression atlas of the central nervous system based on bacterial artificial chromosomes. *Nature* **425**, 917–925.

Goto, S. and Hirano, A. (1991). Catecholaminergic neurons in the parabrachial nucleus of normal individuals and patients with idiopathic Parkinson's disease. *Ann Neurol* **30**, 192–196.

Grace, A. A. and Bunney, B. S. (1984). The control of firing pattern in nigral dopamine neurons: single spike firing. *J. Neurosci.* **4**, 2866–2876.

Gracida, X. and Calarco, J. A. (2017). Cell type-specific transcriptome profiling in C. elegans using the Translating Ribosome Affinity Purification technique. *Methods*.

Greene, J. G., Dingledine, R. and Greenamyre, J. T. (2005). Gene expression profiling of rat midbrain dopamine neurons: Implications for selective vulnerability in parkinsonism. *Neurobiol. Dis.* **18**, 19–31.

Greten-Harrison, B., Polydoro, M., Morimoto-Tomita, M., Diao, L., Williams, A. M., Nie, E. H., Makani, S., Tian, N., Castillo, P. E., Buchman, V. L., et al. (2010). alphabetagamma-Synuclein triple knockout mice reveal age-dependent neuronal dysfunction. *Proc Natl Acad Sci U S A* **107**, 19573–19578.

Grimm, J., Mueller, A., Hefti, F. and Rosenthal, A. (2004). Molecular basis for catecholaminergic neuron diversity. *Proc. Natl. Acad. Sci. U. S. A.* **101**, 13891–6.

Gründemann, J., Schlaudraff, F., Haeckel, O. and Liss, B. (2008). Elevated α-synuclein mRNA levels in individual UV-laser-microdissected dopaminergic substantia nigra neurons in idiopathic Parkinson's disease. *Nucleic Acids Res.* **36**,.

Guardia-Laguarta, C., Area-Gomez, E., Rub, C., Liu, Y., Magrane, J., Becker, D., Voos, W., Schon, E. A. and Przedborski, S. (2014). Alpha-Synuclein Is Localized to Mitochondria-Associated ER Membranes. *J. Neurosci.* **34**, 249–259.

Guardia-Laguarta, C., Area-Gomez, E., Schon, E. A. and Przedborski, S. (2015). A new role for α-synuclein in Parkinson's disease: Alteration of ER–mitochondrial communication. *Mov. Disord.* **30**, 1026–1033.

Guez-Barber, D., Fanous, S., Harvey, B. K., Zhang, Y., Lehrmann, E., Becker, K. G., Picciotto, M. R. and Hope, B. T. (2012). FACS purification of immunolabeled cell types from adult rat brain. *J. Neurosci. Methods* **203**, 10–8.

Gumy, L. F., Yeo, G. S. H., Tung, Y.-C. L., Zivraj, K. H., Willis, D., Coppola, G., Lam, B. Y. H., Twiss, J. L., Holt, C. E. and Fawcett, J. W. (2011). Transcriptome analysis of embryonic and adult sensory axons reveals changes in mRNA repertoire localization. *RNA* **17**, 85–98.

Guzman, J. N., Sanchez-Padilla, J., Chan, C. S. and Surmeier, D. J. (2009). Robust Pacemaking in Substantia Nigra Dopaminergic Neurons. *J. Neurosci.* **29**, 11011–11019.

Gygi, S. P., Rochon, Y., Franza, B. R. and Aebersold, R. (1999). Correlation between Protein and mRNA Abundance in Yeast. *Mol. Cell. Biol.* **19**, 1720–1730.

Haavik, J. and Toska, K. (1998). Tyrosine hydroxylase and Parkinson's disease. *Mol Neurobiol* **16**, 285–309.

Haaxma, C. a, Bloem, B. R., Borm, G. F., Oyen, W. J. G., Leenders, K. L., Eshuis, S., Booij, J., Dluzen, D. E., Horstink, M. W. I. M. and Shulman, L. M. (2007). Gender Differences in Parkinson's Disease. *J. Neurol. Neurosurg. Psychiatry* **78**, 819–24.

Halbeisen, R. E. and Gerber, A. P. (2009). Stress-dependent coordination of transcriptome and translatome in yeast. *PLoS Biol.* **7**,.

Hallett, P. J., McLean, J. R., Kartunen, A., Langston, J. W. and Isacson, O. (2012). Alpha-synuclein overexpressing transgenic mice show internal organ pathology and autonomic deficits. *Neurobiol. Dis.* **47**, 258–267.

Hamilton, B. A. (2004). α-Synuclein A53T substitution associated with Parkinson disease also marks the divergence of Old World and New World primates. *Genomics* **83**, 739–742.

Hamza, T. H., Zabetian, C. P., Tenesa, A., Laederach, A., Montimurro, J., Yearout, D., Kay, D. M., Doheny, K. F., Paschall, J., Pugh, E., et al. (2010). Common genetic variation in the HLA region is associated with late-onset sporadic Parkinson's disease. *Nat. Genet.* **42**, 781–785.

Hansen, C., Angot, E., Bergström, A. L., Steiner, J. A., Pieri, L., Paul, G., Outeiro, T. F., Melki, R., Kallunki, P., Fog, K., et al. (2011). α-Synuclein propagates from mouse brain to grafted dopaminergic neurons and seeds aggregation in cultured human cells. *J. Clin. Invest.* **121**, 715–725.

Hansen, C., Björklund, T., Petit, G. H., Lundblad, M., Murmu, R. P., Brundin, P. and Li, J. Y. (2013). A novel α-synuclein-GFP mouse model displays progressive motor impairment, olfactory dysfunction and accumulation of α-synuclein-GFP. *Neurobiol. Dis.* **56**, 145–155.

Harman, D. (1956). Aging: A Theory Based on Free Radical and Radiation Chemistry. *J. Gerontol.* **11**, 298–300.

Harman, D. (2009). Origin and evolution of the free radical theory of aging: A brief personal history, 1954-2009. *Biogerontology* **10**, 773–781.

Hasegawa, M., Fujiwara, H., Nonaka, T., Wakabayashi, K., Takahashi, H., Lee, V. M.-Y., Trojanowski, J. Q., Mann, D. and Iwatsubo, T. (2002). Phosphorylated alpha-synuclein is ubiquitinated in alpha-synucleinopathy lesions. *J. Biol. Chem.* **277**, 49071–49076.

Hashimoto, M., Hsu, L. J., Xia, Y., Takeda, a, Sisk, a, Sundsmo, M. and Masliah, E. (1999a). Oxidative stress induces amyloid-like aggregate formation of NACP/alpha-synuclein in vitro. *Neuroreport* **10**, 717–721.

Hashimoto, M., Takeda, A., Hsu, L. J., Takenouchi, T. and Masliah, E. (1999b). Role of cytochrome c as a stimulator of α-synuclein aggregation in Lewy body disease. *J. Biol. Chem.* **274**, 28849–28852.

Haywood, A. F. M. and Staveley, B. E. (2004). Parkin counteracts symptoms in a Drosophila model of Parkinson's disease. *BMC Neurosci.* **5**, 14.

Heard, E., Tishkoff, S., Todd, J. A., Vidal, M., Wagner, G. P., Wang, J., Weigel, D. and Young, R. (2010). Ten years of genetics and genomics: What have we achieved and where are we heading? *Nat. Rev. Genet.* **11**, 723–733.

Heiman, M., Schaefer, A., Gong, S., Peterson, J. D., Day, M., Ramsey, K. E., Suárez-Fariñas, M., Schwarz, C., Stephan, D. A., Surmeier, D. J., et al. (2008). A translational profiling approach for the molecular characterization of CNS cell types. *Cell* **135**, 738–48.

Heiman, M., Kulicke, R., Fenster, R. J., Greengard, P. and Heintz, N. (2014). Cell type-specific mRNA purification by translating ribosome affinity purification (TRAP). *Nat Protoc* **9**, 1282–1291.

Heintz, N. (2001). {BAC} to the future: the use of bac transgenic mice for neuroscience research. *Nat. Rev. Neurosci.* **2**, 861–870.

Helferich, A. M., Ruf, W. P., Grozdanov, V., Freischmidt, A., Feiler, M. S., Zondler, L., Ludolph, A. C., McLean, P. J., Weishaupt, J. H. and Danzer, K. M. (2015). α-synuclein interacts with SOD1 and promotes its oligomerization. *Mol. Neurodegener.* **10**, 66.

Henry, G. L., Davis, F. P., Picard, S. and Eddy, S. R. (2012). Cell type-specific genomics of Drosophila neurons. *Nucleic Acids Res.* **40**, 9691–704.

Hernán, M. A., Takkouche, B., Caamaño-Isorna, F. and Gestal-Otero, J. J. (2002). A meta-analysis of coffee drinking, cigarette smoking, and the risk of Parkinson's disease. *Ann. Neurol.* **52**, 276–284.

Hirsch, E., Graybiel, a M. and Agid, Y. a (1988). Melanized dopaminergic neurons are differentially susceptible to degeneration in Parkinson's disease. *Nature* **334**, 345–348.

Hitoshi, N., Ken-ichi, Y. and Jun-ichi, M. (1991). Efficient selection for high-expression transfectants with a novel eukaryotic vector. *Gene* **108**, 193–199.

Holt, C. E. and Schuman, E. M. (2013). The central dogma decentralized: New perspectives on RNA function and local translation in neurons. *Neuron* **80**, 648–657.

Hoogenboom, B. W., Suda, K., Engel, A. and Fotiadis, D. (2007). The Supramolecular Assemblies of Voltage-

dependent Anion Channels in the Native Membrane. *J. Mol. Biol.* **370**, 246–255.

Huang, D. W., Sherman, B. T. and Lempicki, R. A. (2008). Systematic and integrative analysis of large gene lists using DAVID bioinformatics resources. *Nat. Protoc.* **4**, 44–57.

Huang, H. Y., Lin, S. Z., Chen, W. F., Li, K. W., Kuo, J. S. and Wang, M. J. (2011). Urocortin modulates dopaminergic neuronal survival via inhibition of glycogen synthase kinase-3β and histone deacetylase. *Neurobiol. Aging* **32**, 1662–1677.

Hubert, G. W., Jones, D. C., Moffett, M. C., Rogge, G. and Kuhar, M. J. (2008). CART peptides as modulators of dopamine and psychostimulants and interactions with the mesolimbic dopaminergic system. *Biochem. Pharmacol.* **75**, 57–62.

Hupe, M., Li, M. X., Gertow Gillner, K., Adams, R. H. and Stenman, J. M. (2014). Evaluation of TRAP-sequencing technology with a versatile conditional mouse model. *Nucleic Acids Res* **42**, e14.

Iacovitti, L., Wei, X., Cai, J., Kostuk, E. W., Lin, R., Gorodinsky, A., Roman, P., Kusek, G., Das, S. S., Dufour, A., et al. (2014). The hTH-GFP reporter rat model for the study of Parkinson's disease. *PLoS One* **9**,.

Ibáñez, P., Bonnet, a-M., Débarges, B., Lohmann, E., Tison, F., Pollak, P., Agid, Y., Dürr, a and Brice, a (2004). Causal relation between alpha-synuclein gene duplication and familial Parkinson's disease. *Lancet* **364**, 1169–1171.

Iorio, F., Bosotti, R., Scacheri, E., Belcastro, V., Mithbaokar, P., Ferriero, R., Murino, L., Tagliaferri, R., Brunetti-Pierri, N., Isacchi, A., et al. (2010). Discovery of drug mode of action and drug repositioning from transcriptional responses. *Proc. Natl. Acad. Sci.* **107**, 14621–14626.

Janetzky, B., Hauck, S., Youdim, M. B. H., Riederer, P., Jellinger, K., Pantucek, F., Zöchling, R., Boissl, K. W. and Reichmann, H. (1994). Unaltered aconitase activity, but decreased complex I activity in substantia nigra pars compacta of patients with Parkinson's disease. *Neurosci. Lett.* **169**, 126–128.

Janezic, S., Threlfell, S., Dodson, P. D., Dowie, M. J., Taylor, T. N., Potgieter, D., Parkkinen, L., Senior, S. L., Anwar, S., Ryan, B., et al. (2013). Deficits in dopaminergic transmission precede neuron loss and dysfunction in a new Parkinson model. *Proc Natl Acad Sci U S A* **110**, E4016-25.

Jankovic, J. (2008). Parkinson's disease: clinical features and diagnosis. *J. Neurol. Neurosurg. Psychiatry* **79**, 368–376.

Jellinger, K. A. (2009). Formation and development of Lewy pathology: A critical update. In *Journal of Neurology*, .

Jensen, P. H., Hager, H., Nielsen, M. S., Højrup, P., Gliemann, J. and Jakes, R. (1999). Alpha-synuclein binds to tau and stimulates the protein kinase A-catalyzed tau phosphorylation of serine residues 262 and 356. *J. Biol. Chem.* **274**, 25481–25489.

Jo, E., McLaurin, J. A., Yip, C. M., St. George-Hyslop, P. and Fraser, P. E. (2000). α-Synuclein membrane interactions and lipid specificity. *J. Biol. Chem.* **275**, 34328–34334.

Jung, H., Yoon, B. C. and Holt, C. E. (2012). Axonal mRNA localization and local protein synthesis in nervous system assembly, maintenance and repair. *Nat. Rev. Neurosci.* **13**, 308–24.

Justus C. Dachsel, PhD Sarah J. Lincoln, BSc John Gonzalez, BS Owen A. Ross, PhD Dennis W. Dickson, MD Matthew J. Farrer, P. (2007). The Ups and Downs of alpha-Synuclein mRNA Expression. *Mov. Disord.* **22**, 293.

Kahle, P. J., Neumann, M., Ozmen, L., Müller, V., Odoy, S., Okamoto, N., Jacobsen, H., Iwatsubo, T., Trojanowski, J. Q., Takahashi, H., et al. (2001). Selective insolubility of α-synuclein in human lewy body diseases is recapitulated in a transgenic mouse model. *Am. J. Pathol.* **159**, 2215–2225.

Kamp, F., Exner, N., Lutz, A. K., Wender, N., Hegermann, J., Brunner, B., Nuscher, B., Bartels, T., Giese, A., Beyer, K., et al. (2010). Inhibition of mitochondrial fusion by α-synuclein is rescued by PINK1, Parkin and DJ-1. *EMBO J.* **29**, 3571–3589.

Kaneda, N., Sasaoka, T., Kobayashi, K., Kiuchi, K., Nagatsu, I., Kurosawa, Y., Fujita, K., Yokoyama, M., Nomura, T., Katsuki, M., et al. (1991). Tissue-specific and high-level expression of the human tyrosine hydroxylase gene in transgenic mice. *Neuron* **6**, 583–594.

Kara, E., Kiely, A. P., Proukakis, C., Giffin, N., Love, S., Hehir, J., Rantell, K., Pandraud, A., Hernandez, D. G., Nacheva, E., et al. (2014). A 6.4 Mb Duplication of the α-Synuclein Locus Causing Frontotemporal Dementia and Parkinsonism. *JAMA Neurol.* **71**, 1162.

Kellendonk, C., Tronche, F., Reichardt, H. M. and Schütz, G. (1999). Mutagenesis of the glucocorticoid receptor in mice. In *Journal of Steroid Biochemistry and Molecular Biology*, pp. 253–259.

Kelly, B. B., Hedlund, E., Kim, C., Ishiguro, H., Isacson, O., Chikaraishi, D. M., Kim, K. S. and Feng, G. (2006). A tyrosine hydroxylase-yellow fluorescent protein knock-in reporter system labeling dopaminergic neurons reveals potential regulatory role for the first intron of the rodent tyrosine hydroxylase gene. *Neuroscience* **142**, 343–354.

Kennedy, B. K., Berger, S. L., Brunet, A., Campisi, J., Cuervo, A. M., Epel, E. S., Franceschi, C., Lithgow, G. J., Morimoto, R. I., Pessin, J. E., et al. (2014). Geroscience: Linking aging to chronic disease. *Cell* **159**, 709–713.

Kessler, M. A., Yang, M., Gollomp, K. L., Jin, H. and Iacovitti, L. (2003). The human tyrosine hydroxylase gene promoter. *Brain Res Mol Brain Res* **112**, 8–23.

Khateeb, S., Flusser, H., Ofir, R., Shelef, I., Narkis, G., Vardi, G., Shorer, Z., Levy, R., Galil, A., Elbedour, K., et al. (2006). PLA2G6 mutation underlies infantile neuroaxonal dystrophy. *Am. J. Hum. Genet.* **79**, 942–948.

Kim, T. E., Park, M. J., Choi, E. J., Lee, H. S., Lee, S. H., Yoon, S. H., Oh, C. K., Lee, B. J., Kim, S. U., Lee, Y. S., et al. (2003). Cloning and cell type-specific regulation of the human tyrosine hydroxylase gene promoter. *Biochem. Biophys. Res. Commun.* **312**, 1123–1131.

Kim, Y. H., Lussier, S., Rane, A., Choi, S. W. and Andersen, J. K. (2011). Inducible dopaminergic glutathione depletion in an alpha-synuclein transgenic mouse model results in age-related olfactory dysfunction. *Neuroscience* **172**, 379–386.

Kingsbury, A. E., Daniel, S. E., Sangha, H., Eisen, S., Lees, A. J. and Foster, O. J. (2004). Alteration in alpha-synuclein mRNA expression in Parkinson's disease. *Mov. Disord.* **19**, 162–170.

Kirik, D., Rosenblad, C., Burger, C., Lundberg, C., Johansen, T. E., Muzyczka, N., Mandel, R. J. and Björklund, A. (2002). Parkinson-like neurodegeneration induced by targeted overexpression of α-synuclein in the nigrostriatal system. *J. Neurosci.* **22**, 2780–2791.

Kirik, D., Annett, L. E., Burger, C., Muzyczka, N., Mandel, R. J. and Bjorklund, A. (2003). Nigrostriatal alpha-synucleinopathy induced by viral vector-mediated overexpression of human alpha-synuclein: a new primate model of Parkinson's disease. *Proc Natl Acad Sci U S A* **100**, 2884–2889.

Kitada, T., Asakawa, S., Hattori, N., Matsumine, H., Yamamura, Y., Minoshima, S., Yokochi, M., Mizuno, Y. and Shimizu, N. (1998). Mutations in the parkin gene cause autosomal recessive juvenile parkinsonism. *Nature* **392**, 605–608.

Klein, C., Westenberger, A., Hollingworth, P., Harold, D., Jones, L., Owen, M. J., Williams, J., Marques, S. C. F., Oliveira, C. R., Pereira, C. M. F., et al. (2012). Genetics of Parkinson's Disease. *Int. J. Geriatr. Psychiatry* **26**, a008888.

Kleiner-Fisman, G., Herzog, J., Fisman, D. N., Tamma, F., Lyons, K. E., Pahwa, R., Lang, A. E. and Deuschl, G. (2006). Subthalamic nucleus deep brain stimulation: summary and meta-analysis of outcomes. *Mov. Disord.* **21 Suppl 1**, S290-304.

Klivenyi, P., Siwek, D., Gardian, G., Yang, L., Starkov, A., Cleren, C., Ferrante, R. J., Kowall, N. W., Abeliovich, A. and Beal, M. F. (2006). Mice lacking alpha-synuclein are resistant to mitochondrial toxins. *Neurobiol. Dis.* **21**, 541–548.

Kordower, J. H., Chu, Y., Hauser, R. A., Freeman, T. B. and Olanow, C. W. (2008). Lewy body–like pathology in long-term embryonic nigral transplants in Parkinson's disease. *Nat. Med.* **14**, 504–506.

Kordower, J. H., Dodiya, H. B., Kordower, A. M., Terpstra, B., Paumier, K., Madhavan, L., Sortwell, C., Steece-Collier, K. and Collier, T. J. (2011). Transfer of host-derived alpha synuclein to grafted dopaminergic neurons in rat. *Neurobiol. Dis.* **43**, 552–557.

Kruger, R., Kuhn, W., Muller, T., Woitalla, D., Graeber, M., Kosel, S., Przuntek, H., Epplen, J. T., Schols, L. and Riess, O. (1998). Ala30Pro mutation in the gene encoding alpha-synuclein in Parkinson's disease. *Nat Genet* **18**, 106–108.

Krüger, R., Kuhn, W., Müller, T., Woitalla, D., Graeber, M., Kösel, S., Przuntek, H., Epplen, J. T., Schöls, L. and Riess, O. (1998). Ala30Pro mutation in the gene encoding alpha-synuclein in Parkinson's disease. *Nat. Genet.* **18**, 106–108.

Kuo, Y. M., Li, Z., Jiao, Y., Gaborit, N., Pani, A. K., Orrison, B. M., Bruneau, B. G., Giasson, B. I., Smeyne, R. J., Gershon, M. D., et al. (2010). Extensive enteric nervous system abnormalities in mice transgenic for artificial chromosomes containing Parkinson disease-associated α-synuclein gene mutations precede central nervous system changes. *Hum. Mol. Genet.* **19**, 1633–1650.

Lachmann, A., Giorgi, F. M., Lopez, G. and Califano, A. (2016). ARACNe-AP: Gene network reverse engineering through adaptive partitioning inference of mutual information. *Bioinformatics* **32**, 2233–2235.

Lai, B. C. L., Marion, S. A., Teschke, K. and Tsui, J. K. C. (2002). Occupational and environmental risk factors for Parkinson's disease. *Parkinsonism Relat. Disord.* **8**, 297–309.

Lakso, M., Vartiainen, S., Moilanen, A.-M., Sirviö, J., Thomas, J. H., Nass, R., Blakely, R. D. and Wong, G. (2004). Dopaminergic neuronal loss and motor deficits in Caenorhabditis elegans overexpressing human α-synuclein. *J. Neurochem.* **86**, 165–172.

Lamb, J., Crawford, E. D., Peck, D., Modell, J. W., Blat, I. C., Wrobel, M. J., Lerner, J., Brunet, J. P., Subramanian, A., Ross, K. N., et al. (2006). The connectivity map: Using gene-expression signatures to connect small molecules, genes, and disease. *Science (80-.).* **313**, 1929–1935.

Lammel, S., Steinberg, E. E., Földy, C., Wall, N. R., Beier, K., Luo, L. and Malenka, R. C. (2015). Diversity of transgenic mouse models for selective targeting of midbrain dopamine neurons. *Neuron* **85**, 429–438.

Langston, J., Ballard, P., Tetrud, J. and Irwin, I. (1983). Chronic Parkinsonism in humans due to a product of meperidine-analog synthesis. *Science (80-.).* **219**, 979–980.

Lashkari, D. A., DeRisi, J. L., McCusker, J. H., Namath, A. F., Gentile, C., Hwang, S. Y., Brown, P. O. and Davis, R. W. (1997). Yeast microarrays for genome wide parallel genetic and gene expression analysis. *Proc Natl Acad Sci U S A* **94**, 13057–13062.

Lashuel, H. A., Overk, C. R., Oueslati, A. and Masliah, E. (2012). The many faces of α-synuclein: from structure and toxicity to therapeutic target. *Nat. Rev. Neurosci.* **14**, 38–48.

Lau, L. M. L. De and Breteler, M. M. B. (2006). Epidemiology of Parkinson ' s disease. *Lancet. Neurol.* **5**, 525–535.

Lauss, M., Visne, I., Kriegner, A., Ringn??r, M., J??nsson, G. and H??glund, M. (2013). Monitoring of technical

variation in quantitative high-throughput datasets. *Cancer Inform.* **12**, 193–201.

Lavedan, C. (1998). The synuclein family. *Genome Res.* **8**, 871–880.

Lázaro, D. F., Rodrigues, E. F., Langohr, R., Shahpasandzadeh, H., Ribeiro, T., Guerreiro, P., Gerhardt, E., Kröhnert, K., Klucken, J., Pereira, M. D., et al. (2014). Systematic Comparison of the Effects of Alpha-synuclein Mutations on Its Oligomerization and Aggregation. *PLoS Genet.* **10**,.

Lebouvier, T., Chaumette, T., Paillusson, S., Duyckaerts, C., Bruley Des Varannes, S., Neunlist, M. and Derkinderen, P. (2009). The second brain and Parkinson's disease. *Eur. J. Neurosci.* **30**, 735–741.

Lee, M. K., Stirling, W., Xu, Y., Xu, X., Qui, D., Mandir, A. S., Dawson, T. M., Copeland, N. G., Jenkins, N. A. and Price, D. L. (2002). Human α-synuclein-harboring familial Parkinson's disease-linked Ala-53 → Thr mutation causes neurodegenerative disease with α-synuclein aggregation in transgenic mice. *Proc. Natl. Acad. Sci.* **99**, 8968–8973.

Lee, B. K. B., Tiong, K. H., Chang, J. K., Liew, C. S., Abdul Rahman, Z. A., Tan, A. C., Khang, T. F. and Cheong, S. C. (2017). DeSigN: Connecting gene expression with therapeutics for drug repurposing and development. *BMC Genomics* **18**,.

Lesage, S. and Brice, A. (2009). Parkinson's disease: From monogenic forms to genetic susceptibility factors. *Hum. Mol. Genet.* **18**,.

Lesage, S., Anheim, M., Letournel, F., Bousset, L., Honoré, A., Rozas, N., Pieri, L., Madiona, K., Dürr, A., Melki, R., et al. (2013). G51D α-synuclein mutation causes a novel Parkinsonian-pyramidal syndrome. *Ann. Neurol.* **73**, 459–471.

Lewy, F. (1912). Paralysis Agitans Pathologische Anatomie. In *Handbuch der Neurologie*, pp. 920–933.

Li, W., West, N., Colla, E., Pletnikova, O., Troncoso, J. C., Marsh, L., Dawson, T. M., Jakala, P., Hartmann, T., Price, D. L., et al. (2005). Aggregation promoting C-terminal truncation of Alpha-synuclein is a normal cellular process and is enhanced by the familial Parkinson's disease-linked mutations. *Proc. Natl. Acad. Sci.* **102**, 2162–2167.

Li, J.-Y., Englund, E., Holton, J. L., Soulet, D., Hagell, P., Lees, A. J., Lashley, T., Quinn, N. P., Rehncrona, S., Björklund, A., et al. (2008). Lewy bodies in grafted neurons in subjects with Parkinson's disease suggest host-to-graft disease propagation. *Nat. Med.* **14**, 501–503.

Li, X., Qi, J., Yamaguchi, T., Wang, H. L. and Morales, M. (2013). Heterogeneous composition of dopamine neurons of the rat A10 region: Molecular evidence for diverse signaling properties. *Brain Struct. Funct.* **218**, 1159–1176.

Lin, M. T. and Beal, M. F. (2006). Mitochondrial dysfunction and oxidative stress in neurodegenerative diseases. *Nature* **443**, 787–795.

Lindeberg, J., Usoskin, D., Bengtsson, H., Gustafsson, A., Kylberg, A., Söderström, S. and Ebendal, T. (2004). Transgenic expression of Cre recombinase from the tyrosine hydroxylase locus. *Genesis* **40**, 67–73.

Liou, H. H., Tsai, M. C., Chen, C. J., Jeng, J. S., Chang, Y. C., Chen, S. Y. and Chen, R. C. (1997). Environmental risk factors and Parkinson's disease: a case-control study in Taiwan. *Neurology* **48**, 1583–8.

Liu, D., Jin, L., Wang, H., Zhao, H., Zhao, C., Duan, C., Lu, L., Wu, B., Yu, S., Chan, P., et al. (2008). Silencing alpha-synuclein gene expression enhances tyrosine hydroxylase activity in MN9D cells. *Neurochem. Res.* **33**, 1401–9.

Liu, J., Krautzberger, A. M., Sui, S. H., Hofmann, O. M., Chen, Y., Baetscher, M., Grgic, I., Kumar, S., Humphreys, B., Hide, W. A., et al. (2014). Cell-specific translational profiling in acute kidney injury. *J. Clin. Invest.* **124**, 1242–1254.

Lo Bianco, C., Ridet, J.-L., Schneider, B. L., Déglon, N. and Aebischer, P. (2002). a-Synucleinopathy and selective dopaminergic neuron loss in a rat lentiviral-based model of Parkinson's disease. *Proc. Natl. Acad. Sci. USA* **99**, 10813–10818.

Lobo, M. K., Karsten, S. L., Gray, M., Geschwind, D. H. and Yang, X. W. (2006). FACS-array profiling of striatal projection neuron subtypes in juvenile and adult mouse brains. *Nat. Neurosci.* **9**, 443–452.

Long, J. Z., Svensson, K. J., Tsai, L., Zeng, X., Roh, H. C., Kong, X., Rao, R. R., Lou, J., Lokurkar, I., Baur, W., et al. (2014). A smooth muscle-like origin for beige adipocytes. *Cell Metab.* **19**, 810–820.

Love, M. I., Huber, W. and Anders, S. (2014). Moderated estimation of fold change and dispersion for RNA-seq data with DESeq2. *Genome Biol.* **15**, 550.

Lu, T., Pan, Y., Kao, S.-Y., Li, C., Kohane, I., Chan, J. and Yankner, B. A. (2004). Gene regulation and DNA damage in the ageing human brain. *Nature* **429**, 883–891.

Luk, K. C., Song, C., O'Brien, P., Stieber, A., Branch, J. R., Brunden, K. R., Trojanowski, J. Q. and Lee, V. M.-Y. (2009). Exogenous Alpha-synuclein fibrils seed the formation of Lewy body-like intracellular inclusions in cultured cells. *Proc. Natl. Acad. Sci.* **106**, 20051–20056.

Luk, K. C., Kehm, V., Carroll, J., Zhang, B., O'Brien, P., Trojanowski, J. Q. and Lee, V. M.-Y. (2012a). Pathological Alpha-Synuclein Transmission Initiates Parkinson-like Neurodegeneration in Nontransgenic Mice. *Science (80-.).* **338**, 949–953.

Luk, K. C., Kehm, V. M., Zhang, B., O'Brien, P., Trojanowski, J. Q. and Lee, V. M. Y. (2012b). Intracerebral inoculation of pathological α-synuclein initiates a rapidly progressive neurodegenerative α-synucleinopathy in mice. *J. Exp. Med.* **209**, 975–986.

Ma, S. Y., Ciliax, B. J., Stebbins, G., Jaffar, S., Joyce, J. N., Cochran, E. J., Kordower, J. H., Mash, D. C., Levey, A. I. and Mufson, E. J. (1999). Dopamine transporter-immunoreactive neurons decrease with age in the human substantia nigra. *J. Comp. Neurol.* **409**, 25–37.

Maingay, M., Romero-Ramos, M., Carta, M. and Kirik, D. (2006). Ventral tegmental area dopamine neurons are resistant to human mutant alpha-synuclein overexpression. *Neurobiol. Dis.* **23**, 522–532.

Manning-Bog, A. B., McCormack, A. L., Purisai, M. G., Bolin, L. M. and Di Monte, D. a (2003). Alpha-synuclein overexpression protects against paraquat-induced neurodegeneration. *J. Neurosci.* **23**, 3095–9.

Margolin, A. A., Nemenman, I., Basso, K., Wiggins, C., Stolovitzky, G., Favera, R. and Califano, A. (2006). ARACNE: An Algorithm for the Reconstruction of Gene Regulatory Networks in a Mammalian Cellular Context. *BMC Bioinformatics* **7**, S7.

Maroteaux, L., Campanelli, J. T. and Scheller, R. H. (1988). Synuclein: a neuron-specific protein localized to the nucleus and presynaptic nerve terminal. *J. Neurosci.* **8**, 2804–2815.

Marsh, S. E. and Blurton-Jones, M. (2012). Examining the mechanisms that link β-amyloid and α-synuclein pathologies. *Alzheimers. Res. Ther.* **4**, 11.

Masliah, E., Rockenstein, E., Veinbergs, I., Mallory, M., Hashimoto, M., Takeda, a, Sagara, Y., Sisk, a and Mucke, L. (2000). Dopaminergic loss and inclusion body formation in alpha-synuclein mice: implications for neurodegenerative disorders. *Science* **287**, 1265–1269.

Masliah, E., Rockenstein, E., Veinbergs, I., Sagara, Y., Mallory, M., Hashimoto, M. and Mucke, L. (2001). beta-amyloid peptides enhance alpha-synuclein accumulation and neuronal deficits in a transgenic mouse model linking Alzheimer's disease and Parkinson's disease. *Proc. Natl. Acad. Sci. U. S. A.* **98**, 12245–12250.

Masliah, E., Rockenstein, E., Adame, A., Alford, M., Crews, L., Hashimoto, M., Seubert, P., Lee, M., Goldstein, J., Chilcote, T., et al. (2005). Effects of α-synuclein immunization in a mouse model of Parkinson's disease. *Neuron* **46**, 857–868.

Masliah, E., Rockenstein, E., Mante, M., Crews, L., Spencer, B., Adame, A., Patrick, C., Trejo, M., Ubhi, K., Rohn, T. T., et al. (2011). Passive immunization reduces behavioral and neuropathological deficits in an alpha-synuclein transgenic model of lewy body disease. *PLoS One* **6**,.

Masuda-Suzukake, M., Nonaka, T., Hosokawa, M., Oikawa, T., Arai, T., Akiyama, H., Mann, D. M. A. and Hasegawa, M. (2013). Prion-like spreading of pathological alpha-synuclein in brain. *Brain* **136**, 1128–1138.

McCarthy, J. J., Linnertz, C., Saucier, L., Burke, J. R., Hulette, C. M., Welsh-Bohmer, K. A. and Chiba-Falek, O. (2011). The effect of SNCA 3′ region on the levels of SNCA-112 splicing variant. *Neurogenetics* **12**, 59–64.

McDowell, K. a, Shin, D., Roos, K. P. and Chesselet, M.-F. (2014). Sleep dysfunction and EEG alterations in mice overexpressing alpha-synuclein. *J. Parkinsons. Dis.* **4**, 531–9.

McGlinchey, R. P. and Lee, J. C. (2015). Cysteine cathepsins are essential in lysosomal degradation of α-synuclein. *Proc. Natl. Acad. Sci.* **112**, 9322–9327.

Meloni, R., Albanèse, V., Ravassard, P., Treilhou, F. and Mallet, J. (1998). A tetranucleotide polymorphic microsatellite, located in the first intron of the tyrosine hydroxylase gene, acts as a transcription regulatory element in vitro. *Hum. Mol. Genet.* **7**, 423–428.

Meredith, G. E. and Rademacher, D. J. (2011). MPTP mouse models of Parkinson's disease: An update. *J. Parkinsons. Dis.* **1**, 19–33.

Merkwirth, C. and Langer, T. (2009). Prohibitin function within mitochondria: Essential roles for cell proliferation and cristae morphogenesis. *Biochim. Biophys. Acta - Mol. Cell Res.* **1793**, 27–32.

Meyer, R. A., Zaruba, M. E. and McKhann, G. M. (1980). Flow cytometry of isolated cells from the brain. *Anal. Quant. Cytol.* **2**, 66–74.

Meyers, E. N., Lewandoski, M. and Martin, G. R. (1998). An Fgf8 mutant allelic series generated by Cre- and Flp-mediated recombination. *Nat. Genet.* **18**, 136–141.

Miller, D. W., Hague, S. M., Clarimon, J., Baptista, M., Gwinn-Hardy, K., Cookson, M. R. and Singleton, A. B. (2004). Alpha-synuclein in blood and brain from familial Parkinson disease with SNCA locus triplication. *Neurology* **62**, 1835–1838.

Miller, J. A., Ding, S.-L., Sunkin, S. M., Smith, K. A., Ng, L., Szafer, A., Ebbert, A., Riley, Z. L., Royall, J. J., Aiona, K., et al. (2014). Transcriptional landscape of the prenatal human brain. *Nature* **508**, 199–206.

Miyazaki, J., Takaki, S., Araki, K., Tashiro, F., Tominaga, A., Takatsu, K. and Yamamura, K. (1989). Expression vector system based on the chicken beta-actin promoter directs efficient production of interleukin-5. *Gene* **79**, 269–77.

Mizuno, Y., Ohta, S., Tanaka, M., Takamiya, S., Suzuki, K., Sato, T., Oya, H., Ozawa, T. and Kagawa, Y. (1989). Deficiencies in Complex I subunits of the respiratory chain in Parkinson's disease. *Biochem. Biophys. Res. Commun.* **163**, 1450–1455.

Mougenot, A. L., Nicot, S., Bencsik, A., Morignat, E., Verchère, J., Lakhdar, L., Legastelois, S. and Baron, T. (2012). Prion-like acceleration of a synucleinopathy in a transgenic mouse model. *Neurobiol. Aging* **33**, 2225–2228.

Murphy, D. D., Rueter, S. M., Trojanowski, J. Q. and Lee, V. M. (2000). Synucleins are developmentally expressed, and alpha-synuclein regulates the size of the presynaptic vesicular pool in primary hippocampal neurons. *J. Neurosci.* **20**, 3214–3220.

Murray, I. V. J., Giasson, B. I., Quinn, S. M., Koppaka, V., Axelsen, P. H., Ischiropoulos, H., Trojanowski, J. Q. and Lee, V. M.-Y. (2003). C-terminal truncation: Role of alpha-synuclein carboxy-terminus on fibril formation in vitro. *Biochemistry* **42**, 8530–8540.

Mustroph, A., Juntawong, P. and Bailey-Serres, J. (2009). Isolation of plant polysomal mRNA by differential centrifugation and ribosome immunopurification methods. *Methods Mol Biol* **553**, 109–126.

Nagalakshmi, U., Wang, Z., Waern, K., Shou, C., Raha, D., Gerstein, M. and Snyder, M. (2008). The transcriptional landscape of the yeast genome defined by RNA sequencing. *Science (80-.).* **320**, 1344–1349.

Nagatsu, T., Levitt, M. and Udenfriend, S. (1964). Tyrosine Hydroxylase. The Initial Step in Norepinephrine Biosynthesis. *J Biol Chem* **239**, 2910–2917.

Nagatsu, I., Karasawa, N., Yamada, K., Sakai, M., Fujii, T., Takeuchi, T., Arai, R., Kobayashi, K. and Nagatsu, T. (1994). Expression of human tyrosine hydroxylase-chloramphenicol acetyltransferase (CAT) fusion gene in the brains of transgenic mice as examined by CAT immunocytochemistry. *J. Neural Transm.* **96**, 85–104.

Nagy, A., Mar, L. and Watts, G. (2009). Creation and use of a cre recombinase transgenic database. *Methods Mol. Biol.* **530**, 365–378.

Nair-Roberts, R. G., Chatelain-Badie, S. D., Benson, E., White-Cooper, H., Bolam, J. P. and Ungless, M. A. (2008). Stereological estimates of dopaminergic, GABAergic and glutamatergic neurons in the ventral tegmental area, substantia nigra and retrorubral field in the rat. *Neuroscience* **152**, 1024–1031.

Nakamura, K., Nemani, V. M., Azarbal, F., Skibinski, G., Levy, J. M., Egami, K., Munishkina, L., Zhang, J., Gardner, B., Wakabayashi, J., et al. (2011). Direct membrane association drives mitochondrial fission by the Parkinson disease-associated protein α-synuclein. *J. Biol. Chem.* **286**, 20710–20726.

Nalls, M. A., Pankratz, N., Lill, C. M., Do, C. B., Hernandez, D. G., Saad, M., DeStefano, A. L., Kara, E., Bras, J., Sharma, M., et al. (2014). Large-scale meta-analysis of genome-wide association data identifies six new risk loci for Parkinson's disease. *Nat. Genet.* **46**, 989–993.

Naoi, M. and Maruyama, W. (1999). Cell death of dopamine neurons in aging and Parkinson's disease. In *Mechanisms of Ageing and Development*, pp. 175–188.

Narendra, D., Tanaka, A., Suen, D. F. and Youle, R. J. (2008). Parkin is recruited selectively to impaired mitochondria and promotes their autophagy. *J. Cell Biol.* **183**, 795–803.

Nectow, A. R., Ekstrand, M. I. and Friedman, J. M. (2015). Molecular characterization of neuronal cell types based on patterns of projection with Retro-TRAP. *Nat. Protoc.* **10**, 1319–1327.

Nemani, V. M., Lu, W., Berge, V., Nakamura, K., Onoa, B., Lee, M. K., Chaudhry, F. A., Nicoll, R. A. and Edwards, R. H. (2010). Increased Expression of α-Synuclein Reduces Neurotransmitter Release by Inhibiting Synaptic Vesicle Reclustering after Endocytosis. *Neuron* **65**, 66–79.

Neumann, M., Kahle, P. J., Giasson, B. I., Ozmen, L., Borroni, E., Spooren, W., Müller, V., Odoy, S., Fujiwara, H., Hasegawa, M., et al. (2002). Misfolded proteinase K-resistant hyperphosphorylated α-synuclein in aged transgenic mice with locomotor deterioration and in human α-synucleinopathies. *J. Clin. Invest.* **110**, 1429–1439.

Noorian, A. R., Rha, J., Annerino, D. M., Bernhard, D., Taylor, G. M. and Greene, J. G. (2012). Alpha-synuclein transgenic mice display age-related slowing of gastrointestinal motility associated with transgene expression in the vagal system. *Neurobiol. Dis.* **48**, 9–19.

Nuytemans, K., Theuns, J., Cruts, M. and Van Broeckhoven, C. (2010). Genetic etiology of Parkinson disease associated with mutations in the SNCA, PARK2, PINK1, PARK7, and LRRK2 genes: A mutation update. *Hum. Mutat.* **31**, 763–780.

Obrig, T. G., Culp, W. J., McKeehan, W. L. and Hardesty, B. (1971). The mechanism by which cycloheximide and related glutarimide antibiotics inhibit peptide synthesis on reticulocyte ribosomes. *J. Biol. Chem.* **246**, 174–181.

Okaty, B. W., Sugino, K. and Nelson, S. B. (2011). Cell type-specific transcriptomics in the brain. *J. Neurosci.* **31**, 6939–43.

Okita, K., Nakagawa, M., Hyenjong, H., Ichisaka, T. and Yamanaka, S. (2008). Generation of mouse induced pluripotent stem cells without viral vectors. *Science* **322**, 949–53.

Olgiati, S., Thomas, A., Quadri, M., Breedveld, G. J., Graafland, J., Eussen, H., Douben, H., de Klein, A., Onofrj, M. and Bonifati, V. (2015). Early-onset parkinsonism caused by alpha-synuclein gene triplication: Clinical and genetic findings in a novel family. *Park. Relat. Disord.* **21**, 981–986.

Olson, C. B. (1987). A review of why and how we age: A defense of multifactorial aging. *Mech. Ageing Dev.* **41**, 1–28.

Ono, K., Ikeda, T., Takasaki, J. ichi and Yamada, M. (2011). Familial Parkinson disease mutations influence Alpha-Synuclein assembly. *Neurobiol. Dis.* **43**, 715–724.

Ono, K., Takahashi, R., Ikeda, T. and Yamada, M. (2012). Cross-seeding effects of amyloid β-protein and α-synuclein. *J. Neurochem.* **122**, 883–890.

Orban, P. C., Chui, D. and Marth, J. D. (1992). Tissue- and site-specific DNA recombination in transgenic mice. *Proc. Natl. Acad. Sci. U. S. A.* **89**, 6861–5.

Ossowska, K., Śmiałowska, M., Kuter, K., Wierońska, J., Zieba, B., Wardas, J., Nowak, P., Dabrowska, J., Bortel, A., Biedka, I., et al. (2006). Degeneration of dopaminergic mesocortical neurons and activation of compensatory processes induced by a long-term paraquat administration in rats: Implications for Parkinson's

disease. *Neuroscience* **141**, 2155–2165.

Oueslati, A., Fournier, M. and Lashuel, H. a (2010). *Role of post-translational modifications in modulating the structure, function and toxicity of alpha-synuclein: implications for Parkinson's disease pathogenesis and therapies.*

Outeiro, T. F., Putcha, P., Tetzlaff, J. E., Spoelgen, R., Koker, M., Carvalho, F., Hyman, B. T. and McLean, P. J. (2008). Formation of toxic oligomeric α-synuclein species in living cells. *PLoS One* **3**,.

Pacini, C., Iorio, F., Gonçalves, E., Iskar, M., Klabunde, T., Bork, P. and Saez-Rodriguez, J. (2013). DvD: An R/Cytoscape pipeline for drug repurposing using public repositories of gene expression data. *Bioinformatics* **29**, 132–134.

Paisan-Ruiz, C., Bhatia, K. P., Li, A., Hernandez, D., Davis, M., Wood, N. W., Hardy, J., Houlden, H., Singleton, A. and Schneider, S. A. (2009). Characterization of PLA2G6 as a locus for dystonia-parkinsonism. *Ann. Neurol.* **65**, 19–23.

Pan-Montojo, F., Anichtchik, O., Dening, Y., Knels, L., Pursche, S., Jung, R., Jackson, S., Gille, G., Spillantini, M. G., Reichmann, H., et al. (2010). Progression of Parkinson's disease pathology is reproduced by intragastric administration of rotenone in mice. *PLoS One* **5**,.

Pankratz, N., Beecham, G. W., Destefano, A. L., Dawson, T. M., Doheny, K. F., Factor, S. A., Hamza, T. H., Hung, A. Y., Hyman, B. T., Ivinson, A. J., et al. (2012). Meta-analysis of Parkinson's Disease: Identification of a novel locus, RIT2. *Ann. Neurol.* **71**, 370–384.

Parihar, M. S., Parihar, A., Fujita, M., Hashimoto, M. and Ghafourifar, P. (2008). Mitochondrial association of alpha-synuclein causes oxidative stress. *Cell. Mol. Life Sci.* **65**, 1272–1284.

Parkinson, J., Campos, F. L., Coimbra, B., Pêgo, J. M., Rodrigues, C., Lima, R., Rodrigues, A. J., Sousa, N., Salgado, A. J., Parkinson, J., et al. (2002). An Essay on the Shaking Palsy. *J. Neuropsychiatry Clin. Neurosci.* **14**, 223–236.

Parkkinen, L., Pirttilä, T., Tervahauta, M. and Alafuzoff, I. (2005). Widespread and abundant α-synuclein pathology in a neurologically unimpaired subject. *Neuropathology* **25**, 304–314.

Pasanen, P., Myllykangas, L., Siitonen, M., Raunio, A., Kaakkola, S., Lyytinen, J., Tienari, P. J., Pöyhönen, M. and Paetau, A. (2014). A novel α-synuclein mutation A53E associated with atypical multiple system atrophy and Parkinson's disease-type pathology. *Neurobiol. Aging* **35**,.

Patel, M. S., Nemeria, N. S., Furey, W. and Jordan, F. (2014). The pyruvate dehydrogenase complexes: Structure-based function and regulation. *J. Biol. Chem.* **289**, 16615–16623.

Paxinos, G. and Franklin, K. (2012). *Paxinos and Franklin's the Mouse Brain in Stereotaxic Coordinates*.

Peelaerts, W., Bousset, L., Van der Perren, A., Moskalyuk, A., Pulizzi, R., Giugliano, M., Van den Haute, C., Melki, R. and Baekelandt, V. (2015). α-Synuclein strains cause distinct synucleinopathies after local and systemic administration. *Nature* **522**, 340–344.

Perez, R. G., Waymire, J. C., Lin, E., Liu, J. J., Guo, F. and Zigmond, M. J. (2002). A role for alpha-synuclein in the regulation of dopamine biosynthesis. *J. Neurosci.* **22**, 3090–9.

Periquet, M., Fulga, T., Myllykangas, L., Schlossmacher, M. G. and Feany, M. B. (2007). Aggregated Alpha-Synuclein Mediates Dopaminergic Neurotoxicity In Vivo. *J. Neurosci.* **27**, 3338–3346.

Petrucelli, L., O'Farrell, C., Lockhart, P. J., Baptista, M., Kehoe, K., Vink, L., Choi, P., Wolozin, B., Farrer, M., Hardy, J., et al. (2002). Parkin protects against the toxicity associated with mutant Alpha-Synuclein: Proteasome dysfunction selectively affects catecholaminergic neurons. *Neuron* **36**, 1007–1019.

Pissadaki, E. K. and Bolam, J. P. (2013). The energy cost of action potential propagation in dopamine neurons: clues to susceptibility in Parkinson's disease. *Front. Comput. Neurosci.* **7**,.

Polymeropoulos, M. H. (1997). Mutation in the -Synuclein Gene Identified in Families with Parkinson's Disease. *Science (80-.).* **276**, 2045–2047.

Polymeropoulos, M. H., Higgins, J. J., Golbe, L. I., Johnson, W. G., Ide, S. E., Di Iorio, G., Sanges, G., Stenroos, E. S., Pho, L. T., Schaffer, A. A., et al. (1996). Mapping of a Gene for Parkinson's Disease to Chromosome 4q21-q23. *Science (80-.).* **274**, 1197–1199.

Polymeropoulos, M. H., Lavedan, C., Leroy, E., Ide, S. E., Dehejia, A., Dutra, A., Pike, B., Root, H., Rubenstein, J., Boyer, R., et al. (1997). Mutation in the alpha-synuclein gene identified in families with Parkinson's disease. *Science (80-.).* **276**, 2045–2047.

Pomeranz, L. E., Ekstrand, M. I., Latcha, K. N., Smith, G. A., Enquist, L. W. and Friedman, J. M. (2017). Gene Expression Profiling with Cre-Conditional Pseudorabies Virus Reveals a Subset of Midbrain Neurons That Participate in Reward Circuitry. *J. Neurosci.* **37**, 4128–4144.

Poole, A. C., Thomas, R. E., Andrews, L. A., McBride, H. M., Whitworth, A. J. and Pallanck, L. J. (2008). The PINK1/Parkin pathway regulates mitochondrial morphology. *Proc. Natl. Acad. Sci. U. S. A.* **105**, 1638–43.

Poulin, J. F., Zou, J., Drouin-Ouellet, J., Kim, K. Y. A., Cicchetti, F. and Awatramani, R. B. (2014). Defining midbrain dopaminergic neuron diversity by single-cell gene expression profiling. *Cell Rep.* **9**, 930–943.

Prediger, R. D. S. (2010). Effects of caffeine in Parkinson's disease: From neuroprotection to the management of motor and non-motor symptoms. In *Journal of Alzheimer's Disease*, .

Proudfoot, N. J. (2011). Ending the message : poly (A) signals then and now. *Genes Dev.* **25**, 1770–1782.

Proukakis, C., Dudzik, C. G., Brier, T., MacKay, D. S., Cooper, J. M., Millhauser, G. L., Houlden, H. and Schapira, A. H. (2013). A novel α-synuclein missense mutation in Parkinson disease. *Neurology* **80**, 1062–1064.

Quik, M. (2004). Smoking, nicotine and Parkinson's disease. *Trends Neurosci.* **27**, 561–568.

R Development Core Team (2016). R: A Language and Environment for Statistical Computing. *R Found. Stat. Comput. Vienna Austria* **0**, {ISBN} 3-900051-07-0.

Ramirez, A., Heimbach, A., Gründemann, J., Stiller, B., Hampshire, D., Cid, L. P., Goebel, I., Mubaidin, A. F., Wriekat, A.-L., Roeper, J., et al. (2006). Hereditary parkinsonism with dementia is caused by mutations in ATP13A2, encoding a lysosomal type 5 P-type ATPase. *Nat. Genet.* **38**, 1184–1191.

Recchia, A., Debetto, P., Negro, A., Guidolin, D., Skaper, S. D. and Giusti, P. (2004). Alpha-synuclein and Parkinson's disease. *FASEB J.* **18**, 617–26.

Richfield, E. K., Thiruchelvam, M. J., Cory-Slechta, D. a, Wuertzer, C., Gainetdinov, R. R., Caron, M. G., Di Monte, D. a and Federoff, H. J. (2002). Behavioral and neurochemical effects of wild-type and mutated human alpha-synuclein in transgenic mice. *Exp. Neurol.* **175**, 35–48.

Riederer, P. and Laux, G. (2011). MAO-inhibitors in Parkinson's Disease. *Exp. Neurobiol.* **20**, 1–17.

Roberts, R. F., Wade-Martins, R. and Alegre-Abarrategui, J. (2015). Direct visualization of alpha-synuclein oligomers reveals previously undetected pathology in Parkinson's disease brain. *Brain* **138**, 1642–1657.

Robertson, D. C., Schmidt, O., Ninkina, N., Jones, P. A., Sharkey, J. and Buchman, V. L. (2004). Developmental loss and resistance to MPTP toxicity of dopaminergic neurones in substantia nigra pars compacta of gamma-synuclein, alpha-synuclein and double alpha/gamma-synuclein null mutant mice. *J. Neurochem.* **89**, 1126–1136.

Rodriguez, M., Rodriguez-Sabate, C., Morales, I., Sanchez, A. and Sabate, M. (2015). Parkinson's disease as a result of aging. *Aging Cell* **14**, 293–308.

Rogge, G., Jones, D., Hubert, G. W., Lin, Y. and Kuhar, M. J. (2008). CART peptides: regulators of body weight, reward and other functions. *Nat. Rev. Neurosci.* **9**, 747–758.

Roh, H. C., Tsai, L. T. Y., Lyubetskaya, A., Tenen, D., Kumari, M. and Rosen, E. D. (2017). Simultaneous Transcriptional and Epigenomic Profiling from Specific Cell Types within Heterogeneous Tissues In Vivo. *Cell Rep.* **18**, 1048–1061.

Rosen, D. R., Siddique, T., Patterson, D., Figlewicz, D. A., Sapp, P., Hentati, A., Donaldson, D., Goto, J., O'Regan, J. P. and Deng, H. X. (1993). Mutations in Cu/Zn superoxide dismutase gene are associated with familial amyotrophic lateral sclerosis. *Nature* **362**, 59–62.

Rostovtseva, T. K., Gurnev, P. A., Protchenko, O., Hoogerheide, D. P., Yap, T. L., Philpott, C. C., Lee, J. C. and Bezrukov, S. M. (2015). α-synuclein shows high affinity interaction with voltage-dependent anion channel, suggesting mechanisms of mitochondrial regulation and toxicity in Parkinson disease. *J. Biol. Chem.* **290**, 18467–18477.

Rothman, S. M., Griffioen, K. J., Vranis, N., Ladenheim, B., Cong, W. N., Cadet, J. L., Haran, J., Martin, B. and Mattson, M. P. (2013). Neuronal expression of familial Parkinson's disease A53T alpha-synuclein causes early motor impairment, reduced anxiety and potential sleep disturbances in mice. *J Park. Dis* **3**, 215–229.

Roy, P. J., Stuart, J. M., Lund, J. and Kim, S. K. (2002). Chromosomal clustering of muscle-expressed genes in Caenorhabditis elegans. *Nature* **418**, 975–979.

Rutherford, N. J., Moore, B. D., Golde, T. E. and Giasson, B. I. (2015). Divergent effects of the H50Q and G51D SNCA mutations on the aggregation of α-synuclein. *J. Neurochem.* **131**, 859–867.

Ryan, B. J., Louren??o-Venda, L. L., Crabtree, M. J., Hale, A. B., Channon, K. M. and Wade-Martins, R. (2014). Synuclein and mitochondrial bioenergetics regulate tetrahydrobiopterin levels in a human dopaminergic model of Parkinson disease. *Free Radic. Biol. Med.* **67**, 58–68.

Ryan, B. J., Hoek, S., Fon, E. A. and Wade-Martins, R. (2015). Mitochondrial dysfunction and mitophagy in Parkinson's: From familial to sporadic disease. *Trends Biochem. Sci.* **40**, 200–210.

Sadowski, P. D. (1995). The Flp Recombinase of th 2-μm Plasmid of Saccharomyces cerevisiae. *Prog. Nucleic Acid Res. Mol. Biol.* **51**, 53–91.

Sakai, K. and Miyazaki, J. (1997). A transgenic mouse line that retains Cre recombinase activity in mature oocytes irrespective of the cre transgene transmission. *Biochem Biophys Res Commun* **237**, 318–324.

Sakers, K., Lake, A. M., Khazanchi, R., Ouwenga, R., Vasek, M. J., Dani, A. and Dougherty, J. D. (2017). Astrocytes locally translate transcripts in their peripheral processes. *Proc. Natl. Acad. Sci.* **114**, E3830–E3838.

Samii, A., Nutt, J. G. and Ransom, B. R. (2004). Parkinson's disease. *Lancet* **363**, 1783–1793.

Sanz, E., Yang, L., Su, T., Morris, D. R., McKnight, G. S. and Amieux, P. S. (2009). Cell-type-specific isolation of ribosome-associated mRNA from complex tissues. *Proc. Natl. Acad. Sci.* **106**, 13939–13944.

Satake, W., Nakabayashi, Y., Mizuta, I., Hirota, Y., Ito, C., Kubo, M., Kawaguchi, T., Tsunoda, T., Watanabe, M., Takeda, A., et al. (2009). Genome-wide association study identifies common variants at four loci as genetic risk factors for Parkinson's disease. *Nat. Genet.* **41**, 1303–1307.

Sauer, B. and Henderson, N. (1988). Site-specific DNA recombination in mammalian cells by the Cre recombinase of bacteriophage P1. *Proc. Natl. Acad. Sci.* **85**, 5166–5170.

Sawamoto, N., Piccini, P., Hotton, G., Pavese, N., Thielemans, K. and Brooks, D. J. (2008). Cognitive deficits and

striato-frontal dopamine release in Parkinson's disease. *Brain* **131**, 1294–1302.

Saxena, A., Wagatsuma, A., Noro, Y., Kuji, T., Asaka-Oba, A., Watahiki, A., Gurnot, C., Fagiolini, M., Hensch, T. K. and Carninci, P. (2012). Trehalose-enhanced isolation of neuronal sub-types from adult mouse brain. *Biotechniques* **52**, 381–385.

Scannell, J. W., Blanckley, A., Boldon, H. and Warrington, B. (2012). Diagnosing the decline in pharmaceutical R&D efficiency. *Nat. Rev. Drug Discov.* **11**, 191–200.

Schapira, A. H., Cooper, J. M., Dexter, D., Clark, J. B., Jenner, P. and Marsden, C. D. (1990). Mitochondrial complex I deficiency in Parkinson's disease. *J. Neurochem.* **54**, 823–7.

Schlüter, O. M., Fornai, F., Alessandrí, M. G., Takamori, S., Geppert, M., Jahn, R. and Südhof, T. C. (2003). Role of α-synuclein in 1-methyl-4-phenyl-1,2,3,6-tetrahydropyridine-induced Parkinsonism in mice. *Neuroscience* **118**, 985–1002.

Schroeder, A., Mueller, O., Stocker, S., Salowsky, R., Leiber, M., Gassmann, M., Lightfoot, S., Menzel, W., Granzow, M. and Ragg, T. (2006). The RIN: an RNA integrity number for assigning integrity values to RNA measurements. *BMC Mol Biol* **7**, 3.

Scott, D. A., Tabarean, I., Tang, Y., Cartier, A., Masliah, E. and Roy, S. (2010). A Pathologic Cascade Leading to Synaptic Dysfunction in Alpha-Synuclein-Induced Neurodegeneration. *J. Neurosci.* **30**, 8083–8095.

Senior, S. L., Ninkina, N., Deacon, R., Bannerman, D., Buchman, V. L., Cragg, S. J. and Wade-Martins, R. (2008). Increased striatal dopamine release and hyperdopaminergic-like behaviour in mice lacking both alpha-synuclein and gamma-synuclein. *Eur. J. Neurosci.* **27**, 947–957.

Sharon, R., Bar-Joseph, I., Frosch, M. P., Walsh, D. M., Hamilton, J. A. and Selkoe, D. J. (2003). The formation of highly soluble oligomers of α-synuclein is regulated by fatty acids and enhanced in Parkinson's disease. *Neuron* **37**, 583–595.

Shavali, S., Brown-Borg, H. M., Ebadi, M. and Porter, J. (2008). Mitochondrial localization of alpha-synuclein protein in alpha-synuclein overexpressing cells. *Neurosci. Lett.* **439**, 125–128.

Shigeoka, T., Jung, H., Jung, J., Turner-Bridger, B., Ohk, J., Lin, J. Q., Amieux, P. S. and Holt, C. E. (2016). Dynamic Axonal Translation in Developing and Mature Visual Circuits. *Cell* **166**, 181–192.

Shimura, H., Schlossmacher, M. G., Hattori, N., Frosch, M. P., Trockenbacher, a, Schneider, R., Mizuno, Y., Kosik, K. S. and Selkoe, D. J. (2001). Ubiquitination of a new form of alpha-synuclein by parkin from human brain: implications for Parkinson's disease. *Science* **293**, 263–269.

Shizuya, H. and Kouros-Mehr, H. (2001). The development and applications of the bacterial artificial chromosome cloning system. *Keio J. Med.* **50**, 26–30.

Shizuya, H., Birren, B., Kim, U. J., Mancino, V., Slepak, T., Tachiiri, Y. and Simon, M. (1992). Cloning and stable maintenance of 300-kilobase-pair fragments of human DNA in Escherichia coli using an F-factor-based vector. *Proc. Natl. Acad. Sci. U. S. A.* **89**, 8794–7.

Shojaee, S., Sina, F., Banihosseini, S. S., Kazemi, M. H., Kalhor, R., Shahidi, G. A., Fakhrai-Rad, H., Ronaghi, M. and Elahi, E. (2008). Genome-wide Linkage Analysis of a Parkinsonian-Pyramidal Syndrome Pedigree by 500 K SNP Arrays. *Am. J. Hum. Genet.* **82**, 1375–1384.

Simón-Sánchez, J., Schulte, C., Bras, J. M., Sharma, M., Gibbs, J. R., Berg, D., Paisan-Ruiz, C., Lichtner, P., Scholz, S. W., Hernandez, D. G., et al. (2009). Genome-wide association study reveals genetic risk underlying Parkinson's disease. *Nat. Genet.* **41**, 1308–1312.

Simunovic, F., Yi, M., Wang, Y., Macey, L., Brown, L. T., Krichevsky, A. M., Andersen, S. L., Stephens, R. M., Benes, F. M. and Sonntag, K. C. (2009). Gene expression profiling of substantia nigra dopamine neurons: further insights into Parkinson's disease pathology. *Brain* **132**, 1795–1809.

Singleton, B., Farrer, M., Johnson, J., Singleton, A., Hague, S., Kachergus, J., Hulihan, M., Peuralinna, T., Dutra, A., Nussbaum, R., et al. (2003). alpha-Synuclein locus triplication causes Parkinson's disease. *Science* **302**, 841.

Smith, Y. and Kieval, J. Z. (2000). Anatomy of the dopamine system in the basal ganglia. *Trends Neurosci.* **23**, S28-33.

Smith, W. W., Jiang, H., Pei, Z., Tanaka, Y., Morita, H., Sawa, A., Dawson, V. L., Dawson, T. M. and Ross, C. A. (2005). Endoplasmic reticulum stress and mitochondrial cell death pathways mediate A53T mutant alpha-synuclein-induced toxicity. *Hum. Mol. Genet.* **14**, 3801–3811.

Snyder, H., Mensah, K., Theisler, C., Lee, J., Matouschek, A. and Wolozin, B. (2003). Aggregated and monomeric Alpha-synuclein bind to the S6' proteasomal protein and inhibit proteasomal function. *J. Biol. Chem.* **278**, 11753–11759.

Soneson, C., Love, M. I. and Robinson, M. D. (2016). Differential analyses for RNA-seq: transcript-level estimates improve gene-level inferences. *F1000Research* **4**, 1521.

Song, Z., Chen, H., Fiket, M., Alexander, C. and Chan, D. C. (2007). OPA1 processing controls mitochondrial fusion and is regulated by mRNA splicing, membrane potential, and Yme1L. *J. Cell Biol.* **178**, 749–755.

Soriano, P. (1999). Generalized lacZ expression with the ROSA26 Cre reporter strain. *Nat. Genet.* **21**, 70–71.

Specht, C. G. and Schoepfer, R. (2001). Deletion of the alpha-synuclein locus in a subpopulation of C57BL/6J inbred mice. *BMC Neurosci.* **2**, 11.

Spillantini, M. G. and Goedert, M. (2000). The alpha-synucleinopathies: Parkinson's disease, dementia with Lewy bodies, and multiple system atrophy. *Ann N Y Acad Sci* **920**, 16–27.

Spillantini, M. G., Schmidt, M. L., Lee, V. M., Trojanowski, J. Q., Jakes, R. and Goedert, M. (1997). Alpha-synuclein in Lewy bodies. *Nature* **388**, 839–840.

Spillantini, M. G., Crowther, R. A., Jakes, R., Hasegawa, M. and Goedert, M. (1998). alpha-Synuclein in filamentous inclusions of Lewy bodies from Parkinson's disease and dementia with lewy bodies. *Proc. Natl. Acad. Sci. U. S. A.* **95**, 6469–73.

Stanley, S., Domingos, A. I., Kelly, L., Garfield, A., Damanpour, S., Heisler, L. and Friedman, J. (2013). Profiling of glucose-sensing neurons reveals that ghrh neurons are activated by hypoglycemia. *Cell Metab.* **18**, 596–607.

Steiner, F. A., Talbert, P. B., Kasinathan, S., Deal, R. B. and Henikoff, S. (2012). Cell-type-specific nuclei purification from whole animals for genome-wide expression and chromatin profiling. *Genome Res.* **22**, 766–777.

Sternberg, N. and Hamilton, D. (1981). Bacteriophage P1 site-specific recombination. I. Recombination between loxP sites. *J. Mol. Biol.* **150**, 467–486.

Steward, O. and Ribak, C. E. (1986). Polyribosomes associated with synaptic specializations on axon initial segments: localization of protein-synthetic machinery at inhibitory synapses. *J. Neurosci.* **6**, 3079–3085.

Stocchi, F. (2009). Dopamine receptor agonists in the treatment of advanced Parkinson's disease. *Parkinsonism Relat. Disord.* **15**, S54–S57.

Sulzer, D. (2007). Multiple hit hypotheses for dopamine neuron loss in Parkinson's disease. *Trends Neurosci.* **30**, 244–250.

Surmeier, D. J. (2010). α-Synuclein at the Synaptic Gate. *Neuron* **65**, 3–4.

Takahashi, K. and Yamanaka, S. (2006). Induction of pluripotent stem cells from mouse embryonic and adult fibroblast cultures by defined factors. *Cell* **126**, 663–676.

Takahashi, K., Tanabe, K., Ohnuki, M., Narita, M., Ichisaka, T., Tomoda, K. and Yamanaka, S. (2007). Induction of pluripotent stem cells from adult human fibroblasts by defined factors. *Cell* **131**, 861–872.

Tanaka, Y., Engelender, S., Igarashi, S., Rao, R. K., Wanner, T., Tanzi, R. E., Sawa, a, L Dawson, V., Dawson, T. M. and Ross, C. a (2001). Inducible expression of mutant alpha-synuclein decreases proteasome activity and increases sensitivity to mitochondria-dependent apoptosis. *Hum. Mol. Genet.* **10**, 919–926.

Tasic, B., Menon, V., Nguyen, T. N., Kim, T. K., Jarsky, T., Yao, Z., Levi, B., Gray, L. T., Sorensen, S. A., Dolbeare, T., et al. (2016). Adult mouse cortical cell taxonomy revealed by single cell transcriptomics. *Nat. Neurosci.* **19**, 335–346.

Taylor, T. N., Potgieter, D., Anwar, S., Senior, S. L., Janezic, S., Threlfell, S., Ryan, B., Parkkinen, L., Deltheil, T., Cioroch, M., et al. (2014). Region-specific deficits in dopamine, but not norepinephrine, signaling in a novel A30P α-synuclein BAC transgenic mouse. *Neurobiol. Dis.* **62**, 193–207.

Tesson, B. M., Breitling, R. and Jansen, R. C. (2010). DiffCoEx: a simple and sensitive method to find differentially coexpressed gene modules. *BMC Bioinformatics* **11**, 497.

Theillet, F.-X., Binolfi, A., Bekei, B., Martorana, A., Rose, H. M., Stuiver, M., Verzini, S., Lorenz, D., van Rossum, M., Goldfarb, D., et al. (2016). Structural disorder of monomeric α-synuclein persists in mammalian cells. *Nature* **530**, 45–50.

Thomas, B. and Flint Beal, M. (2007). Parkinson's disease. *Hum. Mol. Genet.* **16**,.

Thomas, B., Mandir, A. S., West, N., Liu, Y., Andrabi, S. A., Stirling, W., Dawson, V. L., Dawson, T. M. and Lee, M. K. (2011). Resistance to MPTP-Neurotoxicity in a-Synuclein Knockout Mice Is Complemented by Human α-Synuclein and Associated with Increased b-Synuclein and Akt Activation. *PLoS One* **6**, e16706.

Thomas, A., Lee, P.-J., Dalton, J. E., Nomie, K. J., Stoica, L., Costa-Mattioli, M., Chang, P., Nuzhdin, S., Arbeitman, M. N. and Dierick, H. A. (2012). A versatile method for cell-specific profiling of translated mRNAs in Drosophila. *PLoS One* **7**, e40276.

Tofaris, G. K., Layfield, R. and Spillantini, M. G. (2001). α-Synuclein metabolism and aggregation is linked to ubiquitin-independent degradation by the proteasome. *FEBS Lett.* **509**, 22–26.

Tofaris, G. K., Razzaq, A., Ghetti, B., Lilley, K. S. and Spillantini, M. G. (2003). Ubiquitination of Alpha-Synuclein in Lewy Bodies Is a Pathological Event Not Associated with Impairment of Proteasome Function. *J. Biol. Chem.* **278**, 44405–44411.

Tryon, R. C., Pisat, N., Johnson, S. L. and Dougherty, J. D. (2013). Development of translating ribosome affinity purification for zebrafish. *Genesis* **51**, 187–92.

Tsujimura, A., Taguchi, K., Watanabe, Y., Tatebe, H., Tokuda, T., Mizuno, T. and Tanaka, M. (2015). Lysosomal enzyme cathepsin B enhances the aggregate forming activity of exogenous α-synuclein fibrils. *Neurobiol. Dis.* **73**, 244–253.

Turiault, M., Parnaudeau, S., Milet, A., Parlato, R., Rouzeau, J.-D., Lazar, M. and Tronche, F. (2007). Analysis of dopamine transporter gene expression pattern -- generation of DAT-iCre transgenic mice. *FEBS J.* **274**, 3568–77.

Ueda, K., Fukushima, H., Masliah, E., Xia, Y., Iwai, A., Yoshimoto, M., Otero, D. A., Kondo, J., Ihara, Y. and Saitoh,

T. (1993). Molecular cloning of cDNA encoding an unrecognized component of amyloid in Alzheimer disease. *Proc. Natl. Acad. Sci.* **90**, 11282–11286.

Ungerstedt, U. (1968). 6-Hydroxy-dopamine induced degeneration of central monoamine neurons. *Eur. J. Pharmacol.* **5**, 107–110.

Utomo, a R., Nikitin, a Y. and Lee, W. H. (1999). Temporal, spatial, and cell type-specific control of Cre-mediated DNA recombination in transgenic mice. *Nat. Biotechnol.* **17**, 1091–1096.

Valente, E. M. (2004). Hereditary Early-Onset Parkinson's Disease Caused by Mutations in PINK1. *Science (80-.).* **304**, 1158–1160.

Van Den Eeden, S. K. (2003). Incidence of Parkinson's Disease: Variation by Age, Gender, and Race/Ethnicity. *Am. J. Epidemiol.* **157**, 1015–1022.

Venda, L. L., Cragg, S. J., Buchman, V. L. and Wade-Martins, R. (2010). alpha-Synuclein and dopamine at the crossroads of Parkinson's disease. *Trends Neurosci* **33**, 559–568.

Verma, P. (2005). Axonal Protein Synthesis and Degradation Are Necessary for Efficient Growth Cone Regeneration. *J. Neurosci.* **25**, 331–342.

Vilariño-Güell, C., Wider, C., Ross, O. A., Dachsel, J. C., Kachergus, J. M., Lincoln, S. J., Soto-Ortolaza, A. I., Cobb, S. A., Wilhoite, G. J., Bacon, J. A., et al. (2011). VPS35 mutations in parkinson disease. *Am. J. Hum. Genet.* **89**, 162–167.

Visanji, N. P., Brotchie, J. M., Kalia, L. V., Koprich, J. B., Tandon, A., Watts, J. C. and Lang, A. E. (2016). α-Synuclein-Based Animal Models of Parkinson's Disease: Challenges and Opportunities in a New Era. *Trends Neurosci.* **39**, 750–762.

Volpicelli-Daley, L. A., Luk, K. C., Patel, T. P., Tanik, S. A., Riddle, D. M., Stieber, A., Meaney, D. F., Trojanowski, J. Q. and Lee, V. M. Y. (2011). Exogenous Alpha-Synuclein Fibrils Induce Lewy Body Pathology Leading to Synaptic Dysfunction and Neuron Death. *Neuron* **72**, 57–71.

Walker, B. A., Hengst, U., Kim, H. J., Jeon, N. L., Schmidt, E. F., Heintz, N., Milner, T. A. and Jaffrey, S. R. (2012a). Reprogramming axonal behavior by axon-specific viral transduction. *Gene Ther.* **19**, 947–955.

Walker, B. A., Hengst, U., Kim, H. J., Jeon, N. L., Schmidt, E. F., Heintz, N., Milner, T. A. and Jaffrey, S. R. (2012b). Reprogramming axonal behavior by axon-specific viral transduction. *Gene Ther.* **19**, 947–55.

Wang, L., Fleming, S. M., Chesselet, M.-F. and Taché, Y. (2008). Abnormal colonic motility in mice overexpressing human wild-type alpha-synuclein. *Neuroreport* **19**, 873–6.

Wang, Z., Gerstein, M. and Snyder, M. (2009). RNA-Seq: a revolutionary tool for transcriptomics. *Nat. Rev. Genet.* **10**, 57–63.

Watson, F. L., Mills, E. A., Wang, X., Guo, C., Chen, D. F. and Marsh-Armstrong, N. (2012). Cell type-specific translational profiling in the Xenopus laevis retina. *Dev. Dyn.* **241**, 1960–72.

Weinreb, P. H., Zhen, W., Poon, A. W., Conway, K. A. and Lansbury, P. T. (1996). NACP, a protein implicated in Alzheimer's disease and learning, is natively unfolded. *Biochemistry* **35**, 13709–13715.

Welsh, M. (2004). Parkinson's disease and quality of life: Issues and challenges beyond motor symptoms. *Neurol. Clin.* **22**,.

Wersinger, C. and Sidhu, A. (2003). Attenuation of dopamine transporter activity by alpha-synuclein. *Neurosci. Lett.* **340**, 189–92.

Wersinger, C., Prou, D., Vernier, P. and Sidhu, A. (2003). Modulation of dopamine transporter function by alpha-synuclein is altered by impairment of cell adhesion and by induction of oxidative stress. *Faseb J* **17**, 2151–2153.

Wersinger, C., Banta, M. and Sidhu, A. (2004). Comparative analyses of alpha-synuclein expression levels in rat brain tissues and transfected cells. *Neurosci. Lett.* **358**, 95–8.

Westermann, B. (2010). Mitochondrial fusion and fission in cell life and death. *Nat. Rev. Mol. Cell Biol.* **11**, 872–884.

Winner, B., Jappelli, R., Maji, S. K., Desplats, P. A., Boyer, L., Aigner, S., Hetzer, C., Loher, T., Vilar, M., Campioni, S., et al. (2011). In vivo demonstration that Alpha-synuclein oligomers are toxic. *Proc. Natl. Acad. Sci.* **108**, 4194–4199.

Winslow, A. R., Chen, C. W., Corrochano, S., Acevedo-Arozena, A., Gordon, D. E., Peden, A. A., Lichtenberg, M., Menzies, F. M., Ravikumar, B., Imarisio, S., et al. (2010). α-Synuclein impairs macroautophagy: Implications for Parkinson's disease. *J. Cell Biol.* **190**, 1023–1037.

Wishart, T. M., Macdonald, S. H., Chen, P. E., Shipston, M. J., Coleman, M. P., Gillingwater, T. H. and Ribchester, R. R. (2007). Design of a novel quantitative PCR (QPCR)-based protocol for genotyping mice carrying the neuroprotective Wallerian degeneration slow (Wlds) gene. *Mol Neurodegener* **2**, 21.

Xie, Y. Z. and Zhang, R. X. (2014). Neurodegenerative diseases in a dish: the promise of iPSC technology in disease modeling and therapeutic discovery. *Neurol. Sci.* **36**, 21–27.

Yamada, K. M., Spooner, B. S. and Wessells, N. K. (1971). Ultrastructure and function of growth cones and axons of cultured nerve cells. *J. Cell Biol.* **49**, 614–635.

Yamaguchi, T., Sheen, W. and Morales, M. (2007). Glutamatergic neurons are present in the rat ventral tegmental area. *Eur. J. Neurosci.* **25**, 106–118.

Yamakado, H., Moriwaki, Y., Yamasaki, N., Miyakawa, T., Kurisu, J., Uemura, K., Inoue, H., Takahashi, M. and

Takahashi, R. (2012). Alpha-Synuclein BAC transgenic mice as a model for Parkinson's disease manifested decreased anxiety-like behavior and hyperlocomotion. *Neurosci. Res.* **73**, 173–177.

Yoon, B. C., Jung, H., Dwivedy, A., O'Hare, C. M., Zivraj, K. H. and Holt, C. E. (2012). Local translation of extranuclear lamin B promotes axon maintenance. *Cell* **148**, 752–64.

Yu, S., Zuo, X., Li, Y., Zhang, C., Zhou, M., Zhang, Y. A., Uéda, K. and Chan, P. (2004). Inhibition of tyrosine hydroxylase expression in alpha-synuclein-transfected dopaminergic neuronal cells. *Neurosci. Lett.* **367**, 34–9.

Zambrowicz, B. P., Imamoto, A., Fiering, S., Herzenberg, L. A., Kerr, W. G. and Soriano, P. (1997). Disruption of overlapping transcripts in the ROSA beta geo 26 gene trap strain leads to widespread expression of beta-galactosidase in mouse embryos and hematopoietic cells. *Proc. Natl. Acad. Sci. U. S. A.* **94**, 3789–94.

Zarranz, J. J., Alegre, J., Gomez-Esteban, J. C., Lezcano, E., Ros, R., Ampuero, I., Vidal, L., Hoenicka, J., Rodriguez, O., Atares, B., et al. (2004). The new mutation, E46K, of alpha-synuclein causes Parkinson and Lewy body dementia. *Ann Neurol* **55**, 164–173.

Zhang, S., Xiao, Q. and Le, W. (2015). Olfactory dysfunction and neurotransmitter disturbance in olfactory bulb of transgenic mice expressing human A53T mutant ??-synuclein. *PLoS One* **10**,.

Zharikov, A. D., Cannon, J. R., Tapias, V., Bai, Q., Horowitz, M. P., Shah, V., El Ayadi, A., Hastings, T. G., Greenamyre, J. T. and Burton, E. A. (2015). ShRNA targeting ??-synuclein prevents neurodegeneration in a Parkinson's disease model. *J. Clin. Invest.* **125**, 2721–2735.

Zhou, P., Qian, L., D'Aurelio, M., Cho, S., Wang, G., Manfredi, G., Pickel, V. and Iadecola, C. (2012). Prohibitin reduces mitochondrial free radical production and protects brain cells from different injury modalities. *J. Neurosci.* **32**, 583–92.

Zhou, P., Zhang, Y., Ma, Q., Gu, F., Day, D. S., He, A., Zhou, B., Li, J., Stevens, S. M., Romo, D., et al. (2013). Interrogating translational efficiency and lineage-specific transcriptomes using ribosome affinity purification. *Proc. Natl. Acad. Sci.* **110**, 15395–15400.

Zimprich, A., Biskup, S., Leitner, P., Lichtner, P., Farrer, M., Lincoln, S., Kachergus, J., Hulihan, M., Uitti, R. J., Calne, D. B., et al. (2004). Mutations in LRRK2 cause autosomal-dominant parkinsonism with pleomorphic pathology. *Neuron* **44**, 601–607.

Zivraj, K. H., Tung, Y. C. L., Piper, M., Gumy, L., Fawcett, J. W., Yeo, G. S. H. and Holt, C. E. (2010). Subcellular profiling reveals distinct and developmentally regulated repertoire of growth cone mRNAs. *J. Neurosci.* **30**, 15464–78.

- APPENDIX -

APPENDIX - LIST OF FIGURES

Chapter 5

APPENDIX FIGURE 5. 1 OVERVIEW OVER THE % OF TOTAL COUNTS. VIII
APPENDIX FIGURE 5. 2 SELECTED ASTROCYTE GENE MARKER EXPRESSIONS. XI
APPENDIX FIGURE 5. 3 OTHER SELECTED GENE MARKERS EXPRESSIONS. XII
APPENDIX FIGURE 5. 4 OTHER SELECTED GENE MARKERS EXPRESSIONS. PART II. XIII
APPENDIX FIGURE 5. 5 SELECTED MITOCHONDRIAL GENE MARKER EXPRESSIONS. XIV
APPENDIX FIGURE 5. 6 TH AND DAT GENE EXPRESSION CORRELATION. XVI
APPENDIX FIGURE 5. 7 HIGH CO-EXPRESSION IN THE BRAIN AMONG DIFFERENTIALLY EXPRESSED GENES WITH AGE. XIX
APPENDIX FIGURE 5. 8 FUNCTIONAL ANALYSIS OF GO TERMS FINDS OVERREPRESENTED BIOLOGICAL PROCESSES WITH AGE. XX

APPENDIX - LIST OF TABLES

Chapter 4

APPENDIX TABLE 4. 1 SELECTED MARKERS FOR DOPAMINERGIC NEURONS (DAN) AND NON-DANS. III
APPENDIX TABLE 4. 2 FPKM VALUES FOR DAN AND NON-DAN GENES SHOWN IN SCATTER PLOTS (3 MONTHS). III
APPENDIX TABLE 4. 3 FOLD CHANGES OF FPKM VALUES FOR DAN AND NON-DAN GENES SHOWN IN SCATTER PLOTS (3 MONTHS). III
APPENDIX TABLE 4. 4 FPKM VALUES FOR DAN AND NON-DAN GENES SHOWN IN SCATTER PLOTS (18 MONTHS). IV
APPENDIX TABLE 4. 5 FOLD CHANGES OF FPKM VALUES FOR DAN AND NON-DAN GENES SHOWN IN SCATTER PLOTS IN (18 MONTHS). IV
APPENDIX TABLE 4. 6 MARKER GENES USED FOR THE HEATMAP CLUSTERING. VI

Chapter 5

APPENDIX TABLE 5. 1 SUMMARY OF RNA-SEQ SAMPLE META-DATA. VII
APPENDIX TABLE 5. 2 MARKER GENES TOTAL EXPRESSION ACROSS ALL 40 SAMPLES. X
APPENDIX TABLE 5. 3 OVERVIEW OVER NON-DAN AND DAN MARKERS. XI
APPENDIX TABLE 5. 4 10 MOST UP- AND DOWN-REGULATED GENES FOR THE DEA "DISEASE – 3 MONTHS". XV
APPENDIX TABLE 5. 5 10 MOST UP- AND DOWN-REGULATED GENES FOR THE DEA "DISEASE – 12 MONTHS". XV
APPENDIX TABLE 5. 6 CO-EXPRESSION AMONG DEGS WITH AGE. XVI
APPENDIX TABLE 5. 7 NUMBER OF EDGES IN PPI-NETWORK. XVI
APPENDIX TABLE 5. 8 CLUSTERING IN PPI-NETWORK. XVI
APPENDIX TABLE 5. 9 PDFAM: FAMILIAL PD GENES. XVII
APPENDIX TABLE 5. 10 PDTRAFF: GENES INVOLVED IN INTRACELLULAR TRAFFICKING THAT CONTRIBUTE TO PD. XVII
APPENDIX TABLE 5. 11 PDGWAS: GENES WITHIN LOCI ASSOCIATED TO PD. XVIII

APPENDIX - CHAPTER 4

Symbol	Synonym	ENSEMBL	DAn
Aldh1l1		ENSMUSG00000030088	no
Gfap		ENSMUSG00000020932	no
Slc17a7	Vglut1	ENSMUSG00000070570	no
Thbd		ENSMUSG00000074743	no
Vgat	Slc32a1	ENSMUSG00000037771	no
Calb1	CalbindinD28K	ENSMUSG00000028222	yes
D2	Drd2	ENSMUSG00000032259	yes
Dat	Slc6a3	ENSMUSG00000021609	yes
Foxa2		ENSMUSG00000037025	yes
Girk2	Kcnj6	ENSMUSG00000043301	yes
Nurr1	Nr4a2	ENSMUSG00000026826	yes
Pitx3		ENSMUSG00000025229	yes
Th		ENSMUSG00000000214	yes
Vmat2	Slc18a2	ENSMUSG00000025094	yes

Appendix Table 4. 1 ***Selected markers for dopaminergic neurons (DAn) and non-DAns.***

Symbol	DA	IP-	IP+	IP++	Total-	Total+	Total++
Aldh1l1	no	81.0	38.3	21.8	48.1	51.1	33.8
Gfap	no	91.7	59.1	37.0	155.2	133.8	115.2
Slc17a7	no	4.9	3.7	2.1	5.0	3.9	3.5
Thbd	no	3.7	2.6	2.6	7.3	5.8	7.2
Vgat	no	14.9	11.3	5.4	9.6	7.7	7.8
Calb1	yes	10.1	12.0	26.4	5.6	6.8	10.2
D2	yes	3.9	5.7	9.1	3.7	3.4	4.2
Dat	yes	74.5	67.7	436.9	63.0	71.3	73.6
Foxa2	yes	0.6	0.6	2.4	0.2	0.1	0.4
Girk2	yes	2.5	2.4	3.1	2.2	2.5	1.8
Nurr1	yes	3.6	3.8	10.2	1.8	2.0	2.6
Pitx3	yes	0.0	0.1	0.3	0.1	0.0	0.0
Th	yes	253.7	165.1	858.1	76.7	82.5	67.3
Vmat2	yes	27.7	20.9	64.5	22.0	25.4	21.2

Appendix Table 4. 2 ***FPKM values for DAn and non-DAn genes shown in scatter plots (3 months).***

DAn= dopaminergic neuron. IP= bead-bound or immunoprecipitated RNA fraction. Total= input RNA fraction. Non-tg= non-transgenic (TRAP-negative). ++ or TRAP++= Homozygous THTR mice. + or TRAP+= Hemizygous THTR mice. Analysis performed in collaboration with F. Wessely.

Symbol	DAn	IP-/Total-	IP+/Total+	IP++/Total++
Aldh1l1	no	1.68	0.75	0.65
Gfap	no	0.59	0.44	0.32
Slc17a7	no	0.99	0.94	0.6
Thbd	no	0.5	0.44	0.37
Vgat	no	1.56	1.46	0.69
Calb1	yes	1.8	1.77	2.58
D2	yes	1.05	1.65	2.18
Dat	yes	1.18	0.95	5.94
Foxa2	yes	3.54	11.42	5.65
Girk2	yes	1.1	0.94	1.7
Nurr1	yes	2.02	1.94	3.94
Pitx3	yes	0	2.29	7.38
Th	yes	3.31	2	12.76
Vmat2	yes	1.26	0.82	3.04

Appendix Table 4. 3 ***Fold changes of FPKM values for DAn and non-DAn genes shown in scatter plots (3 months).***

DAn= dopaminergic neuron. IP= bead-bound or immunoprecipitated RNA fraction. Total= input RNA fraction. Non-tg= non-transgenic (TRAP-negative). ++ or TRAP++= Homozygous THTR mice. + or TRAP+= Hemizygous THTR mice. Analysis performed in collaboration with F. Wessely.

Symbol	DAn	IP+ old	Total+ old
Aldh1l1	no	70.8	67.8
Calb1	yes	11.5	4.2
D2	yes	2.4	3.8
Dat	yes	74.3	60.1
Foxa2	yes	1.5	0.2
Gfap	no	107.3	225.1
Girk2	yes	0.7	2.2
Nurr1	yes	5.0	1.7
Pitx3	yes	0.0	0.0
Slc17a7	no	3.6	2.9
Th	yes	226.0	92.8
Thbd	no	3.4	6.7
Vgat	no	10.2	8.8
Vmat2	yes	21.8	23.2

Appendix Table 4. 4 ***FPKM values for DAn and non-DAn genes shown in scatter plots (18 months).***

DAn= dopaminergic neuron. IP= bead-bound or immunoprecipitated RNA fraction. Total= input RNA fraction. F. Wessely.

Symbol	DAn	IP+ old/Total+ old
Aldh1l1	no	1.04
Calb1	yes	2.71
D2	yes	0.63
Dat	yes	1.24
Foxa2	yes	7.9
Gfap	no	0.48
Girk2	yes	0.32
Nurr1	yes	2.97
Pitx3	yes	
Slc17a7	no	1.22
Th	yes	2.44
Thbd	no	0.51
Vgat	no	1.17
Vmat2	yes	0.94

Appendix Table 4. 5 ***Fold changes of FPKM values for DAn and non-DAn genes shown in scatter plots in (18 months).***

DAn= dopaminergic neuron. IP= bead-bound or immunoprecipitated RNA fraction. Total= input RNA fraction. Analysis performed in collaboration with F. Wessely.

Symbol	Description	ENSEMBL
Abcc8	ATP-binding cassette, sub-family C (CFTR/MRP), member 8	ENSMUSG00000040136
Adcyap1	adenylate cyclase activating polypeptide 1	ENSMUSG00000024256
Aldh1a1	aldehyde dehydrogenase family 1, subfamily A1	ENSMUSG00000053279
Aldh1a2	aldehyde dehydrogenase family 1, subfamily A2	ENSMUSG00000013584
Aldh2	aldehyde dehydrogenase 2, mitochondrial	ENSMUSG00000029455
Atp13a2	ATPase type 13A2	ENSMUSG00000036622
B4galt1	UDP-Gal:betaGlcNAc beta 1,4- galactosyltransferase, polypeptide 1	ENSMUSG00000028413
Bag1	BCL2-associated athanogene 1	ENSMUSG00000028416
Bmp2	bone morphogenetic protein 2	ENSMUSG00000027358
Cacna1c	calcium channel, voltage-dependent, L type, alpha 1C subunit	ENSMUSG00000051331
Cacna1d	calcium channel, voltage-dependent, L type, alpha 1D subunit	ENSMUSG00000015968
Calb1	calbindin 1	ENSMUSG00000028222
Calb2	calbindin 2	ENSMUSG00000003657
Cartpt	CART prepropeptide	ENSMUSG00000021647
Cck	cholecystokinin	ENSMUSG00000032532
Chrna4	cholinergic receptor, nicotinic, alpha polypeptide 4	ENSMUSG00000027577
Chrna6	cholinergic receptor, nicotinic, alpha polypeptide 6	ENSMUSG00000031491
Clic3	chloride intracellular channel 3	ENSMUSG00000015093
Clic5	chloride intracellular channel 5	ENSMUSG00000023959
Clptm1l	CLPTM1-like	ENSMUSG00000021610
Clstn2	calsyntenin 2	ENSMUSG00000032452
Cntnap4	contactin associated protein-like 4	ENSMUSG00000031772
Cpne2	copine II	ENSMUSG00000034361
Ddc	dopa decarboxylase	ENSMUSG00000020182
Dlk1	delta-like 1 homolog (Drosophila)	ENSMUSG00000040856
Drd2	dopamine receptor D2	ENSMUSG00000032259
Efnb3	ephrin B3	ENSMUSG00000003934
Egr1	early growth response 1	ENSMUSG00000038418
En1	engrailed 1	ENSMUSG00000058665
En2	engrailed 2	ENSMUSG00000039095
Etv5	ets variant 5	ENSMUSG00000013089
Fam184a	family with sequence similarity 184, member A	ENSMUSG00000019856
Fgf1	fibroblast growth factor 1	ENSMUSG00000036585
Foxa1	forkhead box A1	ENSMUSG00000035451
Foxa2	forkhead box A2	ENSMUSG00000037025
Fzd1	frizzled class receptor 1	ENSMUSG00000044674
Gad1	glutamate decarboxylase 1	ENSMUSG00000070880
Gapdh	glyceraldehyde-3-phosphate dehydrogenase	ENSMUSG00000057666
Gch1	GTP cyclohydrolase 1	ENSMUSG00000037580
Gpr161	G protein-coupled receptor 161	ENSMUSG00000040836
Grb10	growth factor receptor bound protein 10	ENSMUSG00000020176
Grik3	glutamate receptor, ionotropic, kainate 3	ENSMUSG00000001985
Grin2c	glutamate receptor, ionotropic, NMDA2C (epsilon 3)	ENSMUSG00000020734
Grp	gastrin releasing peptide	ENSMUSG00000024517
Gsg1l	GSG1-like	ENSMUSG00000046182
Gucy2c	guanylate cyclase 2c	ENSMUSG00000042638
Igf1	insulin-like growth factor 1	ENSMUSG00000020053
Kcnj11	potassium inwardly rectifying channel, subfamily J, member 11	ENSMUSG00000096146
Kcnj6	potassium inwardly-rectifying channel, subfamily J, member 6	ENSMUSG00000043301
Kcns3	potassium voltage-gated channel, delayed-rectifier, subfamily S, member 3	ENSMUSG00000043673
Lmx1a	LIM homeobox transcription factor 1 alpha	ENSMUSG00000026686
Lmx1b	LIM homeobox transcription factor 1 beta	ENSMUSG00000038765
Lpl	lipoprotein lipase	ENSMUSG00000015568
Lrrc3b	leucine rich repeat containing 3B	ENSMUSG00000045201
Lrrk2	leucine-rich repeat kinase 2	ENSMUSG00000036273
Marcks	myristoylated alanine rich protein kinase C substrate	ENSMUSG00000069662
Ndnf	neuron-derived neurotrophic factor	ENSMUSG00000049001
Nefm	neurofilament, medium polypeptide	ENSMUSG00000022054
Nr4a2	nuclear receptor subfamily 4, group A, member 2	ENSMUSG00000026826
Nrip3	nuclear receptor interacting protein 3	ENSMUSG00000034825
Ntf3	neurotrophin 3	ENSMUSG00000049107
Ntn1	netrin 1	ENSMUSG00000020902
Ntsr1	neurotensin receptor 1	ENSMUSG00000027568

Otx2	orthodenticle homolog 2	ENSMUSG00000021848
Oxr1	oxidation resistance 1	ENSMUSG00000022307
Park2	Parkinson disease (autosomal recessive, juvenile) 2, parkin	ENSMUSG00000023826
Park7	Parkinson disease (autosomal recessive, early onset) 7	ENSMUSG00000028964
Parm1	prostate androgen-regulated mucin-like protein 1	ENSMUSG00000034981
Pink1	PTEN induced putative kinase 1	ENSMUSG00000028756
Pitx3	paired-like homeodomain transcription factor 3	ENSMUSG00000025229
Prkcd	protein kinase C, delta	ENSMUSG00000021948
Pvalb	parvalbumin	ENSMUSG00000005716
Rab3c	RAB3C, member RAS oncogene family	ENSMUSG00000021700
Satb1	special AT-rich sequence binding protein 1	ENSMUSG00000023927
Sdc2	syndecan 2	ENSMUSG00000022261
Sema6d	sema domain, transmembrane domain (TM), and cytoplasmic domain, 6D	ENSMUSG00000027200
Shh	sonic hedgehog	ENSMUSG00000002633
Slc10a4	solute carrier family 10 (sodium/bile acid cotransporter family), member 4	ENSMUSG00000029219
Slc17a6	solute carrier family 17 (sodium-dependent inorganic phosphate	ENSMUSG00000030500
Slc18a2	solute carrier family 18 (vesicular monoamine), member 2	ENSMUSG00000025094
Slc32a1	solute carrier family 32 (GABA vesicular transporter), member 1	ENSMUSG00000037771
Slc6a1	solute carrier family 6 (neurotransmitter transporter, GABA), member 1	ENSMUSG00000030310
Slc6a3	solute carrier family 6 (neurotransmitter transporter, dopamine), member 3	ENSMUSG00000021609
Slit2	slit homolog 2 (Drosophila)	ENSMUSG00000031558
Snca	synuclein, alpha	ENSMUSG00000025889
Sncg	synuclein, gamma	ENSMUSG00000023064
Sox6	SRY (sex determining region Y)-box 6	ENSMUSG00000051910
Syt1	synaptotagmin I	ENSMUSG00000035864
Syt17	synaptotagmin XVII	ENSMUSG00000058420
Tacr3	tachykinin receptor 3	ENSMUSG00000028172
Th	tyrosine hydroxylase	ENSMUSG00000000214
Vgf	VGF nerve growth factor inducible	ENSMUSG00000037428
Vip	vasoactive intestinal polypeptide	ENSMUSG00000019772
Zdhhc2	zinc finger, DHHC domain containing 2	ENSMUSG00000039470
Zfhx3	zinc finger homeobox 3	ENSMUSG00000038872
Zfp746	zinc finger protein 746	ENSMUSG00000057691

Appendix Table 4. 6 Marker genes used for the heatmap clustering.

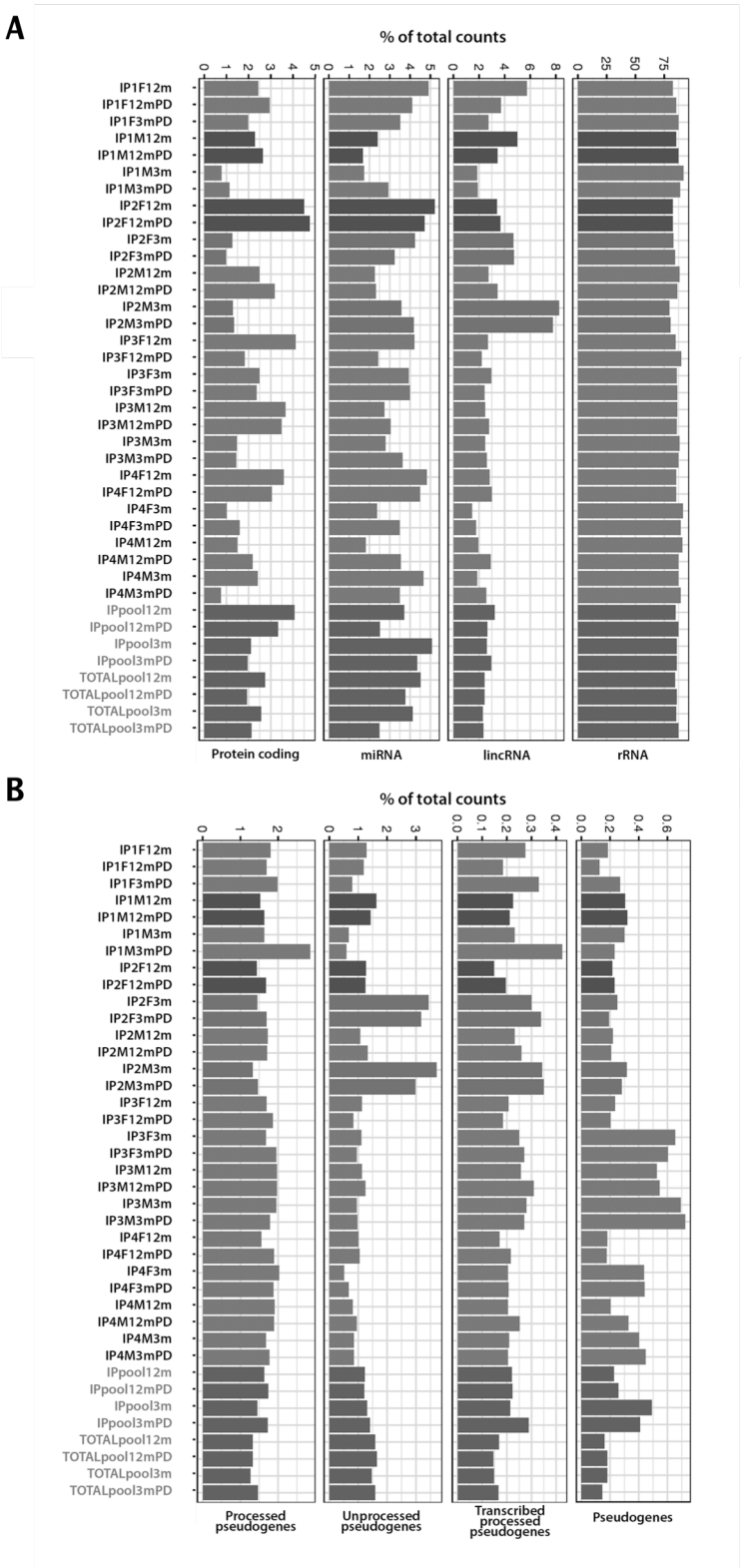
The lists of 96 genes was taken from Poulin et al. REFERNCE: Poulin JF (2014) Defining Midbrain Dopaminergic Neuron Diversity by Single-Cell Gene Expression Profiling. Cell reports.

APPENDIX – CHAPTER 5

Sample name	RIN	Average RNA concentration [ng/µl]	Average RNA amount [ng]	DAT enrichment (qPCR)	TH enrichment (qPCR)
THTR++ A* IP RNA	7.9	0.70	17.43	4.0	8.4
THTR++ B* IP RNA	7.3	3.73	93.37	1.4	2.8
THTR++ C* IP RNA	8.7	2.52	62.88	3.9	7.3
THTR++ D* IP RNA	7.6	2.86	71.59	3.9	5.5
THTR++PD A* IP RNA	7.3	1.87	46.83	2.7	6.0
THTR++PD B* IP RNA	6.0	4.20	104.91	2.4	4.2
THTR++PD C* IP RNA	8.6	0.74	18.45	5.0	11.4
THTR++PD D* IP RNA	7.3	2.49	62.30	3.1	5.1
THTR++ A IP RNA	6.2	1.07	26.68	1.5	3.6
THTR++ B IP RNA	9.1	1.18	29.39	3.6	7.0
THTR++ C IP RNA	8.5	1.30	32.49	4.1	8.5
THTR++ D IP RNA	8.7	1.16	28.98	4.6	7.3
THTR++PD A IP RNA	8.1	5.26	131.51	2.5	3.8
THTR++PD B IP RNA	9.1	0.90	22.48	3.4	7.8
THTR++PD C IP RNA	8.0	1.47	36.75	4.2	7.9
THTR++PD D IP RNA	8.8	0.70	17.39	5.7	11.7
THTR++ a* IP RNA	8.0	0.45	11.27	2.4	28.5
THTR++ b* IP RNA	8.0	0.23	5.75	1.8	9.4
THTR++ c* IP RNA	8.7	1.35	33.77	1.9	3.1
THTR++ d* IP RNA	8.8	1.03	25.79	6.3	10.9
THTR++PD a* IP RNA	9.5	1.06	26.56	5.4	17.1
THTR++PD b* IP RNA	8.2	0.29	7.26	2.3	9.7
THTR++PD c* IP RNA	8.1	1.17	29.18	1.6	4.3
THTR++PD d* IP RNA	8.3	0.86	21.57	5.4	10.0
THTR++ a IP RNA	8.5	0.58	14.54	10.0	10.2
THTR++ b IP RNA	8.5	0.30	7.49	1.5	7.9
THTR++ c IP RNA	8.7	0.77	19.31	2.4	7.9
THTR++ d IP RNA	8.2	1.63	40.82	4.0	10.5
THTR++PD a IP RNA	8.6	0.63	15.64	8.0	9.7
THTR++PD b IP RNA	8.9	0.34	8.39	2.4	6.9
THTR++PD c IP RNA	8.8	0.86	21.53	3.2	9.1
THTR++PD d IP RNA	8.9	0.76	19.01	7.9	12.4
IPpool12m	8.0	1.81	45.35	3.4	6.3
Totalpool12m	9.4	19.84	1090.97		
IPpool12mPD	8.0	2.20	55.08	3.6	7.3
Totalpool12mPD	9.4	15.80	868.77		
IPpool3m	8.4	0.79	19.84	3.8	11.0
Totalpool3m	9.0	21.89	1203.96		
IPpool3mPD	8.7	0.75	18.64	4.5	9.9
Totalpool3mPD	8.6	23.41	1287.36		

Appendix Table 5. 1 Summary of RNA-Seq sample meta-data.

For the pooled samples, average RINs, RNA concentrations/amounts, qPCR enrichemtns are shown. a-d= young mice (3 months). A-D= young mice (12 months).



Appendix Figure 5. 1 Overview over the % of total counts.

The mapping of reads was checked across different gene types sorted by their maximum percentage of total counts across the 40 samples. (A) Overview of protein coding genes, miRNA, lincRNA, and rRNA. (B) Overview of processed pseudogenes, unprocessed pseudogenes, transcribed processed pseudogenes, and pseudogenes. IP= bound or immunoprecipitated RNA fraction. Total= midbrain input RNA fraction. F= female. M= male. 3m= 3 months old mice. 12m= 12 months old mice. PD= Parkinson's disease model. Pool= pooled IP/Total samples across either control or disease model at 3/12 months (grey text). miRNA= microRNA, lincRNA= Long intervening noncoding RNA. rRNA= ribosomal RNA. Analysis performed in collaboration with F. Wessely.

Symbol	Official gene name	ENSEMBL	DAn	# of samples	FC
Acta2	actin, alpha 2, smooth muscle, aorta	ENSMUSG00000035783	fibro	39	0.6
Adgrl4	*adhesion G protein-coupled receptor L4*	*ENSMUSG00000039167*	*endothelial*	*39*	*0.7*
Aldh1l1	aldehyde dehydrogenase 1 family, member L1	ENSMUSG00000030088	astro	39	0.5
Aldoc	aldolase C, fructose-bisphosphate	ENSMUSG00000017390	astro	39	0.6
Aqp4	aquaporin 4	ENSMUSG00000024411	astro	39	0.3
Pygb	brain glycogen phosphorylase	ENSMUSG00000033059	astro	39	0.8
Bysl	bystin-like	ENSMUSG00000023988	astro	39	1.5
Calb1	calbindin 1	ENSMUSG00000028222	DAn	39	4.3
Cd83	CD83 antigen	ENSMUSG00000015396	microglia	39	0.7
Ccl2	*chemokine (C-C motif) ligand 2*	*ENSMUSG00000035385*	*microglia*	*28*	*1.1*
Ccl3	*chemokine (C-C motif) ligand 3*	*ENSMUSG00000000982*	*microglia*	*22*	*0.7*
Cx3cr1	chemokine (C-X3-C motif) receptor 1	ENSMUSG00000052336	microglia	39	0.2
Cck	cholecystokinin	ENSMUSG00000032532	neuron	39	7.5
Cldn5	claudin 5	ENSMUSG00000041378	endothelial	39	0.7
Clu	clusterin	ENSMUSG00000022037	astro	39	0.3
Col1a2	collagen, type I, alpha 2	ENSMUSG00000029661	fibro	39	0.5
Col3a1	*collagen, type III, alpha 1*	*ENSMUSG00000026043*	*fibro*	*38*	*0.6*
C1qa	complement component 1, q subcomponent, alpha polypeptide	ENSMUSG00000036887	microglia	39	0.2
Dio2	deiodinase, iodothyronine, type II	ENSMUSG00000007682	astro	39	0.3
Ddc	dopa decarboxylase	ENSMUSG00000020182	DAn	39	8.3
Drd2	dopamine receptor D2	ENSMUSG00000032259	DAn	39	4.7
Esam	*endothelial cell-specific adhesion molecule*	*ENSMUSG00000001946*	*endothelial*	*39*	*0.7*
Ednrb	endothelin receptor type B	ENSMUSG00000022122	astro	39	0.2
En1	engrailed 1	ENSMUSG00000058665	DAn	39	12.3
En2	engrailed 2	ENSMUSG00000039095	DAn	39	4.8
Fgfr3	fibroblast growth factor receptor 3	ENSMUSG00000054252	astro	39	0.3
Foxa1	forkhead box A1	ENSMUSG00000035451	DAn	38	16.0
Foxa2	forkhead box A2	ENSMUSG00000037025	DAn	39	14.6
Gpr37	G protein-coupled receptor 37	ENSMUSG00000039904	oligo	39	0.3
Gja1	gap junction protein, alpha 1	ENSMUSG00000050953	astro	39	0.2
Gfap	glial fibrillary acidic protein	ENSMUSG00000020932	astro	39	0.8
Gad1	*glutamate decarboxylase 1*	*ENSMUSG00000070880*	*neuron*	*39*	*1.0*
Glul	glutamate-ammonia ligase (glutamine synthetase)	ENSMUSG00000026473	astro	39	0.7
Itm2a	integral membrane protein 2A	ENSMUSG00000031239	endothelial	39	0.6
Icam2	*intercellular adhesion molecule 2*	*ENSMUSG00000001029*	*endothelial*	*35*	*0.6*
Il1a	interleukin 1 alpha	ENSMUSG00000027399	microglia	24	0.7
Lmx1b	LIM homeobox transcription factor 1 beta	ENSMUSG00000038765	DAn	39	5.5
Mlc1	megalencephalic leukoencephalopathy with subcortical cysts 1 homolog (human)	ENSMUSG00000035805	astro	39	0.2
Mbp	myelin basic protein	ENSMUSG00000041607	oligo	39	0.2
Mog	myelin oligodendrocyte glycoprotein	ENSMUSG00000076439	oligo	39	0.3
Mobp	myelin-associated oligodendrocytic basic protein	ENSMUSG00000032517	oligo	39	0.3
Nes	*nestin*	*ENSMUSG00000004891*	*astro*	*39*	*1.2*
Npy	neuropeptide Y	ENSMUSG00000029819	neuron	39	0.6
Nfia	nuclear factor I/A	ENSMUSG00000028565	astro	39	0.5
Nr4a2	nuclear receptor subfamily 4, group A, member 2	ENSMUSG00000026826	DAn	39	7.3

Opalin	oligodendrocytic myelin paranodal and inner loop protein	ENSMUSG00000050121	oligo	39	0.4
Pitx3	paired-like homeodomain transcription factor 3	ENSMUSG00000025229	DAn	38	7.7
Kcnj6	*potassium inwardly-rectifying channel, subfamily J, member 6*	*ENSMUSG00000043301*	*DAn*	*39*	*1.4*
Plp1	proteolipid protein (myelin) 1	ENSMUSG00000031425	oligo	39	0.3
S100a4	*S100 calcium binding protein A4*	*ENSMUSG00000001020*	*fibro*	*32*	*0.8*
S100b	S100 protein, beta polypeptide, neural	ENSMUSG00000033208	astro	39	0.4
Slc1a2	solute carrier family 1 (glial high affinity glutamate transporter), member 2	ENSMUSG00000005089	astro	39	0.2
Slc1a3	solute carrier family 1 (glial high affinity glutamate transporter), member 3	ENSMUSG00000005360	astro	39	0.2
Slc1a1	solute carrier family 1, member 1	ENSMUSG00000024935	neuron	39	0.5
Slc17a7	solute carrier family 17 member 7	ENSMUSG00000070570	other	39	0.7
Slc18a2	solute carrier family 18 (vesicular monoamine), member 2	ENSMUSG00000025094	DAn	39	2.7
Slc32a1	solute carrier family 32 (GABA vesicular transporter), member 1	ENSMUSG00000037771	other	39	1.0
Slc4a4	solute carrier family 4 (anion exchanger), member 4	ENSMUSG00000060961	astro	39	0.5
Slc6a3	solute carrier family 6 (neurotransmitter transporter, dopamine), member 3	ENSMUSG00000021609	DAn	39	5.4
Sst	somatostatin	ENSMUSG00000004366	neuron	39	0.6
Sparcl1	SPARC-like 1	ENSMUSG00000029309	astro	39	0.2
Sox10	*SRY (sex determining region Y)-box 10*	*ENSMUSG00000033006*	*oligo*	*39*	*0.9*
Sox9	SRY (sex determining region Y)-box 9	ENSMUSG00000000567	astro	39	0.6
Stmn2	stathmin-like 2	ENSMUSG00000027500	neuron	39	2.0
Syn1	synapsin I	ENSMUSG00000037217	neuron	39	2.4
Syt1	*synaptotagmin I*	*ENSMUSG00000035864*	*neuron*	*39*	*1.1*
Thbd	thrombomodulin	ENSMUSG00000074743	other	39	0.6
Tlr2	*toll-like receptor 2*	*ENSMUSG00000027995*	*microglia*	*34*	*0.7*
Tmem119	transmembrane protein 119	ENSMUSG00000054675	microglia	39	0.2
Th	tyrosine hydroxylase	ENSMUSG00000000214	DAn	39	14.4
Vim	*vimentin*	*ENSMUSG00000026728*	*astro*	*39*	*0.9*

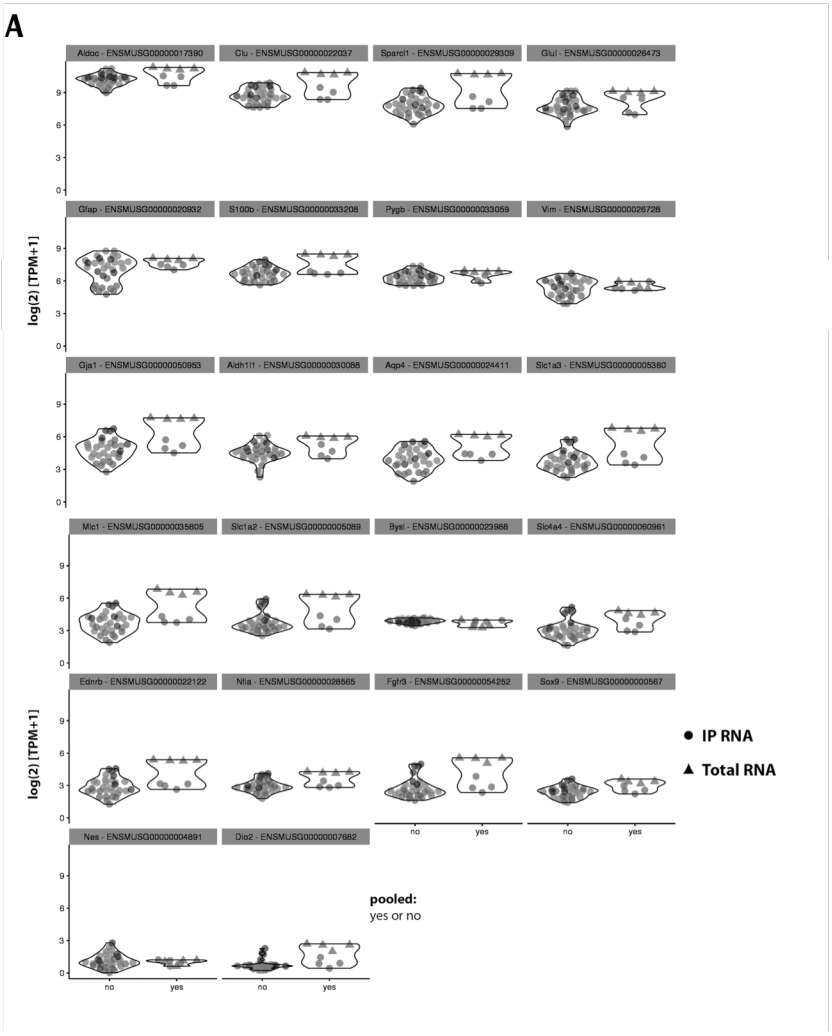
Appendix Table 5. 2 Marker genes total expression across all 40 samples.

Global expression levels of selected marker genes across all samples. The expression rank is based on the mean expression values. Rank 1 refers to the gene with highest mean expression value. Here, the mean expression is based on mean of 'expression' levels, i.e. log2(TPM + 1). DAn= dopaminergic neuron. FC= Fold-change. dark grey+italic= FDR>0.05. Analysis performed in collaboration with F. Wessely and J. Monzon-Sandoval.

Symbol	Synonym	Official gene name	ENSEMBL	DAn
Aldh1l1		Aldehyde dehydrogenase 1 family L1	ENSMUSG00000030088	no
Gad1		Glutamate decarboxylase 1	ENSMUSG00000070880	no
Gfap		Glial fibrillary acidic protein	ENSMUSG00000020932	no
Vglut1	Slc17a7	Vesicular glutamate transporter 1	ENSMUSG00000070570	no
Thbd		Thrombomodulin	ENSMUSG00000074743	no

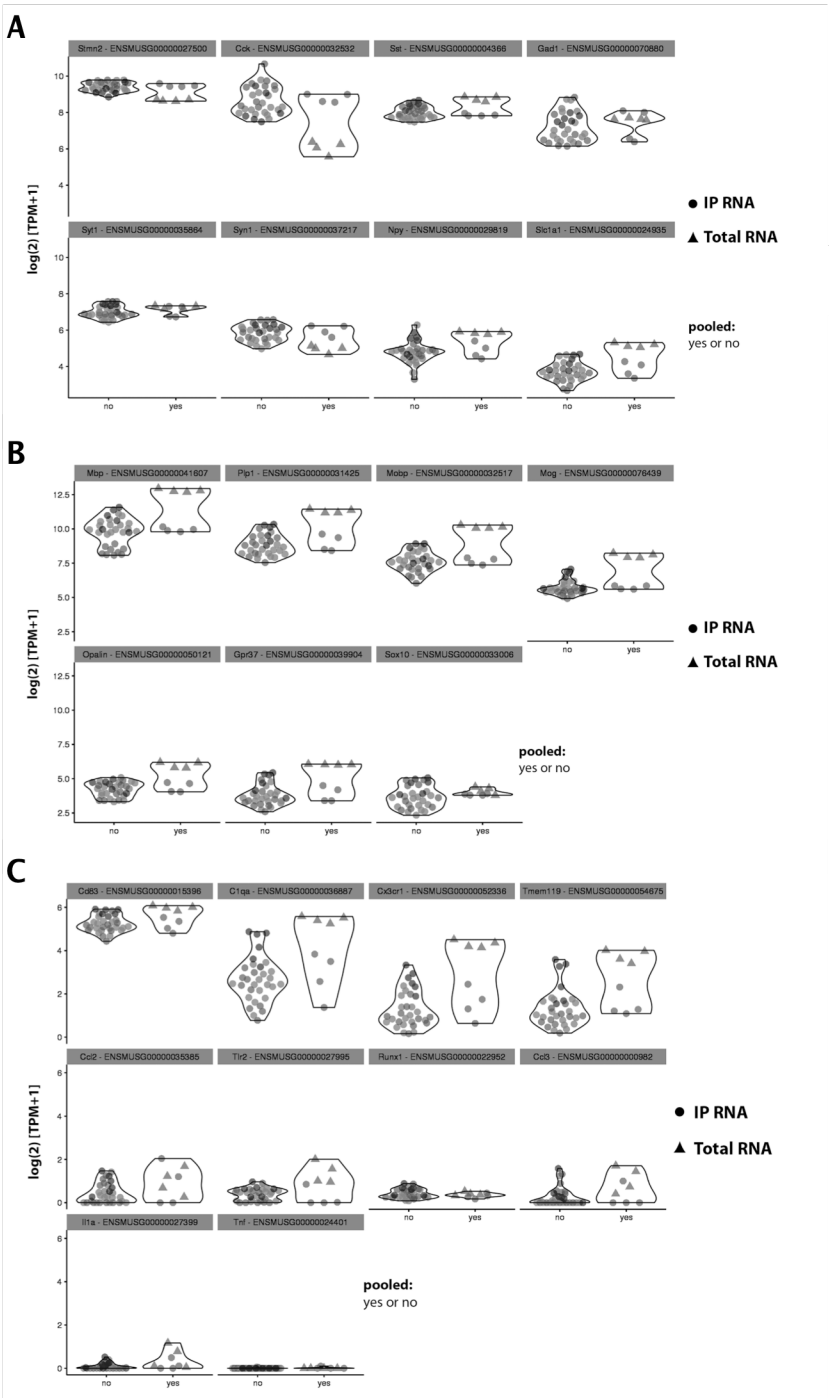
Symbol	Synonym	Official gene name	ENSEMBL	DAn
Dat	Slc6a3	Dopamine transporter	ENSMUSG00000021609	yes
Ddc		Dopa decarboxylase	ENSMUSG00000020182	yes
En1		Engrailed 1	ENSMUSG00000058665	yes
En2		Engrailed 2	ENSMUSG00000039095	yes
Foxa2	HNF-3B/TCF-3B	Forkhead box protein A2	ENSMUSG00000037025	yes
Lmx1b		LIM homeobox transcription factor 1 beta	ENSMUSG00000038765	yes
Nurr1	Nr4a3	Nuclear receptor related-1	ENSMUSG00000026826	yes
Pitx3		Paired like homeodomain 3	ENSMUSG00000025229	yes
TH		Tyrosine hydroxylase	ENSMUSG00000000214	yes
Vmat2	Slc18a2	Vesicular monoamine transporter 2	ENSMUSG00000025094	yes

Appendix Table 5. 3 ***Overview over non-DAn and DAn markers.***



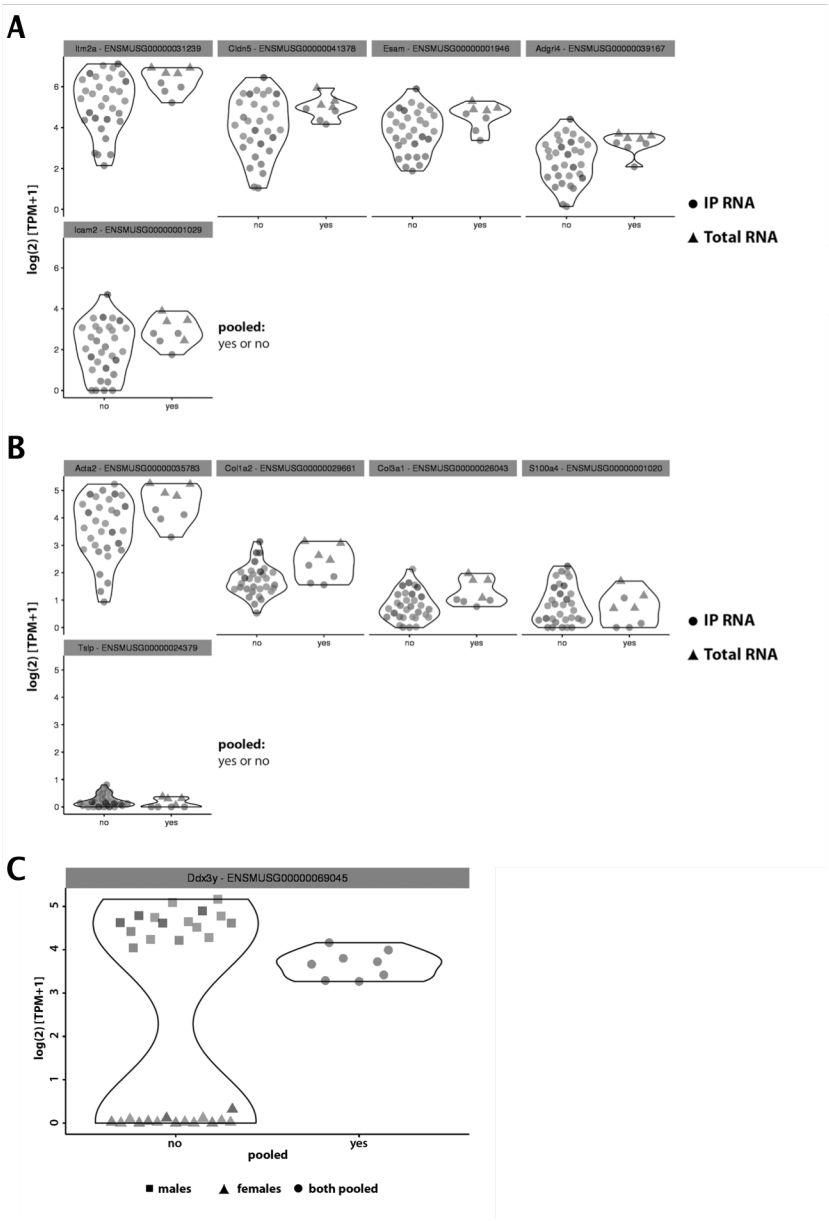
Appendix Figure 5. 2 ***Selected Astrocyte gene marker expressions.***

Global expression levels of 22 selected astrocyte-related marker genes across all 40 samples as the log2 transformed TPM expression [Log2(TPM + 1)]. Left: IP samples (circle). Right: Pooled IP samples (circle) and pooled Total samples (triangle). Most markers show lower expression in the IP fractions compared to the Total fractions. TPM= transcript per million. IP= bound or immunoprecipitated RNA fraction. Total= midbrain input RNA fraction. F= female. Analysis performed in collaboration with F. Wessely.



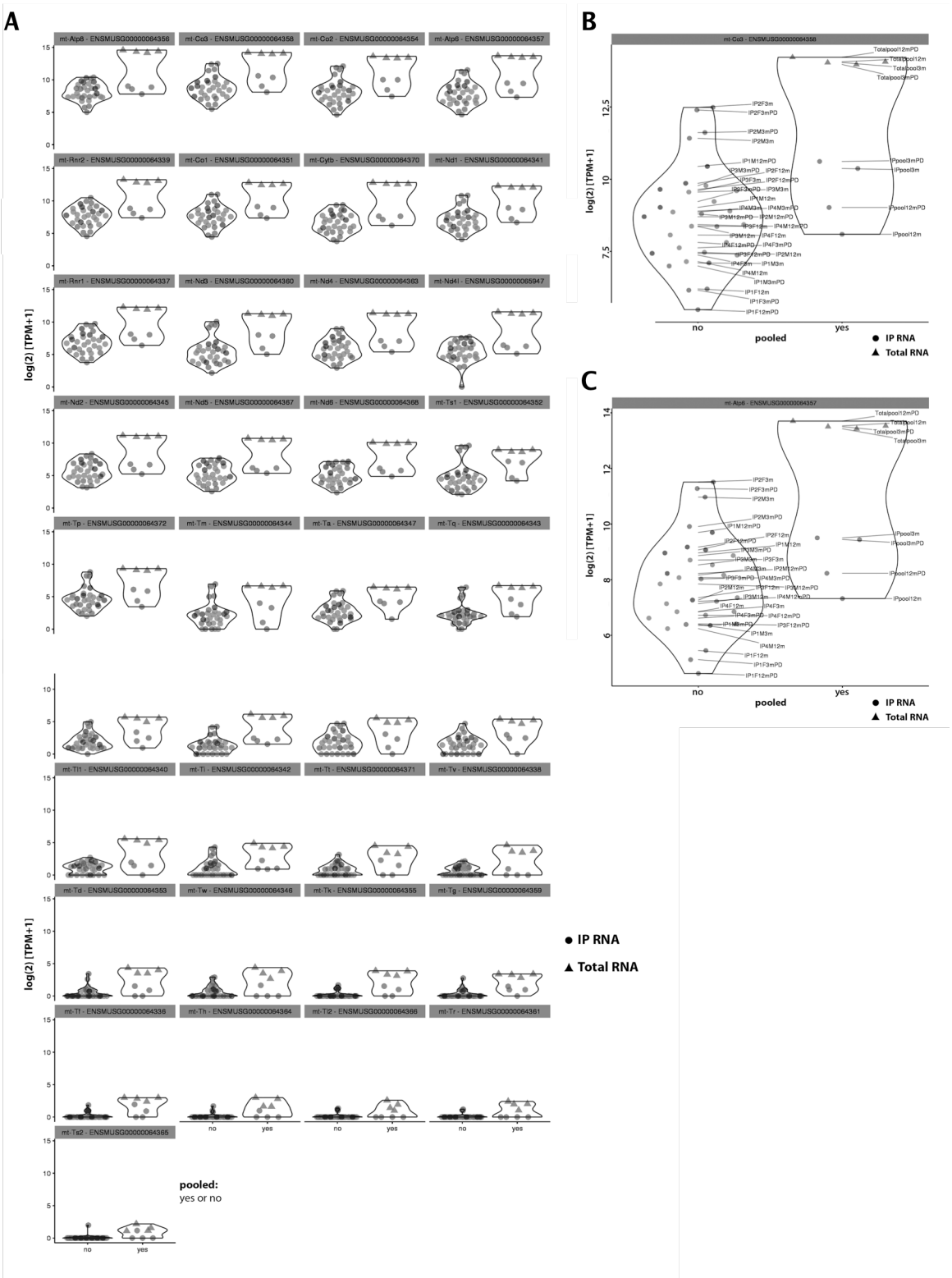
Appendix Figure 5. 3 Other selected gene markers expressions.

Global expression levels of selected neuron/oligodendrocyte/microglia-related marker genes across all 40 samples [Log2(TPM + 1)]. Left: IP samples (circle). Right: Pooled IP (circle) and pooled Total (triangle). (A) Neuron markers. Stmm2, Cck and Syn1 show higher expression in the IP samples, whereas Sst, Npy, and Slc1a1 are higher expressed in the Total samples. All other tested marker genes do not show a clear separation. (B) Oligodendrocyte markers. All 7 tested oligodendrocyte marker genes show a higher expression in the Total fractions, with the exception of Sox10. (C) Microglia/ macrophage markers. There is no clear enrucment profile for any of the markers tested. C1qa, Cx3cr1 and Tmem119 are higher in the Total fractions but show a range of expression across the different IP samples. Many microglia/macrophage-related genes are very lowly expressed overall. TPM= transcript per million. IP= bound or immunoprecipitated RNA fraction. Total= midbrain input RNA fraction. Analysis performed in collaboration with F. Wessely.



Appendix Figure 5. 4 Other selected gene markers expressions. PART II.

Global expression levels of selected endothelial and fibroblast marker genes across all 40 samples as the log2 transformed TPM expression [Log2(TPM + 1)]. Left: IP samples (circle). Right: Pooled IP samples (circle) and pooled Total samples (triangle). (A) Endothelial markers and (B) Fibroblast markers. None of the tested marker genes does show a clear separation. (C) Y chromosome gene. The Y chromosome-specific gene is only enriched in the male samples, as expected. The pooled IP and pooled Total samples show Ddx3y expression but less than compared to its expression in the male-only fractions. TPM= transcript per million. IP= bound or immunoprecipitated RNA fraction. Total= midbrain input RNA fraction. F= female. M= male. 3m= 3 months old mice. 12m= 12 months old mice. PD= Parkinson's disease model. Pool= pooled IP/Total samples across either control or disease model at 3/12 months. Analysis performed in collaboration with F. Wessely.



Appendix Figure 5. 5 Selected Mitochondrial gene marker expressions.

(A) Global expression levels of 37 selected mitochondrial genes across all 40 samples [Log2(TPM + 1)]. Left: IP (circle). Right: Pooled IP (circle) and Total (triangle). Most Total samples show a higher expression of mitochondrial genes. Higher expression for a sub-set of four IP samples for some markers. Sample-specific expression for two selected genes is higher in IP2F3m, IP2F3mPD, IP2M3m, IP2M3mPD. (B) For mt-Co3 and (C) Mt-Atp6 these four samples form a cluster. TPM= transcript per million. IP= bound or immunoprecipitated RNA fraction. Total= midbrain input RNA fraction. F= female. M= male. 3m= 3 months old mice. 12m= 12 months old mice. PD= Parkinson's disease model. Pool= pooled IP/Total samples across either control or disease model at 3/12 months. Analysis performed in collaboration with F. Wessely.

Symbol	ENSEMBL	Log2 FC	FC	p-value	FDR
Snca	ENSMUSG00000025889	8,99	508,81	0,00	0,00
Muc1	ENSMUSG00000042784	5,40	42,14	0,25	1,00
Ces1d	ENSMUSG00000056973	5,40	42,17	0,18	1,00
Foxh1	ENSMUSG00000033837	5,08	33,74	0,20	1,00
Treml1	ENSMUSG00000023993	4,64	24,96	0,30	1,00
Duxbl2	ENSMUSG00000072675	4,35	20,38	0,03	1,00
Gm26602	ENSMUSG00000097854	4,31	19,79	0,19	1,00
Gbgt1	ENSMUSG00000026829	4,09	16,98	0,16	1,00
1700012P22Rik	ENSMUSG00000028589	3,76	13,56	0,36	1,00
Cd86	ENSMUSG00000022901	3,56	11,77	0,04	1,00

Symbol	ENSEMBL	Log2 FC	FC	p-value	FDR
Clec4b1	ENSMUSG00000030147	-3,29	0,10	0,11	1,00
Axdnd1	ENSMUSG00000026601	-3,31	0,10	0,05	1,00
Car9	ENSMUSG00000028463	-3,58	0,08	0,01	1,00
Bdkrb1	ENSMUSG00000041347	-4,11	0,06	0,23	1,00
Klrb1f	ENSMUSG00000030154	-4,14	0,06	0,17	1,00
Syngr4	ENSMUSG00000040231	-4,14	0,06	0,11	1,00
Kiss1	ENSMUSG00000102367	-4,58	0,04	0,19	1,00
Chrna9	ENSMUSG00000029205	-4,72	0,04	0,29	1,00
Duxbl1	ENSMUSG00000048502	-4,93	0,03	0,02	1,00
Crct1	ENSMUSG00000027913	-6,02	0,02	0,09	1,00

Appendix Table 5. 4 10 most up- and down-regulated genes for the DEA "disease – 3 months".

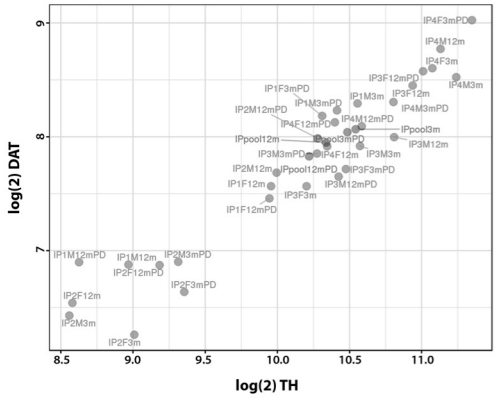
Shown are the log2 FC MLE and the FC MLE (MLE= maximum-likelihood estimate). FDR= false discovery rate. DEA= differential expression analysis. Log2 FC= log2 fold-change. FC= Fold-change. Blue= down-regulated. Red= up-regulated.

Symbol	ENSEMBL	Log2 FC	FC	p-value	FDR
Snca	ENSMUSG00000025889	9,01	514,18	0,00	1,00
Marc1	ENSMUSG00000026621	5,43	43,25	0,04	1,00
Ugt1a7c	ENSMUSG00000090124	4,89	29,68	0,02	1,00
Mc5r	ENSMUSG00000007480	4,76	27,06	0,08	1,00
Klk10	ENSMUSG00000030693	4,57	23,72	0,20	1,00
Evi2b	ENSMUSG00000093938	4,31	19,87	0,07	1,00
Cldn20	ENSMUSG00000091530	3,95	15,43	0,33	1,00
Myo15b	ENSMUSG00000034427	3,93	15,22	0,05	1,00
Lyzl4	ENSMUSG00000032530	3,93	15,20	0,15	1,00
Vipr1	ENSMUSG00000032528	3,86	14,54	0,07	1,00

Symbol	ENSEMBL	Log2 FC	FC	p-value	FDR
Gm9922	ENSMUSG00000053821	-3,36	0,10	0,12	1,00
Gm8439	ENSMUSG00000091297	-3,43	0,09	0,33	1,00
Hmgb4	ENSMUSG00000048686	-3,46	0,09	0,27	1,00
Gm45318	ENSMUSG00000110358	-3,61	0,08	0,26	1,00
Cib3	ENSMUSG00000074240	-3,66	0,08	0,31	1,00
Gm5901	ENSMUSG00000078611	-3,74	0,07	0,24	1,00
Bglap	ENSMUSG00000074483	-3,78	0,07	0,33	1,00
Defb25	ENSMUSG00000074678	-3,82	0,07	0,29	1,00
Tmem217	ENSMUSG00000079580	-3,96	0,06	0,33	1,00
Gm42421	ENSMUSG00000104633	-4,02	0,06	0,15	1,00

Appendix Table 5. 5 10 most up- and down-regulated genes for the DEA "disease – 12 months".

Shown are the log2 FC MLE and the FC MLE (MLE= maximum-likelihood estimate). FDR= false discovery rate. DEA= differential expression analysis. Log2 FC= log2 fold-change. FC= Fold-change. Blue= down-regulated. Red= up-regulated.



Appendix Figure 5. 6 TH and DAT gene expression correlation.

Correlation (Spearman's rank rho= 0.9168067, p-value < 2.2e-16) of the log2 TH and DAT TPM levels from RNA-Seq. The Spearman correlation between two variables is overall very high. A sub-set of 8 samples shows overall lower DAT and TH expression (IP2F3m, IP2F3mPD, IP2M3m, IP2M3mPD, IP2F12m, IP2F12mPD, IP1M12m, IP1M12mPD). TPM= transcript per million. IP= bound or immunoprecipitated RNA fraction. Total= midbrain input RNA fraction. F= female. M= male. 3m= 3 months old mice. 12m= 12 months old mice. PD= Parkinson's disease model. Pool= pooled IP/Total samples across either control or disease model at 3/12 months. Analysis performed in collaboration with F. Wessely.

Sub-set	DEG type	Number of DEGs	Co-expression observed	Co-expression expected	SEM
All	UP	1740	0.0649414	0.0319239	0.0016474
All	DOWN	1582	0.0975324	0.0319239	0.0017533
CTRL	UP	598	0.0673713	0.0319132	0.0029929
CTRL	DOWN	436	0.1981069	0.0319912	0.0035543
PD	UP	510	0.0546696	0.0318859	0.0032570
PD	DOWN	418	0.2281604	0.0319325	0.0036598

Appendix Table 5. 6 Co-expression among DEGs with age.

Analysis performed in collaboration with J. Mozon-Sandoval.

Sub-set	DEG type	Number of DEGs	Co-expression observed	Co-expression expected	SEM
All	UP	24309	22772.8600	259.9660000	< 0.0001
All	DOWN	18718	14948.2600	202.7957000	< 0.0001
CTRL	UP	2956	2778.4720	71.1521400	0.0072
CTRL	DOWN	3294	1567.3200	48.9582800	< 0.0001
PD	UP	1917	1844.3450	52.5085100	0.0889
PD	DOWN	2640	1132.6290	41.0818700	< 0.0001

Appendix Table 5. 7 Number of edges in PPI-network.

Analysis performed in collaboration with J. Mozon-Sandoval.

Sub-set	DEG type	Number of DEGs	Co-expression observed	Co-expression expected	SEM
All	UP	0.1821550	0.2189024	0.0100705	1
All	DOWN	0.4096119	0.2428468	0.0135320	< 0.0001
CTRL	UP	0.1673474	0.2162589	0.0188678	0.997
CTRL	DOWN	0.7042348	0.2210580	0.0231141	< 0.0001
PD	UP	0.1751639	0.2194165	0.0222270	0.9826
PD	DOWN	0.6670189	0.2023067	0.0245829	< 0.0001

Appendix Table 5. 8 Clustering in PPI-network.

Analysis performed in collaboration with J. Mozon-Sandoval.

Symbol	Gene description	ENSEMBL
ASH1L	ASH1 like histone lysine methyltransferase	ENSG00000116539
ATP13A2	ATPase 13A2	ENSG00000159363
BCKDK	branched chain ketoacid dehydrogenase kinase	ENSG00000103507
BST1	bone marrow stromal cell antigen 1	ENSG00000109743
CCDC62	coiled-coil domain containing 62	ENSG00000130783
DLG2	discs large MAGUK scaffold protein 2	ENSG00000150672
FAM47E	family with sequence similarity 47 member E	ENSG00000189157
GCH1	GTP cyclohydrolase 1	ENSG00000131979
GPNMB	glycoprotein nmb	ENSG00000136235
HLA-DQB1	major histocompatibility complex, class II, DQ beta 1	ENSG00000225824
HLA-DQB1	major histocompatibility complex, class II, DQ beta 1	ENSG00000231286
HLA-DQB1	major histocompatibility complex, class II, DQ beta 1	ENSG00000233209
INPP5F	inositol polyphosphate-5-phosphatase F	ENSG00000198825
LRRK2	leucine rich repeat kinase 2	ENSG00000188906
LRRK2	leucine rich repeat kinase 2	ENSG00000188906
MAPT	microtubule associated protein tau	ENSG00000186868
MCCC1	methylcrotonoyl-CoA carboxylase 1	ENSG00000078070
NUCKS1	nuclear casein kinase and cyclin dependent kinase substrate 1	ENSG00000069275
PARK2	parkin RBR E3 ubiquitin protein ligase	ENSG00000185345
PARK7	Parkinsonism associated deglycase	ENSG00000116288
PINK1	PTEN induced putative kinase 1	ENSG00000158828
RIT2	Ras like without CAAX 2	ENSG00000152214
SIPA1L2	signal induced proliferation associated 1 like 2	ENSG00000116991
SNCA	synuclein alpha	ENSG00000145335
STK39	serine/threonine kinase 39	ENSG00000198648
TMEM175	transmembrane protein 175	ENSG00000127419
TMEM229B	transmembrane protein 229B	ENSG00000198133
TMPRSS9	transmembrane protease, serine 9	ENSG00000178297
UBOX5	U-box domain containing 5	ENSG00000185019

Appendix Table 5. 9 ***PDfam: familial PD genes.***

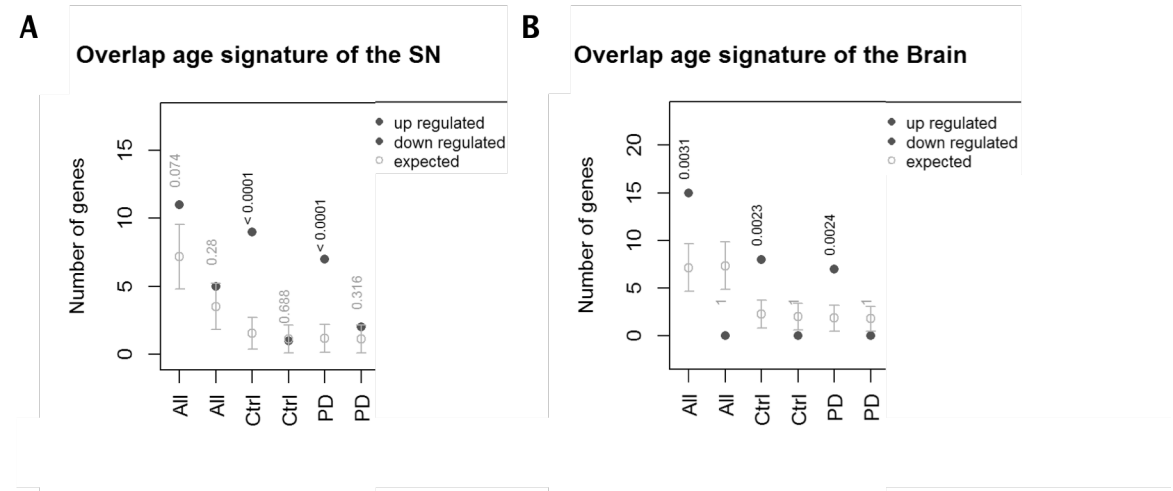
Symbol	Gene description	ENSEMBL
ATP13A2	ATPase 13A2	ENSG00000159363
ATP6AP2	ATPase H+ transporting accessory protein 2	ENSG00000182220
DNAJC13	DnaJ heat shock protein family (Hsp40) member C13	ENSG00000138246
DNAJC6	DnaJ heat shock protein family (Hsp40) member C6	ENSG00000116675
GAK	cyclin G associated kinase	ENSG00000178950
GBA	glucosylceramidase beta	ENSG00000177628
LAMP3	lysosomal associated membrane protein 3	ENSG00000078081
LRRK2	leucine rich repeat kinase 2	ENSG00000188906
MAPT	microtubule associated protein tau	ENSG00000186868
PARK2	parkin RBR E3 ubiquitin protein ligase	ENSG00000185345
PINK1	PTEN induced putative kinase 1	ENSG00000158828
RAB29	RAB29, member RAS oncogene family	ENSG00000117280
RAB39B	RAB39B, member RAS oncogene family	ENSG00000155961
SCARB2	scavenger receptor class B member 2	ENSG00000138760
SNCA	synuclein alpha	ENSG00000145335
SYNJ1	synaptojanin 1	ENSG00000159082
SYT11	synaptotagmin 11	ENSG00000132718
TMEM230	transmembrane protein 230	ENSG00000089063
VPS13C	vacuolar protein sorting 13 homolog C	ENSG00000129003
VPS35	VPS35, retromer complex component	ENSG00000069329

Appendix Table 5. 10 ***PDtraff: genes involved in intracellular trafficking that contribute to PD.***

Reference: Abeliovich et al. (2016).

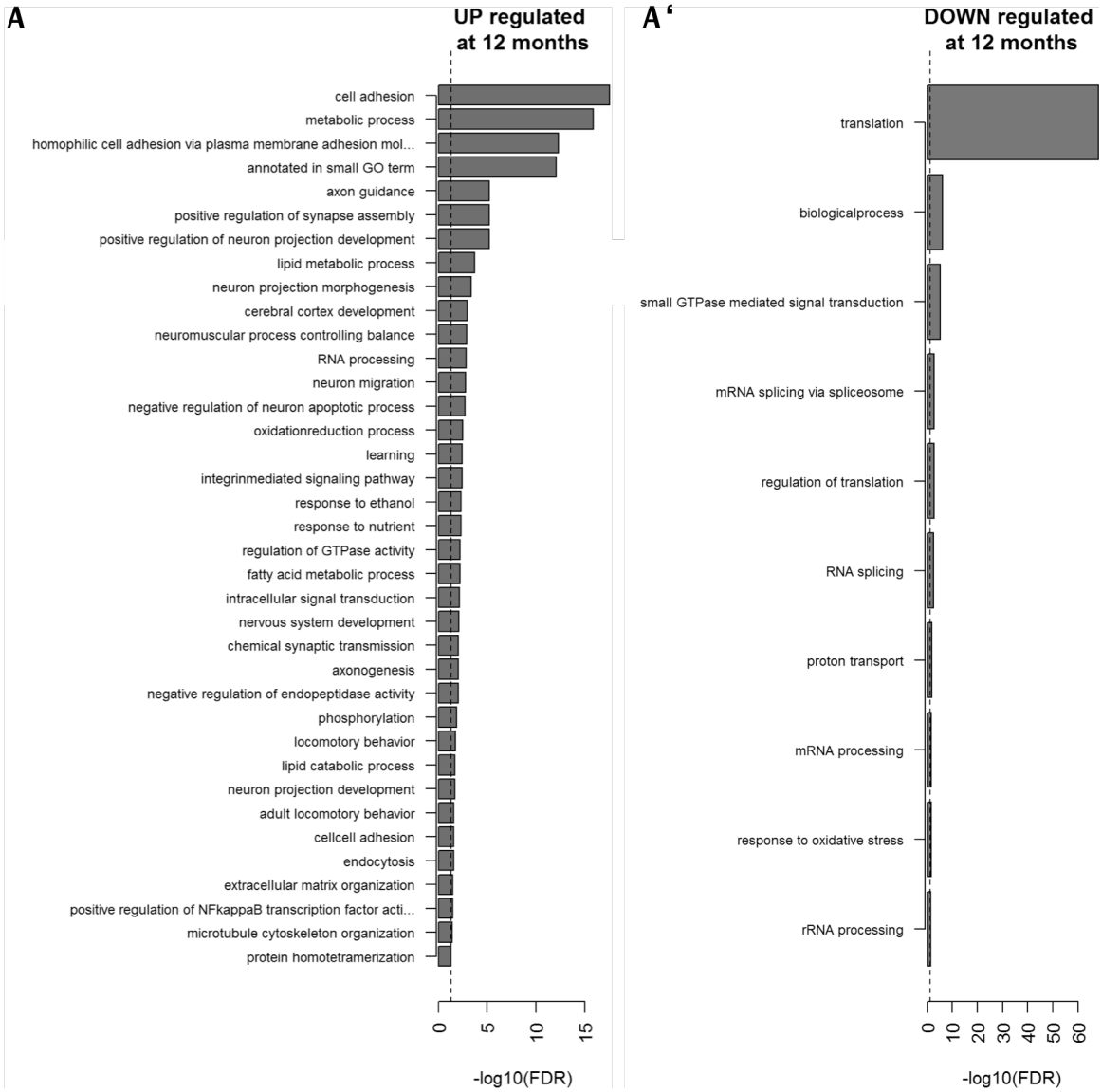
Symbol	Gene description	ENSEMBL
ACMSD	aminocarboxymuconate semialdehyde decarboxylase	ENSG00000153086
BST1	bone marrow stromal cell antigen 1	ENSG00000109743
CCDC62	coiled-coil domain containing 62	ENSG00000130783
CCNT2-AS1	CCNT2 antisense RNA 1	ENSG00000224043
CRHR1	corticotropin releasing hormone receptor 1	ENSG00000120088
DLG2	discs large MAGUK scaffold protein 2	ENSG00000150672
FAM47E	family with sequence similarity 47 member E	ENSG00000189157
FDPSP3	farnesyl diphosphate synthase pseudogene 3	ENSG00000258872
GAK	cyclin G associated kinase	ENSG00000178950
GBA	glucosylceramidase beta	ENSG00000177628
GCH1	GTP cyclohydrolase 1	ENSG00000131979
GPNMB	glycoprotein nmb	ENSG00000136235
HLA-DQA1	major histocompatibility complex, class II, DQ alpha 1	ENSG00000196735
HLA-DQB1-AS1	HLA-DQB1 antisense RNA 1	ENSG00000223534
HLA-DRB5	major histocompatibility complex, class II, DR beta 5	ENSG00000198502
HMGN2P18	high mobility group nucleosomal binding domain 2 pseudogene 18	ENSG00000223452
INPP5F	inositol polyphosphate-5-phosphatase F	ENSG00000198825
ITGA8	integrin subunit alpha 8	ENSG00000077943
LDHAL6DP	lactate dehydrogenase A like 6D, pseudogene	ENSG00000250257
LRRK2	leucine rich repeat kinase 2	ENSG00000188906
LZTS3	leucine zipper tumor suppressor family member 3	ENSG00000088899
MAPT	microtubule associated protein tau	ENSG00000186868
MCCC1	methylcrotonoyl-CoA carboxylase 1	ENSG00000078070
MCCC1-AS1	MCCC1 antisense RNA 1	ENSG00000243368
MED13	mediator complex subunit 13	ENSG00000108510
MIR4308	microRNA 4308	ENSG00000265432
MTCO3P1	mitochondrially encoded cytochrome c oxidase III pseudogene 1	ENSG00000235040
NMD3	NMD3 ribosome export adaptor	ENSG00000169251
PM20D1	peptidase M20 domain containing 1	ENSG00000162877
RAB25	RAB25, member RAS oncogene family	ENSG00000132698
RAB29	RAB29, member RAS oncogene family	ENSG00000117280
RAI1	retinoic acid induced 1	ENSG00000108557
RIT2	Ras like without CAAX 2	ENSG00000152214
RN7SL474P	RNA, 7SL, cytoplasmic 474, pseudogene	ENSG00000264092
SETD1A	SET domain containing 1A	ENSG00000099381
SIPA1L2	signal induced proliferation associated 1 like 2	ENSG00000116991
SLC50A1	solute carrier family 50 member 1	ENSG00000169241
SNCA	synuclein alpha	ENSG00000145335
SREBF1	sterol regulatory element binding transcription factor 1	ENSG00000072310
STK39	serine/threonine kinase 39	ENSG00000198648
TMEM175	transmembrane protein 175	ENSG00000127419
TMEM229B	transmembrane protein 229B	ENSG00000198133
VDAC2P4	voltage dependent anion channel 2 pseudogene 4	ENSG00000234682
ZNF668	zinc finger protein 668	ENSG00000167394

Appendix Table 5. 11 ***PDgwas: genes within loci associated to PD.***



Appendix Figure 5. 7 High co-expression in the brain among differentially expressed genes with age.

The co-expression was measured as the Pearson correlation between sets of DEGs from the TRAP-Seq dataset with DEG levels from the mouse SNc (A) or the whole brain (B). The observed number of overlapping genes to an expected number given 10,000 randomizations was tested. The background gene population has been adjusted to all genes tested in the analysis for which gene expression was also measured in the microarray platform used by Gao et al (2013). The age signature of the SNc has been constructed using microarray data (GeneChip, Mouse Genome 430 2.0 Array) comparing 2 months vs. 18 months old mice (4 replicates (pooled from 4-5 mice) for each age group) Gao et al (2013). The age signature of the mouse brain is based on a meta-analysis comparing brain-specific transcripts from young (2-5 months) and old (24-30 months) mice on a genome-wide base. Only genes identified in at least 3/4 studies, were included in the transcriptional signature of aged mouse brain Gao et al (2013). The observed and expected co-expression levels for each sub-set of DEGs with age and the estimated p-value plotted next to the corresponding co-expression levels (A, B). Grey dots= expected values. Red dots= observed up-resulted values. Blue dots= observed down-regulated values. DEG= differentially expressed gene. PPI= protein-protein interaction network. LD= linkage disequilibrium. SNPs= single nucleotide polymorphisms. SNc= Substantia nigra. REFERENCE: Gao et al. (2013). Analysis performed in collaboration with J. Monzon-Sandoval. Image credit J. Monzon-Sandoval.



Appendix Figure 5. 8 ***Functional analysis of GO terms finds overrepresented biological processes with age.***

Age-related changes comparing 3 and 12 months old mice for DEGs (FDR < 0.05, n >= 2). The UP (A) and DOWN (A') regulation is shown relative to 12 months. Bar plots represent the -log10(FDR), dotted line is drawn at -log10(0.05). The analysis includes all IP samples (CTRL and PD), except outliers (IP1F3m, IP1M12m, IP1M12mPD, IP2F12mPD, IP2F12m) and pooled samples. The bar plots show overrepresented GO terms for UP- or DOWN-regulated genes across all IP samples with age, representing a greater variety of GO terms for UP-regulated than DOWN-regulated genes. FDR= false-discovery rate. GO= gene ontology. bp= biological process. IP= bound or immunoprecipitated RNA fraction. 3m= 3 months old mice. 12m= 12 months old mice. PD= Parkinson's disease model. Analysis performed in collaboration with J. Monzon-Sandoval. Image credit J. Monzon-Sandoval.